TECTONIC CONSTRAINTS FROM THIN GRANITOID SHEETS IN H.U. SVERDRUPFJELLA, WESTERN DRONNING MAUD LAND, ANTARCTICA

by

Erasmus Petrus Burger

Submitted in partial fulfilment of the requirements for the degree
PhD Geology

In the Faculty of Natural & Agricultural Sciences
University of Pretoria
Pretoria

8th of December 2023

I, Erasmus Petrus Burger declare that the thesis/dissertation, which I hereby submit for the degree PhD in Geology at the University of Pretoria, is my own work and has not previously been submitted by me for a degree at this or any other tertiary institution.

SIGNATURE: …………………………..

DATE: …………………………………

Dedication

I would like to dedicate this thesis to my father, Francois Burger. For raising me to a position and enabling me to undertake this adventure and challenge. Thank you for all the support and encouragement over these years.

Acknowledgements

This project was made possible by funding from the National Research Foundation of South Africa, under grants 93079 and 110739. This funding enabled not only the collection of samples in Antarctica, but the preparation of thins sections and analysis of trace and major elements at the Council of Geosciences in Pretoria, the analysis of radiogenic isotopes at the University of Cape Town, and the LA-ICP-MS analysis at the University of Johannesburg. The NRF also provided two years of bursary support for EP Burger under the above grants, and a further 1 year of funding under a free-standing bursary, as well as support for conference attendance in India and Japan. The financial assistance of the National Research Foundation (NRF) towards this research is hereby acknowledged.

Opinions expressed and conclusions arrived at, are those of the author and are not necessarily to be attributed to the NRF.

The South African National Antarctic Program, Department of Environmental Affairs and Starlite Aviation are acknowledged for logistical support during the Antarctic field work.

Dr Kenji Horie of NIPR at Tachikawa, Tokyo, performed the SHRIMP analyses at no cost.

Dr Geoff Grantham for acting as co-supervisor, leading the Antarctic fieldwork and providing guidance and teaching in the field. Dr Grantham, Mike Knoper and Hendrik Smit helped with sample collection and structural measurements, and Dr Grantham collected some samples independently during the project. His guidance and Antarctic knowledge was essential to the project, and his contribution is greatly appreciated

Prof James Roberts provided scientific guidance as well as academic and moral support as the lead supervisor at the University of Pretoria.

Dr. IR Ribbens provided proofreading, advice on structuring and an academic perspective from outside the field of geology.

Finally, I would like to thank my wife, Lindsay, for her patience, support and understanding.

Abstract

This work is a study of granitoid sheets in H.U. Sverdrupfjella. The objectives were to measure the orientations and take samples of the granitoid sheets to produce orientation, geochronological and geochemical data from the granitoids. This data is intended to reveal the nature and timing of emplacement for the granitoid sheets and to provide constraints regarding the tectonic history of the study area.

This work identified three suites of granitoid sheets, namely the Pre-existing Granitoids, Salknappen Pegmatites and Dalmatian Granites:

1) The oldest of these suites is the Pre-existing Granitoids, as is evident from field relationships. Pre-existing Granitoids were only seen at a handful of outcrops at the Rootshorga nunatak, which limited the extent of study possible.
2) Salknappen Pegmatites are weakly deformed, very coarse grained and white in colour. From cross-cutting relationships, Salknappen Pegmatites are older than Dalmatian Granite. SHRIMP geochronology gives ages of 517 ± 3.5 Ma, 507 ± 3.1 Ma and 513 ± 3.7 Ma for the three samples which were dated. Geochemically, Salknappen Pegmatites have two distinct groups, one characterised by positive Eu anomalies (+Eu Salknappen Pegmatites), and another characterised by negative Eu anomalies (-Eu Salknappen Pegmatites). These rocks have a flat REE profile with LREE enrichment. Isotope geochemistry gives a younger model age and higher $^{143}Nd/^{144}Nd$ than Dalmatian Granites and show a similarity to the Rootshorga Complex country rock.
3) Dalmatian Granites crosscut the granitoid suites described above and structural features in the country rock. No deformation is evident in competent country rocks. In the field Dalmatian Granite can be identified by course to very coarse-grained texture and pink colour. SHRIMP dating gives ages of 492 ± 2.1 Ma, 483 ± 2.8 Ma and 483 ± 3.1 Ma for the three samples analysed. The geochemistry of Dalmatian Granite is consistent with an upper crustal source.

The granitoids are interpreted to record the earlier stages of orogeny (Salknappen Pegmatites) followed by the late to post-orogenic stage (Dalmatian Granites). Owing to the ~30 m.y. gap between the emplacements of the two suites, a model involving a diachronous metamorphic event is favoured.

Table of Contents

List of Tables and Figures:

Chapter 1: Introduction

1.1 The Project

In remote locations like Antarctica, where rock exposure is limited and fieldwork constrained, any additional geological information that can be gathered is valuable. Granitic sheets in H.U. Sverdrupfjella, Antarctica, are ubiquitous and interact with country rock over a wide area, which is an advantage compared to using larger intrusions to determine the field relationship with country rocks. Granitic dykes and sills are often a minor component of geologic terranes which can be used to infer the tectonic setting in which they are recognised (e.g., Pearce *et al.*, 1984). Specifically, granitic rocks bear the mark of their source, from which the tectonic setting may be inferred (e.g., Pearce *et al.*, 1984; Chappell and White 2001; Clemens and Stevens, 2012).

The metamorphic country rock and structural geology of the study area, the H.U. Sverdrupfjella in western Dronning Maud Land, Antarctica (Figure 1.1) has already been described, investigated, and mapped (e.g. Board *et.* al. 2005; Grosch *et al.* 2015; Pauly *et al.* 2016; Grantham *et al*. 2019), but the granitic sheets present have been mostly ignored or overlooked. In these relatively thin sheets, the effect of stress during emplacement and subsequent deformation is quite pronounced, making emplacement relative to tectonic activity easier to determine. Absolute ages of the granitic sheets can be used in conjunction with the relative ages from field relationships to constrain models of the tectonic history of the study area. The study area is of interest because of its position adjacent to the Grunehogna province (Figure 1.1) and a history of collision with other parts of Africa. In this work the term “granitoid” refers to rocks that are similar to granite but differ from the formal definition in some way. In this work the word “granitoid” is meant to describe a rock that is similar to granite but is not a granite by strict definition. Rocks described as granitoids in this work are mostly (but not all) too coarse grained to be considered granite by strict definition (i.e., granitic pegmatites).

This project is part of ongoing research projects lead by Dr. Geoff Grantham, in this case a continuation of work in Grantham *et al.* (2008) which describes the mega-nappe hypothesis (reviewed in section 1.4.1). This project intended to revisit the Dalmatian Granites, described by Grantham *et al.,* (1991) and reviewed in Section 1.3.1, and use the granite orientation and geochemistry to gain data and insight into the tectonic history of the study area. During fieldwork additional suites of granitoids were observed and included in this study.

1.2 Geological Setting

There are two significant and distinct geological terranes relevant to the study area (Figure 1.1), the Grunehogna Province and the Maud Belt. The Grunehogna Province is a cratonic fragment that was part of the Kaapvaal Craton, but that was separated during the break-up of Gondwana (Marschall *et al.*, 2010). The Maud Belt is a metamorphic belt adjacent to the Grunehogna Craton that was formed during the formation of Rodinia (~1000 Ma) and later reworked during the formation of Gondwana ~500 Ma) as per Grantham *et al.*, (1995). Geological events affecting the study are summarised in table 1.1.

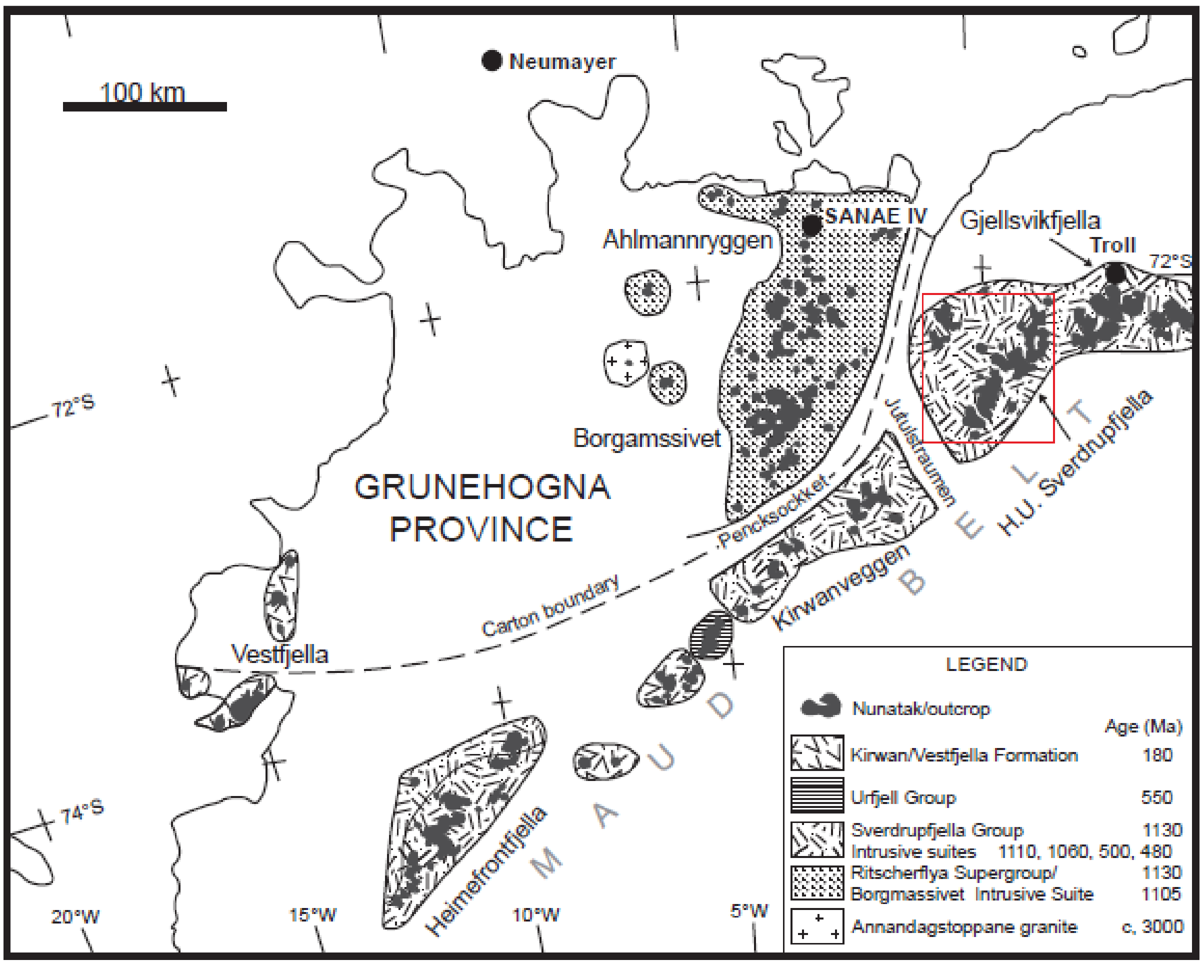

Figure 1.1: A map showing the location and generalised geology of the Grunehogna Province and Maud Belt, after Board *et al*. (2005).

Table 1.1: Chronological summary of geological events in H.U. Sverdrupfjella.

Date:	Event:	Reference:
3450- 2800 Ma	Age of Archaean basement rocks	Halpern (1970)
3067 ± 8 Ma	Age of Annandagstoppane Granite	Marschall *et al*. (2010)
~1130 Ma	Subduction under eastern Grunehogna	Marschall *et al.* (2013)
1130 Ma -1107 Ma	Ahlmannryggen Group deposited	Wolmarans and Kent, (1982)
1130 Ma -1107 Ma	Jutulrøra Complex protolith deposition	Marschall *et al.* (2013)
1180 Ma -1000 Ma	Metamorphism in H.U. Sverdrupfjella	Groenewald (1995)
1127 ± 12 Ma	Emplacement of Sveabreen migmatitic granite	Harris *et al*., (1995)
~1100 Ma	Emplacement of Borgmassivet Intrusive Suite	Riley and Millar, (2004)
1086 ± 4 Ma	Orogeny related to Rodinia assembly	Marschall *et al.* (2013)
~1040 Ma - ~1030 Ma	High grade metamorphic episode in H.U. Sverdrupfjella	Board *et al.* (2005)
1000 Ma - 900 Ma	Period of deformation in H.U. Sverdrupfjella	Grantham *et al.* (1995)
590 Ma - 550 Ma	Posited age of Mega-nappe formation	Grantham *et al.* (2008)
570 ± 7 Ma	Peak metamorphism in H.U. Sverdrupfjella	Pauly *et al.* (2016)
565 Ma - 540 Ma	Metamorphism in eastern H.U. Sverdrupfjella	Grosch *et al.* (2015)
565 Ma - 499 Ma	High grade metamorphic episode in H.U. Sverdrupfjella	Board *et al.* (2005)
550 Ma - 490 Ma	Period of deformation in H.U. Sverdrupfjella	Grantham *et al.* (1995)
~540 Ma	Peak metamorphism in H.U. Sverdrupfjella	Board (2001)
~519 Ma	Emplacement of Brattskarvet intrusive suite	Moyes *et al.* (1993)
~500 Ma	Accretion of the E H.U. Sverdrupfjella onto W H.U. Sverdrupfjella	Grosch *et al.* (2015)
491 ± 27 Ma	High-grade metamorphism in the western H.U. Sverdrupfjella	Grosch *et al.* (2015)
~480 Ma	Emplacement of post-tectonic granitic dykes	Board (2001)
~480 Ma	Ar-Ar isotopic systems reset	Board (2001)
469 ± 5 Ma	Emplacement of Dalmatian Granite	Grantham *et al.* (1991)
~170 Ma	Emplacement of Straumsvola nepheline syenite complex	Harris and Grantham, (1993)

On the Grunehogna Province the Annandagstoppane Granite, the Ritscherflya Supergroup, and the Borgmassivet Intrusive Suite are exposed. Despite extremely limited exposure, ages between ~2950 Ma and ~3100 Ma have been determined for Archaean basement rocks (i.e., Annandagstoppane Granite) by Halpern (1970). Marschall *et al*. (2010) reported an age of 3067 ± 8 Ma for the Annandagstoppane Granite. Based on the limited rock exposure, the Grunehogna Province has been interpreted to be part of the Kaapvaal Craton that detached during the break-up of Gondwana (e.g., Groenewald *et al.,* 1991; Krynauw, 1996; Marschall *et al*., 2010 Marschall *et al*., 2013). The relationships between rock types on the different cratonic blocks are unclear, owing to the lack of exposure, but it was assumed by Wolmarans and Kent (1982) that Archean granite or a granite-greenstone terrane underlies the rocks of the Mesoproterozoic Ritscherflya Supergroup in H.U. Sverdrupfjella.

The Ritscherflya Supergroup consists of the Ahlmannryggen Group overlain by the Jutulstraumen Group (Wolmarans and Kent, 1982) and intruded by the Borgmassivet Intrusive Suite. The Ahlmannryggen

Group consists of rocks consistent with a regressive (marine to braided river) sedimentary cycle (Ferreira, 1988) deposited between 1130 Ma and 1107 Ma (Wolmarans and Kent, 1982). The Jutulstraumen group is characterised by basaltic and andesitic lava flows with minor volcanic units (Watters *et al.,* 1991). Thick mafic and ultramafic rocks of the Borgmassivet Intrusive Suite intruded the Ritscherflya Supergroup at ~1100 Ma (Riley and Millar, 2014) in the form of thick tholeiitic sills with a continental geochemical signature (Krynauw *et al.,* 1991).

Marschall *et al.* (2013) conclude that subduction took place under the eastern margin of the Grunehogna Craton at ~1130 Ma (preceding orogeny associated with Rodinia assembly), based on U-Pb ages of detrital zircon grains from the Ahlmannryggen and Jutulstraumen groups (Ritscherflya Supergroup), as crystallisation ages close to the deposition age of sediments. According to Marschall *et al.* (2013) it also follows that the Ritscherflya Supergroup sediments were deposited in the continental arc setting resulting from the subduction. Marschall *et al.* (2013) also note metamorphic zircon recrystallisation at 1086 ± 4 Ma (in detrital zircons from the Ritscherflya Supergroup), which marks the orogeny related to Rodinia assembly on the eastern margin of the Grunehogna Craton.

The Maud Belt includes (from southwest to northeast) Heimefrontfjella, Kirwanveggen, H.U. Sverdrupfjella, Gjelsvikfjella and western Mühlig-Hofmannfjella. In the H.U. Sverdrupfjella, the Maud Belt is made up of gneisses and other metamorphic rocks (including marbles and amphibolites), which were formed by the ~1000 Ma amalgamation of Rodinia (Grantham *et al.*, 1995). The metamorphic rocks mostly occur as part of three dominant metamorphic complexes; the Jutulrøra Complex (which includes quartz-feldspar gneisses and banded gneisses), the Fuglefjellet Complex (composed of pelitic gneiss and marble with interlayered calc-silicate gneiss) and the Rootshorga Complex (composed of pelitic gneisses, felsic paragneisses and felsic orthogneisses). Marschall *et al.* (2013) suggest that the protolith of the Jutulrøra Complex was derived from a continental arc on the eastern margin of the Grunehogna Craton directly preceding the orogeny associated Rodinia assembly; like the Ritscherflya Supergroup but deposited on the margin of the craton rather than inland.

Several intrusive episodes occurred in H.U. Sverdrupfjella, including the following:

- Intrusions of mafic rocks that are the protolith of what are now amphibolites, with the older amphibolites predating all deformation (Elvevold and Otha, 2010).
- Sveabreen migmatitic granite intruded at 1127 ± 12 Ma (Harris *et al*., 1995). The protolith of younger amphibolites are post-tectonic (with regard to Rodinia amalgamation) and typically occur as boudins (Groenewald, 1995).
- The Brattskarvet intrusive suite, more detail below in section 1.3.1.
- The granitoids considered in this study.
- The ~170 Ma Straumsvola nepheline syenite complex (Harris and Grantham 1993).
- Finally, the Maud Belt was intruded by dolerite dykes associated with the break-up of Gondwana (Groenewald, 1995).

Pauly *et al.* (2016) studied a few samples from northern H.U. Sverdrupfjella and defined a P-T-t path for part of the Rootshorga Complex. Rocks from the area studied by Pauly *et al.* (2016) were subject to eclogite to high-pressure granulite facies (~30-50 km depth at ~800°C); followed by peak conditions (929 ± 23° C and 1.45 GPa) and then decompression and cooling. Ti-in-zircon and Zr-in-rutile thermometry along with U-Pb geochronology from zircon was used to constrain a T-t path for the samples from northern H.U. Sverdrupfjella. The T-t path gives temperatures above 800°C by ~590 Ma, which persisted for at least 40 m.y. The timing for near-peak conditions was constrained to ~570 ± 7 Ma. The near-peak conditions were followed by ~80 m.y. of cooling. The clockwise P-T path in eclogite to high-pressure granulite facies rocks is considered, by Pauly *et al.* (2016), to be characteristic of continent-continent collision, leading to the conclusion that Dronning Maud Land was involved in the amalgamation of a continent at ~570 Ma.

1.3 Previous Work

1.3.1 Earlier work on granitoids

The focus of this study is syn-tectonic and post-tectonic granitoid intrusions associated with the amalgamation of Gondwana. Grantham *et al.* (1991) described Dalmatian Granites (the intended focus of this study) and Moyes *et al.*, (1993) described the Brattskarvet intrusive suite of a similar age. Some authors have mentioned other granitoids similar to those observed in the field during this study (e.g. (Groenewald, 1995; Elvevold and Ohta, 2010), but no detailed study is known to the candidate (which is remedied in this study).

Dalmatian Granites

Grantham *et al.* (1991) described sheet-like intrusions of muscovite and biotite bearing granite that was either magnetite bearing or hosted tourmaline nodules. Grantham *et al.* (1991) named this granite "Dalmatian Granite" and described the following:

"The Dalmatian Granite was present in most of the study area (western and central H.U. Sverdrupfjella), as up to 10m thick "sheet-like bodies" that had varied orientations. The petrographic description noted roughly equal parts of quartz, microcline and plagioclase (An_{20}) with some biotite and muscovite and accessory minerals including apatite, magnetite and zircon. Alteration of plagioclase to muscovite, chloritization of biotite, zoning in plagioclase and diffuse contact with tourmaline nodules (in samples hosting tourmaline) were also noted."

Geochemical data from Grantham *et al.* (1991) will be used below (labelled Grantham *et al., 1*991). From geochemistry, Grantham *et al.* (1991) noted that Dalmatian granites are Fe-rich but show little variation in major element chemistry. More variation was noted in trace elements and an apparent relation to geographical location was noted. Tectonic discrimination plots as per Pearce (1984) indicated a source of rocks associated with syn-collisional environment. REE plots had a steep overall slope, relatively flat HREE patterns and a small positive Eu anomaly. Rb-Sr isotopic data of Dalmatian Granites fall into district geographical groups, a Brekkerista series (initial $^{87}Sr/^{86}Sr$ of 0.7353) and a Kivitjølen series (initial $^{87}Sr/^{86}Sr$ of 0.7140). To produce ages for Dalmatian Granites Grantham *et al.* (1991) consider whole-rock Rb-Sr isotopic data too scattered for reliable geochronology, but used data from muscovite, biotite and feldspar mineral separates from Brekkerista give a preferred age of 469 ± 5 Ma.

Brattskarvet intrusive suite

The Brattskarvet intrusive suite is a large intrusion of alkali granitoids located at Brattskarvet in northern H.U. Sverdrupfjella. Moyes *et al.*, (1993) give and intrusive age of 518 ± 15 Ma from whole-rock Rb-Sr data, 522 ± 120 Ma from whole rock Sm-Nd data and ages of 482-465 Ma from Rb-Sr mineral data (biotite, alkali feldspar and sphene). Moyes *et al.*, (1993) prefer and an intrusive age of ~519 Ma with cooling at ~476 Ma. Therefore, intrusion precedes Gondwana amalgamation.

Moyes *et al.*, (1993) cite low U/Pb ratios as indicating a lower-crustal source. Moyes *et al.*, (1993) also sampled country rock and gneissic xenoliths (which will be compared to data from this study in Chapter 8), which shows that the Brattskarvet intrusive suite is distinct from the country rock. Moyes *et al.*, (1993) conclude that the Brattskarvet intrusive suite is derived from a Sr and Nd depleted “lower-crustal granulite”.

1.3.2 Theses

Grantham PhD thesis

Grantham (1992) studied the stratigraphy and deformation history of the western H.U. Sverdrupfjella. The oldest rocks, according to Grantham (1992), are the gneisses of the Jutulrøra Complex which are considered to record calc-alkaline volcanic and clastic sedimentary protoliths. The Jutulrøra Complex is overlain by the dominant paragneiss and carbonate of the Fuglefjellet Complex. That sequence is overlain by the paragneisses of the Sveabreen Formation. The Roerkulten, Jutulrøra and Brekkerista granites intrude the Jutulrøra Complex as well as various mafic intrusions (now amphibolites), granitic sheets (including the Dalmatian Granites), Jurassic alkaline complexes and dolerite dykes. Grantham (1992) recognises five episodes of deformation. The first two episodes were folding (F_1 and F_2). D_1 and D_2 involved low angle thrust faults and suggest tectonic transport from the SE. Further folding and reverse faulting was recorded as D_3, which suggest transport from the W and NW. D_4 involved basin folding. D_5 involved normal faulting and jointing. Three phases of metamorphism related to the deformation were also recognised.

Groenewald PhD thesis

Groenewald (1995) studied the evolution of metamorphic rocks in the H.U. Sverdrupfjella. A complex metamorphic history that is typical of collision orogeny is reported. Rb-Sr and Sm-Nd isotopes are used to constrain metamorphism to between 1180 Ma and 1000 Ma and model ages suggest residence of protoliths from 1600 to 1400 Ma. The crustal evolution of H.U. Sverdrupfjella is found to be similar enough to that of the Lurio Belt (in Mozambique) to favour juxtaposition of western Dronning Maud Land and SE Africa in Gondwana. Groenewald (1995) describes granite dykes including “microcline pegmatites” that show deformation and Dalmatian Granites. Some of the granitoids described are likely to be the Salknappen Pegmatites described below, but this correlation is uncertain, and the methods of classification do not appear to be compatible. Due to the uncertainty regarding the comparability of data presented by Groenewald (1995) to data from this study, such data will not be included in this study.

Board PhD thesis

Board (2001) studied the tectonic history of southern H.U. Sverdrupfjella using fieldwork, petrography, geochemistry, and geochronology. The high-grade sequence of orthogneisses and paragneisses in southern H.U. Sverdrupfjella are interpreted as a record of a volcanic arc and associated back arc basin between ~1135 Ma and ~1070 Ma. Evidence for a high-grade metamorphic episode between ~1030 Ma and ~1040 Ma is noted but is described by Board (2001) to have been overprinted by a later episode. Petrography and geochemistry suggest a continental-collision-related clockwise P-T path for the later orogeny. Based on U-Pb SHRIMP dating of zircon in syn-tectonic leucosomes and monzonite hosted in fabric-forming minerals, the later metamorphic episode that appears to have begun at ~565 Ma, peaked at ~540 Ma and outlasted deformation. “Post-tectonic granitic dykes” intruded at ~480Ma and are consistent with Dalmatian Granites. In addition, Ar-Ar isotopic systems were reset at ~480 Ma. The final stage of crustal evolution involved the emplacement of N-S trending Jurassic dolerite dykes, indicating continental break-up.

McGibbon MSc thesis

McGibbon (2014) studied shear zones in H.U. Sverdrupfjella and Neumayerskarvet. Two shallow-plunging foliations were identified. A weak E-trending foliation and a well-defined SE-trending foliation. Only the SE-trending foliation occurs in shear zones, which suggests that the SE-trending foliation is associated with a more recent deformation event, i.e. the amalgamation of Gondwana, rather the amalgamation of Rodinia. McGibbon (2014) notes two generations of leucogranites; one that is “mostly foliation-parallel” and a later generation that cross-cuts fabric. The term leucogranite is consistent with the appearance of Salknappen Pegmatites.

Thomas MSc thesis

Thomas (2014) studied melt migration at Nupskåpa (southern H.U. Sverdrupfjella). They describe several intrusive phases including small leucosomes with diffuse boundaries, a network of leucogranite veins and several phases of “composite leucogranite dykes”. The leucosomes are interpreted to represent *in situ* melting during the amalgamation of Rodinia. The leucogranite dykes appear to include the granitoids considered in this work and are interpreted to represent melt transport from 5-15km below Nupskåpa.

Byrnes MSc Thesis

Byrnes (2015) studied the tectono-metamorphic history of Salknappen. They find that earlier metamorphic assemblages are preserved and report no evidence of reworking during a later event. The resulting interpretation is that the grade of metamorphism involved in the amalgamation of Gondwana did not reach the peak temperatures that occurred during the amalgamation of Rodinia. A corollary is that little or insufficient re-hydration occurred at Salknappen to cause melting of the host rocks. However, Byrnes (2015) notes that “megacrystic leucogranite dykes” and “equigranular granite sheets” do record deformation during Gondwana assembly. These are referred to as Salknappen Pegmatites and Dalmatian Granites respectively in the thesis in hand.

1.4 Current models for formation of H.U. Sverdrupfjella

1.4.1 The mega-nappe model

Grantham *et al.* (2008) proposed that a mega-nappe structure exists on the edge of Antarctica, in which part of northern Gondwana, which was thrust ~600 km over southern Gondwana during the amalgamation of the Gondwana supercontinent (between 590 and 550 Ma). Such a radical model was postulated to explain two distinct crustal blocks, correlated over both Mozambique and Antarctica (Figure 1.2). The terrains were correlated by analysing geochronological, lithological, structural, and metamorphic data (summarised below). In addition, Grantham *et al.* (2008) suggest the possibility that the thrust domain extends from the Zambezi Belt, as far west as the Damara Belt and into the Urungwe klippen in northern Zimbabwe.

The evidence found in Grantham *et al.* (2008) for all four types of data will be summarised here. For simplicity the two crustal blocks will be referred to as the Namuno Block (north of the Lurio Belt) and Nampula Block (south of Lurio Belt) and correlated areas on other continents will be referred to as Namuno terrane and Nampula terrane.

Grantham *et al.* (2008) state: *"On a purely lithological composition basis there is little to indicate a major crustal boundary defined by the Lurio Belt."* However, supracrustal rocks containing metapelites and marbles are prevalent in the Namuno Block, whereas the Nampula Block contains relatively alkaline syenitic orthogneiss. The only exceptions to the two noted differences are the Monapo and Mugeba klippen, which are found overlying the Nampula Block (Grantham *et al.,* 2008).

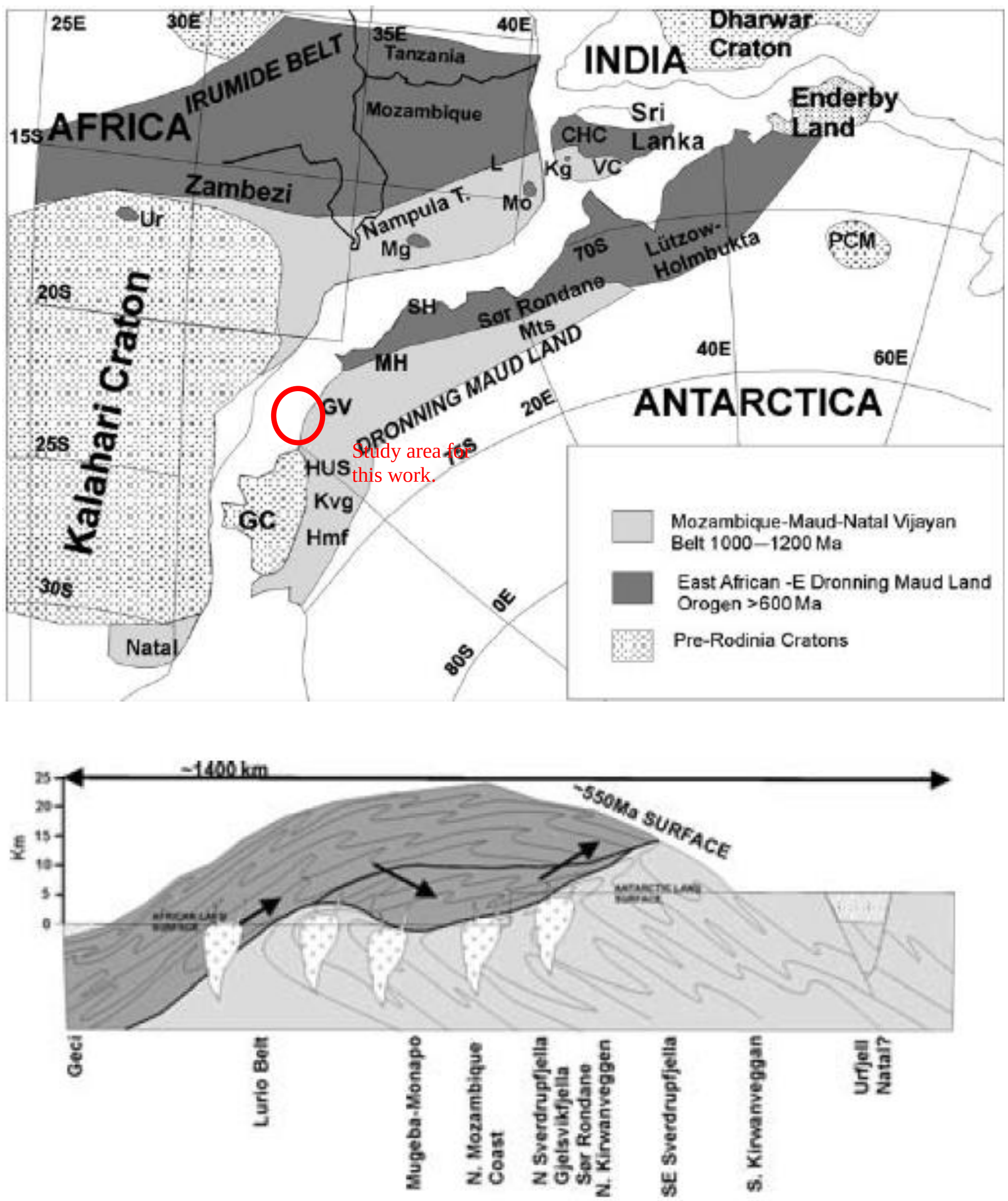

Figure 1.2: Schematic map showing the areas covered by the respective terranes in a reconstruction of Gondwana and cross section of the mega-nappe mode. Note that rocks from northern Gondwana (i.e., the Namuno Block) overlie rocks currently exposed in H.U. Sverdrupfjella, so could not have directly affected the granitoids considered in this study. From Grantham *et al. (*2008).

The boundary between the Namuno and Nampula Blocks in NE Mozambique is marked by the Lurio Belt. The Lurio Belt, like most observed boundaries between the Namuno and Nampula Blocks, is highly sheared (Grantham *et al.,* 2008). In Antarctica, NE and SW Sør Rondane is similarly separated by a ~10 km-wide shear zone (Shiraishi *et al.,* 1991)

Grantham *et al. (*2003) described opposing structural facing directions in northern Mozambique and Dronning Maud Land. Broadly speaking, planar structures in northern Mozambique dip dominantly N and NW, whereas planar structures in Western Dronning Maud Land dip SE. Grantham *et al.* (2008) use the improved amount of structural and geochronology data available to conclude that fabrics in the two areas are not the same age. Whereas deformation in and adjacent to the Lurio Belt must be younger than 630 Ma, two major periods of deformation were identified in H.U. Sverdrupfjella, from 1000 Ma to 900 Ma and from 550 Ma and 490 Ma by Grantham *et al.* (1995). Upon reviewing additional (and more complex) data, Grantham *et al.* (2008) suggest a zone along between northern Mozambique and Dronning Maud Land in which bimodal structural patterns occur due to refolding of earlier planar fabrics, suggesting that multiple directions in the structural data are due to refolding of earlier unimodal structural patterns. Structural data does not appear to support the terrain correlation (nor disprove it), but they support the classification of the discordant (Grantham *et al*. 2007 and Macey *et al*. 2007) Mugeba and Monapo terrains as klippen (Grantham *et al.,* 2008).

According to Grantham *et al.* (2008), the different terrains in Mozambique show significantly different mineral assemblages and metamorphic grades. The Nampula Block is predominantly upper amphibolite facies, but the Mugeba and Monapo klippen are composed of granulite facies orthogneisses and paragneisses. In addition, the Nampula Block hosts an abundance of granitoids with ages ranging from ~495 to ~530 Ma, which show little deformation.

Grantham *et al.* (2008) used metamorphic and crystallization ages to establish characteristic age profiles for the Nampula and Namuno Blocks. The metamorphic age histograms and probability density functions are shown below (Figure 1.3) to illustrate the age characteristics described. Data were published by Grantham *et al.* (2008), predominantly using sensitive high-resolution ion microprobe (SHRIMP), inductive coupled plasma mass spectrometry (ICP-MS) or thermal ionization mass spectrometry (TIMS) analyses.

Grantham *et al.* (2008) describe two groups of ages of ~1150 Ma - 900 Ma and ~650 - 450 Ma, for all areas. The difference lies in the Namuno Block being characterized by ages of ~650 - 900 Ma, a group of ages that are absent from the Nampula Block. Ages of ~630 Ma from the Monapo and Mugeba klippen are reported by Jamal (2005), Grantham et al. (2007) and Macey *et al.* (2007), which Grantham *et al.* (2008) uses to demonstrate that these klippen have age characteristics similar to the Namuno Block.

In summary: The mega-nappe model relies on the correlation of areas in Antarctica with the Nampula and Namuno Blocks in Mozambique. The areas associated with the Namuno Block have a P-T paths interpreted to have significant isobaric cooling at ~550Ma and is characterized by metamorphic and crystallization ages of ~650-900Ma, which are absent from the Nampula Block. Areas associated with the Nampula Block are characterized by granitoid magmatism (at ~500-550Ma).

Grantham *et al.* (2019) added to this model by using the difference in $^{40}Ar/^{39}Ar$ ages of biotite and hornblende to investigate the tectonic history of western Dronning Maud Land. Biotite ages vary between 868-497 Ma in the Kirwanveggen and 547-326 Ma in H.U. Sverdrupfjella. Hornblende ages vary from 1067-480 Ma in the Kirwanveggen and 550-450 Ma in H.U. Sverdrupfjella, increasing from NE to SW. Grantham *et al.* (2019) interpret the larger difference in ages from the Kirwanveggen to imply differential heating due to the area being buried as the footwall of the mega-nappe described by Grantham *et al.* (2008). The similar ages in H.U. Sverdrupfjella are interpreted to record rapid uplift in a single event. Grantham *et al.* (2019) thus conclude in favour of the mega-nappe hypothesis described by Grantham *et al.* (2008).

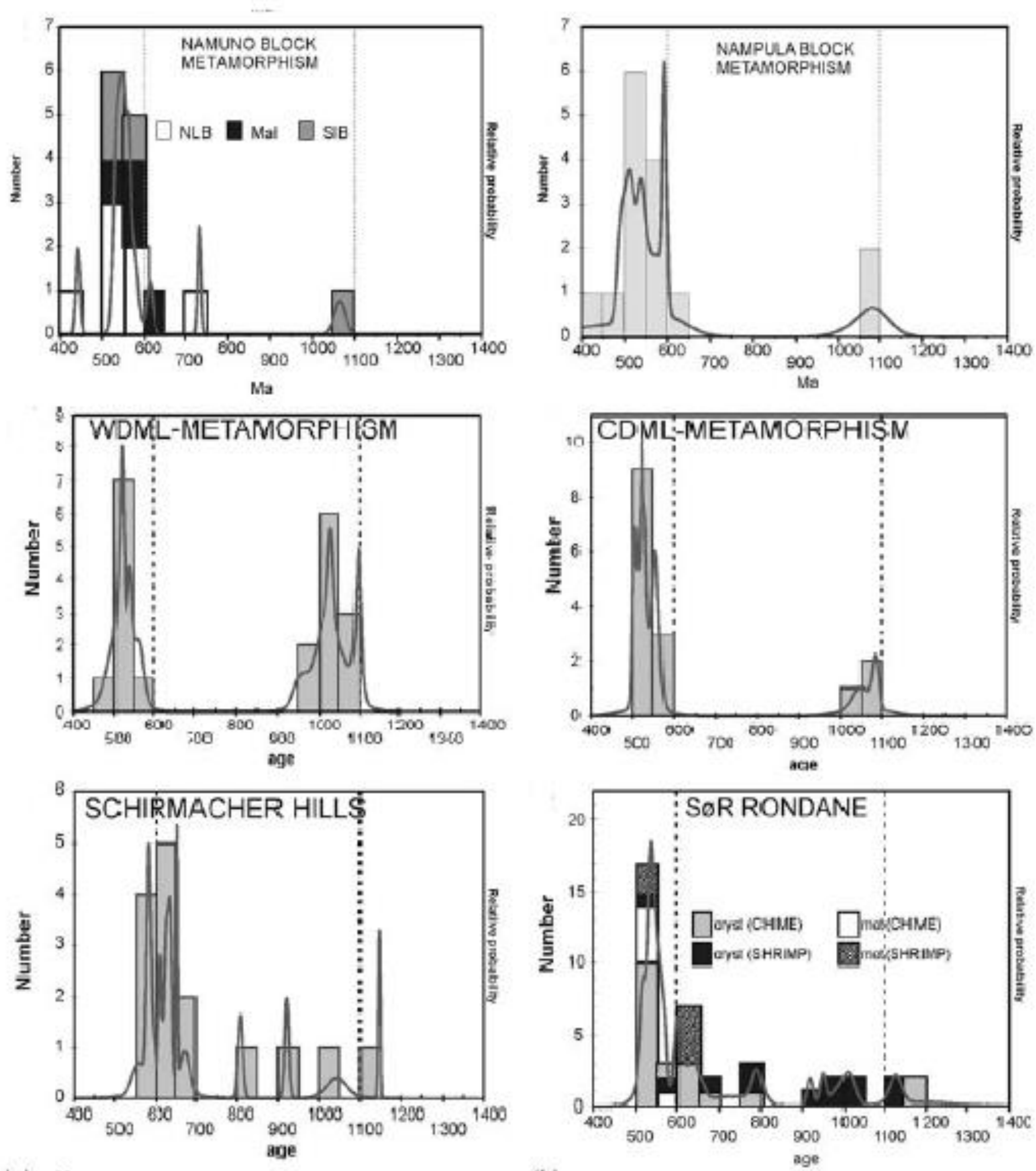

Figure 1.3: Showing histograms (bin size 50 Ma) and probability density distributions of metamorphic age for the applicable areas. Age data for the Nampula block was produced from samples from the area north of the Lurio Block (NLB), a southern Irumide Belt Block (SIB) and Malawi (Mal). Age data for Sør Rondane is subdivided to show different data types. From Grantham *et al.* (2008).

1.4.2 Diachronous orogeny

Board *et al.* (2005) produced new geochronological data on zircon overgrowths from H.U. Sverdrupfjella. That data indicates two distinct phases of high-grade metamorphism (1040 -1030 Ma and 565 -499 Ma).

Board *et al. (*2005) note two tectono-thermal episodes in the late Mesoproterozoic and late Neoproterozoic-Cambrian. Integrated new U-Pb SHRIMP with single zircon and monzonite data plus Ar-Ar data on hornblende and biotite and thermobarometric calculations (on rocks from H.U. Sverdrupfjella) were used to produce a more complex P-T-t path than previously suggested. The presence of 540Ma old monzonite in upper-amphibolite facies rocks implies top to the NW deformation and is cited as evidence for deformation being "Pan-African" (i.e., associated with assembly of Gondwana) rather than "Grenvillian" (i.e., associated with assembly of Rodinia). Strain protected eclogite-facies garnet-omphacite indicates that peak metamorphic conditions were attained around 565Ma. Post-peak K-metasomatism is ascribed to the intrusion of post-orogenic granite at 480Ma. Board *et al.* (2005) argue that extensive Pan-African tectonism casts doubt on previous Rodinia reconstructions in which the Maud Belt takes a pivotal role (between East Antarctica, the Kalahari Craton and Laurentia). The protoliths of the polymetamorphic rocks are largely derived from a ~1140 Ma volcanic arc.

Grosch *et al.* (2015) compared the petrology and metamorphism of Mesoproterozoic metabasic rocks from the eastern margin of the Grunehogna Craton and H.U. Sverdrupfjella (across the Pencksokket-Jutulstraumen Discontinuity. Grosch *et al.* (2015) used laser ablation inductively coupled plasma mass spectrometry U-Pb dating of titanite to yield and an age of 491 ± 27 Ma for high-grade metamorphism in the western H.U. Sverdrupfjella. Grosch *et al.* (2015) cite petrological and geochronological constraints indicating that peak metamorphic conditions in western H.U. Sverdrupfjella occurred at *c.*500 Ma, (*c.* 70-80 Ma after peak metamorphism in eastern H.U. Sverdrupfjella) and used this to argue against models that describe only late Mesoproterozoic (*c.* 1060-1030 Ma) metamorphism in the western H.U. Sverdrupfjella and Grunehogna craton margin and to support a major, diachronous, Pan-African tectonic history. Grosch *et al.* (2015) go on to propose a new geodynamic model for Western Dronning Maud Land. The Grosch *et al.* (2015) model involves earlier metamorphism in a separate eastern H.U. Sverdrupfjella terrane (from 565 Ma to 540 Ma) followed by later accretion of the eastern H.U. Sverdrupfjella onto western H.U. Sverdrupfjella at ~500 Ma.

1.4.3 Indenter escape model

Jacobs and Thomas (2004) proposed a "Himalayan- type indenter-escape tectonics model" for the southern part of the East African-Antarctic orogeny, in which the orogen is characterised by bipolar lateral escape tectonics. Jacobs and Thomas (2004) suggest potential suture zones and potential microplates, which may indicate that the southern end of the East African-Antarctic orogen likely represents a zone of continental fragments that escaped southward. In this model, the Coats Land block (a crustal block within the orogen that was not subject to metamorphic overprinting) can be explained by tectonic translation, allowing the crustal block to escape metamorphic overprinting during the East African-Antarctic collision. The shear zones formed during escape tectonics became zones of weakness, resulting in the microplate pattern produced by the Gondwana break-up and allowing for the detachment of the Grunehogna Craton from the Kaapvaal craton. The dextral Heimefront transpression zone, existing in a generally sinistral setting, can also be explained within the escape-tectonics of the model.

1.5 Aim and Objectives

The purpose of this work is to study relatively thin (5cm to 10m) granitoid sheets in H.U. Sverdrupfjella, in order to provide constraints to the tectonic history of H.U. Sverdrupfjella. The thin granitoid sheets in H.U. Sverdrupfjella will be studied using fieldwork, petrography, geochemistry and geochronology. Insight gained from the study of the granitoid sheets will be used to compare current tectonic models.

The objectives for this project are to:

- Sample and obtain structural measurements on the granitoid sheets in the area, both those previously reported by Grantham *et al.* (1991) and others observed but not previously studied in detail.
- Obtain geochronological data on the different granitoid suites studied.
- Obtain geochemical and petrological data from the granitoids.
- Construct a model for the emplacement of these granitoids and relate their emplacement to the processes of crustal accretion occurring in H.U. Sverdrupfjella at the time of Gondwana assembly.

Chapter 2: Methods

2.1 Fieldwork

Two field seasons were undertaken for this project. Transport to Antarctica was by ship (on the SA Agulhas 2) to the ice shelf, by helicopter to the South African Antarctic base (SANAE IV) and by snowmobile (known colloquially as skidoo) to a base camp. Field work was done by travelling from base camp each day by snowmobile. Transport was arranged by the Department of Environmental Affairs and final packing and logistics were handled at and with support from SANAE IV.

In the first field season the northern (approx.) half of H.U. Sverdrupfjella was the focus; from Brattskarvet to Gordonnuten. Base camp was near Fuglefjellet at 72° 16.15’ S and 00° 48.40’ E. Geologists were in the field from 1 January 2014 to 22 January 2014. Two days were cut short, and four days were unworkable due to weather.

The focus of the second field season was the southern part of H.U. Sverdrupfjella; from Gordonnuten to Nupskåpa. Base camp was near Skarsnuten at 72° 28.72’ S and 00° 20.72’ E. The second field season had geologists in the field from 31 December 2014 to 25 January 2015. One day was cut short and six days were unworkable due to weather.

Samples were taken in way that gave the widest logistically possible geographic variation of both granitoids, and sample locations are shown in Figure 2.1. Samples were taken with a sledgehammer and most weathered material was removed with a geological pick. Further removal of unwanted material was done with a hydraulic rock splitter at the University of Pretoria (UP). The hydraulic rock splitter was cleaned with a brush and a fresh plastic refuse bag was placed under the splitter for each sample. Samples were then washed with deionized water sprayed from a plastic spray bottle and left in sunlight and on plastic sample bags to dry.

The orientations of granitoid sheets were measured in the field using a geological compass, measuring dip and magnetic dip direction. Measurements were converted from the measured magnetic dip direction using Microsoft Excel. The term “true azimuth” is used for the measured azimuth corrected for magnetic declination. The data for the stereonets were imported in a “strike azimuth, dip and dip direction” format. Orientation data were plotted using Stereonet, a computer programme produced by Allmendinger *et al.* (2012)

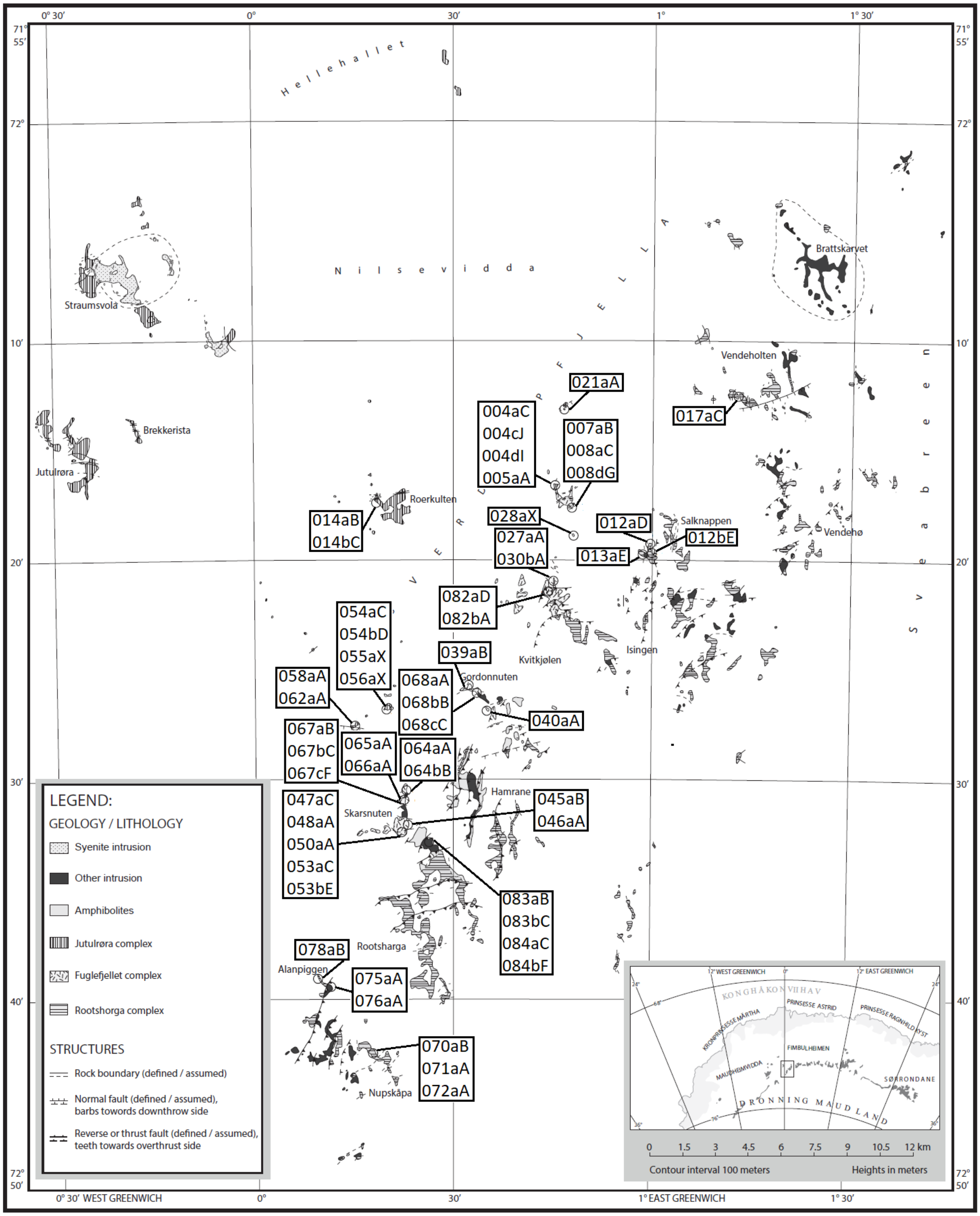

Figure 2.1: Map of H.U. Sverdrupfjella showing relative sample locations, after Elvevold and Ohta (2010). Due to the small surface area of outcrops a map this size does not have the resolution required to show geology in detail; please refer to the map accompanying this thesis (also after Elvevold and Ohta, 2010) to examine the geology of the study area. Please refer to Appendix 3 for the sample list, which includes more location details.

2.2 Analysis

2.2.1 Composition

Samples from H.U. Sverdrupfjella were reduced to coarse crush using a jaw crusher at UP. Between samples the crusher was cleaned by running quartz aggregate and then (after removing jaw) cleaned with compressed air and finally rubbed down with ethanol. Milling was done at UP. A tungsten milling pot (includes ring and puck) in a swing mill was used for two minutes on each sample. The milling pot was cleaned by milling quartz "sand" for one minute, followed by cleaning with ethanol and care was taken not to touch the inside of the pot, the ring or the puck directly.

Major elements (fused beads) and trace elements (pressed pellets) were analysed by X-ray fluorescence spectrometry (XRF), by M Crowley at The Council for Geoscience South Africa (CGS) as per Cloete and Truter (2001).

Trace elements were also analysed at CGS, using the following method: 0.2g of sample (milled powder) prepared using 4 acid digest technique (HCl, HNO_3, $HClO_4$ and HF) and analysed by quantitative ICP-MS. REE*s* were analysed at CGS, using the following method: 0.5 g sample fused with 1.5g 12:22 Lithium meta-/ tetraborate flux, bead dissolved in dilute HNO_3, diluted and analysed for rare earth elements by ICP-MS.

2.2.2 Isotopes

The isotopic analysis was done at the University of Cape Town. Nd and Sr isotope analysis was done as follows: ±50 mg of each sample was prepared for sequential separation by digestion in concentrated HF: HNO_3 for 48 hours at 140ºC in closed Teflon beakers; then dried down and converted to nitrate.

Sequential column separation of Sr and Nd fractions was after Pin *et al.* (2014). Separated elemental fractions were analysed on a Nu Instruments NuPlasma HR. Sr was analysed in a 200 ppb 0.2% HNO_3 solution using NIST SRM987 as reference standard with a $^{87}Sr/^{86}Sr$ normalizing value of 0.710255. Sr isotope data were corrected for Rb interference using the measured signal for ^{85}Rb and the natural $^{85}Rb/^{87}Rb$ ratio; and for instrumental mass fractionation with the exponential law using the measured $^{86}Sr/^{88}Sr$ ratios and an accepted value of 0.1194 for this ratio. Nd isotopes were analysed as 50 ppb 2% HNO_3 solutions using Nu Instruments DSN-100 desolvating nebulizer and JNdi-1 as the reference standard. A $^{143}Nd/^{144}Nd$ normalizing value of 0.512115 was used (Tanaka *et al.,* 2000). Nd isotope data were corrected for Sm and Ce interference and instrumental mass fractionation using the measured signal for ^{147}Sm and ^{140}Ce with natural Sm and Ce isotope abundances and the exponential law with a $^{146}Nd/^{144}Nd$ value of 0.7219, respectively.

2.2.3 Geochronology

Geochronology data were produced by Sensitive High Resolution Ion Microprobe (SHRIMP) as follows: Zircons were separated from coarse crush samples in several stages, at CGS. *Milling* was done with a roller mill. Samples were run five times (a plastic bucket was used to hold samples between runs), but only three times at the finest setting. The roller mill was run with the ventilator on and cleaned using compressed air, after removing the cover. The floor around the roller mill was cleaned with compressed air between each sample. Sieving was done using a stack of two steel sieves (150µm and 250µm), because a second sieve was required to fit in the shaker. Sieves were cleaned using a copper brush and compressed air, cleanliness was checked by holding the sieves against light. Material larger than 250µm was stored and material smaller than 250µm was further separated. *A Wilfley table* was used for further sorting, trays and the table were rinsed between samples and separated material was rinsed with ethanol and dried in a small oven (120ºC) and then sealed with parafilm in a beaker. Other material was stored and labelled "tailings". *Magnetic separation* was done after checking for the presence of zircons with a binocular microscope. A hand magnet (wrapped in plastic) was used initially and then a magnetic separator (set to a 5º inclination) was used. Samples were run through the separator several times, with an increase in current each time. The track and other surfaces were cleaned using compressed air between samples. *Heavy liquids* were used for the final step. After being left to separate, minerals heavier than diiodomethane (bottom half of funnel) were filtered out and rinsed with ethanol. Lighter material was also filtered out and stored. The heavy liquid was reused after filtering.

Analysis for geochronology of the separated zircons was the contribution of National Institute of Polar Research (NIPR) in Japan, for co-authorship of publications. Six samples were analysed by the SHRIMP laboratory at the National Institute of Polar Research (NIPR) in Japan. Prior to analysis, the zircons were embedded in PetroPoxy154, allowed to cure, and then imaged with a JEOL JSM-5900LV SEM with attached Gatan miniCL capacity. An electron beam current of 0.1 nA at 15 Kv of acceleration voltage was used in low vacuum mode on uncoated samples. After imaging, the samples were cleaned in an ultrasonic bath, first with MilliQ then in a 1M HCl solution, allowed to dry and then cleaned in the ultrasonic bath in petroleum ether. Thereafter a gold coating of 135 Å was applied to the samples, and selected spots in several zircons were analysed in the SHRIMP with a spot size of 25 µ (Köhler Ap.: 120 mm) and primary beam intensity of 3.6 nA. The mass resolution for the analysis (M/ΔM) was 5100 at a sensitivity of 18 cps/^{206}Pb ppm/nA. A raster condition of 140 µm was used for 2 minutes. Two standards were used, the TEMORA2 standard (Black *et al.*, 2004) and FC1 (Paces & Miller, 1993). Samples were analysed in two batches: 004cJ, 004dI and 040aA together and 012aD, 012bE and 013aE together (see Chapter 5 for context of samples). The standards used were TEMORA2 and FC1. U-Pb calibration to TEMORA2: 417 ± 0.3 Ma, as per Black *et al.* (2004). FC1's U-Pb calibration was to 1095 ± 7.0 Ma for the former batch and 1098 ± 5.5Ma for the latter batch; with an expected value of 1099 ± 0.6 Ma. Data points with high common Pb (such that it saturates the measurement), Pb instability or low U were excluded from calculations; other data (i.e., that was included) is referred to as "usable" below (in Chapter 5).

Data was processed using SQUID2 (2.50.11.02.04) and then plotted and analysed using Isoplot3. The data was reduced using the weighted average of ^{206}Pb/^{238}U corrected by ^{204}Pb, using the common Pb model of Stacey and Kramers (1975). The Pb/U ratios of some zircons with a U concentration higher than 2500 ppm were corrected for machine-induced bias according to the method of Williams and Hergt (2000). The ages used for publication and in this thesis are those measured and calculated by NIPR as their name and reputation is associated with the results, but calculations were confirmed for this work. The data from NIPR are presented and reviewed in Chapter 5.

Chapter 3: Fieldwork

The purpose of this chapter is to present field work done during this study and to analyse the orientations of the granitoid sheets. This part of the study attempts to use field observations and the orientations of granitoid sheets to infer the stress acting on the area while the granitoids were emplaced, to gain insight regarding the tectonic history of the H.U. Sverdrupfjella. To place the granitoid sheets into context, the field relationships, relative ages, orientations and some structural observations will be described here.

3.1 Field observations

3.1.1 Field relationships

Four different phases of granitoid sheets were identified and designated P0, P1, P2 and P3 in the field. P0s are cross-cut by P1 (Figure 3.1), P1s are cross-cut by P2s (Figure 3.2) and P2s are cross-cut by P3s (Figure 3.3). The field relationships described above were observed to be consistent throughout H.U. Sverdrupfjella.

Note that, in later work, these rocks will be referred to as “Pre-existing Granitoid” (P0), “Salknappen Pegmatite” (P1), P2 will be referred to as “Dalmatian Granite” and P3 as “pegmatitic Dalmatian Granite”. These labels will be explained later in this chapter.

With the possible exception of P0s, the granitoid sheets cut metamorphic fabric. There are no signs of contact metamorphism or metasomatism related to the granitoid sheets considered in this study. Changes in the mineralogy of Dalmatian Granites have been noted with proximity to marble, indicating that chemical exchange has taken place, but no well-developed skarns have been noted.

Figure 3.1: Photograph showing the crosscutting relationships of P0, P1 and P2. Here P0 can be seen to be older than other granitoids. Taken at Skarsnuten.

Figure 3.2: Field photograph (taken at Salknappen) showing that P1 is older than P2, according to the law of cross cutting relationships. Also note that P1 shows deformation, but the P2 does not show noticeable deformation.

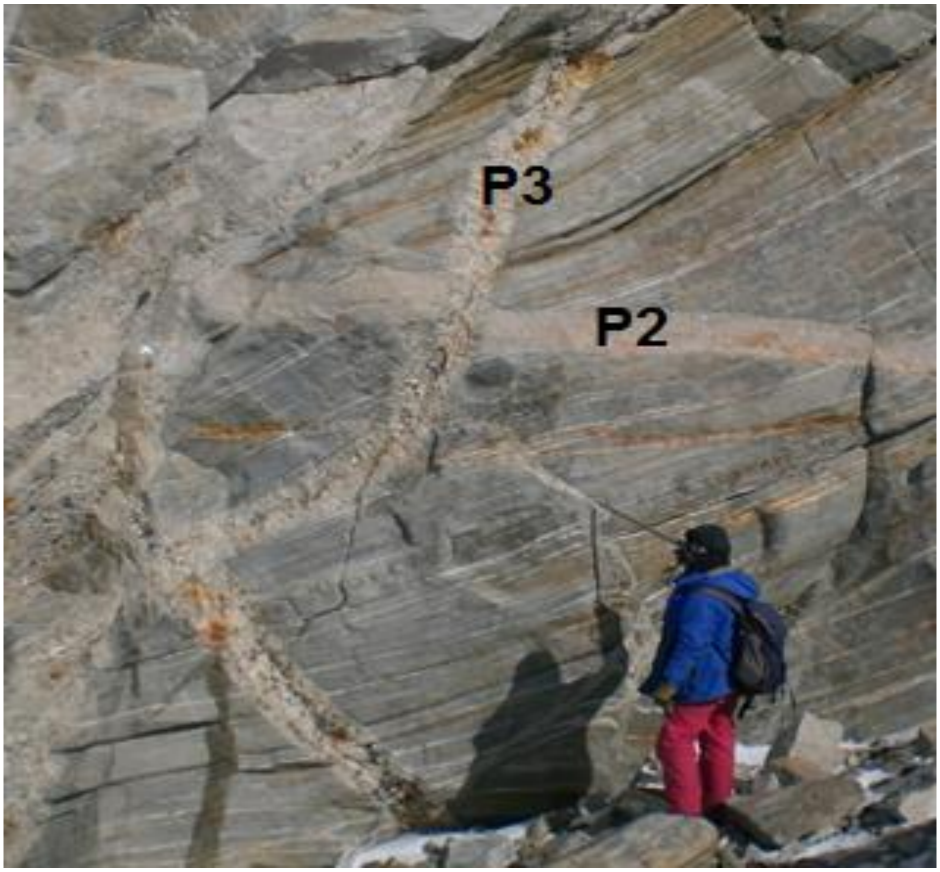

Figure 3.3: A photograph taken at Skarsnuten showing a P3 cross-cutting a P2.

3.1.2 Rock descriptions

P0: The oldest P0 phase comprises sub-horizontal folded granitic sheets with axial planar foliations and was only observed at the Rootshorga nunatak. P0s are predominantly composed of quartz felspars, with accessory biotite. The contacts are sharp and contacts concordant to the gneissic layering in the country, suggesting little or no chemical reactions with country rocks. P0s are deformed and have uniform foliation (stretched quartz lenses and alignment of mica grains) and similar orientation to the metamorphic foliation of the country rock (Figure 3.4); suggesting that granite genesis and emplacement were syn-tectonic.

Figure 3.4: Field photograph taken at way point 067 (Skarsnuten) showing the appearance and foliation of P0s (pre-existing granitoids). Apparent selvage is a coincidental interaction with a gneissic melanosome.

P1: The P1 granitoids are pegmatitic, white in colour and predominantly composed of quartz and feldspar in approximately equal proportions, with subordinate biotite occurring as large books (Figure 3.5). P1s are deformed and predate P2s emplaced into a brittle environment (Figure 3.6). P1s were noted as distinct from P2s at Salknappen and will be referred to as "Salknappen Pegmatites" below.

P2: P2 is correlated with the Cambrian-age Dalmatian Granite described by Grantham *et al*. (1991), due to appearance, texture and mineralogy; therefore P2s will be referred to as "Dalmatian Granite" in the rest of this and future work. Dalmatian Granites are typically granitic (in terms of grain size and mineralogy) and show little deformation. They are syn-tectonic (from field observations). P2s were typically emplaced into a brittle environment as shown by angular contacts in Figure 3.7 and appear to be opportunistic in terms of intrusions pathways, sometimes even intruding along sheets of Salknappen Pegmatites (Figure 3.10). The P2 granites are medium- to coarse-grained, pink to buff in colour and locally exhibit tourmaline "spots", particularly in sheets intruded into carbonates in the Fuglefjellet Complex (Figure 3.8). When tourmaline spots do not occur, Dalmatian Granites typically contain magnetite. Dalmatian granites contain some xenoliths that are the same rock type as the adjacent country rock, but with different fabric orientation, indicating some transport and rotation (Figure 3.2 and Figure 3.7). A contact between Salknappen Pegmatite (below) and Dalmatian Granite (above) is shown in Figure 3.10. The differences in colour, grain size and visible accessory minerals are evident when the granitoids are juxtaposed.

Figure 3.5: Field photograph (taken at Salknappen) showing the appearance of P1 (Salknappen Pegmatite). White square showing photograph number is 10 cm square.

Figure 3.6: Angular contacts with country rocks indicate emplacement of Dalmatian Granite (P2) in a brittle environment (at Skarsnuten). White square showing photograph number is 10cm square.

Figure 3.7: Dalmatian Granite (P2) with tourmaline spots and a xenolith on Fuglefjellet. White square showing photograph number is 10cm square.

Figure 3.8: Dalmatian Granite (P2) without “spots” at Salknappen. White square showing photograph number is 10cm square.

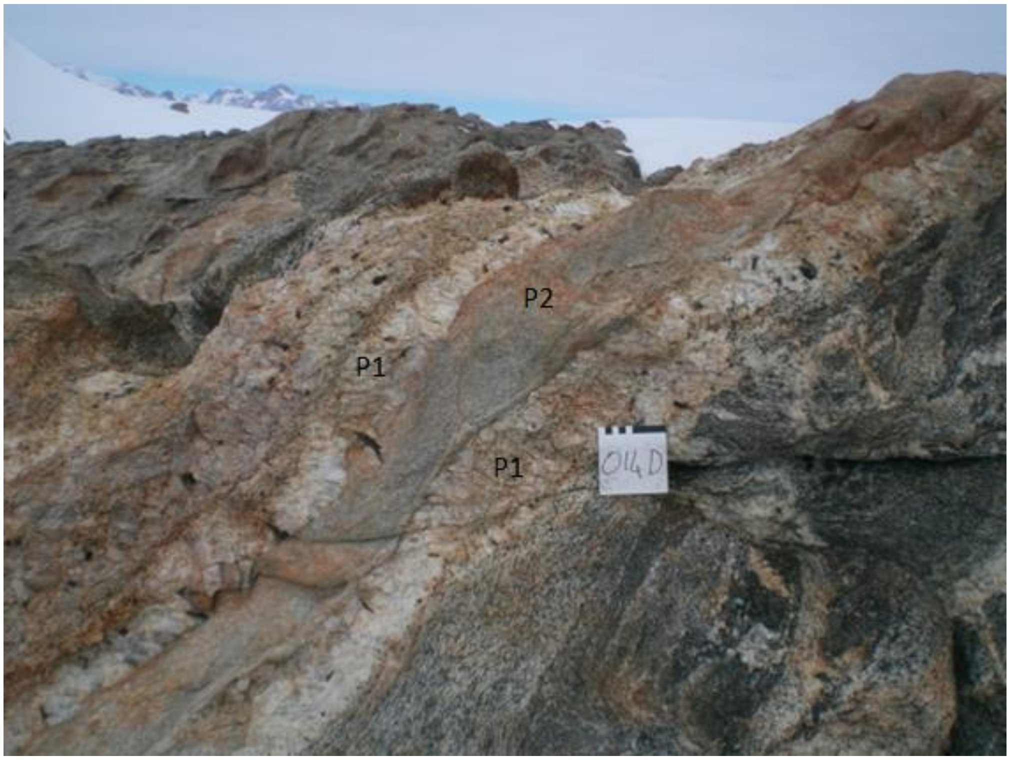

Figure 3.9: Dalmatian Granite (P2) intruding along a Salknappen Pegmatite (P1) at Roerkulten. White square showing photograph number is 10cm square.

Figure 3.10: A contact between Salknappen Pegmatite (below) and Dalmatian Granite (above). The juxtaposition shows the difference in appearance between the two suites.

P3: P3 pegmatites are generally pink in colour. P3s are composed of quartz, feldspar, biotite, muscovite, and some hornblende (Figure 3.11). The P3 veins are typically pegmatitic but have variable grain size (ranging from medium-grained to several cm long grains (Figure 3.12). The P3 intrusions are younger than other phases, according to field relationships and have a similar appearance (when grain sizes are similar) to Dalmatian Granite. P3s are similar to Dalmatian Granites, in terms of appearance and mineralogy and are geochemically similar (Chapter 6). Therefore, P3s will be referred to as “pegmatitic Dalmatian Granites” in the rest of this work and future work; the term will be used below to avoid confusion, even though geochemical similarities are only shown in later chapters.

Figure 3.11: Field photograph showing the appearance, texture and mineralogy of pegmatitic Dalmatian Granite (P3) pegmatite at Jutulrøra.

Figure 3.12: Variable grain size in pegmatitic Dalmatian Granite (P3). Photo taken at Roerkulten and the white square showing photograph number is 10cm square.

3.2 Orientations

3.2.1 H.U. Sverdrupfjella Overall

Stereonets presenting poles to the orientations of Salknappen pegmatites (Figure 3.13) and Dalmatian Granites (Figure 3.14) are presented below. Appendix 2 lists the locations studied (with coordinates) and records the nunataks visited during fieldwork. Data tables are shown in Appendix 3 and orientation data is tabulated in Table A3.2. The plots are scattered, but Salknappen Pegmatites appear to have groups dipping toward NW and S. Dalmatian Granites tend to dip toward the SE, but the data are still widely scattered.

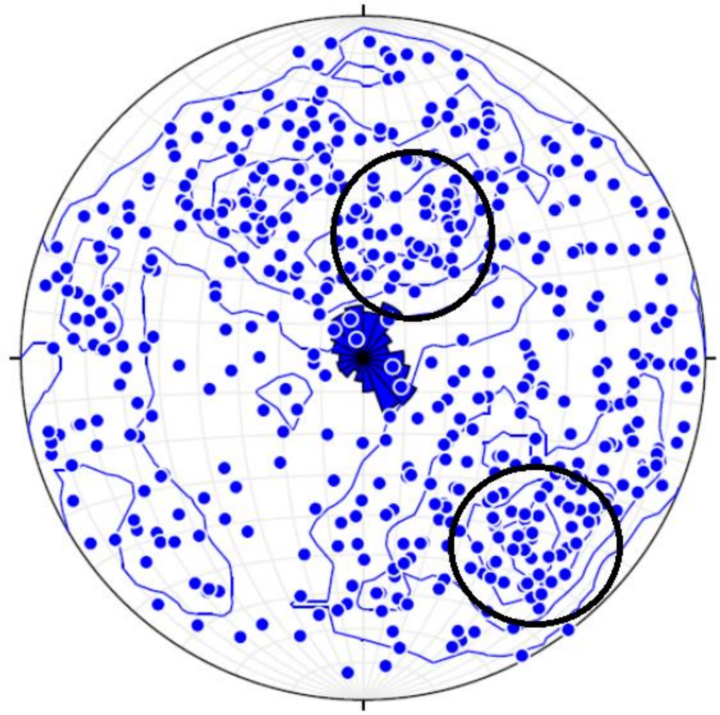

Figure 3.13: The poles to the orientation of Salknappen Pegmatites, showing some grouping. Grouping is only noticeable due to the aid of contours and the rose diagram, dipping towards the S and NW. Groups are marked by black rings.

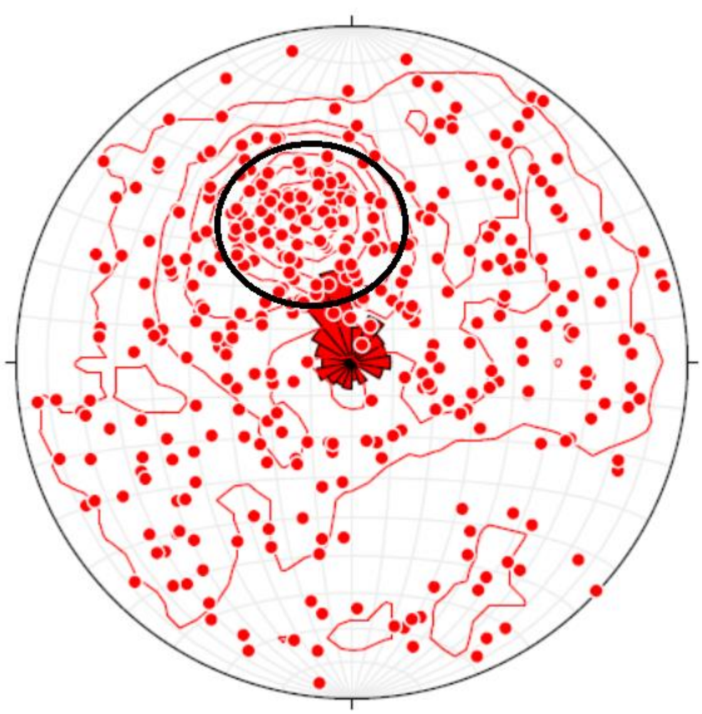

Figure 3.14: Poles to the orientation of Dalmatian Granite. Data is quite scattered, but there is a clear cluster dipping toward the SE (indicated with a black ring).

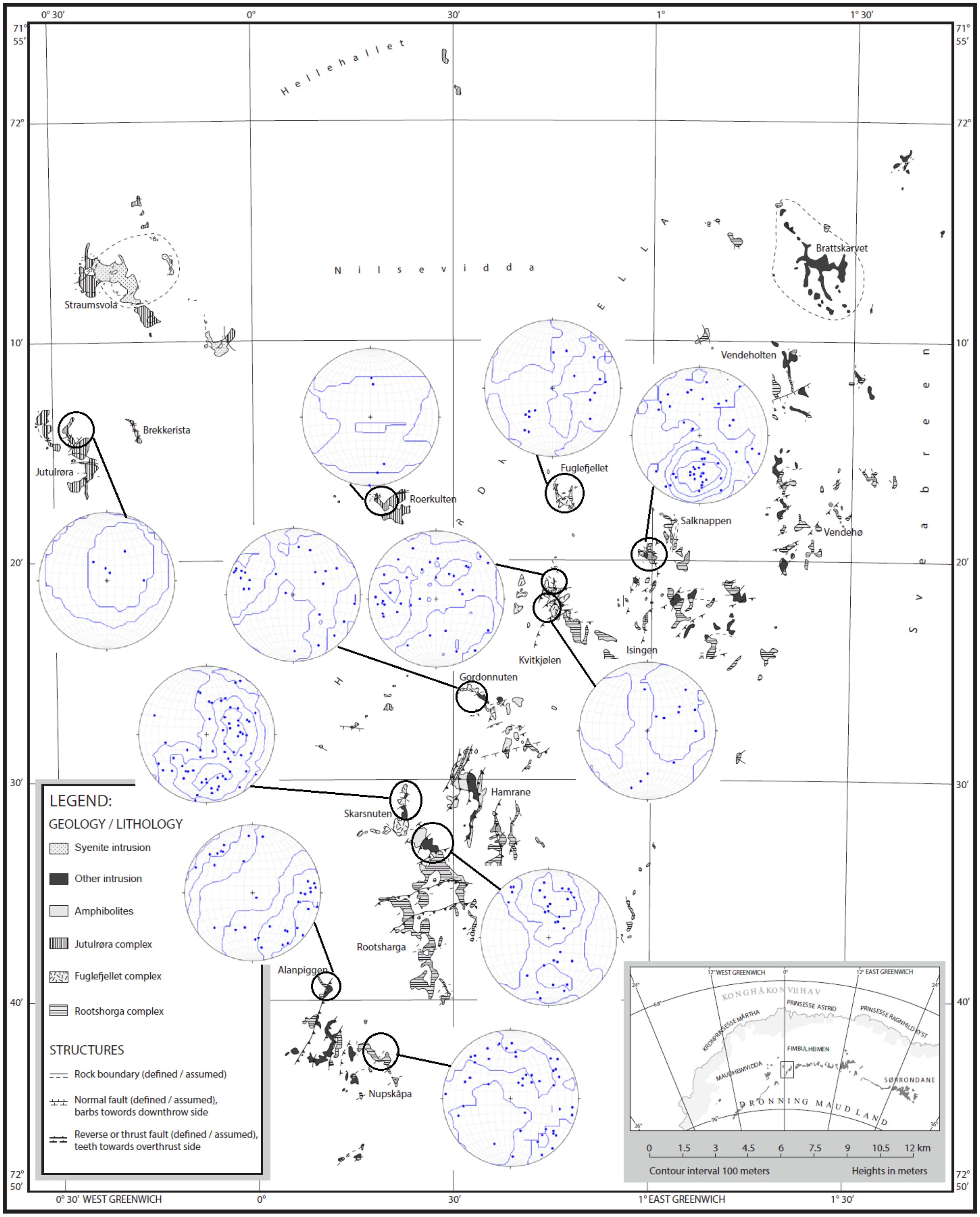

Figure 3.15: Stereonets of poles to sheets of Salknappen Pegmatites arranged on a map of H.U. Sverdrupfjella (after Elvevold and Ohta, 2010) in order to show orientation data in a spatial context. No spatial trend in orientation data for Salknappen Pegmatites is apparent. Please note that this map is being used only to give relative positions within H.U. Sverdrupfjella, please see the map accompanying this thesis for a higher resolution version.

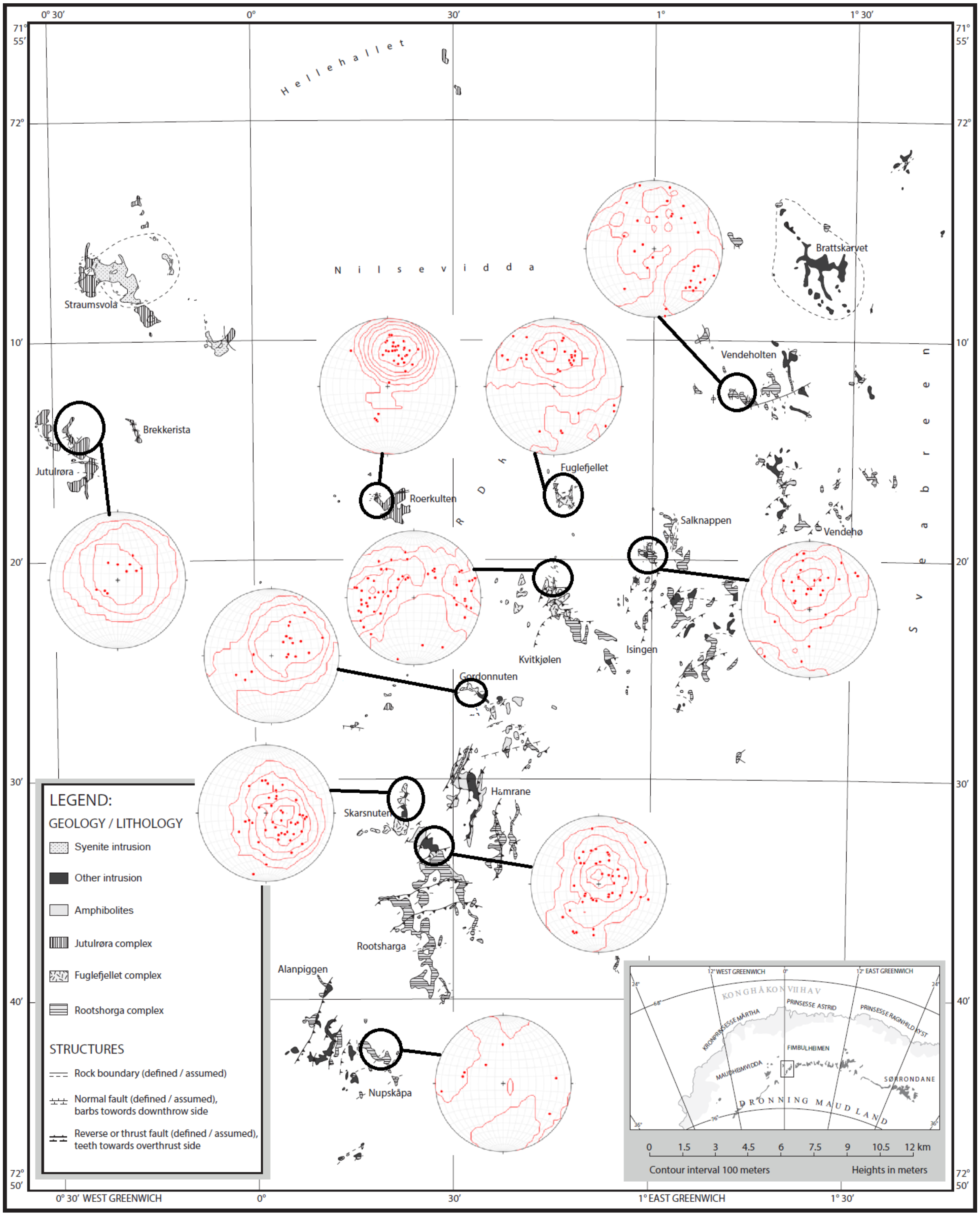

Figure 3.16: To present orientation data of Dalmatian Granites in a spatial context stereonets of poles to sheet orientation are arranged on a map of H.U. Sverdrupfjella (after Elvevold and Ohta, 2010). Data are less variable within nunataks that Salknappen Pegmatites, but the is also no obvious spatial trend in orientation data for Dalmatian Granites. Please note that this map is being used only to give relative positions within H.U. Sverdrupfjella, please see the map accompanying this thesis for a higher resolution version.

3.2.2 Spatial Controls

In order to present orientation data in a spatial context Figure 3.15 and Figure 3.16 show stereonets (plotting poles to granitoid sheet orientation) arranged on maps of H.U. Sverdrupfjella (please see the map attached to this thesis for better resolution) for major nunataks with sufficient data available. Salknappen Pegmatites (in blue, Figure 3.15) do not show an obvious spatial trend in orientations and only orientation data from Salknappen form a cluster of orientation (albeit with significant scatter). Dalmatian Granite orientation data (in red, Figure 3.16) plots in discrete clusters in several nunataks, but also does not show any apparent spatial trend in orientations.

3.2.3 Lithological Controls

Due to the lack of obvious spatial controls on the orientations of granitoid sheets in H.U. Sverdrupfjella, the country rocks will be considered in this section. The study area is predominantly composed of gneisses and other metamorphic rocks, with some granitoid intrusions (other than the granitoids considered in this study). This section will present granitoid orientation data divided by which metamorphic complex hosts the measured sheet, namely the Jutulrøra Complex (composed of quartz feldspar gneiss and banded gneiss), the Fuglefjellet Complex (pelitic gneiss and marbles mixed with calc-silicate gneiss) and the Rootshorga Complex (Pelitic gneiss, felsic paragneiss and felsic orthogneiss).

Salknappen pegmatites in the Jutulrøra Complex (Figure 3.17a) tend to dip toward the S, but there are still scattered data. Salknappen pegmatites in the Fuglefjellet Complex (Figure 3.16B) do not show any obvious preferred orientation. Salknappen pegmatites hosted in the Rootshorga Complex (Figure 3.16C) tend to dip NW, but the data are still scattered; a large proportion of these data dip southward, which may indicate conjugate pairs.

Dalmatian Granite hosted in the Jutulrøra Complex (Figure 3.17a) tends to dip toward SE, making a fairly neat cluster. Dalmatian Granites in the Fuglefjellet Complex (Figure 3.17b) do not show any obvious preferred orientation. Dalmatian Granite hosted in the Rootshorga Complex tends to dip ESE, but there is still significant scatter (Figure 3.17c).

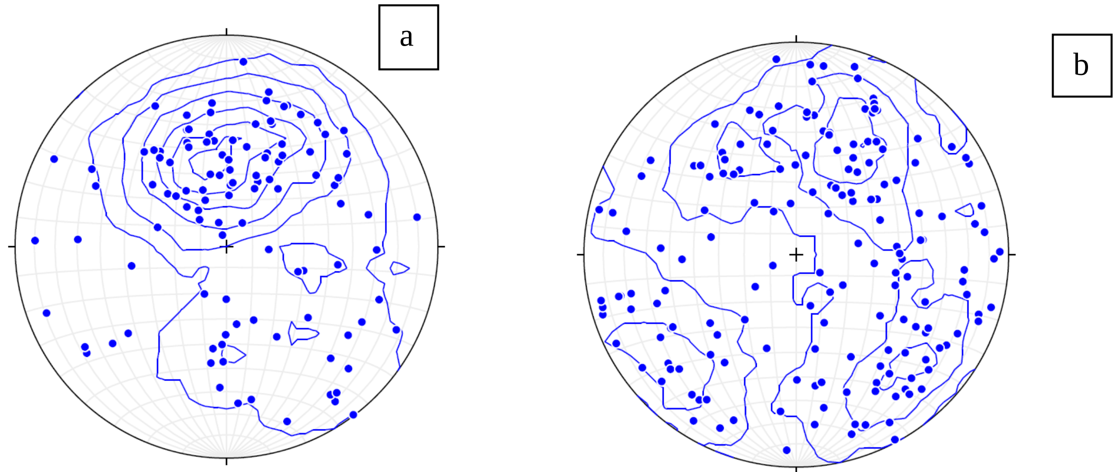

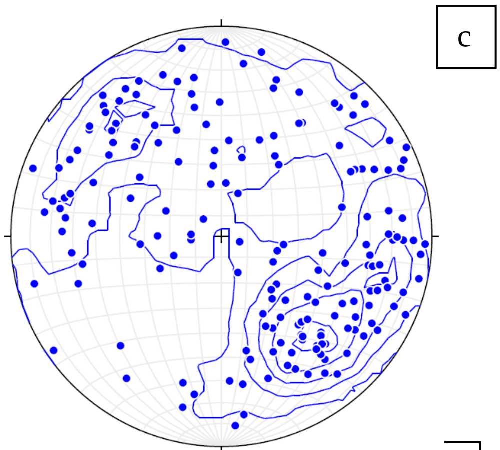

Figure 3.17: Orientation data of H.U. Sverdrupfjella Pegmatites (P1) divided by host rock complex, namely the Jutulrøra Complex (a), the Fuglefjellet Complex (b) and Rootshorga Complex (c).

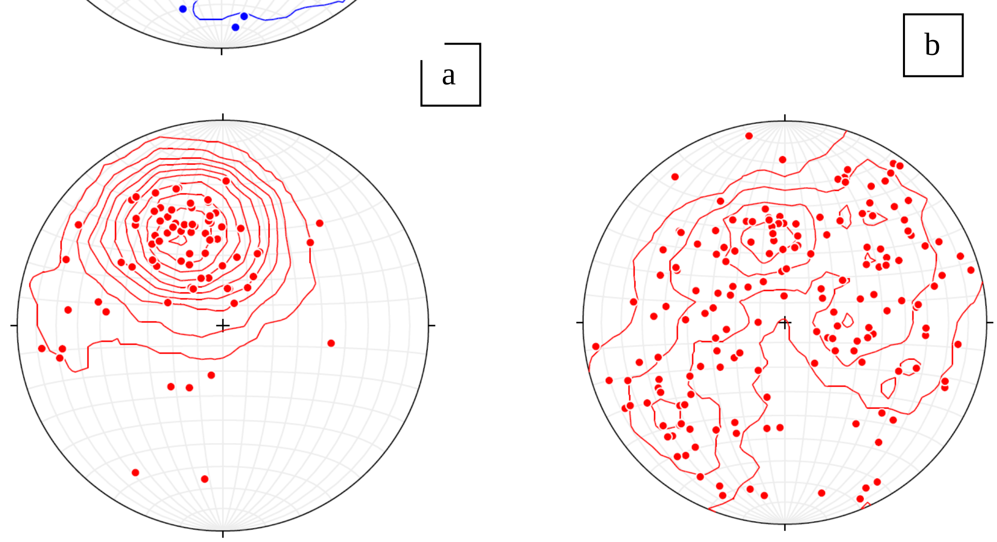

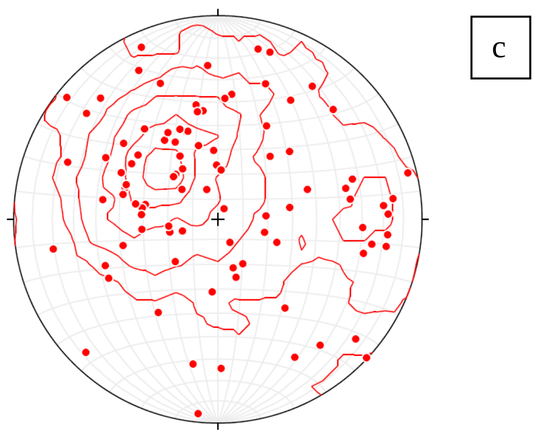

Figure 3.18: Orientation data of Dalmatian Granites divided into which metamorphic complex hosts the sheets measured; the Jutulrøra Complex (a), the Fuglefjellet Complex (b) and Rootshorga Complex (c).

3.3 Orientation Interpretation

The difference in average dips (Figure 3.19) indicates that Salknappen Pegmatites and Dalmatian Granites were emplaced into different stress conditions. The steeper Salknappen Pegmatites are likely to be due to an earlier (crosscutting relationships) tectonic event.

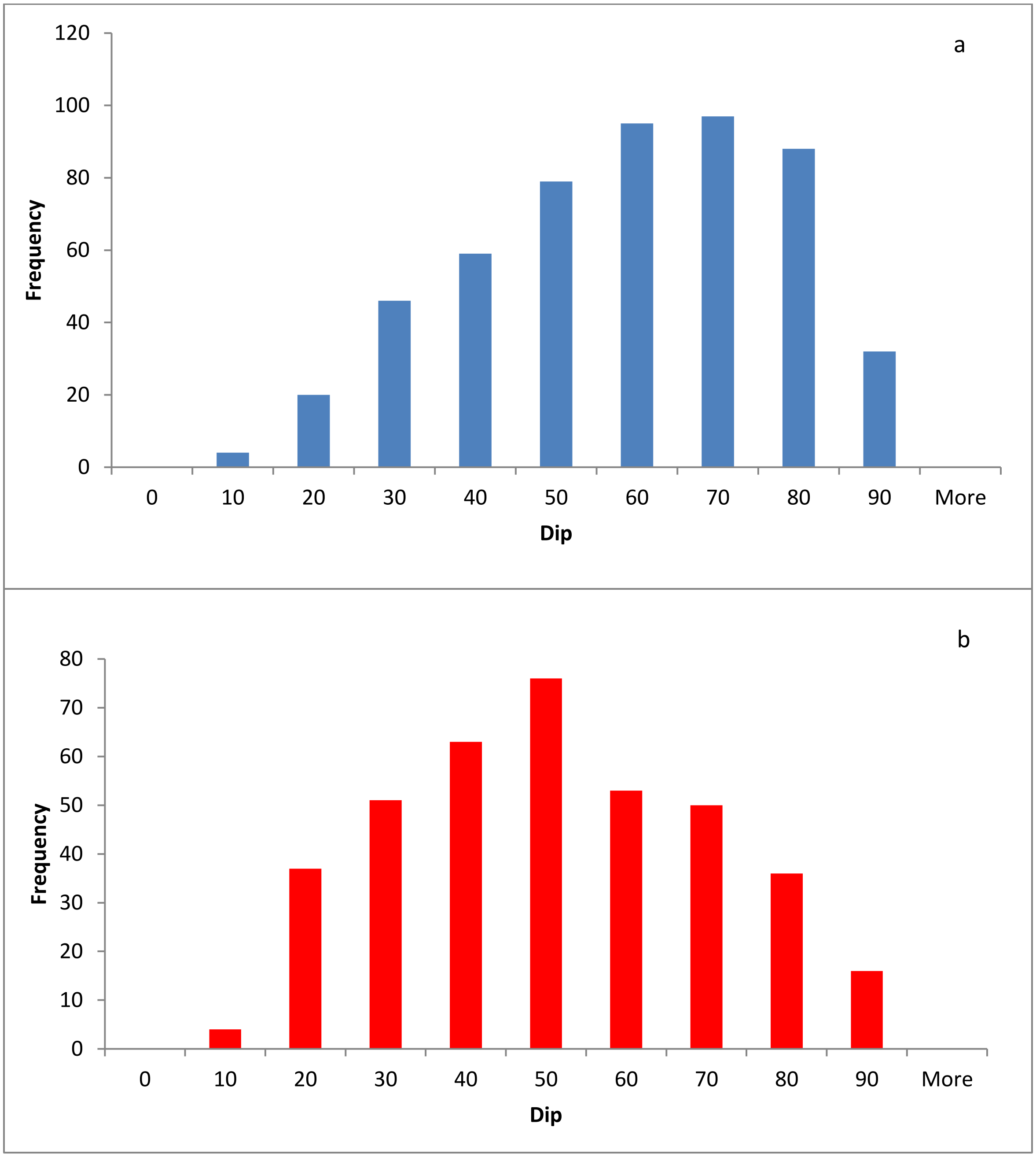

Figure 3.19: A pair of histograms comparing the measured dips of Salknappen Pegmatites (a, in blue) and Dalmatian Granites (b, in red). Note that the while both suites of granitoids have examples varying from near horizontal to near vertical, the Salknappen Pegmatites have a steeper mode of the measured dips than the Dalmatian Granites.

The orientation data does not show a single dominant control, and the scatter in the data demonstrates that several factors control the orientation of granitoid sheets in H.U. Sverdrupfjella. Rock type does appear to be a more significant control than geographical area (which offers no noticeable control). The rocks of Jutulrøra Complex show a more significant influence on the orientation of granitoid sheets than the rocks in the Rootshorga complex. The rocks of the Fuglefjellet Complex offer no noticeable control on the orientation of granitoid sheets, most likely due to the relatively soft marbles mixed with calc-silicate gneiss.

Some of the scatter in the orientation data could be a result of by conjugate pairs of weak planes, which would result in two poles of opposite dip direction, creating orientations opposite to the predominant dip direction. In addition, considering that some granitoid sheets display opportunistic intrusion (as in Figure 3.9), the scatter could be due to localised controls causing some intrusions to deviate from the dominant preference in orientation. For both suites in more competent rocks the dominant preferred orientation in general tends to be near either NW or SE.

3.3.2 Orientations of granitoid sheets

The suites of granitoids sheets have different orientations when seen together in the field. Therefore it may be possible to use orientation to classify and differentiate the different granitoids considered in this study. Salknappen pegmatites have a steeper mode of the measured dips (~70°) than Dalmatian Granites (~55°), as shown in Figure 3.20. The steeper mean dip of Salknappen Pegmatites indicates that the stress acting on the study area during the emplacement of Salknappen pegmatites had a different orientation to the stress acting on the area during emplacement of Dalmatian Granite. Alternatively, the difference in average dip could indicate that some displacement and rotation of the rocks in the study area occurred between the emplacements of the different granitoids.

Though Salknappen Pegmatites and Dalmatian Granites have different average dips, the difference is not great. In addition, both suites of granitoids have single sheets with very steep and very shallow dips. Therefore, while there is an average tendency, the dip of any one granitoid sheet is not a reliable way of classifying that particular granitoid suite. When considered with the variation in orientations, the opportunistic nature of granitoid intrusion and the lithological control on orientation (section 3.2.3 leads to the conclusion that the orientation of granitoid sheets is not a characteristic of the sheets, but rather a circumstance of emplacement, i.e. which rock they were emplaced into.

Chapter 4: Petrography

4.1 Petrography

In this chapter the minerals, mineral interactions, petrogenesis and microscopic properties of the granitoids in this study will be investigated using transmitted light petrography. In addition, an estimation of mineral quantities in the granitoids will be presented in this section. The petrography presented here will be the general descriptions per rock type; for micrographs per sample see Appendix 4.

4.1.1 Pre-existing Granitoids

The Pre-existing Granitoids (P0) consist of biotite, plagioclase, microcline, quartz and muscovite (likely secondary). Quartz intergrowths were observed, often appearing as myrmekite, but not in all examples. Myrmekite is consistent with deformation (Vernon, 2004) as was observed in the field (described in section 3.1.2). However, the foliation observed in the field is not seen in thin section, owing to the scale of that foliation being greater than the size of a thin section.

An early generation of rounded quartz grains are observed. Biotite appears to form early but is rare enough that this observation remains tentative. Microcline and quartz grains are commonly large and interstitial, whereas plagioclase grains are smaller and appear cumulus. Intergrowths of quartz and microcline indicate simultaneous crystallisation. Embayment, myrmekite and one example of what appears to be coronae around inclusions (Figure 4.1) show that some reactions and recrystallization have taken place.

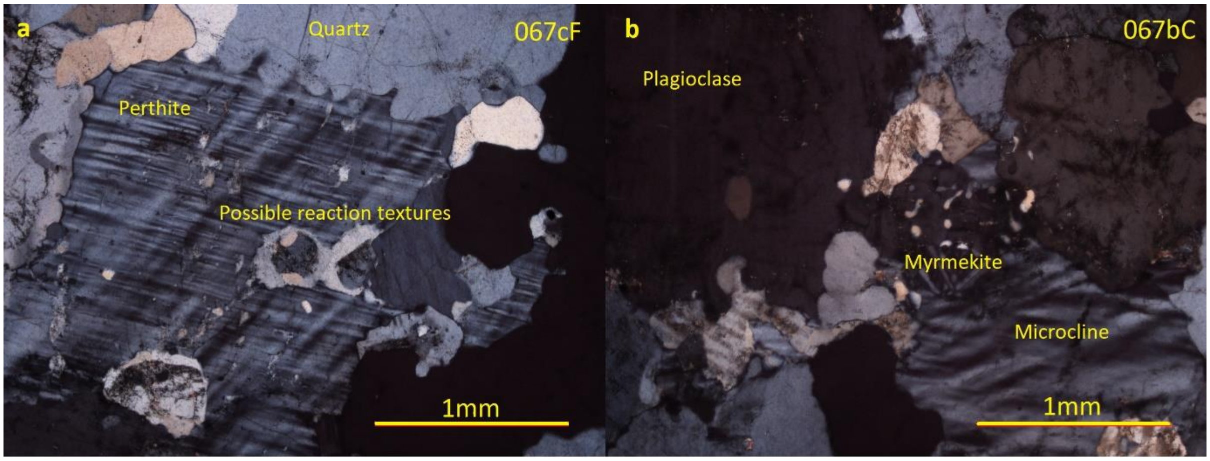

Figure 4.1: A micrograph of a Pre-existing Granitoid. Samples 067cF and 067bC are used to show the mineral relationships and predominant mineralogy of Pre-existing Granitoid. Note the myrmekite and potential corona indicating solid state reactions or recrystallisation.

4.1.2 Salknappen Pegmatite

The grain size in the Salknappen Pegmatite (P1) is very coarse in general, but variable, with an interlocking texture. The following minerals have been observed in Salknappen Pegmatite thin sections: quartz, k-feldspar (microcline and perthite), some plagioclase, biotite (often forming large grains, but no chloritization noted), some muscovite, a few (two or three in a few samples) small grains of amphibole and rare garnet (Figure 4.2). Most plagioclase and some quartz (along cracks and near fractures) host some muscovite and fine-grained minerals with high birefringence. The fine-grained mineral is interpreted to be muscovite or another phyllosilicate. Both muscovite and the fine-grained mineral are considered secondary.

Some quartz grains are relatively large and indicate slightly more strain than smaller grains. Other quartz grains are relatively small and rounded. Large quartz grains are included in and embayed by perthite. There are examples of plagioclase is overgrown by and included in quartz as well as quartz included in and overgrown by plagioclase (Figure 4.2 c and d). Biotite is overgrown by and included in k-feldspar and quartz. Microcline and perthite are interstitial to other minerals. Therefore, early quartz formed first, followed by biotite, then plagioclase with quartz and finally perthite. The early rounded quartz grains could be xenocrysts (from country rock) that were transported by the granitoid magma.

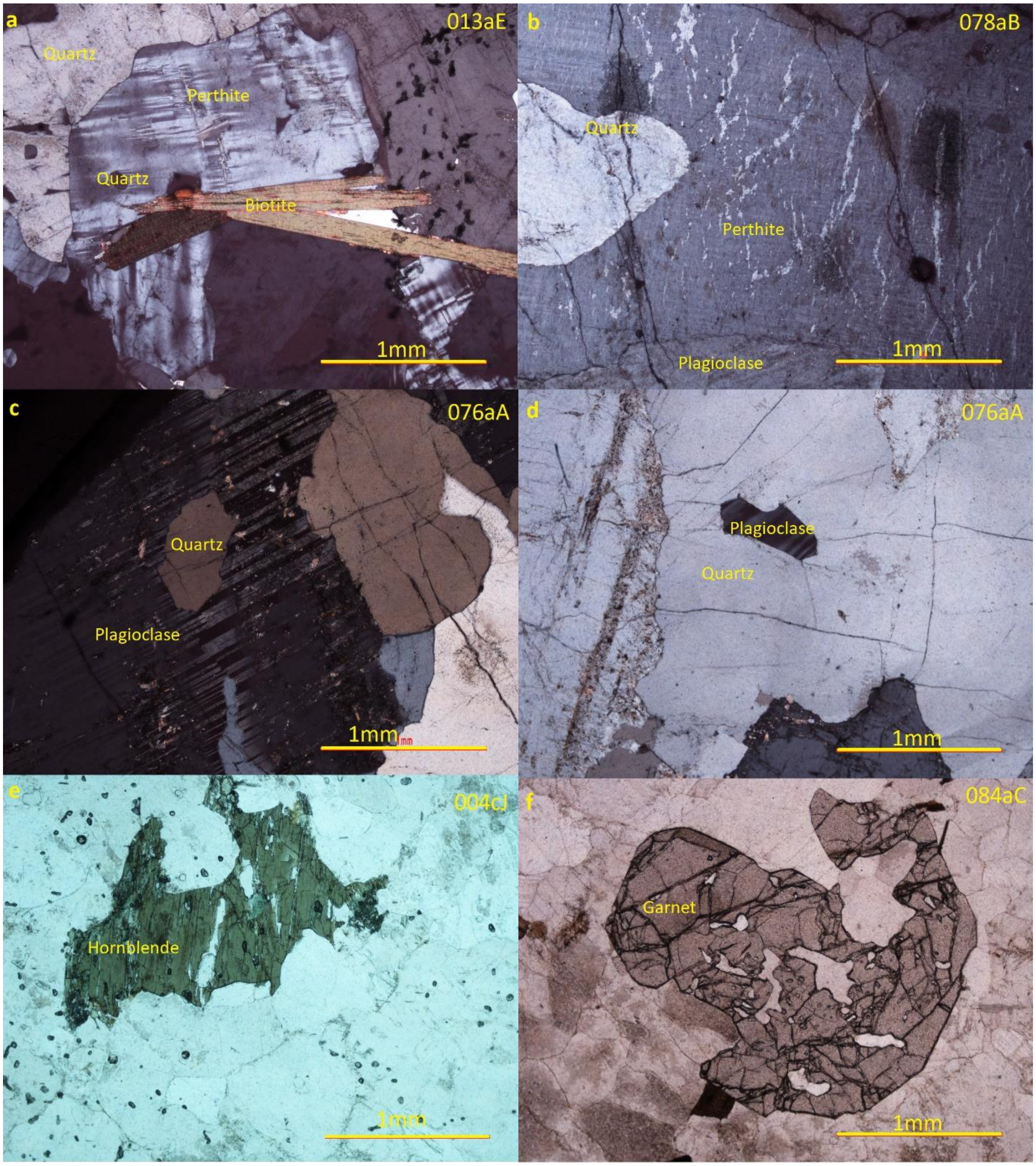

Figure 4.2: Micrograph showing the coarse grain size, large books of biotite (a), perthite (b), presence of hornblende (e) and garnet (f) in Salknappen Pegmatites. Quartz included in plagioclase is shown in c and plagioclase included in quartz is d. These micrographs are from samples 004cJ, 013aE, 76aA, 078aB and 084aC. Micrographs were selected to be specimens that demonstrate observations rather than representative records of Salknappen Pegmatite.

4.1.3 Dalmatian Granite

Dalmatian Granites (P2) have an interlocking texture and varied grain size (coarse in general). Dalmatian Granites samples are generally composed of quartz, microcline as the dominant feldspar (some myrmekite), plagioclase, some biotite (some reacting into chlorite); few zircon grains included in biotite (Figure 5.3). A few grains of haematite observed in the (rare) hornblende in a few samples and some opaque grains were noted in some thin sections. Hornblende was noted, but not in all samples.

Feldspar grains host alteration product including a fine-grained mineral with high birefringence and discernible (>0.25 mm) phyllosilicate grains that appear to be muscovite. Quartz grains are commonly cracked, but do not show very undulose extinction. Dalmatian Granites contain small rounded quartz grains and these are a distinct generation from larger quartz grains. Biotite is usually relatively small, but biotite inclusions are hosted by quartz and plagioclase. Microcline hosts some quartz and some plagioclase inclusions and occurs as large interstitial grains. Plagioclase hosts relatively small quartz inclusions. Cracks in quartz grains host a fine-grained mineral with the same colour, but higher birefringence than quartz.

Rounded quartz is included in microcline, indicating early formation or that it originates from the country rock and was transported. This is interpreted as smaller quartz grains forming first or being inherited, followed by biotite, followed by quartz starting to crystalize, then plagioclase and finally microcline (after biotite stopped forming) and quartz forming until crystallisation stopped. Chlorite and large grains of alteration (phyllosilicate that appears as muscovite) are considered secondary.

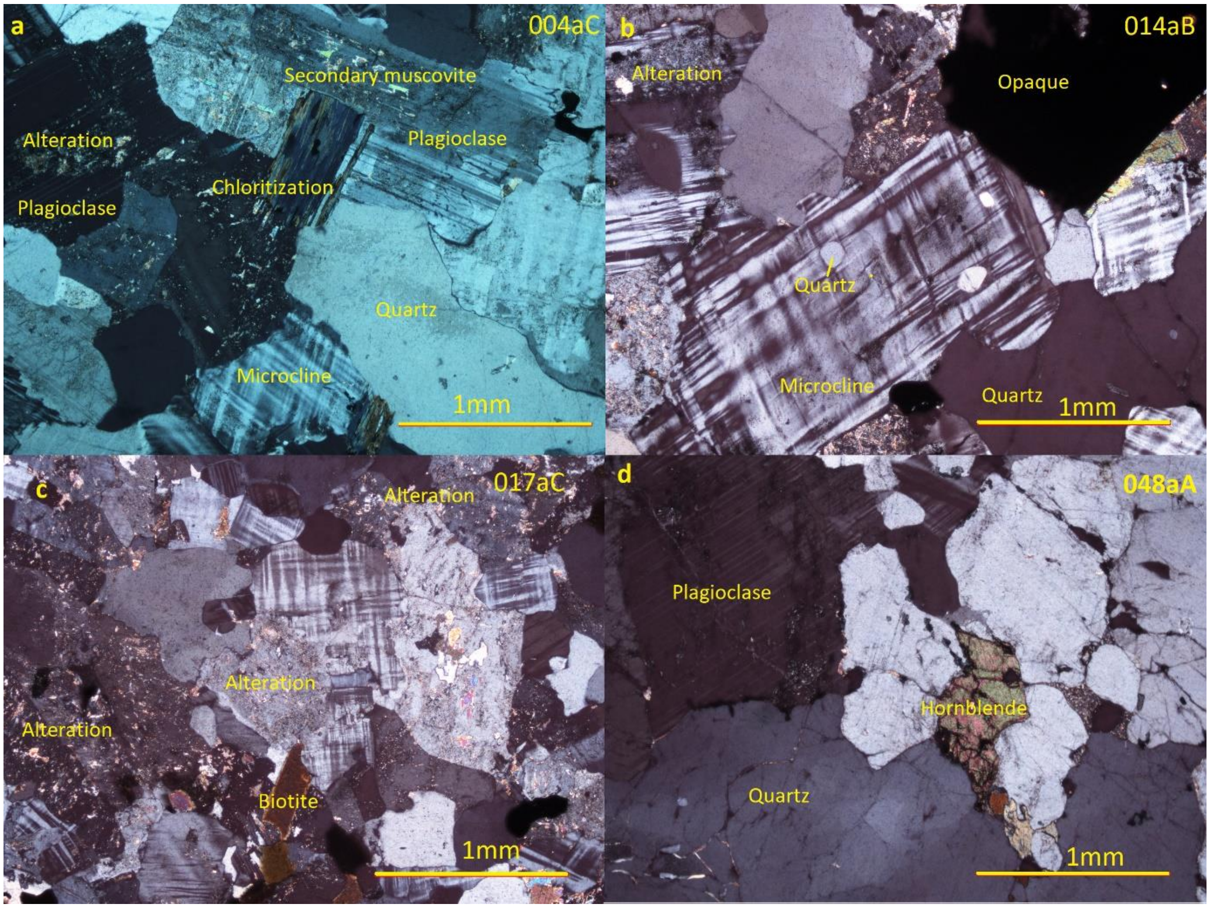

Figure 4.3: Micrographs showing characteristics of Dalmatian Granites, micrographs were chosen purely based on illustrating certain characteristics and are from samples 004aC (a), 014aB (b), 017aC (c) 048aA. The micrographs show the following: Chloritization of biotite and secondary muscovite on feldspar in a. Rounded quartz grains included in microcline, as well as more secondary muscovite in b. Micrograph c shows the mineral relationships and how widespread alteration is and d shows and example of hornblende.

4.1.4 Pegmatitic Dalmatian Granite

One sample of pegmatitic Dalmatian Granite (P3) was taken at Roerkulten (sample 014bC) and a micrograph is shown as Figure 4.4. Sample 014bC is generally coarse grained, but grain size varies. The thin section consists of subhedral quartz, plagioclase, some biotite, much interstitial k-feldspar (some grains showing exsolution), sparse opaque grains and very sparse hornblende. A few zircon grains are visible, and chlorite is replacing biotite. Some alteration forms grains large enough to be birefringent and appear as muscovite.

Quartz is included in microcline, is overgrown by plagioclase and overgrows biotite. Microcline is interstitial to all other minerals. No direct relationship between clinopyroxene, plagioclase and quartz observed. Therefore, biotite crystalized first and microcline last; amphibole, quartz and plagioclase crystalized in an unclear order in between. Chlorite and apparent muscovite are secondary. Pegmatitic Dalmatian Granites (P3s) appear similar to Dalmatian Granites and are grouped with Dalmatian Granites in the discussion that follows.

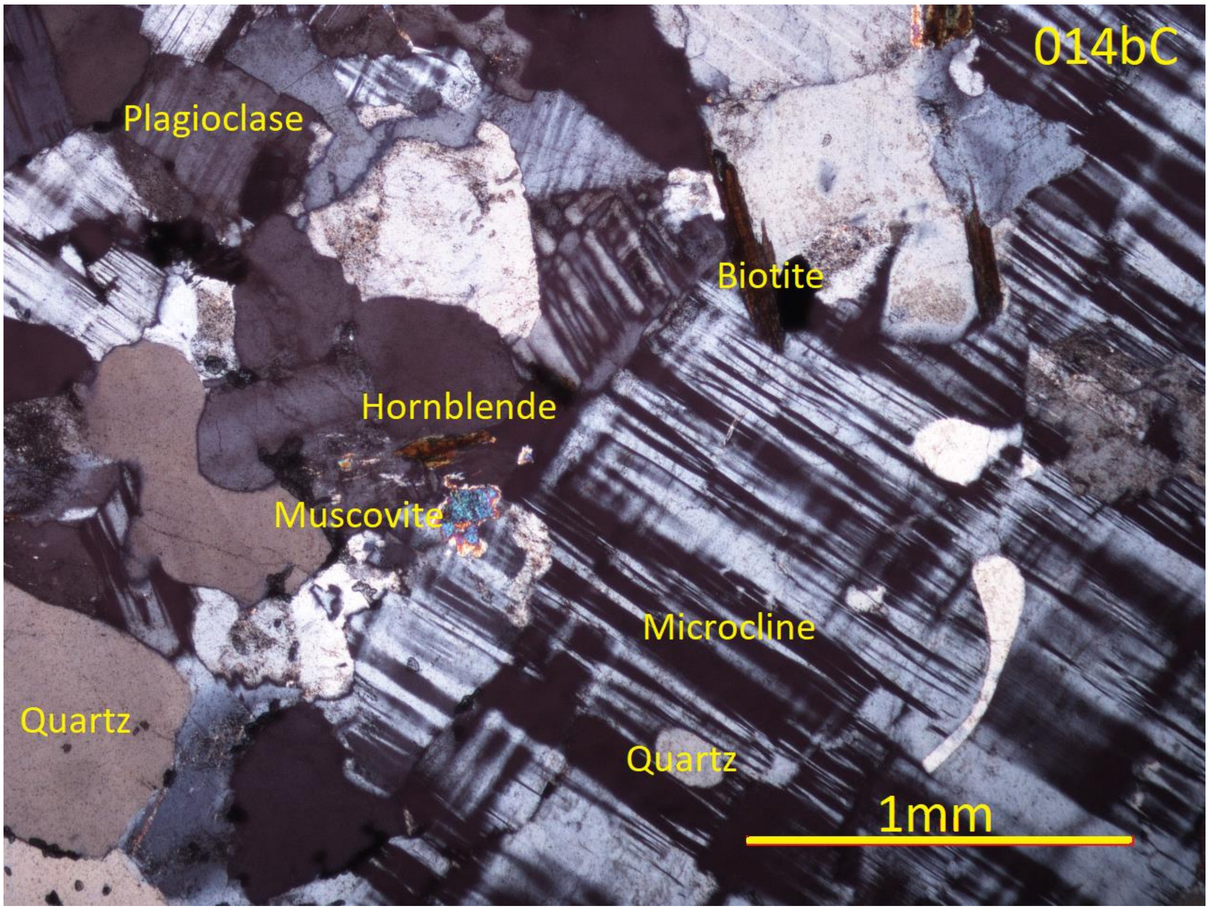

Figure 4.4: Micrograph showing the generally coarse grain size and variation in grain size of pegmatitic Dalmatian Granites. As well as the interstitial nature of microcline and mixed age relationships for other minerals.

4.1.5. Discussion of mineralogy

Both suites of granitoids (Salknappen Pegmatites and Dalmatian Granites) have typical granitoid mineralogy. Mineral composition differs predominantly in the different accessory minerals present. Both suites have an early quartz generation, followed by biotite, then feldspars and more quartz growth. In addition, both granitoids contain hornblende and muscovite.

The differences between the suites of rock are marked by grain size, the habit in which biotite occurs, the feldspar species present, and the accessory and secondary minerals. Salknappen Pegmatites have larger books of and more prominent biotite, which is consistent with the coarser texture. Both suites have large interstitial grains of microcline, but perthite is more commonly visible in Salknappen Pegmatites than in in Dalmatian Granites. More commonly visible perthite is interpreted as more exsolution taking place in Salknappen Pegmatites, likely due to Salknappen Pegmatites having higher Na on average (see Chapter 6). Secondary processes differ in that microcline is more commonly visible in Salknappen Pegmatites and alteration is more extensive in Dalmatian Granites. Magnetite was noted to occur in some Dalmatian Granites in the field (section 3.1.2, some sheets are magnetic), but is not observed in Salknappen Pegmatites. The mineralogy of opaque minerals was not confirmed but could be magnetite. Garnet was observed in Salknappen Pegmatite, but not in Dalmatian Granites.

Owing to the small area sampled in a thin section, the similarity in mineralogy (both suites are granitoids, as defined by mineralogy) and the coarse grain size of granitoids, it is difficult to differentiate granitoids using petrography of any one thin section. However, the petrography is consistent with the field descriptions and appearance above.

4.2 Mineral Estimation

Estimating mineral proportions proved difficult due to grain size relative to the size of a thin section and the smaller size of a micrograph. Accessory minerals are overrepresented if an entire grain is present in a micrograph and including part of a grain gives an arbitrary amount of that mineral.
Therefore, only the major mineral proportions (quartz and feldspars) were estimated for select samples. Estimation using petrography was done using ImageJ software, which calculates the surface area of a manually selected mineral type in the thin section. Proportions are based on the relative area covered by each mineral in the micrograph.

These data are plotted on a QAP diagram below, excluding sections with >60% or <20% quartz which are not considered representative of the host granitoids. The different granitoids do not show a discernible difference and have compositions in most of the range (bar extremes) and between alkali-feldspar and plagioclase in Figure 4.5

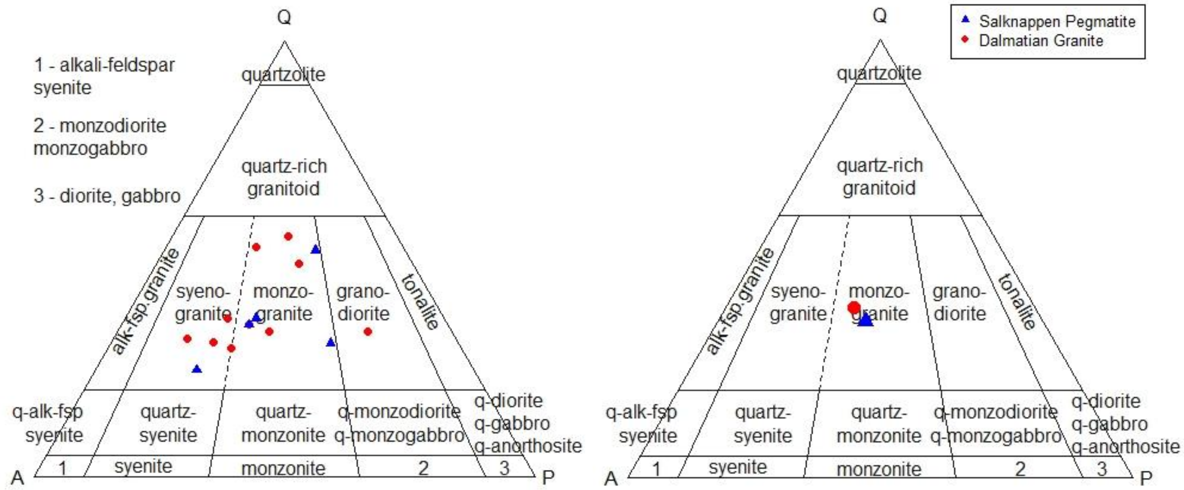

Figure 4.5 QAP diagram for mineral abundances estimated using ImageJ software for Salknappen Pegmatite and Dalmatian Granite (left) and the same data averaged (right). Compositions vary across the range between A and P. Samples with >60% or <20% quartz excluded.

Figure 4.6 shows the CIPW Norm (Johannsen, 1931) derived abundances of major minerals in granitoids done by GCDkit software. There is less variation in that Dalmatian Granites plot mostly (but not exclusively) as monzogranites and Salknappen pegmatites tend to calculate as having more plagioclase (but not always). No samples were not removed for quartz content in this diagram.

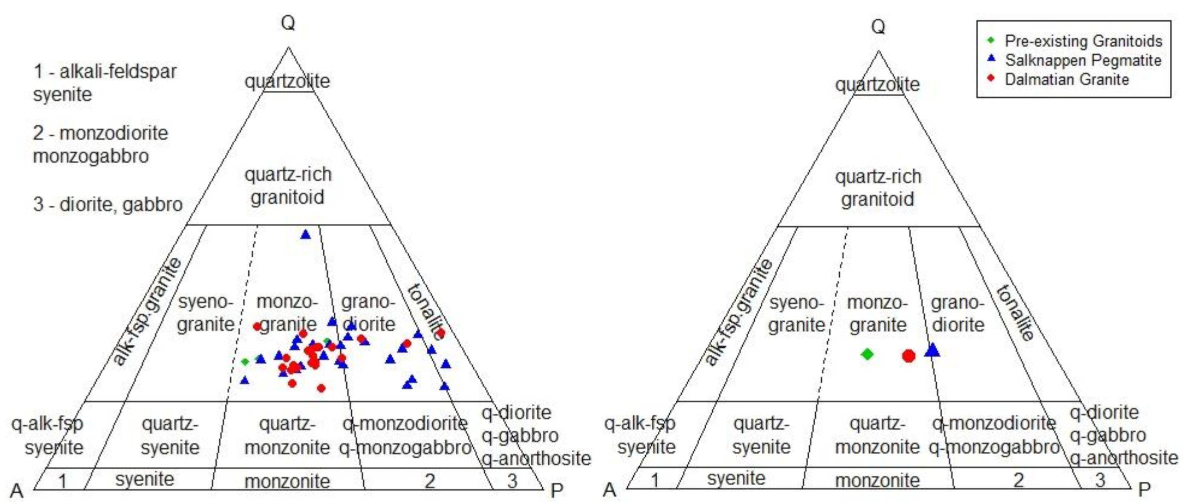

Figure 4.6 QAP diagram of mineral estimates by CIPW Norm calculation by GCDkit software for Pre-existing Granitoids, Salknappen Pegmatites and Dalmatian Granites (left) and averages of the same data (right). Note that the different granitoids behave differently, despite not forming distinct groups. Dalmatian Granites are predominantly monzogranites while Salknappen Pegmatites contain more plagioclase on average.

The mineral abundances calculated from the chemistry are considered to be more reliable than the optically determined abundances. As the mineral proportions based on chemistry are more consistent with more perthite visible in Salknappen Pegmatites in thin section and the colour difference between the granitoids seen in the field (Salknappen Pegmatites are white and Dalmatian Granites are pink). However, it is clear that the rocks analysed are definitely granitoids in composition.

Chapter 5: Geochronology

5.1 Introduction

Six samples, from the first field season, covering the northern part of H.U. Sverdrupfjella (see Figure 5.13), were selected for dating as per the methods described in Chapter 2:

- Three samples of Salknappen Pegmatites were analysed, namely sample 004cJ hosted in the Jutulrøra Complex at Fuglefjellet and samples 012bE and 013aE hosted in the Rootshorga Complex at Salknappen. These 3 samples are all examples of the +Eu Salknappen Pegmatites.
- Three samples, 004dI, 012aD and 040aA, of Dalmatian granite were also analysed by SHRIMP. Sample 004dI, is from Fuglefjellet and hosted in country rock of the Fuglefjellet Complex. Sample 012aD is also from Salknappen and hosted in rocks of the Rootshorga Complex. Sample 040aA is from further South at Gordonnuten and is hosted by rocks of the Fuglefjellet Complex.

The term “usable data” used below refers to data that were not excluded owing to high common Pb. Such data is struck through and the issue noted in table A3.3. Additionally, ages interpreted as inherited (i.e., significantly older than other data) were excluded from weighted mean ages (weighted by error) but are considered further in section 5.3. Outliers were excluded from weighted age for one sample (004cJ), shown in the relevant box plot. The weighted mean is weighted by the error. Error elipses on concordia plots are 68.3% confidence and box heights show a 1σ error.

5.2 SHRIMP Results

5.2.1 Sample 004cJ

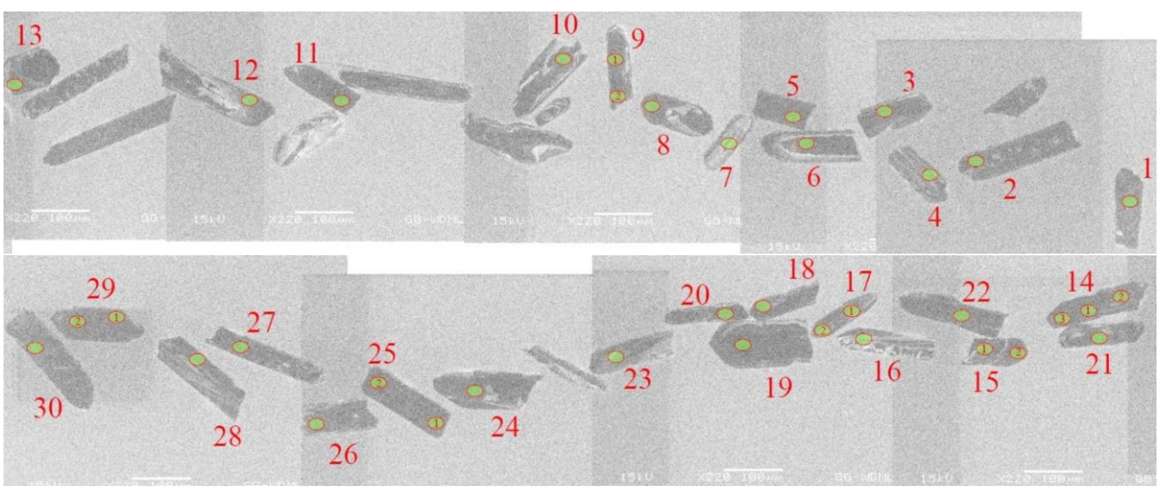

Figure 5.1: A compilation of CL images of zircon grains separated from sample 004cJ and the spots where measurements were attempted. As with sample 004dI, some zoning is visible and different inherited ages were recorded at spots 2 and 7.

For sample 004cJ, 30 grains were analysed, of which 15 produced useable data (Figure 5.1). 20 out of a total of 37 spots were used to calculate an age of 517 ± 3.5 Ma (1.96σ, MSWD=0.37; Figure 5.2). One grain showed an inherited age of ~ 1150 Ma.

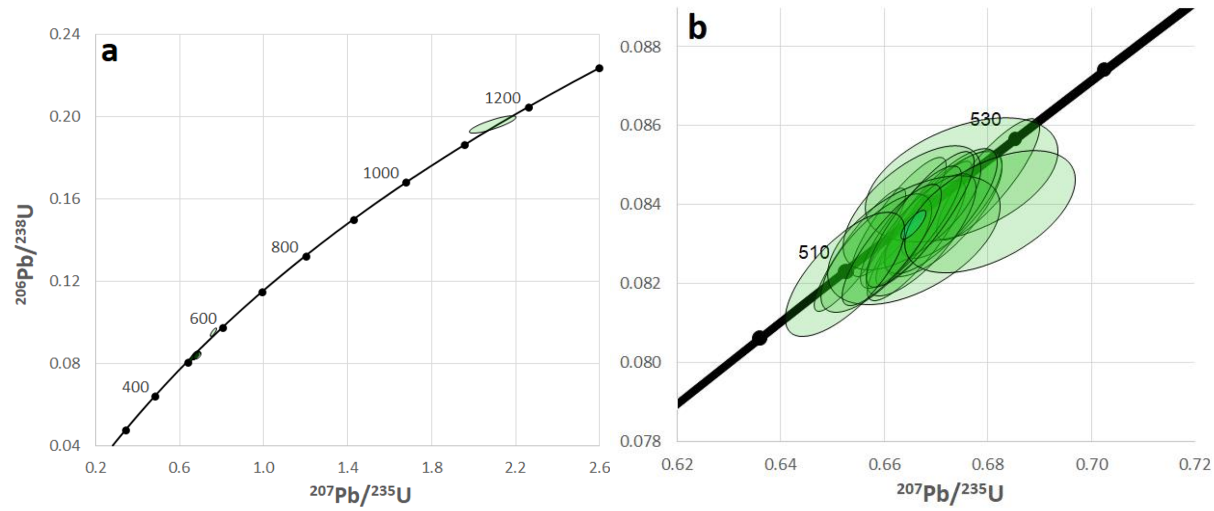

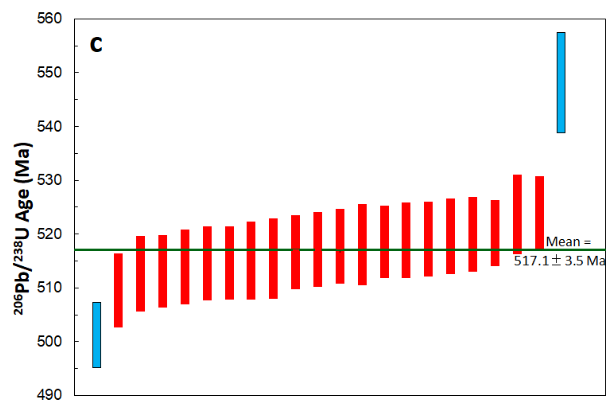

Figure 5.2: Wetherill concordia (a and c) and box plot (c) for sample 004cJ. Two ages were interpreted to be inheritance; these are shown in a but excluded from b. Box plot has MSWD =0.37, probability = 0.991, weighted mean of 517.1 ± 3.5 Ma and boxes show 1σ errors. Two data points were excluded as outliers, shown in blue with a black border.

5.2.2 Sample 012bE

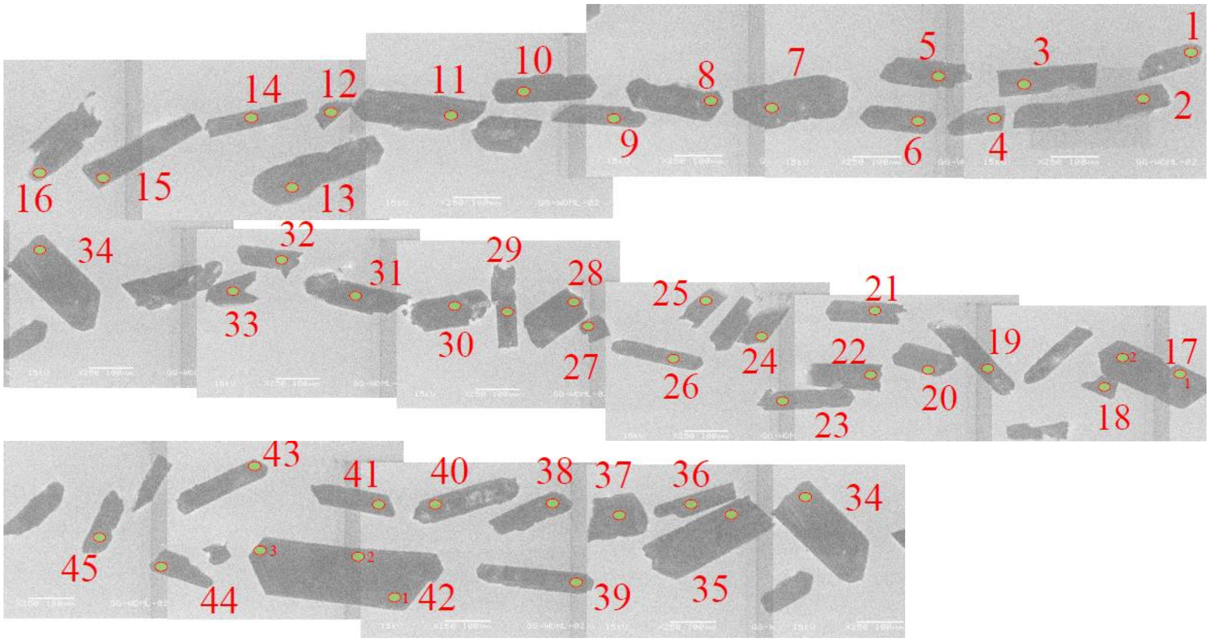

Figure 5.3: A compilation of CL images of zircon grains separated from sample 012bE and the spots where measurements were attempted. Very little zoning is visible and no inheritance was recorded. The first 10 grains shown were not used.

Sample 012bE provided useable data from 25 of 35 grains (Figure 5.3) and 26 points out of 37 spots analyses were used to calculate an age of 507 ± 3.1 Ma (1.96σ, MSWD=0.66; Figure 5.4). No inherited ages were recorded, hence there is only one Wetherill Concordia diagram shown.

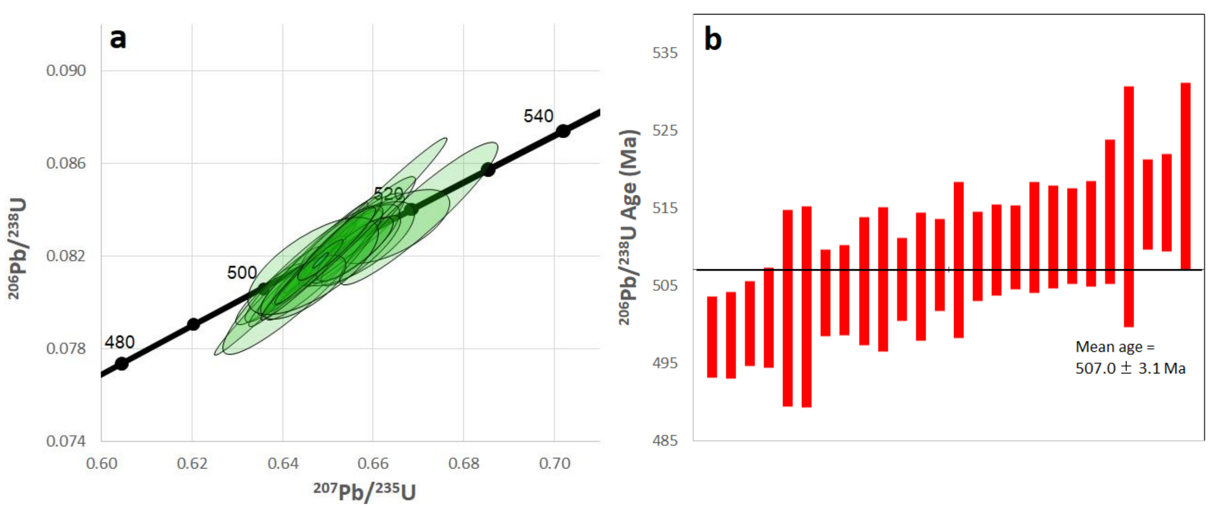

Figure 5.4: Wetherill concordia (a) and box plot (b) for sample 013bE. No inheritance was measured. The weighted mean age is 507.0 ± 3.1 Ma; with MSWD = 0.66, probability = 0.89 and boxes show 1σ error.

5.2.3 Sample 013aE

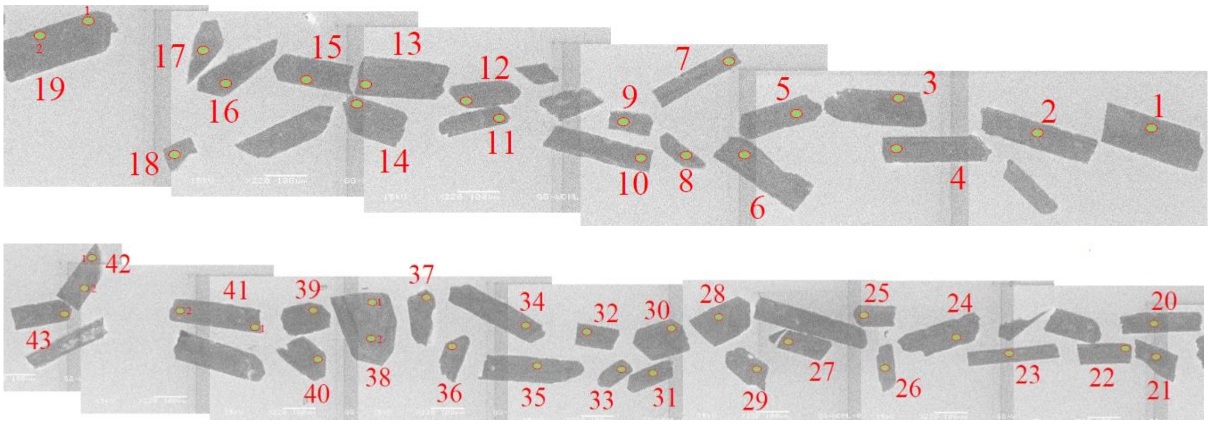

Figure 5.5: A compilation of cathodoluminescence (CL) images of zircon grains separated from sample 013aE and the spots where measurements were attempted. The first 9 grains shown were not used.

Sample 013aE provided useable data from 16 of 34 grains (Figure 5.5) and 17 points out of 38 spot analyses were used to calculate an age of 513 ± 3.7 Ma (1.96t σ, MSWD=0.73; Figure 5.6). No inherited ages were measured. This age has a low MSWD compared to some of the other ages, and visual inspection of the data possible indicates two groups of concordant ages. However, the overlap between these two possible groups means that unravelling the two groups would be extremely speculative.

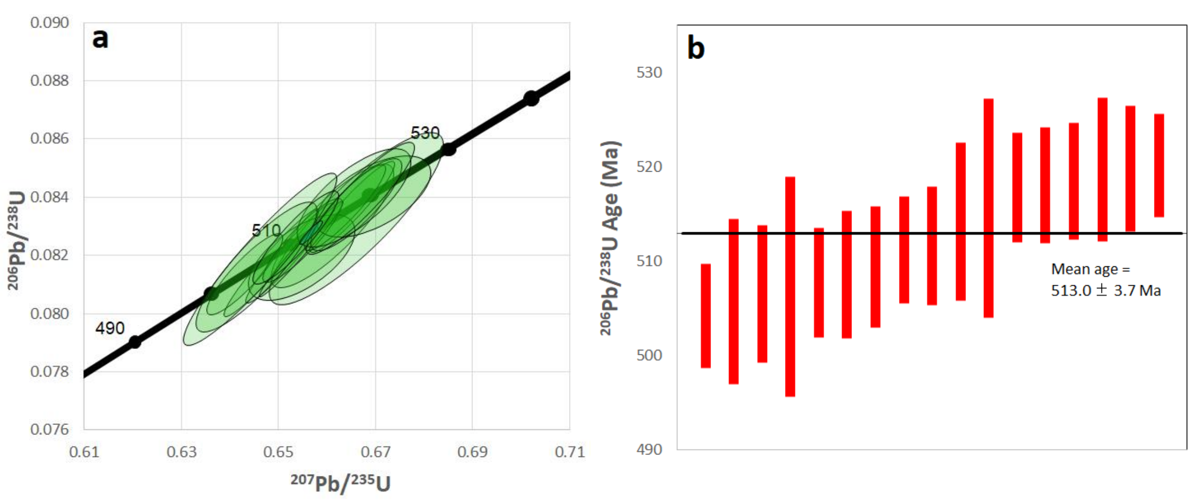

Figure 5.6: Wetherill concordia (a) and box plot (b) for sample 013abE. No inheritance was measured. Weighted mean age is 513.0 ± 3.7 Ma; with MSWD = 0.73, probability = 0.76 and boxes show 1σ error.

5.2.4 Sample 004dI

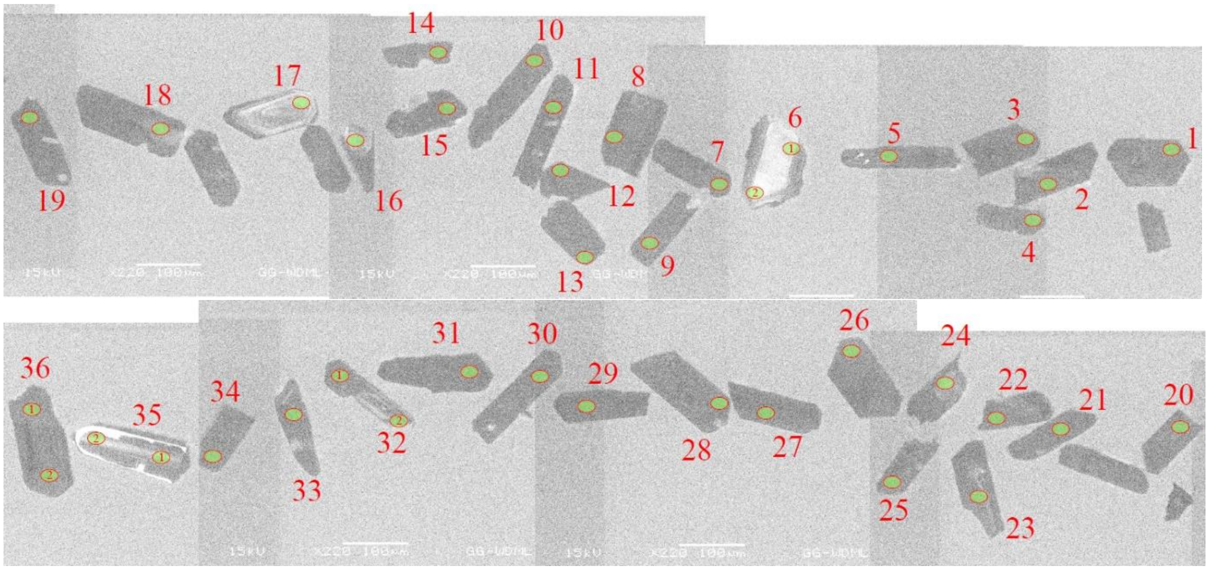

Figure 5.7: A compilation of cathodoluminescence (CL) images of zircon grains separated from sample 004dI and the spots where measurements were attempted. Note some zoning is visible and data from the grain marked 35 gave inherited ages.

Sample 004dI yielded useable data from 27 of 36 grains (Figure 5.7), and 29 out of 40 spot analyses were used to calculate an age of 492 ± 2.9 Ma (1.96σ, MSWD=0.95; Figure 5.8). Useable data refers to data that was not excluded. This age is not perfect, as some spots produced significantly younger ages around 485 Ma, which may indicate late-stage overgrowths. Two spots on one grain (labelled 35 in Figure 5.7) yielded inherited ages of ±1050 Ma (please see data tables in A3.3).

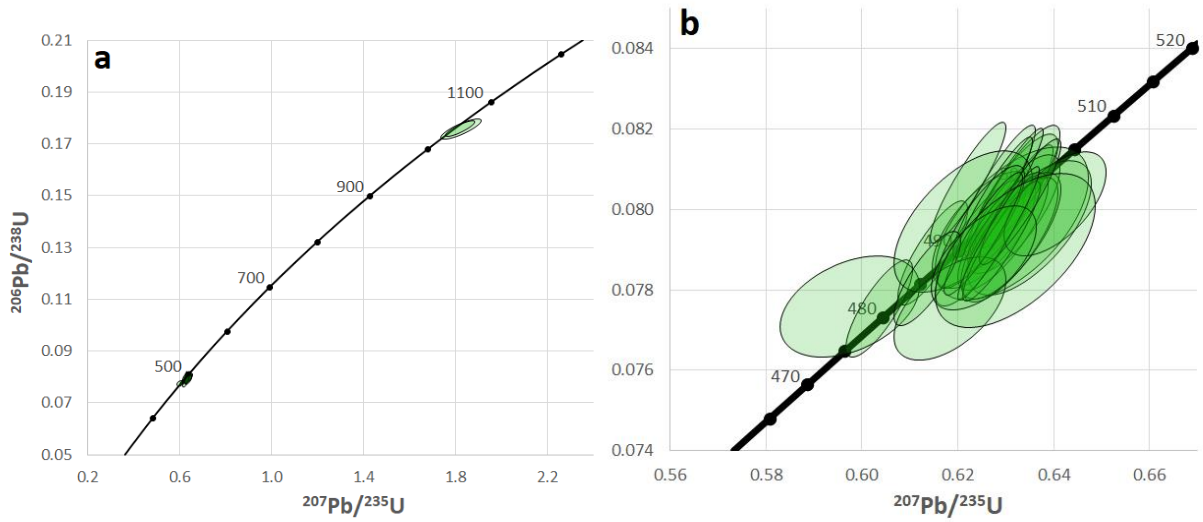

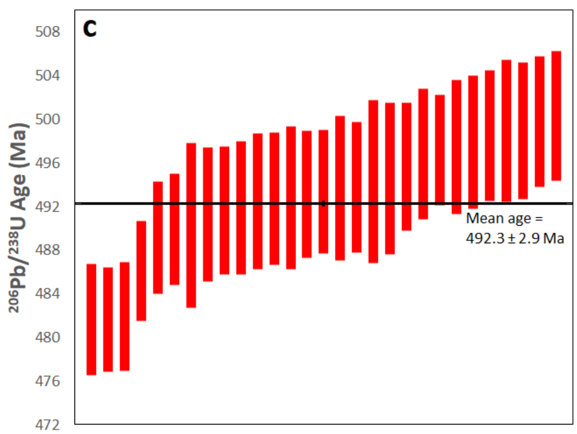

Figure 5.8: Wetherill concordia (a and b) and box plot (c) for sample 004dI. Figure 5.8 a includes points that are considered to be due to inheritance, and b is the Wetherill concordia with inherited ages removed.

The weighted mean age is 492.3 ± 2.9 Ma; with MSWD = 0.95, probability = 0.54 and boxes show a 1σ error.

5.2.5 Sample 012aD

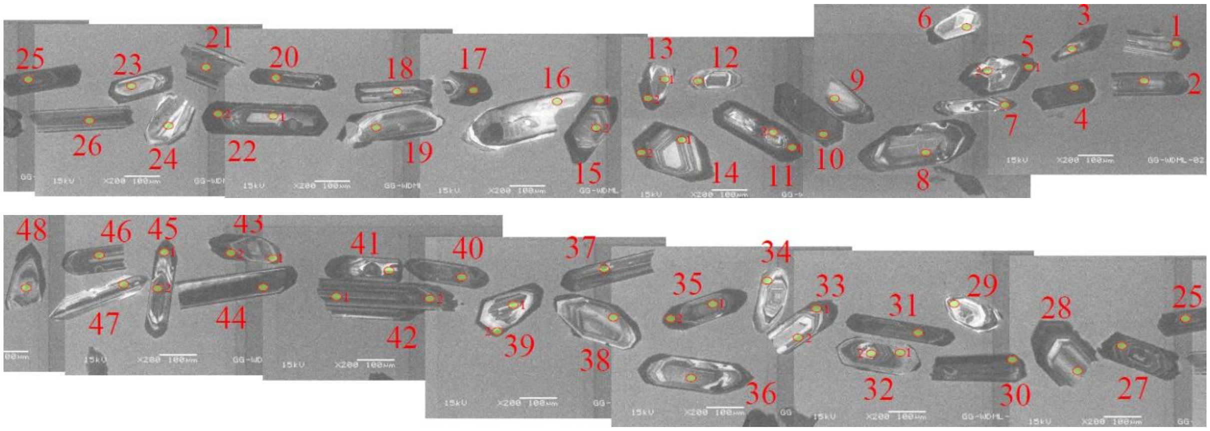

Figure 5.9: A compilation CL images of zircon grains separated from sample 012aD and the spots where measurements were attempted. Significantly more zoning is visible in almost all grains compared to other samples and more inheritance was recorded in the data. Spots 16, 24 and 29 show inherited ages.

Sample 012aD provided useable data from 31 of 37 grains (Figure 5.9), and 36 points out of 48 spot analyses were used to calculate an age of 483 ± 2.8 Ma (t σ, MSWD=1.3; Figure 5.10). Three grains provided inherited ages of 936 ± 17 Ma, 1085 ±60 Ma and 2602 ± 28 Ma.

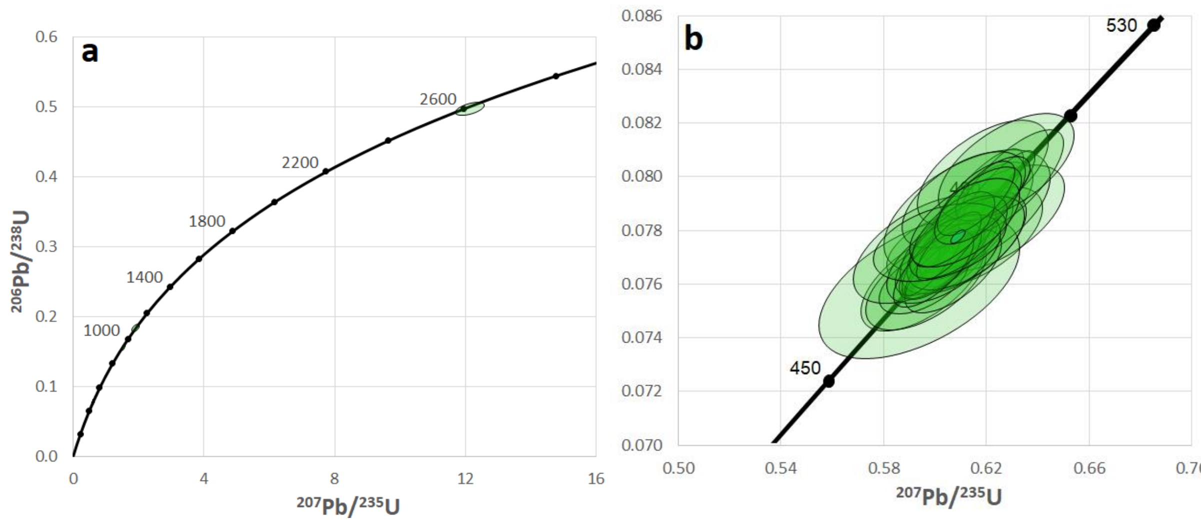

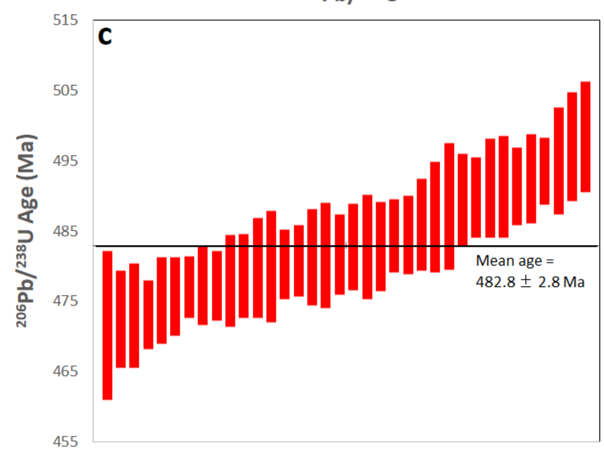

Figure 5.10: Wetherill concordia (a and b) and box plot (c) for sample 012aD. This sample shows more significant inheritence than other samples (a). b shows the Wetherill concordia including only ages that are not interpreted as inheritance. Weighted mean age (c) is 482.6 ± 3.1 Ma; with MSWD = 0.95 and probability = 0.53 and boxes show 1σ error.

5.2.6 Sample 040aA

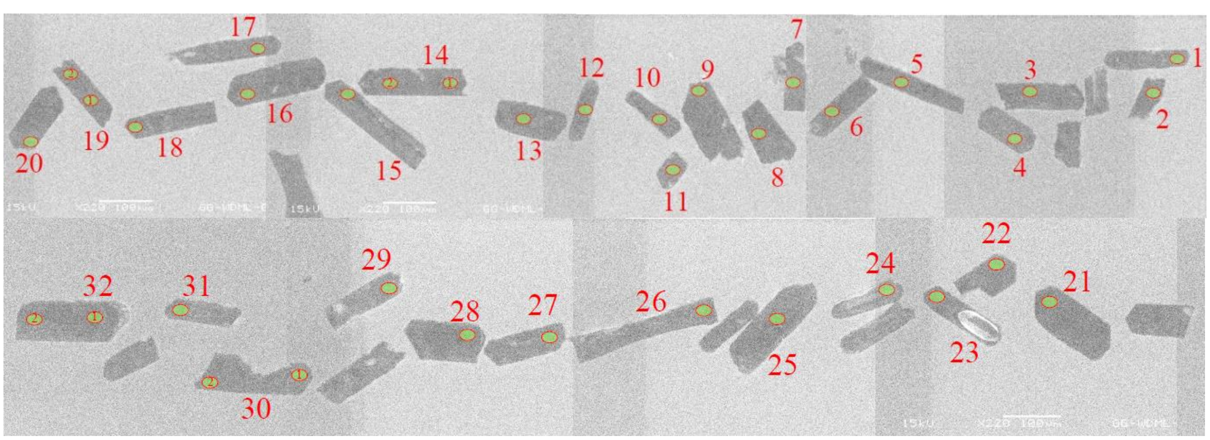

Figure 5.11: A compilation CL images of zircon grains separated from sample 040aA and the spots where measurements were attempted. Little zoning is visible, but inherited ages were recorded at spots 4 and 24.

Sample 040aA provided useable data from 25 out of 32 grains (Figure 5.11), and 26 out of 36 spot analyses were used to calculate an age of 483 ± 3.1 Ma (1.96σ, MSWD=0.95; Figure 5.12). Inherited ages of 1132 ± 13 Ma and 2797 ± 28 Ma were obtained from two zircon grains. This age has a MSWD close to one, but a wide spread of concordant ages can be observed in the concordia plot.

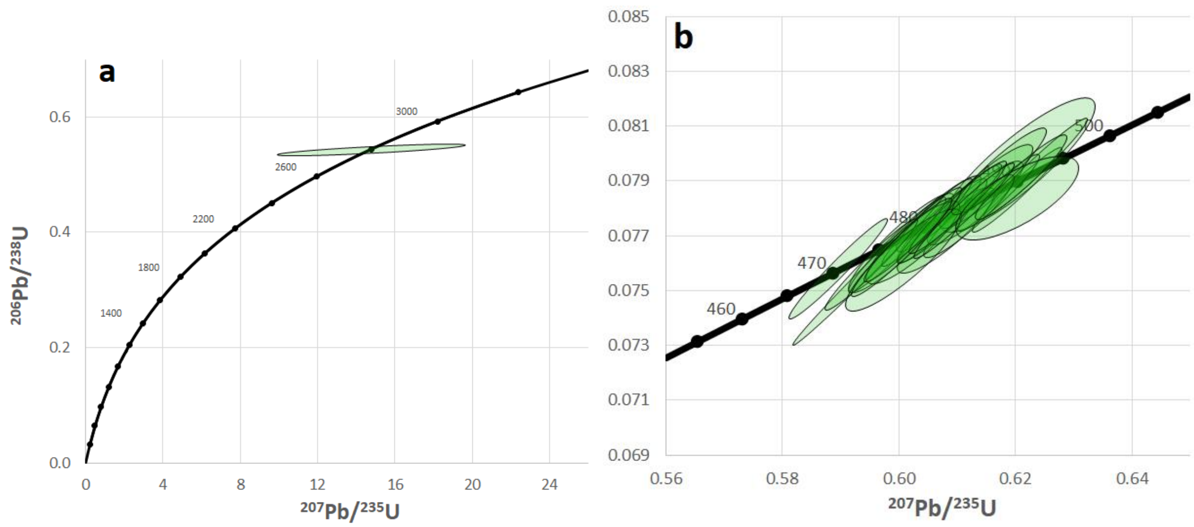

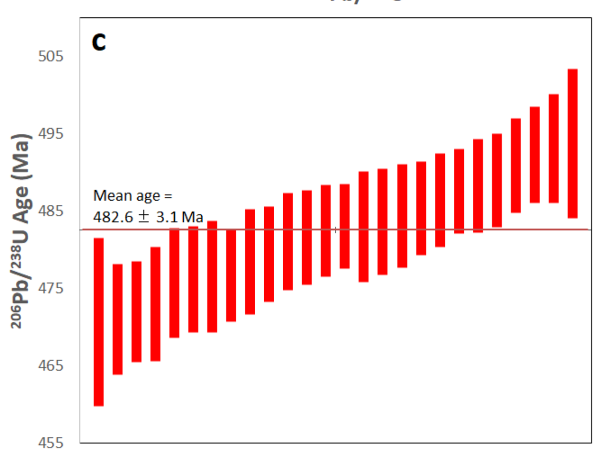

Figure 5.12: Wetherill concordia (a and b) and box plot (c) for sample 040aA. Figure 5.12 a includes points that are considered to be due to ineritance, and b is the Wetherill concordia with inherited ages removed. Weighted mean age is 482.6 ± 3.1 Ma; with MSWD = 0.95 and probability = 0.53. and boxes show 1σ error.

5.3 Summary and interpretation

Table 5.1: SHRIMP geochronology data

Sample	Age (Ma)	Classification	MSWD	Spots Used (n)	Inherited age (Ma)
004cJ	517 ± 2.8	Salknappen Pegmatite	0.37	18	586 ± 7, 1154 ± 15
012bE	507 ± 2.6	Salknappen Pegmatite	0.66	26	None
013aE	513 ± 3.2	Salknappen Pegmatite	0.73	17	None
004dI	492 ± 2.1	Dalmatian Granite	0.95	29	1045 ± 14, 1045 ± 10
012aD	483 ± 2.3	Dalmatian Granite	1.3	36	2602 ± 28, 936 ± 17, 1085 ±60
040aA	483 ± 2.5	Dalmatian Granite	0.95	26	1132 ± 13, 2797 ± 28

The results of the age dating conducted in this study are shown in Table 5.1 and on Figure 5.13. It is important to note that SHRIMP data are from samples collected during the first field season and the samples were selected for analysis in the very early stages of the project. The –Eu subtype of Salknappen Pegmatite, detected in the geochemical data, has not been dated.

The three ages obtained from the Salknappen Pegmatites are 30-40 Ma older (Table 5.1) than the ages for Dalmatian Granites. Salknappen Pegmatites are expected to be older from field relationships (Chapter 3). The age of 469 ± 5 Ma for Dalmatian Granites at Brekkerista (Grantham *et al.,* 1991), is slightly younger that the average age of 483 ± 2.4 Ma for Dalmatian Granites in this study. The difference in ages could be due to a spatial relationship (see Figure 5.13), but it could also be due to a difference in methods; Grantham *et al.,* (1991) used Rb-Sr isotopes to calculate their age. The ages of Dalmatian Granites from this study are very similar to one another, which indicates that the variation is due to the use of different isotopic systems; possibly the rocks sampled by Grantham *et al.* (1991) have experienced some minor loss of Rb, resulting in the younger age. The dataset here is too small to be definitive in either case.

The ages for the Dalmatian Granites are complex, with each of the three samples showing a wide spread of concordant ages. This may indicate that granitic magma flowed through the magma conduits over an extended period, producing several generations of zircons and overgrowths. However, instances where a grain was measured twice give similar ages (see Appendix 3), even for inherited ages from 004dI (grain 35), indicating that zircons that give inherited ages may be xenocrysts with little overgrowth, but from different sources. The ages for the Salknappen Pegmatites samples are much simpler and more reliable, clearly indicating an older age than the Dalmatian Granites samples.

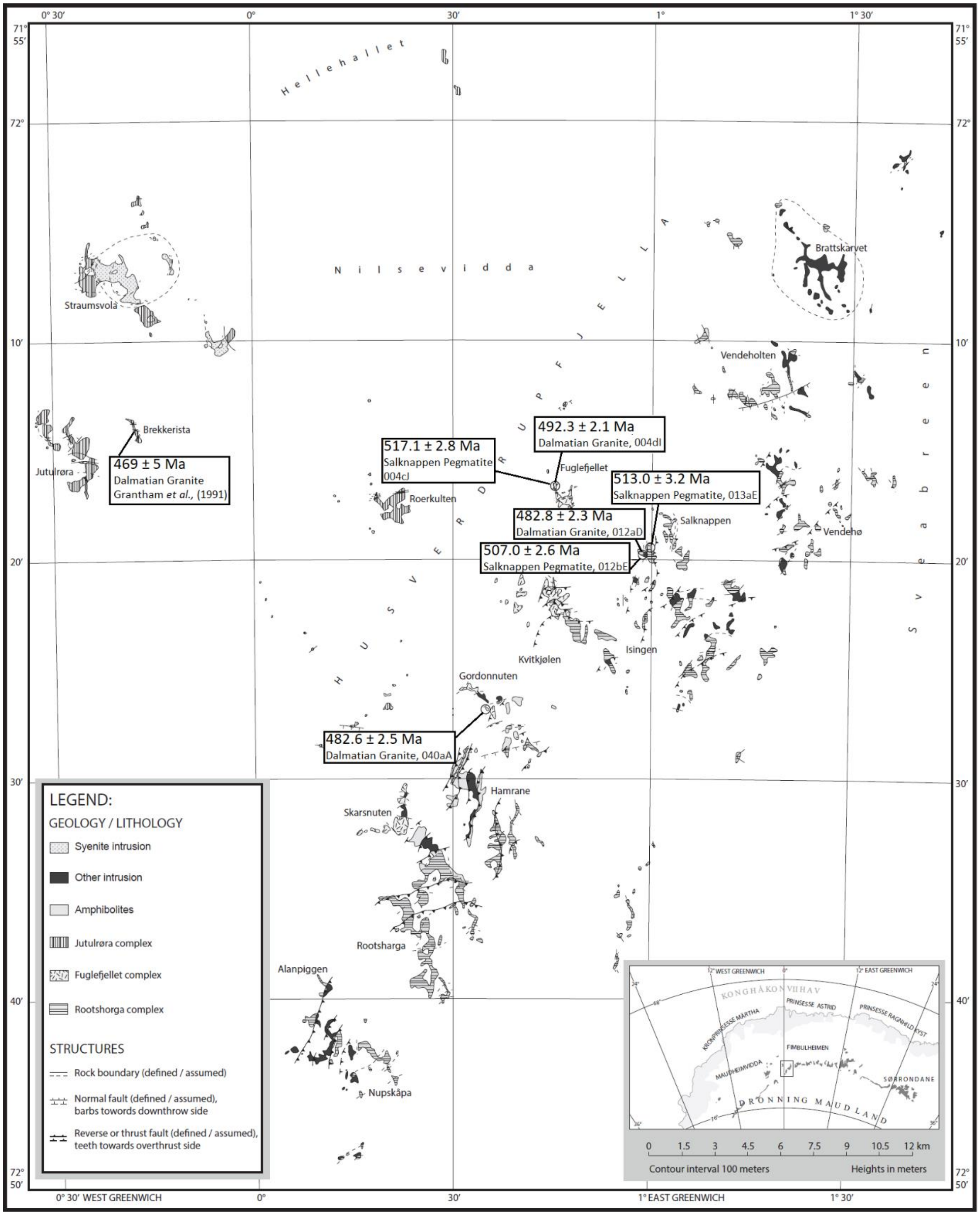

Figure 5.13: A map showing the relative location of and age measured from each sample in the study as well as the age from Grantham *et al.*, (1991). Please note that this image is solely to show spatial relationships; there is a map with better resolution than is possible at this size (due to the small amount of outcrop as a proportion of area) accompanying this thesis. After Elvevold and Ohta, 2010.

Chapter 6: Geochemistry

The focus of this chapter is on reporting the geochemical variation within each of the granitoid suites identified in the field (Chapter 3). Because the petrography reported in Chapter 4 indicates significant overlap between the different groupings of rocks identified in the field (Figure 4.2.2 and 4.2.1), an evaluation will also be made on whether the field classification represents distinct chemical entities, or simply the same group of rocks in varying mineral proportions, i.e. do the Pre-existing Granitoids, the Salknappen Pegmatites and the Dalmatian Granites represent different magmatic events, or simply different expressions of the same event? Interpretation of the data will be presented in the Discussion (Chapter 8).

Sample locations are reported in Chapter 2 and shown on Figure 2.1. Methods used for analysis are presented in Chapter 2, and the full data tables are attached in Appendix 3.

6.1 Major Elements

Major elements control and are controlled by the mineral stoichiometry of the rocks analysed. One way of visualising the variation in major element chemistry between the different suites of rocks, the normative mineralogy calculated by the CIPW norm (Johannsen, 1931), has already been presented in Figure 4.2.2, showing considerable overlap between the Pre-existing Granitoids, Salknappen Pegmatites and the Dalmatian Granites. This would be expected, as all three rocks are dominated by sodic plagioclase, K-feldspar and quartz, with subordinate amphibole and biotite. Any variation in the major elements will be related to the accessory minerals, present in small amounts (Chapter 4).

Similar results can be seen in Harker plots produced for all the samples (Figure 6.1). The different granitoids have similar concentrations of SiO_2 and significant concentrations in only SiO_2, Al_2O_3, Na_2O, K_2O and (to a lesser extent) CaO. Of particular interest is the near complete absence of MgO in most samples, with only some of the Dalmatian Granites from this study and the Grantham *et al*. (1991) study having any appreciable MgO content.

Examining the variation between the five groups plotted in Figure 6.1, a few observations can be made. The Salknappen pegmatites tend to have a higher Al_2O_3 to SiO_2 ratio and apparent trends in Na_2O and CaO (higher concentrations) and K_2O (lower concentrations). The Salknappen Pegmatite samples have no appreciable TiO_2, MgO or P_2O_5 content, and low FeO_t values. This implies that there is very little other than plagioclase, K-feldspar and quartz in these rocks, and, based on the Na content, that plagioclase content will be higher in these rocks than the other granitoids. These observations confirm the observations made in the Petrography chapter.

The Dalmatian Granites identified in this study may be slightly different to the Dalmatian Granites reported in Grantham *et al*., (1991). Though the two groups generally overlap, the Dalmatian Granite rocks for this study have a wider range of SiO_2 values and some samples have higher TiO_2, MgO and FeO_t concentrations. The trends in MgO and P_2O_5 are different for Dalmatian Granites from this study to the trends for the same in data from Grantham *et al*., (1991). This may simply represent a higher concentration of accessory phases in the Dalmatian Granite samples from this study, as this variation is likely caused by the presence of phases such as magnetite (the rocks are magnetic), hornblende and biotite. However, there is a possibility that the two groups of “Dalmatian Granites” may not actually be from the same magma. Dalmatian Granites have trend different to the trends Salknappen Pegmatites in CaO, Na_2O and K_2O. Dalmatian Granites show more variation (i.e. apparent trends) than Salknappen Pegmatites in TiO2, MgO, P_2O_5 and FeO_t.

The last observation on the Harker plots (Figure 6.1) is that neither the pre-existing granitoids nor the pegmatitic Dalmatian Granite samples plot noticeably different from the bulk of the rock. These two groups plot similarly to the Dalmatian Granite samples.

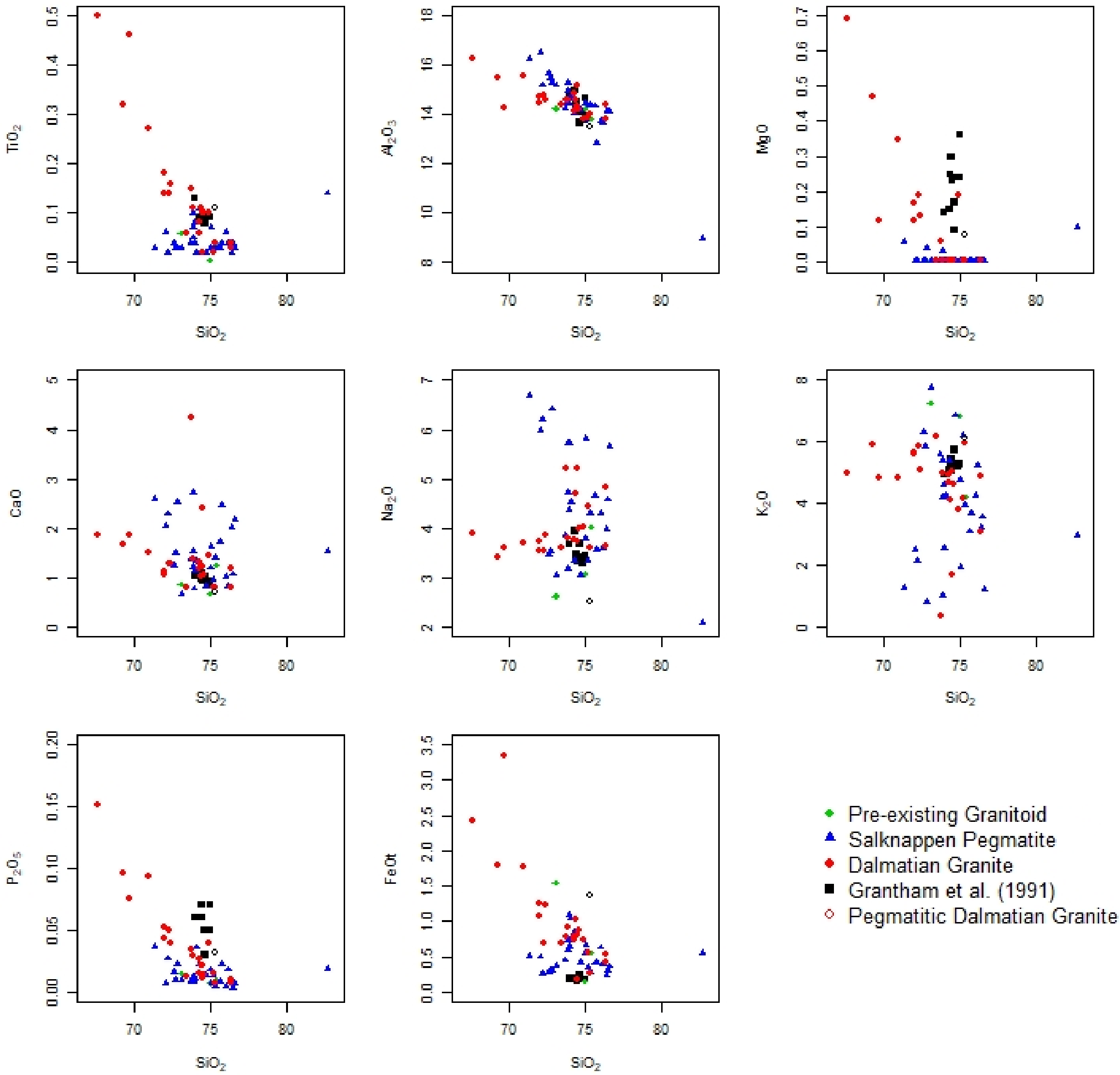

Figure 6.1: A set of Harker plots for the granitoids being studied. Note the different trends for Salknappen Pegmatites and Dalmatian Granites on the plots with CaO, Na_2O and K_2O. Dalmatian Granites also show more variation in $Ti0_2$, P_2O_5, MgO and FeO_t.

A mainstay in granite classification, the degree of Al-saturation as per Shand (1943), also does not show significant differences between groups identified in the field (Figure 6.2). Most samples from all the different granitoids are weakly peraluminous. However, a portion of the Salknappen Pegmatite samples are weakly metaluminous. Samples identified as Dalmatian Granites and Dalmatian Granite from Grantham *et al.* (1991) tend to be more peraluminous. No samples are per-alkaline.

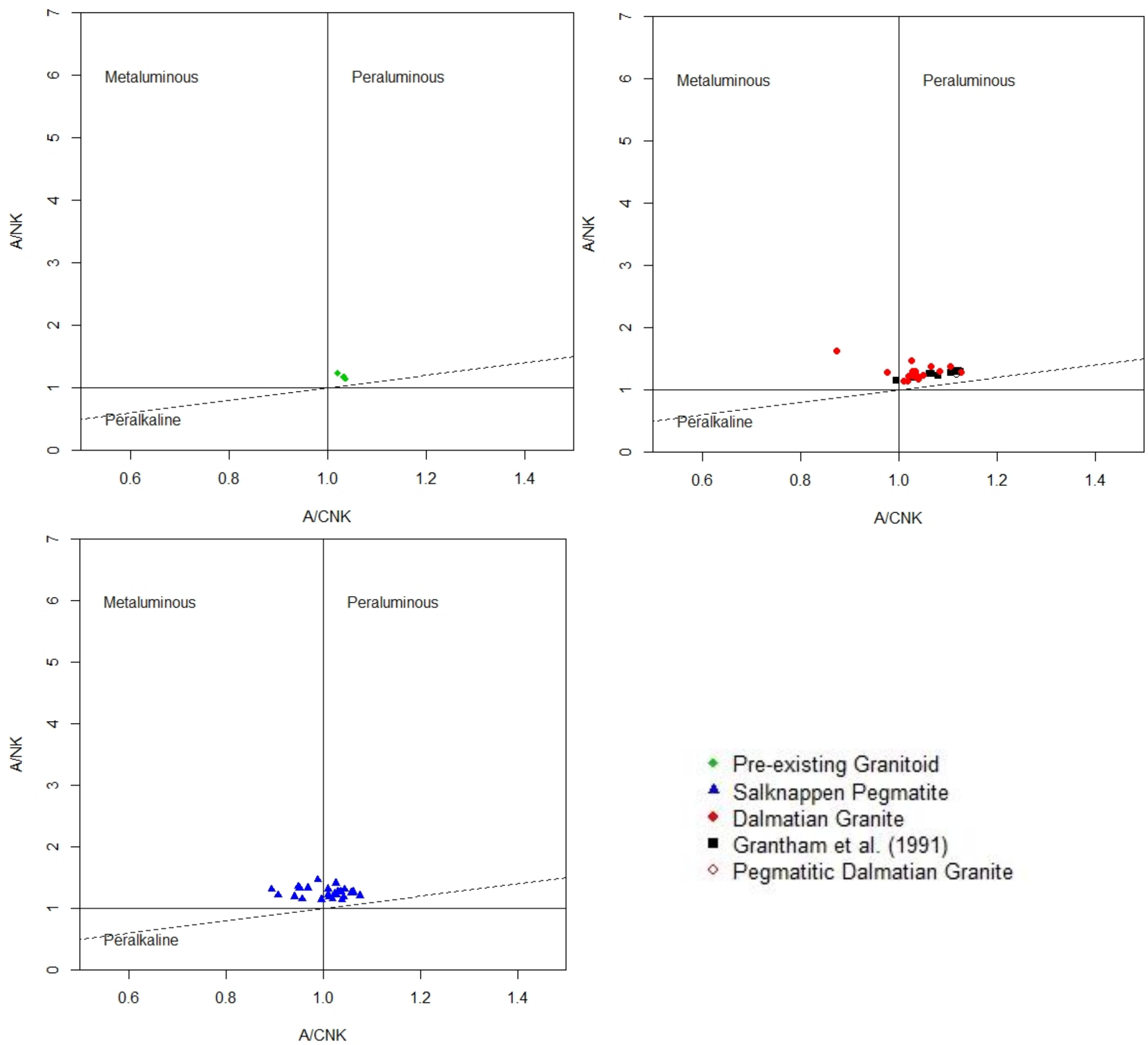

Figure 6.2: A/CNK plotted as per Shand (1943); showing that the Pre-existing Granitoid and Dalmatian Granites are generally weakly peraluminous. Some Salknappen Pegmatites samples are weakly metaluminous while others are weakly peraluminous.

Because no samples are per-alkaline, A/CNK was plotted against maficity (as defined by Clemens and Stevens, 2011) in Figure 6.3 to evaluate the prevalence of Fe-rich minerals. The Dalmatian granites show greater variation in maficity, indicating the presence of Fe-oxides in some samples. Dalmatian Granites are reported to and were observed to contain magnetite, therefore elevated maficity is consistent with both the description by Grantham *et al.* (1991) and field observations in this study. The greater variation in maficity is also consistent with observation from the Harker plots above (Figure 6.1). The two groups of granitoids still share significant overlap. Interestingly, the Dalmatian Granite data from Grantham *et* *al*. (1991) does not show the variation in maficity that would be expected from the observed presence of magnetite. In Figure 6.3, the Grantham data forms a distinct cluster in terms of A/CNK values.

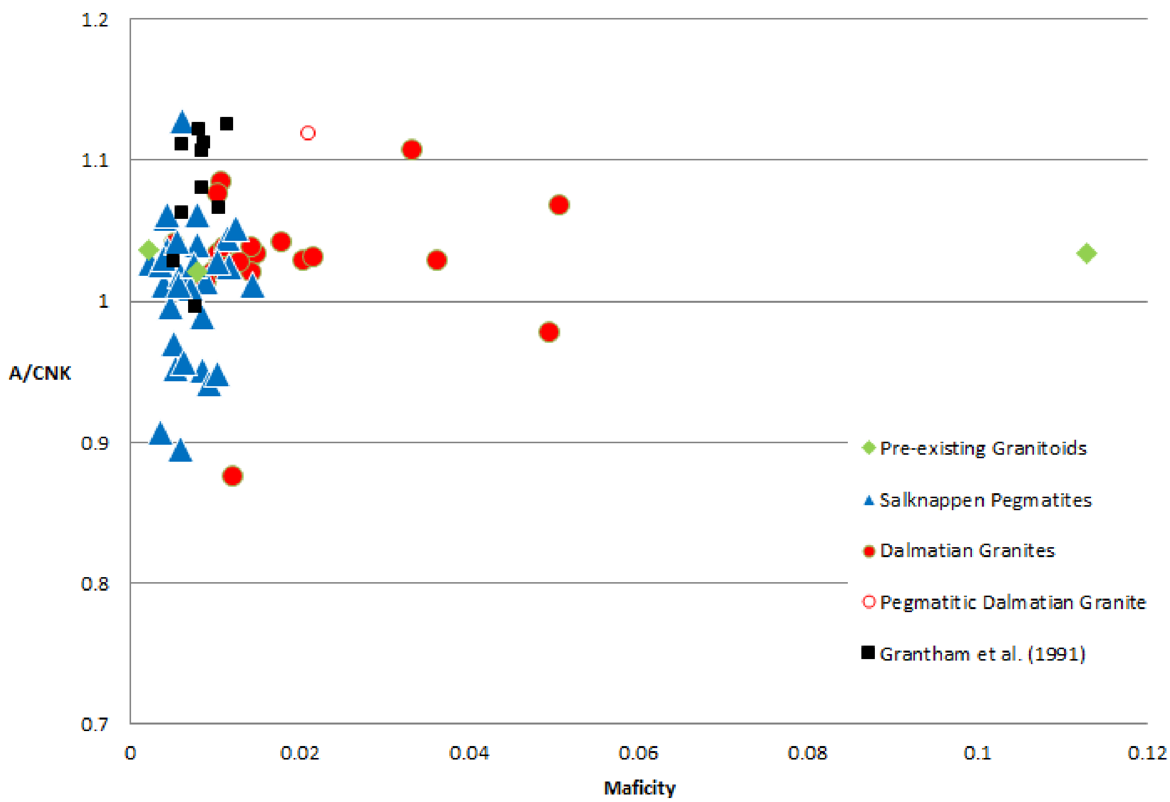

Figure 6.3: A/CNK ratios as per Shand (1943) plotted against maficity (as per Clemens and Stevens, 2012) of the granitoids considered in this study and Dalmatian Granite data from Grantham *et al.*, (1991). Some samples of Dalmatian Granites show high maficity as well as an apparent outlier from the Pre-existing Granitoids.

Frost *et al*. (2001) presents two further major element classification schemes for granites: the Fe-number, and the modified alkali-lime index. These are shown in Figures 6.4. The Fe-number is unfortunately not very useful for this project, due to the low MgO concentrations in samples from this study, and therefore, the Fe-number (FeO/(FeO+MgO) is 1 for most samples, plotting in the "Ferroan" field. Those samples that do have MgO plot in the Ferroan field, or on the boundary between Ferroan and Magnesian. However, the Dalmatian Granite samples from Grantham *et al*. (1991) plot distinctly differently, forming a cluster within the Magnesian field.

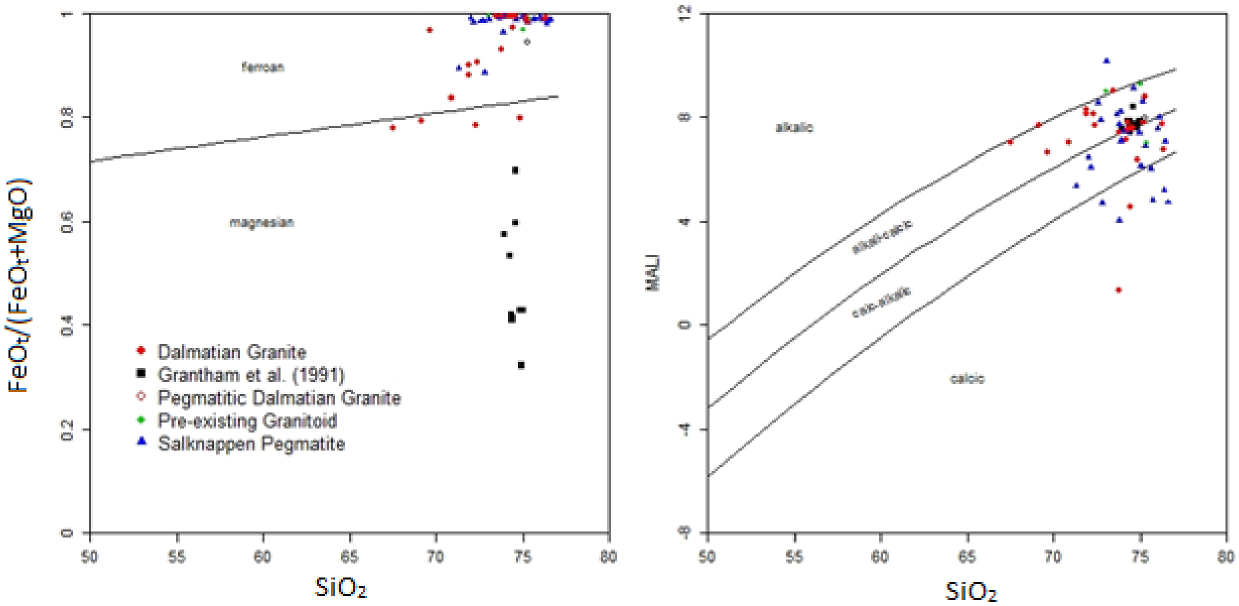

Figure 6.4: Showing Fe-number and the modified alkali-lime index (MALI) against SiO_2 as per Frost *et al*. (2001).

The other discrimination scheme, the Modified Alkali-Lime index (MALI), in Figure 6.4, shows a wide spread of values. The Grantham *et al*. (1991) Dalmatian Granite data plots on the border between alkali-calcic and calc-alkalic, as do the bulk of the other samples. The Salknappen Pegmatite data has a wide spread of values, with points in almost all the fields.

6.2 Trace Elements

While major elements are controlled by mineral proportions, trace elements are controlled by partitioning into either early formed (compatible) or residual (incompatible) minerals. REE plots in Figure 6.5 show clearly different profiles for each suite of granitoids, much more so than major-element analysis. In these diagrams, the Dalmatian Granites are clearly different to the Salknappen Pegmatites. Dalmatian Granite is characterised by a predominantly weak negative Eu anomaly and significant enrichment in light rare earth elements (LREE). LREE enrichment may indicates a crustal source (Rudrick and Fountain, 1995) and a weak negative Eu anomaly indicates middle or lower crustal source, or the loss of cumulus plagioclase before final emplacement. The Dalmatian Granite in this study has a similar profile to the Dalmatian Granite defined by Grantham *et al.,* (1991), though there are only two sample with available REE data from Grantham *et al.,* (1991).

The Salknappen Pegmatites show a flat profile in the light REEs compared to the Dalmatian Granite samples, and a strong upwards profile in the heavy REEs. The Salknappen Pegmatites show two profiles: one with positive Eu anomalies (referred to as +Eu Salknappen Pegmatites below) and another with negative Eu anomalies (referred to as -Eu Salknappen Pegmatites below). +Eu Salknappen Pegmatite shows a positive Eu anomaly and lower REE abundance than the other granitoids in this study. -Eu Salknappen Pegmatite is characterised by predominantly strong negative Eu anomaly and a lack of LREE enrichment. A lack of LREE enrichment and negative Eu anomalies may indicate a low degree of partial melting (without melting plagioclase), a source that has been depleted in LREEs by prior melting, or the removal of plagioclase from the melt before emplacement. The last can be considered unlikely, considering the plagioclase-rich nature of the Salknappen Pegmatite rocks.

The Pre-existing Granitoids are similar in profile to the +Eu Salknappen Pegmatite rocks, with a flattened LREE slope, and an upwards HREE profile.

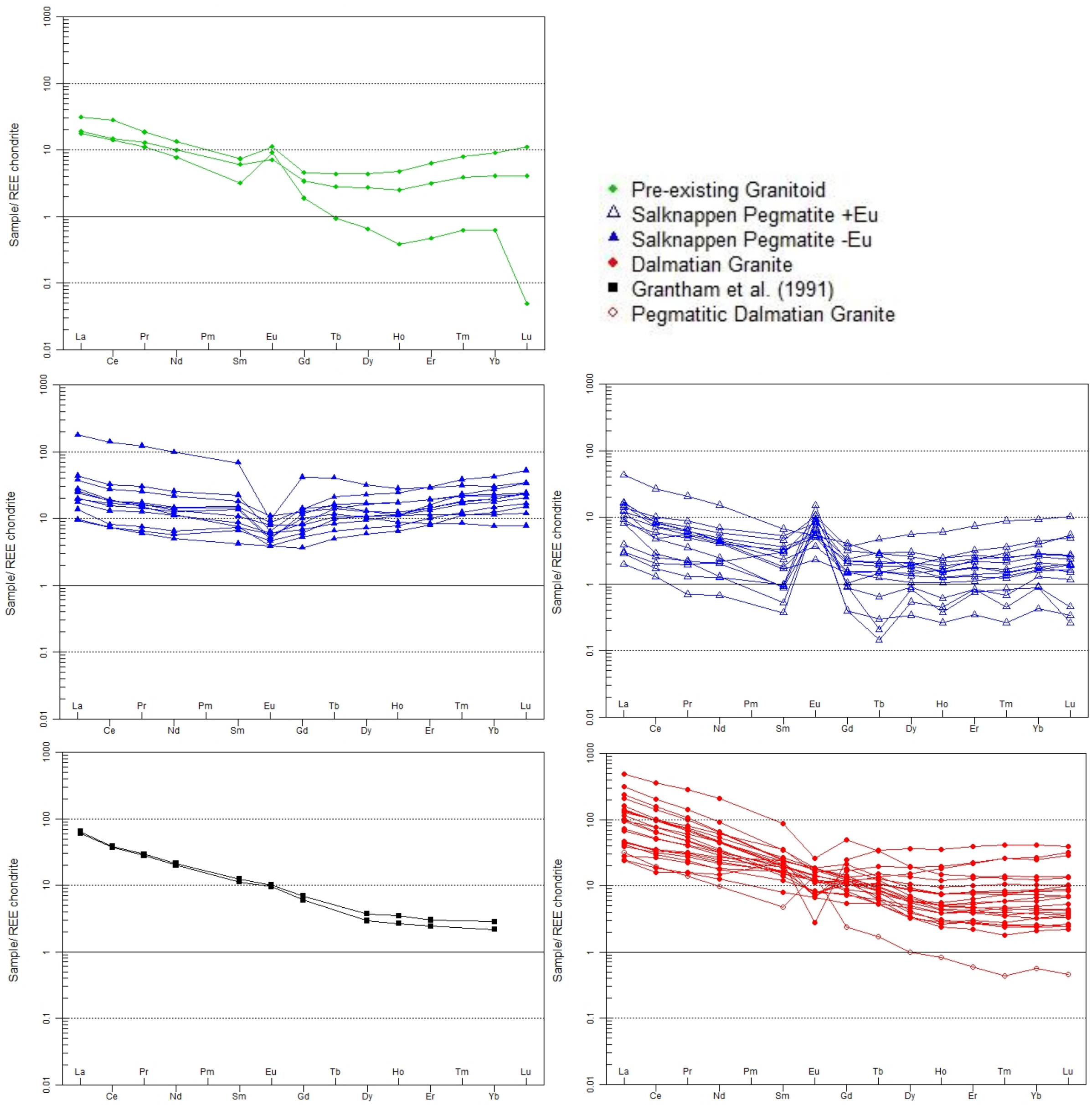

Figure 6.5: REE plots of each group of granitoids. Pre-existing Granitoids have a flat profile with a weak positive Eu anomaly, LREE enrichment and HREE enrichment in most samples. +Eu Salknappen Pegmatite is characterised by a positive Eu anomaly and some LREE enrichment. -Eu Salknappen Pegmatite is characterised by predominantly negative Eu anomaly and a lack of LREE enrichment. Dalmatian Granite is characterised by predominantly weak negative Eu anomaly and significant LREE enrichment.

The difference in LREE and HREE enrichment in the different groups can clearly be seen in Figure 6.6, in which the La/Sm ratio (representing the LREEs) is plotted against Er/Lu (representing the HREE). The -Eu Salknappen Pegmatites are tightly clustered, whereas the +Eu Salknappen Pegmatites are more varied, including two samples showing extreme enrichment in their Er/Lu values. The Dalmatian Granite rocks show a consistent Er/Lu ratio, but a variable La/Sm ratio.

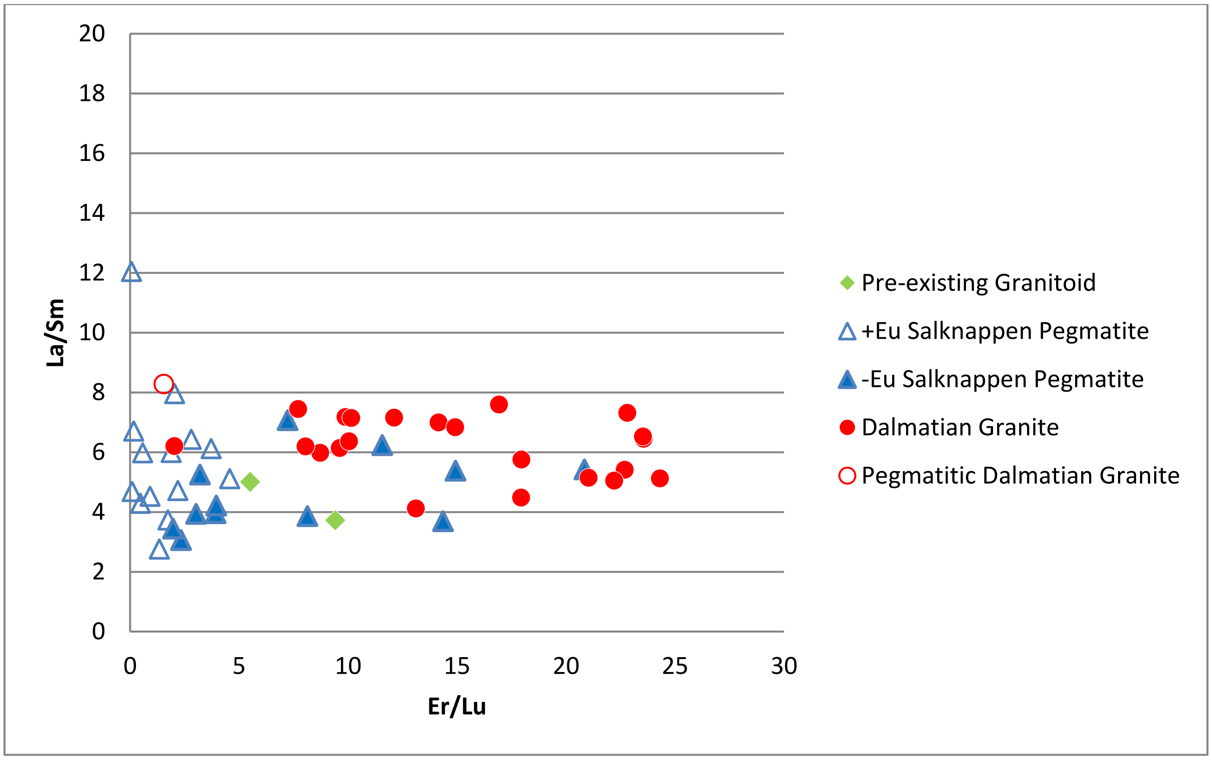

Figure 6.6: a scatter plot of La/Sm ratio against Er/Lu to show LREE and HREE enrichment (respectively). Note the cluster of -Eu Salknappen Pegmatites in contrast in La/Sm variation in other granitoid sheets.

Moving beyond the rare earth elements, Figure 6.7 presents spider diagrams for a wider range of trace elements, normalised to mid ocean ridge basalt (MORB) from Pearce (1984). All four groups from this study are clearly depleted in Ti relative to MORB. All four groups from this study are enriched in K and Rb relative to MORB, two large ion lithophile (LILE) elements which are extremely mobile in aqueous fluids and generally associated with arc magmatism. Ba, another LILE, is quite variable between the groups- The Pre-existing Granitoids and the Dalmatian Granites are enriched in Ba, but the -Eu Salknappen Pegmatites are comparatively depleted in Ba, supporting the idea that a plagioclase-rich source may have melted, and the residual plagioclase retained the Ba (and the Eu). +Eu Salknappen Pegmatites are variable, showing both higher and lower Ba concentrations (but nothing as low as some of the -Eu Salknappen Pegmatites). Eu itself is a LILE, so the strong correlation with Ba is to be expected. The data from Grantham *et al*. (1991) are more akin to Salknappen Pegmatites than Dalmatian Granites from this study with regard to Ba depletion, relative to MORB. Dalmatian Granite data reported by

Grantham *et al*. (1991) is also enriched of LILE and depleted of HFSE relative to MORB but does not show the same depletion of P and Ti as the granitoids from this study.

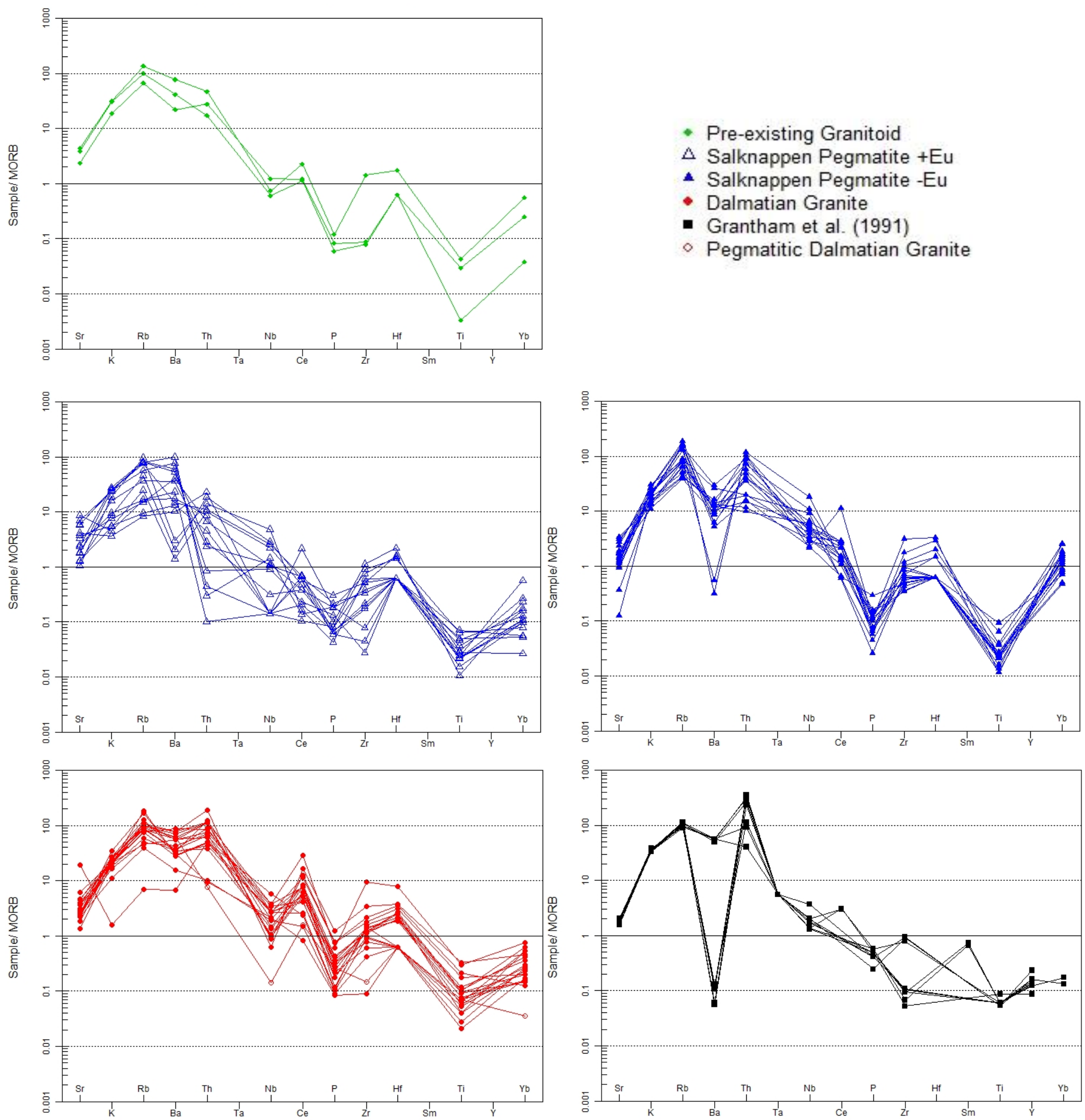

Figure 6.7: MORB normalised spider plots (as per Pearce, 1984). Ta and SM have been excluded for samples from this study as almost all samples are below detection limit. Many samples plotted at half detection limit for Hf.

Among the high field strength elements (HFSE), Th is exceptionally variable in the +Eu Salknappen Pegmatites and is commonly an order of magnitude lower in concentration in this group of rocks. This generally comparable between the other three suites of granitoids. Both Salknappen Pegmatites have higher Nb than the Dalmatian Granites and the Pre-existing Granitoids, but the +Eu Salknappen Pegmatites are again very variable. Ce is quite variable in all rocks, but the -Eu Salknappen Pegmatites have a noticeably higher Ce value than the others. Zr is lower in the +Eu Salknappen Pegmatites relative to the +Eu Salknappen Pegmatites which are similar to the rest. -Eu Salknappen Pegmatites are also higher in Yb than the rest of the rocks.

To examine the two groups of Salknappen Pegmatites further Figure 6.8 is plots maficity against the molar ratio of K with the +Eu and -Eu Salknappen pegmatites plotted separately. Figure 6.8 reveals that the +Eu Salknappen Pegmatites are the group of samples that are weakly metaluminous seen in Figure 6.3 and that the apparent trend of K_2O against SiO_2 in Figure 6.1 is actually a group of samples with low K group, with corresponding higher CaO and Na2O (due the prevalence of feldspar). Figure 6.9 shows the difference in major elements between Salknappen Pegmatites on a Harker plot similar to Figure 6.1.

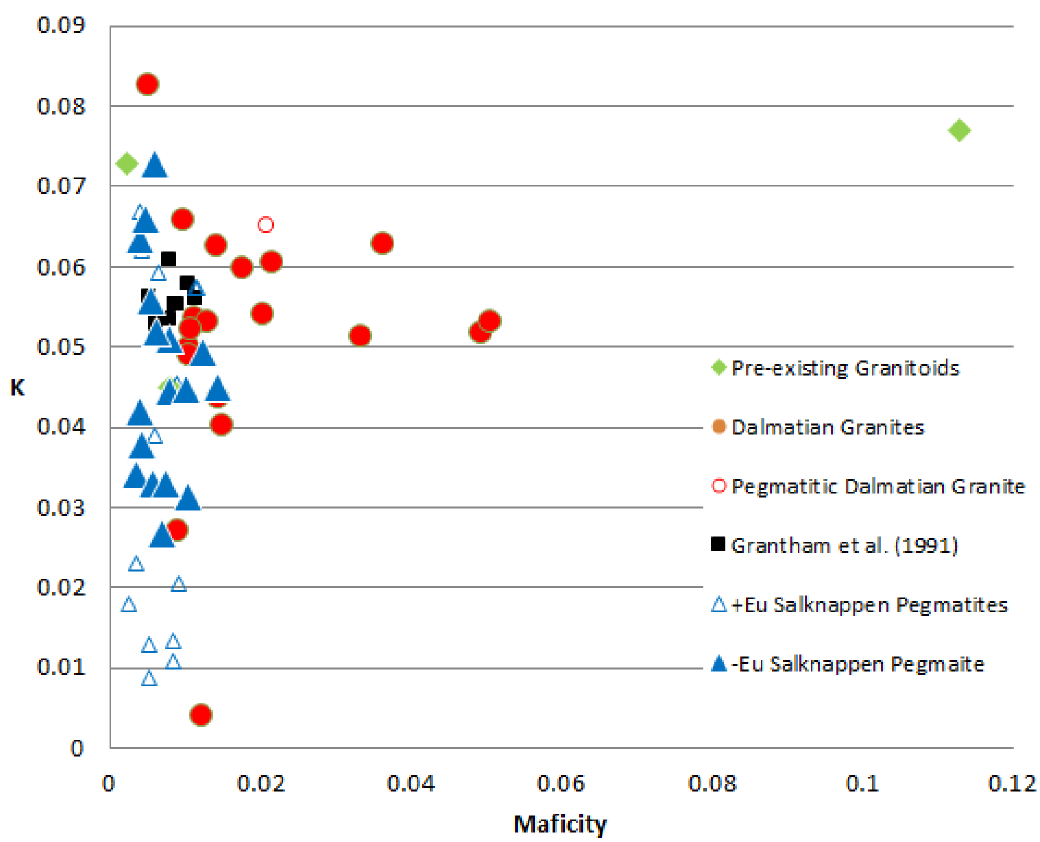

Figure 6.8: Molar ratio of K plotted against maficity (as per Clemens and Stevens, 2012); in order to show the major element variation of the two Salknappen Pegmatites.

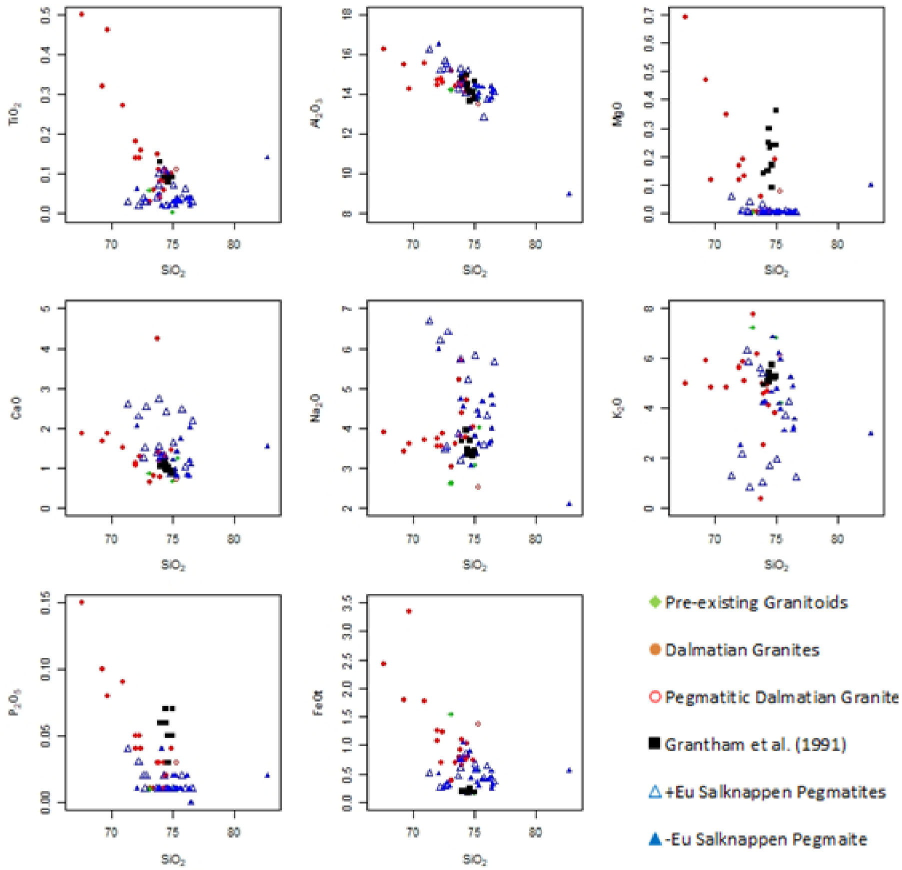

Figure 6.9: Harker plots similar to Figure 6.1, but with different symbols for +Eu Salknappen Pegmatites and -Eu Salknappen Pegmatites. Note the difference in CaO, Na_2O and K_2O.

6.4 Summary of Results

Though the interpretation of these results will be discussed in Chapter 8, there are several clear conclusions from examining the data:

1) The Dalmatian Granites in this study are chemically distinct from the Salknappen Pegmatites sampled in this study.
2) The Dalmatian Granites in this study are slightly different in chemistry to those sampled in Grantham et al. (1991).
3) The Salknappen Pegmatites can be split into two groups based on chemistry, primarily on the behaviour of Eu but also on the behaviour of Ba and Nd.
4) The group of Salknappen Pegmatites with positive Eu anomalies have lower K and are weakly metaluminous.
5) The pre-existing granitoids are similar in chemistry to the Dalmatian Granites, but the amount of data is limited.

Chapter 7: Isotope Chemistry

Besides sending some samples for SHRIMP dating, some samples were also analysed for their $^{143}Nd/^{144}Nd$ and $^{87}Sr/^{86}Sr$ ratios, which allows for the calculation of model ages and initial isotopic ratios. This chapter will present isotopic ratios (Rb-Sr and Sm-Nd isotopic systems) and model ages for select samples. Calculations were done using Geodate software (Eglington and Harmer, 1999). Methods are detailed in Chapter 2, and the data is presented in this chapter. Data for Rb and Sr and the measured $^{87}Sr/^{86}Sr$ ratio is shown in table 7.1; as well as calculated ratios and model ages calculated for chondrite (CHUR) and depleted mantle (DM). Table 7.2 shows similar data, but for the Sm-Nd isotope system. Two samples (027aA and 062aA) produce nonsensical Rb-Sr system model ages and have low Rb concentrations. Samples 027aA and 062aA are considered to have lost Rb and will therefore be excluded from consideration regarding the Rb-Sr isotopic system.

Table 7.1: Rb-Sr system isotopic data for samples from this study. $^{87}Sr/^{86}Sr$ Sr_i and ε_{Sr} calculated at 500 Ma.

Sample	Rb (ppm)	Sr (ppm)	$^{87}Rb/^{86}Sr$	$^{87}Sr/^{86}Sr$	± 2σ	$^{87}Sr/^{86}Sr_i$	ε Sr	T_{CHUR}	T_{DM}	Lithology
004dI	94	328	0.830605	0.725459	0.00001	0.719541	219.35	1933.13	1977.23	Dalmatian Granite
008aC	178	420	1.228438	0.726449	0.00001	0.717696	193.15	1326.56	1375.63	Dalmatian Granite
012aD	138	467	0.856162	0.722001	0.00001	0.715901	167.65	1561.86	1621.13	Dalmatian Granite
017aC	195	539	1.047875	0.718927	0.00001	0.711461	104.59	1032.60	1104.38	Dalmatian Granite
028aX	194	279	2.015406	0.726036	0.00001	0.711676	107.64	773.96	817.78	Dalmatian Granite
040aA	135	159	2.463768	0.737788	0.00001	0.720233	229.18	972.69	1003.93	Dalmatian Granite
070aB	113	105	3.122207	0.735647	0.00001	0.713400	132.14	713.85	743.13	Dalmatian Granite
083aB	112	32	10.203186	0.785218	0.00002	0.712518	119.60	558.17	568.01	Dalmatian Granite
084aC	188	151	3.612422	0.736711	0.00001	0.710972	97.64	636.14	662.71	Dalmatian Granite
014bC	156	265	1.708156	0.737447	0.00001	0.725276	300.80	1406.37	1439.20	Pegmatitic Dalmatian Granite
067aB	96	164	1.697877	0.733438	0.00001	0.721340	244.91	1243.50	1280.99	Pre-existing Granitoid
067bC	131	246	1.543889	0.728746	0.00001	0.717745	193.85	1151.04	1195.30	Pre-existing Granitoid
067cF	143	273	1.518421	0.727301	0.00001	0.716482	175.90	1101.47	1148.15	Pre-existing Granitoid
013aE	146	271	1.561272	0.724382	0.00004	0.713258	130.11	932.50	983.58	+Eu Salknappen Pegmatite
027aA	12	458	0.075824	0.710201	0.00001	0.709661	79.03	-68100.20	9999.00	+Eu Salknappen Pegmatite
053bE	58	104	1.616328	0.725322	0.00001	0.713805	137.89	941.85	990.85	+Eu Salknappen Pegmatite
062aA	19	536	0.102607	0.712487	0.00001	0.711756	108.78	25426.63	379634.12	+Eu Salknappen Pegmatite
068cC	80	148	1.566349	0.723562	0.00001	0.712401	117.95	890.85	943.23	-Eu Salknappen Pegmatite

072aA	138	122	3.282041	0.736880	0.00001	0.713495	133.48	705.23	733.22	-Eu Salknappen Pegmatite

* Samples 027aA and 062aA (marked in yellow) will be excluded from relevant plots below due to evident Rb loss.

Table 7.2: Sm-Nd isotopic system data from this study. $Nd^{143}/Nd^{144}{}_i$ and ε_{Nd} calculated at 500 Ma.

Sample	Sm (ppm)	Nd (ppm)	$^{147}Sm/^{144}Nd$	$^{143}Nd/^{144}Nd$	± 2σ	$^{143}Nd/^{144}Nd_i$	ε Nd	T_{CHUR}	T_{DM}	Lithology
004dI	2.76	19.23	0.086676	0.51158	0.00001	0.511296	-4.47	1466.08	1788.76	Dalmatian Granite
008aC	4.77	39.52	0.072949	0.51126	0.00001	0.511021	-9.84	1695.68	1958.94	Dalmatian Granite
012aD	4.73	38.80	0.073629	0.51122	0.00001	0.510979	-10.67	1754.12	2011.52	Dalmatian Granite
017aC	6.81	55.04	0.074816	0.51131	0.00001	0.511065	-8.99	1659.47	1930.73	Dalmatian Granite
028aX	3.80	26.88	0.085490	0.51146	0.00001	0.51118	-6.74	1613.88	1913.81	Dalmatian Granite
040aA	3.88	19.20	0.122184	0.51154	0.00001	0.51114	-7.52	2240.67	2543.76	Dalmatian Granite
070aB	3.77	14.92	0.152627	0.51204	0.00001	0.51154	0.29	2067.59	2570.14	Dalmatian Granite
083aB	4.70	15.96	0.178080	0.51181	0.00001	0.511227	-5.83	6668.17	5344.65	Dalmatian Granite
084aC	2.34	10.67	0.132450	0.51177	0.00001	0.511336	-3.69	2056.58	2436.65	Dalmatian Granite
014bC	0.93	5.85	0.096128	0.51129	0.00001	0.510975	-10.74	2038.83	2304.06	Pegmatitic Dalmatian Granite
067aB	1.18	6.00	0.118540	0.51219	0.00001	0.511802	5.40	877.82	1414.62	Pre-existing Granitoid
067bC	0.62	4.63	0.080667	0.51207	0.00001	0.511806	5.48	749.29	1149.97	Pre-existing Granitoid
067cF	1.44	8.06	0.107921	0.51207	0.00001	0.511717	3.74	978.580	1445.15	Pre-existing Granitoid
013aE	0.10	0.77	0.078101	0.51225	0.00004	0.511994	9.16	501.99	926.52	Salknappen Pegmatite +Eu
027aA	1.30	9.14	0.086005	0.51212	0.00001	0.511838	6.12	716.61	1138.44	Salknappen Pegmatite +Eu
053bE	0.70	2.96	0.143602	0.51179	0.00001	0.51132	-4.01	2428.37	2778.41	Salknappen Pegmatite +Eu
062aA	0.18	1.21	0.089723	0.51224	0.00003	0.511946	8.22	570.66	1025.43	Salknappen Pegmatite +Eu
068cC	0.82	2.97	0.166233	0.51225	0.00001	0.511706	3.53	1944.90	2635.63	Salknappen Pegmatite -Eu
072aA	2.11	7.97	0.159734	0.51224	0.00001	0.511717	3.75	1645.67	2347.98	Salknappen Pegmatite -Eu

*Sample 083aB (marked in yellow) will be excluded from relevant plots below due to model ages older than Earth.

Plotting $^{143}Nd/^{144}Nd_i$ against $^{87}Sr/^{86}Sr_i$ (Figure 7.1.), as well as using the ε_{Nd} recalculated to 500 Ma (Figure 7.2), shows an isotopic difference between geochemical groups. All samples have negative ε_{Nd}, with +Eu Salknappen Pegmatites having the highest and Dalmatian Granite the lowest ε_{Nd}. ε_{Sr} is generally similar (Figure 7.3), but Pre-existing Granitoids and some Dalmatian Granites have a higher ε_{Sr}. $^{87}Sr/^{86}Sr$ ratios are all above 0.71, indicating a crustal source for all granitoids.

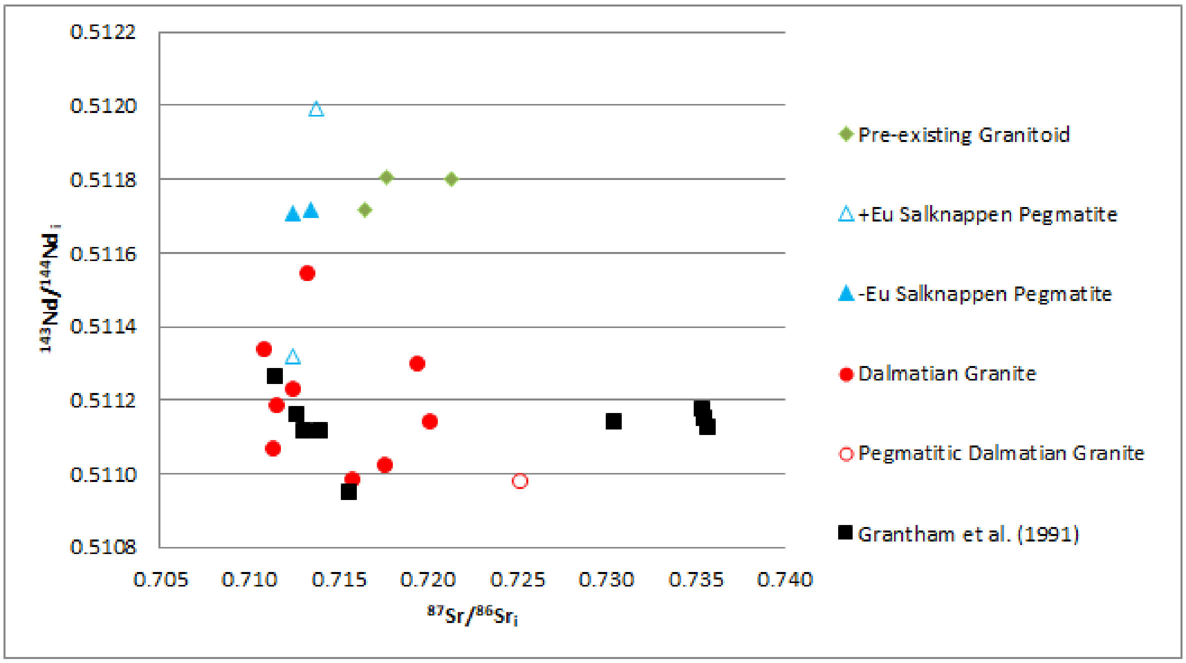

Figure 7.1: $^{143}Nd/^{144}Nd_i$ against $^{87}Sr/^{86}Sr_i$ (recalculated to 500 Ma) showing an isotopic difference between geochemical groups. Dalmatian Granites have lower $^{143}Nd/^{144}Nd_i$ ratios than Salknappen Pegmatites, except for sample 053bE, and Pre-existing Granitoids. However, Dalmatian Granites have more variation in $^{87}Sr/^{86}Sr_I$.

Model ages calculated based on the age relative to either the depleted mantle (T_{DM}) or the chondritic uniform reservoir (T_{CHUR}), as per De Paolo & Wasserburg (1976) can provide an estimate of the age of the protolith to a magma, whereas zircon U-Pb ages reflect the age of crystallisation. The two ages (T_{DM} and T_{CHUR}) differ systematically, so only T_{CHUR} is shown on Figure 7.2 (T_{DM} ages are older). The Sm-Nd model ages for the Pre-existing Granitoids and the +Eu Salknappen Pegmatites are generally less than 1000 Ma, and these rocks are clearly different to the other rocks in the data set, which have much older model ages. This likely reflects very different $^{143}Nd/^{144}Nd$ isotopic ratios in the host rocks for the two groups.

Model ages calculated using the Rb-Sr system (Figure 7.3) do not show as much of a difference. Dalmatian Granites vary more and Pre-existing Granitoids plot as slightly older than Salknappen Pegmatites. However, all the model ages fall into a relatively narrow range. It is possible that this reflects a wide spread metamorphic event resetting the Rb/Sr system in the protolith for the granites, as Rb is notoriously mobile during metamorphism.

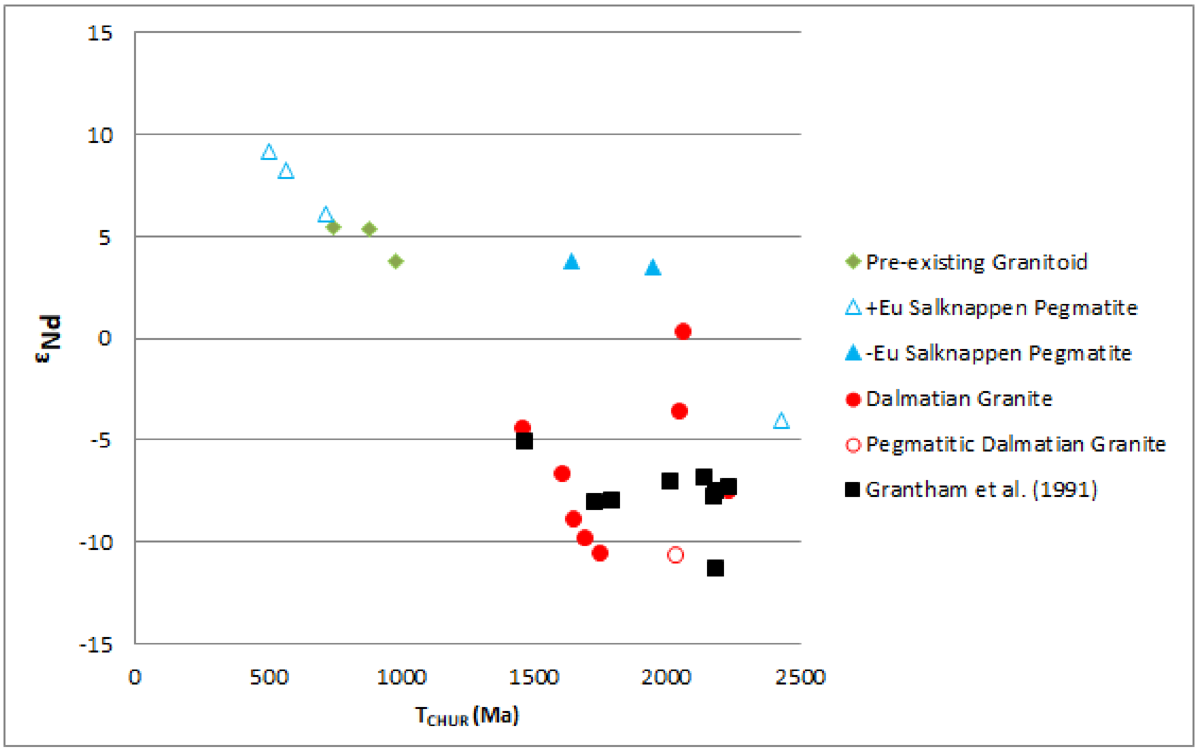

Figure 7.2: ε_{Nd} plotted against Sm-Nd model age (chondrite). Sample 053bE is an outlier again plotting separate form +Eu Salknappen Pegmatites. Salknappen Pegmatites plot with positive ε_{Nd} (calculated to 500Ma) but -Eu Salknappen Pegmatites give similar model ages to Dalmatian Granites. Sample 083aB is excluded due to impossible model ages.

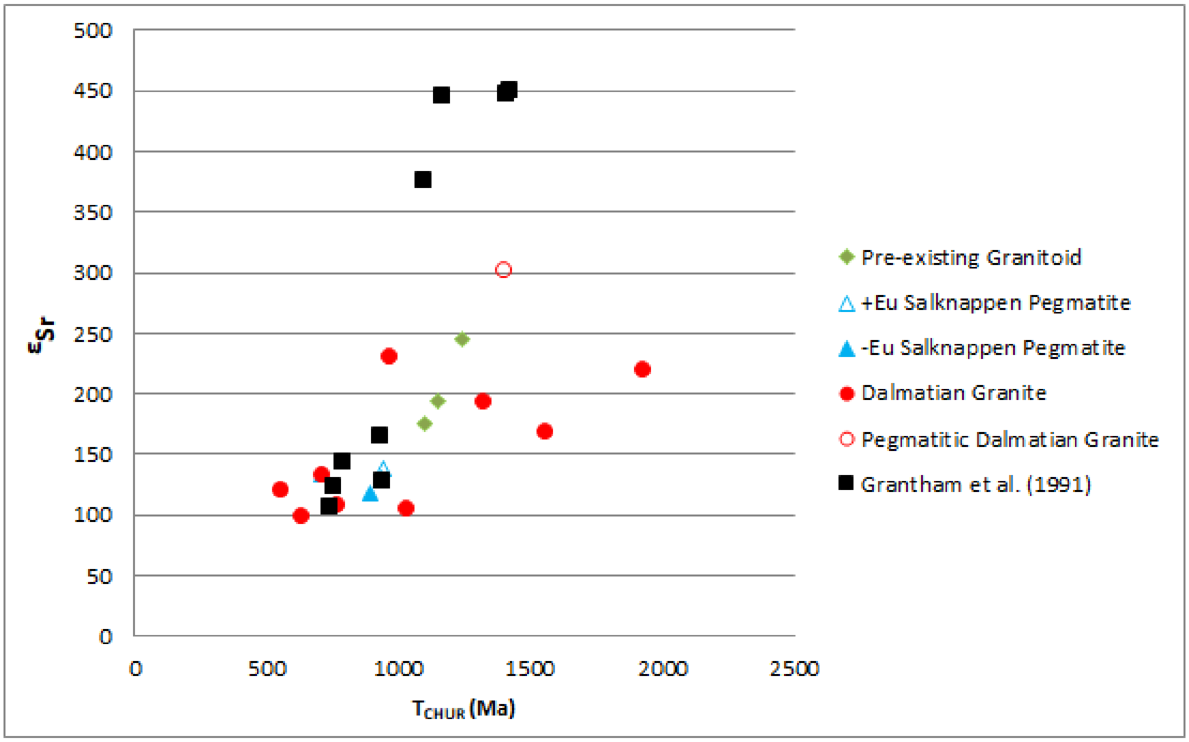

Figure 7.3: ε_{Sr} (calculated to 500 Ma) plotted against Rb-Sr model age (chondrite). The same variation of Rb-Sr isotope ratios in Dalmatian Granites as in Figure 7.1 is evident here as well. While Dalmatian Granites are more varied, Rb-Sr model ages are remarkably similar for different suites compared to Sm-Nd model ages. Samples 027aA and 062aA excluded due to evident Rb loss.

Table 7.3: Comparison of SHRIMP ages and model ages:

Sample	Classification	Age (Ma)	Inherited age(s) (Ma)	Sm-Nd T_{CHUR}	Sm-Nd T_{DM}	Rb-Sr T_{CHUR}
013aE	+Eu Salknappen Pegmatite	513 ± 3.2	None	501.99	926.52	932.50
004dI	Dalmatian Granite	492 ± 2.1	1045 ± 14, 1045 ± 10	1466.08	1788.76	1933.13
012aD	Dalmatian Granite	483 ± 2.3	2602 ± 28, 936 ± 17, 1085 ±60	1754.12	2011.52	1561.86
040aA	Dalmatian Granite	483 ± 2.5	1132 ± 13, 2797 ± 28	2240.67	2543.76	972.69

Table 7.3 compares crystallisation and inherited ages (from SHRIMP data shown in Chapter 5) to model ages from this chapter for samples where both types of data are available. Dalmatian Granites have variable Rb-Sr model ages (Figure 7.3) but do show some higher Sm-Nd model ages in samples with very old inherited zircons. The +Eu Salknappen Pegmatite sample 013aE has a Sm-Nd T_{CHUR} close to crystallisation age and a T_{DM} close to Rodinia assembly. In Table 7.2 other +Eu Salknappen Pegmatite are not as close but have similar data (except for sample 053bE, again). Data is too limited to make reliable generalisations.

Chapter 8 Discussion

8.1 Granitoid Petrogenesis

The most significant finding of this thesis is that the several suites of granitoid sheets in the H.U. Sverdrupfjella area are distinct and represent different aspects of the tectonic history of H.U. Sverdrupfjella. The results of this study need to be considered in terms of granite petrogenesis and compared to existing data, before being used to interpret the tectonic history of the area.

Granitic magmas are commonly accepted as the result of melting supracrustal rocks along the wet solidus (e.g. Nédélec & Bouchez, 2015). In addition, the geochemistry and mineralogy of granitoids reflects the source of the melt (e.g., Chappell & White, 1974; Pearce, 1984), as well as the processes that affect the magma during ascent and emplacement. This has led to a variety of classification schemes (e.g. Garcia-Arias 2020), which can complicate the interpretation of granite origins. However, there are some clear conclusions that can be drawn from the data presented in this study.

Chappell and White (1974; 2001) proposed a classification of granitoids into I- and S-types, based on igneous and sedimentary protoliths, respectively, using mineralogy and chemistry of granites in the Lachlan Fold Belt, Australia, as a case study. In the case of granitoids in this study, the Salknappen Pegmatites would be classified as S-type granitoids as they contain rare garnets, whereas the Dalmatian Granites would be considered I-type, based on the presence of magnetite. However, there are some problems using this classification for this study. Both suites contain hornblende, which is an indicator for the I-types. This contradiction can be resolved if the garnets in the Salknappen Pegmatites are xenolithic or inherited (see Chapter 4), in which case both suites may be considered I-types based on mineralogy alone. This is supported by the low A/CNK ratios (generally less than 1.1; Figure 6.5) for both suites, and the lack of a strong peraluminous signal in the rocks. However, these characteristics are not unique to I-types.

Clemens *et al.* (2011) note that I-types are unlikely to be formed through the melting of mafic rocks like basalt, based on isotope chemistry and melt experiments, as the granites are too enriched in isotopic systems like Rb-Sr and not sodic enough to have been produced by metabasalts or ecologites. Clemens *et al*. (2011) suggest that the I-type granitoids are created from intermediate arc volcanic rocks with varying quantities of entrained clinopyroxene, plagioclase and ilmenite, an idea further fleshed out in Clemens and Stevens (2012). Alternatively, it has been suggested that primary I-type magmas, created by the fractionation of arc magmas, may exist (e.g., Castro 2020), but fluid fluxed melting of andesitic to tonalitic rocks in the crust is strongly supported by experimental data (Castro, 2020).

Based on the work of Clemens and Stevens (2012), it is suggested that Ti can be an important indicator of the entrainment of ilmenite into a granitic magma, and that S- and I-types entrain different amounts of ilmenite. This is presented in Figure 8.1. Barring one outlier (a Pre-existing Granitoid with extreme maficity), the other data plots along a path indicating increasing entrainment of ilmenite. The Dalmatian Granites in this study are the only suite entraining significant amounts of ilmenite, probably indicating a different source. However, what is not seen in this diagram is the lower Ti values often associated with I-types, where hornblende and biotite melt to form clinopyroxene, which is then entrained in the magma (Clemens and Stevens, 2012). Unfortunately, this diagram does not prove or disprove an I-type origin for the rocks in this study.

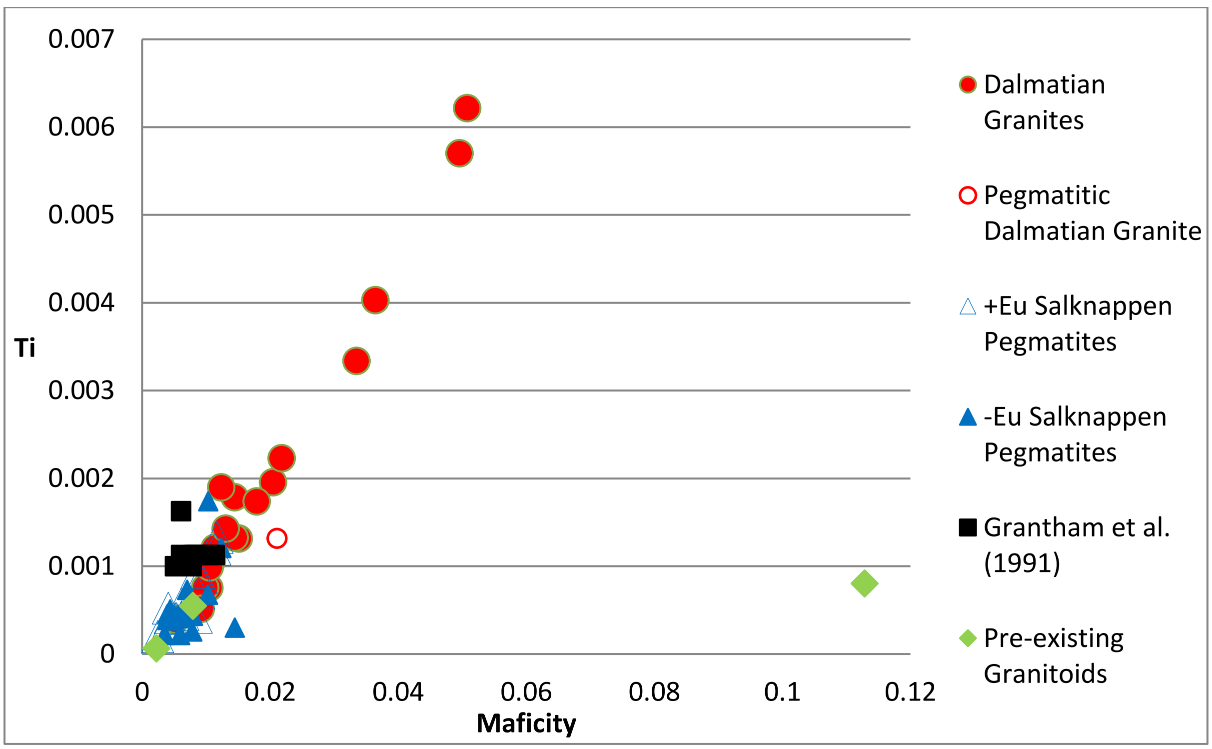

Figure 8.1: Ti vs Maficity for the granitoids in this study (after Clemens and Stevens, 2012). Note how the data plots on a single line, but Dalmatian Granites have a wider spread of both Ti and maficity.

Several other classification schemes have been proposed since the work of Chappell & White (1974). In particular, the work of Frost *et al.* (2001) proposed the use of several other indices for classifying granitoids, a theme that was continued by Bonin *et al*. (2020). These make use of Fe-number and modified alkali-lime index (MALI), see Figure 6.4. Unfortunately, neither of these schemes are particularly useful in this study. The Fe-number is not informative due to the lack of MgO in the samples, and the MALI index does not indicate a consistent clustering of values (which can also be seen in the modal abundances and CIPW norm presented section 4.2).

The only set of data with a consistent grouping in these classification schemes is the peraluminous Dalmatian Granite data of Grantham *et al*. (1991), which is clearly magnesian and plots along the alkali-calcic/calc-alkalic line in Figure 6.4. According to Bonin *et al*. (2020), this suite of rocks would be considered S-type. If we were to consider the other rocks as ferroan, their predominantly peraluminous nature and variable MALI values would indicate they are either I-types, or more likely, unclassified categories (Frost *et al*., 2000; Bonin *et al*., 2020).

An alternative approach to classifying granitoids was proposed by Pearce *et al*. (1984), in which source is correlated to tectonic setting. Figure 8.2 shows tectonic discrimination diagrams as per Pearce *et al.* (1984) and indicates that the +Eu Salknappen Pegmatite group are volcanic arc granites (VAG), with some overlap with the syn-collisional field (syn-COLG). -Eu Salknappen Pegmatites plot as VAG and within plate granites (WPG), but with some samples falling in the syn-COLG field.
Pre-existing granitoids and Dalmatian Granites from this study plot as both VAG and syn-COLG, not favouring either field. In the case of the Pre-existing Granitoids it may be due to a lack of data. Dalmatian Grates from Grantham *et al.*, (1991) plot clearly as syn-COLG. The sample of pegmatitic Dalmatian Granite also plots as syn-COLG.

Pearce (1996) revisited the classification scheme noting insights that are useful here. Pearce (1996) notes that the scheme shows source more than setting, which is consistent with more recent ideas, like Clemens and Stevens (2012). Pearce (1996) notes that the VAG field can also be considered a subduction-related field and that syn-COLG represents the tectonic setting (i.e. sources typically involved in the tectonic setting) after subduction has ceased. From that, the Dalmatian Granites and +Eu Salknappen Pegmatites represent a transition from subduction to continent-continent collision. The data from Dalmatian Granites presented by Grantham *et al.* (1991) plot further into the syn-COLG field than the Dalmatian Granites from this study, which indicates that the Grantham *et al.* (1991) are indeed younger and from later in the orogenic process.

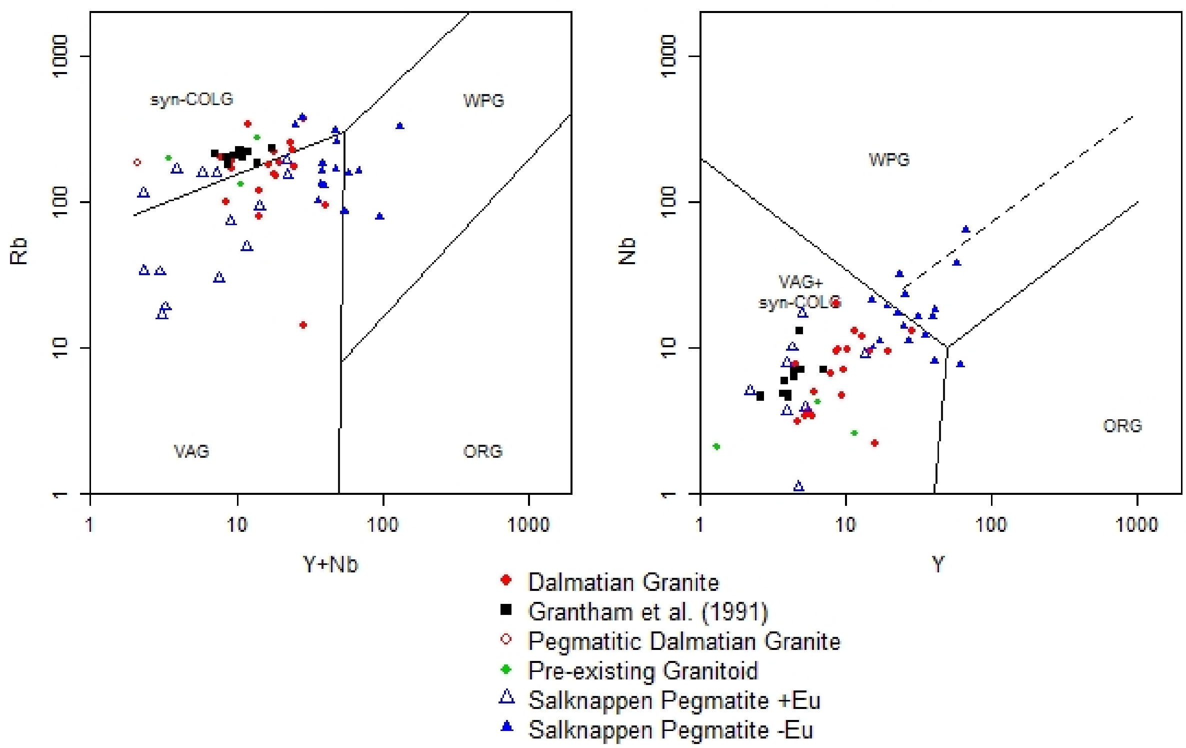

Figure 8.2: Pearce tectonic discrimination diagrams, as per Pearce *et al.* (1984). The below detection limit concentration of Ta present makes the use of diagrams involving Ta impossible. The Pre-existing granitoids, +Eu Salknappen Pegmatites and Dalmatian Granites form this study plot as VAG and syn-COLG. However, the +Eu Salknappen Pegmatites tend more toward VAG. Data from Grantham *et al*. (1991) plot as syn-COLG. -Eu Salknappen Pegmatites plot mostly as VAG and WPG.

The -Eu Salknappen Pegmatites plot separately from the other samples in this study, tending toward the WPG field. This is likely due to a different source, rather than tectonic setting, as the granitoids in this study are spatially and temporally related and therefore must share a tectonic setting. This source is more enriched in HFSE, represented by Y + Nb in Pearce *et al*. (1984) diagrams.

Although not all the granitoids considered in this study are pegmatites, or of economic interest; the pegmatite classification scheme by Černý *et al*. (2012) may allow the source material for the different granitoid suites in this study to be identified. Granitic pegmatites often carry economic mineralisation, and such pegmatites can be classified as either NYF (Nb-Yb-F) or LCT (Li-Cs-Ta) pegmatites, based on the relative concentration of these elements in the rocks. In general, pegmatites are low-temperature, fluid-rich magmas which are unable to assimilate significant amounts of material from country rocks and reflect the trace element composition of their source.

NYF pegmatites (also enriched in Be, REE, Sc, Ti, Zr, Th and U) are formed by A-type magmas with minor input of I-type sources or mantle material (Černý *et al*., 2012), whereas LCT (also enriched in Rb, Be, Sn, B, P and F) pegmatites are formed by the melting of sedimentary sources, and form from S-type peraluminous magmas. To a certain extent, the LCT pegmatites show enriched LILE values, whereas the NYF are enriched in HFSE, which gives us a means to apply this classification scheme to the data in this study despite the lack of a full set of trace element data. Figure 8.3. shows a plot of Ba (for the LILE) vs Yb (for the HFSE) for the granitoids. It can clearly be seen that Ba is enriched in most of the suites, indicating a LCT affinity. This would also be in line with the Ti-depleted nature of the Salknappen Pegmatites (Figure 6.1). However, the -Eu Salknappen Pegmatites are enriched in Yb, and contain significant Nb relative to the other granitoids. The -Eu Salknappen Pegmatites are thus NYF pegmatites, formed from the so-called A-type granites (Eby, 1990) and thus likely created by the melting of gneissic granulite in the lower crust with some mantle input. This is consistent with the source indicated by the Pearce *et al*. (1984) plots (Figure 8.2).

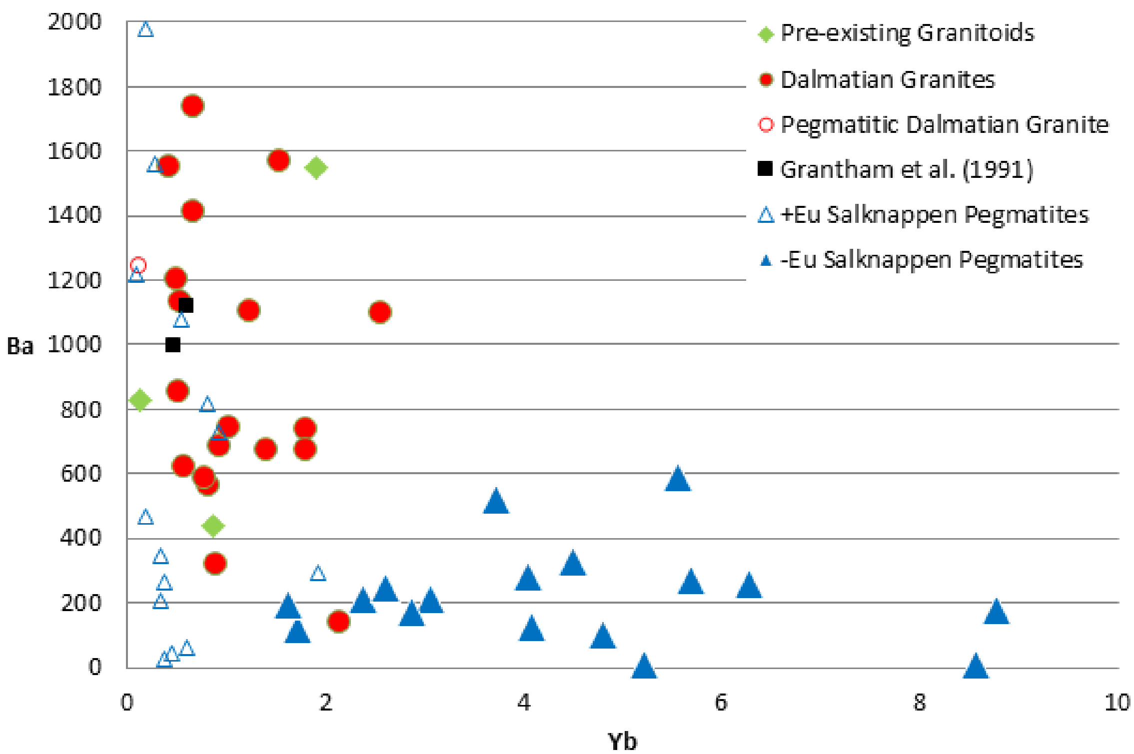

Figure 8.3: A scatter plot to compare the enrichment of LILE (Ba) to the enrichment of HFSE (Yb).

The observation that the -Eu Salknappen Pegmatites are possibly NYF pegmatites whereas the other rocks are likely LCT pegmatites, though done by indirect means, clearly indicates two different sources for the Salknappen Pegmatites.

8.2 Constraints from Geochronology

Geochronology reveals several interesting observations regarding Salknappen Pegmatite and Dalmatian Granite, Including differences in crystallisation ages, the prevalence of inherited zircon and a difference in model ages. The younger group of granitoids, the Dalmatian Granites, is also the suite which contains the older inherited zircons. The Dalmatian Granites were emplaced between 495 Ma and 480 Ma (Table 7.1), an age range older than the previous Rb-Sr age for Dalmatian Granite at Brekkerista (Grantham *et al*., 1991), possibly indicating Rb loss from the rocks studied by Grantham *et al.,* (1991). Dalmatian Granites host older inherited zircon cores giving ages of 1045 ± 14 Ma, 1045 ± 10 Ma, 2602 ± 28 Ma, 936 ± 17 Ma, 1085 ± 60 Ma, 1132 ± 13 Ma, 2797 ± 28 Ma, which roughly divide into two groups of ages: an older group of ages (2.6 – 2.8 Ga), and a younger group (1-1.1 Ga). This compares to the mean Dalmatian Granite Sm-Nd model age calculated for chondrite (T_{CHUR}) of 1819.26 Ma (excluding sample 083aB, as in Chapter 7). The age data and the variable maficity of the Dalmatian Granites indicates that these granitoids either formed from a heterogenous protolith, or (more likely) entrained a lot of xenocrystic material during ascent.

The older group of granitoids, the Salknappen Pegmatites, are relatively free of inherited zircons (one sample reported inherited ages of 586 ± 7 and 1154 ± 15) and have younger model ages than the Dalmatian Granite samples, with mean Sm-Nd T_{CHUR} of 596.42 Ma for +Eu Salknappen Pegmatites (excluding sample 053bE as an outlier, like in Chapter 7). These granitoids are also very homogenous in terms of maficity, and so have not entrained as much material as the Dalmatian Granites (as per the model of Clemens *et al*. (2011)). However, the inherited garnets (figure 4.2) show that there is some xenocrystic content.

However, the -Eu Salknappen Pegmatites are similar to Dalmatian Granites when it comes to model ages. -Eu Salknappen Pegmatites have a mean Sm-Nd T_{CHUR} of 1795.28 Ma but, unfortunately, a SHRIMP zircon age is not available for -Eu Salknappen Pegmatites. From their cross-cutting relationships, the -Eu Salknappen Pegmatites are older than the Dalmatian Granites, but the exact age disparity is unknown.

There is a ~30 m.y. difference in ages between the Salknappen Pegmatites and Dalmatian Granites. To put this age difference in context, consider the following as case studies:

a) Dewey (2005) found that arc-continent collision generates short lived orogeny, in contrast to continent-continent collision. Dewey reports that the Grampian Orogeny lasted ~18 m.y, during which collisional shortening and prograde metamorphism lasted only 8 m.y., before extensional collapse.

b) In contrast, Homke *et al.* (2010) used apatite fission track (AFT) thermochronology to identify denudation episodes in the NW Zargos Belt. Homke *et al.* (2010) found 5 groups of AFT ages: at ~225 Ma to ~171 Ma, ~91 Ma, ~66 Ma, ~38 Ma and ~22 Ma. These ages document at least three denudation periods and evidence a long-lived, but episodic orogeny.

c) According to Schwartz *et al.* (2008) the Pampean Orogen includes a pair of metamorphic belts. A calc-alkaline magmatic belt in the east and a high-grade metasedimentary belt with peraluminous granite intrusion in the west. Zircon ages produced by Schwartz *et al.* (2008) indicate that calc-alkaline arc magmatism was active for at least 30 m.y (from 555 to 525 Ma) and then stopped that the metamorphism and granite magmatism began (525- 515 Ma).

From these examples, two episodes of magmatism recorded by distinct suites of granitoid intrusions 30 m.y apart during the same orogeny would be within precedent for known plate tectonics. However, it is possible that the two suites could represent two different orogenies, if the orogenies were short-lived in nature.

8.3 The granitoids in regional context

The isotopic ratios of data from this study were compared to similar data captured from other work studying the Maud Belt (Figure 8.4). Initial isotopic ratios, $^{87}Sr/^{86}Sr_i$ and $^{143}Nd/^{144}Nd_i$, were all calculated to 500 Ma (as in Chapter 7). Data from Grantham *et al.* (1991) shows two groups of $^{87}Sr/^{86}Sr_i$ ratios in accordance with the isotopic difference between Dalmatian Granites from east H.U. Sverdrupfjella and Dalmatian Granites from west H.U. Sverdrupfjella reported by Grantham *et al.*, (1991). Dalmatian Granite data from this study does not display as stark a difference, but some Dalmatian Granite $^{87}Sr/^{86}Sr_i$ ratios from this study do plot between groups in the Grantham *et al.*, (1991) $^{87}Sr/^{86}Sr_i$ ratios. Dalmatian Granite from as far west as Brekkerista could not be sampled for this study due to logistical constraints. The three Dalmatian Granite samples from this study with the highest $^{87}Sr/^{86}Sr_i$ ratios relative to other Dalmatian Granites from this study are 004dI, 008aC and 040aA. Samples 004dI and 008aC are both from Fuglefjellet (Northwest of H.U. Sverdrupfjella) and sample 040aA is from the Northwest of Gordonnuten but is also hosted by the Fuglefjellet Complex (see the map attached to this thesis). The sample of pegmatitic Dalmatian Granite (014bC) has a higher $^{87}Sr/^{86}Sr_i$ ratio than Dalmatian Granites from this study and is from Roerkulten, which is the furthest West of any sample from this study.

Data from this study therefore confirm the isotopic difference in Dalmatian Granites from eastern H.U. Sverdrupfjella and Dalmatian Granites from western H.U. Sverdrupfjella observed by Grantham *et al.*, (1991). However, data from this study "fills the gap" rather than plotting as distinct groups, which indicates a correlation between $^{87}Sr/^{86}Sr$ ratios in Dalmatian Granite and proximity to the Grunehogna Craton, which supports the proposal by Marschall *et al.* (2013) that the protolith of the Jutulrøra Complex was derived from a continental arc on the eastern margin of the Grunehogna Craton.

From Figure 8.4, it is apparent that Dalmatian Granites have isotope ratios overlapping with those of the Brattskarvet Intrusive Suite and "Sverdrupfjella Gneiss" sampled by Wareham *et al,* (1998). However, it is unclear where in H.U. Sverdrupfjella Wareham *et al,* (1998)'s data is from. In contrast, the Salknappen Pegmatites have isotopic values similar to country rock isotopic data from the Maud Belt.

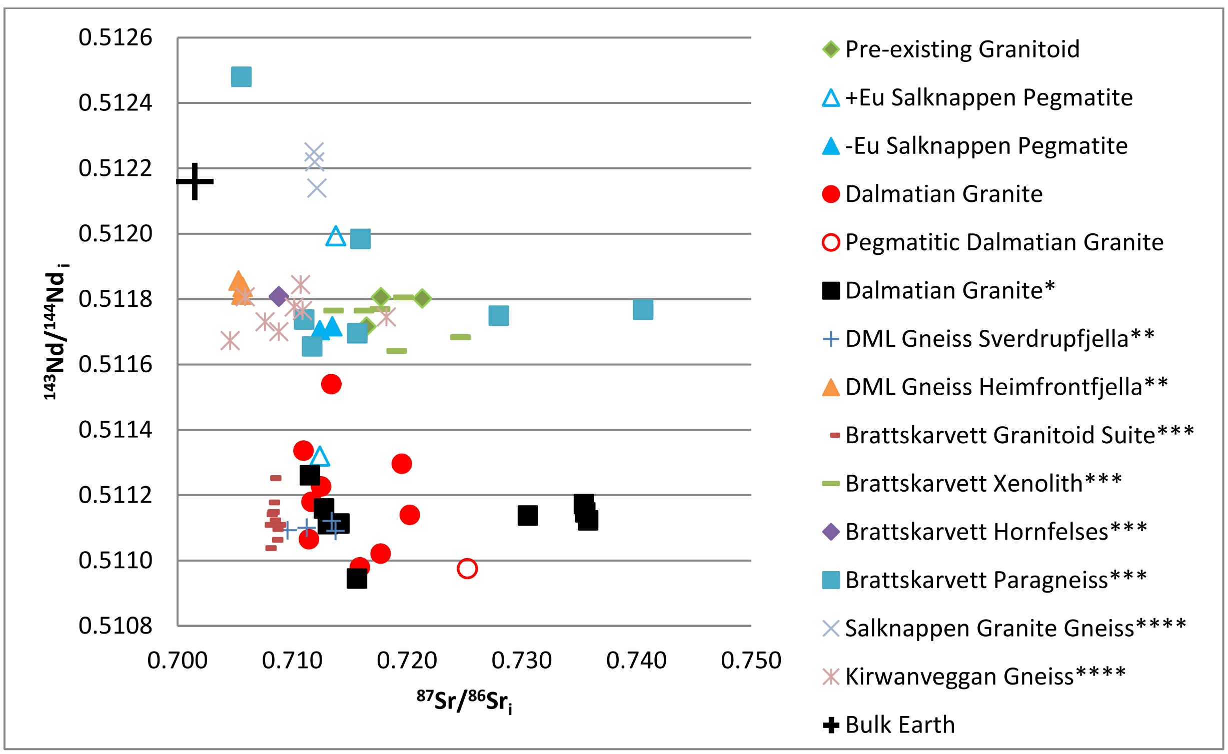

Figure 8.4: Plot comparing initial isotope ratios from this study to initial isotope ratios captured from other work (all calculated for 500 Ma); showing a difference in source between Salknappen Pegmatites and Dalmatian Granites. Except for one outlier, Salknappen Pegmatites show a link to country rock from the Maud Belt. Data was captured from the following publications: Grantham *et al.* (1991)*, Wareham *et al.* (1998)**, Moyes *et al.* (1993)*** and Grantham *et al.* (2019). All initial ratios calculated to 500 Ma. DML = Dronning Maud Land.

In Table 8.1 it is shown that inherited SHRIMP ages are the same age as rocks from the Grunehogna Craton and rocks formed during Rodinia assembly. The crystallisation age of Salknappen Pegmatite falls after peak metamorphism in H.U. Sverdrupfjella as defined by Board *et al*. (2005), Board *et al*. (2005) and Grantham *et al*. (1995), as well as after metamorphism in eastern H.U. Sverdrupfjella reported by Grosch *et al*. (2015), but Salknappen Pegmatites predate metamorphism in the western H.U. Sverdrupfjella that Grosch *et al*. (2015) reported.

Table 8.1: Showing the timing of events affecting H.U. Sverdrupfjella like Table 1.1, but with the addition of Dalmatian Granite and Salknappen Pegmatite SHRIMP ages from this study (highlighted in green).

Date:	Event:	Reference:
3450- 2800 Ma	Age of Archaean basement rocks	Halpern (1970)
3067 ± 8 Ma	Age of Annandagstoppane Granite	Marschall *et al*. (2010)
~2800 Ma – 2600 Ma	Inherited zircon ages in Dalmatian Granite	This study
~1130 Ma	Subduction under eastern Grunehogna	Marschall *et al.* (2013)
1130 Ma -1107 Ma	Ahlmannryggen Group deposited	Wolmarans and Kent, (1982)
1130 Ma -1107 Ma	Jutulrøra Complex protolith deposition	Marschall *et al.* (2013)
1180 Ma -1000 Ma	Metamorphism in H.U. Sverdrupfjella	Groenewald (1995)
1127 ± 12 Ma	Emplacement of Sveabreen migmatitic granite	Harris et al., (1995)
~1100 Ma	Emplacement of Borgmassivet Intrusive Suite	Riley and Millar, (2004)
~1100 Ma – 1000 Ma	Inherited zircon ages in Dalmatian Granite	This study
1086 ± 4 Ma	Orogeny related to Rodinia assembly	Marschall *et al.* (2013)
~1040 Ma - ~1030 Ma	High grade metamorphic episode in H.U. Sverdrupfjella	Board *et al.* (2005)
1000 Ma - 900 Ma	Period of deformation in H.U. Sverdrupfjella	Grantham *et al.* (1995)
590 Ma - 550 Ma	Mega-nappe formation	Grantham *et al.* (2008)
570 ± 7 Ma	Peak metamorphism in H.U. Sverdrupfjella	Pauly *et al.* (2016)
565 Ma - 540 Ma	Metamorphism in eastern H.U. Sverdrupfjella	Grosch *et al.* (2015)
565 Ma - 499 Ma	High grade metamorphic episode in H.U. Sverdrupfjella	Board *et al.* (2005)
550 Ma - 490 Ma	Period of deformation in H.U. Sverdrupfjella	Grantham *et al.* (1995)
~540 Ma	Peak metamorphism in H.U. Sverdrupfjella	Board (2001)
~519 Ma	Emplacement of Brattskarvet intrusive suite	Moyes *et al.* (1993)
~512 Ma	Crystallization of Salknappen Pegmatite	This study
~500 Ma	Accretion of the E H.U. Sverdrupfjella onto W H.U. Sverdrupfjella	Grosch *et al.* (2015)
491 ± 27 Ma	High-grade metamorphism in the western H.U. Sverdrupfjella	Grosch *et al.* (2015)
482.7 ± 2.4 Ma	Crystallization of Dalmatian Granite	This study
~480 Ma	Emplacement of post-tectonic granitic dykes	Board (2001)
~480 Ma	Ar-Ar isotopic systems reset	Board (2001)
469 ± 5 Ma	Emplacement of Dalmatian Granite	Grantham *et al.* (1991)
~170 Ma	Emplacement of Straumsvola nepheline syenite complex	Harris and Grantham, (1993)

One possible model for the emplacement of granitoids into H.U. Sverdrupfjella would be that Salknappen Pegmatites granitoids were intruded during the transition from an arc environment to an orogeny (510- 520 Ma). Then a second granitoid suite was formed in a later stage of orogeny (490- 470 Ma), sourced from the continental crust involved in the continental collision, and emplaced into the same country rock as the earlier granitoids. This fits with the model proposed and dates given by Grosch *et al.*, (2015).

Unfortunately, Grantham *et al*. (2008) does not give characteristics by which to identify a mega-nappe, and the concept does not appear elsewhere in the literature. To explain the occurrence of the granitoid sheets in this study in terms of the mega-nappe hypothesis proposed by Grantham *et al.* (2008), the weight of an overthrust mega-nappe would have pushed underlying rocks to a depth that caused first a lower crust comprised of oceanic floor and subduction-derived sediments to partially melt and produce the Salknappen Pegmatites, and subsequently continuing burial and/or post orogenic collapse causes the upper crust to melt to form the Dalmatian Granites. However, this sequence (mafic and mantle-derived rocks first, continental crust second) is the same as would be expected in a normal subduction related setting. Thus, the geochemical results from this project are ambivalent as to the existence of a mega-nappe in the study area. The same unfortunately holds for the chronology obtained during this study; though there is a clear time difference between the two stages of granitoid formation, it is not possible to relate this time gap uniquely to a mega-nappe process.

In some parts of H.U. Sverdrupfjella, the orientations of Dalmatian Granite and Salknappen Pegmatites are nearly opposite, whereas in parts with different country rocks the orientations are similar. If regional stress exerts some control on at least the mean orientations of granitoid sheets, a simple interpretation is that the dominant stress directions during the emplacement of the two granitoids differ. This would be conformable to any collision with an element of transtension or transpression, as the direction of stress would be expected to change with time as the colliding plates rotate. Such a change in stress fields is common in polymetamorphic belts and would be expected to occur in both a normal subduction setting and the hypothetical mega-nappe scenario.

This interpretation is complicated in that there is a correlation between Salknappen Pegmatite orientation and the metamorphic complex hosting the granitoid sheets, i.e., the granitoids display different orientations in different hosts. Pre-existing weakness does not explain the predominant orientation of the granitoids, because both suites of granitoids all cut across gneiss bands. Alternatively, residual stress (Holzhausen and Johnson, 1979) may have accumulated in the country rock, which could in turn exert control on the orientations of the granitoid sheets. However, there was a change in stress fields between the early Salknappen stage of granitoids and the later Dalmatian stage.

The model by Jacobs and Thomas (2004) is too broad to be supported or refuted directly with this study (as evidence is drawn from a much larger area), but the data here are compatible with the model by Grosh *et al.* (2015). Therefore, this work does not contradict any model that relies on plate tectonics and supports the diachronous event model. Though none of the conclusions here contradict the mega-nappe model either, it is also true that the data does not require the presence of a mega-nappe and can be adequately explained by normal and established plate tectonic processes.

8.4 Inter-continental Context

The tectonic events recorded by the granitoid sheets considered in this study are part of a larger event: the amalgamation of Gondwana. Schmitt *et al.* (2018) have recently reconstructed the amalgamation of Gondwana, as shown in Figure 8.5. Two stages of amalgamation are described, from ~760 to 575 Ma and then from ~575 to 480 Ma. The first stage formed a ”proto-Gondwana core”, to which East Antarctica accreted during the second stage of amalgamation.

During this second stage, East Antarctica was involved in collisions with the Kalahari Craton (then including the Grunehogna Craton), mobile belts between the Tanzania and East Antarctica Cratons, Dharwar Craton, West Australia, South Australia Cratons as well as New Zealand and Patagonia (Figure 8.5). These collisions reworked or resulted in mobile belts that experienced magmatism similar to that considered in this study. The relative timing of this complex series of events is of relevance to the evidence gathered in this study.

Within Antarctica itself, Elburg *et al.,* (2015) studied the Sør Rondane Mountains in Dronning Maud Land to the East of this work’s study area (see Figure 1.2) and report intrusions in that area over 150 m.y. Elburg *et al.,* (2015) demonstrate four “thermal pulses” affected the Sør Rondane Mountains at the following times: 650–600 Ma, 580 –550 Ma, ca. 530 Ma and a “magmatic tail” between 510 Ma and 500 Ma. Elburg *et al.* (2015) point out a lack of igneous U-Pb ages after 500 Ma, although other dating methods by other authors (K-Ar, Ar-Ar, and Rb-Sr) give some younger ages. According to Schmitt *et al.* (2018) the mobile belt that includes Sør Rondane Mountains formed during the older amalgamation event as supported by the older intrusion ages. The “magmatic tail” corresponds to the age of the Salknappen Pegmatites. Further afield in modern Mozambique, the Nampula Block described by Grantham *et al.,* (2008) includes the Murrupula Suite of granitoid intrusions, which have ages that vary from 530 Ma to 495 Ma (Macey *et al., 2007)*. The country rock of the Murrupula Suite was involved in the same collision as H.U. Sverdrupfjella, so similar ages are to be expected.

Further eastwards, Zhao *et al.,* (2023) compiled geochronology data in Sri Lanka and note post tectonic granites in the Highland Complex, Sri Lanka, with zircon U-Pb ages of 558-534 Ma. Yellappa and Mallikharjuna Rao (2018) studied granite magmatism in the Southern Granulite Terrain (India) and complied geochronology data. They present a U–Pb Zircon and Monazite age of syn-tectonic granites at ~570 Ma and post-tectonic granites with ages of ~550 Ma and ~525 Ma in the Madurai Block (Ghosh *et al*., 2004). The youngest granitoid age compiled is a Monazite Th–U–Pb age of ~470 Ma for a granitic Pegmatite in the Trivendrum Block (Braun *et al.*, 1998). Archibald *et al.* (2019) give an age range of 580 Ma to 540 Ma for the syn-collisional Ambalavao Suite of granites in Madagascar. Goodenough *et al.*, (2010) present U-Pb Shrimp ages for the post-collisional granites of the Maevarano Suite in north Madagascar giving emplacement between 537 Ma and 522 Ma.

In the extreme east, Foden *et al.,* (2020) studied magmatism related to the Delamerian Orogen in Australia and report 490 Ma –470 Ma post-tectonic A-type granites. Foden *et al.*, (2002) report the same as well as syn-tectonic I-type and S-type granites, emplaced between 516 Ma and 490 Ma, in the Delamerian Orogen. Paulsen *et al*, (2021) studied geochronology of rocks from the Queen Maud Mountains in the Ross Orogen, Antarctica, opposite modern Australia. They report a $^{206}Pb/^{238}U$ granite sample age of 503 ± 7 Ma. Allibone and Wysoczanski (2002) report SHRIMP U-Pb ages for gneissic granitoid intrusions in the same area that range from 531 ± 10 to 502 ± 9 Ma as well as a granodiorite age of 499 ± 6 Ma.

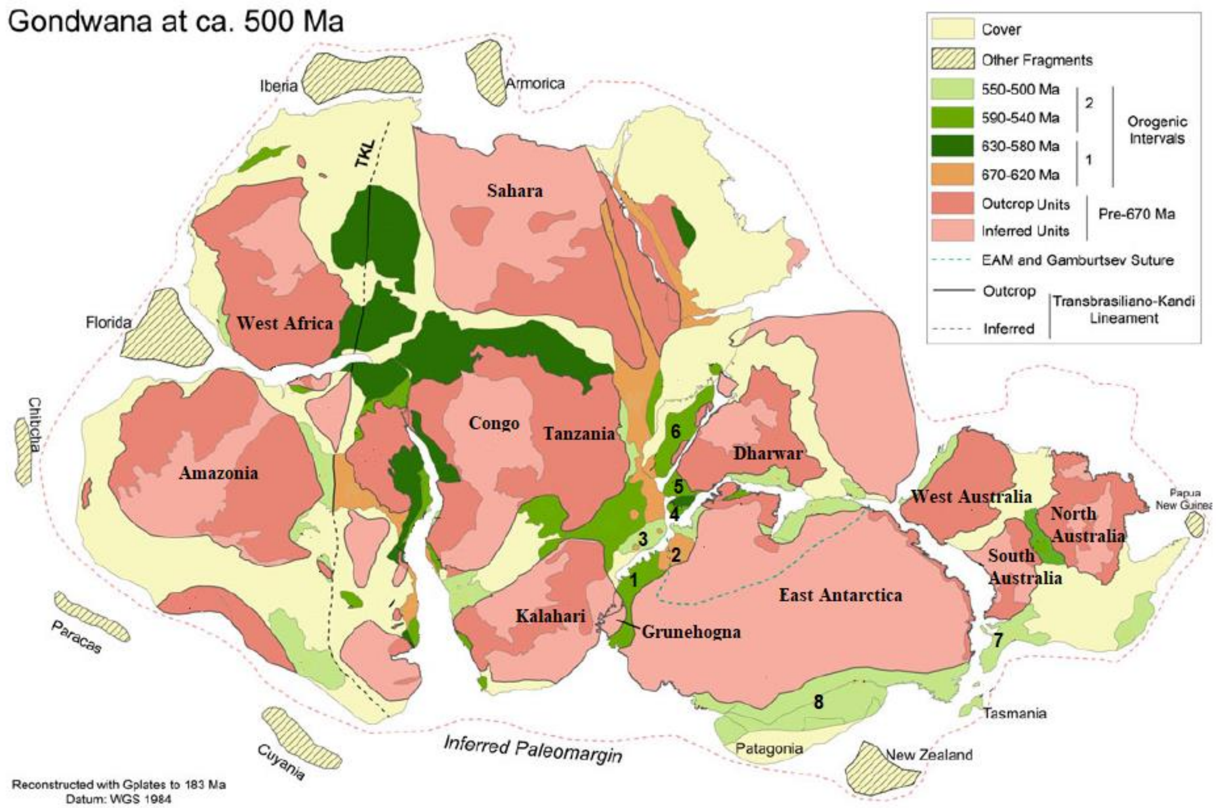

Figure 8.5: a map of Gondwana at 500 Ma modified from Schmitt *et al.,* (2018). Areas of interest are numbered. 1 is the study area, H.U. Sverdrupfjella. 2 is the Sør Rondane Mountains. 3 is the Nampula Block. 4 is Sri Lanka. 5 is the Southern Granulite Terrain (India). 6 is Madagascar. 7 is the Delamerian Orogen. 8 is the Ross orogen.

Thus, there is plenty of granitic magmatism related to Gondwana assembly with similar ages to the granitoid sheets in H.U. Sverdrupfjella. Granitoid magmatism predominantly predates the granitoids considered in this study at Sør Rondane and in Sri Lanka, India and Madagascar, but granitic magmatism of a similar age to the Salknappen Pegmatites (average age of 512 ± 2.9 Ma) occurred in Sør Rondane (the "magmatic tail"), Mozambique, the Delamerian Orogen and the Ross Orogen.

Granitic magmatism of similar age to the Dalmatian Granites dated in this study (average age of 483 ± 2.4 Ma) occurred in Mozambique, India (if the age by Braun *et al.*, 1998, is reliable) and the Delamerian Orogen. This indicates that the collision between the Dharwar Craton and the Tanzania Craton predates the accretion of East Antarctica while orogenies all around East Antarctica were producing granitoids in the same time period.

Chapter 9 Conclusion

A previously under-investigated occurrence of thin granitoid sheets in H.U. Sverdrupfjella has been described. These sheets of white granitoid have been dubbed the Salknappen Pegmatites after the type locality and co-exist with the previously reported but clearly younger Dalmatian Granites. The three ages obtained from the Salknappen Pegmatites granitoids are 30-40 Ma older than the age of 469 ±5 Ma for the Dalmatian Granites and indicate granitoid emplacement over an extended period of time between 517 Ma and 507 Ma.

The evidence supports a two-stage model for formation, in which the Salknappen Pegmatites are formed from Maud Belt country rock either during the early stages of an orogeny or as the crustal pile thickened during subduction leading up to orogeny. Which was prior to the formation of Dalmatian granites during the melting of upper-crustal material, here inferred to be part of or derived from the Grunehogna Craton in the later stages of orogeny or during post-orogenic collapse. Though not being able to disprove the mega-nappe model, the data presented here provide no reason to suspect processes other than established plate tectonics. The magnitude of the difference in ages and different stages of orogeny producing the two suites of granitoids of discussed in this work are consistent with a diachronous metamorphic event as proposed by Grosh *et al.* (2015).

9.1 Further Work

With the appropriate funding and opportunity; sample material remaining from this study could be used for two projects.

Firstly, the petrogenesis and source of granitoids from this study can be further constrained by mineralogical study. Analysis of mineral grains (as opposed to whole rock) for biotite, feldspar, hornblende and garnet (despite rarity) can reveal more about the nature of sources and give more detail on what the production and emplacement of the granitoid sheets represents.

Secondly, SHRIMP geochronology for the -Eu Salknappen Pegmatite group would put that group in context and would reveal more detail in the timing of when the sources of granitoid sheets in this study became involved in orogeny. Additional granularity may reveal spatial variation or confirm a lack thereof.

Production of more comparable data (more modern XRF, ICP-MS and SHRIMP) for Dalmatian Granites from western H.U. Sverdrupfjella would answer questions regarding the nature of the difference to Dalmatian Granites from this study. If available, leftover sample material from Grantham *et al.*, (1991) would be ideal (the most comparable) and logistically far less challenging.

Finally, for the wider research project that this study is a part of: the mega-nappe hypothesis is due significant review. The question posed by this study is why the precedented context of plate tectonics is inadequate in this case?

References

Allibone, A. and Wysoczanski, R. (2002) Initiation of magmatism during the Cambrian–Ordovician Ross orogeny in southern Victoria Land, Antarctica. *GSA Bulletin*. **114 (8):** 1007–1018

Allmendinger, R. W., Cardozo, N., and Fisher, D. (2012). Structural geology algorithms: Vectors and tensors in structural geology. Cambridge University Press. 302pp.

Archibald, D.B,. Collins, A.S., Foden, J.D., Payne, J.L., Holden, P. and Razakamanana, T. (2019). Late syn-to post-collisional magmatism in Madagascar: The genesis of the Ambalavao and Maevarano Suites. *Geoscience Frontiers.* **10:** 2064-2084.

Baba, S., Owada, M., Grew, E. and Shirashi, K. (2006). Sapphirine–orthopyroxene–garnet granulite from Schirmacher Hills, Central Dronning Maud Land. *In: Fütterder, D. K., Damaske, D., Kleinschmidt,G., Miller, H. and Tessensohn, F. (eds) Antarctica: Contributions to Global Earth Sciences. Springer, New York*, 37–44.

Bonin, B., Janoušek, V. and Moyen, J. F. (2020). Chemical variation, modal composition and classification of granitoids. *Geological Society, London, Special Publications*. ***491*(1):** 9-51.

Bisnath, A. and Frimmel, H. E. 2005. Metamorphic evolution of the Maud Belt: P–T–t path for highgrade gneisses in Gjelsvikfjella, Dronning Maud Land, East Antarctica. *Precambrian Research*, **43:**505–524.

Black L.P., Kamo S.L., Allen C.M., Davis D.W., Aleinikoff J.N., Valley J.W., Mundil R., Campbell I.H., Korsch R.J., Williams I.S. and Foudoulis C. (2004). Improved $^{206}Pb/^{238}U$ microprobe geochronology by the monitoring of a trace-element related matrix effect; SHRIMP, ID-TIMS, ELA-ICP-MS, and oxygen isotope documentation for a series of zircon standards. *Chem. Geol*. **205:** 115–140.

Board, W.S. (2001). Tectonothermal evolution of the southern H.U. Sverdrupfjella, western Dronning Maud Land, Antarctica (Ph.D. thesis). University of Cape Town. 205pp.

Board, W. S., Frimmel, H. E. and Armstrong, R. A. (2005). Pan-African Tectonism in the Western Maud Belt: P-T-t Path for High-grade Gneisses in the H.U. Sverdrupfjella, East Antarctica. *Journal of Petrology*. **46**: 671-699.

Boynton, W.V. (1984). Cosmochemistry of the rare earth elements; meteorite studies. *In: Rare earth element geochemistry. Henderson, P. (Editors), Elsevier Sci. Publ. Co., Amsterdam. 63-114.*

Braun, I., Montel, J.M. and Nicollet, C. (1998) Electron probe dating of monazites from high-grade gneisses and pegmatites of the Kerala Khondalite Belt, southern India. *Chemical Geology.* **146:** 65–85.

Byrnes, G. (2015). Tectono-metamorphic history of the reworked, high-grade Maud Belt at central-Eastern H.U. Sverdrupfjella, Antarctica (M.Sc Thesis). *University of Cape Town*. 135pp.

Castro, A. (2020). The dual origin of I-type granites: the contribution from experiments. *Geological Society, London, Special Publications.* **491.1**: 101-145.

Černý, P., David L. and Novák, M. (2012). Granitic pegmatites as reflections of their sources. *Elements* **8**: 289-294.

Clemens, J. D., Stevens, G. and Farina, F. (2011). The enigmatic sources of I-type granites: The peritectic connexion. *Lithos.* **126**:174-181.

Clemens, J. D. and Stevens, G. (2012). What controls chemical variation in granitic magmas? *Lithos* **134**: 317-329.

Cloete, H. C. C. and Truter, J. (2001), Major and Trace Element Analysis by X-ray Fluorescence Spectrometry at the Council for Geoscience. Open File Report 2001 -0074, Council for Geoscience. Pretoria, South Africa, 26pp.

Chappell, B.W. and White, A.J.R. (1974). Two Contrasting Granite Types. *Pacific Geology*. **8:** 173-174.

Chappell, B.W. and White, A.J.R. (2001). Two Contrasting Granite Types: 25 Years Later. *Australian Journal of Earth Sciences*. **48:** 489-499.

DePaolo, D. J. and Wasserburg, G.J. (1976). Nd isotopic variations and petrogenetic models. *Geophysical Research Letters.* **3.5:** 249-252.

Dewey, J. F. (2005). Orogeny can be very short. *Proceedings of the National Academy of Sciences of the United States of America*. **102**: 15286-15293.

Eglington, B.M. and Harmer, R.E. (1999). GEODATE for Windows version 1: Isotope regression and modelling software. Council for Geoscience Open-file report 1999-0206 O. 24 pp

Elburg, M.A., Andersen, T., Jacobs, J., Läufer, A., Ruppel, A., Krohne, N. and Damaske, D. (2015) One Hundred Fifty Million Years of Intrusive Activity in the Sør Rondane Mountains East Antarctica): Implications for Gondwana Assembly. *The Journal of Geology*. **124**: 1–26

Elvevold, S. and Ohta Y. (eds). (2010). Nature environment map H.U. Sverdrupfjella Dronning Maud Land, East Antarctica 1:150 000. *Norwegian Polar Institute.* Temakart 28.

Ferreira, E. P. (1988). The sedimentology and stratigraphy of the Ahlmannryggen Group, Antarctica. (M.Sc Thesis). *University of Stellenbosch*. 193pp.

Foden, J.D., Elburg, M.A., Turner, S.P., Sandiford, M., Callaghan, J.O. and Mitchell. S. (2002). Granite production in the Delamerian Orogen, South Australia. *Journal of the Geological Society*. **159**: 557-575

Foden, J.D., Elburg, M.A., Turner, S.P., Clark, C., Blades, M.L., Cox, G., Collins, A.S., Wolff, K. and George, C. (2020) Cambro-Ordovician magmatism in the Delamerian orogeny: Implications for tectonic development of the southern Gondwanan margin. *Gondwana Research*. **81:** 490–521

Frost, B. R., Barnes, C. G., Collins, W. J., Arculus, R. J., Ellis, D. J. and Frost, C. D. (2001). A geochemical classification for granitic rocks. *Journal of petrology*. ***42*****(11):** 2033-2048.

Garcia-Arias, M. (2020). The never-ending pursuit of a definitive chemical classification system for granites. *Journal of Geosciences* **65.4**: 221-227.

Ghosh, J.G., Maarten De wit, R.E. and Zartman, R.E. (2004) Age and tectonic evolution of neoproterozoic ductile shear zone in Southern Granulite Terrain, India, with implications for Gondwana studies. *Tectonics*. **23:** TC3006.

Goodenough, K.M., Thomas, R.J., De Waele, R.J., Key, R.M., Schofield, D.I., Bauer, W., Tucker, R.D., Rafahatelo, J.-M., Rabarimanana, M., Ralison, A.V. and Randriamananjara, T. (2010). Post-collisional magmatism in the central East African Orogen: The Maevarano Suite of north Madagascar. *Lithos*. **116:** 18-34.

Grantham, G.H., Groenewald, P.B., Hunter, D.R., 1988. Geology of the northern H.U. Sverdrupfjella, western Dronning Maud Land and implications for Gondwana reconstructions. *South African Journal of Antarctic Research.* **18**: 2–10.

Grantham, G. H., Moyes, A. B. and Hunter, D. R. (1991). The age, petrogenesis and emplacement of the Dalmatian Granite, H.U. Sverdrupfjella, Dronning Muad Land, Antarctica. *Antarctic Science*. **3**:197-204.

Grantham, G. H. (1992). Geological evolution of western H.U. Sverdrupfjella (PhD thesis). University of Natal. 332pp.

Grantham, G. H., Jackson, C., Moyes, A. B., Groenewald, P. B., Harris, P. D., Ferrar, G. and Krynauw, J. R. (1995). The tectonothermal evolution of the Kirwanveggan–H.U. Sverdrupfjella areas, Dronning Maud Land, Antarctica. *Precambrian Research*, **75:** 209–230.

Grantham, G. H., Maboko, M. and Eglington, B. M. (2003). A review of the evolution of the Mozambique Belt and implications for the amalgamation of Rodinia and Gondwana. In: Yoshida, M., Windley, B. F. and Dasgupta, S. (eds) Proterozoic East Gondwana: Supercontinent Assembly and Breakup. *Geological Society, London, Special Publications*. **206:** 401–426.

Grantham, G.H., Macey, P.H. and Ingram B. A. Roberts, M.P., Rohwer, M., Opperman, R., Manhica, V., Alvares, S., Bacalhau, C., Du Toit, M. C, Cronwright, M. and Thomas R.J. (2007). Map Explanation of Sheets Meconte (1439) and Nacala (1440). National Directorate of Geology, Republic of Mozambique, Maputo.

Grantham, G. H., Macey, P. H., Ingram, B. A., Roberts, M. P., Armstrong, R. A., Hokada, T., Shiraishi, K., Jackson, C., Bisnath, A. and Manhica (2008). Terrane correlation between Antarctica, Mozambique and Sri Lanka; comparisons of geochronology, lithology, structure and metamorphism and possible implications for the geology of southern Africa and Antarctica. *Geological Society of London, Special Publications*. **308**: 91-119.

Grantham, G.H., Kramers, J.D, Eglington, B. and Burger, E.P. (2019). The Ediacarian-Cambrian uplift history of Western Dronning Maud Land: New 40Ar-39Ar and Sr/Nd data from Sverdrupfjella and Kirwanveggan, the source of the Urfjell Group and tectonic evolution of Dronning Maud Land within the Kuunga Orogeny and Gondwana amalgamation. *Precambrian Research.* **333:** 105-444.

Groenewald, P. B., Grantham, G.H. and Watkeys, M.K. (1991). Geological evidence for a Proterozoic to Mesozoic link between southeastern Africa and Dronning Maud Land, Antarctica. *Geological Society of London*. **148**: 115-1123.

Groenewald, P.B. (1995). The geology of northern H.U. Sverdrupfjella and its bearing on crustal evolution in Dronning Maud Land, Antarctica (PhD thesis). University of Natal. 315pp.

Grosch, E. G., Frimmel, H. E. Abu-Alam, T. and Kosler, J. (2015). Metamorphic and age constraints on crustal reworking in the western H.U. Sverdrupfjella: implications for the evolution of western Dronning Maud Land, Antarctica. *Journal of the Geological Society.* **174**:499-518.

Halpern, M. (1970) Rubidium-strontium date of possibly 3 billion years for a granite rock from Antarctica. *Science*. **169**:977–978.

Harris, C. and Grantham, G.H. (1993). Geology and petrogenesis of the Straumsvola nepheline syenite complex, Dronning Maud Land, Antarctica. *Geol. Mag*. **130 (4):** 513-532.

Harmer, R.E. and Eglington, B.M. (1990). A review of the statistical principles of geochronometry: towards a more consistent approach for reporting geochronological data. *South African Journal of Geology*. **93:** 845-856.

Holzhausen, G.R. and Johnson, A.M. (1979). The concept of residual stress in rock. *Tectonophysics*. **58:** 237-267.

Homke, S., Vergés, J., van der Beek, P., Fernàndez, M., Saura, E., Barnero, L., Badics, B. and Labrin, E. (2010). Insights in the exhumation history of the NW Zagros from bedrock and detrital apatite fission-track analysis: evidence for long-lived orogeny. *Basin Research*. **22**: 659-680.

Jacobs, J. and Thomas, R.J. (2004). Himalayan-type indenter-escape tectonics model for the southern part of the late Neoproterozoic-early Palaeozoic East African-Antarctic orogen. *Geology*. **32**: 721-724.

Janoušek, V., Farrow, C. M. and Erban, V. (2006). Interpretation of whole-rock geochemical data in igneous geochemistry: introducing Geochemical Data Toolkit (GCDkit). *Journal of Petrology* 47(6):1255-1259.

Jamal, D. L. (2005). Crustal studies across selected geotransects in NE Mozambique: Differentiating between Mozambiquan (Kibaran) and Pan African events, with implications for Gondwana studies (PhD thesis). University of Cape Town. 730pp

Johannsen, A. (1931). A Descriptive Petrography of the Igneous Rocks, Vol 1. Introduction, Textures, Classification, and Glossary. *The Journal of Geology.* **40:** 182-185.

Krynauw, J. R. (1996). A review of the geology of East Antarctica, with special reference to the *c*. 1000 Ma and *c*. 500 Ma events. *Terra Antartica.***3**: 77–89.

Macey, P., Ingham, B., Cronwright, M., Botha, G., Roberts, M., Grantham, G., Maree, L., Botha, P., Kota, M., Opperman, R., Haddon, I., Nolte, JC., and Rohwer, M. (2007). Map Explanation of Sheets Alto Molócuè (1537), Murrupula (1538), Nampula (1539), Mogincual (1540), Errego (1637), Gilé

(1638) and Angoche (1639–40). National Directorate of Geology, Republic of Mozambique, Maputo.

Marschall, H.R., Hawkesworth, C.J., Storey, C.D., Dhuime, B., Leat, P.T., Meyers H. and Tamm-Buckle, S. (2010). The Annandagstoppane Granite, East Antarctica: Evidence for Archaean Intracrustal Recycling in the Kaapvaal-Grunehogna Craton from Zircon O and Hf Isotopes. *Journal of Petrology.* **51:** 2277-2301.

Marschall, H.R., Hawkesworth C.J. and Leat P.T. (2013). Mesoproterozoic subduction under the eastern edge of the Kalahari-Grunehogna Craton preceding Rodinia assembly: the Ritscherflya detrital zircon record, Ahlmannryggen (Dronning Maud Land, Antarctica). *Precambrian Research.* **236:** 31-45

McGibbon, D.C. (2014). Shear Zones of the Maud Belt, Antarctica: Kinematics and Deformation Mechanisms. (M.Sc Thesis). *University of Cape Town*. 135pp.

Moyes, A.B., Groenewald, P.B. and Brown, R.W. (1993) Isotopic constraints on the age and origin of the Brattskarvet intrusive suite, Dronning Maud land, Antarctica. *Chemical Geology*. **106:** 453–466.

Nédélec, A. and Bouchez, J. (2015). Origin of granitic magmas., in Peter Bowden (ed.), *Granites: Petrology, Structure, Geological Setting, and Metallogeny.* Oxford University Press. 335pp.

Paces, J.B. and Miller, J.D. (1993). Precise U–Pb ages of Duluth Complex and related mafic intrusions, northeastern Minnesota: Geochronological insights to physical, petrogenetic, paleomagnetic, and tectonomagmatic processes associated with the 1.1 Ga Midcontinent Rift System. *Journal of Geophysics Research.* **98**: 13997–14013.

Paulsen, T., Encarnación, J., Grunow, A.M., Valencia, V.A., Pecha, M.E., Benowitz, J. and Layer, P. (2021). New ages from the Shackleton Glacier area and their context in the regional tectonomagmatic evolution of the Ross orogen of Antarctica. *International Geology Review*. **63(13):** 1596-1618,

Pauly, J., Marschall, H.R., Meyer H.P., Chatterjee, N. and Monteleone B. (2016). Prolonged Ediacaran–Cambrian Metamorphic History and Short-lived High-pressure Granulite facies Metamorphism in the H.U. Sverdrupfjella, Dronning Maud Land (East Antarctica): Evidence for Continental Collision during Gondwana Assembly. *Journal of Petrology*. **57(1):** 185–228.

Pearce, J. A., Harris, N. B. W. and Tindle, A. G. (1984). Trace Element Discrimination Diagrams for the Tectonic Interpretation of Granitic Rocks. *Journal of Petrology*. **25 part 4**: 956-983.

Pearce, J. (1996). Sources and settings of granitic rocks. *Episodes.* **19**:120-125.

Pin, C., Briot, D., Bassin, C. and Poitrasson, F. (1994). Concominant Separation of strontium and samarium–neodymium for isotopic analysis in silicate samples, based on specific extraction chromatography. *Analytica Chimica Acta*. **298**: 209–217.

Pin, C., Gannoun, A. and Dupont, A. (2014). Rapid, simultaneous separation of Sr, Pb, and Nd by extraction chromatography prior to isotope ratios determination by TIMS and MC-ICP-MS. *Journal of Analytical Atomic Spectrometry.* ***29:*** *1858-1870.*

Rudrick, R. L. and Fountain, D. M. (1995). Nature and composition of the continental crust: a lower crustal perspective. *Reviews of Geophysics.* **33, 3w**: 267-309.

Riley, T.R. and Millar, I. L. (2014). Geochemistry of the 1100Ma intrusive rocks from the Ahlmannryggen region, Dronning Maud Land, Antarctica. *Antarctic Science.* **26(4):** 389-399.

Schmitt, R. da S., Fragoso, R. de A. and Collins, A. S. (2018). Suturing Gondwana in the Cambrian: The Orogenic Events of the Final Amalgamation. In: Siegesmund, S. S., Basei, M., Oyhantçabal, P. and Oriolo, S. (eds). *Geology of Southwest Gondwana. Regional Geology Reviews,* Springer, Cham. 411–432.

Shand, S. J. (1943). Eruptive Rocks. Their Genesis, Composition, Classification, and Their Relation to Ore-Deposits with a Chapter on Meteorite. *John Wiley & Sons,* New York.

Shiraishi, K., Asami, M., Ishizuka, H., Kojima, S., Osanai, Y., Sakiyama, T., Takahashi, Y., Yamazaki, M. and Yoshikura, S. (1991). Geology and metamorphism of the Sør Rondane mountains, east Antarctica. In: Thomson, M.R.A., Crame, J.A. and Thomson, J.W. (eds). *Geological Evolution of Antarctica. Cambridge University Press, Cambridge*. 77–82.

Schwartz, J. J., Gromet, L. P. and Miro, R. A. (2008). Timing and Duration of the Calc-Alkaline Arc of the Pampean Orogen: Implications of the Late Neoproterozoic to Cambrian Evolution of Western Gondwana. The *Journal of Geology*. **116**: 39-61.

Stacey, J.S. and Kramers, J.D. (1975). Approximation of Terrestrial Lead Isotope Evolution by a 2-Stage Model. *Earth and Planetary Science Letters* **26(2)**: 207-221.

Sun, S. and McDonough, W. F. (1989). Chemical and isotopic systematics of oceanic basalts: implications for mantle composition and processes. *Geological Society, London, Special Publications*. **42**: 313-345.

Talbot, C.J. (1970). The minimum strain ellipsoid using deformed quartz veins. *Tectonophysics*. **9:** 47-76.

Taylor, S.R. and McLennan, S.M. (1995). The geochemical evolution of the continental crust. *Reviews of Geophysics.***33 (2)**: 241-265.

Tanaka, T., Togashi, S., Kamioka, H., Amakawa, H., Kagami, H., Hamamoto, T., Yuhara, M., Orihashi, Y., Yoneda, S., Shimizu, H,. Kunimaru, T., Takahashi, K., Yanagi, T., Nakano, T., Fujimaki, H., Shinjo, R., Asahara, Y., Tanimizu, M. and Dragusanu, C. (2000) JNdi-1: a neodymium isotopic reference in consistency with LaJolla neodymium. *Chemical Geology*. **168:** 279–28.

Thomas, S.A.J (2014). Metamorphic and melt-migration history of midcrustal migmatitic gneisses from Nupskåpa, the Maud Belt, Antarctica. (M.Sc Thesis). *University of Cape Town*. 159pp.

Vermeesch, P. (2018). IsoplotR : a free and open toolbox for geochronology. *Geoscience Frontiers.* **9:** 1479-1493.

Vernon, R., H. (2004). *A Practical Guide to Rock Microstructure.* Cambridge University Press. 580pp.

Vojtech, J., Colin M., Farrow and Vojtech E., (2006). Interpretation of whole-rock geochemical data in igneous geochemistry: introducing Geochemical Data Toolkit (GCDkit). *Journal of Petrology* **47(6)**: 1255-1259.

Wareham, C. D., Pankhurst, R. J., Thomas, R. J., Storey, B. C., Grantham, G. H., Jacobs, J. and Eglington, B. M. (1998). Pb, Nd, and Sr Isotope Mapping of Grenville-Age Crustal Provinces in Rodinia. *The Journal of Geology*. **106(6):** 647-660.

Watters, B.R., Krynauw, J.R. and Hunter, D.R. (1991). Volcanic rocks of the Proterozoic Jutulstraumen Group in western Dronning Maud Land, Antarctica. *In*: Thomson, M.R.A., Crame, J.A. & Thomson, J.W. (eds) *Geological Evolution of Antarctica*. Cambridge University Press, Cambridge, 41–46.

Wiedenbeck, M., Allé, P., Corfu, F., Griffin, W.L., Meier, M., Oberli, F., von Quadt, A., Roddick, J.C., Spiegel, W. (1995). Three natural zircon standards for U–Th–Pb, Lu–Hf, trace element and REE analyses. *Geostand. Newsl.*, **19:** 1–23.

Williams, I.S. and Hergt, J.M. (2000) U–Pb dating of Tasmanian dolerites: a cautionary tale of SHRIMP analysis of high-U zircon. in: J.D. Woodhead, J.M. Hergt, W.P. Noble. (Eds.), *Beyond 2000: New Frontiers in Isotope Geoscience, Lorne, Abstract Proceedings*. pp. 185–188.

Wolmarans, L.G. and Kent, L.E. 1982. Geological investigations in western Dronning Maud Land, Antarctica: a synthesis. *South African Journal of Antarctic research, Supplement*, 2, 93 pp.

Yellappa, T. and Mallikharjuna Rao, J. (2018). Geochemical characteristics of Proterozoic granite magmatism from Southern Granulite Terrain, India: Implications for Gondwana. *Journal of Earth System Science. **127:** 22*

Zhao, L., Dharmapriya, P.L., Zhang, Y., Zhai, M., Guo, J., Pitawal, A. and Li, X. (2023). Expanding Azania at the heart of Gondwana: Terrane correlation from Southern India to Sri Lanka. *Precambrian Research*. **395:** 107149

Appendix 1 Data Quality

A1.1 XRF Data

Below table A1.1 shows that accuracy of major element oxides, measured by XRF. These data are of good quality, except for Cr_2O_3 measured for the first field season and a high LOI. The elevated LOI is likely due to the high Cr_2O_3 value. Fortunately, the XRF minor element analysis has a reliable data for Cr.

The XRF oxide data has therefore been used and preferred for major element geochemistry in this work.

The trace element XRF data is not as reliable as shown in table A1.2. Accuracy is expressed in the same manner as Table A1.1 but using the reference material GSS-1 (soil reference material from IGGE, China).

Using XRF data for the following elements will be avoided due to poor accuracy: As, Co, Cs, Hf, Ge, Th, U W. In general, however, ICP-MS usually has a lower detection limit; so, will be preferred unless there is a concern regarding the quality of ICPMS data for the element (see section A1.1.2).

Table A1.1: Accuracy of XRF analysis of major elements oxides. Accuracy is expressed as the percentage of certified value that was measured for 12/76 (a secondary amphibolite reference material).

	12/76 for 2014 data			12/76 for 2015 data		
	Certified	Result	% Accuracy	Certified	Result	% Accuracy
SiO2	45.42	45.68	100.5682	45.42	45.90244	101.0622
TiO2	1.54	1.53	99.20961	1.54	1.553139	100.8532
Al2O3	16.62	16.83	101.249	16.62	16.90998	101.7448
Fe2O3	9.73	9.87	101.4141	9.73	9.846748	101.1999
MnO	0.180	0.177	98.53184	0.18	0.174554	96.97456
MgO	8.150	7.98	97.91286	8.15	7.931539	97.3195
CaO	10.93	10.76	98.48753	10.93	10.74959	98.34937
Na2O	3.65	3.29	90.01697	3.65	3.562691	97.60796
K2O	0.70	0.69	98.63238	0.7	0.694286	99.1837
P2O5	0.259	0.280	107.9395	0.259	0.252748	97.58598
Cr2O3	0.074	0.090	121.2868	0.074	0.072775	98.34485
LOI	2.50	2.79	111.6587	2.5	2.45	98

Table A1.2: Minor elements from XRF. GSS-1 is a soil reference material from IGGE, China.

	GSS-1 for 2014 data			GSS-1 for 2015 data		
	Certified	Result	% Accuracy	Certified	Result	% Accuracy
As	**33.5**	39	116.4179	**33.5**	35	104.4776
Ba	**590**	630	106.7797	**590**	625	105.9322
Bi	**1.17**	<3	Below DL	**1.17**	<3	Below DL
Br	**2.9**	<2	Low	**2.9**	<2	Low
Ce	**70**	75	107.1429	**70**	75	107.1429
Co	**14.2**	16	112.6761	**14.2**	16	112.6761
Cr	**62**	61	98.3871	**62**	61	98.3871
Cs	**9**	15	166.6667	**9.0**	12	133.3333
Cu	**21**	21	100	**21**	20	95.2381
Ga	**19.3**	19	98.4456	**19.3**	20	103.6269
Ge	**1.3**	<1	Low	**1.3**	1.9	146.1538
Hf	**6.8**	9.7	142.6471	**6.8**	8.6	126.4706
La	**34**	32	94.11765	**34**	30	88.23529
Mo	**1.4**	<2	Below DL	**1.4**	<2	Below DL
Nb	**16.6**	16	96.38554	**16.6**	17	102.4096
Nd	**28**	28	100	**28**	30	107.1429
Ni	**20.4**	22	107.8431	**20.4**	22	107.8431
Pb	**98**	97	98.97959	**98**	97	98.97959
Rb	**140**	146	104.2857	**140**	145	103.5714
Sc	**11.2**	11	98.21429	**11.2**	13	116.0714
Se	**0.14**	<1	Below DL	**0.14**	1	714.2857
Sm	**5.2**	<10	Below DL	**5.2**	<10	Below DL
Sr	**155**	165	106.4516	**155**	165	106.4516
Ta	**1.4**	<2	Below DL	**1.4**	<2	Below DL
Th	**11.6**	10	86.2069	**11.6**	14	120.6897
Tl	**1**	<3	Below DL	**1.0**	<3	Below DL
U	**3.3**	4	121.2121	**3.3**	2.8	84.84848
V	**86**	87	101.1628	**86**	87	101.1628
W	**3.1**	4.1	132.2581	**3.1**	5.6	180.6452
Y	**25**	26	104	**25**	26	104
Yb	**2.66**	<3	Below DL	**2.66**	<3	Below DL
Zn	**680**	692	101.7647	**680**	695	102.2059
Zr	**245**	260	106.1224	**245**	260	106.1224

A1.2 ICP-MS Data

Due to the number of elements analysed and the number of reference materials, only the average recovery for each element is shown in table A1.3 and A1.4 (these table show the same, but for the first and second field season, respectively) to summarize the recovery of certified reference materials. The full tables can be seen in the next section (A1.3.3).

Two sets of analyses were done using ICP-MS (see section 3.2.1 in the Methods Chapter) one for a variety of elements and another for REEs with Y, Zr and Th.

The REE and Y, Zr and Th data is of good quality (right-most to columns in Table A1.3 and A1.4) as it has been corrected according to certified reference material recovery.

ICP-MS data usually has lower detection limits than XRF, so is generally preferred for minor elements (i.e. elements not covered by XRF oxide analysis).

XRF data will be used for Ba, Fe, K, Mg and Mn. There is not XRF data for Be, so data for Be must be used with caution. The reference material concentration of Bi and Tl are below detection limit for XRF while the ICP-MS data has poor recovery for the certified reference material. The concentration of Ag, Bi and Tl is low for samples in this study, so the data quality of those element is not likely to be relevant in this thesis.

The XRF certified reference material concentration for U is near detection limit and concentrations for many samples is at or near XRF detection limit. Therefore, ICP-MS data has to be used for U, but with caution and an understanding that measured values may be lower than true values. For other minor elements and REE's ICPMS data will be used if available.

Table A1.3: The average % recovery for certified samples measured by ICP-MS analysed with samples from the 2014 field season. The purpose of this table is to be a summary, please see Tables A3.12 and A3.15 for the full data tables.

Li (7)	97	**Mn (55)**	109	**Mo (98)**	102	**Y (89)**	100	**Tb (159)**	101
Be (9)	82	**Fe (57)**	83	**Ag (109)**	125	**Zr (90)**	96	**Dy (163)**	100
Na (23)	91	**Co (59)**	91	**Cd (114)**	100	**La (139)**	100	**Ho (165)**	99
Mg (24)	81	**Ni (60)**	103	**Te (128)**	109	**Ce (140)**	100	**Er (167)**	100
Al (27)	95	**Cu (63)**	106	**Ba (138)**	90	**Pr (141)**	101	**Tm (169)**	94
K (39)	89	**Zn (66)**	96	**Tl (205)**	74	**Nd (146)**	100	**Yb (172)**	96
Ca (43)	95	**Ga (69)**	101	**Pb (208)**	96	**Sm (147)**	100	**Lu (175)**	98
V (51)	95	**Rb (85)**	102	**Bi (209)**	87	**Eu (151)**	100	**Th (232)**	100
Cr (52)	102	**Sr (88)**	91	**U (238)**	90	**Gd (157)**	100		

Table A1.4: The average % recovery for certified samples measured by ICP-MS analysed with samples from the 2015 field season. The purpose of this table is to be a summary, please see Table A3.13 for the full data tables. DL= detection limit.

Li (7)	98	**Mn (55)**	114	**Mo (98)**	102	**Y (89)**	100	**Tb (159)**	100
Be (9)	96	**Fe (57)**	80	**Ag (109)**	Below DL	**Zr (90)**	100	**Dy (163)**	100
Na (23)	94	**Co (59)**	95	**Cd (114)**	102	**La (139)**	100	**Ho (165)**	100
Mg (24)	85	**Ni (60)**	102	**Te (128)**	84	**Ce (140)**	100	**Er (167)**	100
Al (27)	96	**Cu (63)**	104	**Ba (138)**	88	**Pr (141)**	100	**Tm (169)**	101
K (39)	91	**Zn (66)**	102	**Tl (205)**	78	**Nd (146)**	100	**Yb (172)**	100
Ca (43)	96	**Ga (69)**	103	**Pb (208)**	95	**Sm (147)**	100	**Lu (175)**	101
V (51)	98	**Rb (85)**	99	**Bi (209)**	88	**Eu (151)**	100	**Th (232)**	100
Cr (52)	102	**Sr (88)**	97	**U (238)**	81	**Gd (157)**	100		

Appendix 2: Nunatak descriptions

Table A2.1: This table details the coordinates, nunatak and country rock of each way point (where a way point is a location where fieldwork was conducted).

Way Point	Latitude	Longitude	Location	Host Formation
001	-72° 13.62498'	-00° 26.78658'	Jutulrøra	Jutulrøra Complex
002	-72° 14.53320'	-00° 24.51984'	Jutulrøra	Jutulrøra Complex
003	-72° 15.55074'	-00° 23.43654'	Jutulrøra	Jutulrøra Complex
004	-72° 16.36716'	00° 45.78492'	Fuglefjellet	Jutulrøra Complex
005	-72° 16.43184'	00° 45.64284'	Fuglefjellet	Jutulrøra Complex
006	-72° 16.49400'	00° 45.51120'	Fuglefjellet	Jutulrøra Complex
007	-72° 17.52780'	00° 48.87696'	Fuglefjellet	Fuglefjellet Complex
008	-72° 17.67594'	00° 48.23184'	Fuglefjellet	Fuglefjellet Complex
009	-72° 17.73414'	00° 48.26166'	Fuglefjellet	Fuglefjellet Complex
010	-72° 18.02766'	00° 48.85932'	SH 1630	Jutulrøra Complex
011	-72° 19.61316'	00° 59.92656'	Salknappen	Rootshorga Complex
012	-72° 19.60734'	00° 59.96112'	Salknappen	Rootshorga Complex
013	-72° 19.67082'	00° 58.82412'	Salknappen	Rootshorga Complex
014	-72° 17.35068'	00° 18.66756'	Roerkulten	Jutulrøra Complex
015	-72° 17.47626'	00° 18.90510'	Roerkulten	Jutulrøra Complex
016	-72° 17.49738'	00° 19.02360'	Roerkulten	Jutulrøra Complex
017	-72° 12.52434'	01° 12.89556'	Vendeholten	Rootshorga Complex
018	-72° 12.42594'	01° 12.66474'	Vendeholten	Rootshorga Complex
019	-72° 12.29142'	01° 11.82006'	Vendeholten	Rootshorga Complex
020	-72° 12.31764'	01° 12.16584'	Vendeholten	Rootshorga Complex
021	-72° 13.17762'	00° 47.13498'	Dvergen	Jutulrøra Complex
022	-72° 12.92310'	00° 47.28408'	Dvergen	Fuglefjellet Complex
023	-72° 12.96258'	00° 47.48766'	Dvergen	Fuglefjellet Complex
024	-72° 13.05330'	00° 47.43096'	Dvergen	Fuglefjellet Complex
025	-72° 20.49516'	00° 45.72564'	Kivithovden	Fuglefjellet Complex
026	-72° 20.39454'	00° 45.85740'	Kivithovden	Fuglefjellet Complex
027	-72° 20.73858'	00° 45.56712'	Kivithovden	Fuglefjellet Complex
028	-72° 18.95136'	00° 48.60306'	Kivithovden	Fuglefjellet Complex
029	-72° 19.00080'	00° 48.62856'	Kivithovden	Fuglefjellet Complex

030	-72° 20.88846'	00° 45.50538'	Kivithovden	Fuglefjellet Complex
031	-72° 21.10584'	00° 45.57678'	Kivithovden	Fuglefjellet Complex
032	-72° 21.14658'	00° 40.86180'	Dyna	Fuglefjellet Complex
033	-72° 05.65986'	01° 13.39008'	Dyna	Fuglefjellet Complex
034	-72° 05.42370'	01° 12.92400'	Dyna	Fuglefjellet Complex
035	-72° 05.64030'	01° 13.06674'	Tua	Rootshorga Complex
036	-72° 05.45850'	01° 22.15578'	Brattskarvet	Brattskarvet intrusion
037	-72° 23.46492'	00° 50.74002'	Kivitjølen	Rootshorga Complex
038	-72° 25.78518'	00° 32.59428'	Gordonnuten	Fuglefjellet Complex
039	-72° 25.73922'	00° 32.68830'	Gordonnuten	Fuglefjellet Complex
040	-72° 27.01974'	00° 35.74422'	Gordonnuten	Fuglefjellet Complex
041	-72° 26.96586'	00° 35.51466'	Gordonnuten	Fuglefjellet Complex
042	-72° 10.24524'	00 ° 00.57342'	Tvora	Jutulrøra Complex
043	-72° 09.81924'	-00° 14.80770'	Straumsvola	Jutulrøra Complex
044	-72° 09.74532'	-00° 14.87898'	Straumsvola	Jutulrøra Complex
045	-72° 32.13114'	00° 23.28630'	Skarsnuten	Fuglefjellet Complex
046	-72° 32.12562'	00° 23.08632'	Skarsnuten	Fuglefjellet Complex
047	-72° 32.24808'	00° 23.21208'	Skarsnuten	Fuglefjellet Complex
048	-72° 32.32260'	00° 23.53992'	Skarsnuten	Fuglefjellet Complex
049	-72° 30.41130'	00° 22.92066'	Skarsnuten	Fuglefjellet Complex
050	-72° 32.42838'	00° 23.10570'	Skarsnuten	Fuglefjellet Complex
051	-72° 32.46762'	00° 23.09844'	Skarsnuten	Fuglefjellet Complex
052	-72° 32.55282'	00° 23.27604'	Skarsnuten	Fuglefjellet Complex
053	-72° 32.48178'	00° 23.10486'	Skarsnuten	Fuglefjellet Complex
054	-72° 26.92878'	00° 19.93794'	Kvassknatten	Jutulrøra Complex
055	-72° 26.90064'	00° 19.96962'	Kvassknatten	Jutulrøra Complex
056	-72° 26.84952'	00° 20.22468'	Kvassknatten	Jutulrøra Complex
057	-72° 27.38790'	00° 16.40196'	SH 1725	Jutulrøra Complex
058	-72° 27.39984'	00° 16.31496'	SH 1725	Jutulrøra Complex
059	-72° 27.53706'	00° 16.05420'	SH 1725	Jutulrøra Complex
060	-72° 27.58116'	00° 15.67236'	SH 1725	Jutulrøra Complex
061	-72° 27.69786'	00° 15.22104'	SH 1725	Fuglefjellet Complex
062	-72° 27.69366'	00° 14.98962'	SH 1725	Jutulrøra Complex
063	-72° 30.77838'	00° 23.25432'	Skarsnuten	Late Proterozoic Intrusions

064	-72° 30.54714'	00° 22.93674'	Skarsnuten	Fuglefjellet Complex
065	-72° 30.96954'	00° 23.21970'	Skarsnuten	Fuglefjellet Complex
066	-72° 30.84636'	00° 23.07120'	Skarsnuten	Fuglefjellet Complex
067	-72° 31.06410'	00° 23.04762'	Skarsnuten	Late Proterozoic Intrusions
068	-72° 25.98336'	00° 34.23162'	Gordonnuten	Fuglefjellet Complex
069	-72° 26.59302'	00° 35.93034'	Gordonnuten	Fuglefjellet Complex
070	-72° 42.55440'	00° 18.30846'	Nupskåpa	Rootshorga Complex
071	-72° 42.52884'	00° 18.24204'	Nupskåpa	Rootshorga Complex
072	-72° 42.34386'	00° 17.57004'	Nupskåpa	Rootshorga Complex
073	-72° 42.43836'	00° 14.32938'	Nupskåpa	Rootshorga Complex
074	-72° 42.31812'	00° 14.42262'	Nupskåpa	Rootshorga Complex
075	-72° 39.45606'	00° 11.83098'	Alanpiggen	Rootshorga Complex
076	-72° 39.39300'	00° 11.72142'	Alanpiggen	Rootshorga Complex
077	-72° 39.11628'	00° 09.82782'	Alanpiggen	Rootshorga Complex
078	-72° 39.01392'	00° 09.56280'	Alanpiggen	Rootshorga Complex
079	-72° 40.44384'	00° 10.43694'	Alanpiggen	Rootshorga Complex
080	-72° 40.78848'	00° 10.07418'	Alanpiggen	Middle Proterozoic Intrusions
081	-72° 21.06984'	00° 44.56206'	Kivitjølen	Fuglefjellet Complex
082	-72° 21.41820'	00° 44.55774'	Kivitjølen	Fuglefjellet Complex
083	-72° 32.58660'	00° 26.31174'	Rootshorga	Middle Proterozoic Intrusions
084	-72° 32.82042'	00° 27.26466'	Rootshorga	Rootshorga Complex
085	-72° 32.35878'	00° 25.97784'	Rootshorga	Middle Proterozoic Intrusions
086	-72° 32.64144'	00° 24.56448'	Rootshorga	Middle Proterozoic Intrusions
087	-72° 34.53258'	00° 31.93788'	Rootshorga	Middle Proterozoic Intrusions
088	-72° 34.49844'	00° 31.91274'	Rootshorga	Middle Proterozoic Intrusions

In this section the field observations of each nunatak visited will be discussed. As standard and for ease of reference, the way points and granitoid samples taken at each nunatak will be listed in point form under the nunatak's name. In addition, a location of the nunatak being discussed will be displayed on a reduced version of the attached map, to the right of the nunatak's name. Descriptions also include field photographs where relevant or considered interesting and stereonets of poles to the orientation of granitoid sheets measures there.

Dalmatian Granites are always shown in red and to the left of Salknappen Pegmatites (in blue) where measurements for both suites are available.

Some nunataks toward the West are removed from the rest of the mountain range.
These locations include Joungane, Storjoen, Straumsvola, Brekkerista, Tvora, Jutulrøra and Roerkulten. These nunataks will be discussed first; followed by the rest of the nunataks, in order of increasing latitude (starting with Brattskarvet).

A2.1 Straumsvola:

Straumsvola:

Way points: 043 and 044.

Samples: none

Hosts: Jutulrøra Complex

Straumsvola is composed of banded gneisses of the Jutulrøra Complex, with notable mafic boudins. Orientations of pale granitoids were taken; these granitoids appear similar to SP (figure 15). Location, not entirely obvious appearance, and a lack of available chemical data reduces certainty of the classification of these sheets.

Figure A2.1: Field photograph of granitoid sheets at Straumsvola.

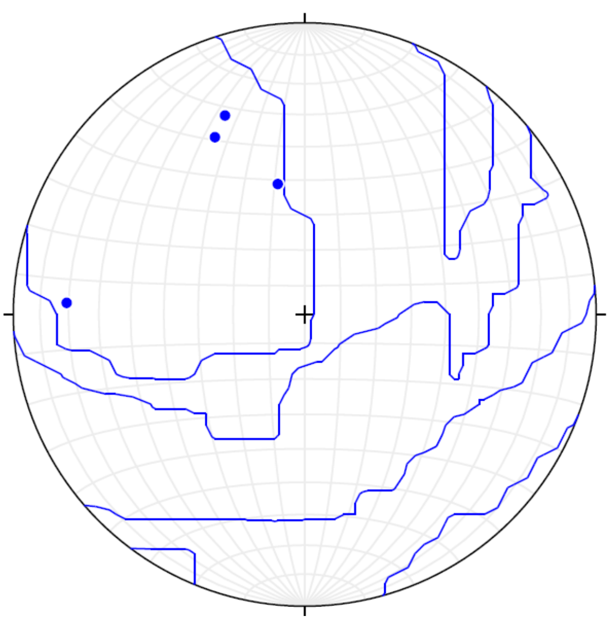

Figure A2.2: Stereonet showing poles to Salknappen Pegmatite sheets at Straumsvola. Orientations are not typical of granitoids hosted by the Jutulrøra complex (typically dip SW).

A2.2 Jutulrøra:

Way points: 001, 002 and 003.

Samples: none

Hosts: Jutulrøra Complex

This nunatak is composed mostly of Jutulrøra Complex quartz-feldspar gneiss. As shown in Figure A2.3, Jutulrøra hosts many Dalmatian Granite sheets (and pegmatitic Dalmatian granites. En echelon margins and branching observed in granite.

Note: (with reference to original field notes) not all distinctions have become evident early into fieldwork, so sheets were classified by field photographs.

Figure A2.3: Showing the prevalence of Dalmatian Granite at Way Point 002.

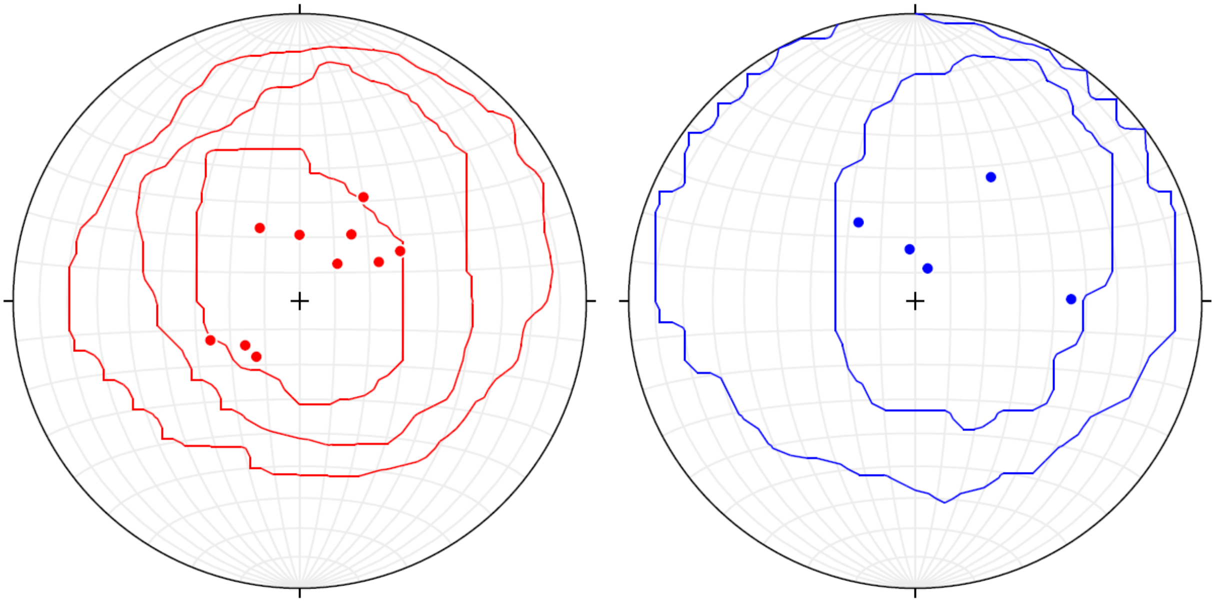

Figure A2.4: Stereonet showing poles to granitoid sheets at Jutulrøra. Orientations of granitoid sheets are similar to other granitoids hosted by the Jutulrøra Complex.

A2.3 Tvora:

Way point: 042

Samples: none

Hosts: Jutulrøra Complex

A small outcrop composed of banded gneiss (Jutulrøra Complex) showing interference folds. A few Salknappen Pegmatites noted and measured (figure 17).

Figure A2.5: Showing uncertain granitoid (probably Salknappen Pegmatite) at Tvora.

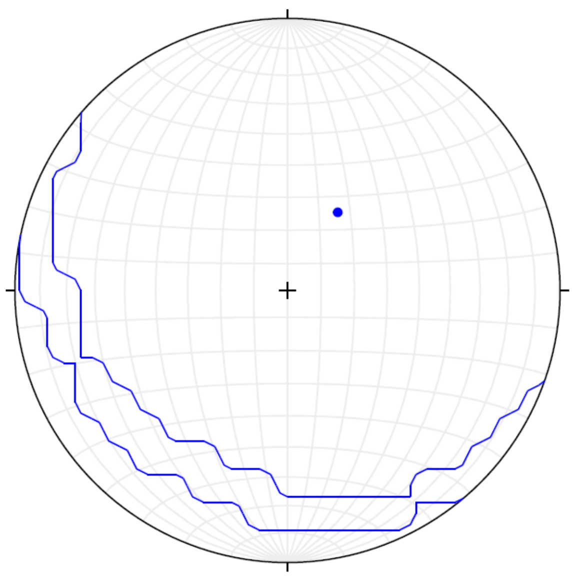

Figure A2.6: Stereonet showing a pole to the Salknappen Pegmatite measured at Tvora. The orientation of the single granitoid sheet measured is similar to other granitoids hosted by the Jutulrøra Complex. The vein was thin and not identified with great certainty.

.

A2.4 Roerkulten:

Way points: 014, 015 and 016.

Sample: 014aB and 014bC.

Hosts: Jutulrøra Complex

This nunatak is composed of quartz-feldspar gneiss of the Jutulrøra Complex. However, a portion of the outcrop is composed of a large (~100m) granite sheet which predates the granitoids in this study (Figure A2.7). Figure A2.8 shows the opportunistic nature of Dalmatian Granites, with an example of a Salknappen Pegmatite being intruded by a Dalmatian Granite along its strike. A significant proportion of the Dalmatian Granite at this outcrop is pegmatitic.

Figure A2.7: Showing the lithology of the outcrop investigated at Roerkulten.

Figure A2.8: Dalmatian Granite intruding along a Salknappen Pegmatite at Roerkulten.

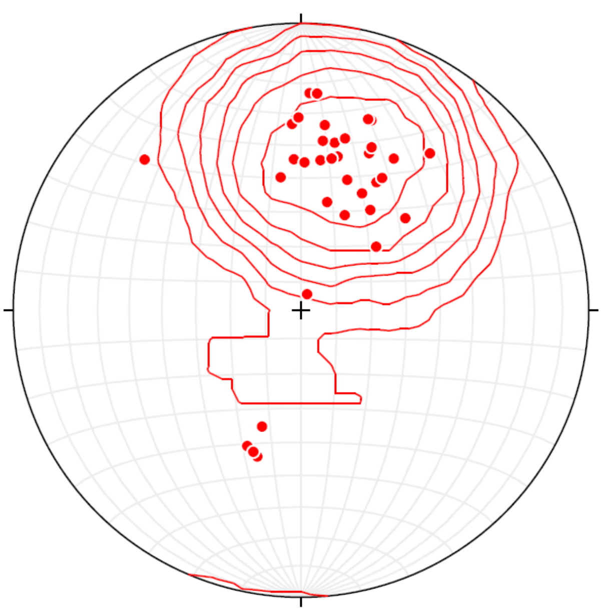

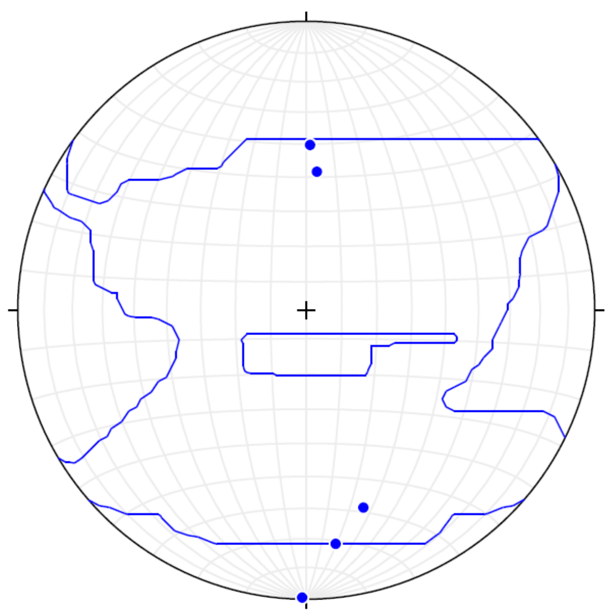

Figure A2.9: Stereonet showing poles to granitoid sheets at Roerkulten. Orientations of granitoid sheets are similar to other granitoids hosted by the Jutulrøra Complex. Salknappen Pegmatites are scarce in western HU Sverdrupfjella.

A2.5 Brattskarvet:

Way point: 036

Sample: 036aC

Hosts: Intrusion

Work was done on the ridge extending northward from Brattskarvet. Country rock is mapped as Brattskarvet granite of the Brattskarvet pluton (which is what this nunatak is predominantly composed of).

However, the sample (of the country rock) taken does not chemically classify as a granite. The country rock is felsic, but has a high proportion of mafic minerals (hornblende); shown in figure A2.10. This area has thin sheets of Dalmatian Granite, Salknappen Pegmatite, syenite and grey aplite. Vertical “dykes” of amphibolite (considered a metamorphosed mafic intrusion) also occur here.

Figure A2.10: Showing the hornblende-rich country rock and thin sheets at Way Point 036.

A2.6 Tua:

Way points: 033, 034 and 035,

Samples: none

Hosts: Rootshorga Complex

This small nunatak is composed of felsic paragneiss of the Rootshorga Complex Felsic gneiss, with fabric evident in the few mafic minerals. Few granitoids noted.

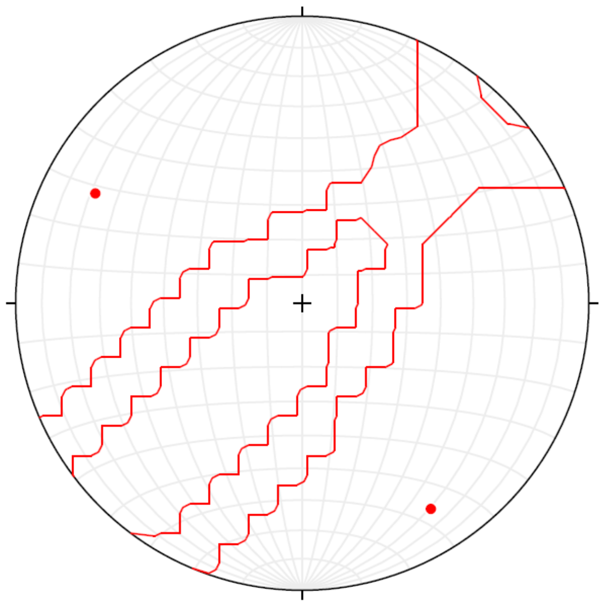

Figure A2.11: Stereonet showing poles to granitoids at Tua. The granitoid orientations from Tua are too few to compare properly and are not distinctly similar or dissimilar to other granitoids hosted by the Rootshorga Complex.

A2.7 Vendeholten:

Way points: 017, 018, 019 and 020.

Samples: 017aC

Hosts: Rootshorga Complex

The outcrops investigated at Vendeholten are composed of Felsic paragneiss (Rootshorga Complex). Many Dalmatian Granites and Salknappen Pegmatites noted and measured.

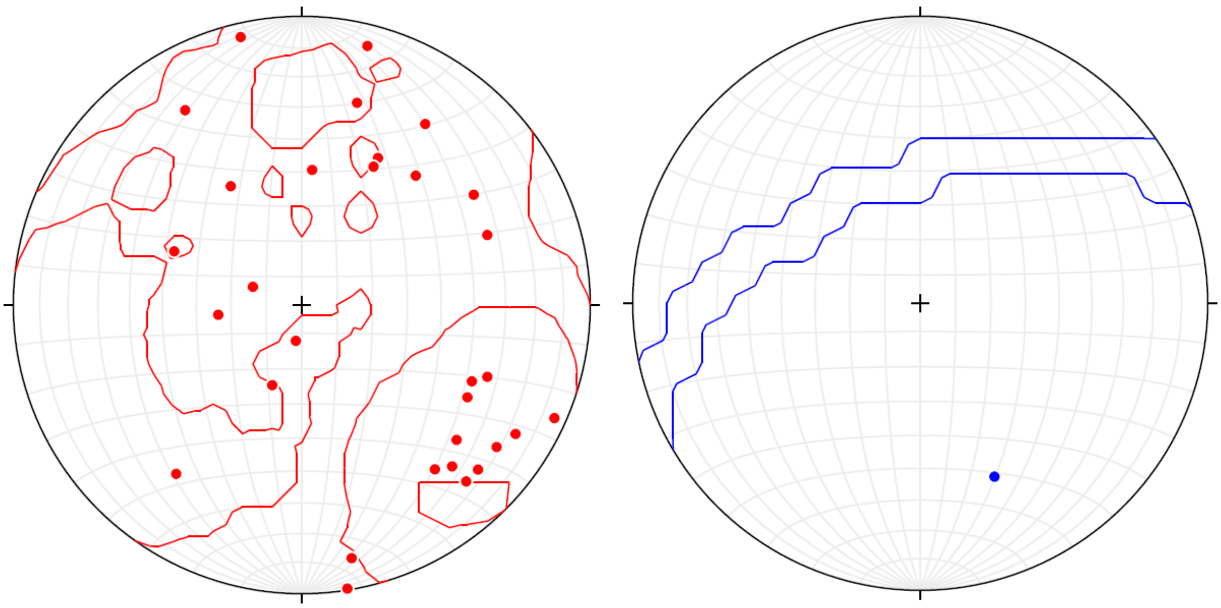

Figure A2.12: Stereonet showing poles to granitoids at Vendeholten. Orientations of some Dalmatian Granite sheets are similar to other Dalmatian Granite sheets hosted by the Rootshorga Complex, but there is a cluster with an opposite dip directions to the bulk of Dalmatian Granites hosted by the Rootshorga Complex.

A2.8 Dvergen:

Way points: 022, 023 and 024.

Samples: 021aA

Hosts: Jutulrøra Complex and Fuglefjellet Complex

Dvergen is a small nunatak composed of Jutulrøra Complex banded gneiss and Fuglefjellet Complex marble. Dalmatian Granites and Salknappen Pegmatites noted and measured. Figure 2.11 shows a Dalmatian Granite crosscutting folding, indicating that Dalmatian granites were emplaced after deformation. Unlike Dalmatian Granites hosted in more competent rocks, but like Dalmatian Granites hosted in marbles at other locations, Dalmatian granite hosted in Marble shows some deformation.

Figure A2.13: Showing a field relationship between Dalmatian Granite and deformation.

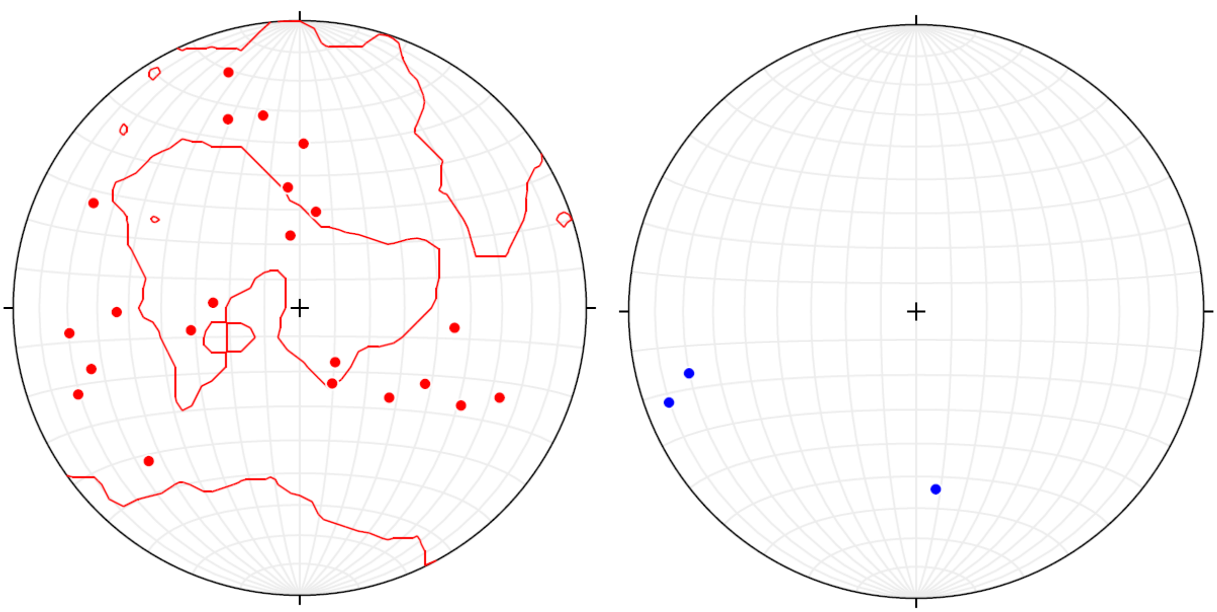

Figure A2.14: Stereonet showing poles to granitoids at Dvergen. Orientations of granitoid sheets are similar to other granitoids hosted by the Fuglefjellet Complex.

A2.9 Fuglefjellet:

Way points: 004, 005, 006, 007, 008 and 009

Samples: 004aC, 004cJ, 004dI, 005aA, 007aB, 008aC and 008dG.

Hosts: Jutulrøra Complex and Fuglefjellet Complex

Fuglefjellet is composed predominantly of marble (Fuglefjellet Complex), interlayered with calc-silicate gneiss. Fuglefjellet also host outcrops of Jutulrøra banded gneiss. Dextral displacement of Salknappen Pegmatite by Dalmatian Granite (or the plane that the Dalmatian Granite intruded along) was noted (figure 22).

Figure A2.15: showing dextral displacement of a Salknappen Pegmatite along a Dalmatian Granite. Photo facing ~W and taken at Fuglefjellet.

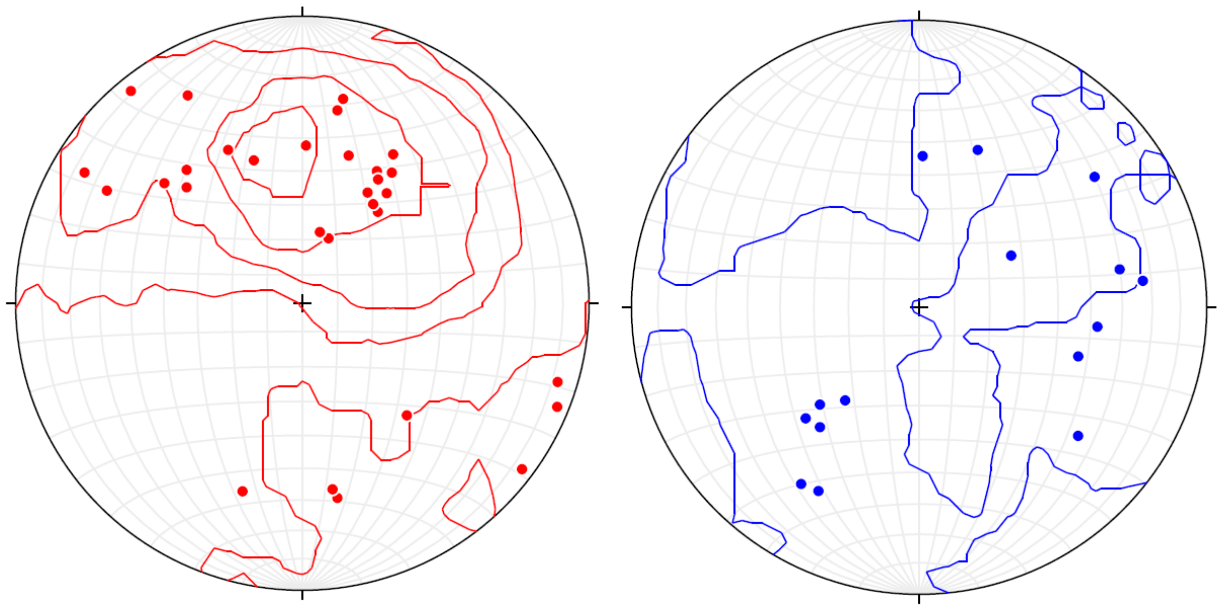

Figure A2.16: Stereonet showing poles to granitoids at Fuglefjellet. Orientations of granitoid sheets are similar to other granitoids hosted by the Fuglefjellet Complex.

A2.10 Salknappen:

Way points: 011, 012 and 013.

Samples: 012aD, 012bE and 013aE.

Hosts: Rootshorga Complex

Salknappen is composed of felsic paragneiss (Rootshorga Complex) with abundant garnet. Boudins of amphibolite, Dalmatian Granites and Salknappen Pegmatites are pervasive. This location is where the difference between Salknappen Pegmatites and Dalmatian Granites is most striking and the difference between the granitoids was noted; this is illustrated well by Figure A2.17 (shown again in this section, for convenience. For this work, Salknappen is considered the type-locality of Salknappen Pegmatites. Displacement of Salknappen Pegmatites was also noted the (also visible in Figure 2.17), this displacement was top to the SE.

Figure A2.17: Field photograph (taken at Salknappen) shown again in this section for convenience.

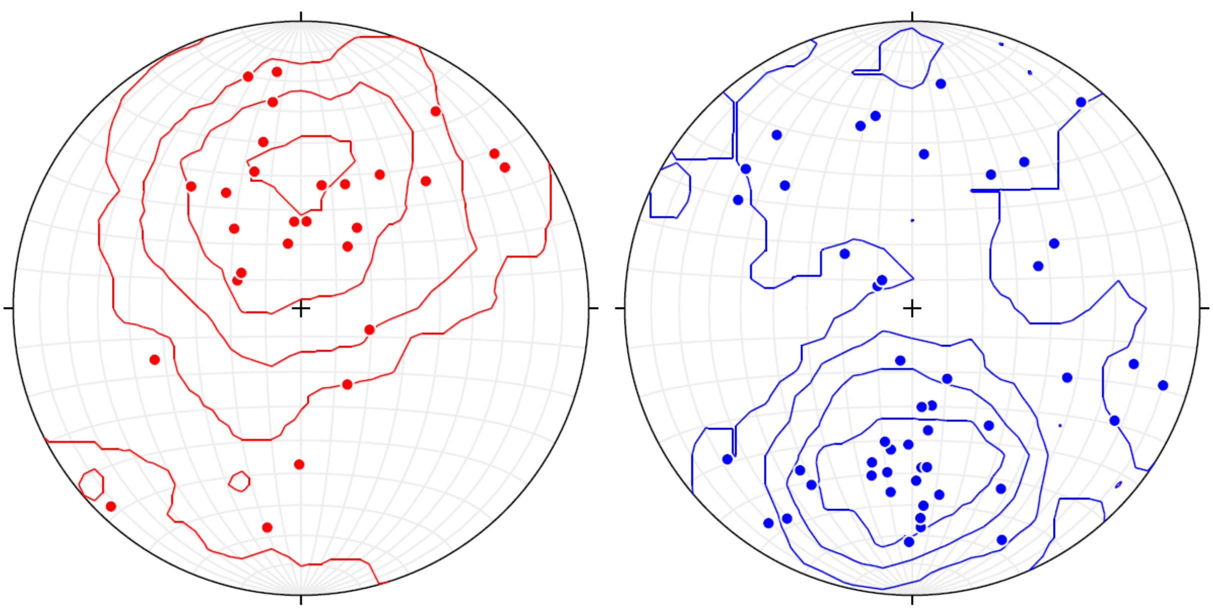

Figure A2.18: Stereonet showing poles to granitoids at Salknappen. Orientations of granitoid sheets are similar to other granitoids hosted by the Rootshorga Complex.

A2.11 Spot Height 1630:

Way point: 010

Samples: none

Hosts: Jutulrøra Complex

Spot Height 1630 is a small outcrop where a Dalmatian Granite sheet crosscuts (with some displacement) thin Salknappen Pegmatites (figure 23). This outcrop is composed of Jutulrøra Complex quartz-feldspar gneiss.

Figure A2.19: Showing the field relationship between Dalmatian Granites and Salknappen Pegmatites (thin veins) at Spot Height 1630.

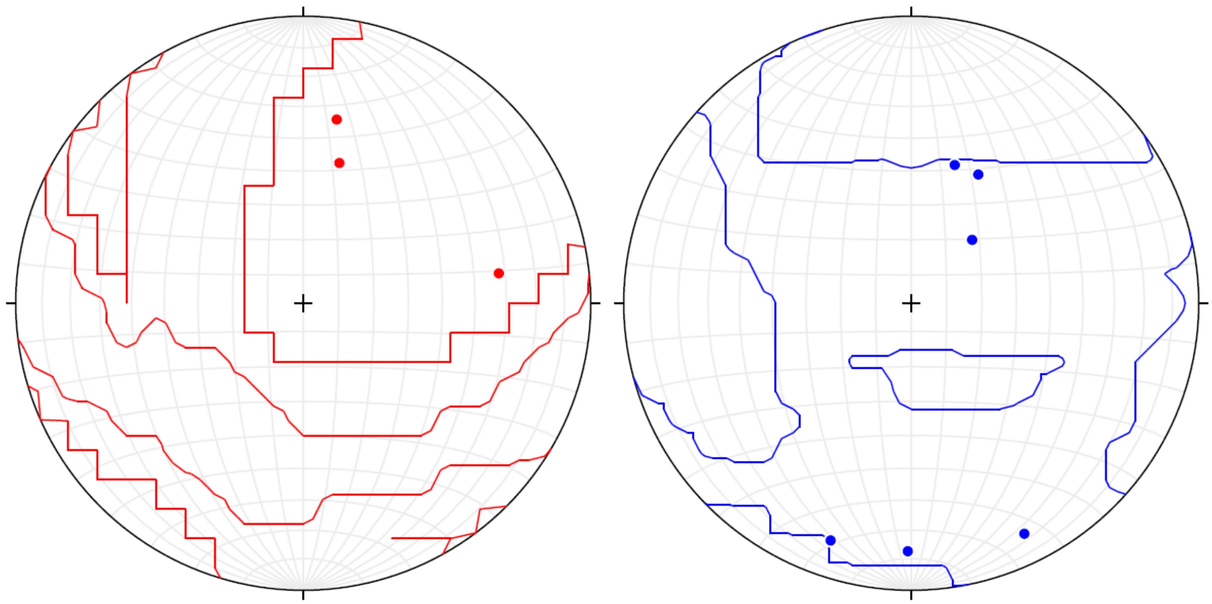

Figure A2.20: Stereonet showing poles to granitoids at Spot Height 1630. Orientations of granitoid sheets are similar to other granitoids hosted by the Jutulrøra Complex, though not much data is available at this location.

A2.12 Kivithovden:

Way points: 025, 026, 027, 028, 029, 030 and 031.

Samples: 027aA, 028aX, 030aA and 030bA.

Hosts: Fuglefjellet Complex

The outcrops studied at Kivithovden are composed of the pelitic gneiss, marble and calc-silicate gneiss of the Fuglefjellet Complex. Deformation of Dalmatian Granites hosted in marbles was noted. Figure 2.21 shows dextral shear evident in granites outcropping in marble. Folding of Dalmatian Granite was noted at Way Point 030 and a sample was taken for geochronology (Figure 2.22).

Figure A2.21: Sigmoidal tension gashes displayed by Dalmatian Granite in hosted in marble at Kivithovden.

Figure A2.22: Folded Dalmatian Granite; sample 030aA was taken here.

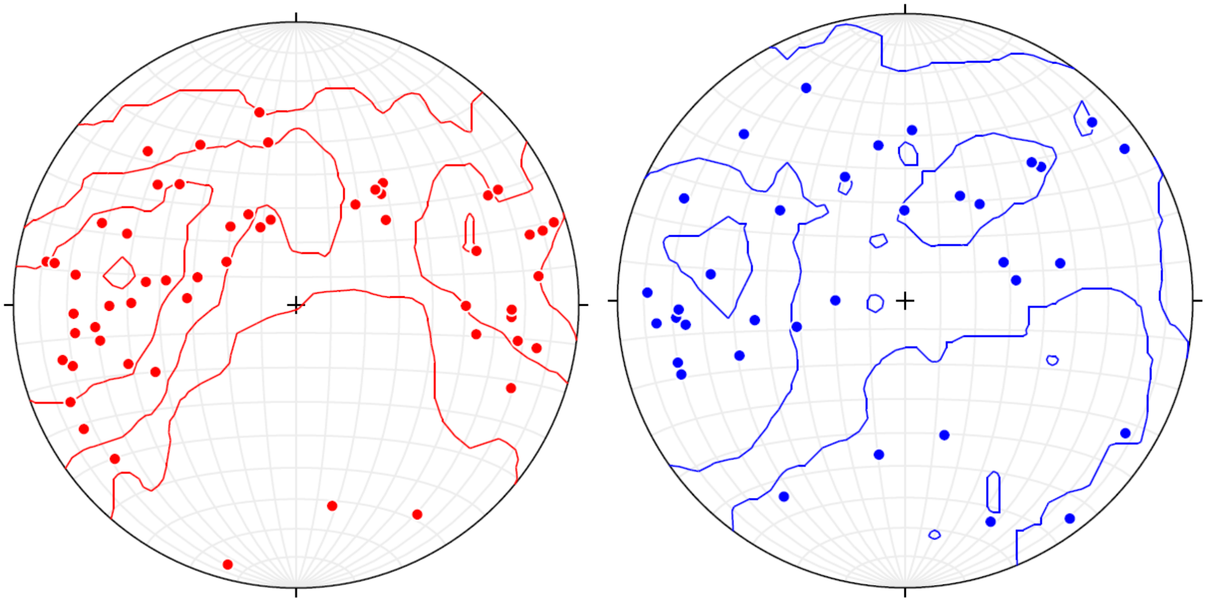

Figure A2.23: Stereonet showing poles to granitoids at Kivithovden. Orientations of granitoid sheets are similar to other granitoids hosted by the Fuglefjellet Complex.

A2.13 Dyna:

Way points: 032, 033 and 034.

Samples: none

Hosts: Fuglefjellet Complex

Dyna is composed of pelitic gneiss from the Fuglefjellet Complex. Dalmatian Granites and a few Salknappen Pegmatites were noted and measured.

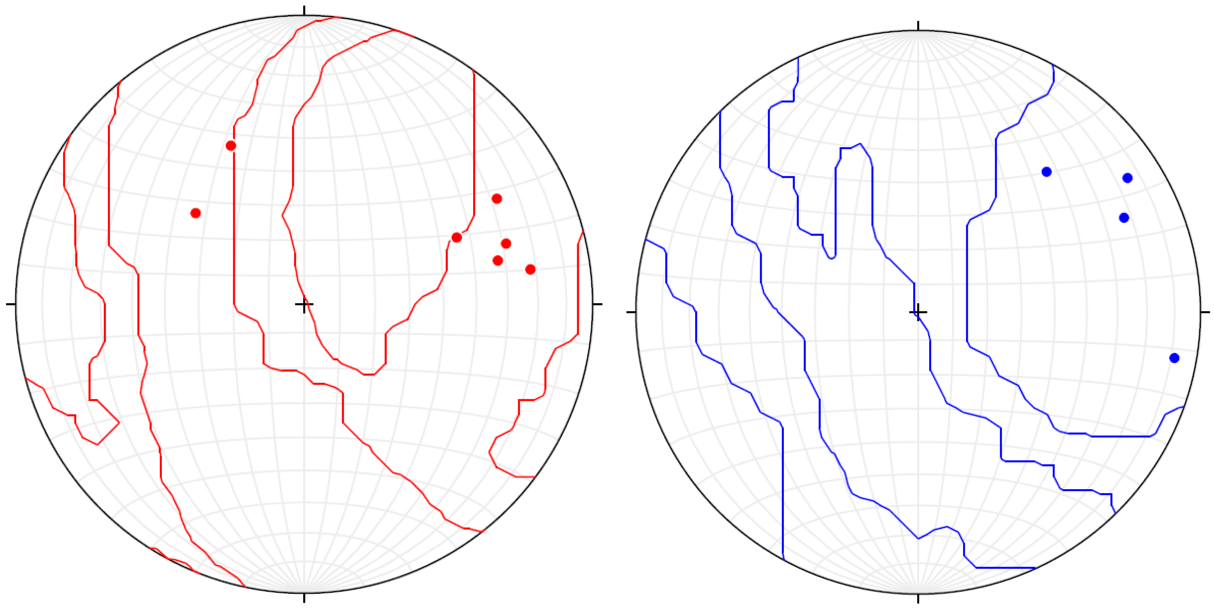

Figure A2.24: Stereonet showing poles to granitoids at Dyna. Orientations of granitoid sheets are similar to other granitoids hosted by the Fuglefjellet Complex, though the data set from Dyna is too small to provide certainty.

A2.14 Kivitjølen:

Way points: 037, 081 and 082.

Samples: 082aD and 082bA.

Hosts: Rootshorga Complex

This nunatak hosts both Fuglefjellet Complex and Rootshorga Complex rocks (pelitic gneiss and felsic paragneiss, respectively). Dalmatian granites and Salknappen Pegmatites hosted in pelitic gneiss were noted and measured during the first field season. Salknappen Pegmatites involved in a shear zone were investigated in the second field season (Figure A2.25). The involvement of the granitoid sheet in the shear makes it possible to date the shear, unfortunately project constraints and scope did not allow for further work regarding the age of this shear zone.

Figure A2.25: showing a Salknappen Pegmatite involved in deformation.

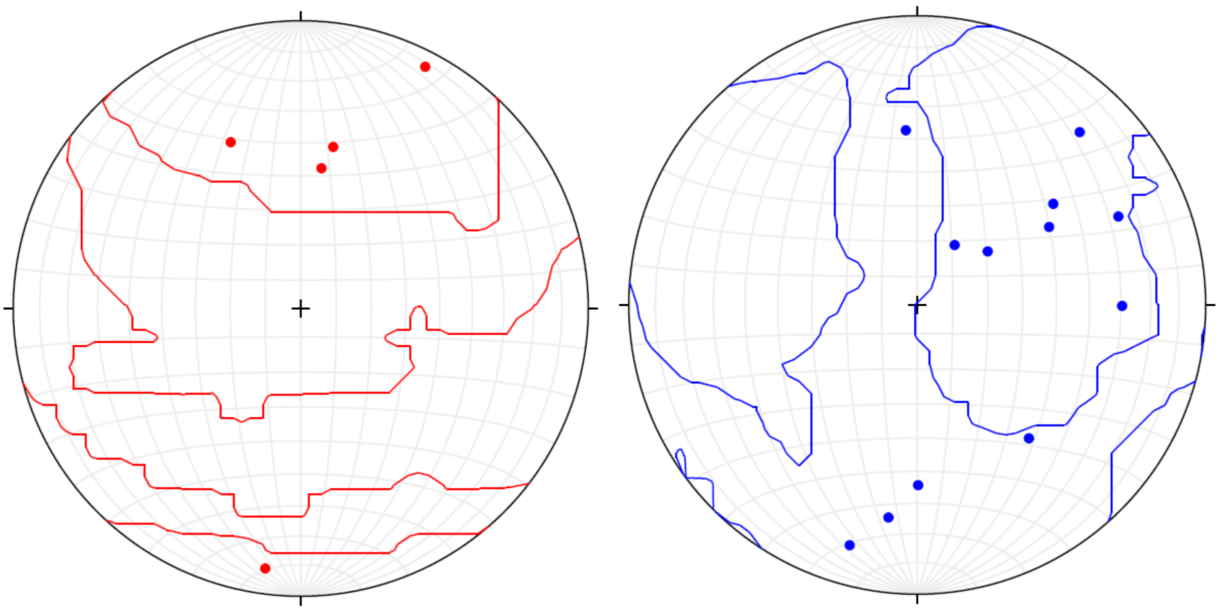

Figure A2.26: Stereonet showing poles to granitoid sheets at Kivitjølen. Orientations of granitoid sheets are not inconsistent to other granitoids hosted by the Rootshorga Complex.

A2.15 Kvassknatten:

Way points: 054, 055, 056

Samples: 054aC, 054bD, 055aX and 056aX.

Hosts: Jutulrøra Complex

Kvassknatten is a small nunatak composed of quartz-feldspar gneiss of the Jutulrøra complex. Dalmatian Granites and Salknappen Pegmatites were noted, measured and sampled.

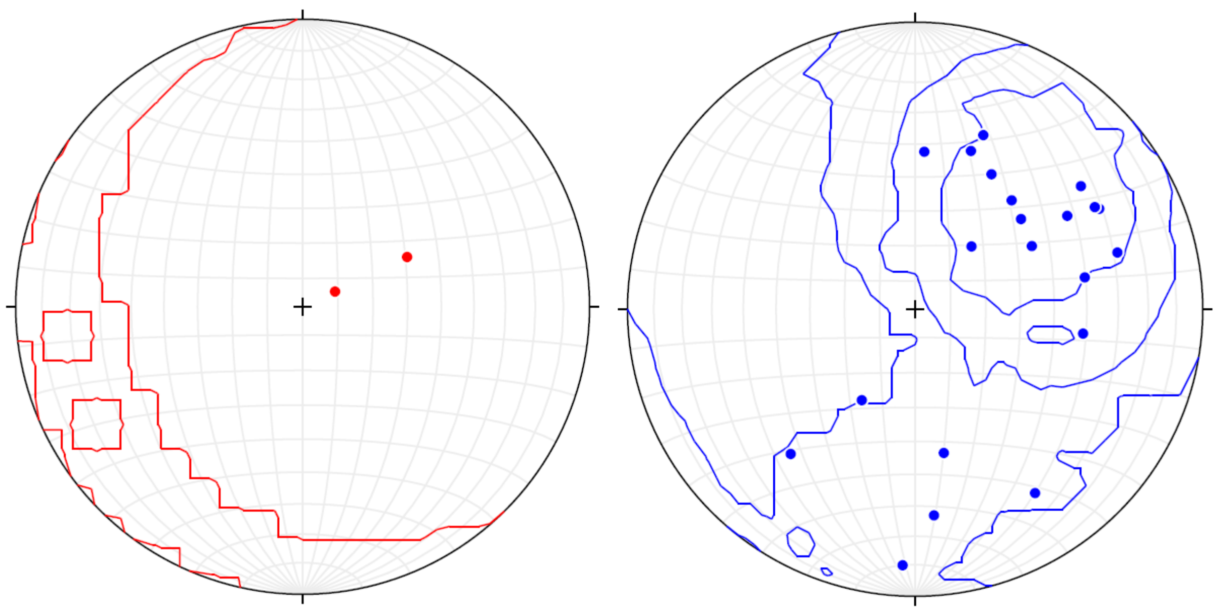

Figure A2.27: Stereonet showing poles to granitoid sheets at Kvassknatten. Orientations of granitoid sheets are similar to other granitoids hosted by the Jutulrøra Complex.

A2.16 Spot Height 1725:

Way points: 057, 058, 059, 060, 061 and 062.

Samples: 057aC, 058aAand 062aA

Hosts: Fuglefjellet Complex

Spot Height 1725 is on the same ridge as Kvassknatten and is composed of quartz-feldspar gneiss of the Jutulrøra complex and toward the southern part of the ride of Fuglefjellet Complex marble. Dalmatian Granites and Salknappen Pegmatites were noted, measured and sampled. Large blocks of perthite (hosted in a Salknappen Pegmatite) were found and sampled (sample 057aC).

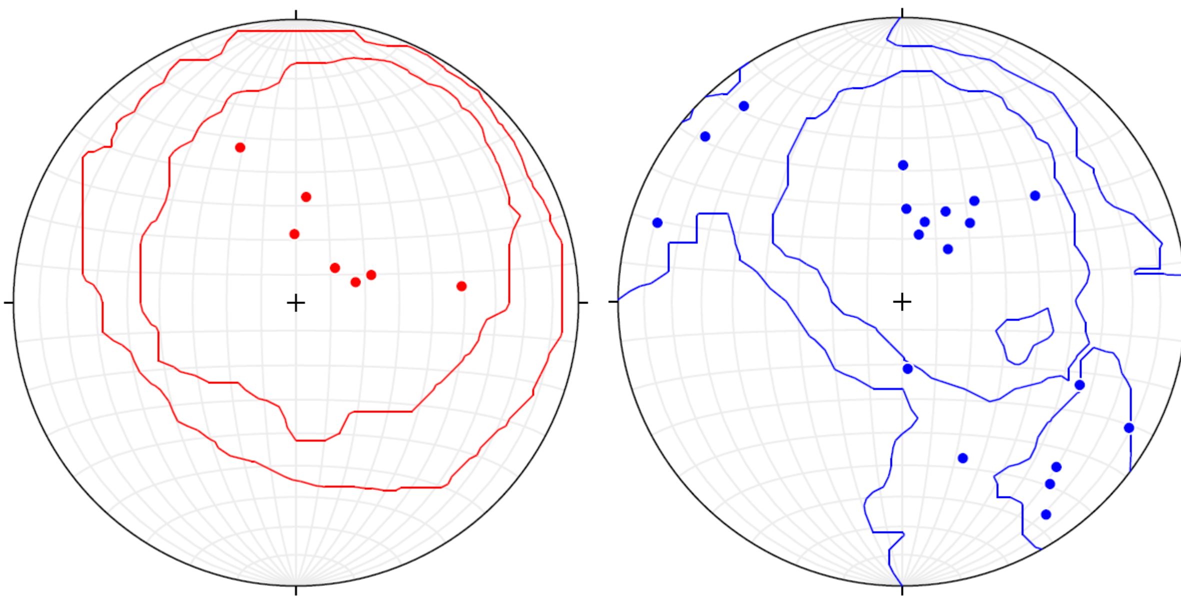

Figure A2.28: Stereonet showing poles to granitoids at Spot Height 1725. Orientations of granitoid sheets are similar to other granitoids hosted by the Fuglefjellet Complex.

A2.17 Gordonnuten:

Way points: 038, 039, 040, 041, 068 and 069.

Samples: 039aB, 040aA, 068aA, 068bB and 068cC.

Hosts: Fuglefjellet Complex

Gordonnuten was visited during both field seasons. Dalmatian Granites and Salknappen Pegmatites hosted in Fuglefjellet Complex pelitic gneiss were measured and sampled.

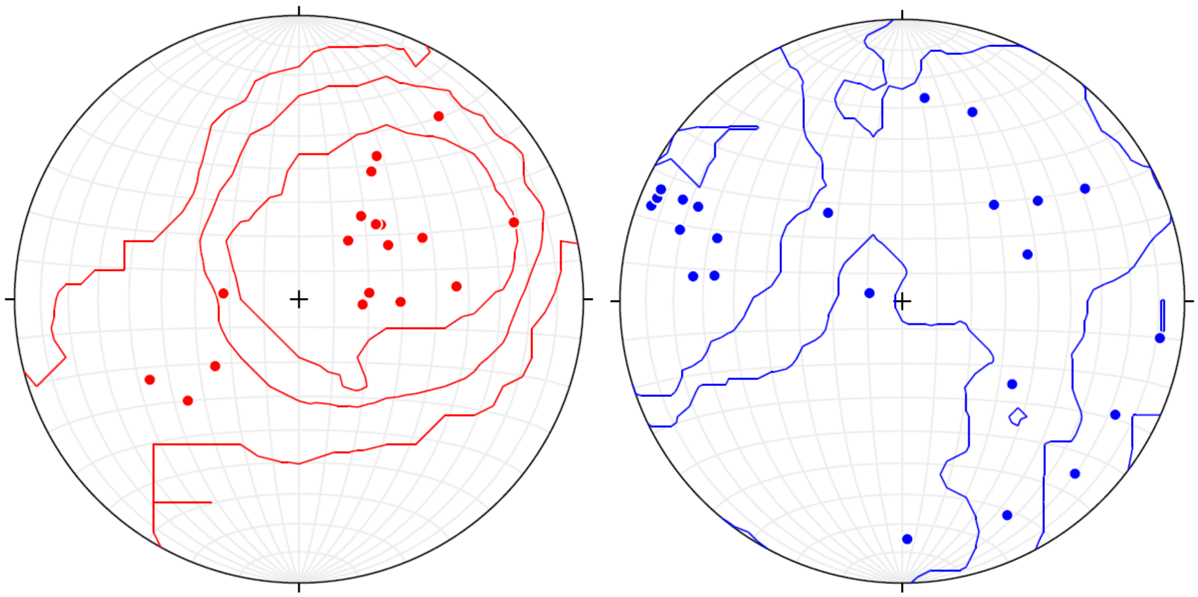

Figure A2.29: Stereonet showing poles to granitoid sheets at Gordonnuten. Orientations of granitoid sheets are similar to other granitoids hosted by the Fuglefjellet Complex.

A2.18 Skarsnuten:

Way points: 045, 046, 047, 048, 049, 050, 051, 052, 053, 063, 064, 065, 066 and 067.

Samples: 045aB, 046aA, 047aC, 048aA, 050aA, 053aC, 053bE, 064aA, 064bB, 065aA, 066aA, 067aB, 067bC and 067cF.

Hosts: Fuglefjellet Complex

Skarsnuten presented good exposure of Fuglefjellet Complex rocks and large granitoid intrusions (not the focus of this study). Due to the good outcrop, this nunatak was worked on extensively. The pre-existing granitoids were found along this ridge at Way Point 067. Top to the North displacement of Salknappen Pegmatite by Dalmatian granite noted (figure 27).

Figure A2.30: Top to the N displacement of Salknappen Pegmatite by Dalmatian granite. Facing W and taken at Skarsnuten.

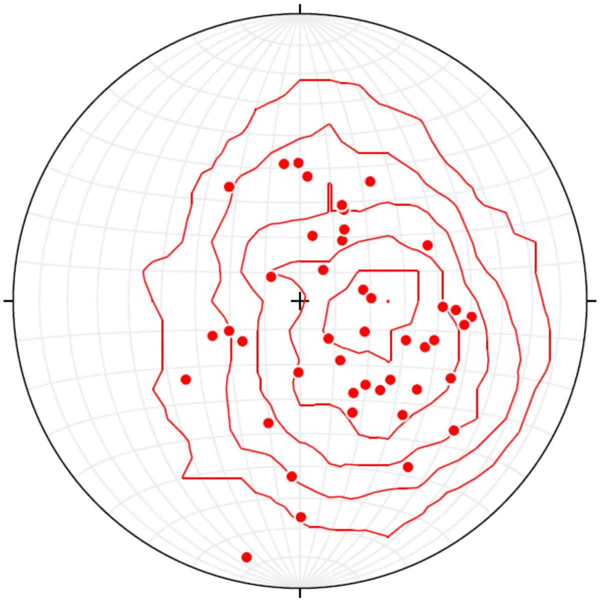

Figure A2.31: Stereonet showing poles to granitoids at Skarsnuten. Orientations of granitoid sheets are similar to other granitoids hosted by the Fuglefjellet Complex.

A2.19 Rootshorga:

Way points: 083, 084, 085, 086, 087 and 088

Samples: 083aB, 083bC, 084aC and 084bF.

Hosts: Rootshorga Complex

Rootshorga is predominantly composed of felsic paragneisses of the Rootshorga Complex. A few pre-existing granitoids identified by field relationships. Dalmatian Granites and Salknappen Pegmatites noted, measured and sampled. Dalmatian Granite intruding along Salknappen Pegmatite at Rootshorga noted (figure 28).

Figure A2.32: Dalmatian Granite intruding along Salknappen Pegmatite at Rootshorga.

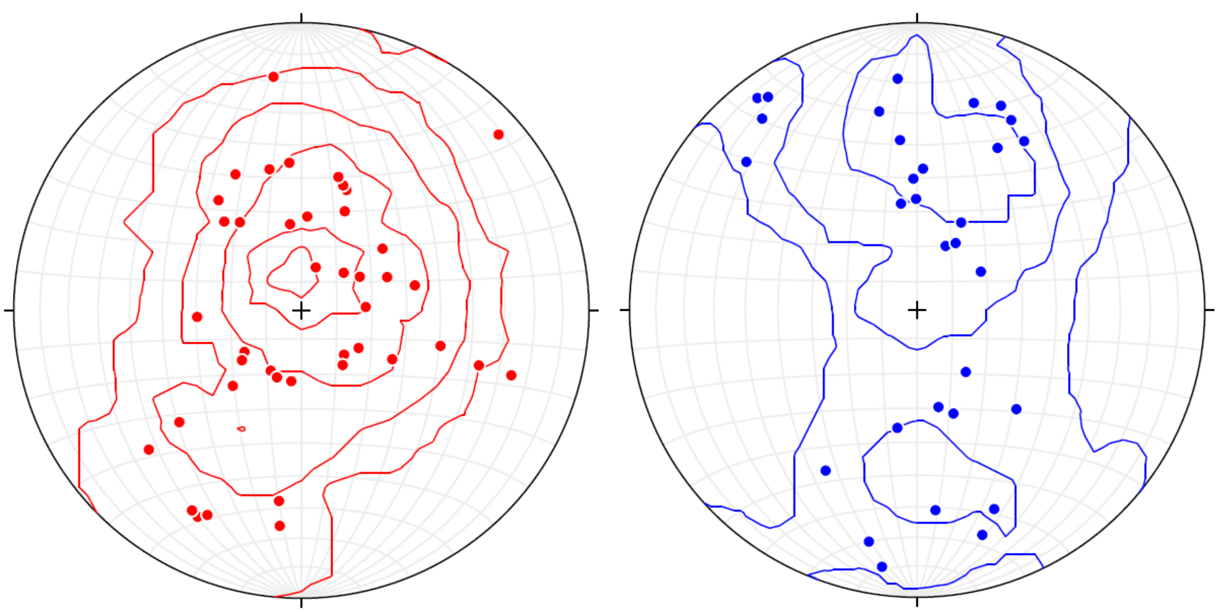

Figure A2.33: Stereonet showing poles to granitoids at Rootshorga. Orientations of granitoid sheets are similar to other granitoids hosted by the Rootshorga Complex, but both suites of granitoids have a more even distribution between predominant and conjugate dip direction.

A2.20 Alanpiggen:

Way points: 075, 076, 077, 078, 079 and 080.

Samples: 075aA, 076aA, 078aB and 080aA.

Hosts: Rootshorga Complex

This peak is composed mostly of felsic paragneiss of the Rootshorga Complex. Dalmatian Granites are sparse. Salknappen Pegmatites were measured and samples at this nunatak.

Salknappen Pegmatites hosted other (older) granites (mapped as Sveabreen granites) were measured and sampled.

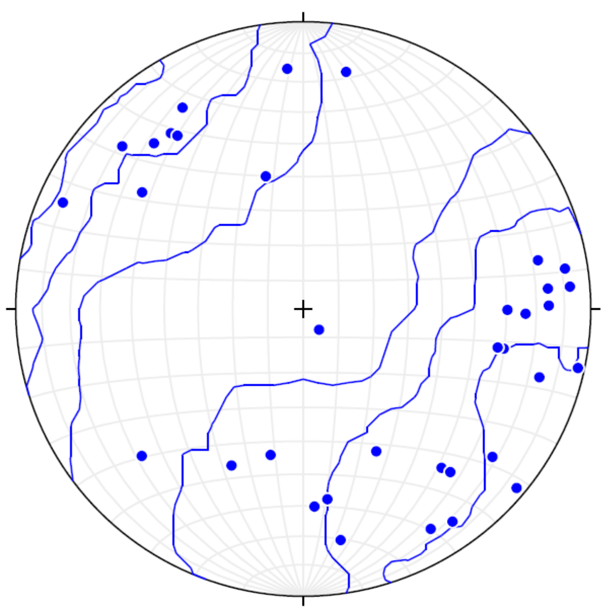

Figure A2.34: Stereonet showing poles to granitoids at Alanpiggen. Orientations of Salknappen Pegmatites are not typical to other Salknappen Pegmatites hosted by the Rootshorga Complex, but still plot within scatter. Dalmatian Granites are scarce in southern HU Sverdrupfjella.

A2.21 Nupskåpa:

Way points: 070, 071, 072, 073 and 074.

Samples: 070aB, 071aA, 072aA and 074aA.

Hosts: Rootshorga Complex

The southernmost nunatak in investigated in this study. This nunatak is composed predominantly of Rootshorga Complex rocks. Dalmatian Granites are sparse and dip steeply. A Dalmatian Granite intruding along a Salknappen Pegmatite was sampled. Salknappen pegmatites were prevalent.

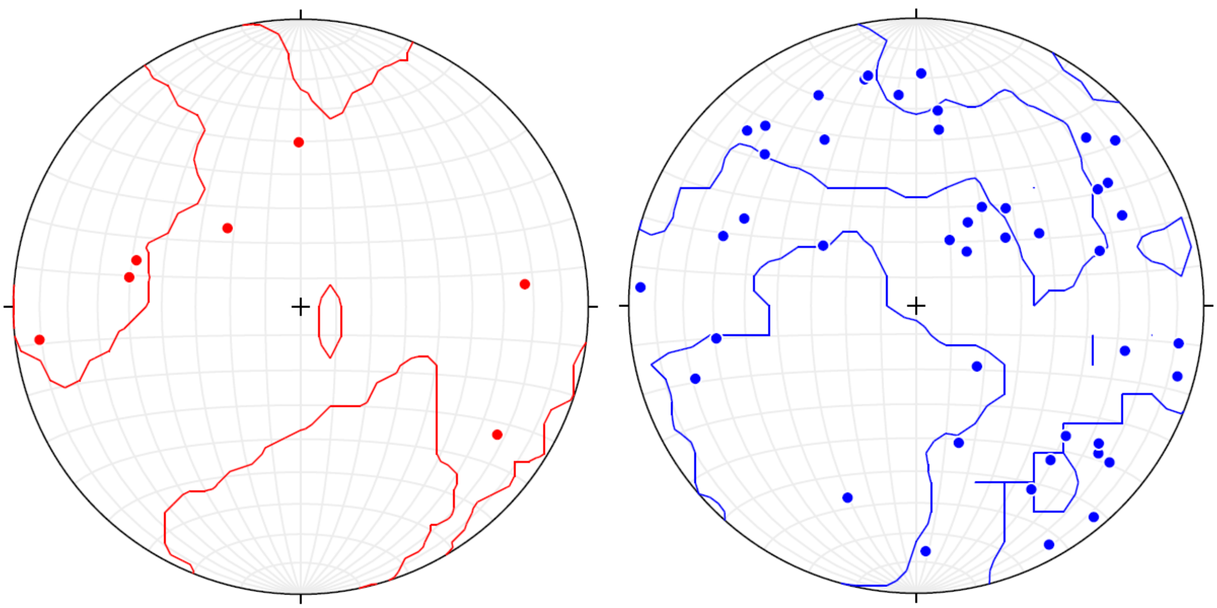

Figure A2.35: Stereonet showing poles to granitoids at Nupskåpa. Orientations of Salknappen Pegmatites are not typical to other Salknappen Pegmatites hosted by the Rootshorga Complex, but the data is within scatter for other Salknappen Pegmatites hosted by the Rootshorga Complex. Dalmatian Granites are scarce in southern HU Sverdrupfjella.

Appendix 3: Data tables

A3.1 Sample list:

Table A3.1: A list of samples taken, analysed and of which data was presented in this thesis.

Sample	Latitude	Longitude	Location	Host Formation	Classification
004aC	-72° 16.36716'	00° 45.78492'	Fuglefjellet	Jutulrøra Complex	Dalmatian Granite
004cJ	-72° 16.36716'	00° 45.78492'	Fuglefjellet	Jutulrøra Complex	Salknappen Pegmatite +Eu
005aA	-72° 16.43184'	00° 45.64284'	Fuglefjellet	Jutulrøra Complex	Dalmatian Granite
007aB	-72° 17.52780'	00° 48.87696'	Fuglefjellet	Fuglefjellet Complex	Salknappen Pegmatite -Eu
008aC	-72° 17.67594'	00° 48.23184'	Fuglefjellet	Fuglefjellet Complex	Dalmatian Granite
008dG	-72° 17.67594'	00° 48.23184'	Fuglefjellet	Fuglefjellet Complex	Salknappen Pegmatite +Eu
012aD	-72° 19.60734'	00° 59.96112'	Salknappen	Rootshorga Complex	Dalmatian Granite
012bE	-72° 19.60734'	00° 59.96112'	Salknappen	Rootshorga Complex	Salknappen Pegmatite +Eu
013aE	-72° 19.67082'	00° 58.82412'	Salknappen	Rootshorga Complex	Salknappen Pegmatite +Eu
014aB	-72° 17.35068'	00° 18.66756'	Roerkulten	Jutulrøra Complex	Dalmatian Granite
014bC	-72° 17.35068'	00° 18.66756'	Roerkulten	Jutulrøra Complex	Dalmatian Granite
017aC	-72° 12.52434'	01° 12.89556'	Vendeholten	Rootshorga Complex	Dalmatian Granite
021aA	-72° 13.17762'	00° 47.13498'	Dvergen	Jutulrøra Complex	Dalmatian Granite
027aA	-72° 20.73858'	00° 45.56712'	Kivithovden	Fuglefjellet Complex	Salknappen Pegmatite +Eu
028aX	-72° 18.95136'	00° 48.60306'	Kivithovden	Fuglefjellet Complex	Dalmatian Granite
030bA	-72° 20.88846'	00° 45.50538'	Kivithovden	Fuglefjellet Complex	Salknappen Pegmatite +Eu
039aB	-72° 25.78518'	00° 32.59428'	Gordonnuten	Fuglefjellet Complex	Salknappen Pegmatite -Eu
040aA	-72° 27.01974'	00° 35.74422'	Gordonnuten	Fuglefjellet Complex	Dalmatian Granite
045aB	-72° 32.13114'	00° 23.28630'	Skarsnuten	Fuglefjellet Complex	Salknappen Pegmatite -Eu
046aA	-72° 32.12562'	00° 23.08632'	Skarsnuten	Fuglefjellet Complex	Salknappen Pegmatite -Eu
047aC	-72° 32.24808'	00° 23.21208'	Skarsnuten	Fuglefjellet Complex	Salknappen Pegmatite +Eu
048aA	-72° 32.32260'	00° 23.53992'	Skarsnuten	Fuglefjellet Complex	Dalmatian Granite
050aA	-72° 32.42838'	00° 23.10570'	Skarsnuten	Fuglefjellet Complex	Salknappen Pegmatite +Eu
053aC	-72° 32.48178'	00° 23.10486'	Skarsnuten	Fuglefjellet Complex	Dalmatian Granite
053bE	-72° 32.48178'	00° 23.10486'	Skarsnuten	Fuglefjellet Complex	Salknappen Pegmatite +Eu
054aC	-72° 26.92878'	00° 19.93794'	Kvassknatten	Jutulrøra Complex	Salknappen Pegmatite +Eu
054bD	-72° 26.92878'	00° 19.93794'	Kvassknatten	Jutulrøra Complex	Salknappen Pegmatite +Eu
055aX	-72° 26.90064'	00° 19.96962'	Kvassknatten	Jutulrøra Complex	Dalmatian Granite
056aX	-72° 26.84952'	00° 20.22468'	Kvassknatten	Jutulrøra Complex	Salknappen Pegmatite -Eu
058aA	-72° 27.39984'	00° 16.31496'	SH 1725	Jutulrøra Complex	Salknappen Pegmatite -Eu
062aA	-72° 27.69366'	00° 14.98962'	SH 1725	Jutulrøra Complex	Salknappen Pegmatite +Eu
064aA	-72° 30.54714'	00° 22.93674'	Skarsnuten	Fuglefjellet Complex	Dalmatian Granite
064bB	-72° 30.54714'	00° 22.93674'	Skarsnuten	Fuglefjellet Complex	Dalmatian Granite
065aA	-72° 30.96954'	00° 23.21970'	Skarsnuten	Fuglefjellet Complex	Dalmatian Granite
066aA	-72° 30.84636'	00° 23.07120'	Skarsnuten	Fuglefjellet Complex	Dalmatian Granite
067aB	-72° 31.06410'	00° 23.04762'	Skarsnuten	Late Proterozoic Intrusions	Pre-existing Granitoid
067bC	-72° 31.06410'	00° 23.04762'	Skarsnuten	Late Proterozoic Intrusions	Pre-existing Granitoid
067cF	-72° 31.06410'	00° 23.04762'	Skarsnuten	Late Proterozoic Intrusions	Pre-existing Granitoid
068aA	-72° 25.98336'	00° 34.23162'	Gordonnuten	Fuglefjellet Complex	Dalmatian Granite
068bB	-72° 25.98336'	00° 34.23162'	Gordonnuten	Fuglefjellet Complex	Salknappen Pegmatite -Eu

068cC	-72° 25.98336'	00° 34.23162'	Gordonnuten	Fuglefjellet Complex	Salknappen Pegmatite -Eu
070aB	-72° 42.55440'	00° 18.30846'	Nupskåpa	Rootshorga Complex	Salknappen Pegmatite -Eu
071aA	-72° 42.52884'	00° 18.24204'	Nupskåpa	Rootshorga Complex	Salknappen Pegmatite +Eu
072aA	-72° 42.34386'	00° 17.57004'	Nupskåpa	Rootshorga Complex	Salknappen Pegmatite -Eu
075aA	-72° 39.45606'	00° 11.83098'	Alanpiggen	Rootshorga Complex	Salknappen Pegmatite -Eu
076aA	-72° 39.39300'	00° 11.72142'	Alanpiggen	Rootshorga Complex	Salknappen Pegmatite -Eu
078aB	-72° 39.01392'	00° 09.56280'	Alanpiggen	Rootshorga Complex	Salknappen Pegmatite -Eu
082aD	-72° 21.41820'	00° 44.55774'	Kivitjølen	Fuglefjellet Complex	Salknappen Pegmatite -Eu
082bA	-72° 21.41820'	00° 44.55774'	Kivitjølen	Fuglefjellet Complex	Salknappen Pegmatite -Eu
083aB	-72°°32.58660'	00° 26.31174'	Rootshorga	Middle Proterozoic Intrusions	Salknappen Pegmatite -Eu
083bC	-72° 32.58660'	00° 26.31174'	Rootshorga	Middle Proterozoic Intrusions	Salknappen Pegmatite -Eu
084aC	-72° 32.82042'	00° 27.26466'	Rootshorga	Rootshorga Complex	Dalmatian Granite
084bF	-72° 32.82042'	00° 27.26466'	Rootshorga	Rootshorga Complex	Salknappen Pegmatite -Eu

A3.2 Granitoid orientation data:

Table A3.2: orientations of granitoid sheets measured for this study.

Data #	True Azimuth	Strike	Dip	Dip Direction	Type	Location
831	126	216	59	SE	Salknappen Pegmatite	Alanpiggen
834	149	239	71	SE	Salknappen Pegmatite	Alanpiggen
835	143	233	66	SE	Salknappen Pegmatite	Alanpiggen
837	013	283	43	N	Salknappen Pegmatite	Alanpiggen
838	271	181	66	W	Salknappen Pegmatite	Alanpiggen
840	269	179	74	W	Salknappen Pegmatite	Alanpiggen
841	132	222	74	SE	Salknappen Pegmatite	Alanpiggen
781	286	196	74	W	Salknappen Pegmatite	Alanpiggen
784	270	180	60	W	Salknappen Pegmatite	Alanpiggen
785	258	168	72	W	Salknappen Pegmatite	Alanpiggen
786	265	175	82	W	Salknappen Pegmatite	Alanpiggen
787	281	191	60	W	Salknappen Pegmatite	Alanpiggen
790	190	280	73	S	Salknappen Pegmatite	Alanpiggen
795	176	266	73	S	Salknappen Pegmatite	Alanpiggen
799	333	243	46	NW	Salknappen Pegmatite	Alanpiggen
801	351	261	70	N	Salknappen Pegmatite	Alanpiggen
802	282	192	87	W	Salknappen Pegmatite	Alanpiggen
803	357	267	58	N	Salknappen Pegmatite	Alanpiggen
805	353	263	56	N	Salknappen Pegmatite	Alanpiggen
806	138	228	67	SE	Salknappen Pegmatite	Alanpiggen
807	144	234	64	SE	Salknappen Pegmatite	Alanpiggen
810	261	171	81	W	Salknappen Pegmatite	Alanpiggen
811	325	235	79	NW	Salknappen Pegmatite	Alanpiggen
812	308	218	72	NW	Salknappen Pegmatite	Alanpiggen
813	319	229	62	NW	Salknappen Pegmatite	Alanpiggen
814	114	204	81	SE	Salknappen Pegmatite	Alanpiggen
816	281	191	58	W	Salknappen Pegmatite	Alanpiggen
818	310	220	86	NW	Salknappen Pegmatite	Alanpiggen
823	323	233	07	NW	Salknappen Pegmatite	Alanpiggen
824	048	138	65	NE	Salknappen Pegmatite	Alanpiggen
825	025	115	50	NE	Salknappen Pegmatite	Alanpiggen
827	164	254	40	S	Salknappen Pegmatite	Alanpiggen
828	265	175	74	W	Salknappen Pegmatite	Alanpiggen
829	318	228	65	NW	Salknappen Pegmatite	Alanpiggen
830	330	240	77	NW	Salknappen Pegmatite	Alanpiggen
273	070	160	81	E	Salknappen Pegmatite	Dvergen
274	075	165	71	E	Salknappen Pegmatite	Dvergen
275	354	264	52	N	Salknappen Pegmatite	Dvergen

263	172	262	21	S	Dalmatian Granite	Dvergen
264	174	264	35	S	Dalmatian Granite	Dvergen
265	294	204	65	NW	Dalmatian Granite	Dvergen
266	315	225	36	NW	Dalmatian Granite	Dvergen
267	094	184	25	E	Dalmatian Granite	Dvergen
268	277	187	45	W	Dalmatian Granite	Dvergen
269	301	211	55	NW	Dalmatian Granite	Dvergen
270	337	247	23	NW	Dalmatian Granite	Dvergen
271	327	237	18	NW	Dalmatian Granite	Dvergen
272	074	164	65	E	Dalmatian Granite	Dvergen
276	181	271	48	S	Dalmatian Granite	Dvergen
277	169	259	58	S	Dalmatian Granite	Dvergen
278	159	249	60	S	Dalmatian Granite	Dvergen
279	089	179	54	E	Dalmatian Granite	Dvergen
280	301	211	42	NW	Dalmatian Granite	Dvergen
281	084	174	70	E	Dalmatian Granite	Dvergen
255	189	279	28	S	Dalmatian Granite	Dvergen
261	069	159	72	E	Dalmatian Granite	Dvergen
262	079	169	32	E	Dalmatian Granite	Dvergen
256	163	253	75	S	Dalmatian Granite	Dvergen
259	045	135	64	NE	Dalmatian Granite	Dvergen
260	117	207	70	SE	Dalmatian Granite	Dvergen
409	280	190	81	W	Salknappen Pegmatite	Dyna
411	237	147	77	SW	Salknappen Pegmatite	Dyna
415	245	155	69	SW	Salknappen Pegmatite	Dyna
416	222	132	57	SW	Salknappen Pegmatite	Dyna
403	257	167	58	W	Dalmatian Granite	Dyna
404	261	171	68	W	Dalmatian Granite	Dyna
407	130	220	41	SE	Dalmatian Granite	Dyna
408	155	245	51	SE	Dalmatian Granite	Dyna
414	241	151	65	SW	Dalmatian Granite	Dyna
419	246	156	48	SW	Dalmatian Granite	Dyna
420	253	163	62	W	Dalmatian Granite	Dyna
71	018	288	58	N	Salknappen Pegmatite	Fuglefjellet
73	350	260	58	N	Salknappen Pegmatite	Fuglefjellet
74	350	260	58	N	Salknappen Pegmatite	Fuglefjellet
75	141	231	85	SE	Salknappen Pegmatite	Fuglefjellet
76	131	221	54	SE	Salknappen Pegmatite	Fuglefjellet
69	351	261	55	N	Dalmatian Granite	Fuglefjellet
70	209	119	44	SW	Dalmatian Granite	Fuglefjellet
72	154	244	50	SE	Dalmatian Granite	Fuglefjellet
79	210	120	37	SW	Dalmatian Granite	Fuglefjellet
80	190	280	58	S	Dalmatian Granite	Fuglefjellet
81	197	287	45	S	Dalmatian Granite	Fuglefjellet
83	287	197	82	W	Dalmatian Granite	Fuglefjellet
84	292	202	85	W	Dalmatian Granite	Fuglefjellet
82	307	217	85	NW	Dalmatian Granite	Fuglefjellet
29	259	169	60	W	Salknappen Pegmatite	Fuglefjellet
34	040	130	45	NE	Salknappen Pegmatite	Fuglefjellet
35	039	129	34	NE	Salknappen Pegmatite	Fuglefjellet
36	046	136	40	NE	Salknappen Pegmatite	Fuglefjellet
37	046	136	46	NE	Salknappen Pegmatite	Fuglefjellet
42	029	119	62	NE	Salknappen Pegmatite	Fuglefjellet
43	034	124	63	NE	Salknappen Pegmatite	Fuglefjellet
44	309	219	60	NW	Salknappen Pegmatite	Fuglefjellet
53	276	186	52	W	Salknappen Pegmatite	Fuglefjellet
54	287	197	48	W	Salknappen Pegmatite	Fuglefjellet
60	181	271	44	S	Salknappen Pegmatite	Fuglefjellet
61	263	173	67	W	Salknappen Pegmatite	Fuglefjellet
62	200	110	49	S	Salknappen Pegmatite	Fuglefjellet
63	233	143	65	SW	Salknappen Pegmatite	Fuglefjellet
68	240	150	30	SW	Salknappen Pegmatite	Fuglefjellet
23	219	129	34	SW	Dalmatian Granite	Fuglefjellet

28	191	281	62	S	Dalmatian Granite	Fuglefjellet
31	317	227	44	NW	Dalmatian Granite	Fuglefjellet
32	215	125	35	SW	Dalmatian Granite	Fuglefjellet
45	151	241	72	SE	Dalmatian Granite	Fuglefjellet
46	121	211	78	SE	Dalmatian Granite	Fuglefjellet
47	120	210	68	SE	Dalmatian Granite	Fuglefjellet
48	135	225	48	SE	Dalmatian Granite	Fuglefjellet
49	139	229	52	SE	Dalmatian Granite	Fuglefjellet
50	161	251	44	S	Dalmatian Granite	Fuglefjellet
51	181	271	46	S	Dalmatian Granite	Fuglefjellet
55	211	121	51	SW	Dalmatian Granite	Fuglefjellet
56	211	121	42	SW	Dalmatian Granite	Fuglefjellet
64	217	127	40	SW	Dalmatian Granite	Fuglefjellet
65	214	124	46	SW	Dalmatian Granite	Fuglefjellet
66	201	111	20	S	Dalmatian Granite	Fuglefjellet
67	193	283	21	S	Dalmatian Granite	Fuglefjellet
443	098	188	57	E	Salknappen Pegmatite	Gordonnuten
445	115	205	69	SE	Salknappen Pegmatite	Gordonnuten
447	109	199	59	E	Salknappen Pegmatite	Gordonnuten
448	140	230	34	SE	Salknappen Pegmatite	Gordonnuten
449	108	198	72	E	Salknappen Pegmatite	Gordonnuten
450	238	148	65	SW	Salknappen Pegmatite	Gordonnuten
451	315	225	75	NW	Salknappen Pegmatite	Gordonnuten
452	200	110	61	S	Salknappen Pegmatite	Gordonnuten
453	223	133	39	SW	Salknappen Pegmatite	Gordonnuten
460	334	244	73	NW	Salknappen Pegmatite	Gordonnuten
461	105	195	10	E	Salknappen Pegmatite	Gordonnuten
462	359	269	73	N	Salknappen Pegmatite	Gordonnuten
684	115	205	75	SE	Salknappen Pegmatite	Gordonnuten
686	111	201	85	E	Salknappen Pegmatite	Gordonnuten
687	113	203	84	SE	Salknappen Pegmatite	Gordonnuten
688	278	188	81	W	Salknappen Pegmatite	Gordonnuten
693	298	208	74	NW	Salknappen Pegmatite	Gordonnuten
694	115	205	84	SE	Salknappen Pegmatite	Gordonnuten
695	097	187	64	E	Salknappen Pegmatite	Gordonnuten
701	307	217	40	NW	Salknappen Pegmatite	Gordonnuten
707	186	276	62	S	Salknappen Pegmatite	Gordonnuten
710	233	143	50	SW	Salknappen Pegmatite	Gordonnuten
711	249	159	39	W	Salknappen Pegmatite	Gordonnuten
454	062	152	50	NE	Dalmatian Granite	Gordonnuten
455	095	185	22	E	Dalmatian Granite	Gordonnuten
456	052	142	31	NE	Dalmatian Granite	Gordonnuten
457	048	138	44	NE	Dalmatian Granite	Gordonnuten
459	250	160	69	W	Dalmatian Granite	Gordonnuten
683	243	153	40	SW	Dalmatian Granite	Gordonnuten
685	208	118	48	SW	Dalmatian Granite	Gordonnuten
689	216	126	30	SW	Dalmatian Granite	Gordonnuten
690	209	119	43	SW	Dalmatian Granite	Gordonnuten
699	265	175	46	W	Dalmatian Granite	Gordonnuten
702	274	184	18	W	Dalmatian Granite	Gordonnuten
704	217	127	70	SW	Dalmatian Granite	Gordonnuten
706	271	181	29	W	Dalmatian Granite	Gordonnuten
713	227	137	32	SW	Dalmatian Granite	Gordonnuten
714	238	148	30	SW	Dalmatian Granite	Gordonnuten
715	219	129	22	SW	Dalmatian Granite	Gordonnuten
697	264	174	20	W	Dalmatian Granite	Gordonnuten
698	225	135	31	SW	Dalmatian Granite	Gordonnuten
1	269	179	45	W	Salknappen Pegmatite	Jutulrøra
4	211	121	42	SW	Salknappen Pegmatite	Jutulrøra
5	199	289	10	S	Salknappen Pegmatite	Jutulrøra
8	173	263	15	S	Salknappen Pegmatite	Jutulrøra
11	179	269	19	S	Dalmatian Granite	Jutulrøra
13	243	153	32	SW	Dalmatian Granite	Jutulrøra

14	067	157	28	E	Dalmatian Granite	Jutulrøra
15	052	142	20	NE	Dalmatian Granite	Jutulrøra
16	217	127	24	SW	Dalmatian Granite	Jutulrøra
17	211	121	35	SW	Dalmatian Granite	Jutulrøra
18	224	134	15	SW	Dalmatian Granite	Jutulrøra
19	243	153	25	SW	Dalmatian Granite	Jutulrøra
20	039	129	20	NE	Dalmatian Granite	Jutulrøra
2	144	234	28	SE	Salknappen Pegmatite	Jutulrøra
12	151	241	24	SE	Dalmatian Granite	Jutulrøra
842	211	121	20	SW	Salknappen Pegmatite	Kivitjølen
843	232	142	25	SW	Salknappen Pegmatite	Kivitjølen
844	233	143	49	SW	Salknappen Pegmatite	Kivitjølen
845	270	180	60	W	Salknappen Pegmatite	Kivitjølen
846	016	286	75	N	Salknappen Pegmatite	Kivitjølen
847	239	149	44	SW	Salknappen Pegmatite	Kivitjølen
850	223	133	71	SW	Salknappen Pegmatite	Kivitjølen
856	008	278	63	N	Salknappen Pegmatite	Kivitjølen
860	246	156	65	SW	Salknappen Pegmatite	Kivitjølen
848	207	117	84	SW	Dalmatian Granite	Kivitjølen
849	191	281	48	S	Dalmatian Granite	Kivitjølen
853	008	278	80	N	Dalmatian Granite	Kivitjølen
438	000	270	52	N	Salknappen Pegmatite	Kivitjølen
439	176	266	51	S	Salknappen Pegmatite	Kivitjølen
440	320	230	50	NW	Salknappen Pegmatite	Kivitjølen
436	157	247	53	S	Dalmatian Granite	Kivitjølen
441	188	278	41	S	Dalmatian Granite	Kivitjølen
528	003	273	78	N	Salknappen Pegmatite	Kvassknatten
529	183	273	46	S	Salknappen Pegmatite	Kvassknatten
530	278	188	49	W	Salknappen Pegmatite	Kvassknatten
533	041	131	56	NE	Salknappen Pegmatite	Kvassknatten
534	199	289	49	S	Salknappen Pegmatite	Kvassknatten
535	209	119	45	SW	Salknappen Pegmatite	Kvassknatten
536	201	111	55	S	Salknappen Pegmatite	Kvassknatten
537	031	121	30	NE	Salknappen Pegmatite	Kvassknatten
539	355	265	61	N	Salknappen Pegmatite	Kvassknatten
540	349	259	42	N	Salknappen Pegmatite	Kvassknatten
561	229	139	40	SW	Salknappen Pegmatite	Kvassknatten
563	221	131	24	SW	Salknappen Pegmatite	Kvassknatten
564	241	151	38	SW	Salknappen Pegmatite	Kvassknatten
565	233	143	61	SW	Salknappen Pegmatite	Kvassknatten
566	221	131	42	SW	Salknappen Pegmatite	Kvassknatten
567	327	237	65	NW	Salknappen Pegmatite	Kvassknatten
568	238	148	52	SW	Salknappen Pegmatite	Kvassknatten
569	241	151	62	SW	Salknappen Pegmatite	Kvassknatten
574	254	164	62	W	Salknappen Pegmatite	Kvassknatten
575	240	150	61	SW	Salknappen Pegmatite	Kvassknatten
576	259	169	50	W	Salknappen Pegmatite	Kvassknatten
560	243	153	10	SW	Dalmatian Granite	Kvassknatten
577	244	154	33	SW	Dalmatian Granite	Kvassknatten
282	301	211	78	NW	Salknappen Pegmatite	Kivithovden
283	075	165	71	E	Salknappen Pegmatite	Kivithovden
284	115	205	74	SE	Salknappen Pegmatite	Kivithovden
285	084	174	66	E	Salknappen Pegmatite	Kivithovden
286	179	269	26	S	Salknappen Pegmatite	Kivithovden
334	217	127	35	SW	Salknappen Pegmatite	Kivithovden
335	083	173	44	E	Salknappen Pegmatite	Kivithovden
336	072	162	71	E	Salknappen Pegmatite	Kivithovden
337	072	162	51	E	Salknappen Pegmatite	Kivithovden
342	085	175	76	E	Salknappen Pegmatite	Kivithovden
344	339	249	71	N	Salknappen Pegmatite	Kivithovden
345	323	233	84	NW	Salknappen Pegmatite	Kivithovden
346	155	245	71	SE	Salknappen Pegmatite	Kivithovden
348	225	135	56	SW	Salknappen Pegmatite	Kivithovden

349	222	132	55	SW	Salknappen Pegmatite	Kivithovden
359	182	272	50	S	Salknappen Pegmatite	Kivithovden
360	170	260	46	S	Salknappen Pegmatite	Kivithovden
361	207	117	34	SW	Salknappen Pegmatite	Kivithovden
362	086	176	69	E	Salknappen Pegmatite	Kivithovden
363	084	174	66	E	Salknappen Pegmatite	Kivithovden
367	154	244	40	SE	Salknappen Pegmatite	Kivithovden
368	136	226	70	SE	Salknappen Pegmatite	Kivithovden
369	259	169	32	W	Salknappen Pegmatite	Kivithovden
370	092	182	79	E	Salknappen Pegmatite	Kivithovden
371	248	158	30	W	Salknappen Pegmatite	Kivithovden
372	256	166	46	W	Salknappen Pegmatite	Kivithovden
373	235	145	82	SW	Salknappen Pegmatite	Kivithovden
374	126	216	45	SE	Salknappen Pegmatite	Kivithovden
375	010	280	45	N	Salknappen Pegmatite	Kivithovden
384	032	122	69	NE	Salknappen Pegmatite	Kivithovden
385	091	181	20	E	Salknappen Pegmatite	Kivithovden
386	344	254	40	N	Salknappen Pegmatite	Kivithovden
387	077	167	32	E	Salknappen Pegmatite	Kivithovden
395	098	188	58	E	Salknappen Pegmatite	Kivithovden
396	088	178	68	E	Salknappen Pegmatite	Kivithovden
402	226	136	79	SW	Salknappen Pegmatite	Kivithovden
287	091	181	49	E	Dalmatian Granite	Kivithovden
288	131	221	55	SE	Dalmatian Granite	Kivithovden
289	136	226	65	SE	Dalmatian Granite	Kivithovden
290	253	163	80	W	Dalmatian Granite	Kivithovden
292	071	161	53	E	Dalmatian Granite	Kivithovden
295	065	155	46	NE	Dalmatian Granite	Kivithovden
296	149	239	56	SE	Dalmatian Granite	Kivithovden
297	169	259	59	S	Dalmatian Granite	Kivithovden
298	170	260	49	S	Dalmatian Granite	Kivithovden
301	279	189	68	W	Dalmatian Granite	Kivithovden
302	098	188	68	E	Dalmatian Granite	Kivithovden
303	090	180	56	E	Dalmatian Granite	Kivithovden
304	050	140	73	NE	Dalmatian Granite	Kivithovden
305	330	240	74	NW	Dalmatian Granite	Kivithovden
306	075	165	71	E	Dalmatian Granite	Kivithovden
308	100	190	79	E	Dalmatian Granite	Kivithovden
309	273	183	65	W	Dalmatian Granite	Kivithovden
310	015	285	84	N	Dalmatian Granite	Kivithovden
311	279	189	54	W	Dalmatian Granite	Kivithovden
312	271	181	65	W	Dalmatian Granite	Kivithovden
314	263	173	75	W	Dalmatian Granite	Kivithovden
316	077	167	74	E	Dalmatian Granite	Kivithovden
318	253	163	75	W	Dalmatian Granite	Kivithovden
319	280	190	75	W	Dalmatian Granite	Kivithovden
320	084	174	61	E	Dalmatian Granite	Kivithovden
322	067	157	76	E	Dalmatian Granite	Kivithovden
323	060	150	76	NE	Dalmatian Granite	Kivithovden
325	100	190	76	E	Dalmatian Granite	Kivithovden
326	240	150	67	SW	Dalmatian Granite	Kivithovden
327	291	201	70	W	Dalmatian Granite	Kivithovden
328	113	203	55	SE	Dalmatian Granite	Kivithovden
330	215	125	41	SW	Dalmatian Granite	Kivithovden
331	113	203	64	SE	Dalmatian Granite	Kivithovden
333	253	163	56	W	Dalmatian Granite	Kivithovden
339	152	242	30	SE	Dalmatian Granite	Kivithovden
350	226	136	36	SW	Dalmatian Granite	Kivithovden
352	210	120	34	SW	Dalmatian Granite	Kivithovden
353	215	125	44	SW	Dalmatian Granite	Kivithovden
354	122	212	24	SE	Dalmatian Granite	Kivithovden
357	217	127	41	SW	Dalmatian Granite	Kivithovden
376	083	173	68	E	Dalmatian Granite	Kivithovden

377	350	260	61	N	Dalmatian Granite	Kivithovden
380	106	196	30	E	Dalmatian Granite	Kivithovden
381	270	180	50	W	Dalmatian Granite	Kivithovden
382	155	245	25	SE	Dalmatian Granite	Kivithovden
383	163	253	26	S	Dalmatian Granite	Kivithovden
388	088	178	68	E	Dalmatian Granite	Kivithovden
397	099	189	45	E	Dalmatian Granite	Kivithovden
398	080	170	60	E	Dalmatian Granite	Kivithovden
399	101	191	39	E	Dalmatian Granite	Kivithovden
400	214	124	41	SW	Dalmatian Granite	Kivithovden
401	094	184	32	E	Dalmatian Granite	Kivithovden
340	252	162	85	W	Dalmatian Granite	Kivithovden
341	140	230	30	SE	Dalmatian Granite	Kivithovden
343	240	150	71	SW	Dalmatian Granite	Kivithovden
365	136	226	50	SE	Dalmatian Granite	Kivithovden
716	230	140	79	SW	Salknappen Pegmatite	Nupskåpa
717	167	257	70	S	Salknappen Pegmatite	Nupskåpa
718	331	241	84	NW	Salknappen Pegmatite	Nupskåpa
719	253	163	56	W	Salknappen Pegmatite	Nupskåpa
722	222	132	21	SW	Salknappen Pegmatite	Nupskåpa
723	155	245	70	SE	Salknappen Pegmatite	Nupskåpa
725	187	277	52	S	Salknappen Pegmatite	Nupskåpa
726	186	276	58	S	Salknappen Pegmatite	Nupskåpa
728	168	258	71	S	Salknappen Pegmatite	Nupskåpa
732	211	121	28	SW	Salknappen Pegmatite	Nupskåpa
733	232	142	32	SW	Salknappen Pegmatite	Nupskåpa
734	237	147	68	SW	Salknappen Pegmatite	Nupskåpa
736	175	265	63	S	Salknappen Pegmatite	Nupskåpa
737	282	192	63	W	Salknappen Pegmatite	Nupskåpa
738	239	149	41	SW	Salknappen Pegmatite	Nupskåpa
739	181	271	70	S	Salknappen Pegmatite	Nupskåpa
741	072	162	70	E	Salknappen Pegmatite	Nupskåpa
743	315	225	24	NW	Salknappen Pegmatite	Nupskåpa
745	222	132	38	SW	Salknappen Pegmatite	Nupskåpa
746	343	253	41	N	Salknappen Pegmatite	Nupskåpa
747	206	116	21	SW	Salknappen Pegmatite	Nupskåpa
748	135	225	64	SE	Salknappen Pegmatite	Nupskåpa
749	110	200	61	E	Salknappen Pegmatite	Nupskåpa
750	151	241	56	SE	Salknappen Pegmatite	Nupskåpa
751	213	123	34	SW	Salknappen Pegmatite	Nupskåpa
752	319	229	60	NW	Salknappen Pegmatite	Nupskåpa
753	285	195	83	W	Salknappen Pegmatite	Nupskåpa
754	278	188	81	W	Salknappen Pegmatite	Nupskåpa
755	311	221	58	NW	Salknappen Pegmatite	Nupskåpa
756	246	156	67	SW	Salknappen Pegmatite	Nupskåpa
757	328	238	64	NW	Salknappen Pegmatite	Nupskåpa
758	117	207	57	SE	Salknappen Pegmatite	Nupskåpa
759	309	219	75	NW	Salknappen Pegmatite	Nupskåpa
760	081	171	60	E	Salknappen Pegmatite	Nupskåpa
761	225	135	72	SW	Salknappen Pegmatite	Nupskåpa
762	320	230	85	NW	Salknappen Pegmatite	Nupskåpa
763	309	219	70	NW	Salknappen Pegmatite	Nupskåpa
764	237	147	64	SW	Salknappen Pegmatite	Nupskåpa
765	307	217	68	NW	Salknappen Pegmatite	Nupskåpa
766	358	268	74	N	Salknappen Pegmatite	Nupskåpa
772	136	226	74	SE	Salknappen Pegmatite	Nupskåpa
774	140	230	71	SE	Salknappen Pegmatite	Nupskåpa
777	094	184	86	E	Salknappen Pegmatite	Nupskåpa
778	123	213	32	SE	Salknappen Pegmatite	Nupskåpa
779	020	110	60	N	Salknappen Pegmatite	Nupskåpa
731	264	174	67	W	Dalmatian Granite	Nupskåpa
767	100	190	51	E	Dalmatian Granite	Nupskåpa
768	083	173	81	E	Dalmatian Granite	Nupskåpa

769	106	196	50	E	Dalmatian Granite	Nupskåpa
770	303	213	70	NW	Dalmatian Granite	Nupskåpa
771	179	269	48	S	Dalmatian Granite	Nupskåpa
775	137	227	31	SE	Dalmatian Granite	Nupskåpa
193	353	263	70	N	Salknappen Pegmatite	Roerkulten
194	344	254	60	N	Salknappen Pegmatite	Roerkulten
199	001	271	89	N	Salknappen Pegmatite	Roerkulten
201	181	271	48	S	Salknappen Pegmatite	Roerkulten
202	184	274	40	S	Salknappen Pegmatite	Roerkulten
206	181	271	48	S	Salknappen Pegmatite	Roerkulten
197	202	292	42	N	Dalmatian Granite	Roerkulten
198	197	287	44	N	Dalmatian Granite	Roerkulten
200	229	139	28	SW	Dalmatian Granite	Roerkulten
176	134	224	65	SE	Dalmatian Granite	Roerkulten
177	203	113	50	SW	Dalmatian Granite	Roerkulten
178	207	117	38	SW	Dalmatian Granite	Roerkulten
179	219	129	60	SW	Dalmatian Granite	Roerkulten
180	199	289	40	S	Dalmatian Granite	Roerkulten
181	211	121	52	SW	Dalmatian Granite	Roerkulten
182	193	283	32	S	Dalmatian Granite	Roerkulten
183	210	120	43	SW	Dalmatian Granite	Roerkulten
184	207	117	38	SW	Dalmatian Granite	Roerkulten
185	200	110	60	S	Dalmatian Granite	Roerkulten
186	191	281	50	S	Dalmatian Granite	Roerkulten
187	193	283	46	S	Dalmatian Granite	Roerkulten
188	228	138	40	SW	Dalmatian Granite	Roerkulten
189	204	114	30	SW	Dalmatian Granite	Roerkulten
190	214	124	35	SW	Dalmatian Granite	Roerkulten
191	199	289	60	S	Dalmatian Granite	Roerkulten
192	191	281	45	S	Dalmatian Granite	Roerkulten
195	209	109	35	N	Dalmatian Granite	Roerkulten
196	201	109	43	N	Dalmatian Granite	Roerkulten
203	187	277	44	S	Dalmatian Granite	Roerkulten
204	177	267	44	S	Dalmatian Granite	Roerkulten
205	171	261	39	S	Dalmatian Granite	Roerkulten
207	211	121	45	SW	Dalmatian Granite	Roerkulten
208	203	113	52	SW	Dalmatian Granite	Roerkulten
209	187	277	55	S	Dalmatian Granite	Roerkulten
210	177	267	55	S	Dalmatian Granite	Roerkulten
211	182	272	65	S	Dalmatian Granite	Roerkulten
212	179	269	57	S	Dalmatian Granite	Roerkulten
213	197	287	05	S	Dalmatian Granite	Roerkulten
214	187	277	50	S	Dalmatian Granite	Roerkulten
215	184	274	65	S	Dalmatian Granite	Roerkulten
216	191	281	45	S	Dalmatian Granite	Roerkulten
217	194	284	52	S	Dalmatian Granite	Roerkulten
218	181	271	43	S	Dalmatian Granite	Roerkulten
931	152	242	54	SE	Pre-existing Granitoid	Rootshorga
863	203	113	20	SW	Salknappen Pegmatite	Rootshorga
864	178	268	38	S	Salknappen Pegmatite	Rootshorga
865	209	119	22	SW	Salknappen Pegmatite	Rootshorga
866	238	148	21	SW	Salknappen Pegmatite	Rootshorga
867	179	269	32	S	Salknappen Pegmatite	Rootshorga
869	206	116	63	SW	Salknappen Pegmatite	Rootshorga
870	348	258	28	N	Salknappen Pegmatite	Rootshorga
871	344	254	70	N	Salknappen Pegmatite	Rootshorga
875	206	116	28	SW	Salknappen Pegmatite	Rootshorga
918	012	282	71	N	Salknappen Pegmatite	Rootshorga
924	195	285	64	S	Salknappen Pegmatite	Rootshorga
928	212	122	59	SW	Salknappen Pegmatite	Rootshorga
932	030	120	54	NE	Salknappen Pegmatite	Rootshorga
933	131	221	68	SE	Salknappen Pegmatite	Rootshorga
937	169	259	60	S	Salknappen Pegmatite	Rootshorga

939	008	278	79	N	Salknappen Pegmatite	Rootshorga
940	341	251	31	N	Salknappen Pegmatite	Rootshorga
950	143	233	82	SE	Salknappen Pegmatite	Rootshorga
951	141	231	75	SE	Salknappen Pegmatite	Rootshorga
952	182	272	41	S	Salknappen Pegmatite	Rootshorga
953	171	261	31	S	Salknappen Pegmatite	Rootshorga
954	145	235	80	SE	Salknappen Pegmatite	Rootshorga
955	315	225	40	NW	Salknappen Pegmatite	Rootshorga
874	027	117	69	NE	Dalmatian Granite	Rootshorga
876	173	263	71	S	Dalmatian Granite	Rootshorga
915	284	194	41	W	Dalmatian Granite	Rootshorga
921	048	138	48	NE	Dalmatian Granite	Rootshorga
925	145	235	31	SE	Dalmatian Granite	Rootshorga
926	175	265	43	S	Dalmatian Granite	Rootshorga
929	183	273	27	S	Dalmatian Granite	Rootshorga
941	006	276	64	N	Dalmatian Granite	Rootshorga
942	029	119	68	NE	Dalmatian Granite	Rootshorga
943	007	277	56	N	Dalmatian Granite	Rootshorga
944	028	118	19	NE	Dalmatian Granite	Rootshorga
945	055	145	20	NE	Dalmatian Granite	Rootshorga
946	087	177	30	E	Dalmatian Granite	Rootshorga
948	266	176	18	W	Dalmatian Granite	Rootshorga
949	051	141	22	NE	Dalmatian Granite	Rootshorga
956	287	197	65	W	Dalmatian Granite	Rootshorga
957	316	226	17	NW	Dalmatian Granite	Rootshorga
958	232	142	29	SW	Dalmatian Granite	Rootshorga
959	248	158	26	W	Dalmatian Granite	Rootshorga
960	287	197	54	W	Dalmatian Granite	Rootshorga
919	200	110	37	S	Dalmatian Granite	Rootshorga
920	227	137	16	SW	Dalmatian Granite	Rootshorga
930	228	138	81	SW	Dalmatian Granite	Rootshorga
947	239	149	19	SW	Dalmatian Granite	Rootshorga
962	025	115	67	NE	Dalmatian Granite	Rootshorga
879	355	265	59	N	Salknappen Pegmatite	Rootshorga
880	010	280	34	N	Salknappen Pegmatite	Rootshorga
885	206	116	53	SW	Salknappen Pegmatite	Rootshorga
887	339	249	63	N	Salknappen Pegmatite	Rootshorga
890	202	112	66	S	Salknappen Pegmatite	Rootshorga
902	322	232	22	NW	Salknappen Pegmatite	Rootshorga
906	174	264	50	S	Salknappen Pegmatite	Rootshorga
907	175	265	70	S	Salknappen Pegmatite	Rootshorga
892	043	133	29	NE	Dalmatian Granite	Rootshorga
893	139	229	34	SE	Dalmatian Granite	Rootshorga
897	303	213	19	NW	Dalmatian Granite	Rootshorga
910	021	111	20	N	Dalmatian Granite	Rootshorga
911	167	257	42	S	Dalmatian Granite	Rootshorga
912	048	138	61	NE	Dalmatian Granite	Rootshorga
913	257	167	33	W	Dalmatian Granite	Rootshorga
914	198	288	38	S	Dalmatian Granite	Rootshorga
877	172	262	25	S	Dalmatian Granite	Rootshorga
878	009	279	20	N	Dalmatian Granite	Rootshorga
894	203	113	31	SW	Dalmatian Granite	Rootshorga
896	323	233	19	NW	Dalmatian Granite	Rootshorga
899	298	208	29	NW	Dalmatian Granite	Rootshorga
900	195	285	40	S	Dalmatian Granite	Rootshorga
903	143	233	40	SE	Dalmatian Granite	Rootshorga
905	154	244	44	SE	Dalmatian Granite	Rootshorga
908	197	287	13	S	Dalmatian Granite	Rootshorga
96	357	267	46	N	Salknappen Pegmatite	Salknappen
97	217	127	54	SW	Salknappen Pegmatite	Salknappen
98	009	279	41	N	Salknappen Pegmatite	Salknappen
99	007	277	54	N	Salknappen Pegmatite	Salknappen
100	014	284	50	N	Salknappen Pegmatite	Salknappen

102	001	271	70	N	Salknappen Pegmatite	Salknappen
103	353	263	35	N	Salknappen Pegmatite	Salknappen
104	327	237	40	NW	Salknappen Pegmatite	Salknappen
105	219	129	82	SW	Salknappen Pegmatite	Salknappen
106	051	141	72	NE	Salknappen Pegmatite	Salknappen
107	358	268	65	N	Salknappen Pegmatite	Salknappen
111	130	220	65	SE	Salknappen Pegmatite	Salknappen
112	014	284	15	N	Salknappen Pegmatite	Salknappen
113	349	259	28	N	Salknappen Pegmatite	Salknappen
114	009	279	48	N	Salknappen Pegmatite	Salknappen
123	352	262	55	N	Salknappen Pegmatite	Salknappen
124	359	269	50	N	Salknappen Pegmatite	Salknappen
125	245	155	45	SW	Salknappen Pegmatite	Salknappen
126	030	120	60	NE	Salknappen Pegmatite	Salknappen
127	002	272	39	N	Salknappen Pegmatite	Salknappen
128	355	265	46	N	Salknappen Pegmatite	Salknappen
137	012	282	39	N	Salknappen Pegmatite	Salknappen
138	015	285	46	N	Salknappen Pegmatite	Salknappen
139	031	121	74	NE	Salknappen Pegmatite	Salknappen
140	357	267	58	N	Salknappen Pegmatite	Salknappen
141	358	268	62	N	Salknappen Pegmatite	Salknappen
142	164	254	56	S	Salknappen Pegmatite	Salknappen
143	169	259	58	S	Salknappen Pegmatite	Salknappen
144	184	274	45	S	Salknappen Pegmatite	Salknappen
145	129	219	25	SE	Salknappen Pegmatite	Salknappen
146	123	213	12	SE	Salknappen Pegmatite	Salknappen
147	133	223	12	SE	Salknappen Pegmatite	Salknappen
148	142	232	66	SE	Salknappen Pegmatite	Salknappen
149	122	212	61	SE	Salknappen Pegmatite	Salknappen
150	334	244	59	NW	Salknappen Pegmatite	Salknappen
151	299	209	69	NW	Salknappen Pegmatite	Salknappen
152	134	224	52	SE	Salknappen Pegmatite	Salknappen
153	287	197	80	W	Salknappen Pegmatite	Salknappen
163	294	204	49	NW	Salknappen Pegmatite	Salknappen
164	210	120	45	SW	Salknappen Pegmatite	Salknappen
168	334	244	22	NW	Salknappen Pegmatite	Salknappen
169	251	161	38	W	Salknappen Pegmatite	Salknappen
170	187	277	68	S	Salknappen Pegmatite	Salknappen
171	355	265	28	N	Salknappen Pegmatite	Salknappen
172	284	194	68	W	Salknappen Pegmatite	Salknappen
173	034	124	79	NE	Salknappen Pegmatite	Salknappen
174	035	125	58	NE	Salknappen Pegmatite	Salknappen
175	339	249	75	N	Salknappen Pegmatite	Salknappen
94	175	265	25	S	Dalmatian Granite	Salknappen
95	071	161	45	E	Dalmatian Granite	Salknappen
101	044	134	85	NE	Dalmatian Granite	Salknappen
109	183	273	25	S	Dalmatian Granite	Salknappen
115	216	126	22	SW	Dalmatian Granite	Salknappen
116	235	145	75	SW	Dalmatian Granite	Salknappen
117	161	251	42	S	Dalmatian Granite	Salknappen
118	189	279	36	S	Dalmatian Granite	Salknappen
119	199	289	38	S	Dalmatian Granite	Salknappen
120	147	237	40	SE	Dalmatian Granite	Salknappen
121	140	230	30	SE	Dalmatian Granite	Salknappen
131	114	204	20	SE	Dalmatian Granite	Salknappen
132	121	211	20	SE	Dalmatian Granite	Salknappen
133	329	239	25	NW	Dalmatian Granite	Salknappen
134	167	257	50	S	Dalmatian Granite	Salknappen
136	138	228	48	SE	Dalmatian Granite	Salknappen
154	214	124	28	SW	Dalmatian Granite	Salknappen
155	221	197	20	W	Dalmatian Granite	Salknappen
156	190	124	72	SW	Dalmatian Granite	Salknappen
157	231	141	75	SW	Dalmatian Granite	Salknappen

159	009	279	66	N	Dalmatian Granite	Salknappen
160	001	271	45	N	Dalmatian Granite	Salknappen
161	174	264	72	S	Dalmatian Granite	Salknappen
162	168	258	19	S	Dalmatian Granite	Salknappen
165	210	120	45	SW	Dalmatian Granite	Salknappen
166	224	134	52	SW	Dalmatian Granite	Salknappen
167	167	257	72	S	Dalmatian Granite	Salknappen
110	172	262	62	S	Dalmatian Granite	Salknappen
86	197	287	42	S	Salknappen Pegmatite	SH 1630
88	019	109	76	N	Salknappen Pegmatite	SH 1630
89	207	117	42	SW	Salknappen Pegmatite	SH 1630
90	223	133	25	SW	Salknappen Pegmatite	SH 1630
92	001	271	75	N	Salknappen Pegmatite	SH 1630
93	334	244	78	NW	Salknappen Pegmatite	SH 1630
85	261	171	58	W	Dalmatian Granite	SH 1630
87	194	284	42	S	Dalmatian Granite	SH 1630
91	190	280	55	S	Dalmatian Granite	SH 1630
596	321	231	71	NW	Salknappen Pegmatite	SH 1725
597	180	270	40	S	Salknappen Pegmatite	SH 1725
598	326	236	79	NW	Salknappen Pegmatite	SH 1725
599	141	231	78	SE	Salknappen Pegmatite	SH 1725
600	339	249	49	N	Salknappen Pegmatite	SH 1725
602	317	227	68	NW	Salknappen Pegmatite	SH 1725
603	356	266	19	N	Salknappen Pegmatite	SH 1725
579	130	220	80	SE	Salknappen Pegmatite	SH 1725
583	182	272	27	S	Salknappen Pegmatite	SH 1725
584	205	115	29	SW	Salknappen Pegmatite	SH 1725
585	215	125	36	SW	Salknappen Pegmatite	SH 1725
586	220	130	20	SW	Salknappen Pegmatite	SH 1725
587	231	141	50	SW	Salknappen Pegmatite	SH 1725
588	195	285	24	S	Salknappen Pegmatite	SH 1725
589	193	283	20	S	Salknappen Pegmatite	SH 1725
590	295	205	58	NW	Salknappen Pegmatite	SH 1725
593	299	209	80	NW	Salknappen Pegmatite	SH 1725
595	220	130	30	SW	Salknappen Pegmatite	SH 1725
604	108	198	80	E	Salknappen Pegmatite	SH 1725
578	264	174	49	W	Dalmatian Granite	SH 1725
580	249	159	23	W	Dalmatian Granite	SH 1725
581	250	160	18	W	Dalmatian Granite	SH 1725
582	227	137	15	SW	Dalmatian Granite	SH 1725
591	185	275	31	S	Dalmatian Granite	SH 1725
592	178	268	20	S	Dalmatian Granite	SH 1725
594	160	250	49	S	Dalmatian Granite	SH 1725
475	341	251	21	N	Salknappen Pegmatite	Skarsnuten
476	347	257	67	N	Salknappen Pegmatite	Skarsnuten
477	059	149	72	NE	Salknappen Pegmatite	Skarsnuten
478	000	270	60	N	Salknappen Pegmatite	Skarsnuten
479	319	229	44	NW	Salknappen Pegmatite	Skarsnuten
481	028	118	62	NE	Salknappen Pegmatite	Skarsnuten
482	246	156	67	SW	Salknappen Pegmatite	Skarsnuten
483	212	122	82	SW	Salknappen Pegmatite	Skarsnuten
484	184	274	40	S	Salknappen Pegmatite	Skarsnuten
485	207	117	50	SW	Salknappen Pegmatite	Skarsnuten
486	030	120	52	NE	Salknappen Pegmatite	Skarsnuten
487	016	286	28	N	Salknappen Pegmatite	Skarsnuten
491	297	207	24	NW	Salknappen Pegmatite	Skarsnuten
493	328	238	54	NW	Salknappen Pegmatite	Skarsnuten
494	244	154	30	SW	Salknappen Pegmatite	Skarsnuten
495	318	228	39	NW	Salknappen Pegmatite	Skarsnuten
496	254	164	40	W	Salknappen Pegmatite	Skarsnuten
497	355	265	68	N	Salknappen Pegmatite	Skarsnuten
498	293	203	60	NW	Salknappen Pegmatite	Skarsnuten
499	250	160	53	W	Salknappen Pegmatite	Skarsnuten

500	313	223	68	NW	Salknappen Pegmatite	Skarsnuten
501	255	165	20	W	Salknappen Pegmatite	Skarsnuten
502	303	213	39	NW	Salknappen Pegmatite	Skarsnuten
503	169	259	54	S	Salknappen Pegmatite	Skarsnuten
505	255	165	29	W	Salknappen Pegmatite	Skarsnuten
509	301	211	50	NW	Salknappen Pegmatite	Skarsnuten
510	273	183	38	W	Salknappen Pegmatite	Skarsnuten
511	023	113	20	NE	Salknappen Pegmatite	Skarsnuten
512	253	163	55	W	Salknappen Pegmatite	Skarsnuten
517	203	113	45	SW	Salknappen Pegmatite	Skarsnuten
519	190	280	19	S	Salknappen Pegmatite	Skarsnuten
520	171	261	52	S	Salknappen Pegmatite	Skarsnuten
521	349	259	71	N	Salknappen Pegmatite	Skarsnuten
522	001	271	55	N	Salknappen Pegmatite	Skarsnuten
523	230	140	50	SW	Salknappen Pegmatite	Skarsnuten
619	038	128	49	NE	Salknappen Pegmatite	Skarsnuten
620	006	276	60	N	Salknappen Pegmatite	Skarsnuten
621	110	200	71	E	Salknappen Pegmatite	Skarsnuten
623	328	238	80	NW	Salknappen Pegmatite	Skarsnuten
627	339	249	55	N	Salknappen Pegmatite	Skarsnuten
629	314	224	30	NW	Salknappen Pegmatite	Skarsnuten
631	079	169	52	E	Salknappen Pegmatite	Skarsnuten
637	044	134	63	NE	Salknappen Pegmatite	Skarsnuten
642	355	265	75	N	Salknappen Pegmatite	Skarsnuten
643	010	280	88	N	Salknappen Pegmatite	Skarsnuten
644	271	181	49	W	Salknappen Pegmatite	Skarsnuten
649	301	211	49	NW	Salknappen Pegmatite	Skarsnuten
656	309	219	82	NW	Salknappen Pegmatite	Skarsnuten
659	009	279	79	N	Salknappen Pegmatite	Skarsnuten
660	027	117	51	NE	Salknappen Pegmatite	Skarsnuten
661	269	179	44	W	Salknappen Pegmatite	Skarsnuten
662	337	247	60	NW	Salknappen Pegmatite	Skarsnuten
473	000	270	64	N	Dalmatian Granite	Skarsnuten
474	003	273	51	N	Dalmatian Granite	Skarsnuten
488	330	240	30	NW	Dalmatian Granite	Skarsnuten
489	002	272	20	N	Dalmatian Granite	Skarsnuten
504	130	220	11	SE	Dalmatian Granite	Skarsnuten
508	214	124	21	SW	Dalmatian Granite	Skarsnuten
513	205	115	29	SW	Dalmatian Granite	Skarsnuten
514	179	269	40	S	Dalmatian Granite	Skarsnuten
524	183	273	36	S	Dalmatian Granite	Skarsnuten
525	210	120	40	SW	Dalmatian Granite	Skarsnuten
526	190	280	19	S	Dalmatian Granite	Skarsnuten
527	173	263	40	S	Dalmatian Granite	Skarsnuten
618	297	207	49	NW	Dalmatian Granite	Skarsnuten
622	311	221	34	NW	Dalmatian Granite	Skarsnuten
624	275	185	50	W	Dalmatian Granite	Skarsnuten
625	015	285	36	N	Dalmatian Granite	Skarsnuten
632	272	182	41	W	Dalmatian Granite	Skarsnuten
634	215	125	11	SW	Dalmatian Granite	Skarsnuten
638	326	236	20	NW	Dalmatian Granite	Skarsnuten
639	318	228	34	NW	Dalmatian Granite	Skarsnuten
640	295	205	20	NW	Dalmatian Granite	Skarsnuten
645	290	200	38	W	Dalmatian Granite	Skarsnuten
646	290	200	32	W	Dalmatian Granite	Skarsnuten
647	278	188	48	W	Dalmatian Granite	Skarsnuten
648	335	245	35	NW	Dalmatian Granite	Skarsnuten
650	310	220	59	NW	Dalmatian Granite	Skarsnuten
651	322	232	30	NW	Dalmatian Granite	Skarsnuten
653	327	237	58	NW	Dalmatian Granite	Skarsnuten
655	323	233	13	NW	Dalmatian Granite	Skarsnuten
657	148	238	39	SE	Dalmatian Granite	Skarsnuten
658	068	158	22	E	Dalmatian Granite	Skarsnuten

515	012	282	80	N	Dalmatian Granite	Skarsnuten
663	200	110	40	S	Pre-existing Granitoid	Skarsnuten
678	229	139	64	SW	Pre-existing Granitoid	Skarsnuten
680	246	156	44	SW	Pre-existing Granitoid	Skarsnuten
682	273	183	75	W	Pre-existing Granitoid	Skarsnuten
963	257	167	45	W	Pre-existing Granitoid	Skarsnuten
969	223	133	36	SW	Pre-existing Granitoid	Skarsnuten
972	063	153	59	NE	Pre-existing Granitoid	Skarsnuten
978	244	154	47	SW	Pre-existing Granitoid	Skarsnuten
984	254	164	41	W	Pre-existing Granitoid	Skarsnuten
987	227	137	42	SW	Pre-existing Granitoid	Skarsnuten
993	249	159	39	W	Pre-existing Granitoid	Skarsnuten
999	215	125	41	SW	Pre-existing Granitoid	Skarsnuten
1002	220	130	31	SW	Pre-existing Granitoid	Skarsnuten
1005	249	159	40	W	Pre-existing Granitoid	Skarsnuten
1014	254	164	67	W	Pre-existing Granitoid	Skarsnuten
1020	239	149	55	SW	Pre-existing Granitoid	Skarsnuten
1023	229	139	36	SW	Pre-existing Granitoid	Skarsnuten
1031	215	125	42	SW	Pre-existing Granitoid	Skarsnuten
1034	024	114	78	NE	Pre-existing Granitoid	Skarsnuten
1035	215	125	35	SW	Pre-existing Granitoid	Skarsnuten
1038	243	153	70	SW	Pre-existing Granitoid	Skarsnuten
1041	242	152	31	SW	Pre-existing Granitoid	Skarsnuten
1044	344	254	85	N	Pre-existing Granitoid	Skarsnuten
1047	235	145	42	SW	Pre-existing Granitoid	Skarsnuten
1050	177	267	64	S	Pre-existing Granitoid	Skarsnuten
1053	229	139	48	SW	Pre-existing Granitoid	Skarsnuten
1056	238	148	48	SW	Pre-existing Granitoid	Skarsnuten
1059	238	148	45	SW	Pre-existing Granitoid	Skarsnuten
1062	004	274	70	N	Pre-existing Granitoid	Skarsnuten
605	051	141	72	NE	Salknappen Pegmatite	Skarsnuten
606	346	256	55	N	Salknappen Pegmatite	Skarsnuten
609	246	156	42	SW	Salknappen Pegmatite	Skarsnuten
612	055	145	50	NE	Salknappen Pegmatite	Skarsnuten
613	021	111	47	N	Salknappen Pegmatite	Skarsnuten
667	189	279	39	S	Salknappen Pegmatite	Skarsnuten
669	266	176	41	W	Salknappen Pegmatite	Skarsnuten
672	221	131	44	SW	Salknappen Pegmatite	Skarsnuten
676	052	142	30	NE	Salknappen Pegmatite	Skarsnuten
677	209	119	76	SW	Salknappen Pegmatite	Skarsnuten
679	226	136	30	SW	Salknappen Pegmatite	Skarsnuten
607	203	113	30	SW	Dalmatian Granite	Skarsnuten
608	307	217	42	NW	Dalmatian Granite	Skarsnuten
611	211	121	24	SW	Dalmatian Granite	Skarsnuten
614	286	196	40	W	Dalmatian Granite	Skarsnuten
617	259	169	18	W	Dalmatian Granite	Skarsnuten
665	069	159	27	E	Dalmatian Granite	Skarsnuten
666	273	183	45	W	Dalmatian Granite	Skarsnuten
668	318	228	44	NW	Dalmatian Granite	Skarsnuten
673	056	146	40	NE	Dalmatian Granite	Skarsnuten
674	267	177	20	W	Dalmatian Granite	Skarsnuten
675	056	146	20	NE	Dalmatian Granite	Skarsnuten
664	246	156	40	SW	Dalmatian Granite	Skarsnuten
468	153	243	58	SE	Salknappen Pegmatite	Straumsvola
469	158	248	63	S	Salknappen Pegmatite	Straumsvola
470	168	258	38	S	Salknappen Pegmatite	Straumsvola
471	093	183	71	E	Salknappen Pegmatite	Straumsvola
423	062	152	78	NE	Salknappen Pegmatite	Tua
424	341	251	69	N	Salknappen Pegmatite	Tua
421	328	238	73	NW	Dalmatian Granite	Tua
425	118	208	71	SE	Dalmatian Granite	Tua
465	212	122	28	SW	Salknappen Pegmatite	Tvora
227	337	247	55	NW	Salknappen Pegmatite	Vendeholten

223	195	285	62	S	Dalmatian Granite	Vendeholten
225	084	174	24	E	Dalmatian Granite	Vendeholten
228	311	221	60	NW	Dalmatian Granite	Vendeholten
231	021	111	24	N	Dalmatian Granite	Vendeholten
232	306	216	72	NW	Dalmatian Granite	Vendeholten
233	317	227	72	NW	Dalmatian Granite	Vendeholten
234	149	239	68	SE	Dalmatian Granite	Vendeholten
235	291	201	58	W	Dalmatian Granite	Vendeholten
236	301	211	75	NW	Dalmatian Granite	Vendeholten
237	317	227	65	NW	Dalmatian Granite	Vendeholten
238	184	274	39	S	Dalmatian Granite	Vendeholten
239	313	223	72	NW	Dalmatian Granite	Vendeholten
241	111	201	15	E	Dalmatian Granite	Vendeholten
245	294	204	85	NW	Dalmatian Granite	Vendeholten
246	221	131	50	SW	Dalmatian Granite	Vendeholten
247	299	209	55	NW	Dalmatian Granite	Vendeholten
249	249	159	58	W	Dalmatian Granite	Vendeholten
250	294	204	54	NW	Dalmatian Granite	Vendeholten
251	149	239	40	SE	Dalmatian Granite	Vendeholten
252	207	117	48	SW	Dalmatian Granite	Vendeholten
253	113	203	40	SE	Dalmatian Granite	Vendeholten
254	321	231	62	NW	Dalmatian Granite	Vendeholten
219	349	259	78	N	Dalmatian Granite	Vendeholten
220	351	261	89	N	Dalmatian Granite	Vendeholten
222	214	124	65	SW	Dalmatian Granite	Vendeholten
226	037	127	62	NE	Dalmatian Granite	Vendeholten
229	194	284	82	S	Dalmatian Granite	Vendeholten
240	237	147	60	SW	Dalmatian Granite	Vendeholten
243	207	117	45	SW	Dalmatian Granite	Vendeholten
244	011	281	10	N	Dalmatian Granite	Vendeholten
248	167	257	85	S	Dalmatian Granite	Vendeholten

A3.3 SHRIMP Data:

Table A3.3: SHRIMP data for sample 004cJ. Errors are 1-sigma; PF_{BC} and Pb^{*} indicate the common and radiogenic Pb, respectively. The error in Standard calibration was 0.20% (not included in above errors but required when comparing data from different mounts). (1) indicates that common Pb was corrected using measured ^{204}Pb.

Comment	Spot	$^{206}Pb_c$ (%)	U (ppm)	Th (ppm)	4 corr $^{206}Pb^*$ (ppm)	$^{232}Th/^{238}U$	$^{206}Pb/^{238}U$ Age (Ma) (1)		Discor-dant %	$^{238}U/^{206}Pb^*$ (1)	±%	$^{207}Pb^*/^{206}Pb^*$ (1)	±%	$^{207}Pb^*/^{235}U$ (1)	±%	$^{206}Pb^*/^{238}U$ (1)	±%	Error Corr.
	004cJ-1.1	0.16	1515	28	109	0.02	518	±6	+3	11.9	1.3	0.0581	1.1	0.671	1.1	0.0838	1.3	0.75
High U, inheritance	004cJ-2.1	0.11	3412	120	294	0.04	586	±7	-13	10.5	1.3	0.0577	0.8	0.756	1.1	0.0952	1.3	0.83
High Pb_c	~~004cJ-3.1~~	~~2.52~~	~~9211~~	~~171~~	~~413~~	~~0.02~~	~~283~~	~~±10~~	~~+75~~	~~22.2~~	~~3.5~~	~~0.0774~~	~~15.0~~	~~0.480~~	~~7.4~~	~~0.0450~~	~~3.5~~	~~0.19~~
High Pb_c	~~004cJ-4.1~~	~~3.18~~	~~1126~~	~~93~~	~~86~~	~~0.09~~	~~547~~	~~±7~~	~~-6~~	~~11.3~~	~~1.3~~	~~0.0577~~	~~5.9~~	~~0.704~~	~~4.2~~	~~0.0885~~	~~1.3~~	~~0.22~~
High U	004cJ-5.1	0.21	2836	63	213	0.02	517	±6	+2	12.0	1.2	0.0580	0.6	0.668	0.9	0.0835	1.2	0.89
High Pb_c	~~004cJ-6.1~~	~~2.44~~	~~1545~~	~~22~~	~~109~~	~~0.01~~	~~507~~	~~±6~~	~~-22~~	~~12.2~~	~~1.3~~	~~0.0551~~	~~3.5~~	~~0.621~~	~~2.3~~	~~0.0818~~	~~1.3~~	~~0.34~~
Inheritance	004cJ-7.1	0.01	392	170	66	0.45	1154	±15	-3	5.1	1.4	0.0771	0.9	2.085	3.5	0.1960	1.4	0.83
High Pb_c	~~004cJ-8.1~~	~~6.99~~	~~2268~~	~~102~~	~~156~~	~~0.05~~	~~496~~	~~±6~~	~~+9~~	~~12.5~~	~~1.3~~	~~0.0584~~	~~9.7~~	~~0.644~~	~~6.3~~	~~0.0799~~	~~1.3~~	~~0.13~~
High U	004cJ-9.1	0.10	3025	66	229	0.02	520	±5	+3	11.9	1.1	0.0581	0.9	0.673	0.9	0.0840	1.1	0.74
	004cJ-10.1	0.09	4106	61	311	0.02	513	±6	-2	12.1	1.2	0.0574	0.6	0.655	0.9	0.0829	1.2	0.90
	004cJ-11.1	0.18	2452	42	176	0.02	518	±6	-2	11.9	1.2	0.0574	0.7	0.663	0.9	0.0837	1.2	0.87
h High Pb_c	~~004cJ-12.1~~	~~2.26~~	~~1023~~	~~26~~	~~70~~	~~0.03~~	~~497~~	~~±6~~	~~+26~~	~~12.5~~	~~1.3~~	~~0.0618~~	~~2.1~~	~~0.684~~	~~1.7~~	~~0.0802~~	~~1.3~~	~~0.51~~
	004cJ-13.1	0.25	1521	22	111	0.02	524	±6	+3	11.8	1.2	0.0582	0.8	0.680	1.0	0.0846	1.2	0.85
	004cJ-14.1	0.04	1602	32	114	0.02	515	±6	+4	12.0	1.2	0.0581	0.7	0.666	0.9	0.0831	1.2	0.85
	004cJ-15.1	0.35	2341	73	170	0.03	524	±6	-0	11.8	1.2	0.0578	2.4	0.675	1.8	0.0846	1.2	0.46
High Pb_c	~~004cJ-16.1~~	~~14.22~~	~~1299~~	~~268~~	~~91~~	~~0.21~~	~~508~~	~~±12~~	~~-231~~	~~12.2~~	~~2.5~~	~~0.0491~~	~~46.8~~	~~0.555~~	~~26.0~~	~~0.0820~~	~~2.5~~	~~0.05~~
	004cJ-17.1	0.23	1255	26	90	0.02	519	±6	+2	11.9	1.2	0.0580	1.0	0.671	1.1	0.0838	1.2	0.78
	004cJ-18.1	0.19	1202	22	87	0.02	520	±6	-2	11.9	1.2	0.0575	1.5	0.665	1.3	0.0839	1.2	0.63
High Pb_c, high UO/U	~~004cJ-19.1~~	~~4.53~~	~~8431~~	~~213~~	~~313~~	~~0.03~~	~~239~~	~~±28~~		~~26.5~~	~~11.9~~	~~0.0182~~	~~59.7~~	~~0.095~~	~~5.8~~	~~0.0378~~	~~11.9~~	~~0.17~~
High U	004cJ-20.1	0.22	3291	44	247	0.01	515	±6	+4	12.0	1.2	0.0581	1.0	0.667	1.0	0.0832	1.2	0.77
High UO/U	004cJ-9.2	0.34	1675	38	128	0.02	548	±9	-9	11.3	1.8	0.0572	2.9	0.700	2.4	0.0888	1.8	0.53
	004cJ-14.2	0.25	1595	30	114	0.02	517	±6	+1	12.0	1.2	0.0578	0.8	0.665	1.0	0.0834	1.2	0.84
	004cJ-14.3	0.11	1647	34	117	0.02	513	±6	+1	12.1	1.2	0.0577	1.1	0.658	1.1	0.0828	1.2	0.73
	004cJ-21.1	0.29	2173	64	155	0.03	515	±6	+3	12.0	1.3	0.0581	2.1	0.666	1.6	0.0831	1.3	0.53
High U	004cJ-15.2	0.34	7436	146	601	0.02	518	±7	+1	12.0	1.4	0.0578	0.7	0.667	1.0	0.0836	1.4	0.85
High Pb_c	~~004cJ-22.1~~	~~3.05~~	~~2911~~	~~94~~	~~220~~	~~0.03~~	~~522~~	~~±7~~	~~+6~~	~~11.9~~	~~1.3~~	~~0.0587~~	~~3.6~~	~~0.682~~	~~2.6~~	~~0.0843~~	~~1.3~~	~~0.33~~
High Pb_c, low UO/U	~~004cJ-23.1~~	~~16.92~~	~~1022~~	~~110~~	~~72~~	~~0.11~~	~~511~~	~~±6~~		~~12.1~~	~~1.2~~	~~0.0244~~	~~113.2~~	~~0.278~~	~~31.5~~	~~0.0826~~	~~1.2~~	~~0.01~~
High Pb_c, high UO/U	~~004cJ-24.1~~	~~13.40~~	~~6153~~	~~75~~	~~281~~	~~0.01~~	~~304~~	~~±21~~	~~+34~~	~~20.7~~	~~7.0~~	~~0.0563~~	~~23.9~~	~~0.375~~	~~9.3~~	~~0.0483~~	~~7.0~~	~~0.25~~
	004cJ-25.1	0.03	2094	44	149	0.02	514	±6	+2	12.1	1.2	0.0578	0.8	0.661	1.0	0.0830	1.2	0.84
High Pb_c	~~004cJ-17.2~~	~~6.03~~	~~1115~~	~~43~~	~~79~~	~~0.04~~	~~509~~	~~±6~~	~~+11~~	~~12.2~~	~~1.3~~	~~0.0591~~	~~8.9~~	~~0.670~~	~~6.0~~	~~0.0822~~	~~1.3~~	~~0.15~~
High UO/U	004cJ-25.2	0.08	7014	343	560	0.05	515	±7	+1	12.0	1.3	0.0577	0.7	0.662	1.0	0.0832	1.3	0.87
High UO/U	004cJ-26.1	0.09	2755	54	200	0.02	501	±6	+4	12.4	1.3	0.0577	1.0	0.644	1.0	0.0809	1.3	0.76
High Pb_c, high UO/U	~~004cJ-27.1~~	~~7.43~~	~~4342~~	~~220~~	~~337~~	~~0.05~~	~~523~~	~~±6~~	~~-1~~	~~11.8~~	~~1.3~~	~~0.0576~~	~~3.1~~	~~0.671~~	~~2.3~~	~~0.0845~~	~~1.3~~	~~0.36~~
High Pb_c	~~004cJ-28.1~~	~~10.98~~	~~2074~~	~~47~~	~~143~~	~~0.02~~	~~499~~	~~±8~~	~~+6~~	~~12.4~~	~~1.6~~	~~0.0581~~	~~19.2~~	~~0.644~~	~~12.4~~	~~0.0805~~	~~1.6~~	~~0.08~~
	004cJ-29.1	0.30	1506	11	106	0.01	509	±6	+0	12.2	1.3	0.0575	1.3	0.652	1.2	0.0822	1.3	0.71
High UO/U	004cJ-29.2	0.02	7680	204	627	0.03	520	±7	-1	11.9	1.3	0.0576	0.3	0.667	0.9	0.0840	1.3	0.96
	004cJ-30.1	0.29	1540	30	111	0.02	519	±6	+8	11.9	1.2	0.0589	2.0	0.680	1.6	0.0838	1.2	0.52

Table A3.4: SHRIMP data for sample 012bE. Notes from NiPR are as follows: Errors are 1-sigma; Pb_c and Pb^* indicate the common and radiogenic Pb, respectively. The error in Standard calibration was 0.20% (not included in above errors but required when comparing data from different mounts). (1) indicates that common Pb was corrected using measured ^{204}Pb.

Comment	Spot	$^{206}Pb_c$ (%)	U (ppm)	Th (ppm)	4 corr $^{206}Pb^*$ (ppm)	$^{232}Th/^{238}U$	$^{206}Pb/^{238}U$ Age (Ma) (1)	Discor-dant %	$^{238}U/^{206}Pb^*$ (1)	±%	$^{207}Pb^*/^{206}Pb^*$ (1)	±%	$^{207}Pb^*/^{235}U$ (1)	±%	$^{206}Pb^*/^{238}U$ (1)	±%	Error Corr.
	012bE-11.1	0.03	7989	361	637	0.05	506 ±8	+0	12.2	1.7	0.0574	0.2	0.65	1.1	0.082	1.7	1.0
	012bE-12.1	0.25	6138	197	477	0.03	509 ±6	+1	12.2	1.2	0.0576	0.5	0.65	0.8	0.082	1.2	0.9
	012bE-13.1	0.03	2059	44	144	0.02	506 ±5	+1	12.3	1.1	0.0575	0.3	0.65	0.7	0.082	1.1	1.0
	012bE-14.1	0.04	2083	35	144	0.02	498 ±5	+2	12.4	1.1	0.0575	0.6	0.64	0.8	0.080	1.1	0.9
	012bE-15.1	0.38	6661	245	529	0.04	515 ±6	-2	12.0	1.2	0.0573	0.7	0.66	0.9	0.083	1.2	0.8
High Pb_c	~~012bE-16.1~~	~~5.49~~	~~6662~~	~~233~~	~~626~~	~~0.04~~	~~606 ±8~~	~~-8~~	~~10.2~~	~~1.3~~	~~0.0589~~	~~12.1~~	~~0.80~~	~~9.7~~	~~0.099~~	~~1.3~~	~~0.1~~
	012bE-17.1	0.11	5525	172	431	0.03	516 ±6	+2	12.0	1.3	0.0578	1.4	0.66	1.3	0.083	1.3	0.6
	012bE-18.1	0.01	7588	345	600	0.05	506 ±9	+2	12.3	1.9	0.0577	0.6	0.65	1.3	0.082	1.9	0.9
High Pb_c	~~012bE-19.1~~	~~2.93~~	~~5983~~	~~237~~	~~347~~	~~0.04~~	~~384 ±4~~	~~+31~~	~~16.3~~	~~1.2~~	~~0.0588~~	~~2.5~~	~~0.50~~	~~1.4~~	~~0.061~~	~~1.2~~	~~0.4~~
	012bE-20.1	0.29	11084	630	923	0.06	501 ±6	+2	12.4	1.3	0.0575	0.5	0.64	0.9	0.081	1.3	0.9
	012bE-21.1	0.08	7519	301	601	0.04	511 ±7	+1	12.1	1.5	0.0577	1.3	0.66	1.3	0.083	1.5	0.7
	012bE-22.1	0.08	10549	440	889	0.04	511 ±7	+1	12.1	1.4	0.0576	0.9	0.66	1.1	0.083	1.4	0.8
	012bE-23.1	0.02	6823	275	525	0.04	499 ±6	+4	12.4	1.2	0.0577	0.4	0.64	0.8	0.080	1.2	0.9
	012bE-24.1	0.30	8952	359	723	0.04	504 ±6	+2	12.3	1.2	0.0575	0.5	0.65	0.8	0.081	1.2	0.9
High Pb_c	~~012bE-25.1~~	~~4.24~~	~~4518~~	~~144~~	~~305~~	~~0.03~~	~~456 ±9~~	~~+24~~	~~13.6~~	~~2.0~~	~~0.0599~~	~~4.7~~	~~0.61~~	~~3.1~~	~~0.073~~	~~2.0~~	~~0.4~~
	012bE-26.1	0.05	8436	327	680	0.04	508 ±6	-0	12.2	1.2	0.0574	0.2	0.65	0.8	0.082	1.2	1.0
High Pb_c	~~012bE-27.1~~	~~9.19~~	~~6197~~	~~217~~	~~163~~	~~0.04~~	~~177 ±2~~	~~+78~~	~~35.9~~	~~1.2~~	~~0.0658~~	~~3.7~~	~~0.25~~	~~1.0~~	~~0.028~~	~~1.2~~	~~0.3~~
High Pb_c	~~012bE-28.1~~	~~5.39~~	~~6701~~	~~319~~	~~178~~	~~0.05~~	~~177 ±2~~	~~-13~~	~~36.0~~	~~1.3~~	~~0.0492~~	~~11.0~~	~~0.19~~	~~2.1~~	~~0.028~~	~~1.3~~	~~0.1~~
	012bE-29.1	0.04	10631	366	897	0.04	512 ±7	-2	12.1	1.4	0.0573	0.3	0.65	0.9	0.083	1.4	1.0
	012bE-30.1	0.09	9539	399	786	0.04	510 ±6	+3	12.2	1.2	0.0579	0.6	0.66	0.9	0.082	1.2	0.9
	012bE-31.1	0.00	10915	520	908	0.05	502 ±13	+1	12.3	2.7	0.0575	0.3	0.64	1.7	0.081	2.7	1.0
	012bE-32.1	0.13	6074	254	477	0.04	514 ±9	-2	12.0	1.9	0.0573	0.6	0.66	1.3	0.083	1.9	0.9
	012bE-33.1	0.39	5426	222	425	0.04	519 ±12	+2	11.9	2.4	0.0580	0.9	0.67	1.7	0.084	2.4	0.9
unstable	~~012bE-34.1~~	~~--~~	~~5008~~	~~158~~	~~360~~	~~0.03~~	~~481 ±15~~	~~+25~~	~~12.9~~	~~3.2~~	~~0.0610~~	~~17.4~~	~~0.65~~	~~11.5~~	~~0.077~~	~~3.2~~	~~0.2~~
	012bE-35.1	0.25	7400	252	587	0.04	508 ±10	-1	12.2	2.1	0.0573	0.6	0.65	1.4	0.082	2.1	1.0
High Pb_c	~~012bE-36.1~~	~~2.01~~	~~6621~~	~~268~~	~~351~~	~~0.04~~	~~349 ±4~~	~~+32~~	~~18.0~~	~~1.1~~	~~0.0575~~	~~1.9~~	~~0.44~~	~~1.0~~	~~0.056~~	~~1.1~~	~~0.5~~
	012bE-37.1	0.17	10160	642	834	0.07	502 ±13	+3	12.3	2.6	0.0577	1.0	0.64	1.8	0.081	2.6	0.9
	012bE-38.1	0.25	5866	229	455	0.04	510 ±5	+2	12.1	1.1	0.0578	0.7	0.66	0.9	0.082	1.1	0.8
	012bE-39.1	0.68	7153	278	555	0.04	500 ±5	+5	12.4	1.1	0.0580	1.0	0.64	1.0	0.081	1.1	0.7
High Pb_c	~~012bE-40.1~~	~~2.16~~	~~7067~~	~~274~~	~~272~~	~~0.04~~	~~253 ±7~~	~~-1~~	~~25.0~~	~~2.7~~	~~0.0512~~	~~12.0~~	~~0.28~~	~~3.5~~	~~0.040~~	~~2.7~~	~~0.2~~
High Pb_c	~~012bE-41.1~~	~~15.71~~	~~5036~~	~~170~~	~~107~~	~~0.03~~	~~146 ±12~~	~~+47~~	~~43.6~~	~~8.6~~	~~0.0518~~	~~7.8~~	~~0.16~~	~~1.9~~	~~0.023~~	~~8.6~~	~~0.7~~
	012bE-42.1	0.53	9550	355	781	0.04	506 ±8	+1	12.3	1.7	0.0575	1.5	0.65	1.5	0.082	1.7	0.7
	012bE-42.2	0.14	6124	214	482	0.04	515 ±15	-3	12.0	3.1	0.0572	0.5	0.66	2.1	0.083	3.1	1.0
High Pb_c	~~012bE-42.3~~	~~3.83~~	~~6818~~	~~254~~	~~504~~	~~0.04~~	~~480 ±5~~	~~+13~~	~~13.0~~	~~1.1~~	~~0.0586~~	~~3.1~~	~~0.62~~	~~2.1~~	~~0.077~~	~~1.1~~	~~0.3~~
High Pb_c	~~012bE-43.1~~	~~3.28~~	~~7462~~	~~267~~	~~222~~	~~0.04~~	~~195 ±3~~	~~-112~~	~~32.5~~	~~1.8~~	~~0.0479~~	~~14.5~~	~~0.20~~	~~3.0~~	~~0.031~~	~~1.8~~	~~0.1~~
	012bE-44.1	0.06	8619	365	692	0.04	504 ±6	+2	12.3	1.2	0.0576	0.3	0.65	0.8	0.081	1.2	1.0
	012bE-45.1	0.01	6725	291	530	0.04	511 ±6	-2	12.1	1.3	0.0573	0.4	0.65	0.9	0.083	1.3	0.9

Table A3.5: SHRIMP data for sample 013aE. Notes from NiPR are as follows: Errors are 1-sigma; Pb_c and Pb^* indicate the common and radiogenic Pb, respectively. The error in Standard calibration was 0.20% (not included in above errors but required when comparing data from different mounts). (1) means that common Pb was corrected using measured ^{204}Pb.

Comment	Spot	$^{206}Pb_c$ (%)	U (ppm)	Th (ppm)	4 corr $^{206}Pb^*$ (ppm)	$^{232}Th/^{238}U$	$^{206}Pb/^{238}U$ Age (Ma) (1)		Discor-dant %	$^{238}U/^{206}Pb^*$ (1)	±%	$^{207}Pb^*/^{206}Pb^*$ (1)	±%	$^{207}Pb^*/^{235}U$ (1)	±%	$^{206}Pb^*/^{238}U$ (1)	±%	Error Corr.
	013aE-9.1	0.16	10088	229	848	0.02	514	±8	+1	12.0	1.7	0.0577	0.9	0.66	1.3	0.083	1.7	0.8
	013aE-10.1	0.04	15076	530	1374	0.04	509	±7	+1	12.2	1.4	0.0576	0.3	0.65	0.9	0.082	1.4	1.0
High Pb_c	013aE-11.1	27.08	10182	740	247	0.08	153	±6	+81	41.7	4.2	0.0662	36.3	0.22	8.0	0.024	4.2	0.1
High Pb_c	013aE-12.1	7.54	5544	158	406	0.03	485	±6	+7	12.8	1.3	0.0577	11.7	0.62	7.3	0.078	1.3	0.1
	013aE-13.1	0.25	4424	30	339	0.01	516	±12	+3	12.0	2.3	0.0580	1.3	0.67	1.8	0.083	2.3	0.9
High Pb_c	013aE-14.1	24.98	8285	171	257	0.02	201	±3	+66	31.6	1.4	0.0595	8.7	0.26	2.3	0.032	1.4	0.1
	013aE-15.1	0.03	6186	169	479	0.03	506	±7	+1	12.2	1.5	0.0575	0.4	0.65	1.0	0.082	1.5	1.0
	013aE-16.1	0.27	10734	241	920	0.02	518	±6	-0	12.0	1.2	0.0576	0.4	0.67	0.9	0.084	1.2	0.9
High Pb_c	013aE-17.1	3.30	16269	379	970	0.02	330	±4	+23	19.1	1.4	0.0554	1.2	0.40	0.7	0.052	1.4	0.6
High Pb_c	013aE-18.1	6.16	11745	242	713	0.02	365	±5	+17	17.2	1.4	0.0556	7.3	0.45	3.3	0.058	1.4	0.1
High Pb_c	013aE-19.1	8.28	1868	69	133	0.04	514	±6	+18	12.0	1.1	0.0607	8.0	0.69	5.6	0.083	1.1	0.1
High Pb_c	013aE-19.2	8.06	2251	204	157	0.09	505	±8	+30	12.3	1.6	0.0634	25.3	0.71	18.1	0.081	1.6	0.1
	013aE-20.1	0.06	12698	340	1104	0.03	508	±6	+4	12.2	1.2	0.0579	1.2	0.65	1.1	0.082	1.2	0.6
	013aE-21.1	0.04	10201	367	842	0.04	504	±6	-0	12.3	1.1	0.0573	0.5	0.64	0.8	0.081	1.1	0.9
High Pb_c	013aE-22.1	33.30	2471	36	148	0.02	434	±43	+312	14.3	10.2	0.0424	180.4	0.41	73.6	0.070	10.2	0.1
High Pb_c	013aE-23.1	4.04	8499	141	943	0.02	689	±8	-43	8.9	1.2	0.0567	1.5	0.88	1.7	0.113	1.2	0.6
High Pb_c	013aE-24.1	5.97	12880	268	802	0.02	366	±6	+35	17.1	1.7	0.0588	6.5	0.47	3.2	0.058	1.7	0.2
High Pb_c	013aE-25.1	1.45	5796	94	528	0.02	596	±7	+1	10.3	1.2	0.0599	1.7	0.80	1.7	0.097	1.2	0.5
	013aE-26.1	0.04	6002	102	474	0.02	518	±6	-1	12.0	1.2	0.0575	0.5	0.66	0.8	0.084	1.2	0.9
	013aE-28.1	0.10	7626	147	610	0.02	511	±6	+0	12.1	1.2	0.0575	0.5	0.65	0.8	0.083	1.2	0.9
High Pb_c	013aE-29.1	8.06	11648	268	338	0.02	177	±8	+65	35.9	4.5	0.0575	28.7	0.22	6.4	0.028	4.5	0.1
	013aE-30.1	0.02	14572	413	1317	0.03	509	±6	+2	12.2	1.3	0.0577	0.2	0.65	0.9	0.082	1.3	1.0
High Pb_c	013aE-31.1	4.67	5309	117	393	0.02	492	±31	+26	12.6	6.6	0.0618	28.6	0.67	19.8	0.079	6.6	0.2
	013aE-32.1	0.26	7682	171	627	0.02	520	±5	+0	11.9	1.1	0.0578	1.3	0.67	1.2	0.084	1.1	0.6
High Pb_c	013aE-33.1	34.52	2044	50	136	0.03	482	±5	+68	12.9	1.1	0.0945	16.8	1.01	17.0	0.078	1.1	0.1
	013aE-34.1	0.30	12000	364	1053	0.03	518	±6	-0	11.9	1.2	0.0577	0.7	0.67	0.9	0.084	1.2	0.8
High Pb_c	013aE-35.1	56.72	3122	42	200	0.01	443	±19	+149	14.1	4.5	0.0326	92.7	0.32	29.7	0.071	4.5	0.0
High Pb_c	013aE-36.1	25.29	1502	74	102	0.05	490	±12	+372	12.7	2.5	0.0428	54.4	0.47	25.4	0.079	2.5	0.0
High Pb_c	013aE-37.1	71.18	6496	240	243	0.04	249	±57	+84	25.4	23.4	0.0987	154.7	0.54	83.8	0.039	23.4	0.1
	013aE-38.1	0.35	6667	110	534	0.02	520	±7	-2	11.9	1.3	0.0575	1.1	0.67	1.2	0.084	1.3	0.7
	013aE-39.1	0.03	12806	348	1111	0.03	506	±9	-0	12.3	1.8	0.0574	0.8	0.65	1.3	0.082	1.8	0.9
High Pb_c	013aE-40.1	33.75	3996	75	222	0.02	380	±9	+62	16.5	2.4	0.0722	23.0	0.60	13.9	0.061	2.4	0.1
	013aE-38.2	0.01	4442	61	343	0.01	520	±8	-1	11.9	1.5	0.0576	0.7	0.67	1.1	0.084	1.5	0.9
	013aE-41.1	0.04	13154	346	1152	0.03	507	±12	-1	12.2	2.4	0.0572	0.7	0.65	1.6	0.082	2.4	0.9
High Pb_c	013aE-41.2	14.38	3810	63	423	0.02	742	±52	-250	8.2	7.5	0.0504	55.4	0.85	47.3	0.122	7.5	0.1
	013aE-42.1	0.01	13572	276	1209	0.02	512	±6	-1	12.1	1.3	0.0574	0.5	0.65	0.9	0.083	1.3	0.9
High Pb_c	013aE-42.2	9.06	9784	158	419	0.02	268	±39	+81	23.5	14.8	0.0892	85.5	0.52	45.3	0.042	14.8	0.1
High Pb_c	013aE-43.1	--	10470	184	385	0.02	229	±136		27.7	60.7	0.0022	3680.7	0.01	40.0	0.036	60.7	0.0

Table A3.6: SHRIMP data for sample 004dI. Notes from NiPR are as follows: Errors are 1-sigma; Pb_c and Pb^* indicate the common and radiogenic Pb, respectively. The error in Standard calibration was 0.20% (not included in above errors but required when comparing data from different mounts). (1) Common Pb corrected using measured 204Pb.

Comment	Spot	U (ppm)	Th (ppm)	4 corr $^{206}Pb^*$ (ppm)	$^{232}Th/^{238}U$	$^{206}Pb/^{238}U$ Age (Ma) (1)		Discor-dant %	$^{238}U/^{206}Pb^*$ (1)	±%	$^{207}Pb^*/^{206}Pb^*$ (1)	±%	$^{207}Pb^*/^{235}U$ (1)	±%	$^{206}Pb^*/^{238}U$ (1)	±%	Error Corr.
	004dI-1.1	1130	142	78	0.13	497	±6	+0	12.5	1.3	0.0571	0.6	0.631	0.9	0.0801	1.3	0.91
	004dI-2.1	3794	993	273	0.27	490	±5	-4	12.7	1.1	0.0565	0.7	0.615	0.8	0.0790	1.1	0.83
	004dI-3.1	2559	326	177	0.13	482	±5	-3	12.9	1.0	0.0564	0.7	0.604	0.8	0.0776	1.0	0.81
High Pb_c	~~004dI-4.1~~	~~2762~~	~~666~~	~~172~~	~~0.25~~	~~433~~	~~±6~~	~~+4~~	~~14.4~~	~~1.3~~	~~0.0560~~	~~6.5~~	~~0.537~~	~~3.6~~	~~0.0695~~	~~1.3~~	~~0.19~~
	004dI-5.1	1312	746	91	0.59	499	±6	-2	12.4	1.2	0.0569	0.9	0.631	1.0	0.0804	1.2	0.82
	004dI-6.1	231	100	16	0.45	494	±7	+3	12.5	1.6	0.0574	2.1	0.631	1.7	0.0797	1.6	0.59
	004dI-6.2	173	67	12	0.40	482	±5	-8	12.9	1.1	0.0558	2.5	0.597	1.6	0.0776	1.1	0.40
High U	004dI-7.1	3293	281	237	0.09	493	±6	-0	12.6	1.2	0.0570	1.4	0.625	1.1	0.0795	1.2	0.64
Pb unstable, high U	~~004dI-8.1~~	~~3202~~	~~708~~	~~168~~	~~0.23~~	~~365~~	~~±24~~	~~+53~~	~~17.2~~	~~6.9~~	~~0.0652~~	~~22.3~~	~~0.524~~	~~12.2~~	~~0.0583~~	~~6.9~~	~~0.28~~
High Pb_c, high U	~~004dI-9.1~~	~~2695~~	~~571~~	~~152~~	~~0.22~~	~~394~~	~~±4~~	~~-50~~	~~15.9~~	~~1.1~~	~~0.0515~~	~~2.6~~	~~0.447~~	~~1.2~~	~~0.0630~~	~~1.1~~	~~0.37~~
High U	004dI-10.1	5368	556	397	0.11	491	±6	+2	12.6	1.3	0.0572	0.9	0.625	1.0	0.0792	1.3	0.80
High U	004dI-11.1	6486	2427	497	0.39	499	±7	-5	12.4	1.4	0.0566	0.5	0.627	0.9	0.0805	1.4	0.92
High U	004dI-12.1	3725	794	274	0.22	500	±6	-11	12.4	1.2	0.0559	0.5	0.622	0.8	0.0807	1.2	0.91
High U	004dI-13.1	2768	214	198	0.08	496	±6	+2	12.5	1.2	0.0573	1.0	0.631	1.0	0.0799	1.2	0.76
High U	004dI-14.1	3279	389	239	0.12	500	±6	-3	12.4	1.2	0.0569	0.7	0.632	0.9	0.0806	1.2	0.85
High U	004dI-15.1	6303	317	481	0.05	499	±6	-4	12.4	1.3	0.0567	0.4	0.629	0.9	0.0805	1.3	0.94
	004dI-16.1	355	161	24	0.47	494	±7	+6	12.6	1.4	0.0578	1.6	0.635	1.3	0.0796	1.4	0.66
	004dI-17.1	298	194	20	0.67	495	±7	-5	12.5	1.5	0.0565	2.0	0.621	1.5	0.0797	1.5	0.59
High Pb_c	~~004dI-18.1~~	~~471~~	~~134~~	~~29~~	~~0.29~~	~~448~~	~~±7~~	~~-672~~	~~13.9~~	~~1.7~~	~~0.0472~~	~~35.6~~	~~0.468~~	~~16.7~~	~~0.0719~~	~~1.7~~	~~0.05~~
High U	004dI-19.1	4341	2420	320	0.58	498	±6	-4	12.5	1.3	0.0567	0.5	0.627	0.8	0.0803	1.3	0.93
	004dI-20.1	1319	720	90	0.56	493	±6	+3	12.6	1.2	0.0574	1.0	0.629	1.0	0.0795	1.2	0.79
High U	004dI-21.1	3521	826	253	0.24	492	±6	+5	12.6	1.3	0.0577	1.0	0.631	1.0	0.0793	1.3	0.76
High U	004dI-22.1	4227	1047	308	0.26	492	±6	+5	12.6	1.3	0.0576	1.1	0.631	1.1	0.0794	1.3	0.74
	004dI-23.1	1239	598	85	0.50	494	±6	-1	12.6	1.3	0.0569	0.9	0.625	1.0	0.0796	1.3	0.82
	004dI-24.1	498	51	33	0.10	482	±5	+8	12.9	1.1	0.0578	1.7	0.618	1.2	0.0776	1.1	0.55
High U	004dI-25.1	3429	1084	246	0.33	492	±6	+4	12.6	1.2	0.0576	0.5	0.629	0.9	0.0792	1.2	0.91
High Pb_c	~~004dI-26.1~~	~~8698~~	~~442~~	~~627~~	~~0.05~~	~~454~~	~~±6~~	~~-121~~	~~13.7~~	~~1.4~~	~~0.0502~~	~~1.7~~	~~0.505~~	~~1.1~~	~~0.0730~~	~~1.4~~	~~0.57~~
High U	004dI-27.1	3441	864	250	0.26	497	±5	+5	12.5	1.1	0.0579	1.3	0.640	1.1	0.0802	1.1	0.60
High Pb_c, high U	~~004dI-28.1~~	~~4379~~	~~1407~~	~~141~~	~~0.33~~	~~221~~	~~±3~~	~~+58~~	~~28.6~~	~~1.2~~	~~0.0578~~	~~2.8~~	~~0.278~~	~~0.9~~	~~0.0349~~	~~1.2~~	~~0.38~~
High U	004dI-29.1	3424	381	249	0.11	497	±6	+0	12.5	1.3	0.0572	0.6	0.633	0.9	0.0802	1.3	0.90
High U	004dI-30.1	4807	611	354	0.13	493	±6	+0	12.6	1.3	0.0571	0.5	0.625	0.9	0.0794	1.3	0.91
High U	004dI-31.1	9271	791	735	0.09	493	±7	+3	12.6	1.4	0.0574	0.4	0.628	0.9	0.0794	1.4	0.95
	004dI-32.1	2004	1238	135	0.64	486	±5	-0	12.8	1.0	0.0568	0.7	0.614	0.8	0.0783	1.0	0.80
	004dI-32.2	629	767	43	1.26	489	±5	+4	12.7	1.1	0.0575	1.5	0.625	1.2	0.0788	1.1	0.59
	004dI-33.1	1474	800	100	0.56	490	±8	+7	12.7	1.6	0.0580	2.2	0.632	1.7	0.0790	1.6	0.58
High Pb_c	~~004dI-34.1~~	~~2123~~	~~404~~	~~136~~	~~0.20~~	~~463~~	~~±6~~	~~-446~~	~~13.4~~	~~1.2~~	~~0.0477~~	~~3.9~~	~~0.490~~	~~2.0~~	~~0.0744~~	~~1.2~~	~~0.30~~
inheritance	004dI-35.1	368	203	56	0.57	1045	±14	+2	5.7	1.5	0.0749	1.0	1.817	3.2	0.1759	1.5	0.83
inheritance	004dI-35.2	340	112	51	0.34	1045	±10	+1	5.7	1.1	0.0747	0.6	1.813	2.3	0.1760	1.1	0.86

High Pb_c	~~004dl-36.1~~	~~7384~~	~~796~~	~~393~~	~~0.11~~	~~346~~	~~±5~~	~~+25~~	~~18.1~~	~~1.4~~	~~0.0563~~	~~5.7~~	~~0.427~~	~~2.5~~	~~0.0551~~	~~1.4~~	~~0.21~~
High Pb_c	~~004dl-36.2~~	~~9379~~	~~866~~	~~522~~	~~0.10~~	~~349~~	~~±5~~	~~+28~~	~~18.0~~	~~1.4~~	~~0.0568~~	~~1.5~~	~~0.436~~	~~0.9~~	~~0.0557~~	~~1.4~~	~~0.61~~

Table A3.7: SHRIMP data for sample 012aD. Notes from NiPR are as follows: Errors are 1-sigma; Pb_c and Pb^* indicate the common and radiogenic Pb, respectively. The error in Standard calibration was 0.20% (not included in above errors but required when comparing data from different mounts). (1) Common Pb corrected using measured 204Pb.

Comment	Spot	$^{206}Pb_c$ (%)	U (ppm)	Th (ppm)	4 corr $^{206}Pb^*$ (ppm)	$^{232}Th/^{238}U$	$^{206}Pb/^{238}U$ Age (Ma) (1)		Discor-dant %	$^{238}U/^{206}Pb^*$ (1)	±%	$^{207}Pb^*/^{206}Pb^*$ (1)	±%	$^{207}Pb^*/^{235}U$ (1)	±%	$^{206}Pb^*/^{238}U$ (1)	±%	Error Corr.
	012aD-12.1	0.05	424	81	29	0.20	489	±7	-1	12.7	1.4	0.0568	1.6	0.62	2.1	0.079	1.4	0.7
High Pb_c	~~012aD-13.1~~	~~8.77~~	~~208~~	~~157~~	~~13~~	~~0.78~~	~~468~~	~~±8~~	~~+52~~	~~13.3~~	~~1.7~~	~~0.0704~~	~~23.4~~	~~0.73~~	~~23.5~~	~~0.075~~	~~1.7~~	~~0.1~~
	012aD-13.2	0.11	1649	821	110	0.51	480	±5	-4	12.9	1.1	0.0563	1.8	0.60	2.1	0.077	1.1	0.5
	012aD-14.1	0.10	295	183	20	0.64	483	±7	+5	12.9	1.6	0.0575	2.2	0.62	2.7	0.078	1.6	0.6
hi U	~~012aD-14.2~~	~~0.18~~	~~1323~~	~~249~~	~~94~~	~~0.19~~	~~514~~	~~±6~~	~~+6~~	~~12.0~~	~~1.2~~	~~0.0585~~	~~1.5~~	~~0.67~~	~~1.9~~	~~0.083~~	~~1.2~~	~~0.6~~
hi U	~~012aD-15.1~~	~~0.11~~	~~2009~~	~~535~~	~~142~~	~~0.28~~	~~510~~	~~±6~~	~~-1~~	~~12.1~~	~~1.1~~	~~0.0573~~	~~0.8~~	~~0.65~~	~~1.4~~	~~0.082~~	~~1.1~~	~~0.8~~
	012aD-15.2	0.07	246	128	17	0.54	487	±8	+5	12.7	1.7	0.0576	2.4	0.62	2.9	0.078	1.7	0.6
inheritance	012aD-16.1	0.04	121	68	52	0.58	2602	±28	+1	2.0	1.3	0.1770	2.0	12.14	2.4	0.497	1.3	0.5
	012aD-17.1	0.03	3537	345	233	0.10	477	±4	+4	13.0	1.0	0.0571	1.4	0.60	1.7	0.077	1.0	0.6
	012aD-18.1	--	197	81	13	0.42	473	±7	+1	13.1	1.6	0.0567	2.1	0.59	2.7	0.076	1.6	0.6
	012aD-19.1	0.05	213	80	14	0.39	472	±11	+2	13.2	2.3	0.0567	3.7	0.59	4.3	0.076	2.3	0.5
High Pb_c	~~012aD-20.1~~	~~6.55~~	~~545~~	~~403~~	~~36~~	~~0.76~~	~~479~~	~~±7~~	~~-20~~	~~13.0~~	~~1.5~~	~~0.0548~~	~~11.7~~	~~0.58~~	~~11.8~~	~~0.077~~	~~1.5~~	~~0.1~~
	012aD-21.1	0.15	304	168	20	0.57	472	±7	+3	13.2	1.5	0.0569	2.1	0.60	2.6	0.076	1.5	0.6
	012aD-22.1	0.05	96	50	7	0.54	489	±9	-4	12.7	1.9	0.0564	2.9	0.61	3.5	0.079	1.9	0.5
	012aD-22.2	0.14	1665	511	109	0.32	473	±5	+2	13.1	1.1	0.0567	1.6	0.60	1.9	0.076	1.1	0.6
	012aD-23.1	0.13	185	104	12	0.58	480	±8	-7	12.9	1.7	0.0559	2.6	0.60	3.1	0.077	1.7	0.6
inheritance	012aD-24.1	0.03	144	158	19	1.14	936	±17	+1	6.4	1.9	0.0706	1.9	1.52	2.7	0.156	1.9	0.7
High Pb_c	~~012aD-25.1~~	~~3.17~~	~~534~~	~~109~~	~~36~~	~~0.21~~	~~487~~	~~±10~~	~~-47~~	~~12.7~~	~~2.1~~	~~0.0531~~	~~8.2~~	~~0.58~~	~~8.5~~	~~0.078~~	~~2.1~~	~~0.2~~
	012aD-26.1	0.04	498	378	33	0.78	479	±6	-0	13.0	1.3	0.0566	1.4	0.60	1.9	0.077	1.3	0.7
	012aD-27.1	0.02	525	160	35	0.32	483	±6	+2	12.9	1.4	0.0571	1.4	0.61	2.0	0.078	1.4	0.7
	012aD-28.1	0.07	287	69	19	0.25	481	±7	+3	12.9	1.6	0.0571	2.1	0.61	2.7	0.078	1.6	0.6
inheritance	012aD-29.1	--	99	59	16	0.62	1085	±21	-0	5.5	2.1	0.0756	3.0	1.91	3.7	0.183	2.1	0.6
	012aD-30.1	0.04	1552	86	104	0.06	484	±5	+2	12.8	1.1	0.0571	0.8	0.61	1.4	0.078	1.1	0.8
	012aD-31.1	--	696	546	47	0.81	491	±7	-4	12.6	1.5	0.0565	1.1	0.62	1.9	0.079	1.5	0.8
	012aD-32.1	--	203	72	13	0.37	480	±7	+1	12.9	1.5	0.0568	1.3	0.61	2.0	0.077	1.5	0.8
	012aD-32.2	0.05	170	65	12	0.40	497	±8	-11	12.5	1.6	0.0560	2.2	0.62	2.7	0.080	1.6	0.6
	012aD-33.1	0.01	1203	430	82	0.37	492	±6	-0	12.6	1.3	0.0570	0.8	0.62	1.6	0.079	1.3	0.8
	012aD-33.2	0.08	190	148	13	0.80	495	±8	+1	12.5	1.6	0.0572	1.4	0.63	2.2	0.080	1.6	0.7
	012aD-34.1	0.00	175	66	12	0.39	498	±8	-5	12.4	1.6	0.0566	2.2	0.63	2.8	0.080	1.6	0.6
	012aD-35.1	--	346	222	23	0.66	475	±6	+8	13.1	1.3	0.0575	1.6	0.61	2.1	0.076	1.3	0.7
	012aD-35.2	0.01	2581	1057	170	0.42	477	±5	-0	13.0	1.1	0.0566	0.6	0.60	1.2	0.077	1.1	0.9
	012aD-36.1	0.09	220	119	15	0.56	491	±7	-9	12.6	1.5	0.0560	2.1	0.61	2.6	0.079	1.5	0.6
High Pb_c	~~012aD-37.1~~	~~6.57~~	~~762~~	~~421~~	~~46~~	~~0.57~~	~~436~~	~~±6~~	~~+233~~	~~14.3~~	~~1.5~~	~~0.0400~~	~~17.3~~	~~0.39~~	~~17.3~~	~~0.070~~	~~1.5~~	~~0.1~~
	012aD-38.1	--	221	126	15	0.59	481	±7	+4	12.9	1.5	0.0572	2.0	0.61	2.5	0.078	1.5	0.6
High Pb_c	~~012aD-39.1~~	~~0.24~~	~~216~~	~~102~~	~~14~~	~~0.49~~	~~475~~	~~±7~~	~~+1~~	~~13.1~~	~~1.4~~	~~0.0567~~	~~2.2~~	~~0.60~~	~~2.6~~	~~0.076~~	~~1.4~~	~~0.5~~

	012aD-39.2	0.12	627	123	41	0.20	477 ±6	+1	13.0	1.2	0.0568	1.3	0.60	1.8	0.077	1.2	0.7
	012aD-40.1	0.01	609	407	42	0.69	494 ±5	-3	12.6	1.0	0.0567	1.2	0.62	1.5	0.080	1.0	0.7
	012aD-41.1	0.17	245	119	16	0.50	478 ±7	+2	13.0	1.4	0.0568	2.0	0.60	2.4	0.077	1.4	0.6
	012aD-42.1	0.01	567	487	37	0.89	476 ±6	+1	13.1	1.2	0.0568	1.2	0.60	1.7	0.077	1.2	0.7
High Pb_c	~~012aD-42.2~~	~~1.13~~	~~601~~	~~354~~	~~40~~	~~0.61~~	~~481 ±5~~	~~-7~~	~~12.9~~	~~1.2~~	~~0.0559~~	~~3.2~~	~~0.60~~	~~3.4~~	~~0.077~~	~~1.2~~	~~0.3~~
	012aD-43.1	0.00	301	118	20	0.40	483 ±6	+0	12.9	1.3	0.0568	1.6	0.61	2.0	0.078	1.3	0.6
High Pb_c	~~012aD-43.2~~	~~11.88~~	~~1352~~	~~455~~	~~89~~	~~0.35~~	~~474 ±14~~		~~13.1~~	~~3.0~~	~~0.0236~~	~~103.5~~	~~0.25~~	~~103.5~~	~~0.076~~	~~3.0~~	~~0.0~~
	012aD-45.1	0.07	448	220	30	0.51	482 ±6	-4	12.9	1.2	0.0563	2.5	0.60	2.8	0.078	1.2	0.4
	012aD-45.2	0.08	525	385	35	0.76	484 ±6	-3	12.8	1.2	0.0564	1.3	0.61	1.7	0.078	1.2	0.7
	012aD-46.1	0.01	620	223	42	0.37	491 ±5	-5	12.6	1.2	0.0564	1.1	0.62	1.6	0.079	1.2	0.7
	012aD-47.1	0.10	458	422	31	0.95	490 ±6	-3	12.7	1.2	0.0566	1.4	0.62	1.8	0.079	1.2	0.7
	012aD-48.1	0.07	221	127	15	0.59	486 ±7	-2	12.8	1.4	0.0566	1.8	0.61	2.3	0.078	1.4	0.6

Table A3.8: SHRIMP data for sample 040aA. Notes from NiPR are as follows: Errors are 1-sigma; Pbc and Pb* indicate the common and radiogenic Pb, respectively. The error in Standard calibration was 0.20% (not included in above errors but required when comparing data from different mounts). (1) Common Pb corrected using measured 204Pb.

Comment	**Spot**	**$^{206}Pb_c$ (%)**	**U (ppm)**	**Th (ppm)**	**4 corr $^{206}Pb^*$ (ppm)**	**$^{232}Th/^{238}U$**	**$^{206}Pb/^{238}U$ Age (Ma) (1)**		**Discor-dant %**	**$^{238}U/^{206}Pb^*$ (1)**	**±%**	**$^{207}Pb^*/^{206}Pb^*$ (1)**	**±%**	**$^{207}Pb^*/^{235}U$ (1)**	**±%**	**$^{206}Pb^*/^{238}U$ (1)**	**±%**	**Error Corr.**
High U	040aA-1.1	0.01	14115	3461	1180	0.25	477	±7	+1	13.0	1.6	0.0567	0.5	0.600	1.0	0.0767	1.6	0.92
Pb unstable, High U	~~040aA-2.1~~	~~0.10~~	~~8261~~	~~1016~~	~~561~~	~~0.13~~	~~431~~	~~±20~~	~~+33~~	~~14.4~~	~~4.7~~	~~0.0610~~	~~5.1~~	~~0.582~~	~~4.1~~	~~0.0692~~	~~4.7~~	~~0.62~~
High U	040aA-3.1	0.05	5317	1028	391	0.20	488	±6	+2	12.7	1.3	0.0572	0.3	0.620	0.8	0.0787	1.3	0.97
Inheritance	040aA-4.1	0.00	1073	302	177	0.29	1132	±13	+0	5.2	1.3	0.0775	0.6	2.050	2.9	0.1919	1.3	0.91
High U	040aA-5.1	0.03	14652	1125	1223	0.08	471	±7	-1	13.2	1.6	0.0564	0.3	0.590	0.9	0.0758	1.6	0.97
High U	040aA-6.1	0.06	7116	730	545	0.11	494	±10	-4	12.6	2.0	0.0565	1.0	0.620	1.4	0.0796	2.0	0.87
High U	040aA-7.1	0.07	4898	752	355	0.16	485	±6	-0	12.8	1.3	0.0568	0.6	0.613	0.9	0.0782	1.3	0.89
High U	040aA-8.1	0.01	7882	784	593	0.10	479	±6	+3	13.0	1.3	0.0571	0.7	0.608	0.9	0.0772	1.3	0.87
	040aA-9.1	0.25	2189	229	146	0.11	483	±5	-2	12.9	1.2	0.0566	0.5	0.607	0.8	0.0778	1.2	0.91
High Pb_c, High U	~~040aA-10.1~~	~~1.27~~	~~4842~~	~~569~~	~~384~~	~~0.12~~	~~529~~	~~±7~~	~~+17~~	~~11.7~~	~~1.3~~	~~0.0609~~	~~2.2~~	~~0.718~~	~~1.8~~	~~0.0856~~	~~1.3~~	~~0.48~~
High U	040aA-11.1	0.06	5211	564	377	0.11	482	±6	+0	12.9	1.3	0.0568	0.5	0.607	0.8	0.0776	1.3	0.93
High U	040aA-12.1	0.16	5543	941	409	0.18	489	±6	-3	12.7	1.3	0.0566	0.6	0.615	0.9	0.0788	1.3	0.90
High U	040aA-13.1	0.02	12005	2644	1000	0.23	493	±7	-1	12.6	1.5	0.0569	0.3	0.623	0.9	0.0795	1.5	0.98
Pb unstable High U	~~040aA-14.1~~	~~0.02~~	~~4172~~	~~466~~	~~292~~	~~0.12~~	~~474~~	~~±27~~	~~+5~~	~~13.1~~	~~5.9~~	~~0.0573~~	~~2.7~~	~~0.603~~	~~3.9~~	~~0.0764~~	~~5.9~~	~~0.90~~
High Pb_c, High U	~~040aA-15.1~~	~~7.62~~	~~6616~~	~~1131~~	~~363~~	~~0.18~~	~~361~~	~~±5~~	~~+8~~	~~17.4~~	~~1.4~~	~~0.0545~~	~~5.0~~	~~0.433~~	~~2.3~~	~~0.0576~~	~~1.4~~	~~0.24~~
High U	040aA-16.1	0.04	13784	1756	1144	0.13	476	±7	+1	13.0	1.5	0.0567	0.3	0.600	0.9	0.0767	1.5	0.96
High U	040aA-17.1	0.04	9797	501	775	0.05	488	±5	+0	12.7	1.2	0.0570	0.3	0.617	0.7	0.0786	1.2	0.95
High U	040aA-18.1	0.06	8673	1677	664	0.20	481	±6	-1	12.9	1.4	0.0566	0.4	0.605	0.9	0.0775	1.4	0.96
High U	040aA-19.1	0.06	5279	703	383	0.14	482	±6	+3	12.9	1.3	0.0571	0.5	0.612	0.8	0.0777	1.3	0.92
High U	040aA-20.1	0.11	6572	296	496	0.05	491	±6	-1	12.6	1.3	0.0569	0.4	0.621	0.8	0.0791	1.3	0.94
High U	040aA-21.1	0.02	7641	692	562	0.09	471	±11	+4	13.2	2.4	0.0569	0.2	0.595	1.4	0.0757	2.4	0.99
Disc. High U	~~040aA-22.1~~	~~0.31~~	~~5483~~	~~852~~	~~300~~	~~0.16~~	~~366~~	~~±5~~	~~+15~~	~~17.1~~	~~1.3~~	~~0.0554~~	~~0.6~~	~~0.447~~	~~0.6~~	~~0.0584~~	~~1.3~~	~~0.89~~
High U	040aA-23.1	0.05	5891	1244	426	0.22	477	±6	+2	13.0	1.3	0.0569	0.7	0.602	0.9	0.0767	1.3	0.86
Inheritance	040aA-24.1	0.00	1215	58	567	0.05	2797	±28	+0	1.8	1.2	0.1968	0.8	14.740	21.7	0.5432	1.2	0.82
High U	040aA-25.1	0.06	7872	1428	597	0.19	483	±7	-0	12.9	1.5	0.0567	0.4	0.609	1.0	0.0778	1.5	0.96
High U	040aA-26.1	0.03	11028	2872	862	0.27	472	±7	+3	13.2	1.4	0.0568	0.3	0.595	0.9	0.0760	1.4	0.97
High U	040aA-14.2	0.32	2933	296	201	0.10	473	±7	+5	13.1	1.6	0.0572	0.9	0.601	1.1	0.0761	1.6	0.88
Disc. High U	~~040aA-19.2~~	~~0.28~~	~~5967~~	~~1063~~	~~269~~	~~0.18~~	~~301~~	~~±4~~	~~+18~~	~~20.9~~	~~1.4~~	~~0.0539~~	~~0.9~~	~~0.355~~	~~0.6~~	~~0.0478~~	~~1.4~~	~~0.82~~
High U	040aA-27.1	0.06	5322	635	394	0.12	492	±6	-5	12.6	1.3	0.0564	0.5	0.617	0.9	0.0794	1.3	0.92
High U	040aA-28.1	0.05	10705	1274	855	0.12	484	±7	-1	12.8	1.4	0.0567	0.3	0.610	0.9	0.0780	1.4	0.96
High Pb_c, High U	~~040aA-29.1~~	~~6.30~~	~~9689~~	~~482~~	~~477~~	~~0.05~~	~~308~~	~~±22~~	~~-15~~	~~20.4~~	~~7.3~~	~~0.0516~~	~~24.1~~	~~0.348~~	~~8.8~~	~~0.0490~~	~~7.3~~	~~0.25~~
High U	040aA-30.1	0.14	10700	1617	843	0.16	478	±7	+0	13.0	1.5	0.0567	0.3	0.602	0.9	0.0770	1.5	0.96
High U	040aA-30.2	0.03	11523	1422	932	0.13	484	±7	+1	12.8	1.5	0.0569	0.3	0.611	0.9	0.0779	1.5	0.97
	040aA-31.1	0.20	1250	144	84	0.12	486	±6	+4	12.8	1.3	0.0574	1.3	0.620	1.1	0.0784	1.3	0.72
High Pb_c High U	~~040aA-32.1~~	~~0.81~~	~~9402~~	~~1655~~	~~386~~	~~0.18~~	~~259~~	~~±4~~	~~-6~~	~~24.4~~	~~1.4~~	~~0.0511~~	~~2.8~~	~~0.289~~	~~0.9~~	~~0.0410~~	~~1.4~~	~~0.40~~
High U	040aA-32.2	0.09	14210	2492	1188	0.18	476	±7	+2	13.1	1.5	0.0569	0.4	0.600	1.0	0.0766	1.5	0.96

A3.4 Major and trace element data:

A3.4 Major and trace element data

Table A3.9: Major element XRF data in wt%. Samples marked with * are from Grantham *et al.* (1991):

Sample	SiO_2	TiO_2	Al_2O_3	Fe_2O_3	MnO	MgO	CaO	Na_2O	K_2O	P_2O_5	Cr_2O_3	LOI	Total	H_2O-
004aC	72.38	0.16	14.59	1.38	0.012	0.13	1.28	3.88	5.07	0.040	0.0005	0.73	99.65	0.28
004cJ	71.28	0.03	16.22	0.56	0.012	0.06	2.59	6.67	1.27	0.037	0.0005	0.44	99.17	0.20
004dI	74.84	0.10	13.82	0.83	0.014	0.19	1.45	4.03	3.79	0.040	0.0005	0.30	99.41	0.22
005aA	72.30	0.14	14.80	0.77	0.009	0.19	1.28	3.54	5.88	0.050	0.0005	0.35	99.32	0.21
007aB	75.19	0.02	13.85	0.62	0.076	0.005	0.82	4.43	4.18	0.015	0.0005	0.43	99.55	0.21
008aC	69.18	0.32	15.45	1.99	0.023	0.47	1.66	3.42	5.90	0.096	0.0005	0.88	99.39	0.28
008P2	74.43	0.02	15.17	0.19	0.004	0.005	2.40	5.21	1.70	0.012	0.0005	0.55	99.63	0.18
012aD	70.86	0.27	15.56	1.98	0.026	0.35	1.50	3.72	4.82	0.094	0.0005	0.67	99.85	0.21
012bE	75.74	0.04	12.84	0.47	0.031	0.005	2.47	3.58	3.67	0.022	0.0005	0.40	99.27	0.18
013aE	72.55	0.04	15.65	0.32	0.010	0.005	1.24	3.47	6.31	0.016	0.0005	0.42	99.97	0.38
014aB	69.63	0.46	14.24	3.73	0.061	0.12	1.86	3.61	4.86	0.075	0.0005	0.41	99.04	0.17
014bC	75.27	0.11	13.48	1.52	0.013	0.08	0.71	2.52	6.13	0.032	0.0005	0.39	100.25	0.23
017aC	67.52	0.50	16.24	2.69	0.054	0.69	1.87	3.90	5.00	0.151	0.0005	1.21	99.81	0.29
021aA	71.93	0.14	14.70	1.19	0.022	0.12	1.05	3.73	5.63	0.052	0.0005	0.53	99.09	0.22
027aA	72.82	0.03	15.28	0.34	0.013	0.04	2.54	6.41	0.82	0.022	0.0005	0.38	98.71	0.14
028aX	71.91	0.18	14.47	1.40	0.032	0.17	1.13	3.55	5.68	0.044	0.0005	0.73	99.30	0.21
030bA	72.13	0.02	15.17	0.28	0.006	0.005	2.29	6.20	2.17	0.027	0.0005	0.42	98.66	0.19

032aB	62.68	0.13	16.48	12.22	0.101	0.87	0.82	2.63	2.55	0.017	0.0005	0.28	98.78	0.22
036aC	58.60	0.38	14.49	5.77	0.221	1.47	6.31	3.12	8.00	0.623	0.0005	0.15	99.15	0.15
039aB	74.96	0.03	14.42	0.62	0.046	0.005	1.20	3.78	4.79	0.018	0.0005	0.25	100.08	0.11
040aA	74.25	0.06	14.15	0.83	0.017	0.005	1.33	3.78	4.69	0.027	0.0005	0.51	99.61	0.16
045aB	75.30	0.04	14.02	0.30	0.014	<0.01	0.81	3.61	5.97	0.008	0.011	0.25	100.18	0.24
046aA	75.15	0.03	13.90	0.38	0.020	<0.01	0.95	3.35	6.20	0.014	0.005	0.23	100.11	0.19
047aC	76.00	0.06	13.75	0.70	0.012	<0.01	1.03	4.30	4.27	0.005	0.009	0.31	100.29	0.26
048aA	73.78	0.15	14.58	0.88	0.047	0.06	4.23	5.23	0.36	0.034	0.004	0.71	100.05	0.21
050aA	76.60	0.03	14.12	0.40	0.012	<0.01	2.17	5.67	1.21	0.007	0.004	0.18	100.30	0.18
053aC	74.49	0.10	14.32	0.90	0.029	<0.01	1.21	3.74	5.05	0.022	0.003	0.45	100.24	0.22
053bE	75.03	0.07	13.77	0.73	0.024	<0.01	1.63	5.81	1.94	0.007	0.004	0.27	99.23	0.26
054aC	72.71	0.03	15.44	0.34	0.006	<0.01	1.51	3.55	5.84	0.010	0.002	0.42	99.74	0.24
054bD	73.87	0.10	14.49	0.85	0.010	0.03	1.53	3.19	5.40	0.010	0.004	0.51	99.99	0.14
055aX	73.45	0.06	14.39	0.78	0.011	<0.01	0.82	3.61	6.19	0.013	0.003	0.54	99.77	0.24
056aX	82.70	0.14	8.96	0.62	0.016	0.10	1.54	2.09	2.96	0.019	0.005	0.60	99.76	0.19
057aC	65.53	<0.01	18.95	0.05	0.002	<0.01	0.13	2.25	13.31	0.010	0.004	0.11	100.14	0.15
058aA	76.40	0.02	14.10	0.27	0.044	<0.01	2.03	3.99	3.22	0.008	0.004	0.25	100.19	0.15
062aA	73.82	0.07	15.28	0.67	0.013	<0.01	2.72	5.71	1.02	0.008	0.007	0.40	99.72	0.20
064aA	74.31	0.11	14.56	1.15	0.026	<0.01	1.02	4.70	4.10	0.022	0.005	0.30	100.15	0.16
064bB	73.91	0.04	14.40	0.72	0.026	<0.01	1.14	5.71	2.54	0.011	0.004	0.24	98.58	0.15

065aA	73.79	0.11	14.55	1.03	0.022	<0.01	1.38	3.80	5.00	0.029	0.007	0.51	100.21	0.20
066aA	73.06	0.03	15.17	0.41	0.011	<0.01	0.66	3.04	7.76	0.010	0.006	0.24	100.25	0.19
067aB	75.40	0.04	13.79	0.62	0.018	<0.01	1.26	4.03	4.24	0.010	0.004	0.27	99.56	0.08
067bC	75.02	<0.01	14.22	0.17	0.004	<0.01	0.67	3.08	6.86	0.007	0.003	0.29	100.14	0.14
067cF	73.06	0.06	14.23	1.73	0.052	<0.01	0.87	2.63	7.26	0.015	0.004	0.29	100.09	0.14
068aA	74.28	0.08	14.83	0.86	0.014	<0.01	1.19	3.76	4.92	0.015	0.005	0.44	100.35	0.21
068bB	76.43	0.04	14.14	0.34	0.021	<0.01	1.07	4.58	3.56	0.003	0.004	0.22	100.26	0.17
068cC	75.27	0.03	14.36	0.31	0.018	<0.01	1.41	4.32	3.95	0.005	0.005	0.68	100.22	0.10
070aB	76.30	0.04	14.37	0.48	0.010	<0.01	0.80	3.65	4.88	0.010	0.009	0.51	100.92	0.10
071aA	74.29	0.11	14.05	0.93	0.016	<0.01	1.31	3.34	5.40	0.023	0.004	0.27	99.72	0.15
072aA	76.13	0.04	13.68	0.44	0.025	<0.01	0.84	3.60	5.25	0.018	0.004	0.26	100.15	0.16
074aA	75.09	0.02	14.22	0.64	0.082	<0.01	0.77	3.78	5.48	0.016	0.004	0.29	100.22	0.14
075aA	74.07	0.02	14.67	1.15	0.033	<0.01	1.35	4.54	4.24	0.036	0.004	0.25	100.19	0.11
076aA	73.67	0.04	14.25	0.50	0.026	<0.01	1.36	3.87	5.58	0.008	0.003	0.36	99.52	0.15
078aB	74.65	0.02	14.18	0.46	0.054	<0.01	0.82	3.04	6.85	0.014	0.004	0.24	100.19	0.12
080aA	64.95	0.14	19.78	1.17	0.022	0.11	2.59	5.15	5.61	0.034	0.004	0.42	99.98	0.10
082aD	72.01	0.06	16.47	0.55	0.012	<0.01	2.06	5.98	2.52	0.007	0.004	0.51	100.10	0.16
082bA	75.63	0.03	14.33	0.45	0.010	<0.01	1.74	4.65	3.10	0.009	0.004	0.30	100.11	0.14
083aB	76.34	0.03	13.81	0.60	0.052	<0.01	1.19	4.82	3.11	0.008	0.003	0.27	100.09	0.14
083bC	73.81	0.05	14.94	0.81	0.068	<0.01	1.22	4.72	4.21	0.012	0.003	0.34	100.07	0.14

084aC	73.90	0.08	14.61	1.21	0.077	<0.01	0.78	4.37	4.60	0.012	0.003	0.39	99.96	0.10
084bF	74.60	0.10	14.20	0.98	0.021	<0.01	1.06	3.99	4.64	0.014	0.005	0.43	99.98	0.14
BK4*	73.98	0.13	14.79	0.21	0.01	0.14	1.05	3.68	4.94	0.06			99.52	
BK56*	74.35	0.09	14.40	0.20	0.00	0.25	0.97	3.36	5.22	0.06			99.41	
BK57*	74.84	0.09	14.10	0.20	0.01	0.24	0.92	3.29	5.22	0.05			99.47	
BK58*	74.95	0.09	14.64	0.19	0.01	0.36	0.89	3.44	5.29	0.07			100.42	
BK59*	74.47	0.09	14.17	0.18	0.01	0.23	0.94	3.31	5.05	0.06			98.97	
BK60*	75.02	0.09	13.77	0.20	0.01	0.24	0.83	3.39	5.23	0.05			99.33	
BK61*	74.31	0.09	14.98	0.19	0.00	0.15	1.16	3.95	5.07	0.06			100.43	
BK62*	74.41	0.09	14.50	0.23	0.01	0.30	1.08	3.47	5.47	0.07			100.20	
DVG-2*	74.63	0.08	14.08	0.28	0.06	0.17	1.02	3.69	5.74	0.03			100.43	
DVGD*	74.63	0.08	13.65	0.23	0.05	0.09	1.03	3.43	5.32	0.05			99.15	

Table A3.10: Trace element XRF data in ppm. Samples marked with * are from Grantham *et al.* (1991):

Sample	004aC	004cJ	004dI	005aA	007aB	008aC	008P2	012aD	012bE	013aE	014aB	014bC	017aC	021aA	027aA	028aX	030bA	032aB	036aC	039aB
As	<4	<4	<4	<4	<4	<4	<4	<4	<4	<4	<4	<4	<4	<4	<4	<4	<4	<4	<4	<4
Ba	669	263	850	1,411	6.3	1,551	818	1,735	728	1,220	1,094	1,241	1,566	1,203	205	1,102	348	2,729	11,369	211
Bi	<3	<3	<3	<3	<3	<3	<3	<3	<3	<3	<3	<3	<3	<3	<3	<3	<3	<3	<3	<3
Br	<2	<2	<2	<2	<2	<2	<2	<2	<2	<2	<2	<2	<2	<2	<2	<2	<2	<2	<2	<2
Ce	61	<10	43	50	14	108	<10	76	<10	<10	243	<10	120	<102	23	60	<10	112	731	17
Co	70	69	93	79	97	92	79	71	92	137	85	110	72	78	72	85	60	92	53	74
Cr	9.5	12	12	11	12	11	20	11	16	11	<3	6.7	8.1	7	15	7.8	13	14	<3	16
Cs	5.7	<5	<5	5	10	5.9	<5	5.8	<5	<5	9.5	<5	6.6	<5	<5	8.6	<5	<5	<5	<5
Cu	9.5	<2	6.3	4.3	<2	<2	3.1	3.6	3.3	2.3	27	<2	3.4	2	<2	3.1	<2	<2	2.4	7.6
Ga	26	15	19	22	27	22	16	23	12	13	17	17	24	22	15	21	19	28	23	20
Ge	1.3	<1	<1	<1	1.6	<1	1.3	<1	<1	<1	2	1.1	<1	1.5	<1	<1	1.4	1.9	1.5	1.5
Hf	4.8	<3	<3	6.1	<3	8.4	5.3	7.5	3.7	<3	19	<3	9.1	4.7	<3	5.2	<3	7.4	21	3.6
La	34	<10	26	27	<10	68	<10	47	<10	<10	122	<10	71	31	<10	40	<10	48	341	<10
Mo	<2	<2	<2	<2	<2	<2	<2	<2	<2	<2	<2	<2	<2	<2	<2	<2	<2	<2	<2	<2
Nb	9.6	<1	3.4	3.4	64	3.1	3.7	9.4	3.9	3.2	13	<1	2.2	5	<1	13	<1	28	<1	19
Nd	24	<10	15	22	<10	36	<10	31	<10	<10	107	<10	44	22	12	24	<10	61	403	<10
Ni	3.6	2.7	4.7	3	4.7	5.7	4.3	18	25	4.8	4.4	3.7	5.6	3.5	4.6	3.4	2.9	5.1	8.4	4.8
Pb	27	17	18	25	60	33	32	46	54	61	22	45	48	50	17	31	20	7.3	48	54
Rb	164	15	94	168	298	178	26	138	69	146	90	156	195	176	12	194	30	83	185	144
Sc	<3	<3	<3	<3	<3	<3	<3	<3	<3	<3	3.6	<3	<3	<3	<3	<3	<3	<3	4.3	<3
Se	1.2	<1	1.6	1.4	<1	1.5	2.2	1.5	<1	1	1.1	1.5	<1	<1	1.2	1.7	1.3	<1	<1	1.4
Sm	<10	<10	<10	<10	<10	<10	<10	<10	<10	<10	19	<10	<10	<10	<10	<10	<10	13	62	<10
Sr	203	442	328	366	16	420	382	467	213	271	311	265	539	303	458	279	299	52	3,504	131
Ta	<2	<2	<2	<2	<2	<2	<2	<2	<2	<2	<2	<2	<2	<2	<2	<2	<2	<2	<2	<2
Th	25	<3	16	25	27	23	<3	17	<3	<3	14	<3	35	24	4.5	22	<3	7.9	97	3.2
Tl	33	33	46	37	48	45	39	33	44	66	44	56	32	38	35	41	31	46	12	38
U	<2	<2	<2	2.5	12	2.3	3.2	2.6	<2	<2	2.9	<2	2.6	2.2	<2	2	<2	3.3	13	8.3
V	5.8	3.2	5.9	8	<3	15	<3	14	<3	<3	6.6	<3	26	3.2	<3	4.7	<3	<3	82	<3
W	453	411	585	488	614	574	506	430	555	810	552	700	445	498	454	542	391	533	209	470
Y	10	2.2	4.6	5.4	66	4.2	3.6	8	4.8	<1	25	1.4	16	5.2	2.3	11	2.1	154	54	18
Yb	4.2	<3	5.1	4.6	9.9	4.3	3.2	4.5	4.8	5.5	8.1	5.2	5.5	4	<3	3.7	<3	18	5.6	4.7
Zn	11	5.9	7.5	6.1	31	39	<3	30	4.9	4.5	39	22	54	25	8.4	19	<3	20	108	5
Zr	108	52	73	109	90	200	102	170	74	3.6	685	9.1	311	114	35	127	33	345	583	63

Table A3.10 continued (1).

Sample	040aA	045aB	046aA	047aC	048aA	050aA	053aC	053bE	054aC	054bD	055aX	056aX	057aC	058aA	062aA	064aA	064bB	065aA	066aA	067aB	067bC
As	<4	<4	<4	<4	<4	<4	5.2	<4	<4	<4	<4	<4	<4	<4	<4	<4	<4	5.4	<4	<4	<4
Ba	561	121	194	60	135	28	735	41	1,080	1,561	672	214	2,875	269	469	685	316	1,130	622	440	830
Bi	<3	<3	<3	<3	<3	<3	<3	<3	<3	<3	<3	<3	<3	<3	<3	<3	<3	<3	<3	<3	<3
Br	<2	<2	<2	<2	<2	<2	<2	<2	<2	<2	<2	<2	<2	<2	<2	<2	<2	<2	<2	<2	<2
Ce	36	14	13	<10	47	<10	29	<10	<10	<10	12	19	<10	<10	<10	24	12	42	<10	<10	<10
Co	79	113	77	110	79	82	70	101	98	91	79	98	18	78	72	81	84	100	65	81	84
Cr	8	<3	35	<3	<3	<3	34	<3	<3	88	<3	<3	<3	29	<3	<3	5.5	<3	<3	<3	<3
Cs	<5	<5	<5	<5	<5	<5	<5	<5	<5	<5	<5	<5	<5	<5	<5	<5	<5	<5	<5	<5	<5
Cu	<2	6	4.6	4	<2	<2	2.1	<2	18	43	<2	3.2	<2	<2	<2	<2	<2	<2	<2	3.5	<2
Ga	18	19	19	20	25	21	18	21	16	14	19	13	14	18	13	18	19	18	16	15	13
Ge	1.2	<1	<1	<1	<1	<1	<1	<1	<1	<1	<1	<1	<1	<1	<1	<1	<1	1	1.1	1.1	<1
Hf	<3	7.1	<3	<3	6.5	<3	<3	<3	3.8	3.4	6	<3	<3	<3	<3	<3	<3	4.5	<3	<3	<3
La	16	<10	<10	<10	22	<10	19	<10	<10	<10	<10	<10	<10	<10	<10	11	<10	27	<10	<10	<10
Mo	<2	<2	<2	<2	<2	<2	<2	<2	<2	<2	<2	<2	<2	<2	<2	<2	<2	<2	<2	<2	<2
Nb	9.7	10	11	17	9.4	7.8	12	10	1.1	<1	9.3	17	<1	11	<1	4.7	6.6	3.7	7.6	4.3	2.1
Nd	18	<10	<10	<10	18	<10	15	<10	<10	<10	<10	13	<10	<10	<10	15	<10	23	<10	<10	<10
Ni	3.2	<2	5.8	<2	<2	<2	<2	<2	<2	15	<2	2.2	<2	3.8	<2	<2	<2	<2	<2	<2	<2
Pb	59	46	46	41	16	34	50	35	42	30	68	34	123	59	19	27	26	41	69	30	37
Rb	135	175	197	129	9.5	31	154	58	108	78	157	83	247	77	19	73	45	102	167	96	131
Sc	<3	<3	<3	<3	<3	<3	<3	<3	<3	<3	<3	<3	<3	<3	<3	<3	<3	<3	<3	<3	<3
Se	2	1.1	<1	<1	<1	<1	<1	1.2	<1	<1	<1	<1	<1	<1	<1	<1	<1	<1	<1	<1	<1
Sm	<10	<10	<10	<10	<10	<10	<10	<10	<10	<10	<10	<10	<10	<10	<10	<10	<10	<10	<10	<10	<10
Sr	159	114	157	87	1,175	110	214	104	382	476	302	220	409	183	536	228	135	377	161	164	246
Ta	<2	<2	<2	<2	<2	<2	<2	<2	<2	<2	<2	<2	<2	<2	<2	<2	<2	<2	<2	<2	<2
Th	12	9.6	9.7	<3	14	<3	12	4.7	<3	<3	7.6	11	<3	3.6	<3	3.3	<3	9.9	3	5.2	<3
Tl	42	53	36	55	37	41	34	52	45	46	41	49	9.6	38	35	41	41	52	33	42	44
U	<2	3.2	3.1	3.7	4.3	<2	<2	2.9	<2	<2	5.6	3.4	<2	2.3	<2	<2	<2	<2	<2	<2	<2
V	<3	<3	<3	<3	4.2	<3	<3	<3	<3	6.7	<3	<3	<3	<3	4.1	<3	<3	<3	<3	<3	<3
W	527	534	369	553	373	406	343	516	453	461	419	499	88	388	353	410	416	521	330	418	441
Y	9	11	16	3.9	19	3.4	11	3.5	2.5	1.7	10	17	<1	23	1.1	4.6	6.7	4.5	3.8	4.4	<1
Yb	4.9	<3	<3	<3	<3	<3	<3	<3	<3	<3	<3	<3	<3	3.3	<3	<3	<3	<3	<3	<3	<3
Zn	20	7.1	10	3.1	45	8.5	22	19	3.9	9.2	6.4	15	<3	4.2	13	19	12	22	4.5	6.6	<3
Zr	56	122	34	44	100	4.2	75	16	33	52	104	29	<2	28	3.8	61	25	103	9.5	3.9	5.7

Table A3.10 continued (2).

Sample	067cF	068aA	068bB	068cC	070aB	071aA	072aA	074aA	075aA	076aA	078aB	080aA	082aD	082bA	083aB	083bC	084aC	084bF
As	<4	<4	<4	<4	<4	<4	<4	<4	<4	<4	<4	<4	<4	5.5	<4	4.6	<4	<4
Ba	1,552	741	281	250	171	1,982	519	848	104	296	259	2,699	176	326	11	123	583	591
Bi	<3	<3	<3	<3	<3	<3	<3	<3	<3	<3	<3	<3	<3	<3	<3	<3	<3	<3
Br	<2	<2	<2	<2	<2	<2	<2	<2	<2	<2	<2	<2	<2	<2	<2	<2	<2	<2
Ce	<10	<109	<10	<10	21	<10	<10	21	<10	<10	104	<10	12	16	13	13	11	17
Co	67	96	106	80	74	88	89	108	76	92	81	52	69	76	125	79	69	89
Cr	<3	<3	<3	<3	<3	<3	<3	16	<3	4.5	<3	<3	<3	<3	9	<3	<3	<3
Cs	<5	<5	<5	<5	<5	<5	<5	<5	<5	<5	5.8	<5	<5	<5	<5	<5	<5	<5
Cu	<2	<2	5.9	<2	3.8	<2	3.2	9.5	<2	<2	3.3	<2	4.9	12	<2	<2	<2	<2
Ga	13	18	20	19	18	12	14	23	15	14	19	22	27	22	22	24	23	23
Ge	<1	<1	1.8	<1	1	<1	<1	1.8	<1	<1	1.6	<1	1.1	<1	<1	<1	<1	1.8
Hf	4.2	5.1	<3	<3	<3	<3	<3	<3	<3	<3	7.9	3.8	4.8	<3	<3	<3	<3	3.5
La	10	31	<10	<10	<10	<10	<10	16	<10	<10	50	<10	<10	<10	<10	<10	<10	11
Mo	<2	<2	<2	<2	<2	<2	<2	<2	<2	<2	<2	<2	<2	<2	<2	<2	<2	<2
Nb	2.6	7.1	32	21	23	5.1	14	24	8.1	9	7.5	1.4	38	16	18	16	20	12
Nd	<10	30	<10	<10	13	<10	<10	16	<10	<10	53	<10	<10	12	<10	<10	11	<10
Ni	<2	<2	<2	<2	<2	<2	<2	3.1	<2	<2	<2	<2	3.1	<2	2.5	<2	<2	<2
Pb	36	55	51	41	55	36	51	76	77	58	55	42	43	41	58	68	87	48
Rb	143	109	58	80	113	106	138	146	170	114	115	107	59	71	112	151	188	160
Sc	<3	<3	<3	<3	<3	<3	<3	<3	<3	<3	<3	<3	<3	<3	<3	<3	<3	<3
Se	<1	<1	1.2	<1	<1	<1	<1	<1	<1	<1	<1	<1	<1	1.1	1.3	<1	<1	<1
Sm	<10	<10	<10	<10	<10	<10	<10	<10	<10	<10	13	<10	<10	<10	<10	<10	<10	<10
Sr	273	251	117	148	105	399	122	238	89	131	121	634	133	160	32	80	151	178
Ta	<2	<2	<2	<2	<2	<2	<2	<2	<2	<2	<2	<2	<2	<2	<2	<2	<2	<2
Th	9.7	17	<3	3.2	8.5	<3	4.5	10	<3	3.7	24	<3	17	7.4	15	19	17	11
Tl	35	49	56	42	40	47	47	54	38	45	41	26	33	38	64	38	37	45
U	3.4	<2	11	4.2	3.5	<2	5.5	14	3.1	3.3	7.3	<2	11	5.8	17	10	4.1	3.2
V	4.7	<3	<3	<3	<3	<3	<3	<3	<3	<3	<3	9	<3	<3	<3	<3	<3	<3
W	343	504	561	432	399	448	463	553	382	461	428	254	356	401	650	406	376	465
Y	9.2	8.8	18	12	19	2.2	20	70	34	11	57	6.3	51	32	33	32	25	8.2
Yb	<3	<3	3.1	<3	<3	<3	<3	6	<3	<3	4.3	<3	8.3	4.5	3.7	<3	3.5	<3
Zn	8.3	16	<3	3.2	6.7	16	9.1	4.8	5.1	7.8	18	17	8.7	7.2	16	21	27	26
Zr	87	113	41	41	52	6.7	29	47	44	13	238	57	92	47	71	52	79	78

Table A3.10 continued (3) for data from Grantham *et al.,* (1991).

Sample	BK4*	BK56*	BK57*	BK58*	BK59*	BK60*	BK61*	BK62*	DVG-2*	DVGD*
Ba	1.10	1.20	1125.00	1001.00	1121.00	2.10	2.40	1133.00	1127.00	2.60
Nb	4.60	5.90	6.20	7.10	4.80	6.80	4.60	4.80	7.00	12.90
Rb	212.00	207.00	222.00	220.00	200.00	201.00	180.00	200.00	184.00	231.00
Sc	1164.00	1203.00	2.00	1.60	0.80	1129.00	925.00	ND	2.90	1097.00
Sr	209.00	224.00	217.00	185.00	190.00	187.00	209.00	220.00	236.00	244.00
Th	47.00	67.00	63.00	53.00	64.00	65.00	72.00	8.10	18.70	23.00
Y	2.60	3.80	4.40	4.90	3.70	4.40	4.10	4.00	7.00	4.80
Zn	24.00	32.00	27.00	23.00	31.00	35.00	25.00	32.00	28.00	48.00
Zr	4.70	8.60	9.70	6.10	8.40	9.50	9.30	71.00	82.00	85.00

Table A3.11: Trace element ICP-MS data. Values below detection limit given as half of detection limit.

Sample	Li (7) ppb	Be (9) ppb	Na (23) ppb	Mg (24) ppb	Al (27) ppb	K (39) ppb	Ca (43) ppb	V (51) ppb	Cr (52) ppb	Mn (55) ppb
004aC	5786	5306	31161163	1290033	65870737	33445804	9107143	9460	5 000	75533
004cJ	6881	4986	39239296	853353	72080930	10272886	17742385	7928	5 000	77462
004dI	6485	4088	31517733	1615844	61009140	25557946	10233093	11192	5 000	84628
005aA	7598	3237	26318292	1498150	66085441	39460370	8843517	12458	5 000	57299
007aB	25933	7291	34228781	65408	61281936	33140270	5773785	2318	5 000	644980
008aC	15727	2183	25135827	3066280	67348778	40020704	11722508	21296	5 000	175011
008P2	4691	3926	40954217	229332	66973199	13687495	16361845	4352	5 000	68784
012aD	16527	3119	29088078	2276463	70891942	33116260	10543306	18348	5 000	199290
012bE	4442	2185	25353811	475976	57844868	28464261	9858246	4699	5 000	255687
013aE	6889	2167	27440893	315225	68213305	42923280	8698557	3387	5 000	50544
014aB	16414	2211	25970966	1146773	64023206	37540363	12434203	11284	5 000	474926
014bC	16601	1652	20581309	1006460	74989911	42822983	5194589	6856	5 000	94415
017aC	18477	3732	30306688	4732638	71560168	34482841	13216031	35033	5 000	427256
021aA	10170	2652	26933973	1199481	62969672	37441229	7337965	5731	5 000	140145
027aA	8111	3320	44150071	778011	68790913	6356218	17015488	6720	5 000	116236
028aX	13266	4108	25915758	1431319	63586242	37593305	7568257	9265	5 000	199720
030bA	4298	4054	41108439	303463	68240361	16646088	14710117	4073	5 000	22571
032aB	14718	911	17948704	5368377	72296831	19508129	5238054	2145	5 000	800865
036aC	8488	7153	20128598	8113876	72062046	53597605	39338076	91638	5 000	1681313
039aB	10601	2922	28710127	237063	64310492	32798387	8194286	3580	5 000	380916
040aA	6348	4514	28228180	420184	72309694	35620907	8712022	4407	5 000	116961
045aB	12698	6658	28837626	267833	25000	18846879	7653540	2964	5000	121514
046aA	14328	6875	25882391	511204	59341120	36398462	9023004	3263	5000	184760
047aC	30697	8876	33825509	237539	60591128	37941093	9540651	3657	5000	63025
048aA	24102	20413	42076161	1848628	57333583	3991302	39905516	12197	5000	581732
050aA	16986	9920	26867632	529653	62230795	12087418	15764553	3448	5000	101060
053aC	21040	5317	22089579	735837	73891997	6560300	8192554	5996	5000	189811
053bE	24785	9168	43350004	1005331	59150911	19188703	14819718	4120	5000	195692
054aC	5924	5538	27615849	509354	66179829	34111300	14169578	6407	5000	44517

054bD	15001	3634	23816784	1472544	60191482	31477076	13691656	13844	5000	85307
055aX	1450	9083	27772724	783398	60203539	34686271	7768508	9187	5000	85160
056aX	15018	5770	16855663	1876367	64902535	31380336	14597130	8683	5000	349043
057aC	3607	688	17472300	51488	109473970	103204675	1805861	3295	5000	10166
058aA	12305	14433	34953156	355705	66569935	36220494	20971528	4437	5000	514477
062aA	13082	6523	46531045	1582461	72955198	11559646	27323523	13729	5000	129648
064aA	22767	3657	39906499	519692	69650045	25347841	10443010	6127	5000	322265
064bB	7962	5763	35848484	271939	67809512	30585924	12345372	4320	5000	323264
065aA	15642	4256	33402827	1326472	67549183	30159901	14547830	10494	5000	223344
066aA	6707	3927	25485128	297492	70254167	50226938	6371966	4154	5000	70204
067aB	6864	3883	29433276	387956	62875591	40583324	11214731	5581	5000	147821
067bC	4947	2136	24760347	158616	64310729	41756139	6738530	3630	5000	24018
067cF	6589	1580	22516355	719511	65731755	44358641	9513866	12999	5000	677007
068aA	13887	5859	32525418	1084890	68144395	29845506	12468239	8146	5000	143941
068bB	7069	5275	33528900	405438	65251650	34067235	9854606	5315	5000	178459
068cC	6762	5548	29018460	380628	69163446	32333196	11167777	4969	5000	112513
070aB	3601	6690	29676147	340079	98206350	31117014	7234897	3626	5000	90805
071aA	7993	1791	25234020	1252171	39579771	17657416	12397309	7972	5000	135334
072aA	4124	4710	24813965	392211	31321475	31404594	6895838	3157	5000	244220
074aA	1450	11873	26949248	193261	31918410	31970820	6900556	3634	5000	869892
075aA	1450	2468	20510176	236184	40496373	40513014	6687608	2284	5000	562621
076aA	5040	3588	24969576	364998	30594831	30585874	10803645	3351	5000	182051
078aB	4753	7715	34393334	194510	25140951	25115039	12117472	9167	10168	389783
080aA	17159	5758	36224559	2108048	31145349	31073653	22251394	19572	5000	175269
082aD	8554	12056	33606294	578496	15807423	22015430	16436807	6649	5000	86192
082bA	8850	7418	27894622	265223	18718742	24425246	12577041	4481	5000	67863
083aB	20423	8973	36058578	271006	16984482	28417893	10346714	3268	5000	580748
083bC	18565	7859	39298449	672401	25059301	24908623	12083397	4981	5000	892888
084aC	30373	5495	35540904	940523	26428686	26241363	7882058	8498	5000	935100
084bF	61000	7499	30474436	1054348	27431514	27208238	10211863	8181	5000	189520

Table A3.11 continued (1):

Sample	Fe (57) ppb	Co (59) ppb	Ni (60) ppb	Cu (63) ppb	Zn (66) ppb	Ga (69) ppb	Rb (85) ppb	Sr (88) ppb	Mo (98) ppb	Ag (109) ppb
004aC	9321351	69386	2 500	12031	16966	28485	182343	218891	200	250
004cJ	3549892	67638	7853	2 500	12043	17409	18975	449526	200	250
004dI	5209360	93647	6062	8125	24613	22810	98993	344965	200	250
005aA	4664162	78111	2 500	5461	9865	25039	189900	380271	200	250
007aB	3739472	94627	13083	2 500	33596	29817	326469	15004	464	250
008aC	13636791	91124	2 500	2 500	47812	25432	201235	432170	916	250
008P2	1331116	80623	2 500	2 500	10000	17544	29846	393826	428	250
012aD	13139152	66757	23452	7083	50711	25152	152876	478300	628	250
012bE	2907721	92222	27603	2 500	13294	13506	73296	223836	200	250
013aE	1872263	137068	2 500	2 500	10241	15466	164291	280609	200	250
014aB	25171362	82660	2 500	30173	48925	20119	92430	324428	1376	250
014bC	10898361	112376	12094	2 500	32052	19792	180450	285517	200	250
017aC	18583606	72115	2 500	5747	61687	26967	218962	556500	200	250
021aA	8022952	77055	7259	2 500	34122	25295	199970	323028	200	250
027aA	2229122	74353	11316	2 500	10610	17100	16616	495207	200	250
028aX	9172855	84431	2 500	7479	93331	24679	225177	301154	619	250
030bA	1683397	60485	2 500	2 500	2 500	20283	33059	300954	200	250
032aB	79724956	82591	2 500	2 500	27368	27322	85444	51743	200	250
036aC	35687132	41218	5135	2 500	96434	25734	203235	3366994	200	250
039aB	4036955	69737	2 500	9906	14392	21548	160858	134981	200	250
040aA	4850693	75486	2 500	2 500	26926	19983	150318	164520	200	250
045aB	2205511	182707	2500	2500	22219	30610	335870	165982	1146	250
046aA	2674494	119275	2500	2500	18843	30123	373263	282388	998	250
047aC	4947805	179905	2500	2500	5897	30291	192343	125476	1141	250
048aA	6882645	129366	2500	2500	71041	41275	13998	2306974	200	250
050aA	2693313	129496	2500	2500	14924	32433	49450	157064	200	250
053aC	5037927	80224	2500	2500	27145	22077	171260	277426	200	250
053bE	5305604	171019	2500	2500	30432	34234	92326	151508	200	250
054aC	2448155	156343	2500	23606	7020	23676	157960	688612	200	250

054bD	5814574	144980	2500	64766	16449	19833	113468	840164	200	250
055aX	5796100	130888	2500	2500	13200	29997	254820	545191	200	250
056aX	5016863	162299	2500	2500	27497	20614	128741	407711	938	250
057aC	235330	26890	2500	2500	2500	20431	465345	738371	1074	250
058aA	2152571	143189	2500	2500	8246	32487	130928	373637	418	250
062aA	5668973	125657	2500	2500	23296	22832	33572	1042789	200	250
064aA	9090320	138993	2500	2500	35454	29073	117573	438653	1045	250
064bB	6107568	145874	2500	2500	24296	31811	78021	269053	851	250
065aA	8375242	175974	2500	2500	39621	31827	169656	750254	991	250
066aA	2928520	113432	2500	2500	9589	27414	338075	314044	718	250
067aB	4383442	119995	2500	2500	11858	22591	133863	281315	200	250
067bC	1129969	141537	2500	2500	2500	20694	200612	461836	200	250
067cF	18084343	110474	2500	2500	19616	23294	272254	533665	590	250
068aA	6690275	165658	2500	2500	36240	29128	177238	479020	200	250
068bB	2314907	167156	2500	2500	9549	28208	86314	203971	200	250
068cC	1761778	112700	2500	2500	5680	24279	102030	211846	200	250
070aB	3139781	117478	2500	2500	11962	27462	164369	142848	200	250
071aA	6975514	137608	2500	2500	27395	19277	158552	719868	200	250
072aA	2718873	126058	2500	2500	14056	21040	180162	151260	200	250
074aA	3926110	152698	2500	5608	10194	32159	193830	388460	1338	250
075aA	2888724	104977	2500	2500	8753	22762	256987	110344	200	250
076aA	3091776	130726	2500	2500	13130	21011	152000	211413	200	250
078aB	8085878	123300	2500	2500	34011	29203	163036	178863	200	250
080aA	7793757	76894	2500	2500	27789	29898	143320	1037991	200	250
082aD	3373620	96227	2500	2500	11865	36227	78008	209231	200	250
082bA	2477310	96967	2500	8150	8505	26359	84300	225060	412	250
083aB	4009407	190710	2500	2500	25303	32344	158330	44088	200	250
083bC	6148905	139400	2500	2500	36531	37992	309180	119281	200	250
084aC	12093821	115191	2500	2500	46930	37352	367066	277344	200	250
084bF	7261190	144954	2500	2500	45503	36540	305837	331877	200	250

Table A3.11 continued (2):

Sample	Cd (114) ppb	Te (128) ppb	Ba (138) ppb	Tl (205) ppb	Pb (208) ppb	Bi (209) ppb	U (238) ppb
004aC	10	13	697130	551	27271	53	1415
004cJ	22	5	284934	61	16708	39	627
004dI	43	5	893917	312	17995	21	732
005aA	10	5	1481805	497	24264	22	1809
007aB	10	5	4000	1279	60968	632	11290
008aC	10	5	1563129	748	31914	28	1072
008P2	10	12	871079	121	30101	28	2841
012aD	87	5	1712625	612	44791	23	1976
012bE	63	11	766850	298	53045	21	1039
013aE	70	5	1356934	611	58802	33	183
014aB	59	5	1064666	347	22143	139	1656
014bC	10	5	1304092	611	45278	10	275
017aC	10	5	1563599	838	47829	24	2031
021aA	48	15	1268076	774	48427	37	2391
027aA	10	5	231423	75	17409	10	699
028aX	10	5	1206686	715	34856	37	1325
030bA	20	5	370704	105	19027	10	663
032aB	125	16	2507356	334	6967	33	1716
036aC	82	35	9355264	854	49248	95	6928
039aB	32	13	241409	524	50583	20	7737
040aA	72	5	603373	566	56322	57	1387
045aB	34	5	181028	1259	60471	41	4420
046aA	28	5	298667	1391	59937	36	3798
047aC	10	48	77407	915	52821	95	4478
048aA	54	5	216865	48	19052	36	2951
050aA	10	5	37746	228	43961	10	1147
053aC	36	5	817504	838	48554	10	1917
053bE	25	5	55027	440	47610	10	2942
054aC	32	5	1708245	701	54707	10	1144

054bD	40	5	2371264	432	36833	10	691
055aX	30	5	1064425	1007	87735	10	6576
056aX	54	5	336762	627	44256	58	5189
057aC	10	5	4490544	1718	161544	10	199
058aA	79	5	467844	593	86017	10	3566
062aA	31	5	799951	150	29358	10	54
064aA	48	5	1123793	518	38645	10	512
064bB	76	5	568206	350	37173	88	670
065aA	26	5	1879832	826	57034	10	1111
066aA	10	5	1060679	1234	94574	10	1727
067aB	39	5	650717	606	35940	10	1709
067bC	10	5	1345196	934	47321	10	421
067cF	78	5	2524227	1090	48756	10	4412
068aA	10	5	1262822	870	76863	10	2229
068bB	10	5	421558	324	62488	10	13444
068cC	10	5	358402	405	43836	10	5388
070aB	35	5	269097	693	67711	10	5739
071aA	28	5	3072828	727	47442	30	295
072aA	52	5	723264	891	54722	61	6442
074aA	60	5	1186937	883	86096	42	15223
075aA	66	5	108564	1120	86573	87	3504
076aA	35	5	422647	751	68101	29	3555
078aB	111	5	390035	791	67629	91	9641
080aA	46	5	3679301	627	48463	10	1118
082aD	28	5	239478	276	45385	310	11551
082bA	29	5	402733	279	40052	435	5282
083aB	63	5	11581	674	67474	72	18135
083bC	93	5	210111	1145	91444	26	12843
084aC	129	5	973529	1392	115303	32	5422
084bF	62	5	920781	1173	62054	46	3812

Table A3.12: Trace element ICP-MS data certified reference materials for the 2014 field season in ppb:

Certified Reference Samples	**Li (7)**	**Be (9)**	**Na (23)**	**Mg (24)**	**Al (27)**	**K (39)**	**Ca (43)**	**V (51)**	**Cr (52)**
GSD 09 measured	31548.21	1734.474	10109940	14121634	56311940	15516009	37307201	98429.47	83172.44
NCS DC 73307 (GSD-09 river sediment) cert.	30000	1800	10682784	14415763	55992534	16519985	38235915	97000	85000
recovery %	105.1607	96.35967	94.63769	97.95967	100.5704	93.92266	97.5711	101.4737	97.84993
GSD 10 measured	12327.91	597.6084	296488.4	490919.7	13908078	898792.7	4620659	101997.8	138108.7
NCS DC 73308 (GSD-10 stream sediment) cert.	13000	900	296744	723804	15030132	1037688	5002830	107000	136000
recovery %	94.83011	66.40094	99.91388	67.82496	92.53464	86.61496	92.36091	95.32508	101.5505
GSD 11 measured	64574.24	20206.26	2820620	2995296	49709847	22989719	3193073	40884.77	44151.47
NCS DC 73309 (GSD-11 soil sediment) cert.	70600	26000	3412556	3739654	54881151	27228920	3359043	46800	40000
recovery %	91.46493	77.7164	82.65416	80.09554	90.57727	84.43126	95.05902	87.36062	110.3787
GSD 12 measured	37855.67	7232.996	2888786	2234339	47596688	22321798	7951005	44469.19	34291.6
NCS DC 73310 (GSD-12 sediment) cert.	39000	8200	3264184	2834899	49218390	24157365	8290404	46600	35000
recovery %	97.06581	88.20727	88.4995	78.81548	96.70509	92.40163	95.90612	95.42745	97.97601
Certified Reference Samples	**Mn (55)**	**Fe (57)**	**Co (59)**	**Ni (60)**	**Cu (63)**	**Zn (66)**	**Ga (69)**	**Rb (85)**	**Sr (88)**
GSD 09 measured	702830.5	33119931	13616.77	35510.37	38603.27	85891.99	14840.31	82609.2	172230.3
NCS DC 73307 (GSD-09 river sediment) cert.	619600	33992444	14400	32300	32100	78000	14000	80000	166000
recovery %	113.4329	97.43321	94.56089	109.9392	120.2594	110.1179	106.0022	103.2615	103.7532
GSD 10 measured	1092135	25261405	14237.06	28706.75	22804.49	41588.66	6303.47	8511.451	21993.44
NCS DC 73308 (GSD-10 stream sediment) cert.	1006850	34732666	15300	30200	22600	46000	6400	9200	25300
recovery %	108.4705	72.73097	93.0527	95.05546	100.9048	90.41014	98.49171	92.51577	86.93059
GSD 11 measured	2570711	27164266	7471.709	15321.66	75970.78	331086.4	17674.45	414238.7	24472.76
NCS DC 73309 (GSD-11 soil sediment) cert.	2478400	30705109	8500	14400	78600	373000	18500	408000	29000
recovery %	103.7246	88.46823	87.90246	106.4004	96.65494	88.76312	95.53755	101.5291	84.38881
GSD 12 measured	1541757	32416930	7860.388	13002.67	1319807	464123.9	14399.44	295119.2	21703.34
NCS DC 73310 (GSD-12 sediment) cert.	1394100	43910728	8800	12800	1230000	498000	14100	270000	24400
recovery %	110.5915	73.82463	89.32259	101.5834	107.3014	93.19757	102.1237	109.3034	88.94811
Certified Reference Samples	**Mo (98)**	**Ag (109)**	**Cd (114)**	**Te (128)**	**Ba (138)**	**Tl (205)**	**Pb (208)**	**Bi (209)**	**U (238)**
GSD 09 measured	629.7638	727.5931	258.0053	39.76743	424883.8	351.3847	20862.73	479.2899	2176.283
NCS DC 73307 (GSD-09 river sediment) cert.	640	89	260	40	430000	490	23000	420	2600

recovery %	98.40059		99.23283	99.41856	98.81018	71.71117	90.70752	114.1166	83.70321
GSD 10 measured	1241.304	< 500	1168.469	95.51201	32073.37	144.0285	24197.94	302.2966	1889.38
NCS DC 73308 (GSD-10 stream sediment) cert.	1200	270	1120	90	42000	210	27000	380	2100
recovery %	103.442		104.3276	106.1245	76.36517	68.585	89.622	79.55174	89.97048
GSD 11 measured	6178.566	2804.496	2187.768	459.5288	230175.1	2228.325	628650.1	37858.77	8509.399
NCS DC 73309 (GSD-11 soil sediment) cert.	5900	3200	2300	380	260000	2900	636000	50000	9100
recovery %	104.7215	87.6405	95.12035	120.9286	88.5289	76.8388	98.84435	75.71754	93.50988
GSD 12 measured	8650.5	1873.65	4017.377	313.3598	197022.4	1416.83	297866.6	8467.673	7364.684
NCS DC 73310 (GSD-12 sediment) cert.	8400	1150	4000	290	206000	1800	285000	10900	7800
recovery %	102.9821	162.9261	100.4344	108.0551	95.64194	78.71276	104.5146	77.68507	94.41902

Table A3.13: Trace element ICP-MS data certified reference materials for the 2015 field season in ppb:

Certified Reference Samples	**Li (7)**	**Be (9)**	**Na (23)**	**Mg (24)**	**Al (27)**	**K (39)**	**Ca (43)**	**V (51)**	**Cr (52)**
GSD 09 measured	30201.89	1966.519	8422752	15191538	55563920	14826626	36045566	98153.4	93715.62
NCS DC 73307 (GSD-09 river sediment) cert.	30000	1800	10682784	14415763	55992534	16519985	38235915	97000	85000
recovery %	100.673	109.2511	78.84417	105.3814	99.23452	89.74963	94.27149	101.1891	110.2537
GSD 10 measured	11585.21	708.8074	359702	504880.2	13804151	972718.6	4848428	102509.9	121730.1
NCS DC 73308 (GSD-10 stream sediment) cert.	13000	900	296744	723804	15030132	1037688	5002830	107000	136000
recovery %	89.117	78.75638	121.2163	69.75372	91.84318	93.73907	96.91372	95.80364	89.50743
GSD 12 measured	40948.9	8122.751	2634874	2252646	48433667	21487392	8008200	44965.84	37007.36
NCS DC 73310 (GSD-12 sediment) cert.	39000	8200	3264184	2834899	49218390	24157365	8290404	46600	35000
recovery %	104.9972	99.05794	80.72077	79.46125	98.40563	88.94758	96.59601	96.49322	105.7353
Certified Reference Samples	**Mn (55)**	**Fe (57)**	**Co (59)**	**Ni (60)**	**Cu (63)**	**Zn (66)**	**Ga (69)**	**Rb (85)**	**Sr (88)**
GSD 09 measured	702649.5	32154583	13725.04	36981.67	35813.5	82748.03	14669.57	75250.34	188804.8
NCS DC 73307 (GSD-09 river sediment) cert.	619600	33992444	14400	32300	32100	78000	14000	80000	166000
recovery %	113.4037	94.59333	95.31276	114.4943	111.5685	106.0872	104.7827	94.06293	113.7378
GSD 10 measured	1138903	25008395	14812.39	32777.34	18214.22	44918.08	6394.913	7667.888	21883.03
NCS DC 73308 (GSD-10 stream sediment) cert.	1006850	34732666	15300	30200	22600	46000	6400	9200	25300
recovery %	113.1155	72.00252	96.81302	108.5342	80.59389	97.648	99.92051	83.34661	86.4942
GSD 12 measured	1622537	32674716	8094.828	10558.37	1474111	507620.9	14838.08	321981.9	21961.99

NCS DC 73310 (GSD-12 sediment) cert.	1394100	43910728	8800	12800	1230000	498000	14100	270000	24400
recovery %	116.386	74.41169	91.98668	82.48728	119.8464	101.9319	105.2346	119.2526	90.00814
Certified Reference Samples	**Mo (98)**	**Ag (109)**	**Cd (114)**	**Te (128)**	**Ba (138)**	**Tl (205)**	**Pb (208)**	**Bi (209)**	**U (238)**
GSD 09 measured	599.35	< 500	259.1837	19.07919	422924.4	369.1751	19540.91	397.6174	1924.118
NCS DC 73307 (GSD-09 river sediment) cert.	640	89	260	40	430000	490	23000	420	2600
recovery %	93.64844		99.68605	47.69798	98.35451	75.34185	84.96047	94.6708	74.00454
GSD 10 measured	1230.644	< 500	1140.197	79.74792	28187.9	141.2041	22382.68	306.2332	1692.214
NCS DC 73308 (GSD-10 stream sediment) cert.	1200	270	1120	90	42000	210	27000	380	2100
recovery %	102.5537		101.8033	88.6088	67.11404	67.24003	82.89881	80.58767	80.58163
GSD 12 measured	9329.986	< 500	4198.854	337.8842	204623.3	1668.887	329784.8	9554.145	6874.351
NCS DC 73310 (GSD-12 sediment) cert.	8400	1150	4000	290	206000	1800	285000	10900	7800
recovery %	111.0713	< 500	104.9713	116.5118	99.33171	92.71595	115.714	87.65271	88.13271

Table A3.14: REE and Th ICP-MS data; data is in ppm and was corrected in accordance with CRM results:

Sample	Y	Zr	La	Ce	Pr	Nd	Sm	Eu	Gd	Tb	Dy	Ho	Er	Tm	Yb	Lu	Th
004aC	10.4	102.8	43.1	78.7	8.7	28.3	4.2	0.9	2.8	0.4	1.8	0.4	1.2	0.2	1.4	0.2	24.3
004cJ	2.7	47.4	4.7	5.8	0.7	2.5	0.3	0.2	0.4	0.1	0.4	0.1	0.3	0.0	0.4	0.1	0.9
004dI	5.2	69.9	31.3	53.4	5.8	19.2	2.8	0.6	2.0	0.2	1.1	0.2	0.6	0.1	0.5	0.1	14.1
005aA	6.0	108.9	36.3	62.3	6.7	21.2	2.9	0.9	2.2	0.3	1.0	0.2	0.6	0.1	0.7	0.1	22.7
007aB	66.3	86.8	7.5	13.0	2.0	8.8	4.3	0.2	6.4	1.7	11.8	2.5	8.2	1.3	8.6	1.3	23.6
008aC	4.6	192.8	74.3	125.9	13.0	39.5	4.8	1.3	3.2	0.3	1.1	0.2	0.5	0.1	0.4	0.1	23.5
008dG	3.9	101.7	5.2	6.6	0.8	2.6	0.4	0.4	0.4	0.1	0.5	0.1	0.5	0.1	0.8	0.2	1.3
012aD	8.6	163.0	64.2	113.7	12.0	38.8	4.7	1.3	3.7	0.4	1.8	0.3	0.8	0.1	0.7	0.1	16.9
012bE	5.2	68.5	3.9	3.9	0.4	1.5	0.2	0.5	0.3	0.1	0.6	0.2	0.7	0.1	0.9	0.2	0.5
013aE	0.7	2.5	2.5	2.3	0.3	0.8	0.1	0.7	0.1	0.0	0.1	0.0	0.1	0.0	0.1	0.0	0.2
014aB	28.5	866.3	150.4	291.0	34.4	125.4	17.1	1.9	12.9	1.6	6.4	1.1	2.9	0.4	2.6	0.4	14.9
014bC	1.6	13.1	9.9	15.7	1.7	5.8	0.9	1.1	0.6	0.1	0.3	0.1	0.1	0.0	0.1	0.0	1.5
017aC	16.0	312.8	97.1	166.3	17.4	55.0	6.8	1.4	5.5	0.6	3.0	0.5	1.6	0.2	1.5	0.2	38.1
021aA	6.1	106.8	50.7	82.8	8.6	27.8	3.9	1.0	2.9	0.3	1.2	0.2	0.6	0.1	0.5	0.1	22.8
027aA	2.6	34.5	13.3	21.7	2.5	9.1	1.3	0.4	1.1	0.1	0.5	0.1	0.3	0.0	0.3	0.1	4.6
028aX	11.6	126.9	43.9	77.6	8.2	26.9	3.8	1.0	3.0	0.4	1.9	0.4	1.1	0.2	1.2	0.2	22.2
030bA	2.5	30.3	5.1	6.8	0.8	2.6	0.4	0.3	0.4	0.1	0.3	0.1	0.2	0.0	0.3	0.1	1.7
039aB	19.2	63.8	8.6	15.3	1.8	6.8	1.5	0.3	1.4	0.3	2.3	0.6	2.1	0.4	3.1	0.5	3.0
040aA	9.0	54.1	21.2	41.0	5.1	19.2	3.9	0.8	3.1	0.5	2.0	0.3	0.9	0.1	0.8	0.1	9.9
045aB	15.3	158.8	8.8	21.6	2.7	10.9	3.2	0.6	2.6	0.5	2.8	0.5	1.7	0.3	1.7	0.3	9.6
046aA	17.1	32.5	6.0	13.6	1.9	8.5	2.8	0.4	2.6	0.6	3.3	0.6	1.8	0.3	1.6	0.3	7.2
047aC	5.0	54.1	0.9	1.7	0.2	1.3	0.6	0.5	0.6	0.1	1.0	0.2	0.6	0.1	0.6	0.1	2.8
048aA	19.7	107.0	29.0	51.8	5.9	20.3	3.7	0.5	3.2	0.6	3.4	0.7	2.1	0.3	2.1	0.3	10.0
050aA	4.0	4.0	2.5	4.8	0.6	2.4	0.6	0.4	0.6	0.1	0.7	0.1	0.4	0.0	0.4	0.0	2.1
053aC	13.0	86.6	22.6	41.9	4.9	17.1	3.2	0.9	2.3	0.4	1.9	0.4	1.3	0.2	1.8	0.3	13.1
053bE	4.3	15.7	3.2	5.8	0.7	3.0	0.7	0.4	0.5	0.1	0.6	0.1	0.4	0.1	0.4	0.1	3.7
054aC	4.7	46.9	2.9	3.8	0.7	2.7	0.6	0.6	0.6	0.1	0.7	0.1	0.5	0.1	0.5	0.1	0.6
054bD	1.8	82.3	0.6	1.0	0.1	0.4	0.1	0.7	0.1	0.0	0.2	0.0	0.2	0.0	0.3	0.0	0.1
055aX	14.5	142.7	12.0	25.8	3.4	13.1	3.3	0.9	2.7	0.5	2.8	0.5	1.7	0.3	1.8	0.3	8.7
056aX	22.5	45.4	13.5	26.1	3.7	15.3	4.4	0.5	3.7	0.7	4.2	0.8	2.4	0.4	2.4	0.4	11.6
058aA	27.0	39.1	5.4	10.6	1.6	6.6	1.7	0.4	1.8	0.4	3.0	0.8	3.3	0.8	5.7	1.1	2.3
062aA	1.8	17.1	1.2	2.0	0.3	1.2	0.2	0.8	0.2	0.0	0.3	0.0	0.2	0.0	0.2	0.0	0.0
064aA	9.5	131.5	30.1	62.4	7.4	27.3	4.6	1.3	3.4	0.5	2.1	0.4	1.0	0.1	0.9	0.1	7.7

064bB	8.0	37.4	7.8	15.1	1.9	7.6	1.5	0.5	1.4	0.3	1.5	0.3	0.9	0.1	0.9	0.1	2.0
065aA	5.6	127.1	41.4	77.8	9.2	32.4	5.2	1.4	3.4	0.4	1.3	0.2	0.6	0.1	0.5	0.1	12.1
066aA	4.5	8.0	4.4	8.2	1.1	4.1	1.0	0.6	0.8	0.1	0.8	0.2	0.5	0.1	0.6	0.1	1.9
067aB	6.4	7.9	5.9	12.0	1.6	6.0	1.2	0.5	0.9	0.1	0.9	0.2	0.7	0.1	0.9	0.1	5.5
067bC	1.3	7.1	5.5	11.4	1.4	4.6	0.6	0.7	0.5	0.0	0.2	0.0	0.1	0.0	0.1	0.0	3.5
067cF	11.5	129.3	9.7	22.8	2.3	8.1	1.4	0.8	1.2	0.2	1.4	0.3	1.3	0.3	1.9	0.4	9.4
068aA	9.6	126.2	39.9	80.4	9.9	36.6	7.0	1.2	4.7	0.6	2.3	0.3	1.0	0.2	1.0	0.2	17.9
068bB	23.4	54.0	2.9	6.0	0.8	3.5	1.3	0.3	1.6	0.5	3.5	0.8	3.0	0.6	4.0	0.8	3.9
068cC	15.1	44.2	3.0	6.0	0.7	3.0	0.8	0.3	0.9	0.2	1.9	0.5	1.7	0.4	2.6	0.5	2.0
070aB	25.2	57.2	14.1	27.4	3.8	14.9	3.8	0.5	3.5	0.7	4.4	0.9	2.8	0.5	2.9	0.4	8.0
071aA	2.2	7.0	0.9	1.4	0.2	0.7	0.2	1.1	0.2	0.0	0.3	0.0	0.2	0.0	0.2	0.0	0.1
072aA	25.0	31.0	7.5	15.2	2.0	8.0	2.1	0.6	2.1	0.5	3.5	0.8	2.8	0.5	3.7	0.7	3.9
075aA	40.1	43.7	4.2	6.6	0.9	3.9	1.4	0.4	2.2	0.7	5.3	1.2	4.1	0.7	4.8	0.8	3.2
076aA	13.6	19.5	3.8	7.0	0.9	3.5	0.9	0.8	0.9	0.2	1.8	0.4	1.6	0.3	1.9	0.3	2.2
078aB	61.0	281.3	55.4	113.1	14.9	59.1	13.3	0.7	10.7	1.9	10.3	2.0	6.0	1.0	6.3	1.1	20.8
082aD	57.5	107.4	8.1	14.6	2.1	8.8	2.9	0.6	3.5	1.0	7.3	1.7	6.2	1.2	8.8	1.7	14.4
082bA	39.1	75.9	6.2	12.7	1.8	7.5	2.6	0.4	3.0	0.8	5.5	1.2	4.0	0.7	4.5	0.7	14.9
083aB	41.0	59.3	13.7	28.8	3.9	16.0	4.7	0.5	4.4	0.9	6.2	1.4	4.7	0.9	5.2	0.9	21.0
083bC	31.2	52.2	11.7	22.1	3.1	13.0	3.5	0.8	3.3	0.7	4.1	0.9	3.0	0.6	4.1	0.8	8.1
084aC	8.7	82.1	13.2	24.0	2.9	10.7	2.3	0.6	1.8	0.3	1.6	0.3	0.8	0.1	0.8	0.1	10.1
084bF	35.1	93.6	14.6	28.1	3.6	13.6	3.2	0.6	2.9	0.7	4.9	1.3	4.6	0.8	5.6	1.0	17.9

Table A3.14 continued, data from Grantham *et al.,* (1991), data is in ppm:

Sample	Y	Zr	La	Ce	Pr	Nd	Sm	Eu	Gd	Dy	Ho	Er	Yb	Th
BK58	4.90	6.10	18.85	29.95	3.40	11.98	2.19	0.70	1.54	0.94	0.19	0.51	0.45	53.00
BK59	3.70	8.40	19.87	31.12	3.59	12.81	2.41	0.74	1.78	1.20	0.25	0.63	0.59	64.00

Table A3.15: REE and Th ICP-MS data certified reference materials for the 2014 field season:

Samples	**Y (89)**	**Zr (90)**	**La (139)**	**Ce (140)**	**Pr (141)**	**Nd (146)**	**Sm (147)**	**Eu (151)**	**Gd (157)**	**Tb (159)**	**Dy (163)**	**Ho (165)**	**Er (167)**	**Tm (169)**	**Yb (172)**	**Lu (175)**	**Th (232)**
GSD 09 Avg	**27426**	**387019**	**40188**	**78197**	**9563**	**35649**	**6571**	**1321**	**5662**	**939**	**5124**	**978**	**2877**	**437**	**2791**	**441**	**12400**
NCS DC 73307 (GSD-09 river sediment) cert.	27000	370000	40000	78000	9200	34000	6300	1330	5500	870	5100	960	2800	440	2800	450	12400
recovery %	102	105	100	100	104	105	104	99	103	108	100	102	103	99	100	98	100

GSD 10 Avg	**13204**	**70535**	**13998**	**37845**	**3016**	**11793**	**2312**	**455**	**2186**	**382**	**2227**	**430**	**1277**	**185**	**1175**	**177**	**4895**
NCS DC 73308 (GSD-10 stream sediment) cert.	14000	70000	13000	38000	3200	11800	2400	470	2200	420	2200	450	1300	200	1200	190	5000
recovery %	94	101	108	100	94	100	96	97	99	91	101	96	98	92	98	93	98
GSD 11 Avg	**43637**	**152480**	**28724**	**57428**	**7306**	**26888**	**6203**	**605**	**5905**	**1222**	**7522**	**1470**	**4649**	**764**	**5104**	**799**	**22765**
NCS DC 73309 (GSD-11 soil sediment) cert.	43000	153000	30000	58000	7400	27000	6200	600	5900	1130	7200	1400	4600	740	5100	780	23300
recovery %	101	100	96	99	99	100	100	101	100	108	104	105	101	103	100	102	98
GSD 12 Avg	**29666**	**237606**	**31261**	**60657**	**7235**	**25471**	**4994**	**597**	**4473**	**815**	**4866**	**982**	**3198**	**539**	**3722**	**601**	**21036**
NCS DC 73310 (GSD-12 sediment) cert.	29000	234000	32700	61000	6900	26000	5000	610	4400	820	4800	940	3100	530	3700	580	21400
recovery %	102	102	96	99	105	98	100	98	102	99	101	104	103	102	101	104	98
GSR-1 Avg	**67748**	**167809**	**53991**	**109482**	**13084**	**46799**	**9784**	**832**	**8987**	**1711**	**10202**	**2016**	**6556**	**1104**	**7539**	**1192**	**53048**
NCS DC73301 (GSR-1 granite) cert.	62000	167000	54000	108000	12700	47000	9700	850	9300	1650	10200	2050	6500	1060	7400	1150	54000
recovery %	109	100	100	101	103	100	101	98	97	104	100	98	101	104	102	104	98
GSR-2 Avg	**8552**	**92683**	**22329**	**39821**	**4907**	**18753**	**3324**	**1088**	**2652**	**370**	**1736**	**299**	**829**	**111**	**723**	**111**	**2884**
NCS DC73302 (GSR-2 andesite) cert.	9300	99000	22000	40000	4900	19000	3400	1020	2700	410	1850	340	850	150	890	120	2600
recovery %	92	94	101	100	100	99	98	107	98	90	94	88	98	74	81	92	111
GSR-3 Avg	**22231**	**163948**	**55994**	**105859**	**13268**	**53823**	**10319**	**3241**	**8614**	**1234**	**5556**	**842**	**1935**	**229**	**1230**	**167**	**5892**
NCS DC73303 (GSR-3 basalt) cert.	22000	277000	56000	105000	13200	54000	10200	3200	8500	1200	5600	880	2000	280	1500	190	6000
recovery %	101	59	100	101	101	100	101	101	101	103	99	96	97	82	82	88	98
NCS DC 73307 (GSD-09 river sediment) cert.	27000	370000	40000	78000	9200	34000	6300	1330	5500	870	5100	960	2800	440	2800	450	12400
recovery %	101	109	101	98	101	103	101	95	102	101	99	101	103	96	101	102	100

Table A3.16: REE ICP-MS data certified reference materials for the 2015 field season:

Samples	Y (89)	Zr (90)	La (139)	Ce (140)	Pr (141)	Nd (146)	Sm (147)	Eu (151)	Gd (157)	Tb (159)	Dy (163)	Ho (165)	Er (167)	Tm (169)	Yb (172)	Lu (175)	Th (232)
GSD-09 avg	**26995**	**384510**	**40134**	**76244**	**9363**	**34799**	**6388**	**1349**	**5455**	**923**	**4931**	**958**	**2797**	**448**	**2791**	**465**	**12123**
NCS DC 73307 (GSD-09 river sediment) cert.	27000	370000	40000	78000	9200	34000	6300	1330	5500	870	5100	960	2800	440	2800	450	12400
recovery %	100	104	100	98	102	102	101	101	99	106	97	100	100	102	100	103	98
GSD-10 avg	**13389**	**66004**	**13059**	**38541**	**2980**	**11687**	**2313**	**449**	**2176**	**383**	**2172**	**417**	**1231**	**182**	**1156**	**166**	**5110**
NCS DC 73308 (GSD-10 stream sediment) cert.	14000	70000	13000	38000	3200	11800	2400	470	2200	420	2200	450	1300	200	1200	190	5000
recovery %	96	94	100	101	93	99	96	95	99	91	99	93	95	91	96	87	102
GSD 12 Avg	**30394**	**239459**	**32444**	**61553**	**7313**	**25660**	**5122**	**631**	**4486**	**853**	**5037**	**1022**	**3289**	**578**	**3857**	**654**	**21428**
NCS DC 73310 (GSD-12 sediment) cert.	29000	234000	32700	61000	6900	26000	5000	610	4400	820	4800	940	3100	530	3700	580	21400
recovery %	105	102	99	101	106	99	102	103	102	104	105	109	106	109	104	113	100

A3.5 Isotope data

Table A3.17: Rb-Sr isotope data that was produced for this study as well as data from other authors that was captured for this study. $^{87}Sr/^{86}Sr_i$ calculated to 500 Ma.

Sample	Rb (ppm)	Sr (ppm)	$^{87}Rb/^{86}Sr$	$^{87}Sr/^{86}Sr$	2σ	$^{87}Sr/^{86}Sr_i$	Lithology	Location	Author(s)
004dI	94.0	328.0	0.830605	0.725459	0.00001	0.719541	Dalmatian Granite	Fuglefjellet	This study
008aC	178.0	420.0	1.228438	0.726449	0.00001	0.717696	Dalmatian Granite	Fuglefjellet	This study
012aD	138.0	467.0	0.856162	0.722001	0.00001	0.715901	Dalmatian Granite	Salknappen	This study
017aC	195.0	539.0	1.047875	0.718927	0.00001	0.711461	Dalmatian Granite	Vendeholten	This study
028aX	194.0	279.0	2.015406	0.726036	0.00001	0.711676	Dalmatian Granite	Kivithovden	This study
040aA	135.0	159.0	2.463768	0.737788	0.00001	0.720233	Dalmatian Granite	Gordonnuten	This study
070aB	113.0	105.0	3.122207	0.735647	0.00001	0.713400	Dalmatian Granite	Nupskåpa	This study
083aB	112.0	32.0	10.203186	0.785218	0.00002	0.712518	Dalmatian Granite	Rootshorga	This study
084aC	188.0	151.0	3.612422	0.736711	0.00001	0.710972	Dalmatian Granite	Rootshorga	This study
014bC	156.0	265.0	1.708156	0.737447	0.00001	0.725276	Pegmatitic Dalmatian Granite	Roerkulten	This study
067aB	96.0	164.0	1.697877	0.733438	0.00001	0.721340	Pre-existing Granitoid	Skarsnuten	This study
067bC	131.0	246.0	1.543889	0.728746	0.00001	0.717745	Pre-existing Granitoid	Skarsnuten	This study
067cF	143.0	273.0	1.518421	0.727301	0.00001	0.716482	Pre-existing Granitoid	Skarsnuten	This study
013aE	146.0	271.0	1.561272	0.724382	0.00004	0.713258	Salknappen Pegmatite +Eu	Salknappen	This study
027aA	12.0	458.0	0.075824	0.710201	0.00001	0.709661	Salknappen Pegmatite +Eu	Kivithovden	This study
053bE	58.0	104.0	1.616328	0.725322	0.00001	0.713805	Salknappen Pegmatite +Eu	Skarsnuten	This study
062aA	19.0	536.0	0.102607	0.712487	0.00001	0.711756	Salknappen Pegmatite +Eu	SH 1725	This study
068cC	80.0	148.0	1.566349	0.723562	0.00001	0.712401	Salknappen Pegmatite -Eu	Gordonnuten	This study
072aA	138.0	122.0	3.282041	0.736880	0.00001	0.713495	Salknappen Pegmatite -Eu	Nupskåpa	This study
JW1	91.0	410.0	0.64283	0.718353	0.00003	0.713773	DML Gneisses	Sverdrupfjella	Wareham et al. (1998)
JW4	72.0	508.0	0.41033	0.714171	0.00003	0.711247	DML Gneisses	Sverdrupfjella	Wareham et al. (1998)
JW5	47.0	863.0	0.15762	0.710711	0.00003	0.709588	DML Gneisses	Sverdrupfjella	Wareham et al. (1998)
JE13	79.0	477.0	0.47961	0.716867	0.00003	0.713450	DML Gneisses	Sverdrupfjella	Wareham et al. (1998)
J7.2.94/1	49.0	511.0	0.27742	0.707303	0.00003	0.705326	DML Gneisses	Heimefrontfjella	Wareham et al. (1998)
J7.2.94/2	53.0	510.0	0.30067	0.707717	0.00003	0.705575	DML Gneisses	Heimefrontfjella	Wareham et al. (1998)
J7.2.94/8	55.0	503.0	0.31637	0.707947	0.00003	0.705693	DML Gneisses	Heimefrontfjella	Wareham et al. (1998)
SF847WR	251.0	1081.0	0.67213	0.712800	0.00001	0.708011	Granitoid Suite	Brattskarvet	Moyes et al. (1993)
SF8437	173.0	2921.0	0.17138	0.709380	0.00001	0.708159	Granitoid Suite	Brattskarvet	Moyes et al.

									(1993)
SF85117	147.0	1063.0	0.40022	0.710750	0.00001	0.707898	Granitoid Suite	Brattskarvet	Moyes et al. (1993)
SF8662WR	274.0	1645.0	0.48208	0.711110	0.00001	0.707675	Granitoid Suite	Brattskarvet	Moyes et al. (1993)
SF8663WR	243.0	2931.0	0.23991	0.709450	0.00002	0.707741	Granitoid Suite	Brattskarvet	Moyes et al. (1993)
SF8665	223.0	890.0	0.72534	0.713300	0.00001	0.708132	Granitoid Suite	Brattskarvet	Moyes et al. (1993)
SF8666	294.0	748.0	1.13813	0.716160	0.00001	0.708051	Granitoid Suite	Brattskarvet	Moyes et al. (1993)
SF8696	158.0	1496.0	0.30566	0.710750	0.00001	0.708572	Granitoid Suite	Brattskarvet	Moyes et al. (1993)
SF8698	191.0	2466.0	0.22414	0.709950	0.00001	0.708353	Granitoid Suite	Brattskarvet	Moyes et al. (1993)
ABM89-38	210.0	3769.0	0.16123	0.709000	0.00004	0.707851	Granitoid Suite	Brattskarvet	Moyes et al. (1993)
ABM89-40	153.0	1633.0	0.27114	0.710270	0.00002	0.708338	Granitoid Suite	Brattskarvet	Moyes et al. (1993)
ABM89-32	95.0	349.0	0.78865	0.721880	0.00002	0.716261	Xenolith	Brattskarvet	Moyes et al. (1993)
ABM89-33	114.0	338.0	0.97759	0.726070	0.00002	0.719104	Xenolith	Brattskarvet	Moyes et al. (1993)
ABM89-34	99.0	160.0	1.79541	0.737450	0.00002	0.724657	Xenolith	Brattskarvet	Moyes et al. (1993)
ABM89-35	68.0	233.0	0.84570	0.723670	0.00004	0.717644	Xenolith	Brattskarvet	Moyes et al. (1993)
ABM89-36	111.0	245.0	1.31356	0.729040	0.00002	0.719681	Xenolith	Brattskarvet	Moyes et al. (1993)
ABM89-37	46.0	330.0	0.40365	0.716470	0.00002	0.713594	Xenolith	Brattskarvet	Moyes et al. (1993)
ABM89-39	115.0	1014.0	0.32824	0.711180	0.00002	0.708841	Hornfelses	Brattskarvet	Moyes et al. (1993)
ABM89-41	100.0	886.0	0.32666	0.711160	0.00003	0.708832	Hornfelses	Brattskarvet	Moyes et al. (1993)
SLK5	76.0	287.0	0.76682	0.716510	0.00002	0.711046	Sveabreen Paragneiss	Brattskarvet	Moyes et al. (1993)
SLK10	4.8	61.0	0.22765	0.707190	0.00001	0.705568	Sveabreen Paragneiss	Brattskarvet	Moyes et al. (1993)
SF8537	124.0	281.0	1.27887	0.724790	0.00001	0.715678	Sveabreen Paragneiss	Brattskarvet	Moyes et al. (1993)
SF8538	116.0	259.0	1.29804	0.725210	0.00001	0.715961	Sveabreen Paragneiss	Brattskarvet	Moyes et al. (1993)
SF8564	75.0	275.0	0.78981	0.717350	0.00001	0.711722	Sveabreen Paragneiss	Brattskarvet	Moyes et al. (1993)
SF8597WR	321.1	31.7	30.79697	1.227480	0.00008	1.008043	Sveabreen Paragneiss	Brattskarvet	Moyes et al. (1993)
SF85126	38.0	26.0	4.25475	0.770900	0.00002	0.740584	Sveabreen Paragneiss	Brattskarvet	Moyes et al. (1993)
SF8642	121.0	152.0	2.31147	0.744480	0.00004	0.728010	Sveabreen Paragneiss	Brattskarvet	Moyes et al. (1993)
dvg2	182.3	273.4	1.93329	0.729420	0.00001	0.715645	Dalmatian Granite	Dvergen	Grantham et al. (1991)
dig-dal	231.4	271.4	2.47264	0.731730	0.00001	0.714112	Dalmatian Granite	Dvergen	Grantham et al. (1991)
kk7	202.8	389.4	1.50919	0.723860	0.00001	0.713107	Dalmatian Granite	Kivitjølen	Grantham et al. (1991)
kk6	185.1	244.5	2.19453	0.727180	0.00015	0.711543	Dalmatian Granite	Kivitjølen	Grantham et al. (1991)
kk5	208.9	249.0	2.43263	0.730100	0.00001	0.712767	Dalmatian Granite	Kivitjølen	Grantham et al. (1991)
bk62	199.2	235.4	2.45925	0.753310	0.00001	0.735787	Dalmatian Granite	Brekkerista	Grantham et al. (1991)
bk59	214.1	196.4	3.16801	0.753100	0.00001	0.730527	Dalmatian	Brekkerista	Grantham et al.

							Granite		(1991)
bk58	219.5	192.2	3.32082	0.759080	0.00003	0.735418	Dalmatian Granite	Brekkerista	Grantham et al. (1991)
bk4	198.4	233.2	2.47244	0.753150	0.00001	0.735533	Dalmatian Granite	Brekkerista	Grantham et al. (1991)
SA 10	107.0	293.0	1.05782	0.719690	0.00001	0.712153	Salknappen Granite Gneiss	Salknappen	Grantham et al. (2019)
SA 09	111.0	300.0	1.07175	0.719600	0.00003	0.711963	Salknappen Granite Gneiss	Salknappen	Grantham et al. (2019)
SA 08	108.0	274.0	1.14178	0.720030	0.00001	0.711894	Salknappen Granite Gneiss	Salknappen	Grantham et al. (2019)
93/29	50.0	895.8	0.16146	0.705730	0.00015	0.704580	Orthogneiss	Kvervelnatten	Grantham et al. (2019)
93/36	59.4	748.7	0.22954	0.707530	0.00013	0.705894	Orthogneiss	Kvervelnatten	Grantham et al. (2019)
92/81	111.2	491.8	0.65456	0.713490	0.00020	0.708826	Granite Gneiss	Issfosnippa	Grantham et al. (2019)
92/86	144.7	238.4	1.76006	0.730760	0.00190	0.718219	Granite Gneiss	Issfosnippa	Grantham et al. (2019)
92/14	76.1	363.2	0.606616	0.714480	0.00016	0.710158	Megacrystic Orthogneiss	Kirwanveggan	Grantham et al. (2019)
92/17	84.6	395.3	0.619463	0.712060	0.00017	0.707646	Megacrystic Orthogneiss	Kirwanveggan	Grantham et al. (2019)
92/18	95.2	307.0	0.898019	0.717120	0.00150	0.710721	Megacrystic Orthogneiss	Kirwanveggan	Grantham et al. (2019)
92/19	101.6	310.0	0.949164	0.717650	0.00014	0.710887	Megacrystic Orthogneiss	Kirwanveggan	Grantham et al. (2019)

Table A3.18: Sm-Nd isotope data that was produced for this study as well as data from other authors that was captured for this study. $^{143}Nd/^{144}Nd_i$ calculated to 500 Ma.

Sample	Sm (ppm)	Nd (ppm)	$^{147}Sm/^{144}Nd$	$^{143}Nd/^{144}Nd$	2σ	$^{143}Nd/^{144}Nd_i$	Lithology	Location	Author(s)
004dI	2.758	19.232	0.086676	0.51158	0.00001	0.511296	Dalmatian Granite	Fuglefjellet	This study
008aC	4.770	39.518	0.072949	0.51126	0.00001	0.511021	Dalmatian Granite	Fuglefjellet	This study
012aD	4.727	38.800	0.073629	0.51122	0.00001	0.510979	Dalmatian Granite	Salknappen	This study
017aC	6.814	55.044	0.074816	0.51131	0.00001	0.511065	Dalmatian Granite	Vendeholten	This study
028aX	3.802	26.879	0.085490	0.51146	0.00001	0.51118	Dalmatian Granite	Kivithovden	This study
040aA	3.881	19.198	0.122184	0.51154	0.00001	0.51114	Dalmatian Granite	Gordonnuten	This study
070aB	3.768	14.923	0.152627	0.51204	0.00001	0.51154	Dalmatian Granite	Nupskåpa	This study
083aB	4.703	15.963	0.178080	0.51181	0.00001	0.511227	Dalmatian Granite	Rootshorga	This study
084aC	2.339	10.674	0.132450	0.51177	0.00001	0.511336	Dalmatian Granite	Rootshorga	This study
014bC	0.930	5.847	0.096128	0.51129	0.00001	0.510975	Pegmatitic Dalmatian Granite	Roerkulten	This study
067aB	1.176	5.997	0.118540	0.51219	0.00001	0.511802	Pre-existing Granitoid	Skarsnuten	This study
067bC	0.618	4.631	0.080667	0.51207	0.00001	0.511806	Pre-existing Granitoid	Skarsnuten	This study
067cF	1.439	8.060	0.107921	0.51207	0.00001	0.511717	Pre-existing Granitoid	Skarsnuten	This study

013aE	0.100	0.774	0.078101	0.51225	0.00004	0.511994	Salknappen Pegmatite +Eu	Salknappen	This study
027aA	1.300	9.137	0.086005	0.51212	0.00001	0.511838	Salknappen Pegmatite +Eu	Kivithovden	This study
053bE	0.703	2.959	0.143602	0.51179	0.00001	0.51132	Salknappen Pegmatite +Eu	Skarsnuten	This study
062aA	0.179	1.206	0.089723	0.51224	0.00003	0.511946	Salknappen Pegmatite +Eu	SH 1725	This study
068cC	0.817	2.971	0.166233	0.51225	0.00001	0.511706	Salknappen Pegmatite -Eu	Gordonnuten	This study
072aA	2.106	7.970	0.159734	0.51224	0.00001	0.511717	Salknappen Pegmatite -Eu	Nupskåpa	This study
JW1	5.061	27.880	0.109714	0.51145	0.00001	0.511091	DML Gneisses	Sverdrupfjella	Wareham et al. (1998)
JW4	6.154	32.102	0.115863	0.51148	0.00001	0.511101	DML Gneisses	Sverdrupfjella	Wareham et al. (1998)
JW5	6.275	33.823	0.112129	0.51146	0.00001	0.511093	DML Gneisses	Sverdrupfjella	Wareham et al. (1998)
JE13	6.031	31.520	0.115645	0.51150	0.00001	0.511121	DML Gneisses	Sverdrupfjella	Wareham et al. (1998)
J7.2.94/1	4.953	23.720	0.126228	0.51227	0.00001	0.511857	DML Gneisses	Heimefront-fjella	Wareham et al. (1998)
J7.2.94/2	5.019	26.426	0.114810	0.51219	0.00001	0.511814	DML Gneisses	Heimefront-fjella	Wareham et al. (1998)
J7.2.94/8	5.455	26.180	0.125957	0.51225	0.00001	0.511837	DML Gneisses	Heimefront-fjella	Wareham et al. (1998)
SF847WR	108.000	381.000	0.171333	0.51171	0.00002	0.511149	Granitoid Suite	Brattskarvet	Moyes et al. (1993)
SF8437	22.700	162.000	0.084691	0.51153	0.00002	0.511253	Granitoid Suite	Brattskarvet	Moyes et al. (1993)
SF85117	36.200	263.000	0.083189	0.51142	0.00002	0.511148	Granitoid Suite	Brattskarvet	Moyes et al. (1993)
SF8662WR	175.000	1644.00	0.064334	0.51132	0.00002	0.511109	Granitoid Suite	Brattskarvet	Moyes et al. (1993)
SF8663WR	55.600	390.000	0.086162	0.51132	0.00001	0.511038	Granitoid Suite	Brattskarvet	Moyes et al. (1993)
SF8665	11.300	87.200	0.078320	0.51138	0.00002	0.511123	Granitoid Suite	Brattskarvet	Moyes et al. (1993)
SF8666	11.800	89.100	0.080042	0.51144	0.00001	0.511178	Granitoid Suite	Brattskarvet	Moyes et al. (1993)
SF8696	13.300	101.000	0.079586	0.51137	0.00002	0.511109	Granitoid Suite	Brattskarvet	Moyes et al. (1993)
SF8698	12.300	92.400	0.080453	0.51136	0.00002	0.511096	Granitoid Suite	Brattskarvet	Moyes et al. (1993)
ABM89-38	35.400	227.000	0.094253	0.51145	0.00002	0.511141	Granitoid Suite	Brattskarvet	Moyes et al. (1993)
ABM89-40	11.500	105.000	0.066192	0.51128	0.00002	0.511063	Granitoid Suite	Brattskarvet	Moyes et al. (1993)
ABM89-32	4.200	22.800	0.111353	0.51213	0.00001	0.511765	Xenolith	Brattskarvet	Moyes et al. (1993)
ABM89-33	5.100	26.700	0.115461	0.51202	0.00003	0.511642	Xenolith	Brattskarvet	Moyes et al. (1993)
ABM89-34	8.500	44.700	0.114945	0.51206	0.00001	0.511684	Xenolith	Brattskarvet	Moyes et al. (1993)

ABM89-35	9.100	40.900	0.134497	0.51221	0.00001	0.511769	Xenolith	Brattskarvet	Moyes et al. (1993)
ABM89-36	6.100	32.200	0.114516	0.51218	0.00003	0.511805	Xenolith	Brattskarvet	Moyes et al. (1993)
ABM89-37	6.500	27.700	0.141850	0.51223	0.00003	0.511765	Xenolith	Brattskarvet	Moyes et al. (1993)
ABM89-39	14.600	92.300	0.095617	0.51212	0.00002	0.511807	Hornfelses	Brattskarvet	Moyes et al. (1993)
ABM89-41	14.100	89.900	0.094808	0.51212	0.00003	0.511809	Hornfelses	Brattskarvet	Moyes et al. (1993)
SLK5	19.800	86.700	0.138051	0.51219	0.00001	0.511738	Sveabreen Paragneiss	Brattskarvet	Moyes et al. (1993)
SLK10	2.300	6.900	0.201543	0.51314	0.00001	0.51248	Sveabreen Paragneiss	Brattskarvet	Moyes et al. (1993)
SF8537	19.400	100.000	0.117269	0.51208	0.00001	0.511696	Sveabreen Paragneiss	Brattskarvet	Moyes et al. (1993)
SF8538	5.400	25.700	0.127021	0.51240	0.00003	0.511984	Sveabreen Paragneiss	Brattskarvet	Moyes et al. (1993)
SF8564	38.000	186.100	0.123429	0.51206	0.00001	0.511656	Sveabreen Paragneiss	Brattskarvet	Moyes et al. (1993)
SF8597WR	4.030	14.700	0.165730	0.51240	0.00001	0.511857	Sveabreen Paragneiss	Brattskarvet	Moyes et al. (1993)
SF85126	203.000	852.000	0.144030	0.51224	0.00001	0.511768	Sveabreen Paragneiss	Brattskarvet	Moyes et al. (1993)
SF8642	8.500	42.000	0.122337	0.51215	0.00002	0.511749	Sveabreen Paragneiss	Brattskarvet	Moyes et al. (1993)
dvg2	2.405	14.205	0.102323	0.51128	0.00003	0.510945	Dalmatian Granite	Dvergen	Grantham et al. (1991)
dig-dal	2.368	15.270	0.093725	0.51142	0.00003	0.511113	Dalmatian Granite	Dvergen	Grantham et al. (1991)
kk7	3.406	23.352	0.088152	0.51140	0.00003	0.511111	Dalmatian Granite	Kivitjølen	Grantham et al. (1991)
kk6	3.671	27.022	0.082109	0.51153	0.00002	0.511261	Dalmatian Granite	Kivitjølen	Grantham et al. (1991)
kk5	4.580	24.481	0.113074	0.51153	0.00004	0.51116	Dalmatian Granite	Kivitjølen	Grantham et al. (1991)
bk62	3.265	16.695	0.118201	0.51151	0.00003	0.511123	Dalmatian Granite	Brekkerista	Grantham et al. (1991)
bk59	1.874	9.464	0.119680	0.51153	0.00003	0.511138	Dalmatian Granite	Brekkerista	Grantham et al. (1991)
bk58	2.135	10.654	0.121120	0.51157	0.00002	0.511173	Dalmatian Granite	Brekkerista	Grantham et al. (1991)
bk4	1.375	6.768	0.122792	0.51155	0.00003	0.511148	Dalmatian Granite	Brekkerista	Grantham et al. (1991)
SA 10	9.252	37.962	0.147324	0.51214	0.00002	0.511657	Salknappen Granite Gneiss	Salknappen	Grantham et al. (2019)
SA 09	6.243	25.523	0.147862	0.51222	0.00002	0.511736	Salknappen Granite Gneiss	Salknappen	Grantham et al. (2019)
SA 08	5.293	23.575	0.135722	0.51225	0.00002	0.511805	Salknappen Granite Gneiss	Salknappen	Grantham et al. (2019)
93/29	5.966	37.290	0.096708	0.51199	0.00003	0.511673	Orthogneiss	Kvervelnatten	Grantham et al. (2019)
93/36	9.718	44.400	0.132310	0.51224	0.00001	0.511807	Orthogneiss	Kvervelnatten	Grantham et al. (2019)
92/81	8.039	51.340	0.094650	0.51201	0.00002	0.5117	Granite Gneiss	Issfosnippa	Grantham et al. (2019)
92/86	2.651	15.670	0.102264	0.51208	0.00001	0.511745	Granite Gneiss	Issfosnippa	Grantham et al. (2019)

92/14	10.790	51.560	0.126503	0.51219	0.00006	0.511776	Megacrystic Orthogneiss	Kirwanveggan	Grantham et al. (2019)
92/17	11.940	56.450	0.127858	0.51215	0.00002	0.511731	Megacrystic Orthogneiss	Kirwanveggan	Grantham et al. (2019)
92/18	14.740	70.210	0.126911	0.51226	0.00001	0.511844	Megacrystic Orthogneiss	Kirwanveggan	Grantham et al. (2019)
92/19	14.110	64.250	0.132754	0.51220	0.00004	0.511765	Megacrystic Orthogneiss	Kirwanveggan	Grantham et al. (2019)

Appendix 4: Micrographs

Here follows a collection of micrographs for each sample.

004aC - Dalmatian Granite

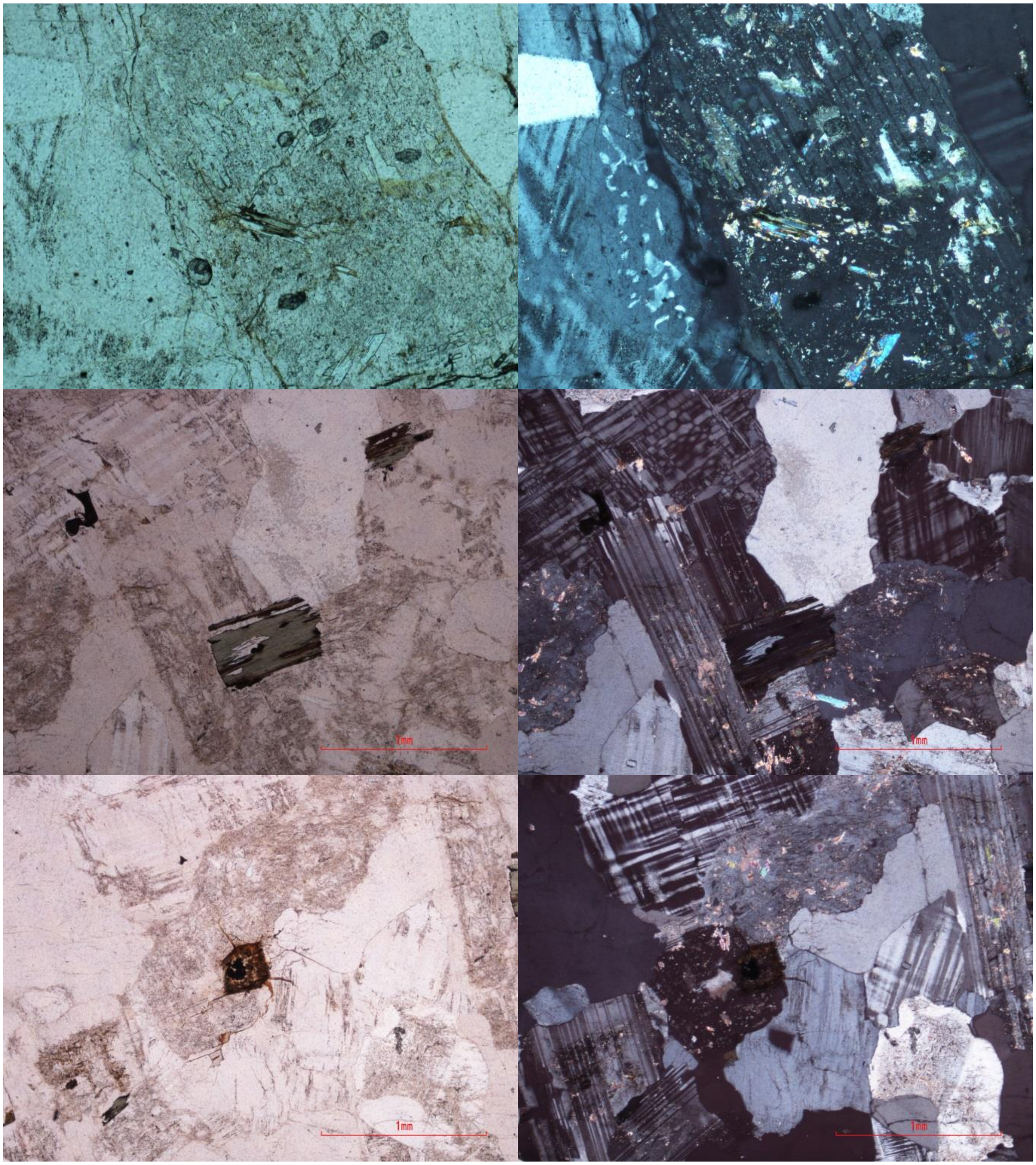

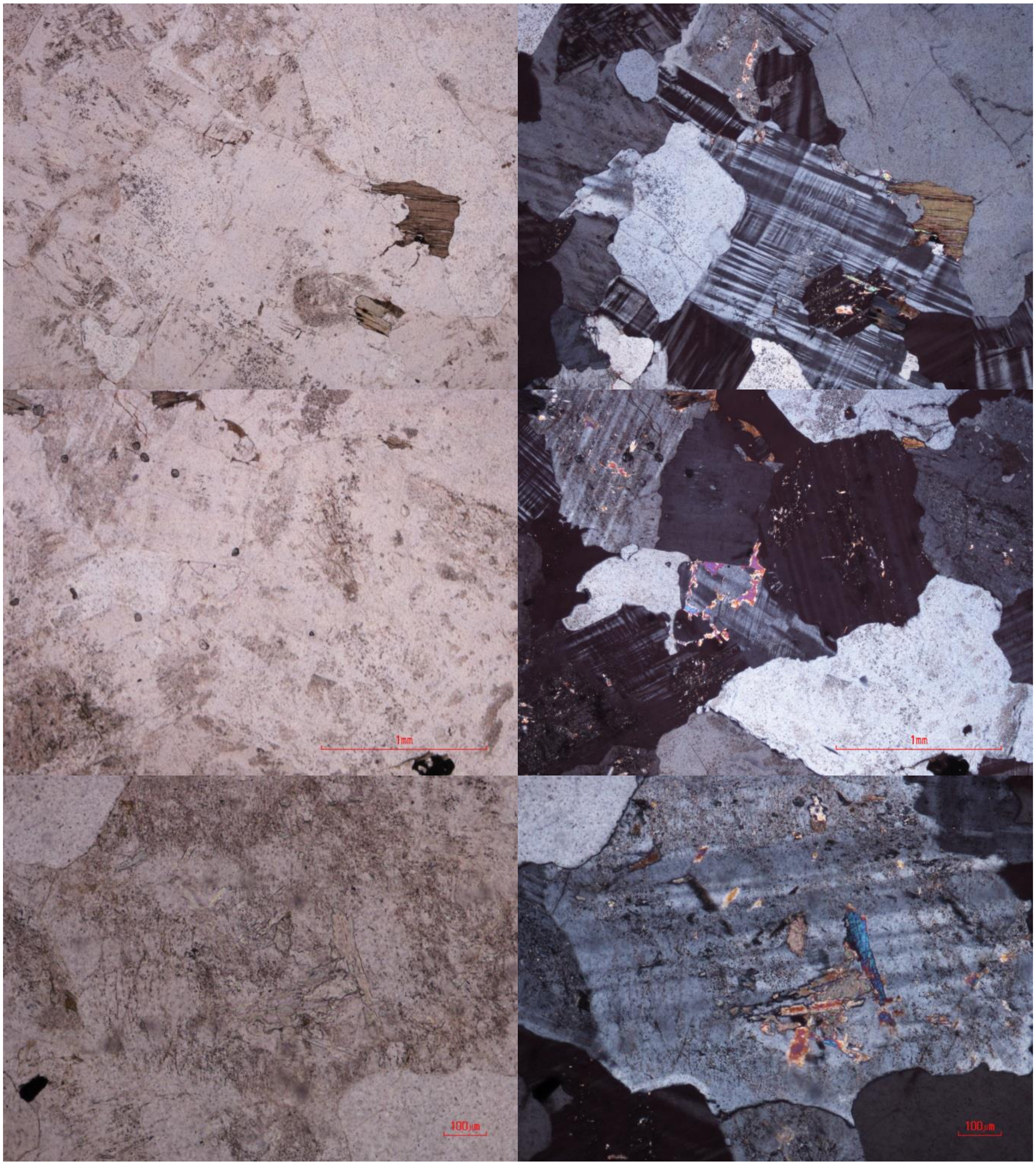
1mm
1mm
100μm
100μm

004cJ - Salknappen Pegmatite

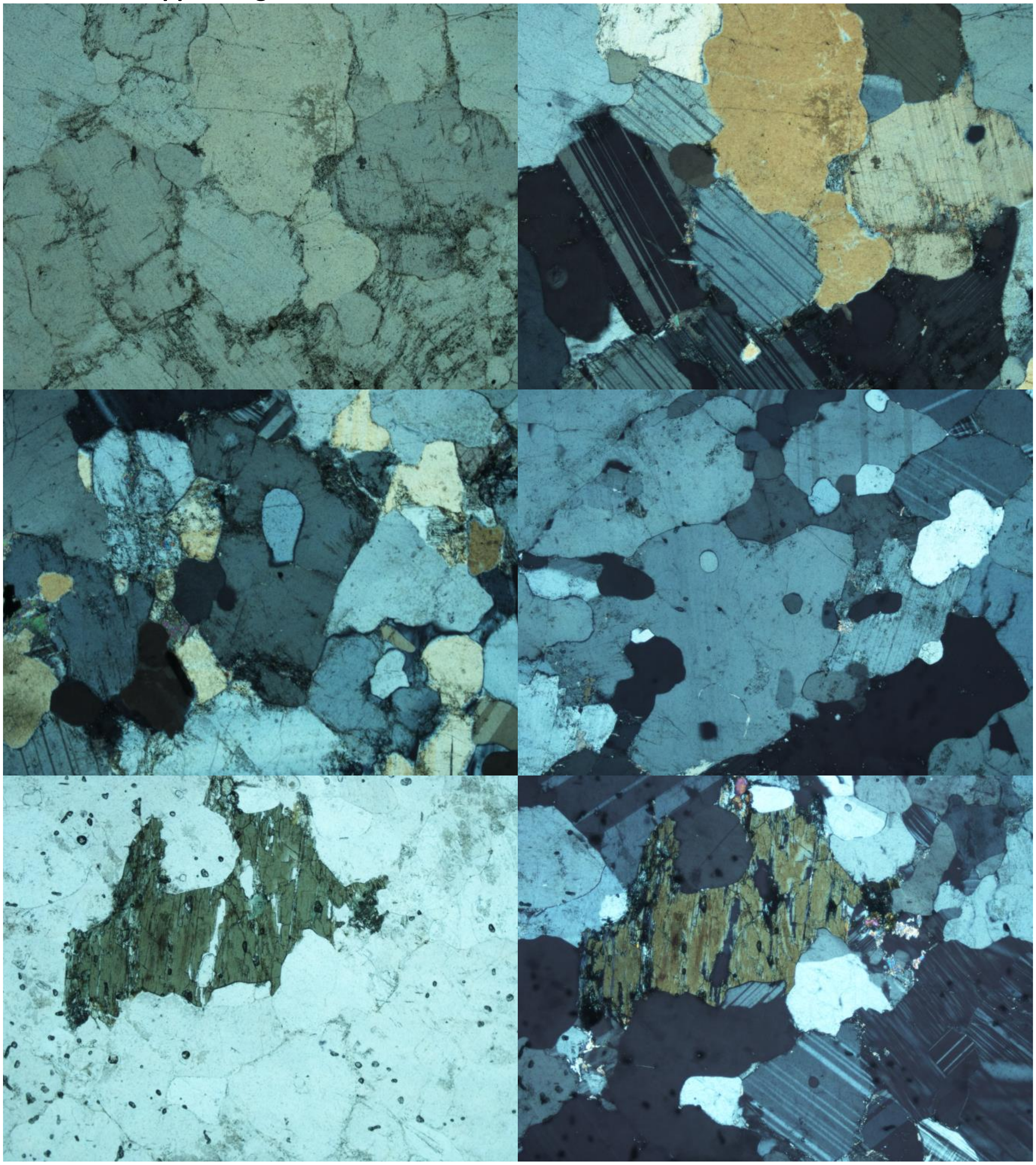

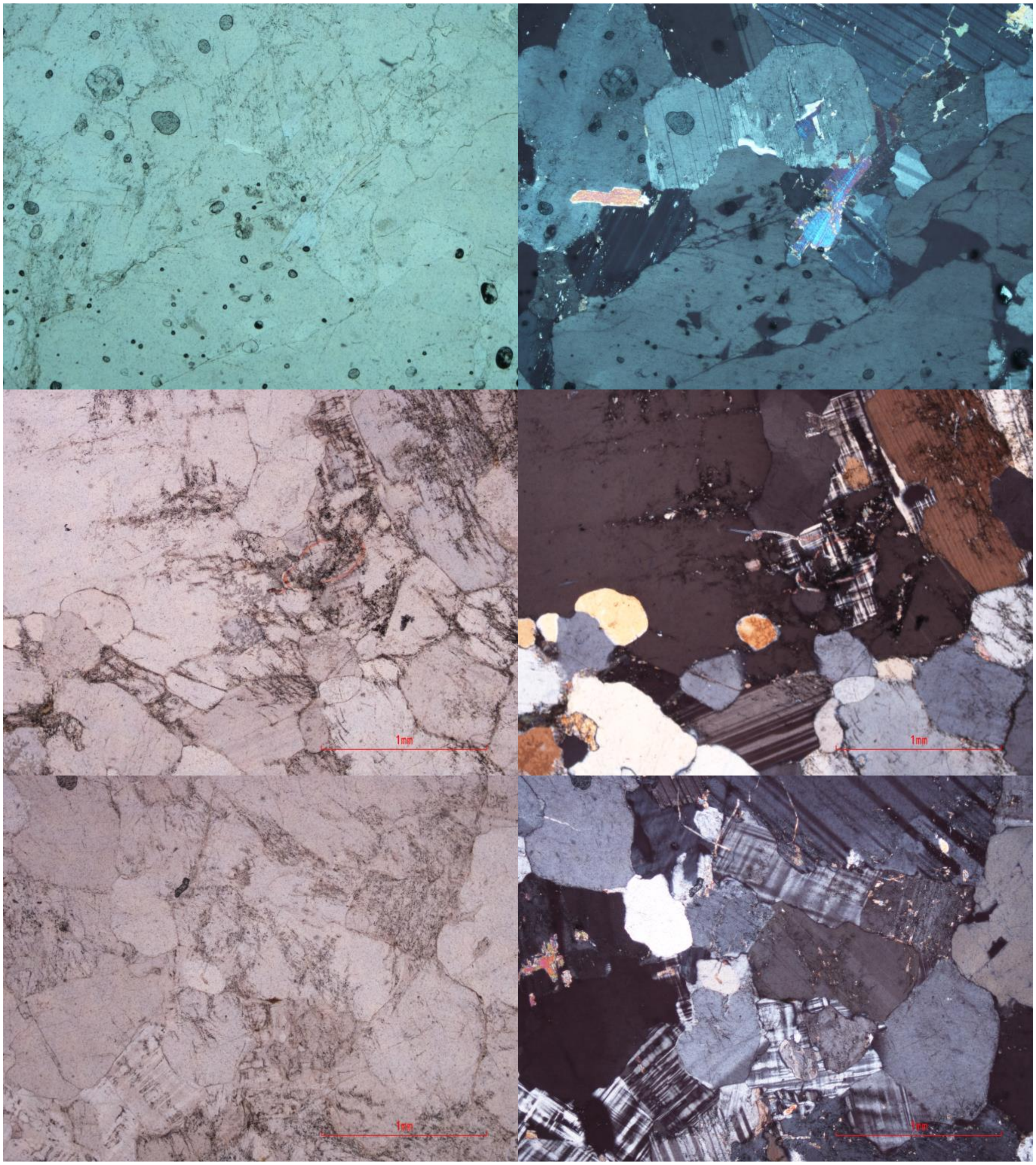
1mm
1mm
1mm
1mm

004dl – Dalmatian Granite

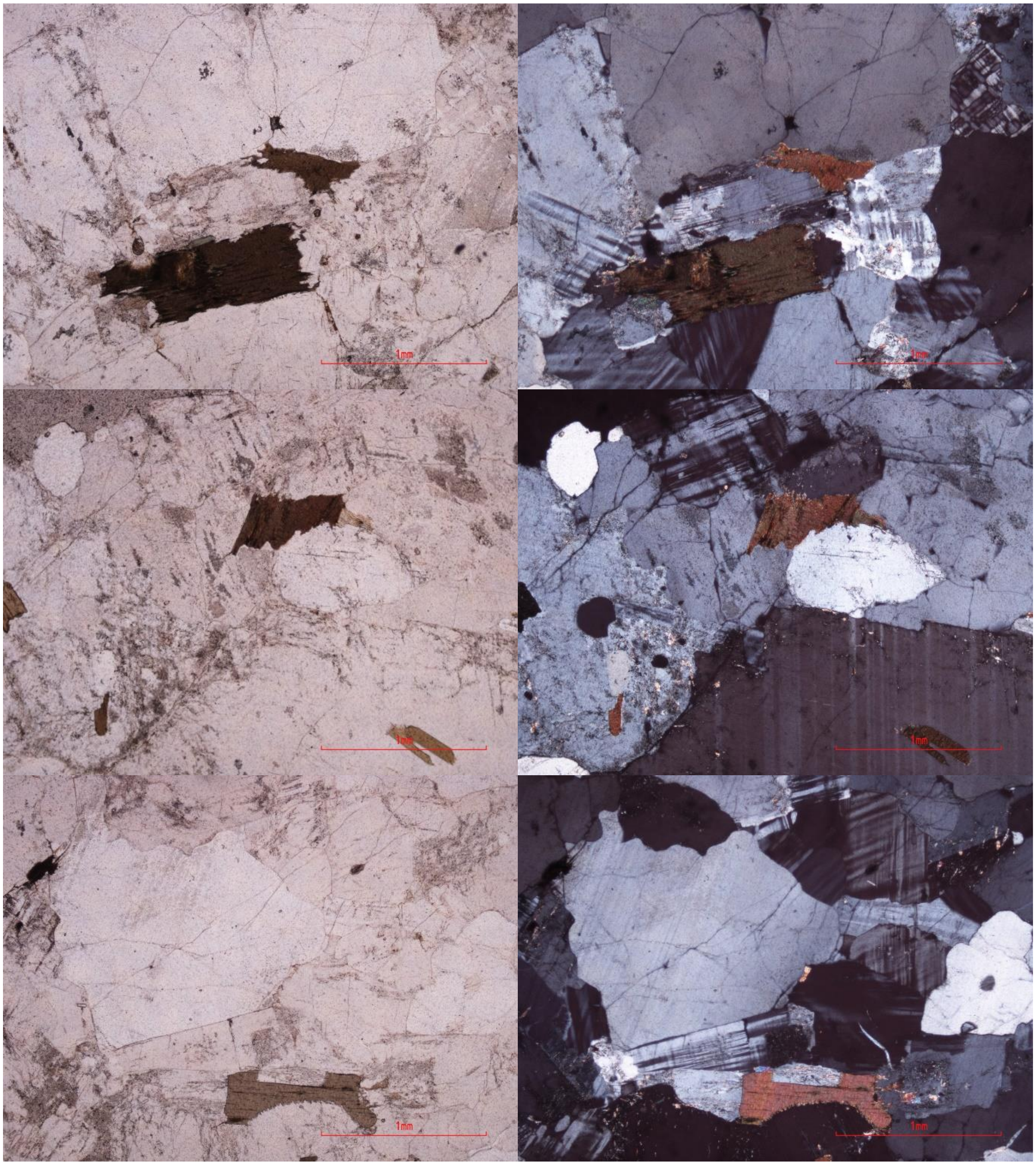

005aA - Dalmatian Granite

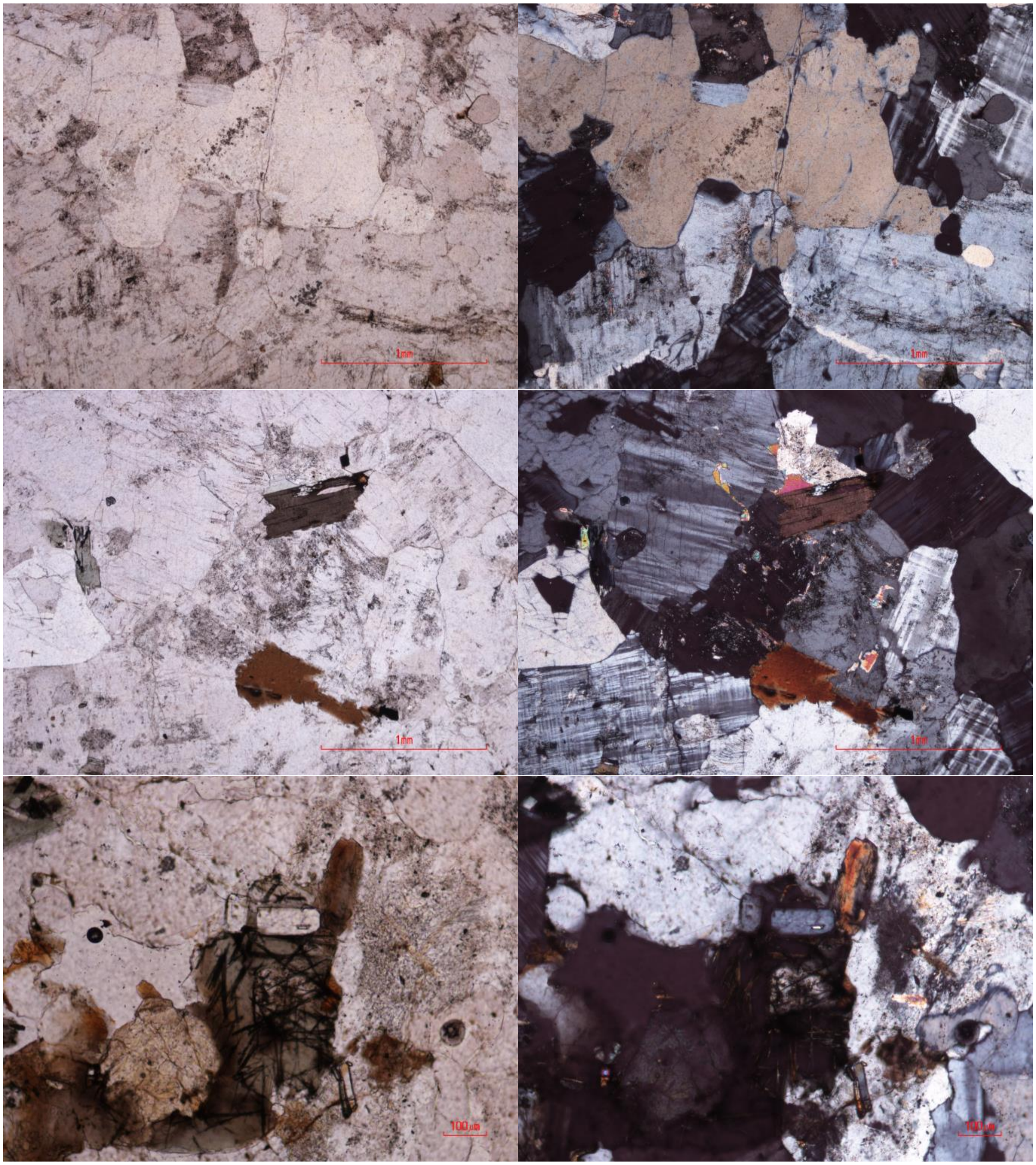

007aB - Dalmatian Granite

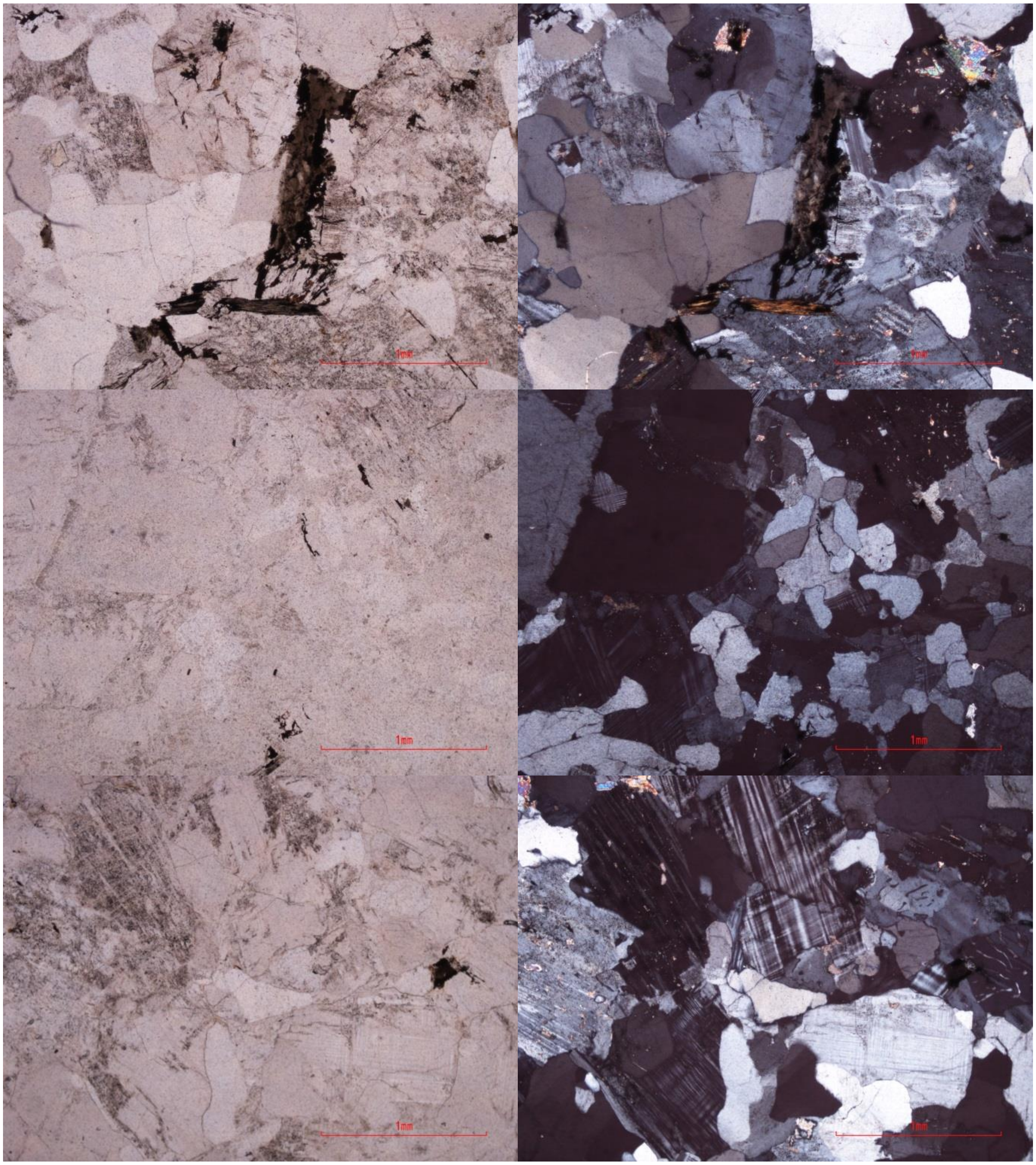

008aC - Dalmatian Granite

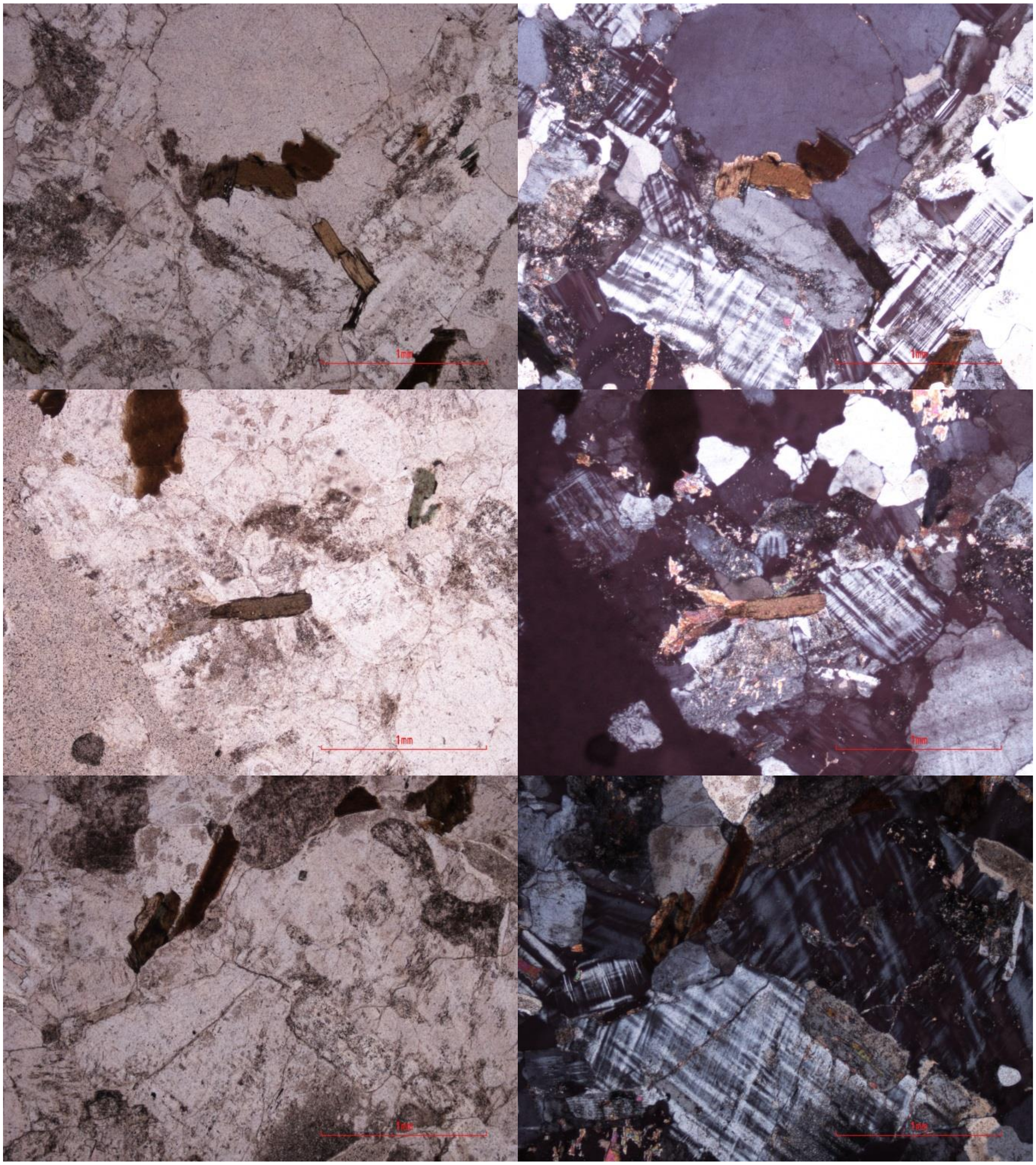

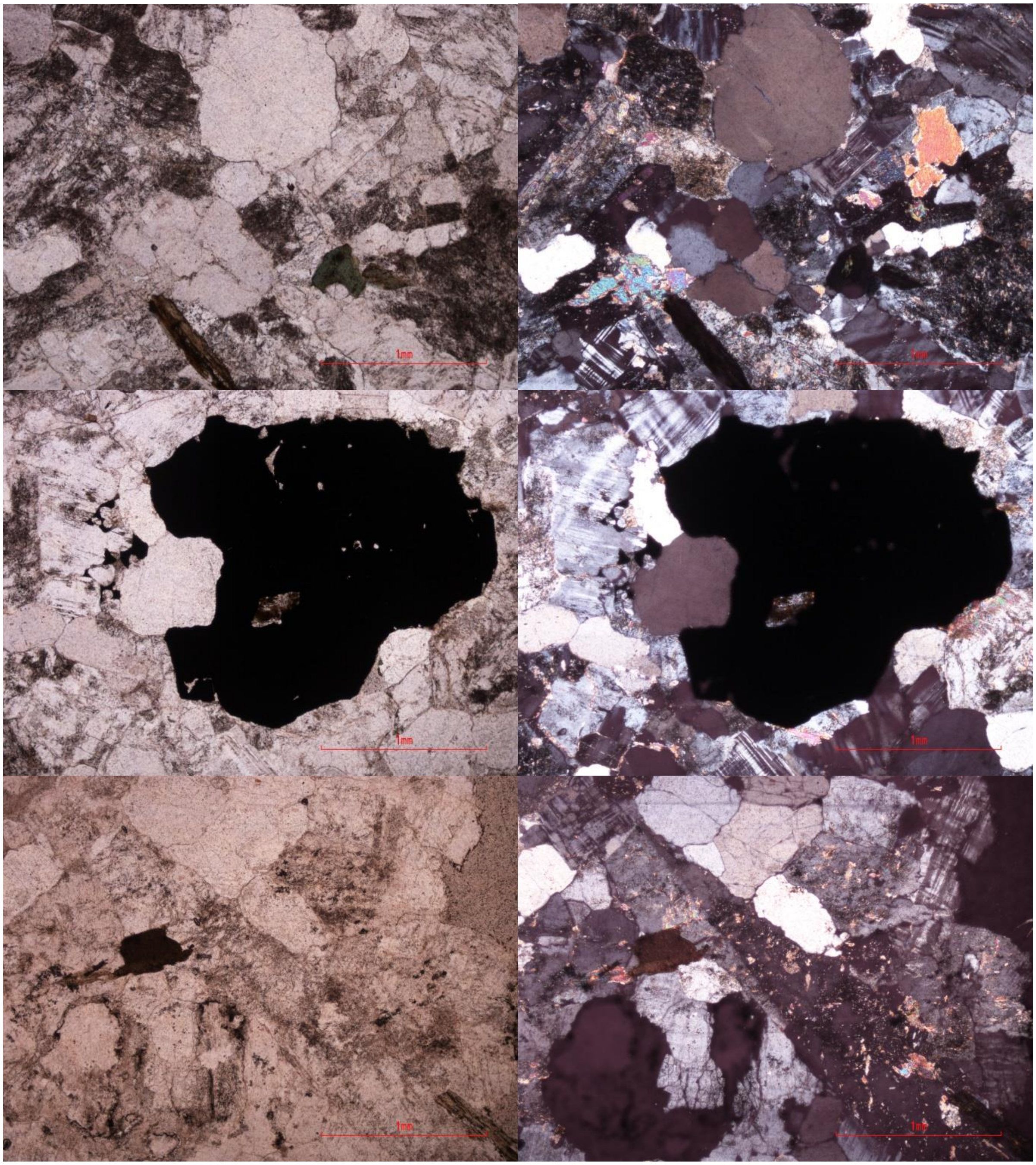
1mm
1mm
1mm
1mm
1mm
1mm

008dG - Dalmatian Granite

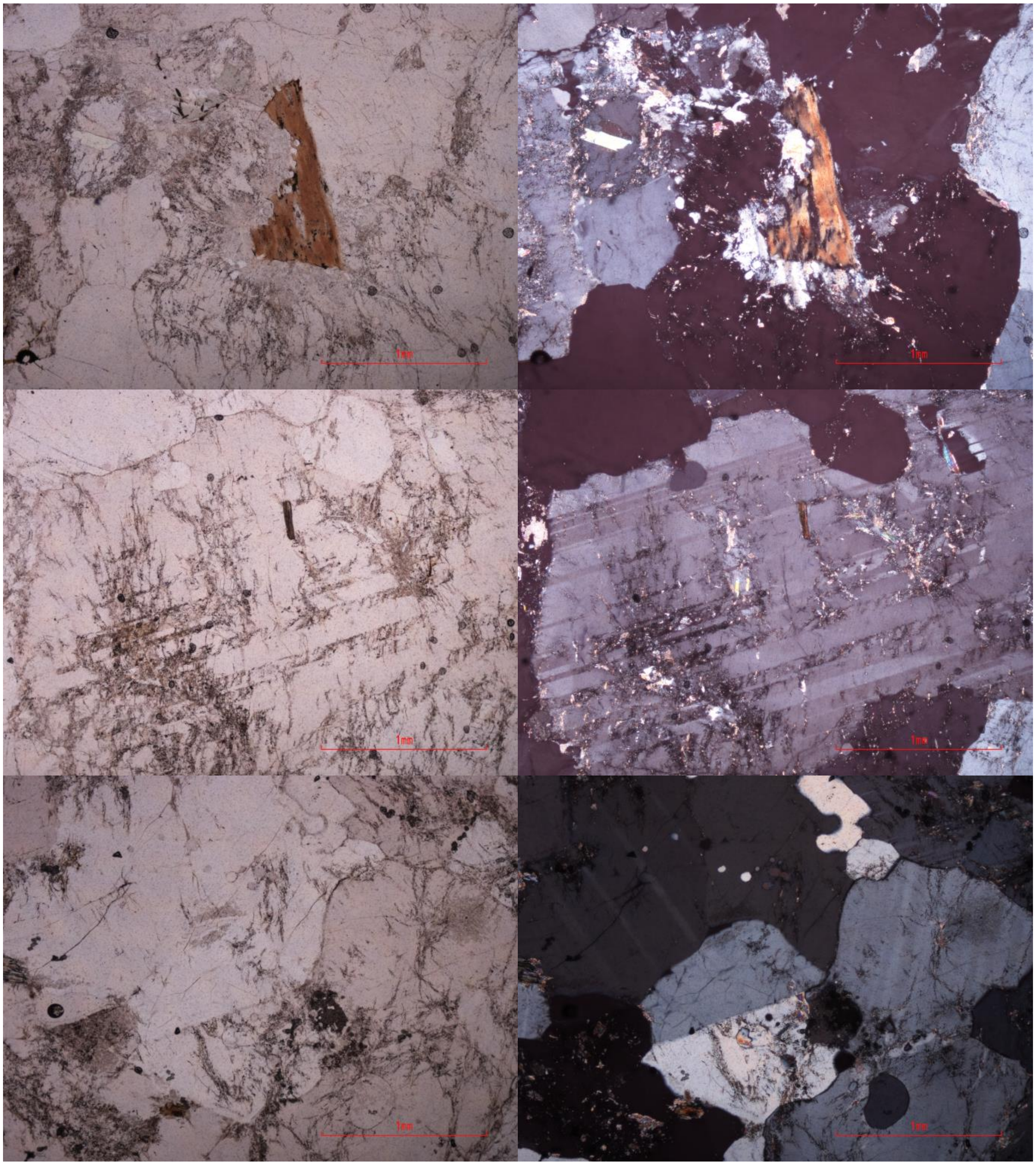

012aD - Dalmatian Granite

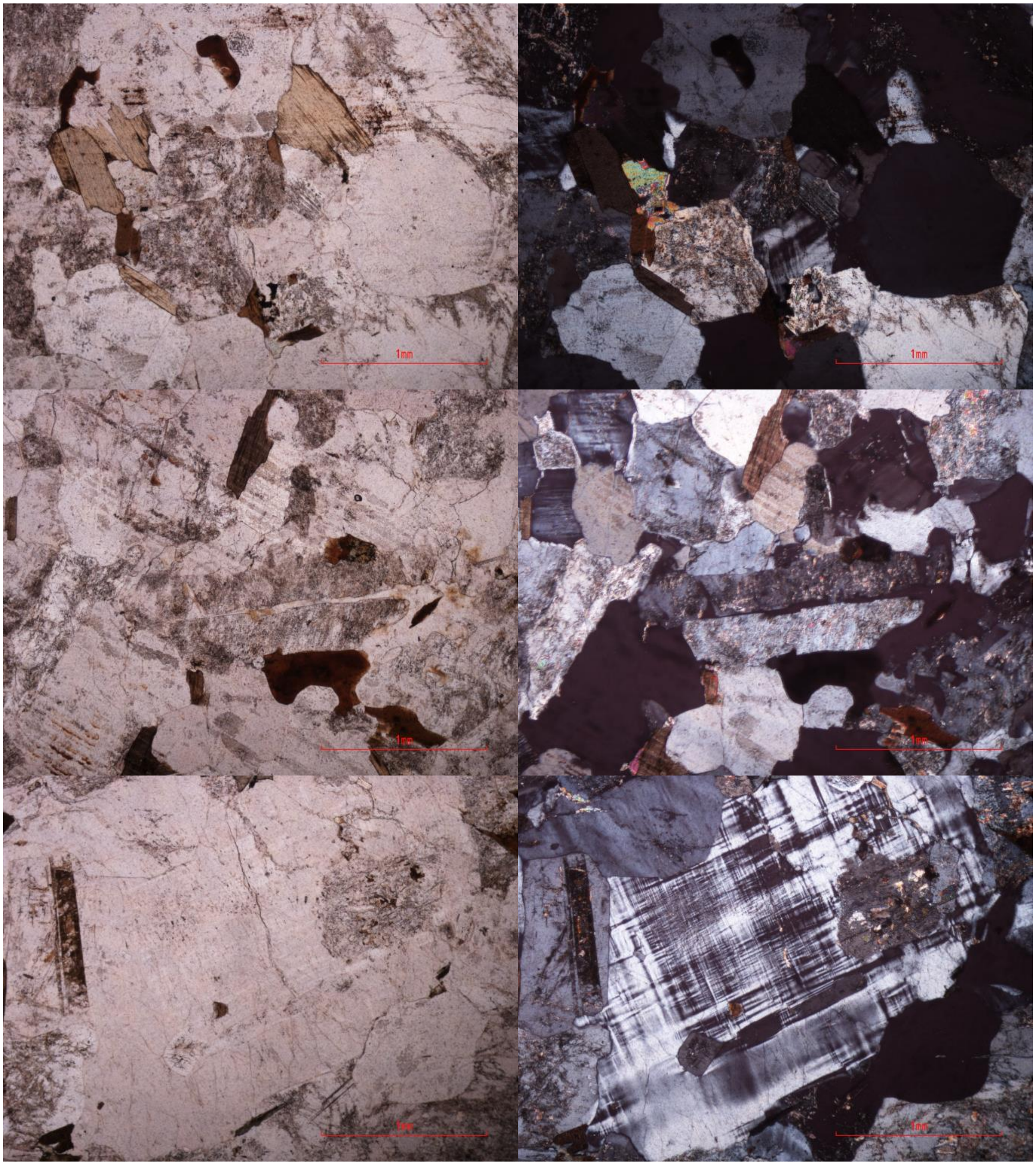

012bE - Salknappen Pegmatite

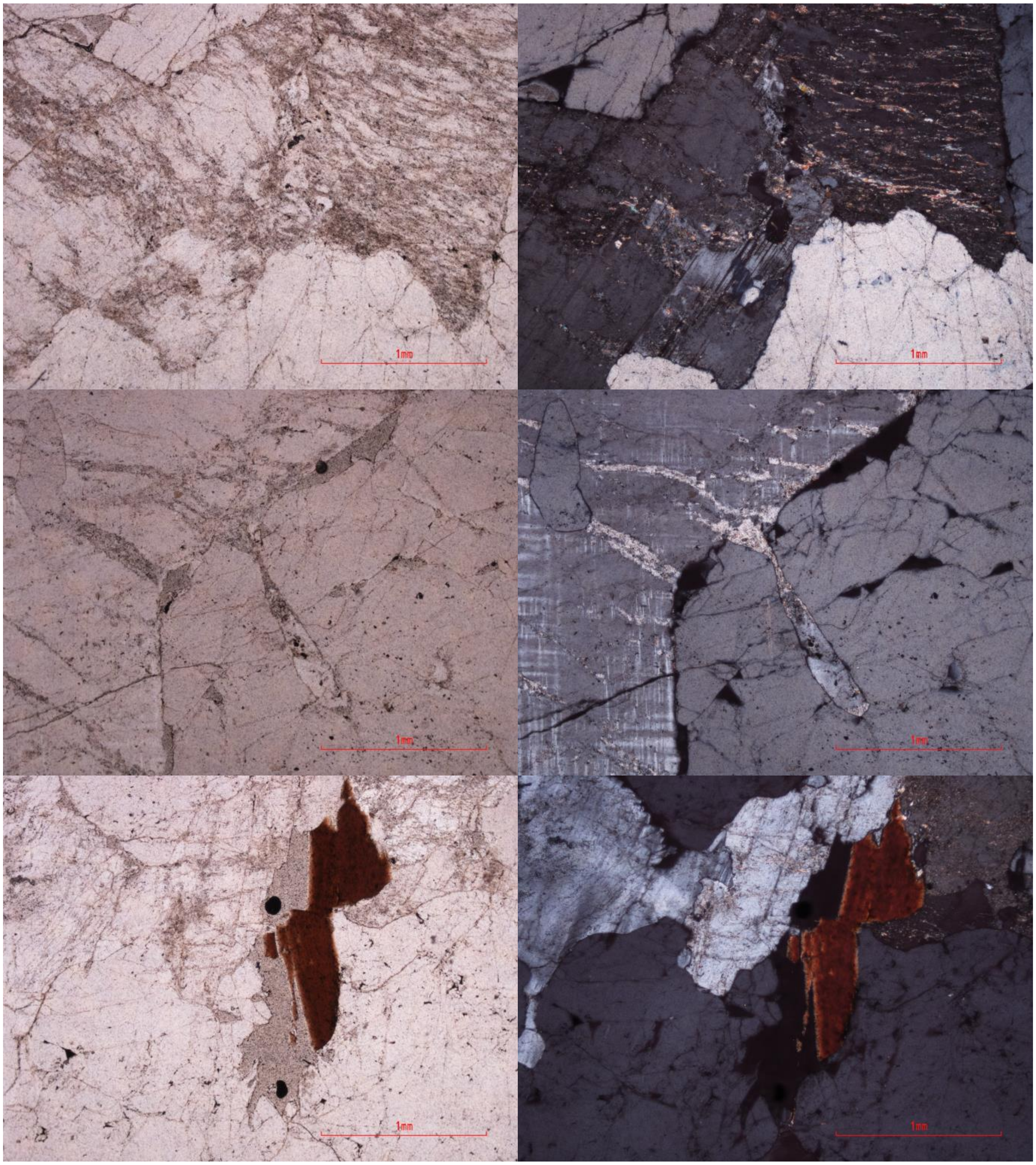
1mm
1mm
1mm
1mm
1mm
1mm

013aE - Salknappen Pegmatite

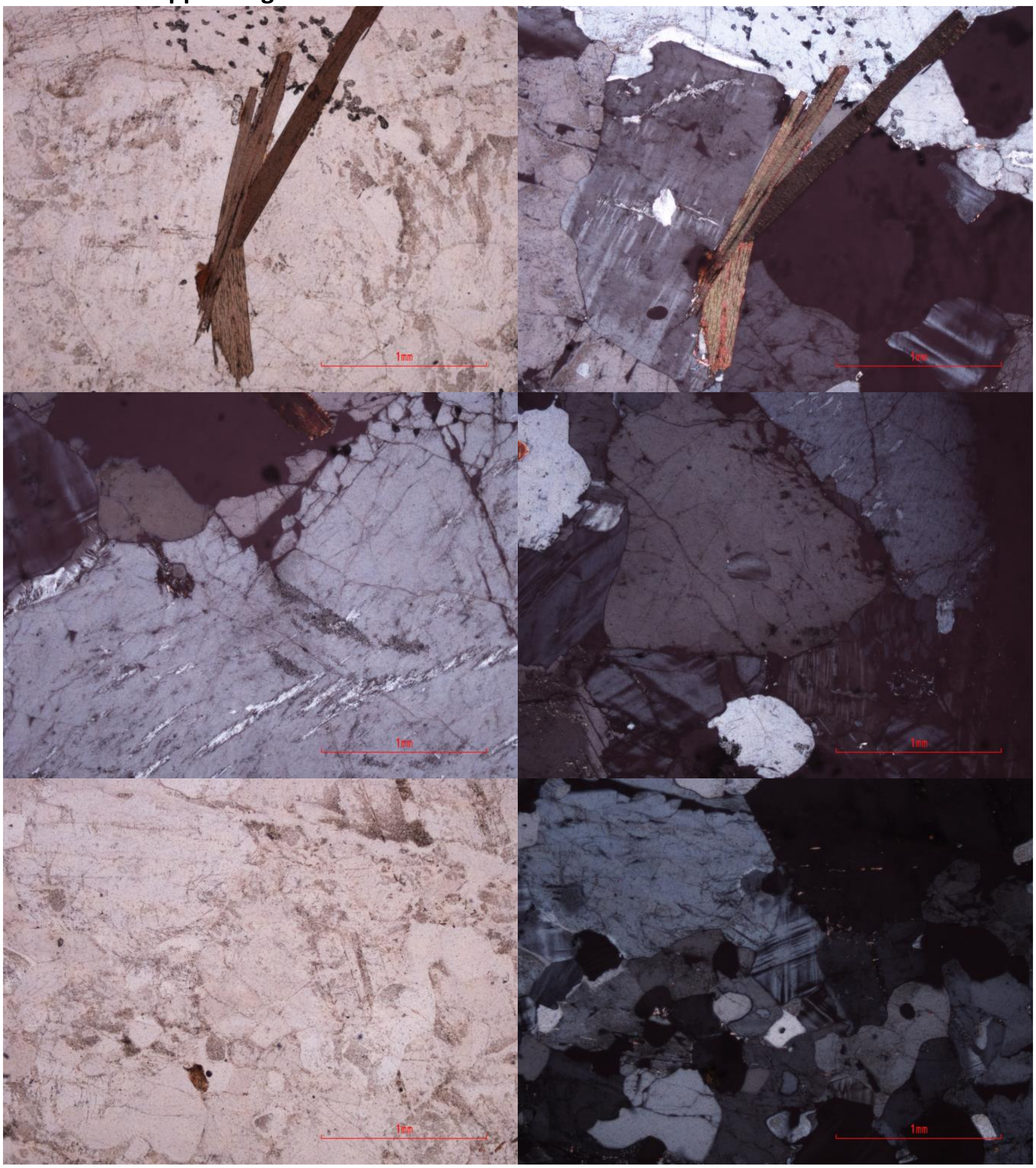

014aB – Dalmatian Granite

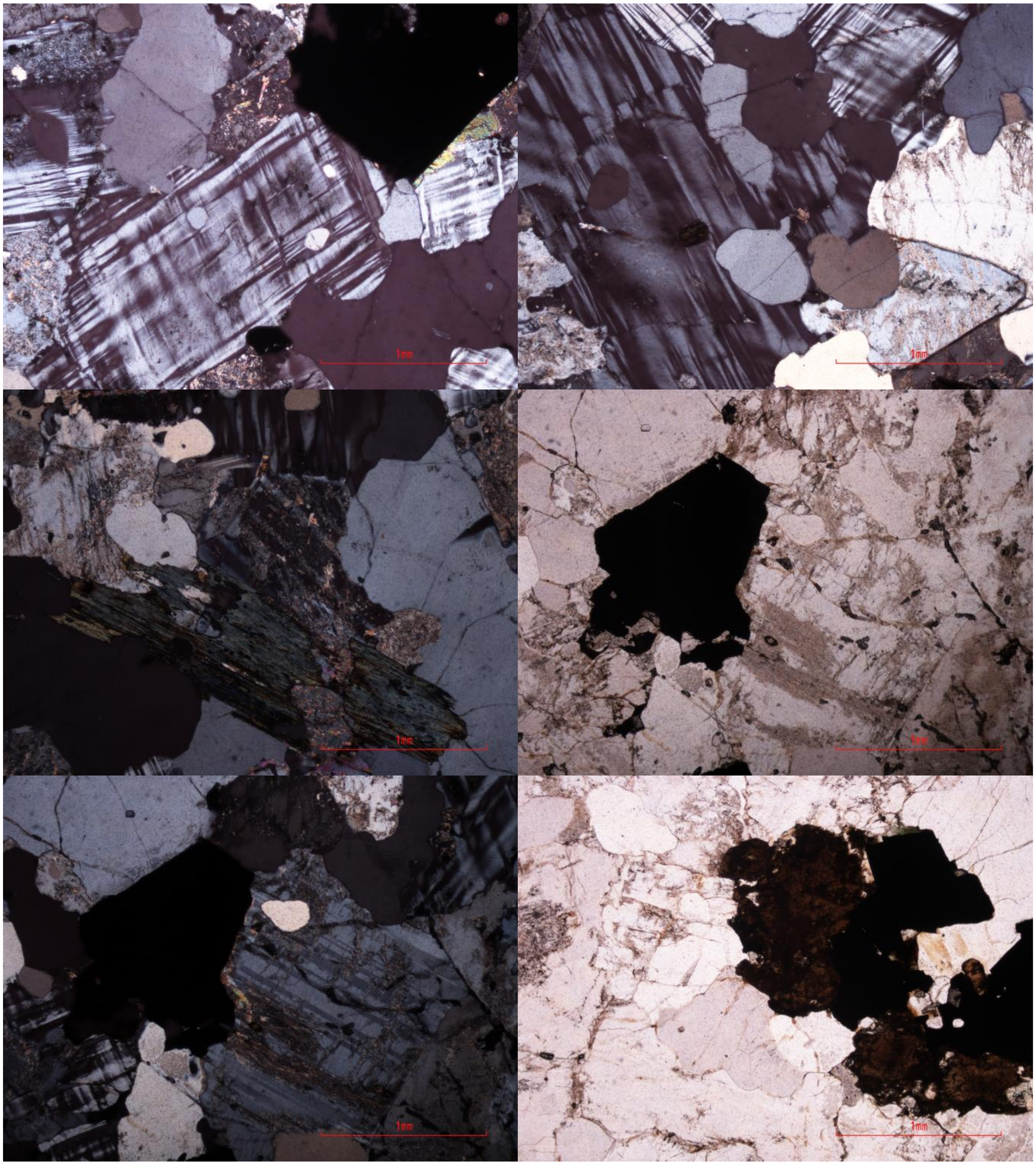

014bC – Pegmatitic Dalmatian Granite

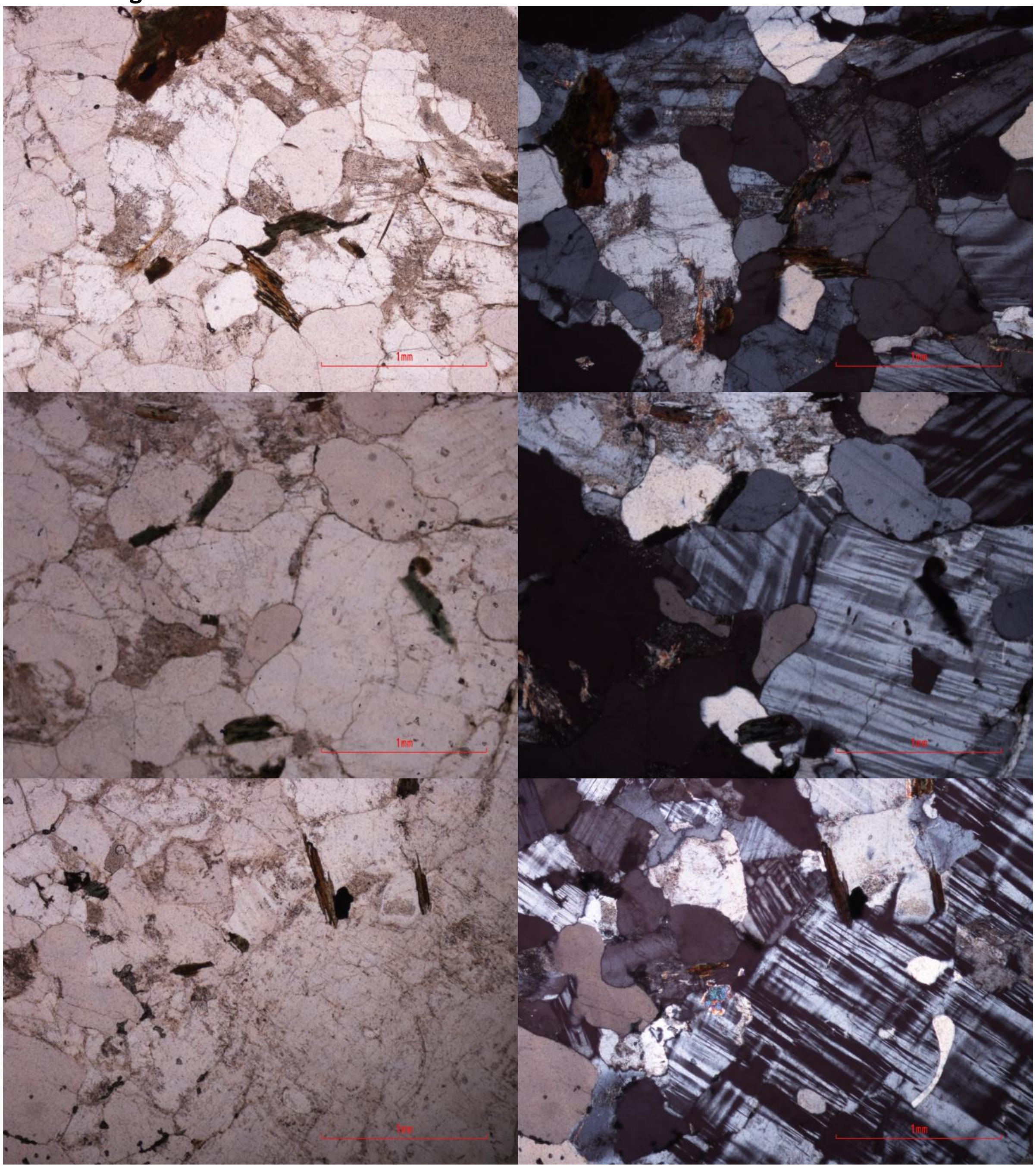

017aC - Dalmatian Granite

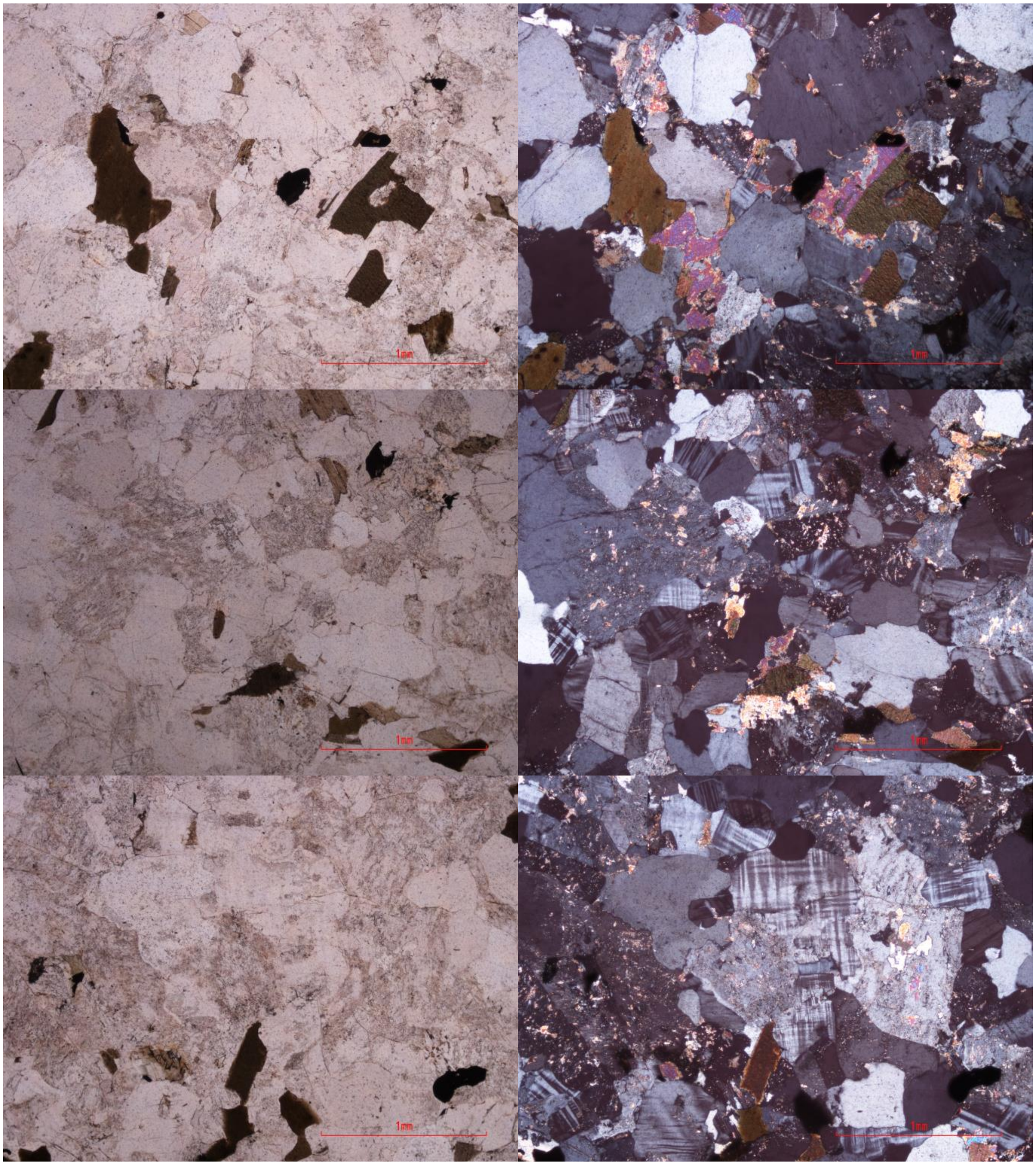

021aA - Dalmatian Granite

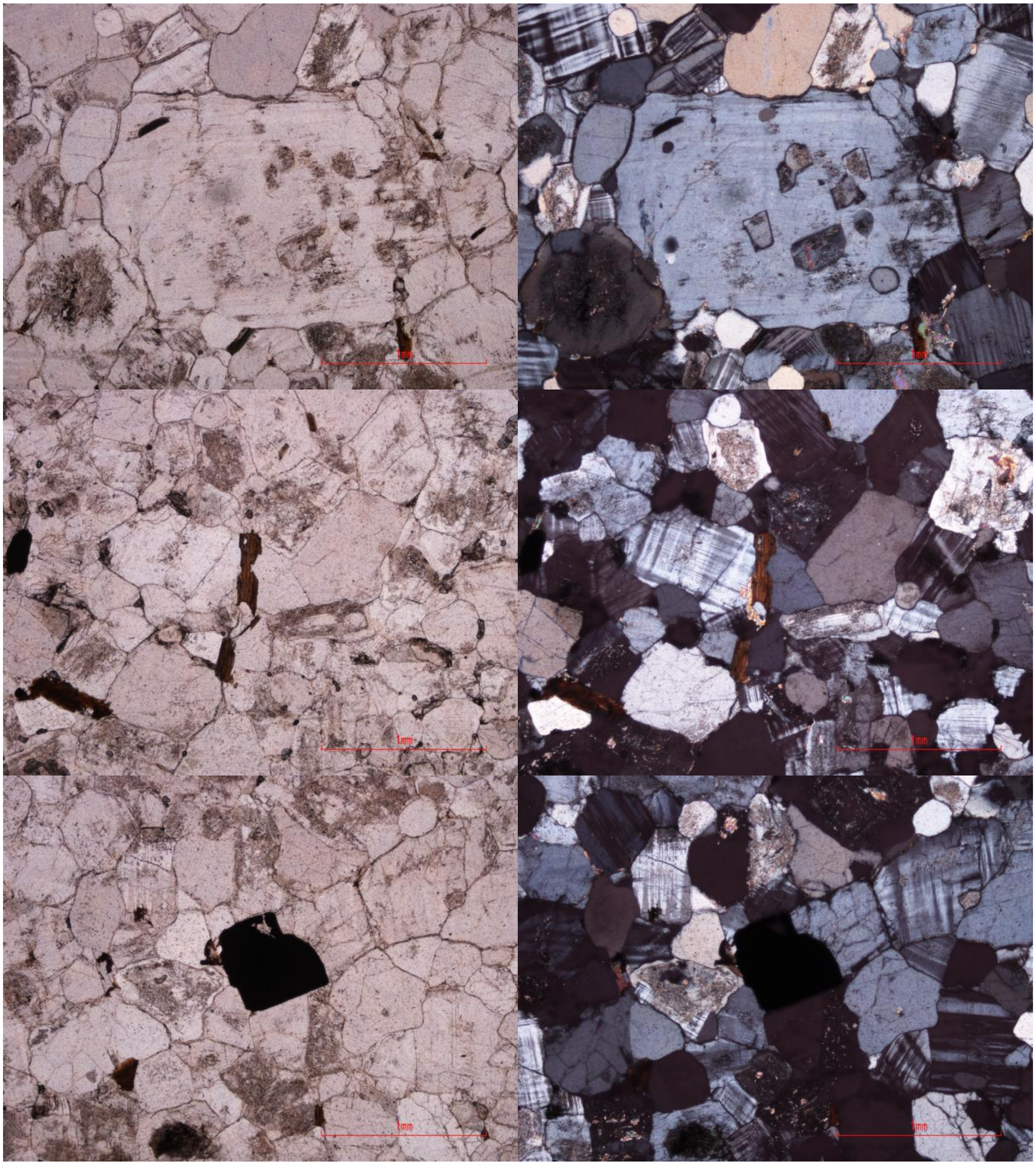

027aA - Salknappen Pegmatite

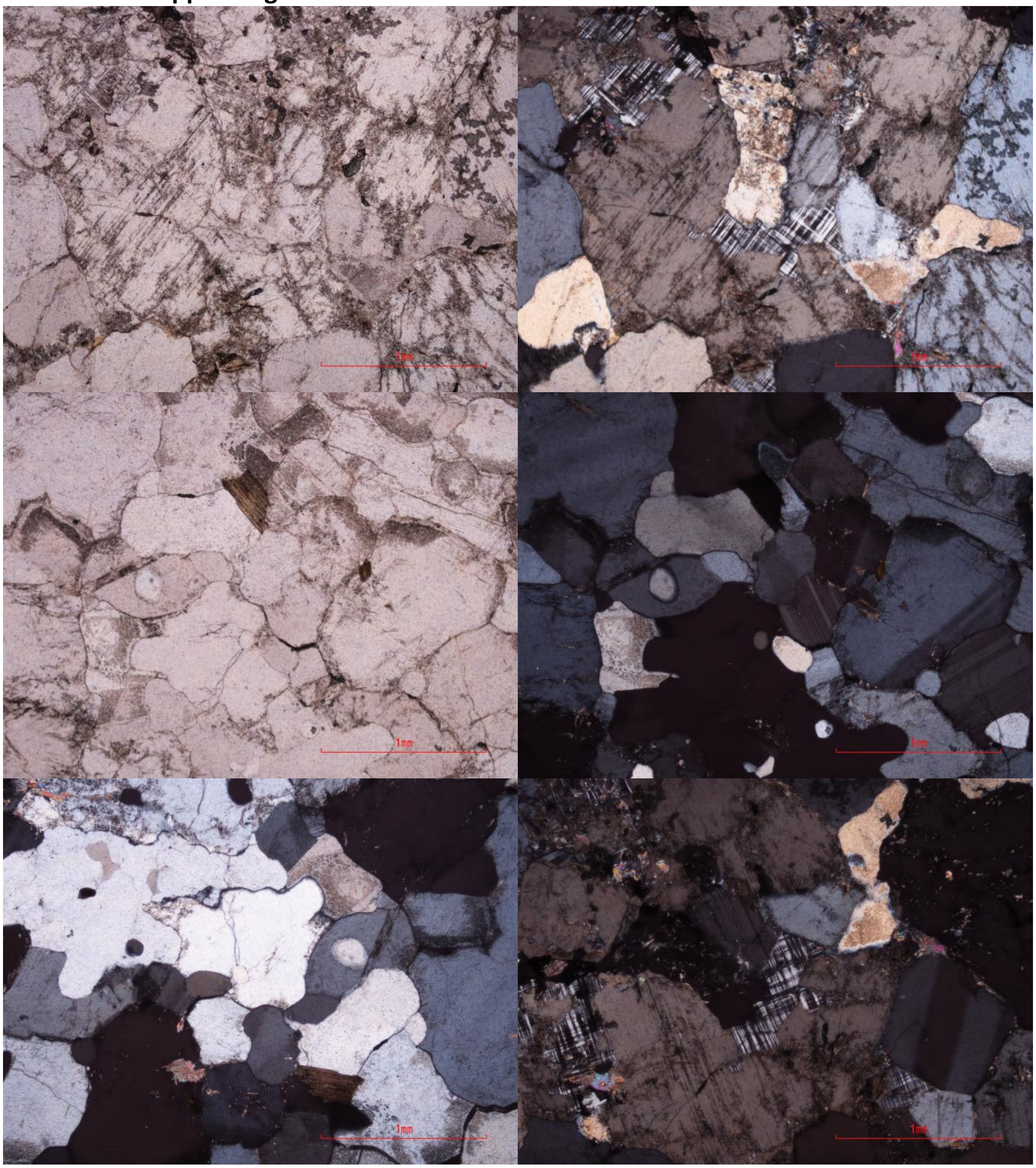

028aX - Dalmatian Granite

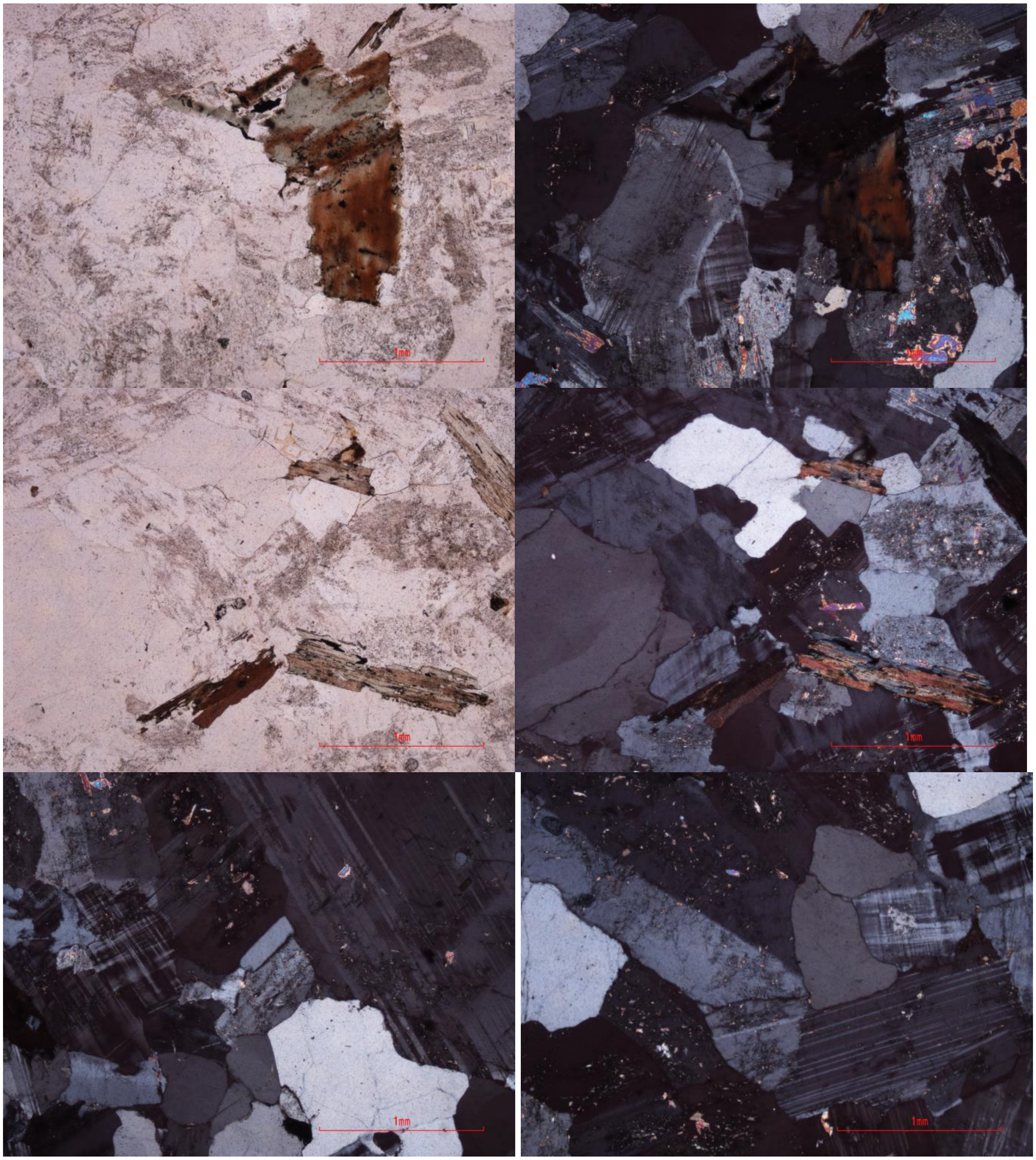

030aA - Dalmatian Granite

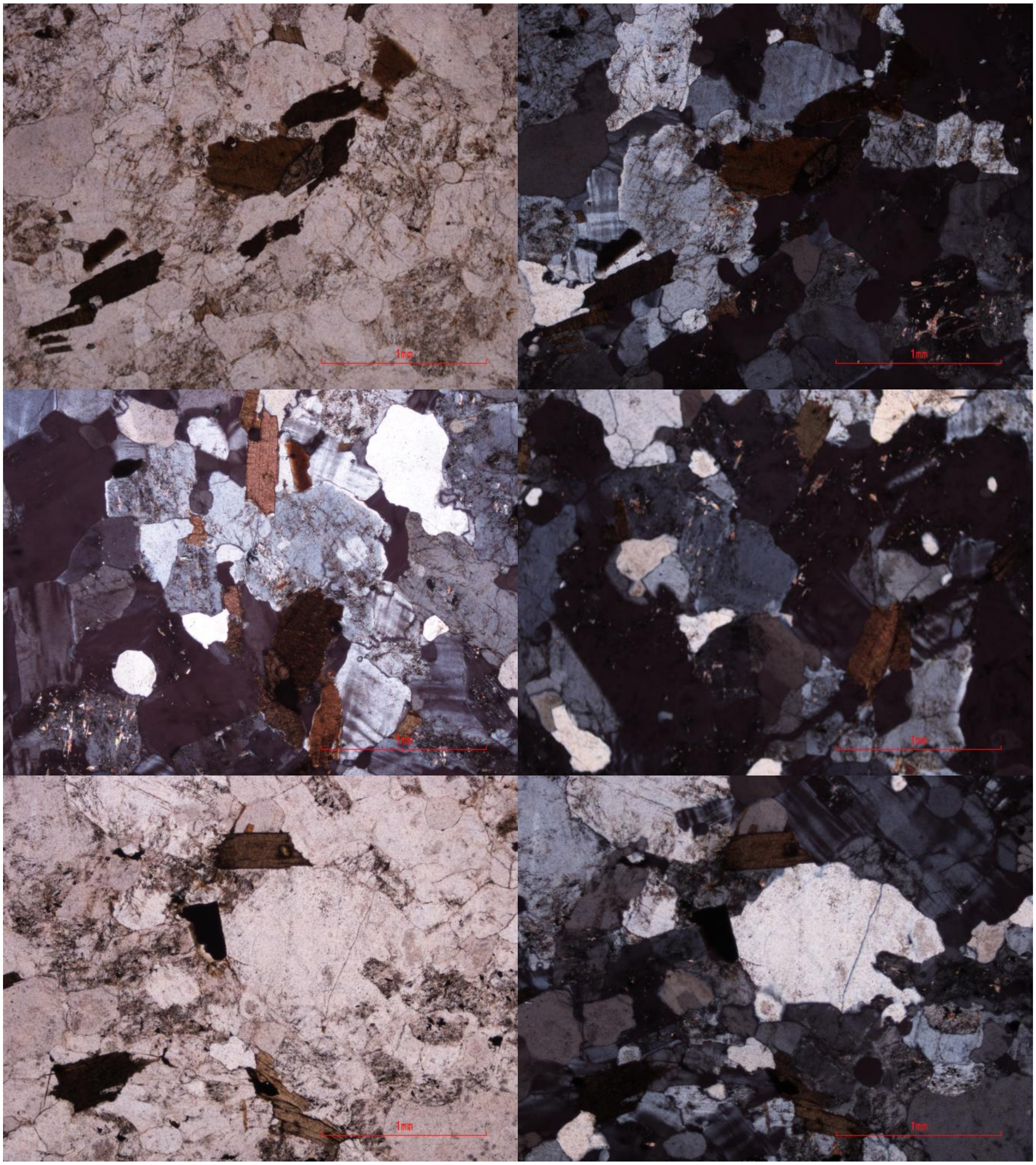

030bA - Dalmatian Granite

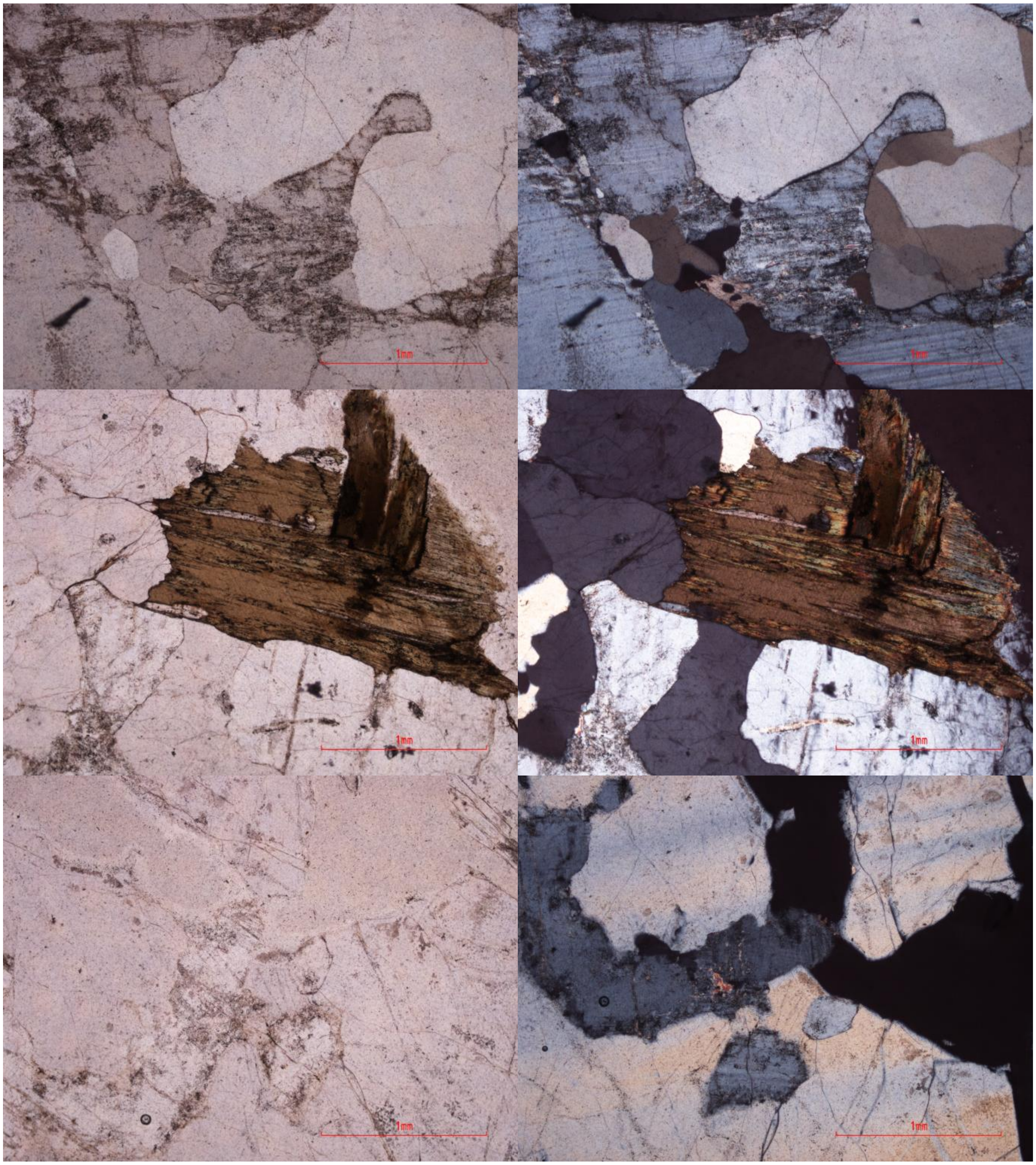

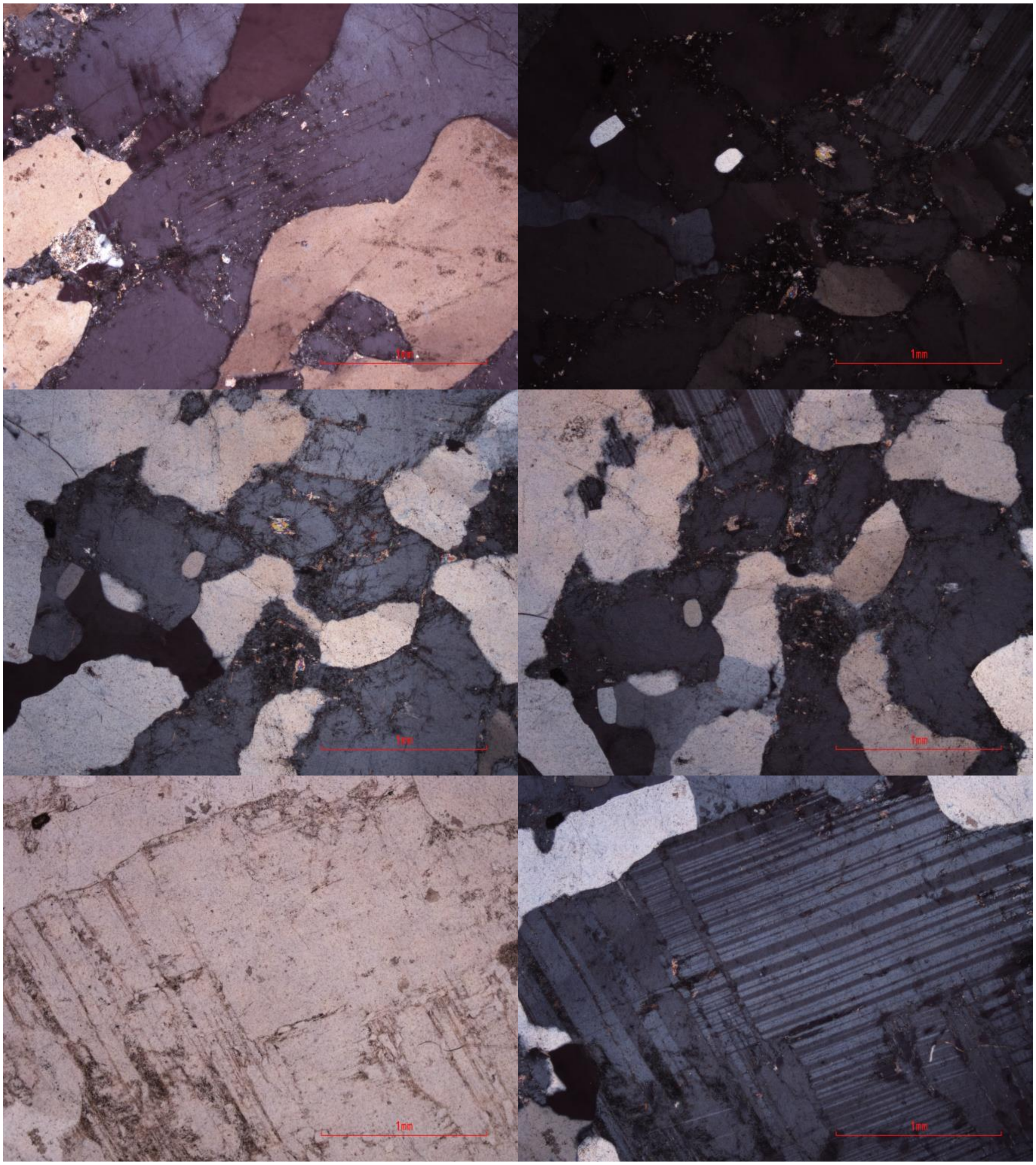

039aB - Salknappen Pegmatite

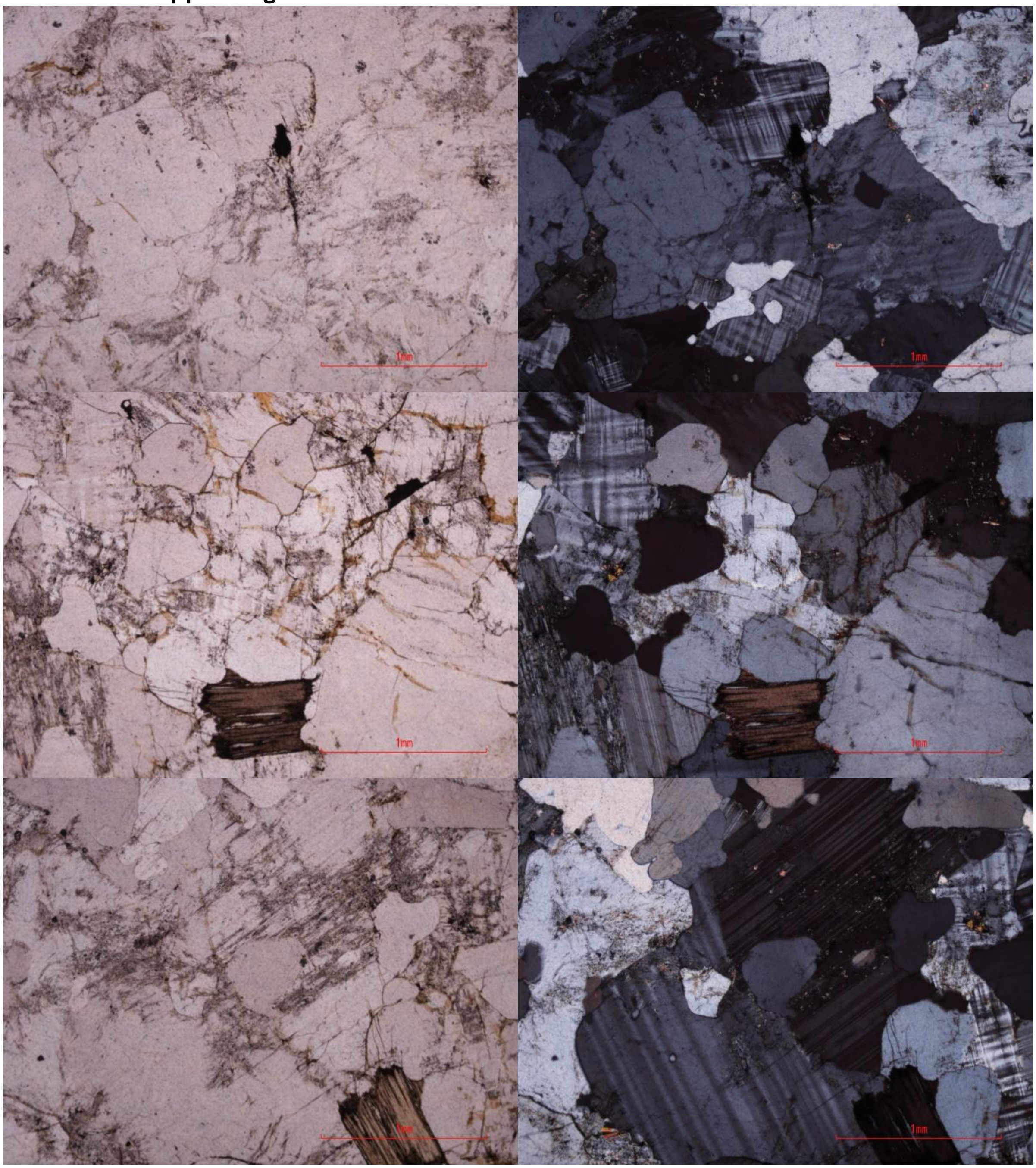

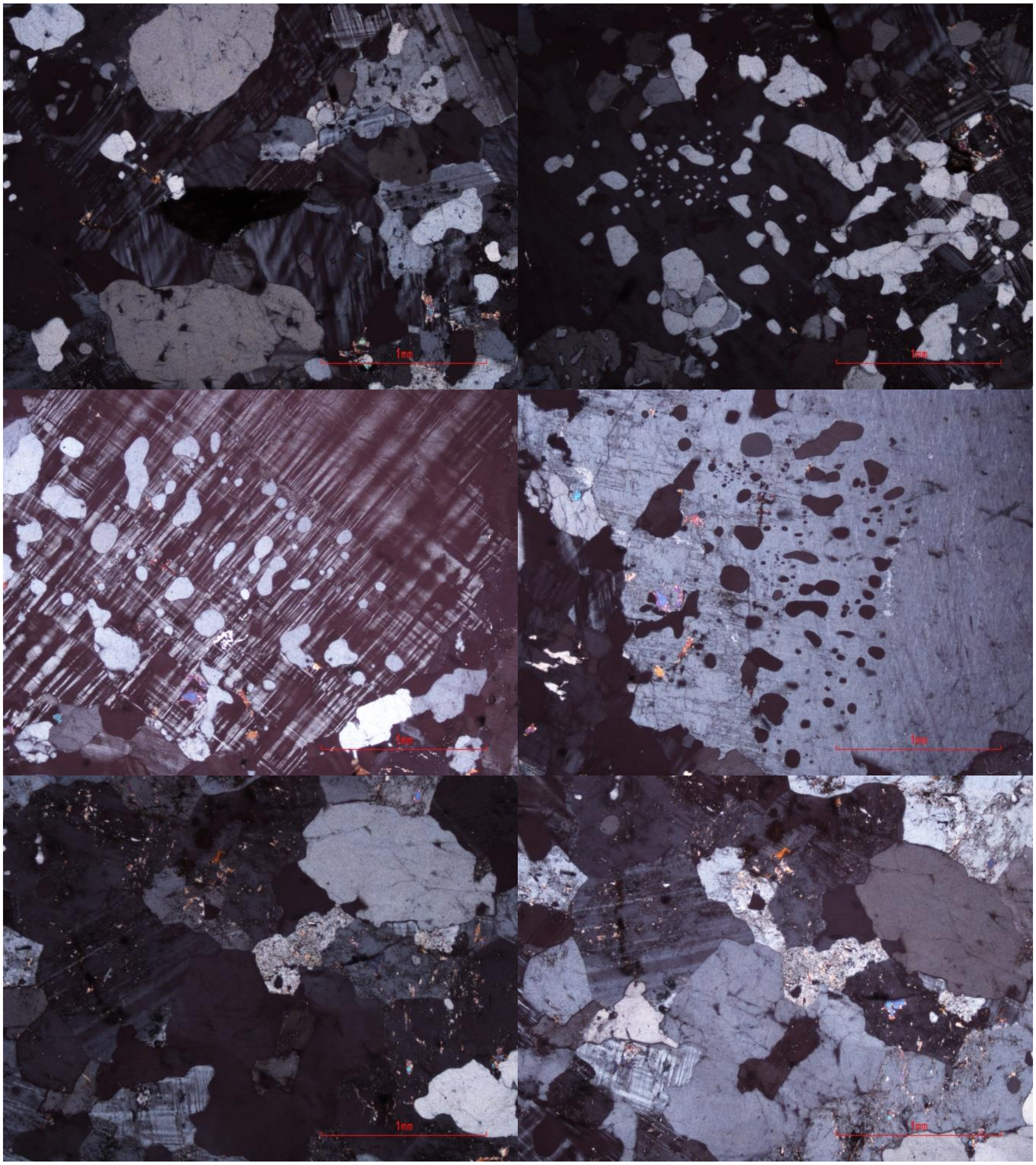
1mm
1mm
1mm
1mm
1mm

040aA - Dalmatian Granite

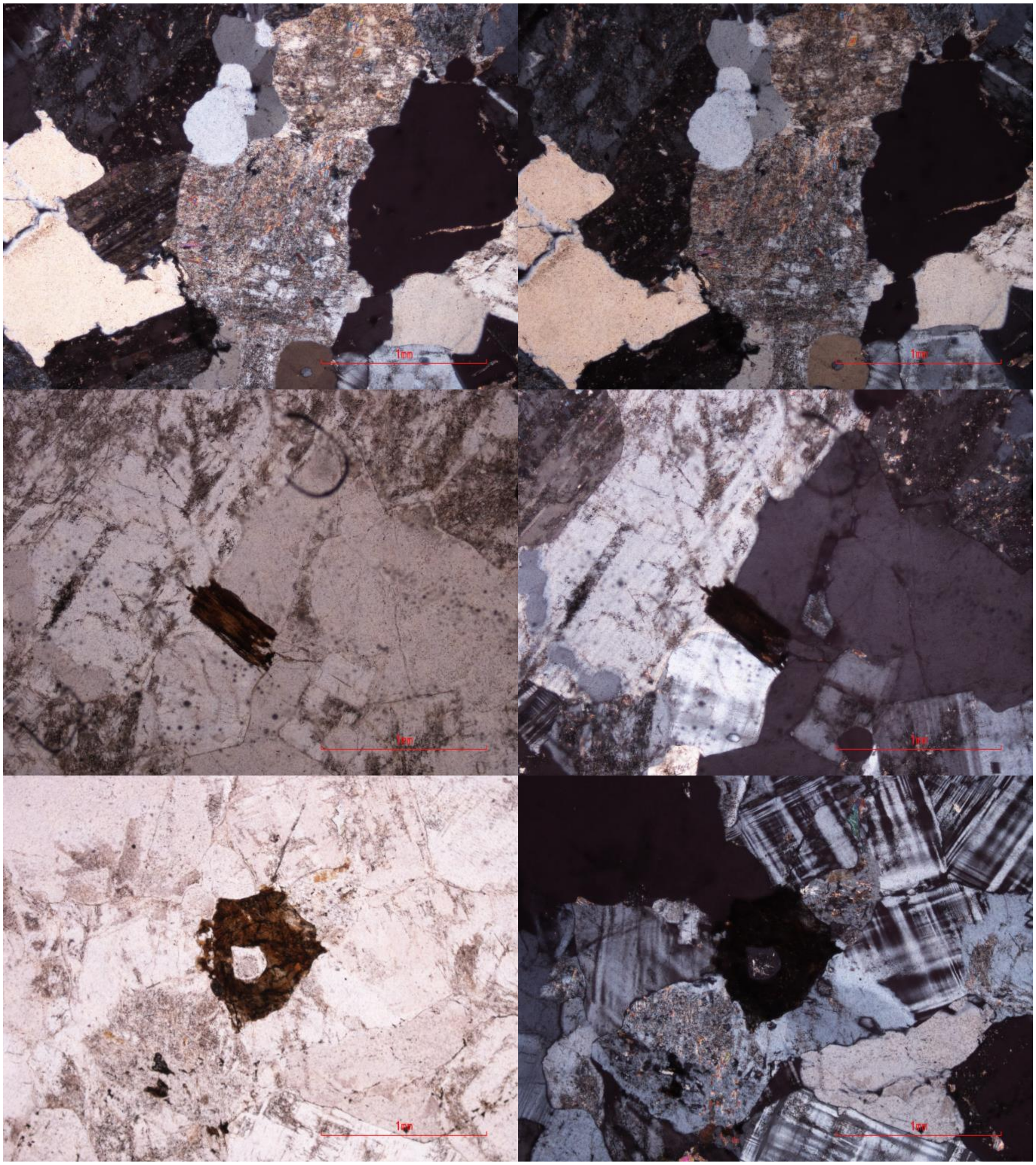

045aB - Dalmatian Granite

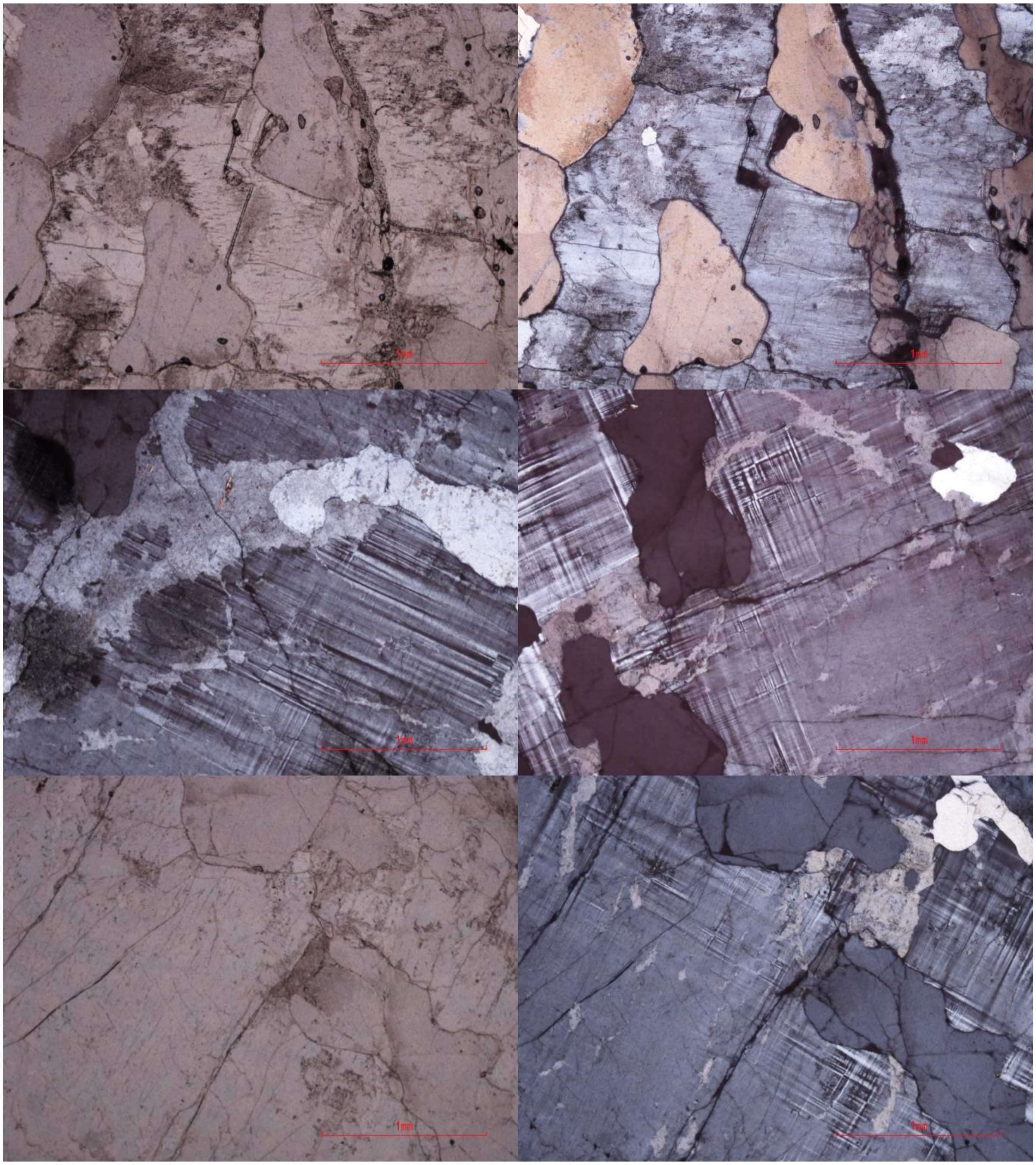

046aA - Salknappen Pegmatite

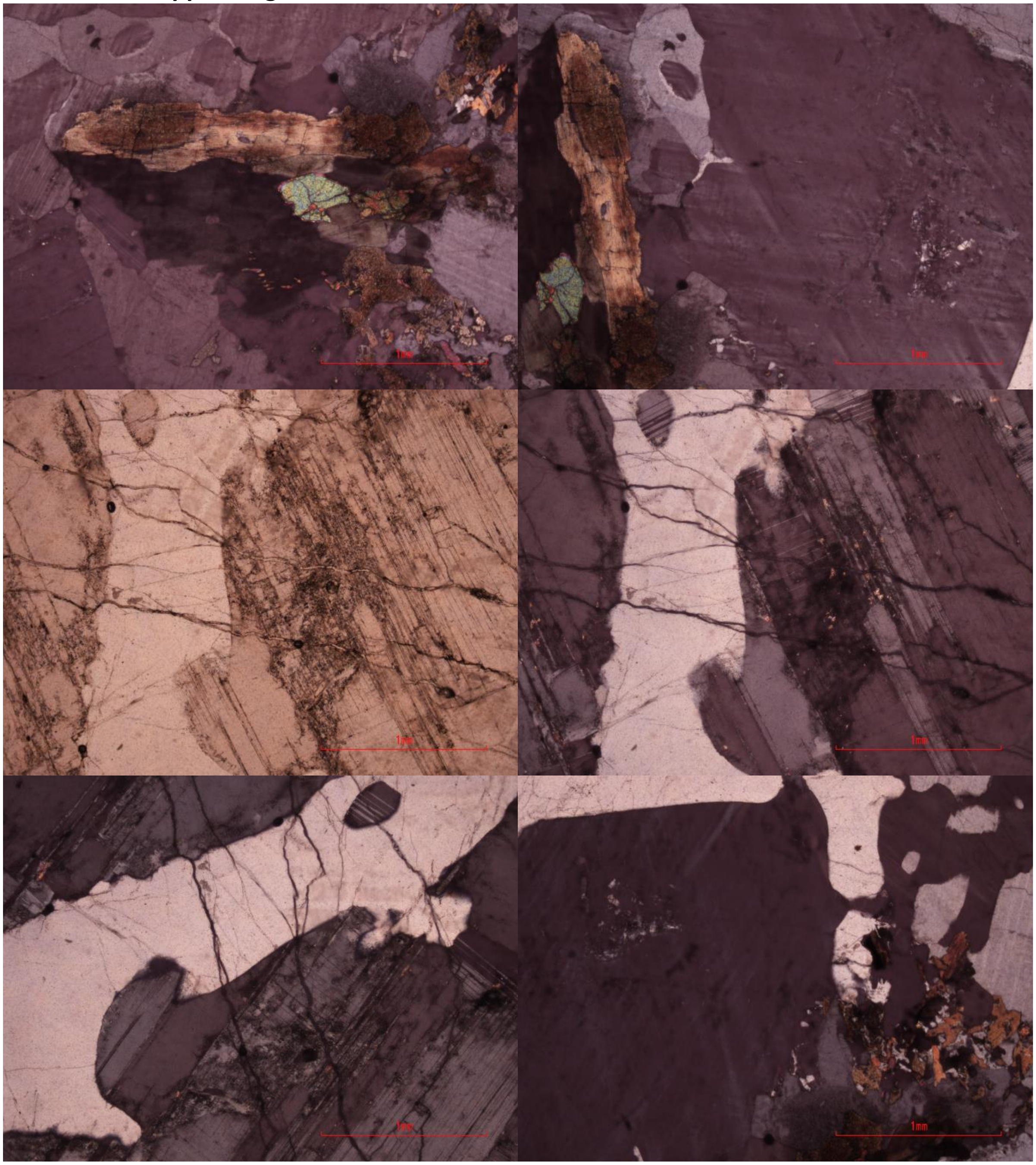

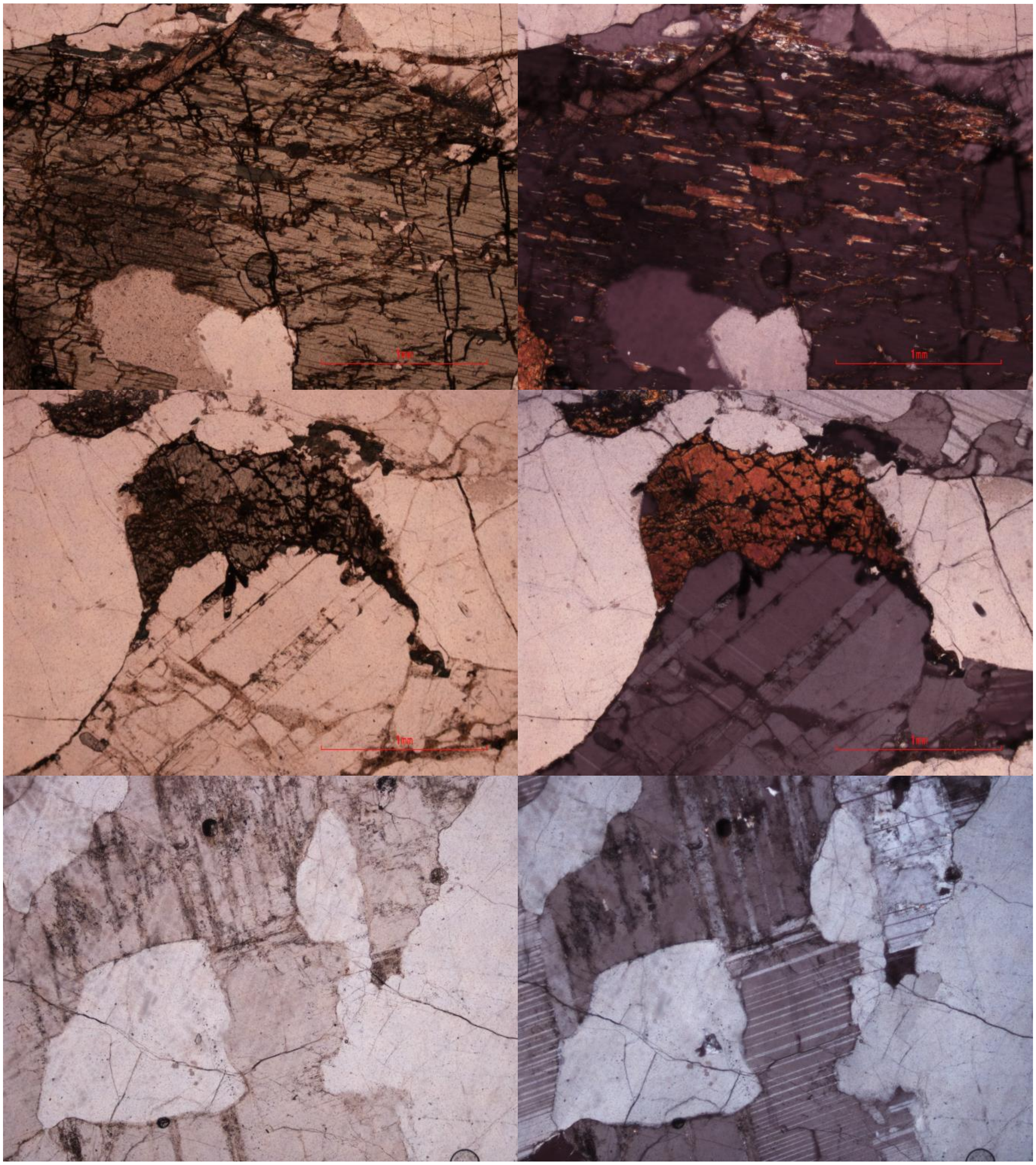
1mm
1mm
1mm
1mm

047aC - Salknappen Pegmatite

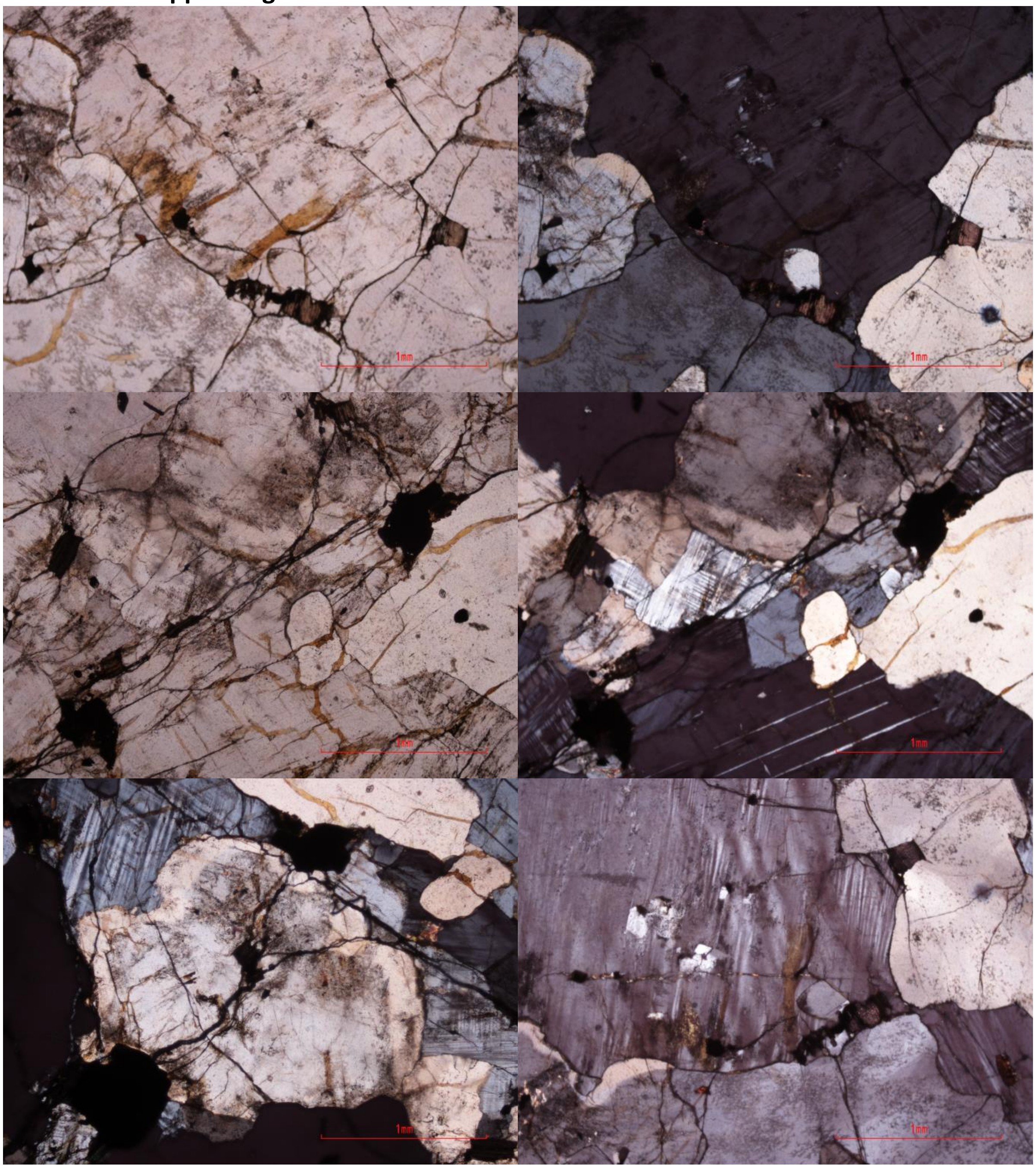

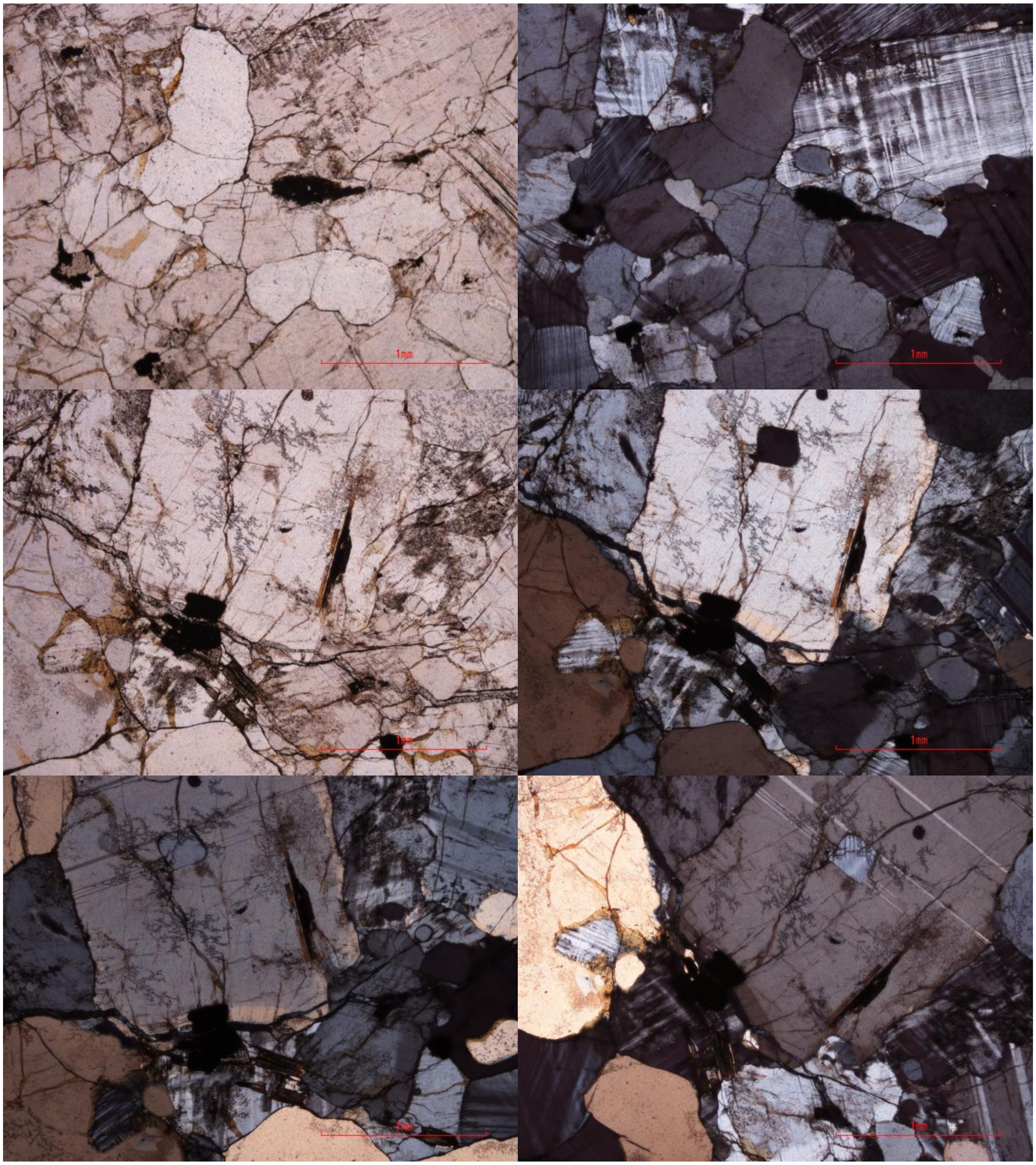
1mm
1mm
1mm
1mm

048aA - Dalmatian Granite

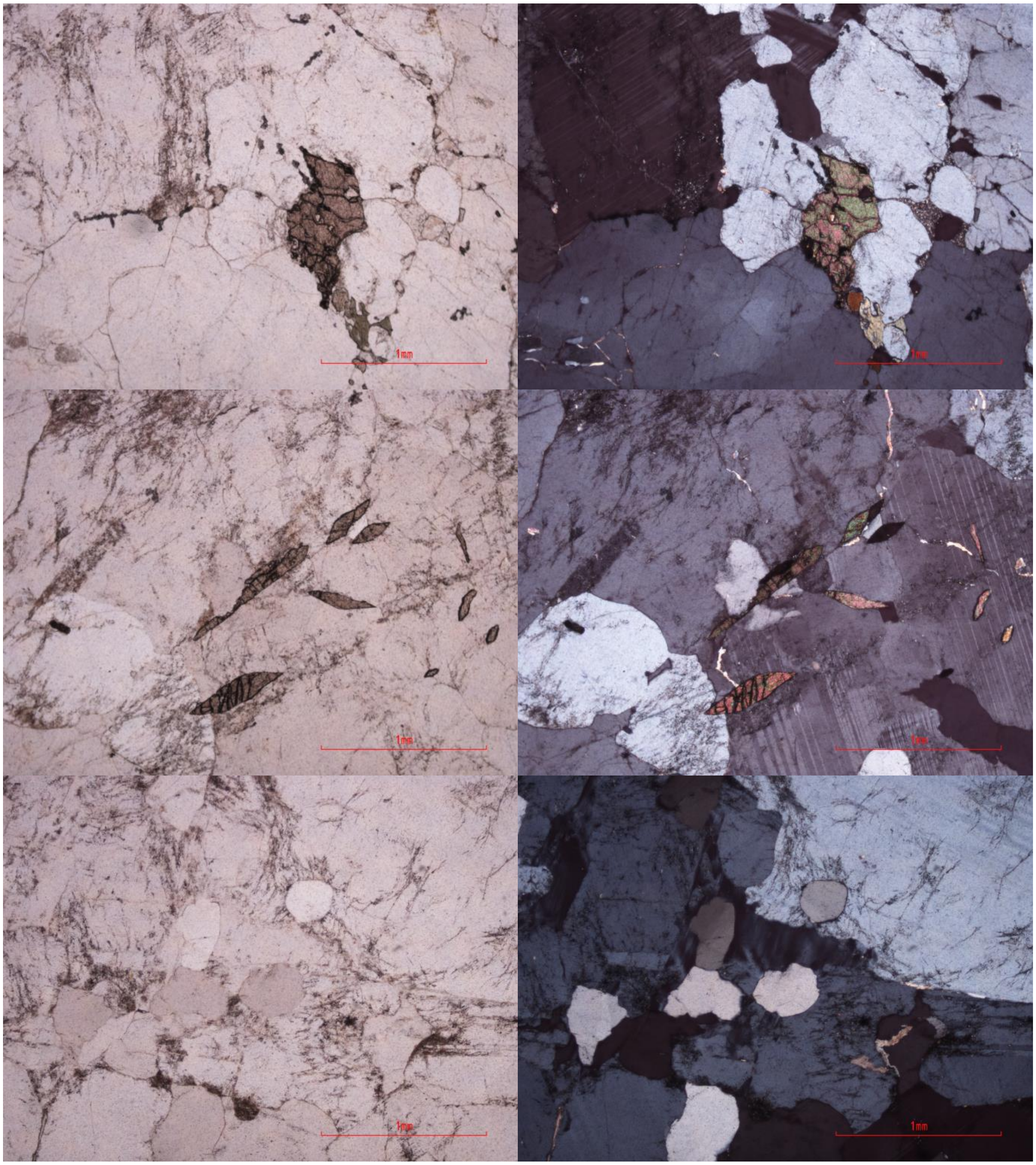

050aA - Salknappen Pegmatite

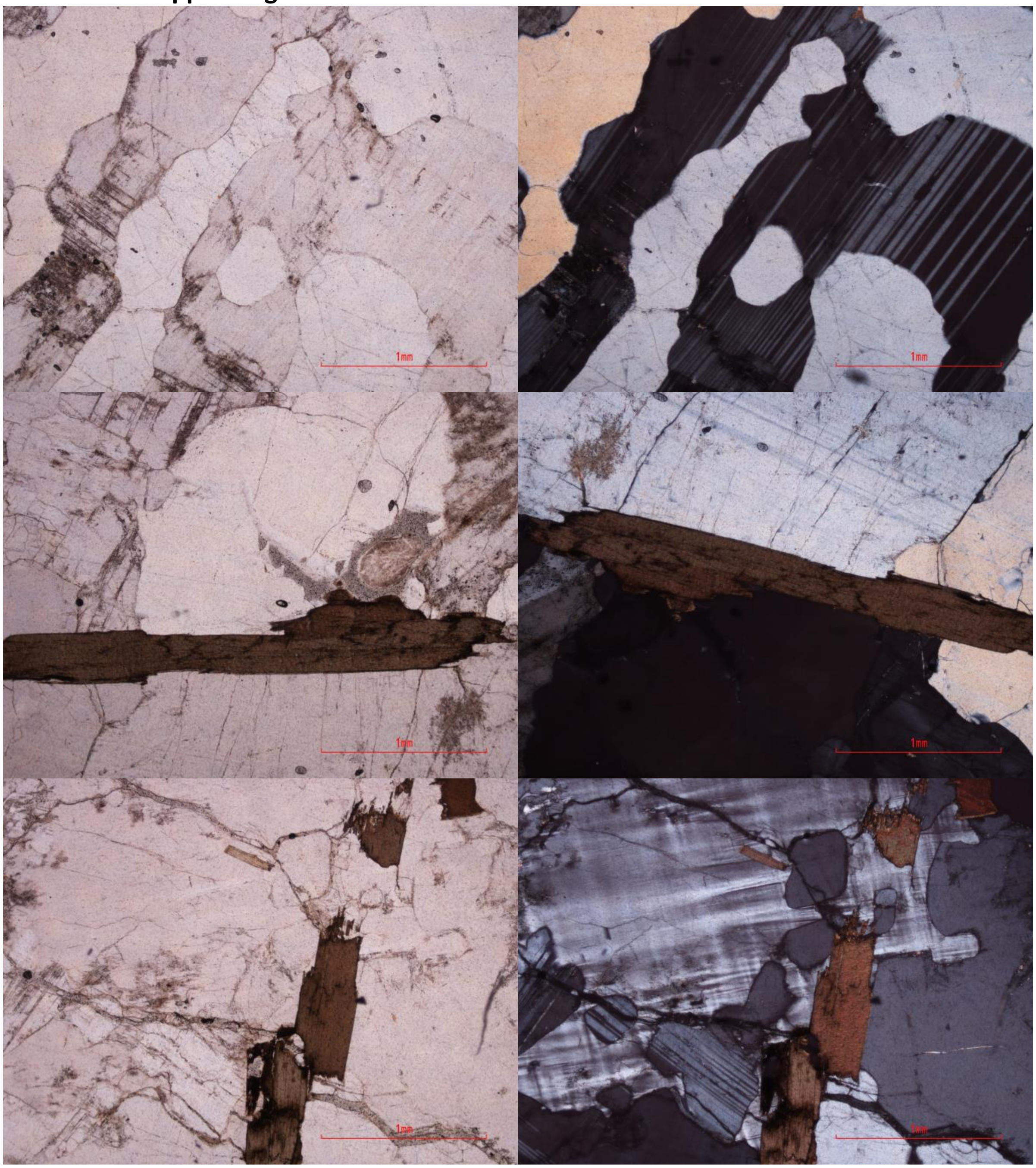

053aC - Dalmatian Granite

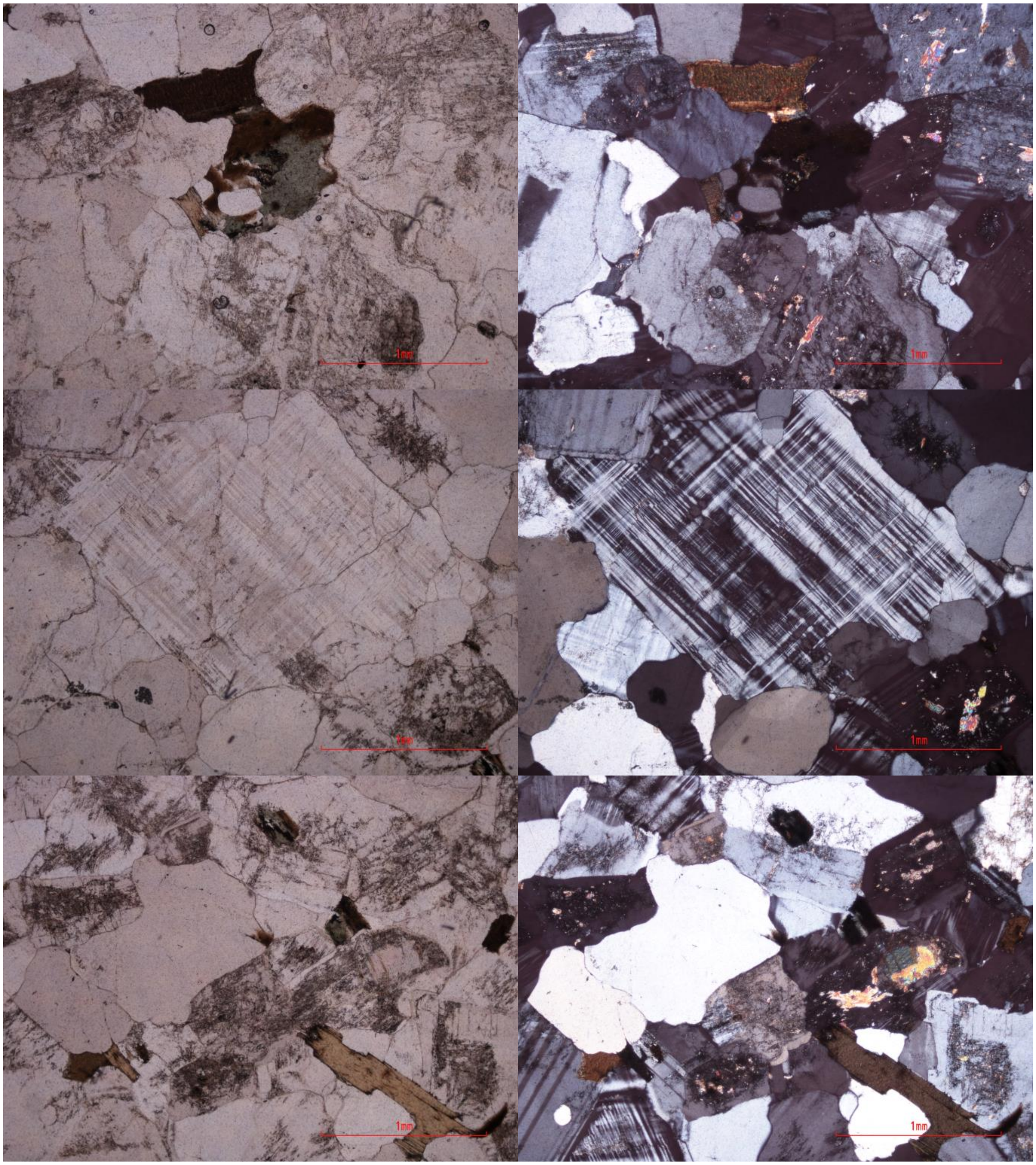

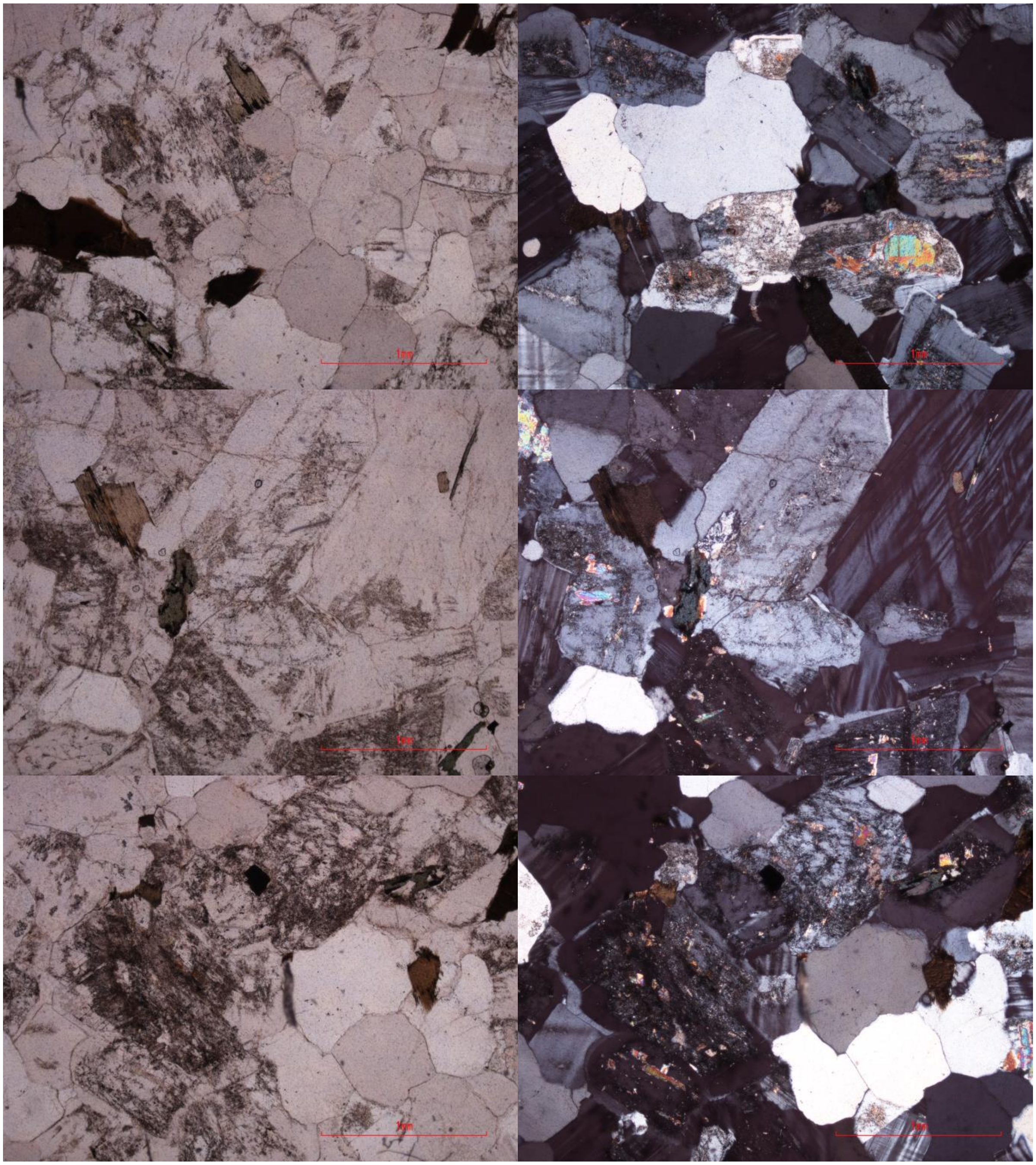

053bE - Salknappen Pegmatite

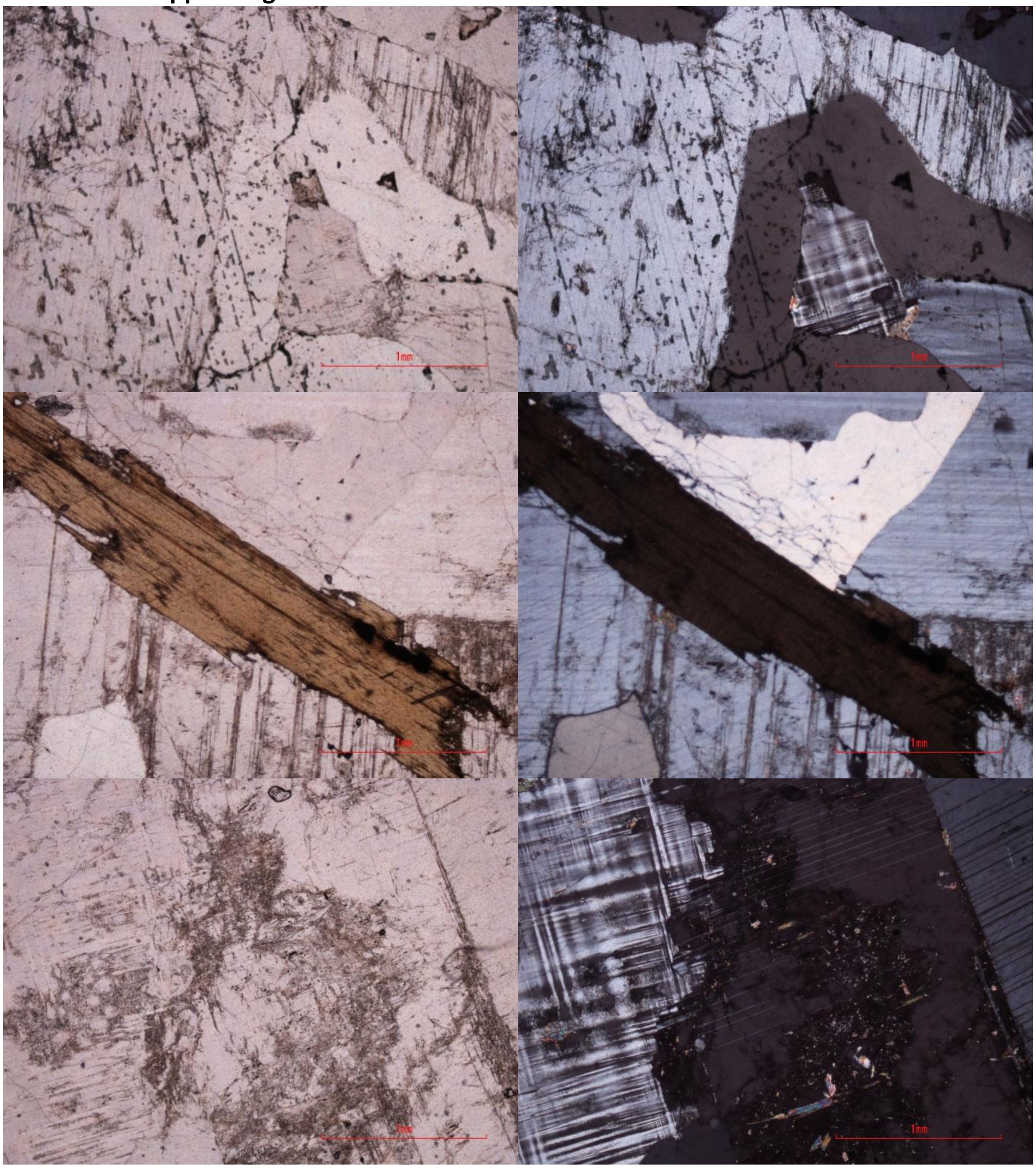

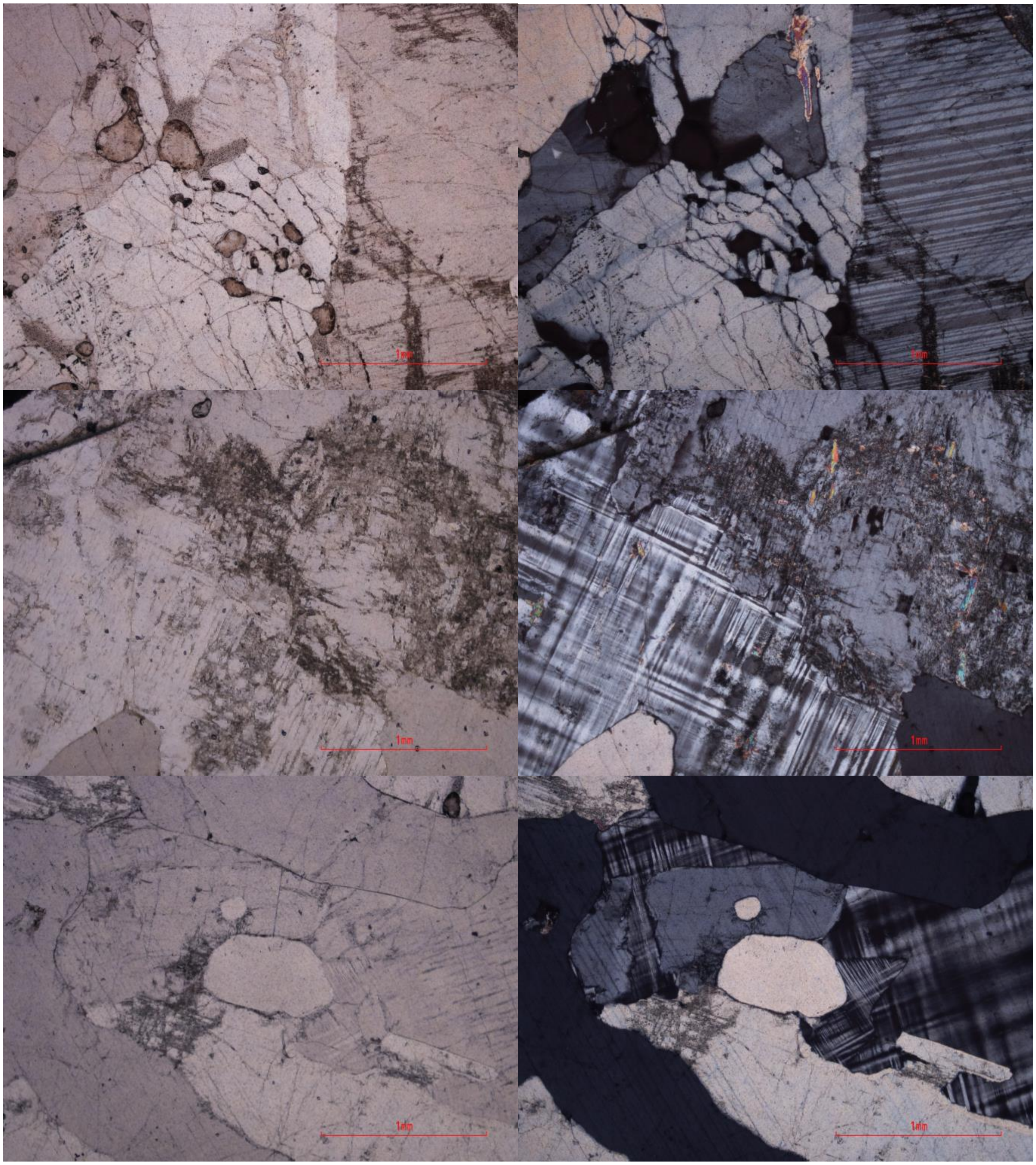
1mm
1mm
1mm
1mm
1mm
1mm

054aC - Salknappen Pegmatite

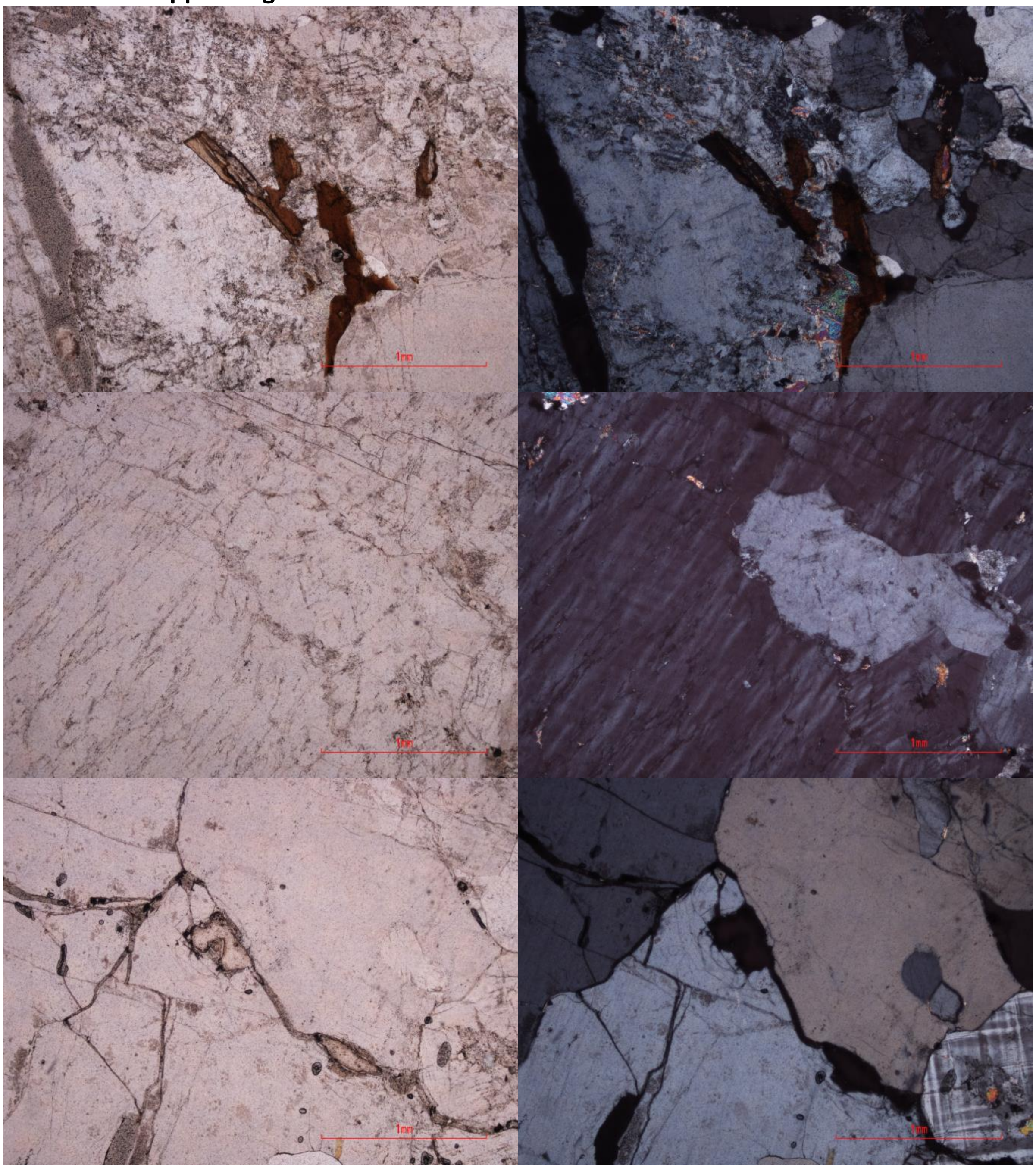

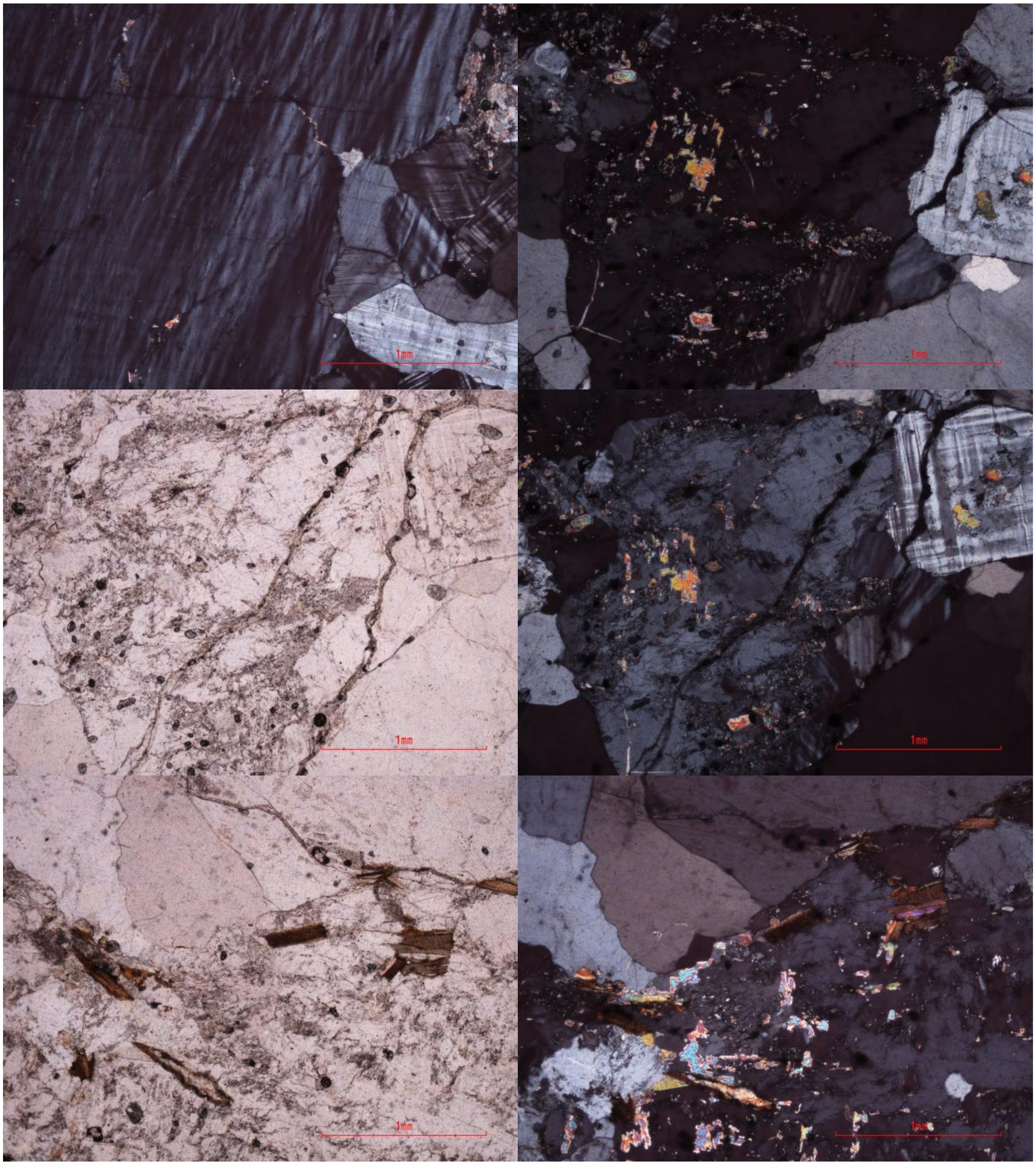
1mm
1mm
1mm
1mm
1mm
1mm

054bD - Salknappen Pegmatite

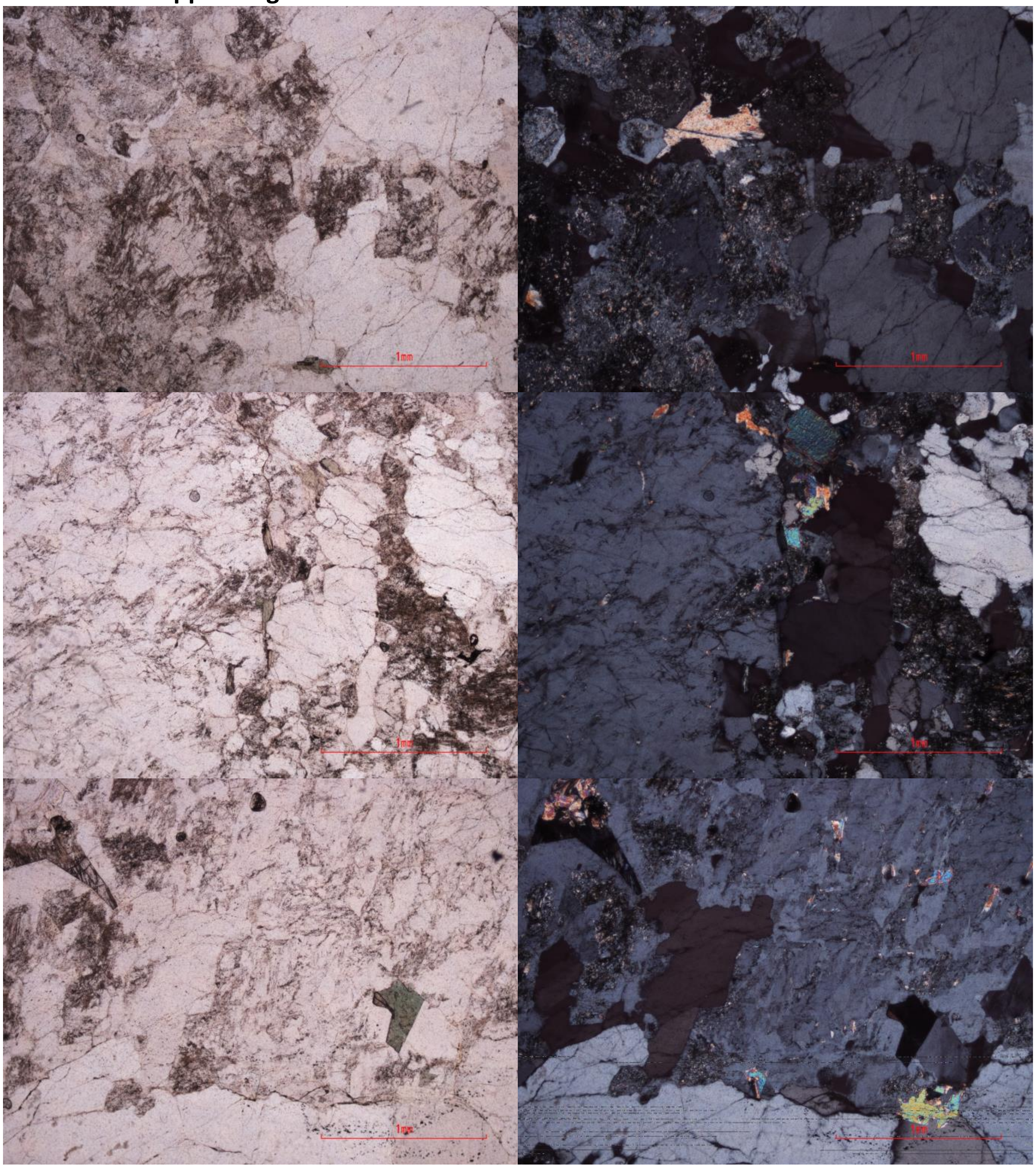

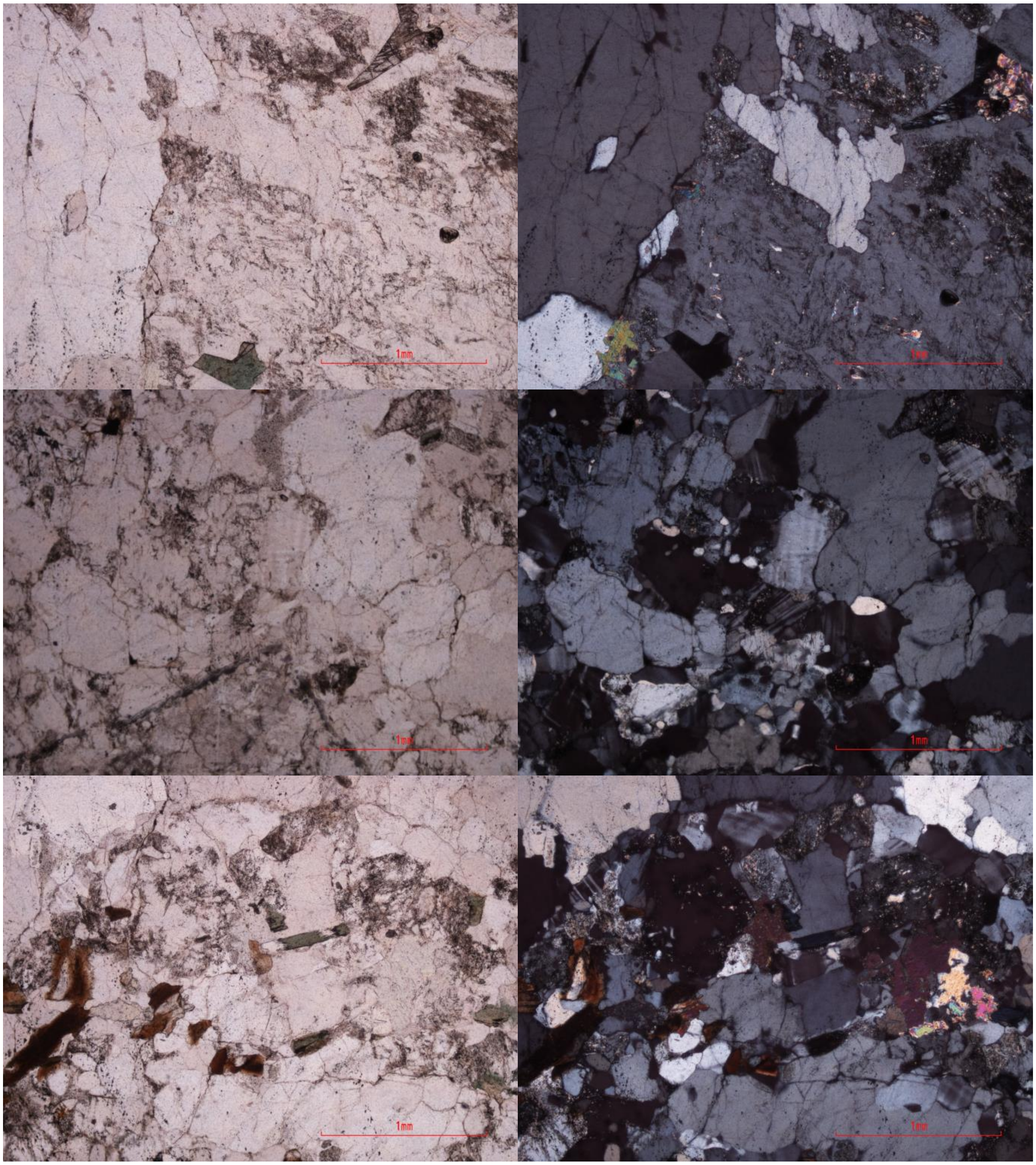
1mm

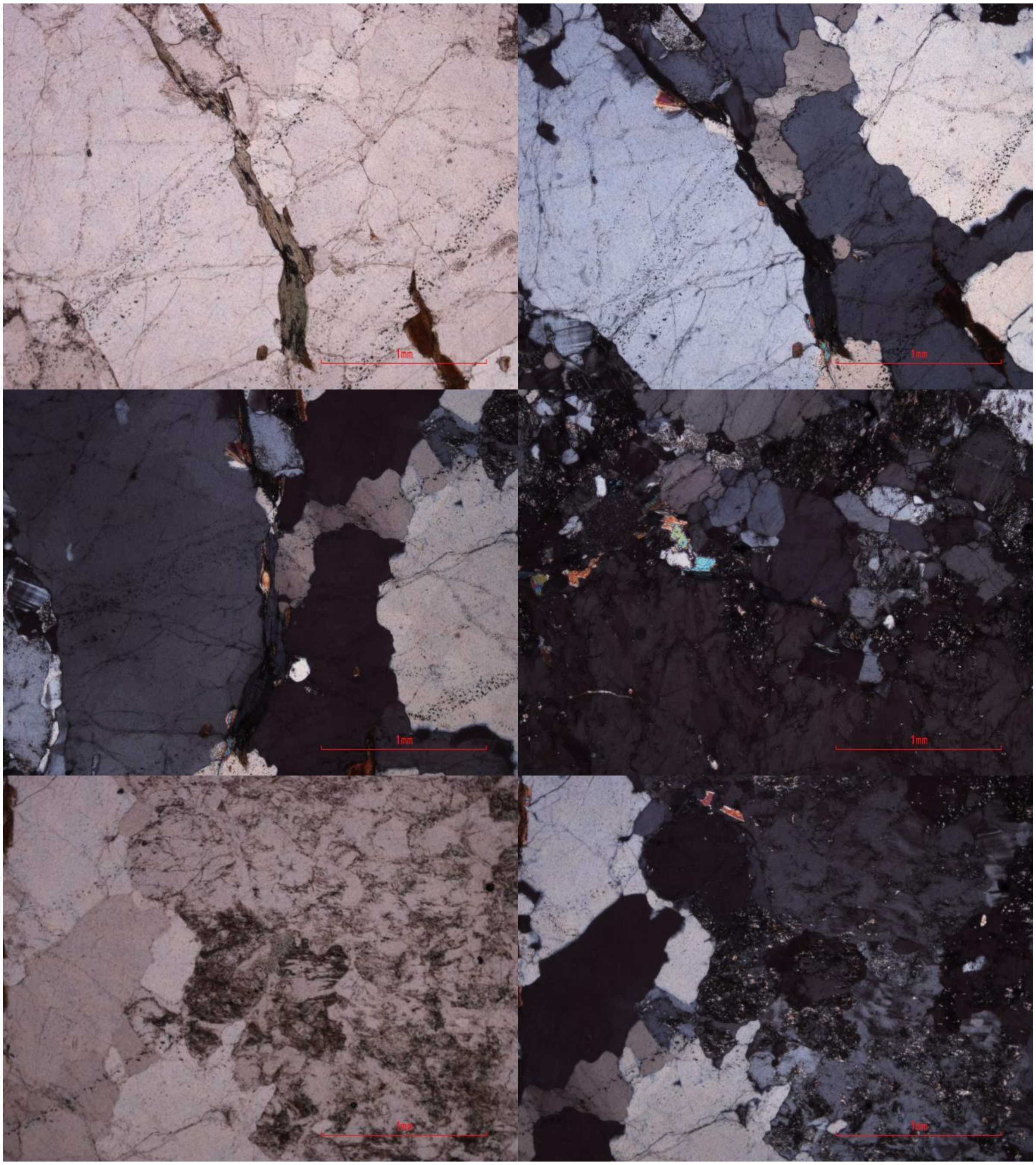
1mm
1mm
1mm
1mm
1mm
1mm

055aX - Dalmatian Granite

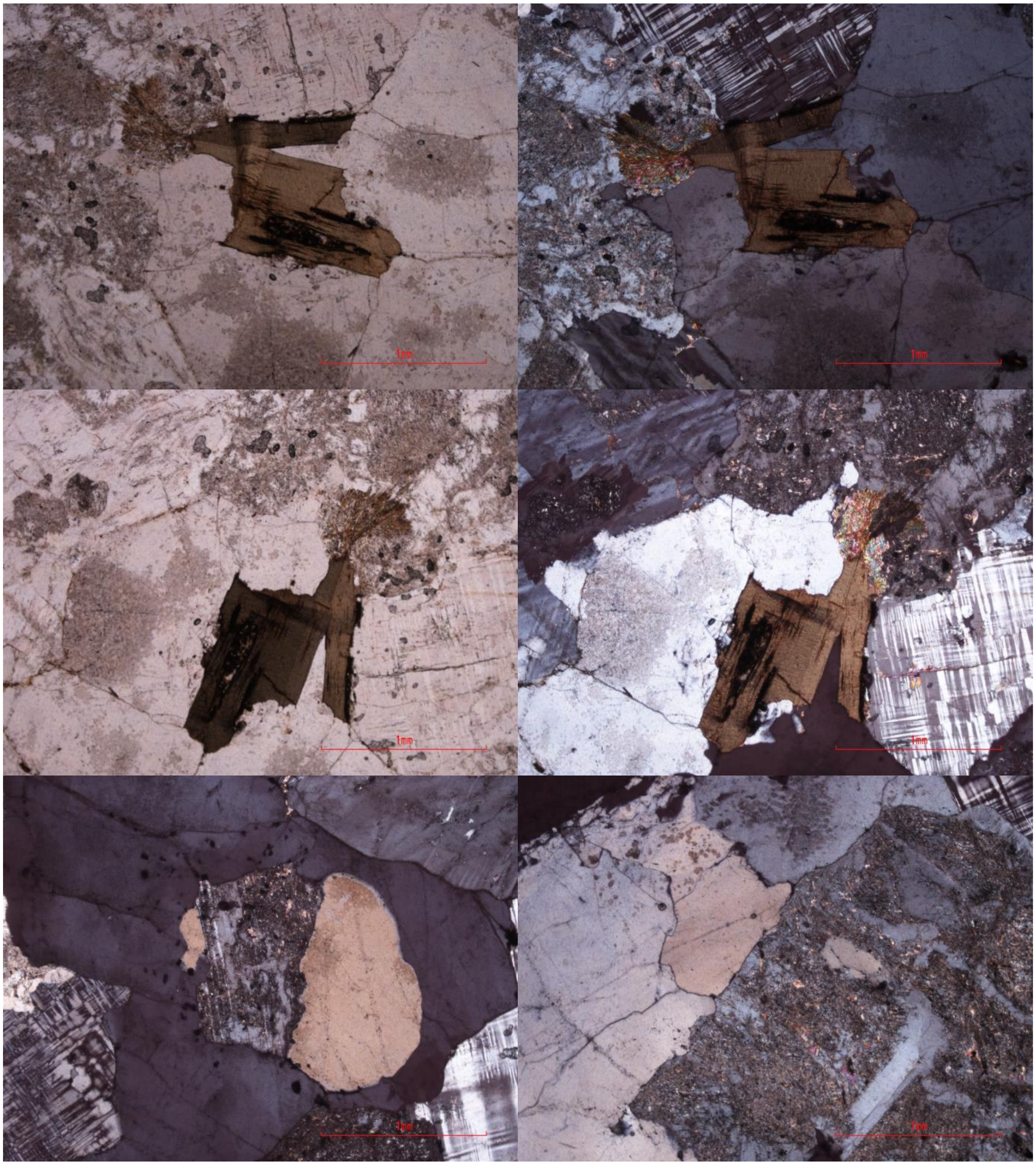

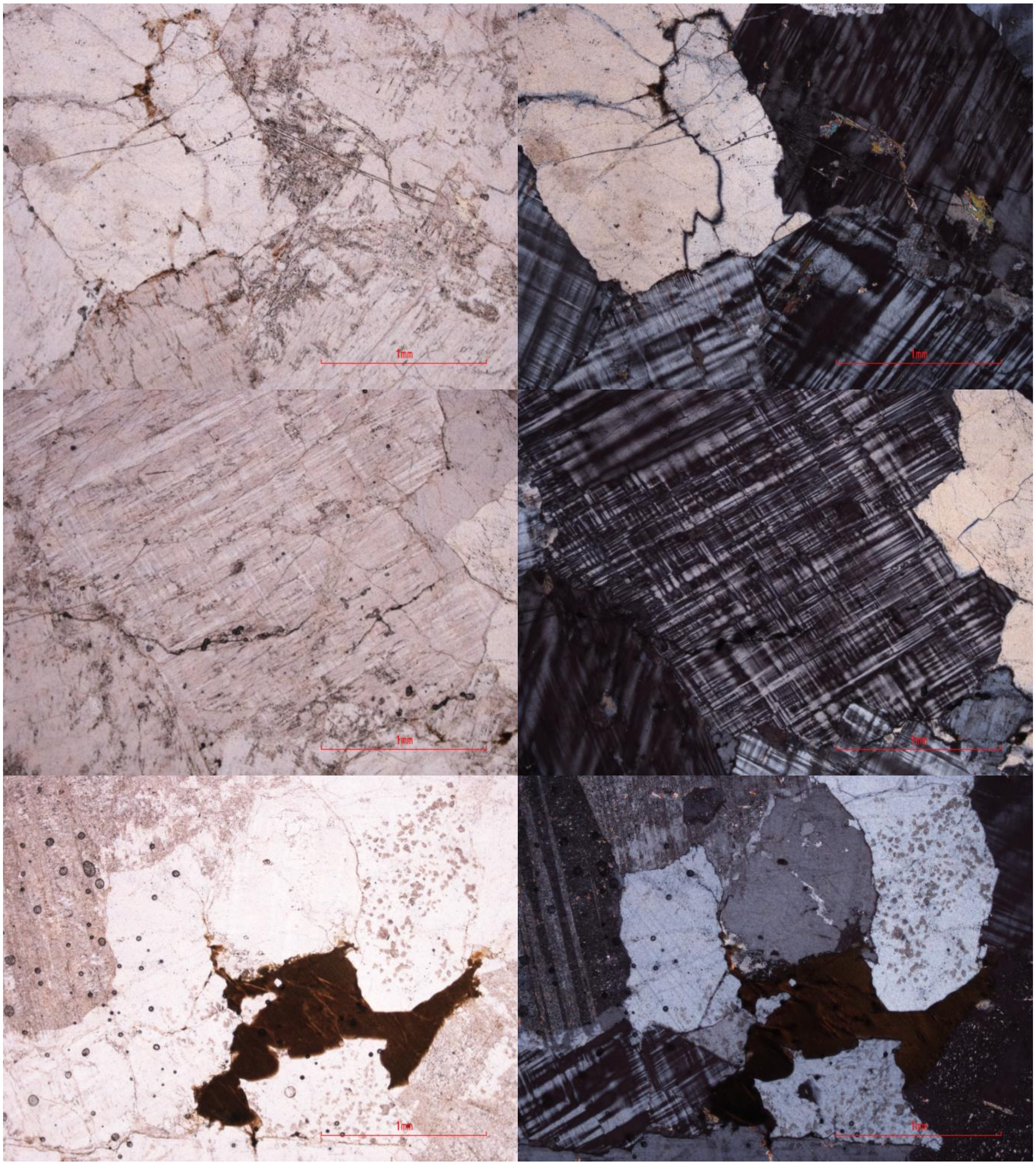
1mm
1mm
1mm
1mm
1mm
1mm

056aX - Salknappen Pegmatite

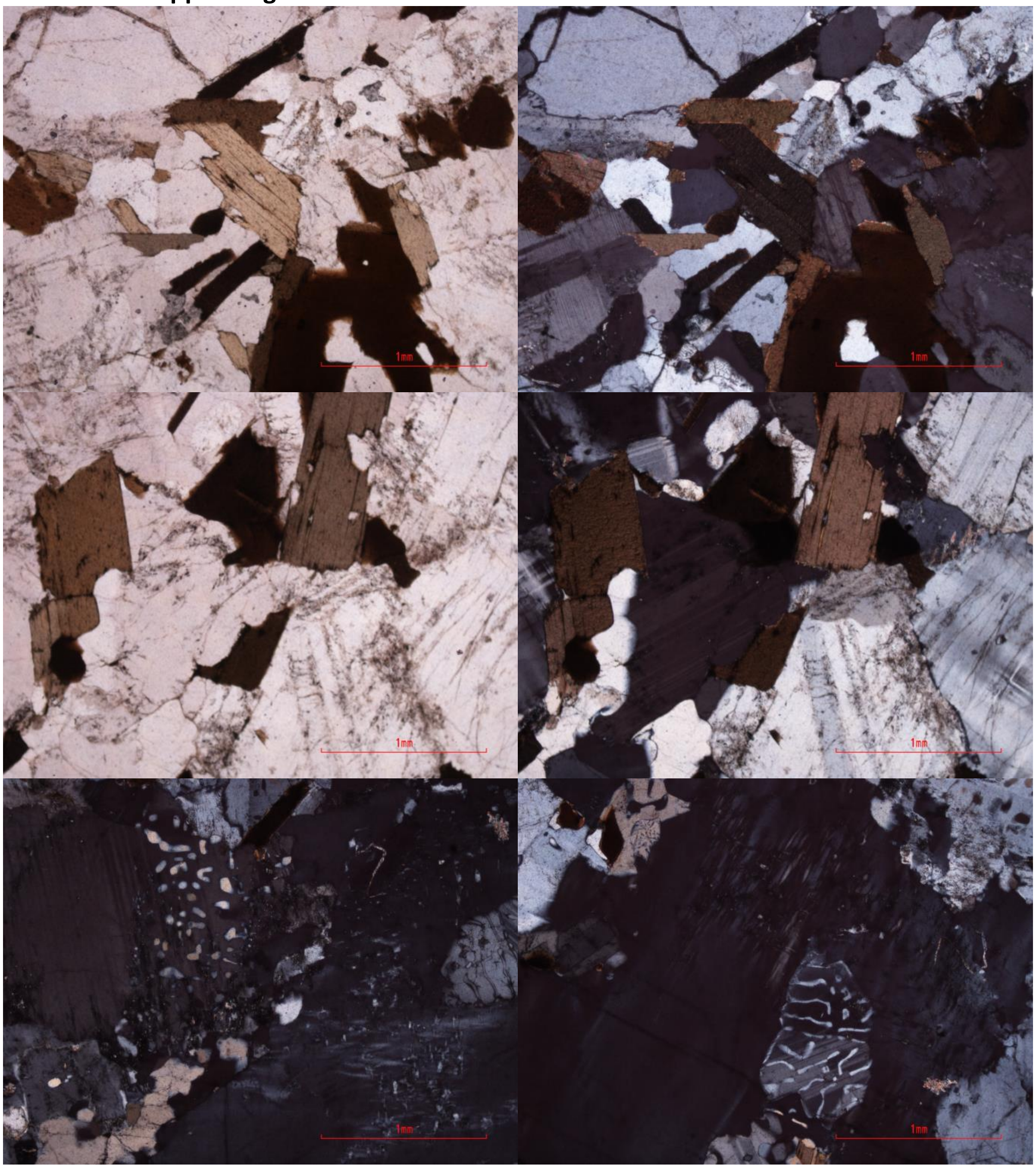

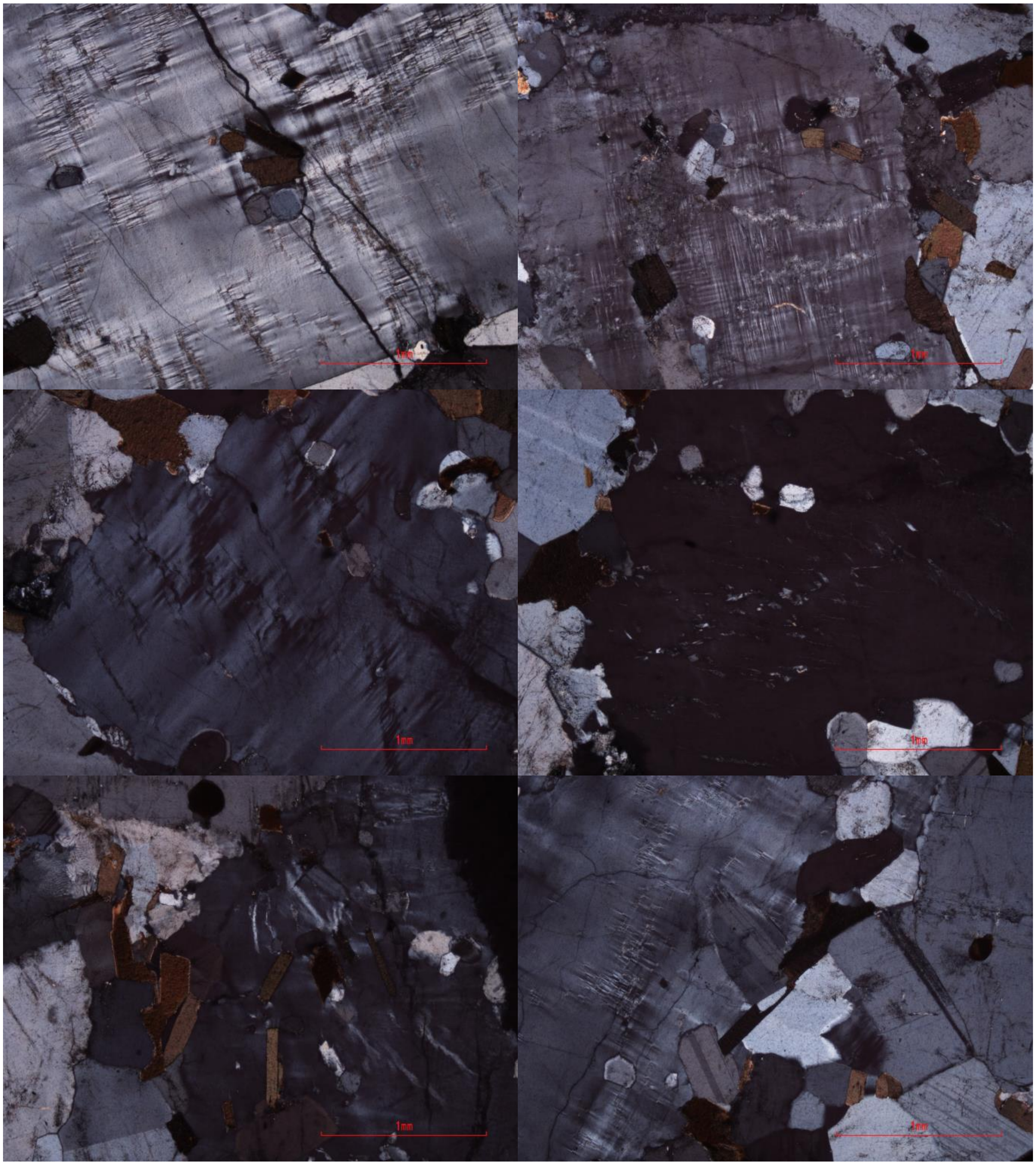
1mm
1mm
1mm

058aA - Salknappen Pegmatite

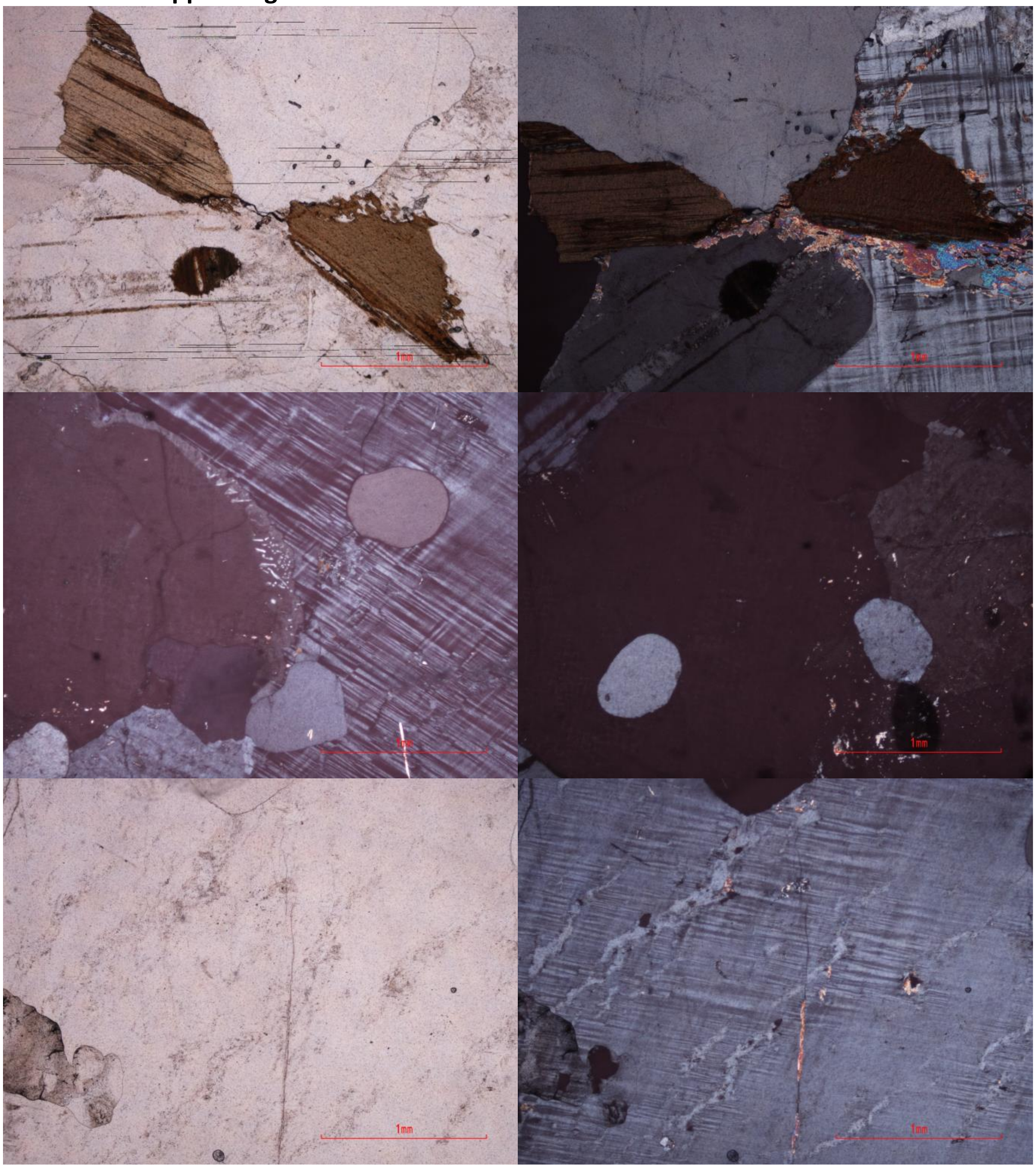

062aA - Salknappen Pegmatite

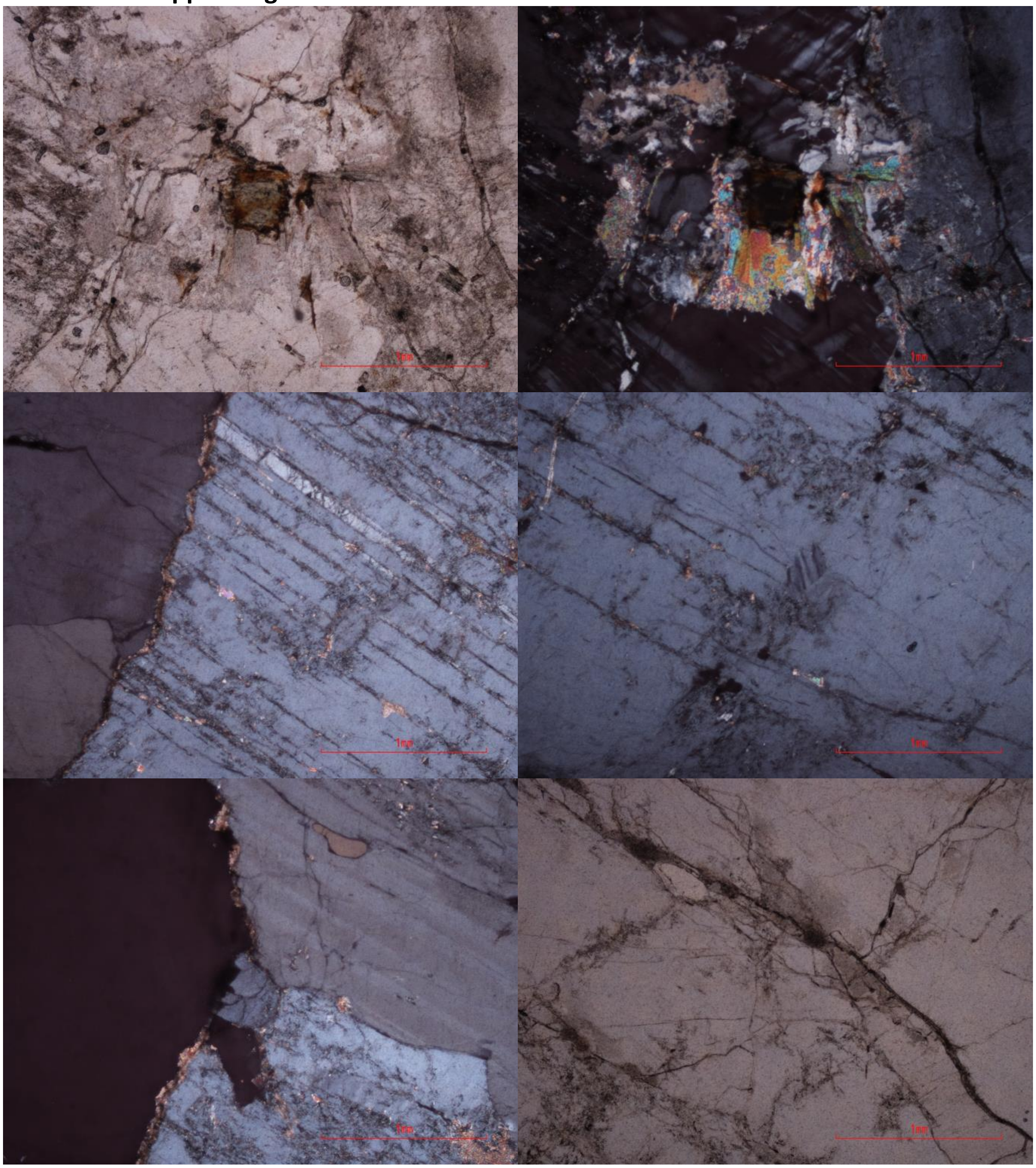


1mm
1mm
1mm
1mm
1mm
1mm

064aA - Dalmatian Granite

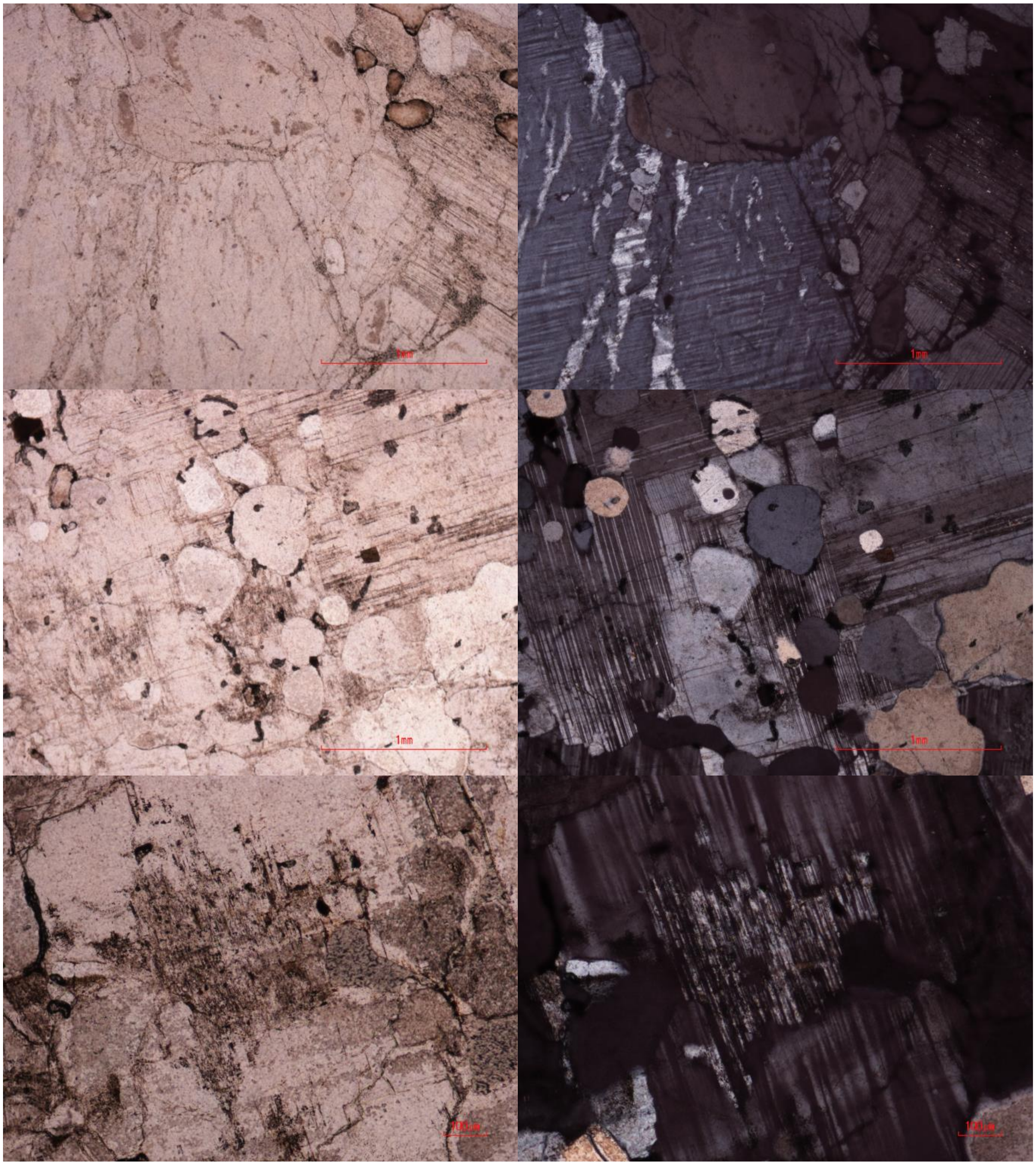

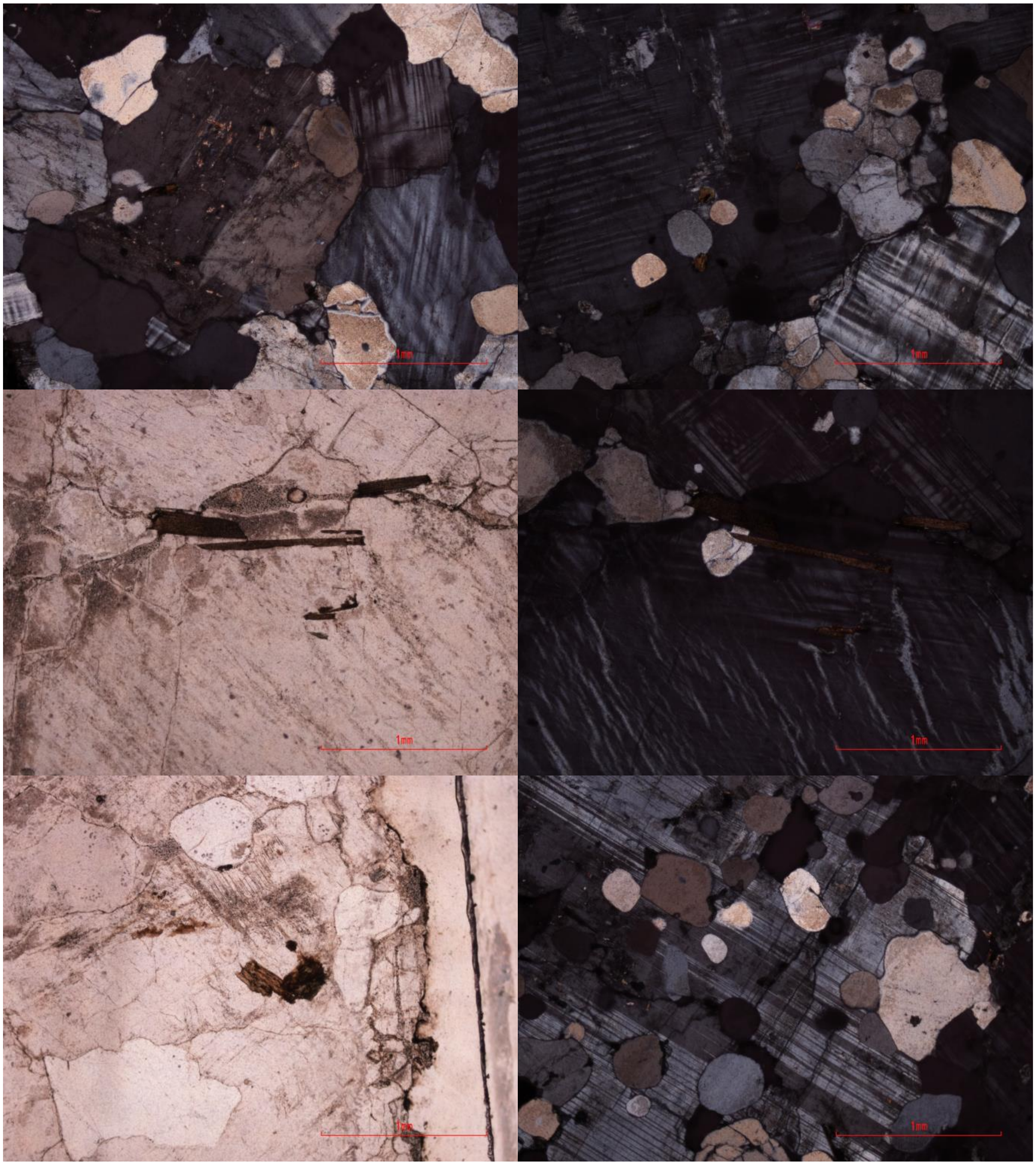

065aA - Dalmatian Granite

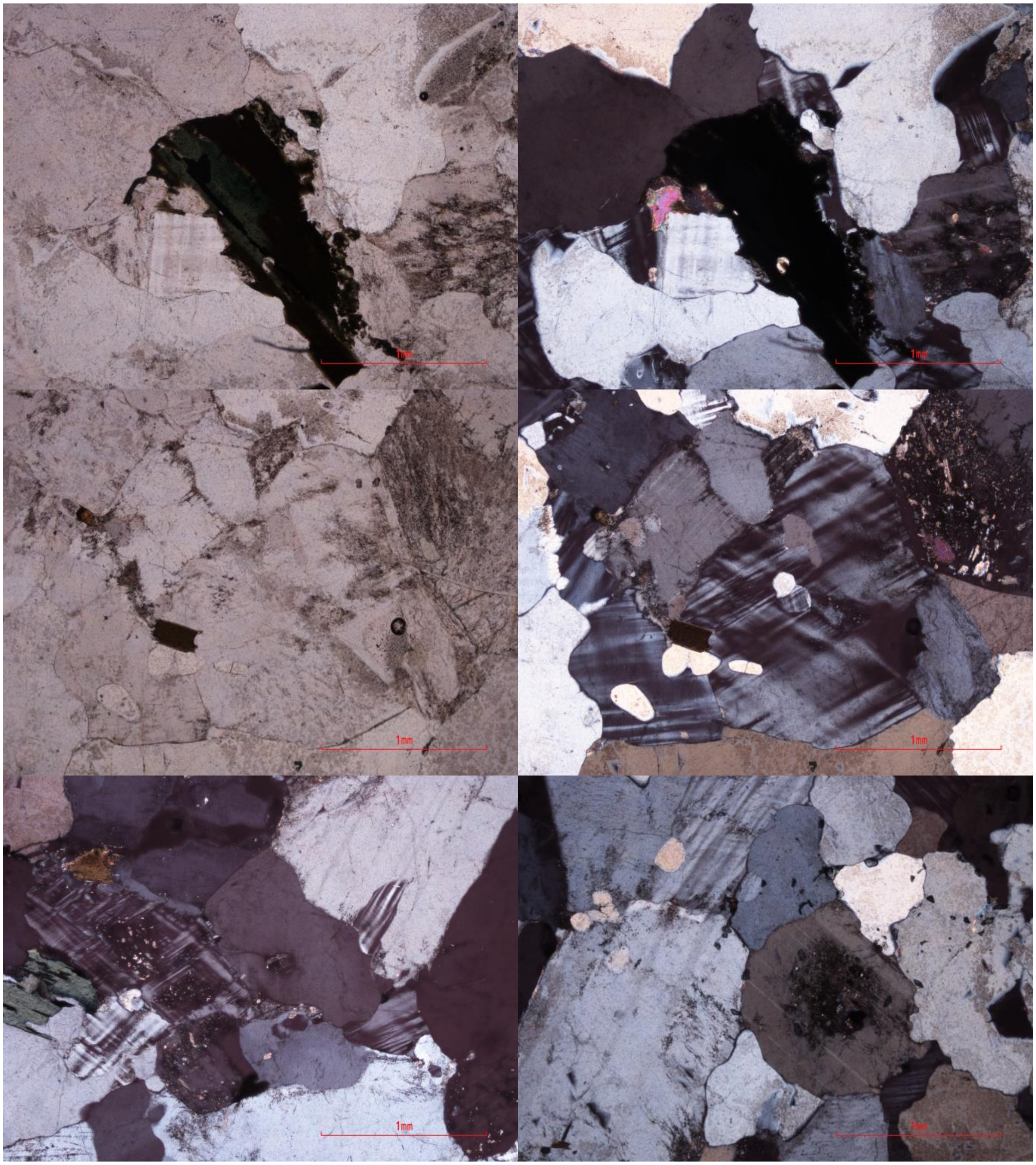

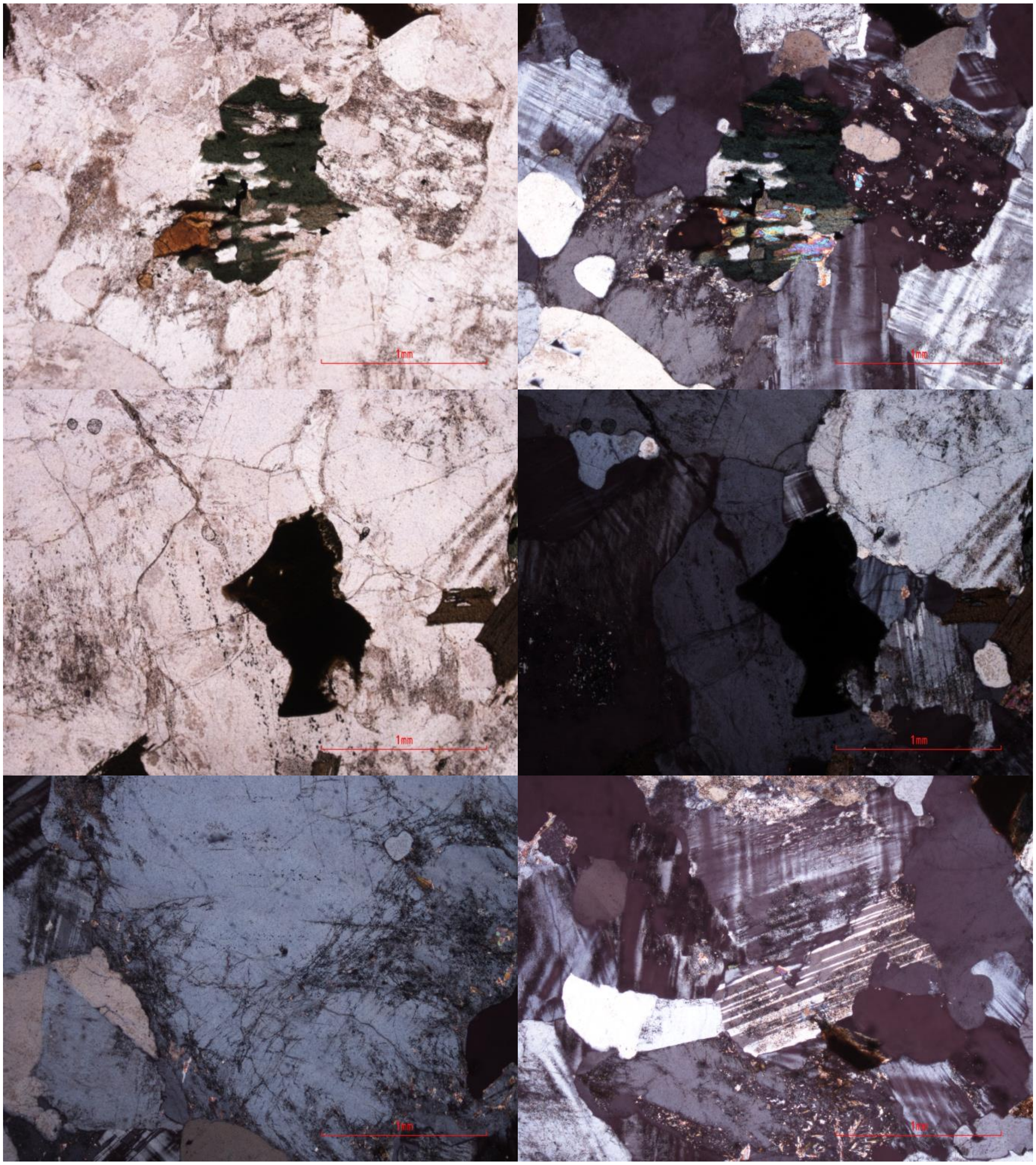
1mm
1mm
1mm
1mm
1mm
1mm

066aA - Salknappen Pegmatite

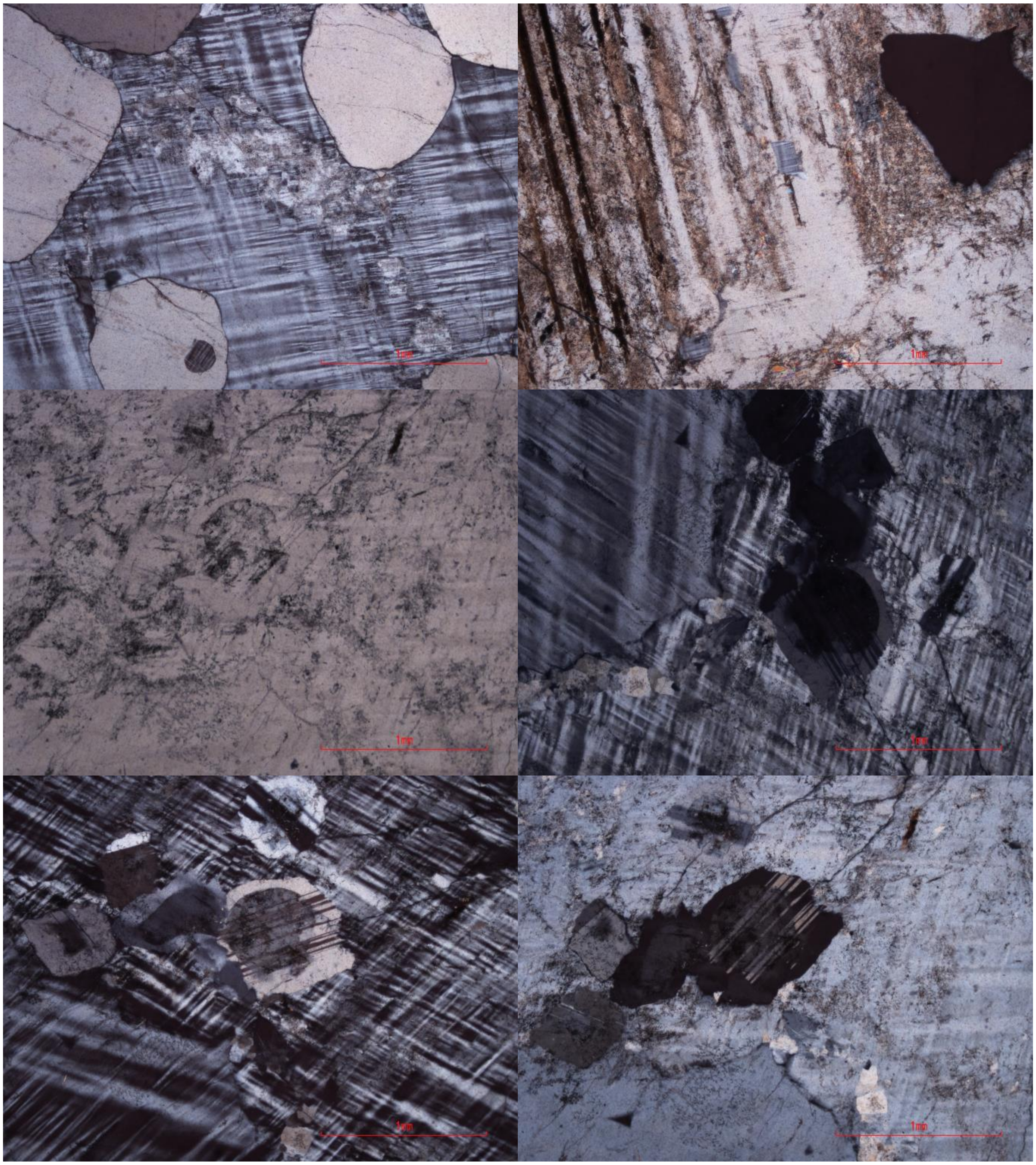
1mm
1mm
1mm
1mm
1mm
1mm

067aB – Pre-existing Granitoid

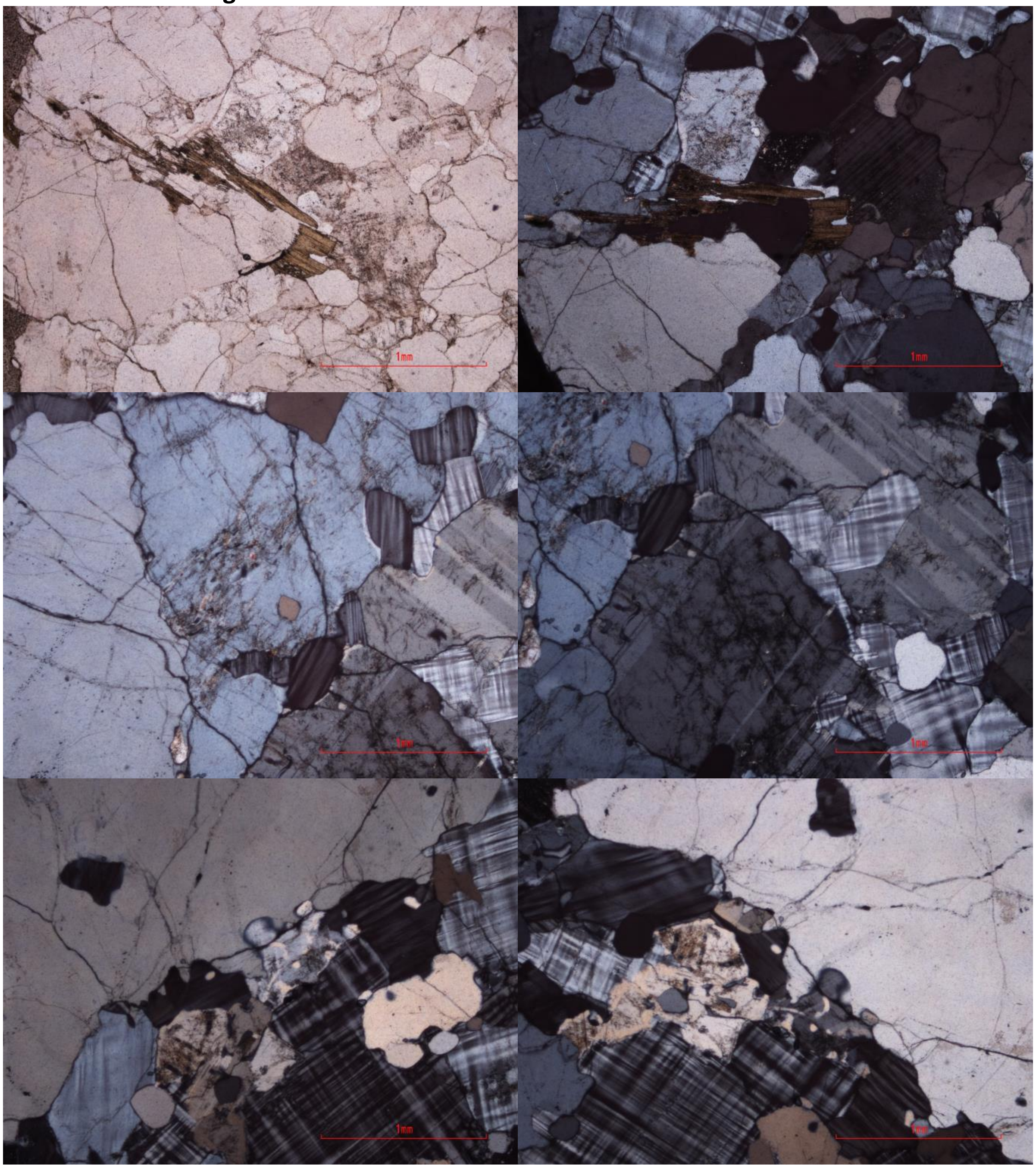

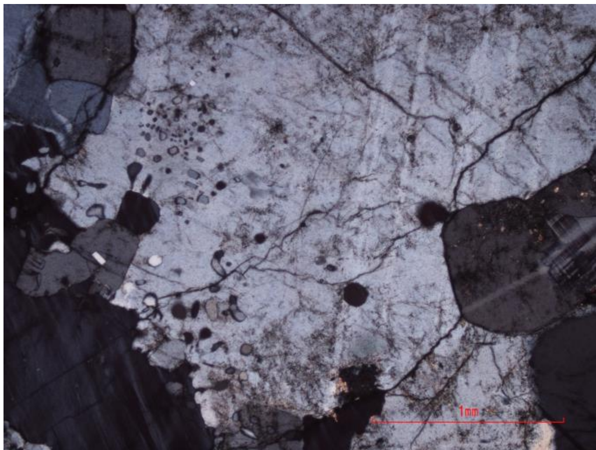
1mm
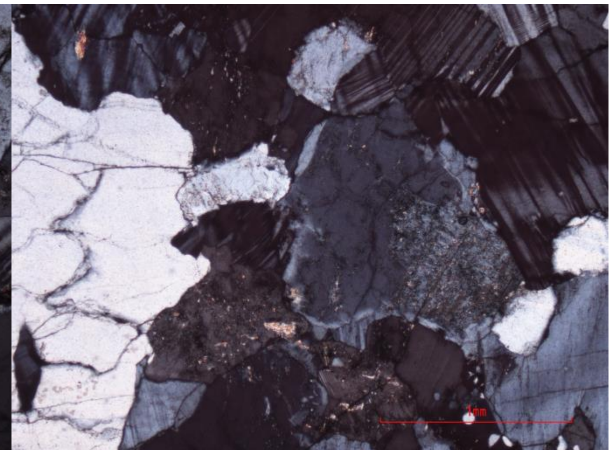
1mm
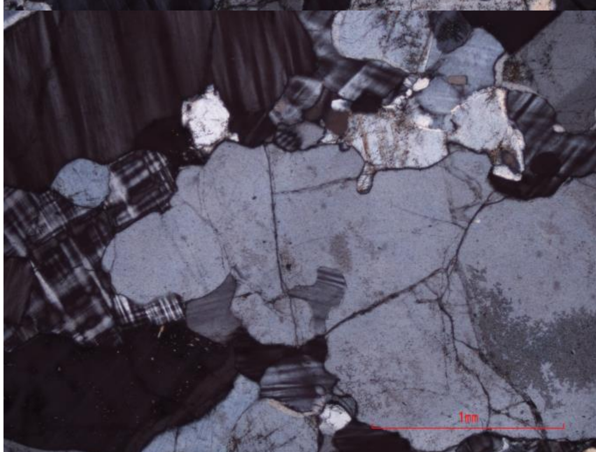
1mm
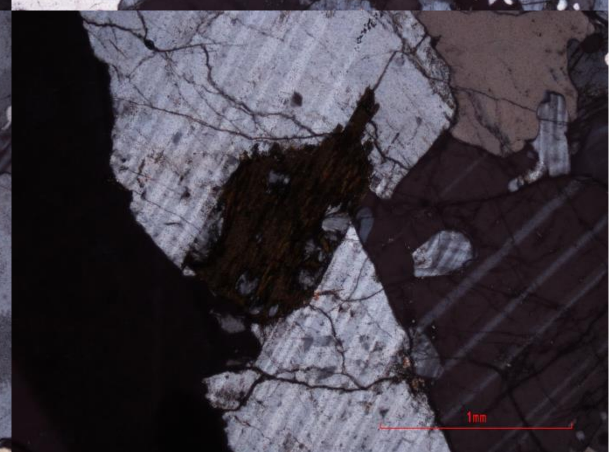
1mm
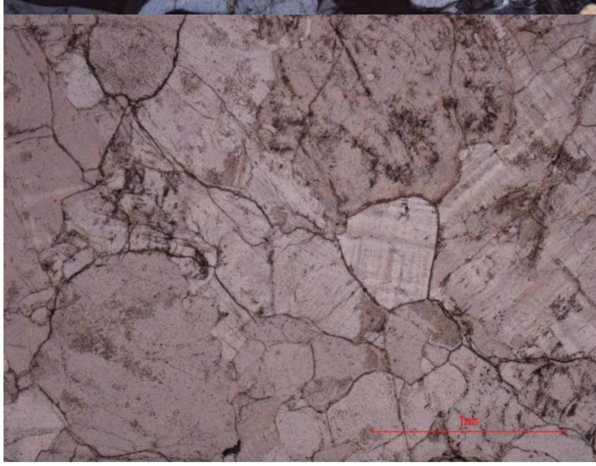
1mm
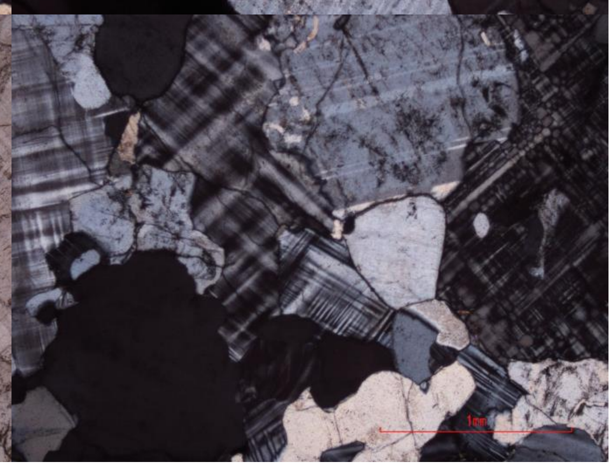
1mm

067bC – Pre-existing Granitoid

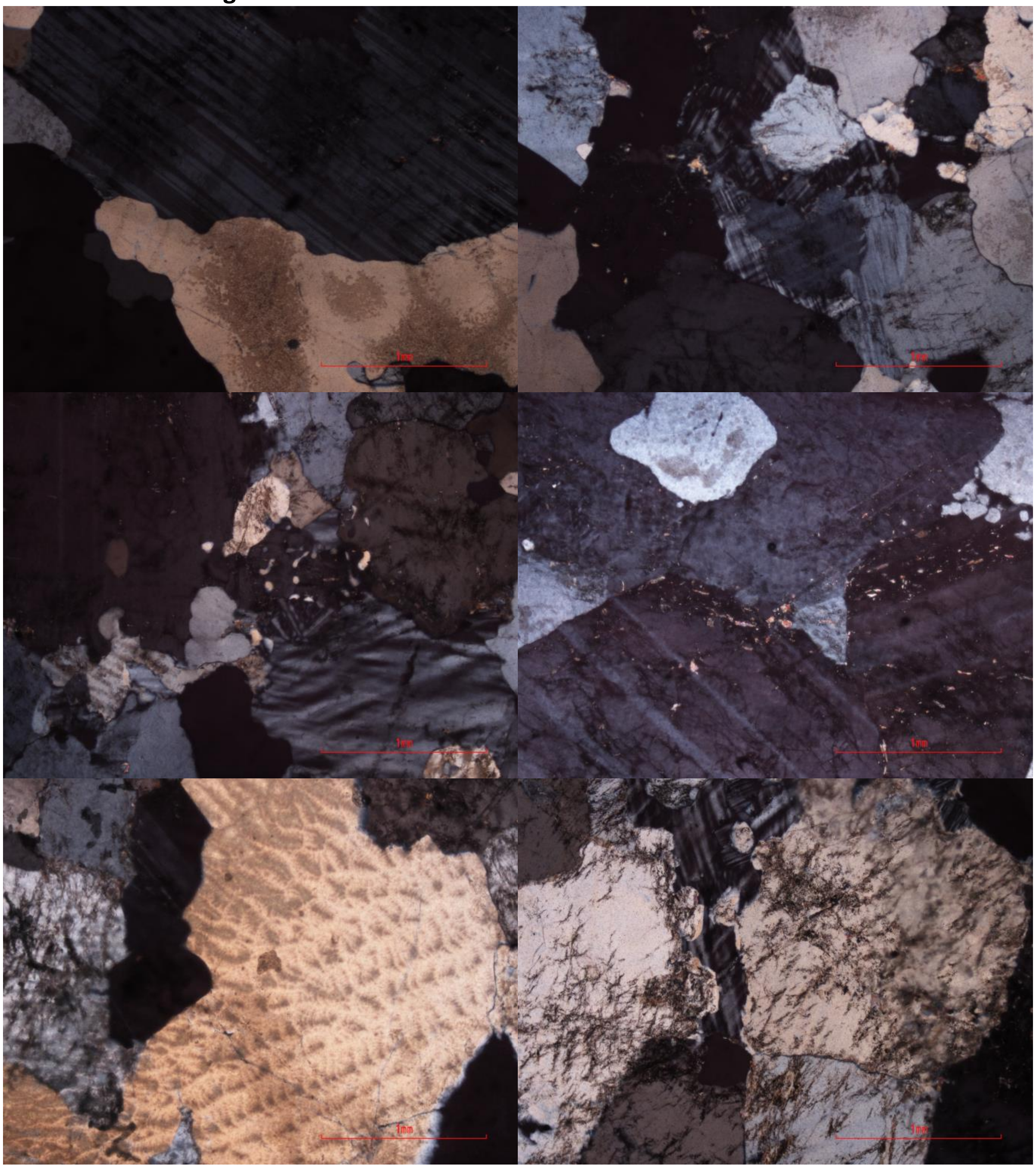

067cF – Pre-existing Granitoid

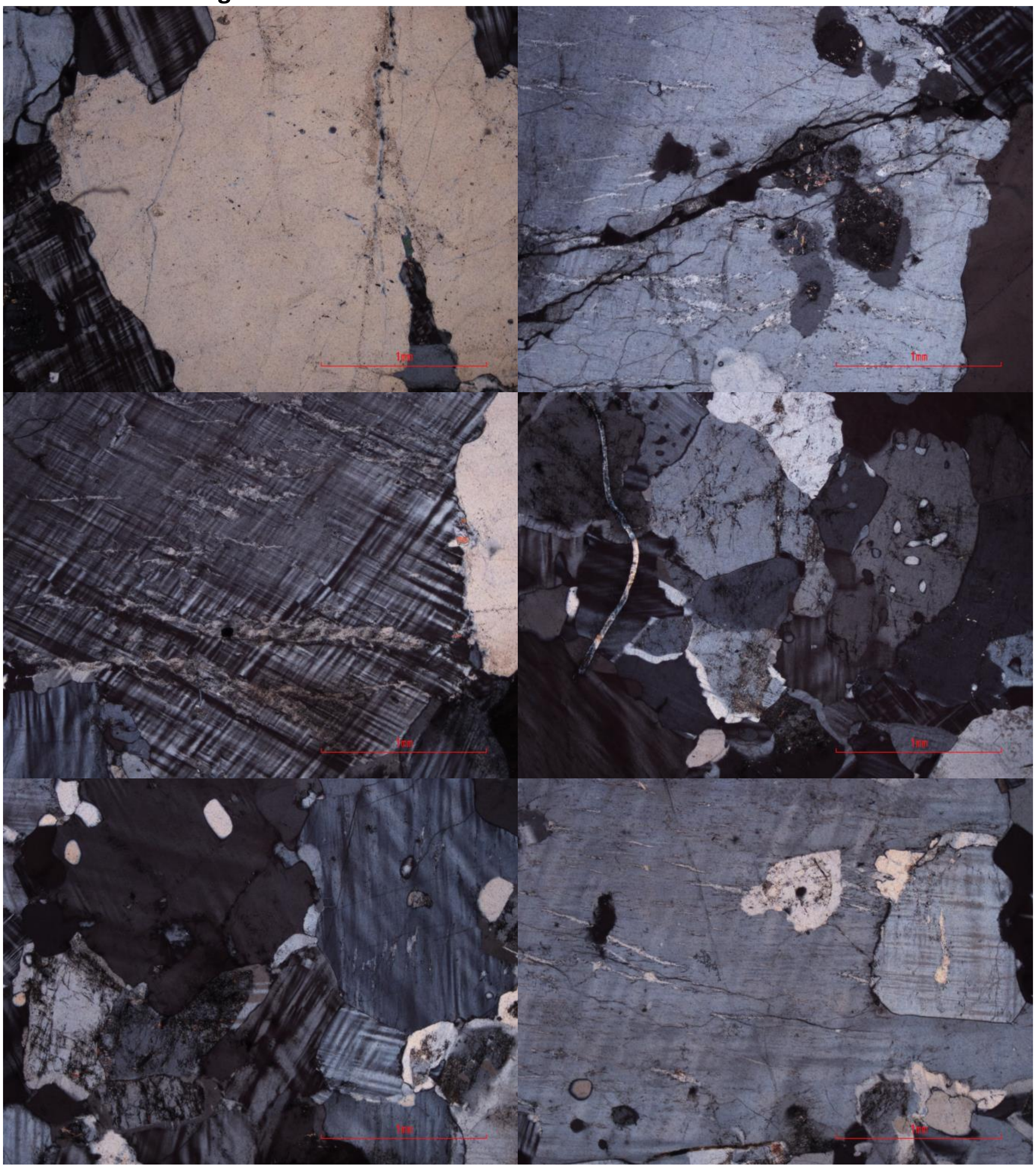

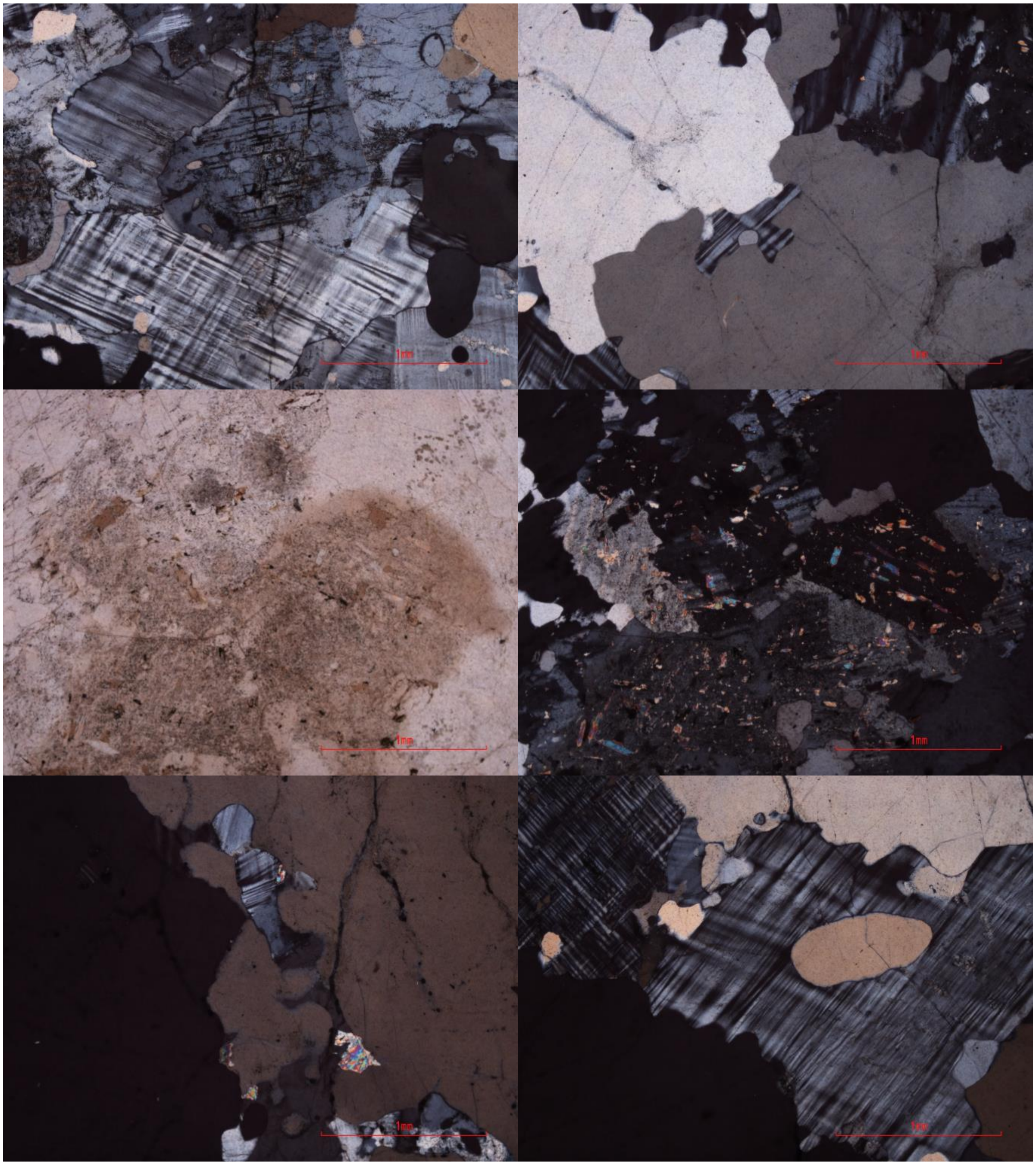
1mm
1mm
1mm

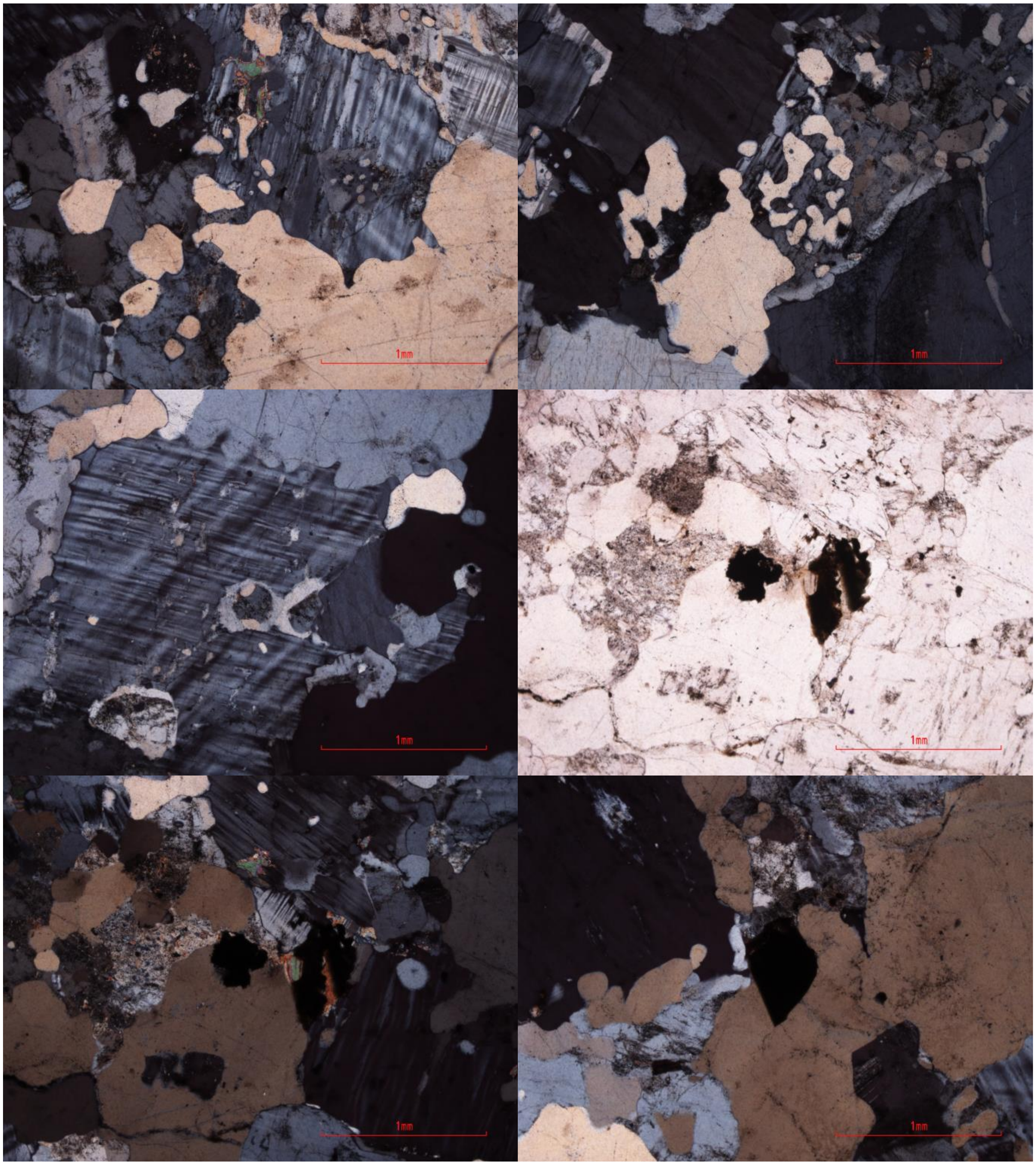
1mm
1mm
1mm
1mm
1mm
1mm

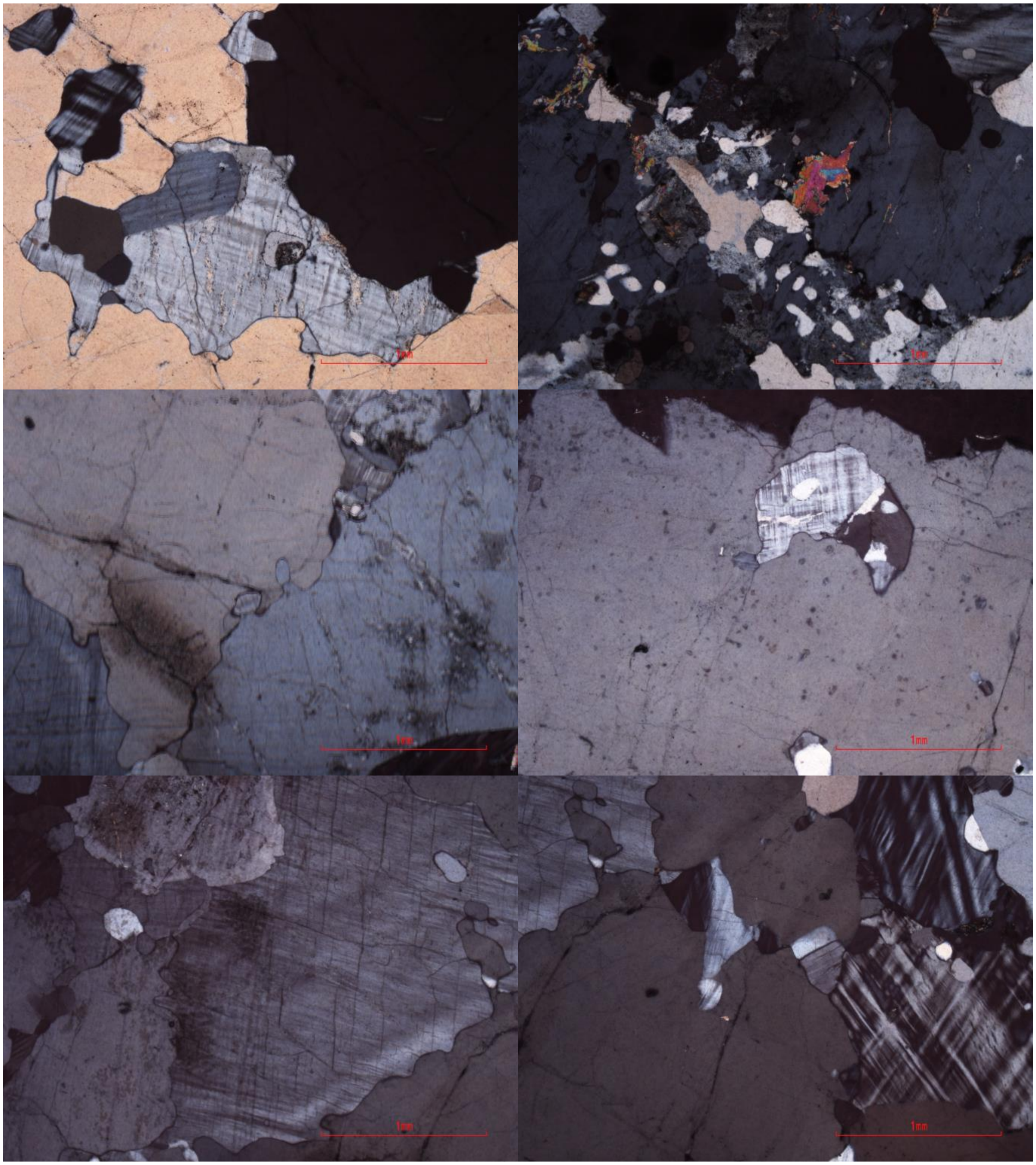
1mm
1mm
1mm
1mm
1mm
1mm

068aA - Dalmatian Granite

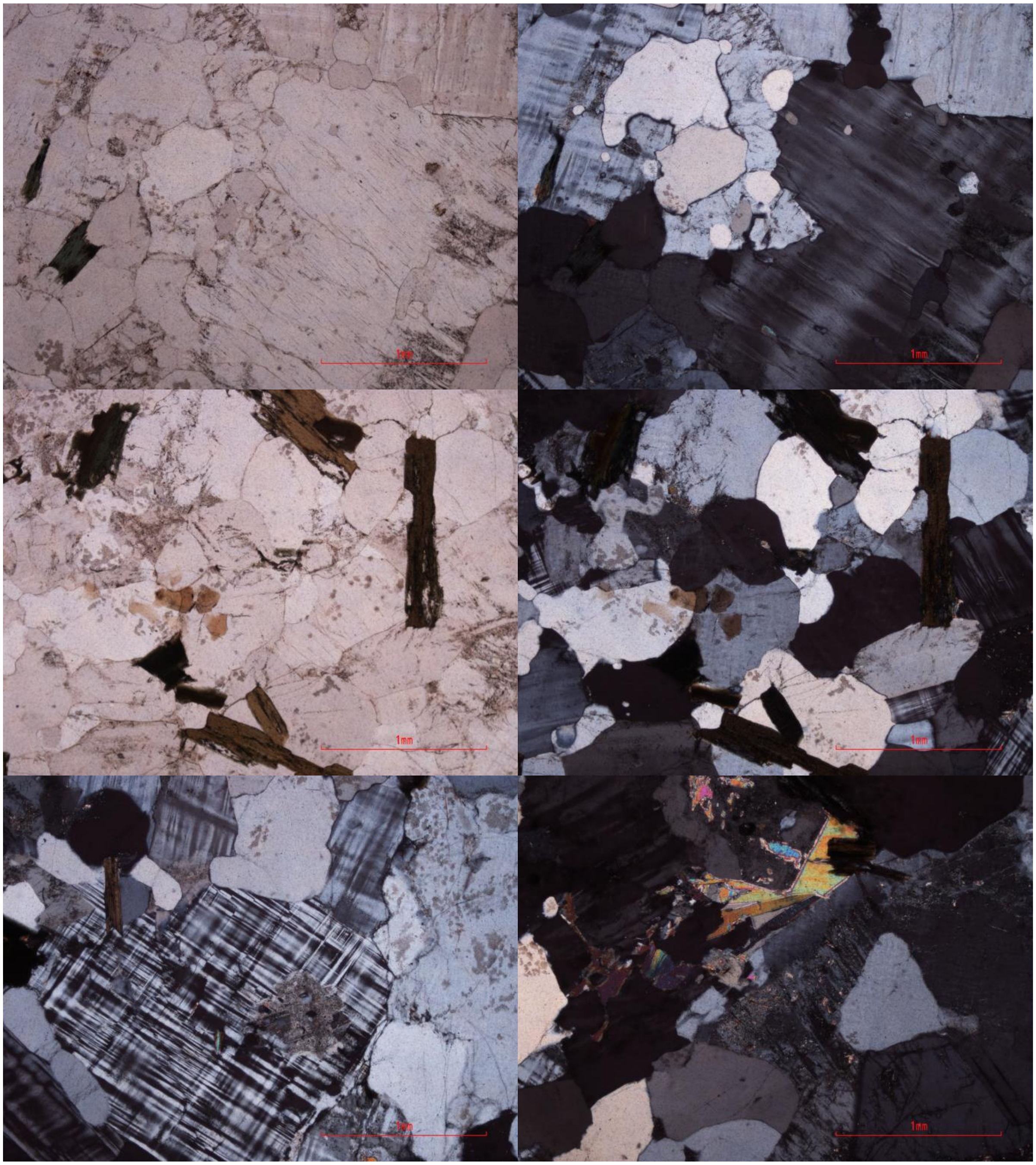

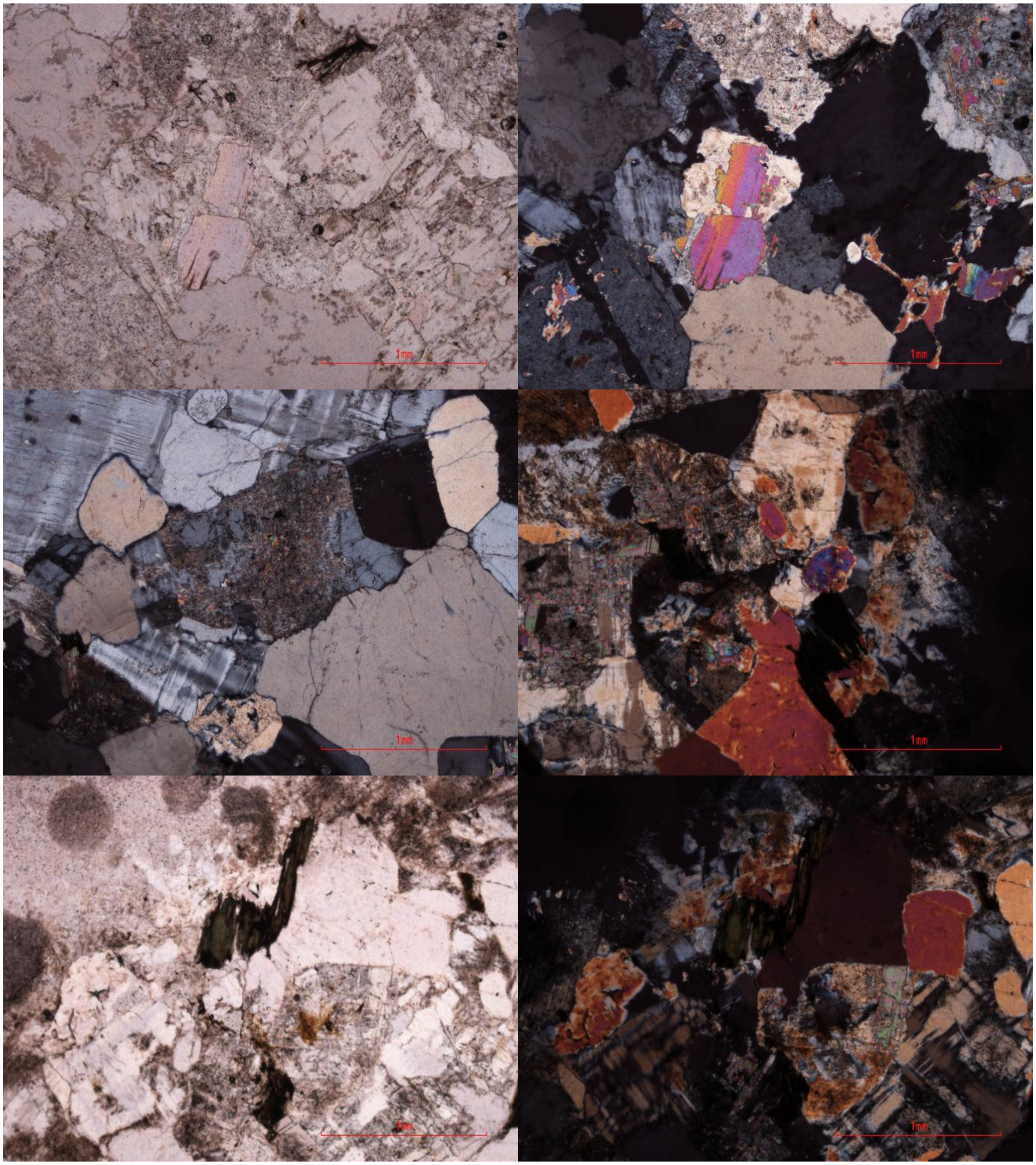
1mm
1mm
1mm
1mm

068bB - Salknappen Pegmatite

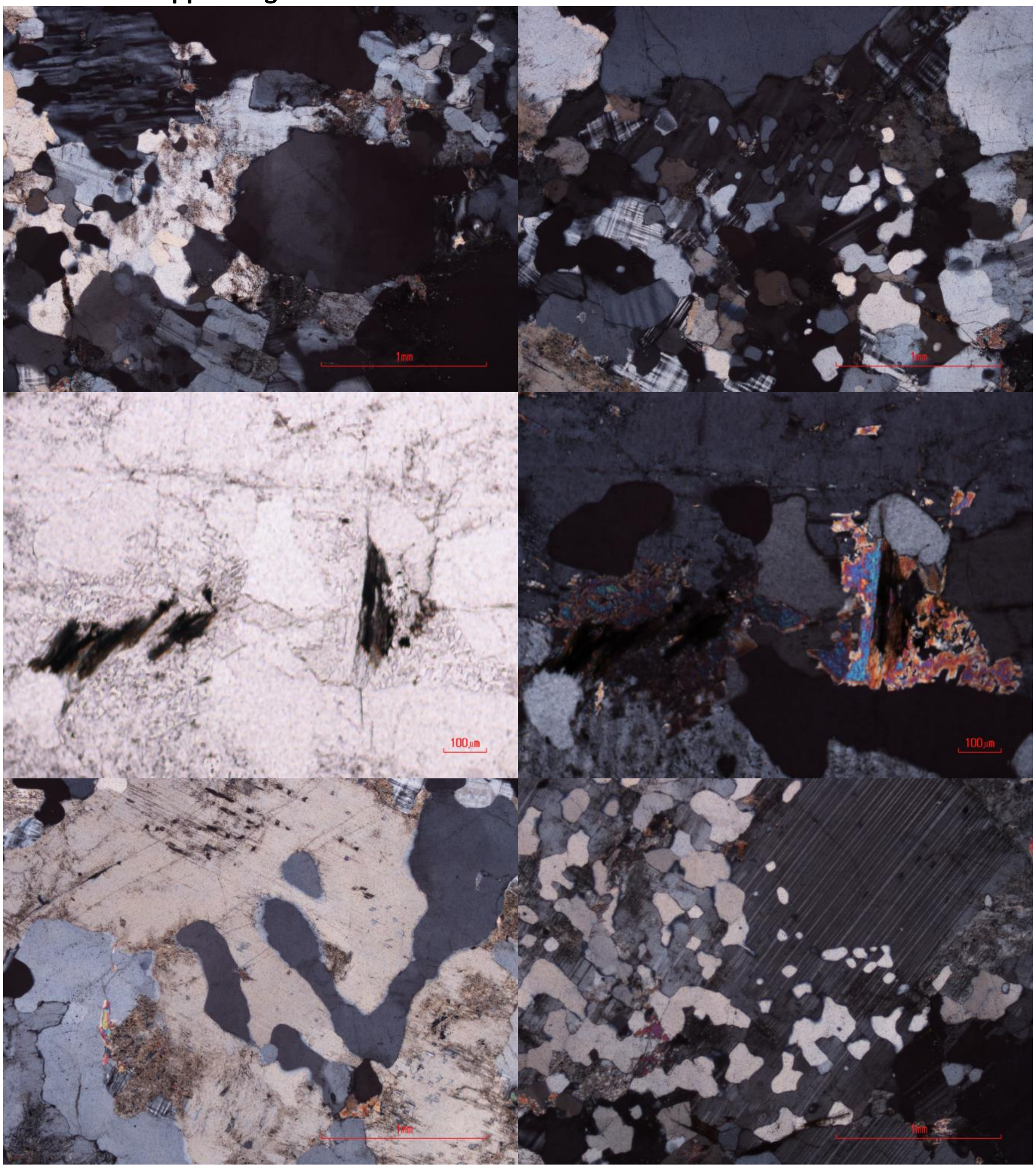

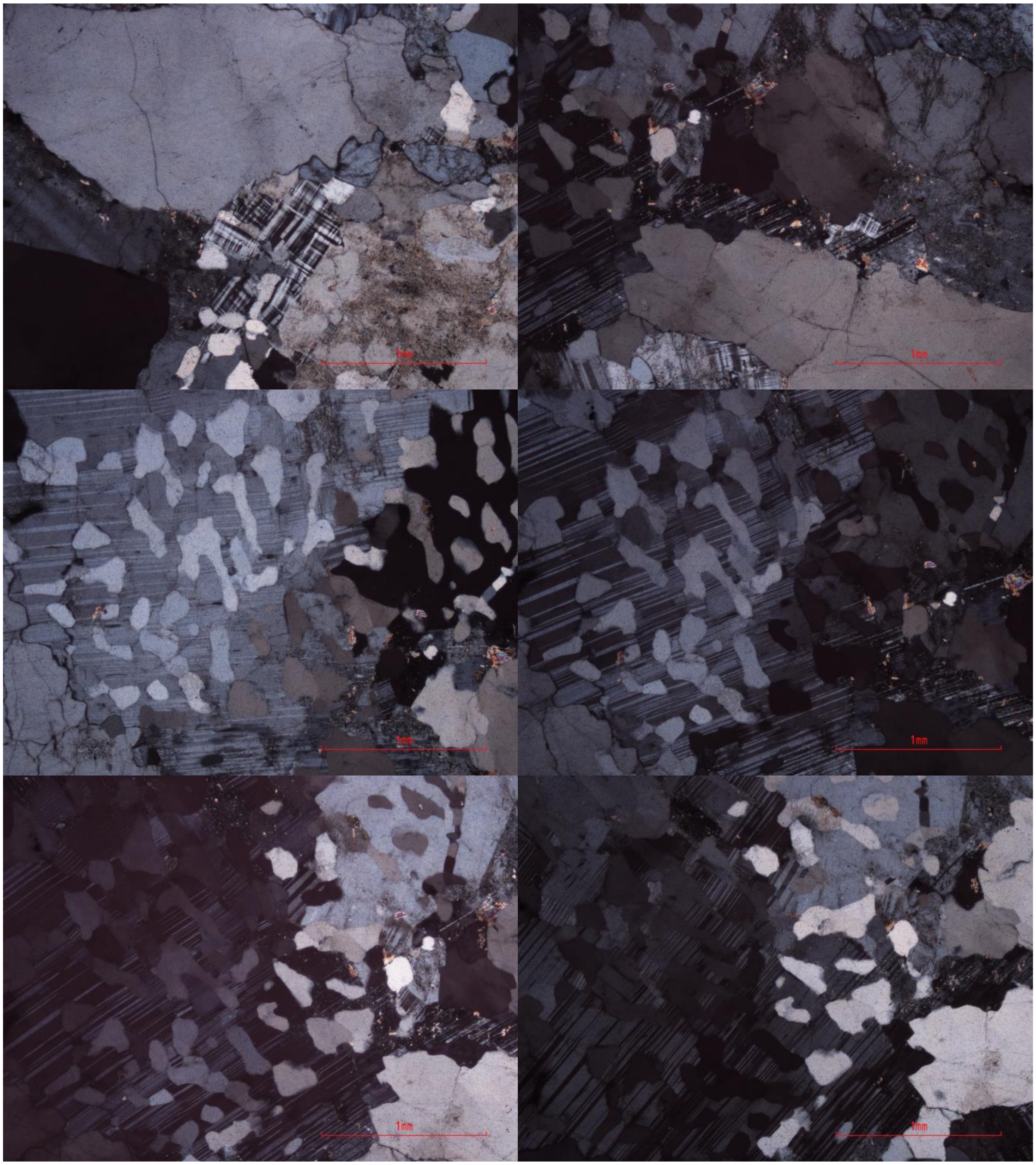
1mm
1mm
1mm
1mm
1mm
1mm

068cC - Salknappen Pegmatite

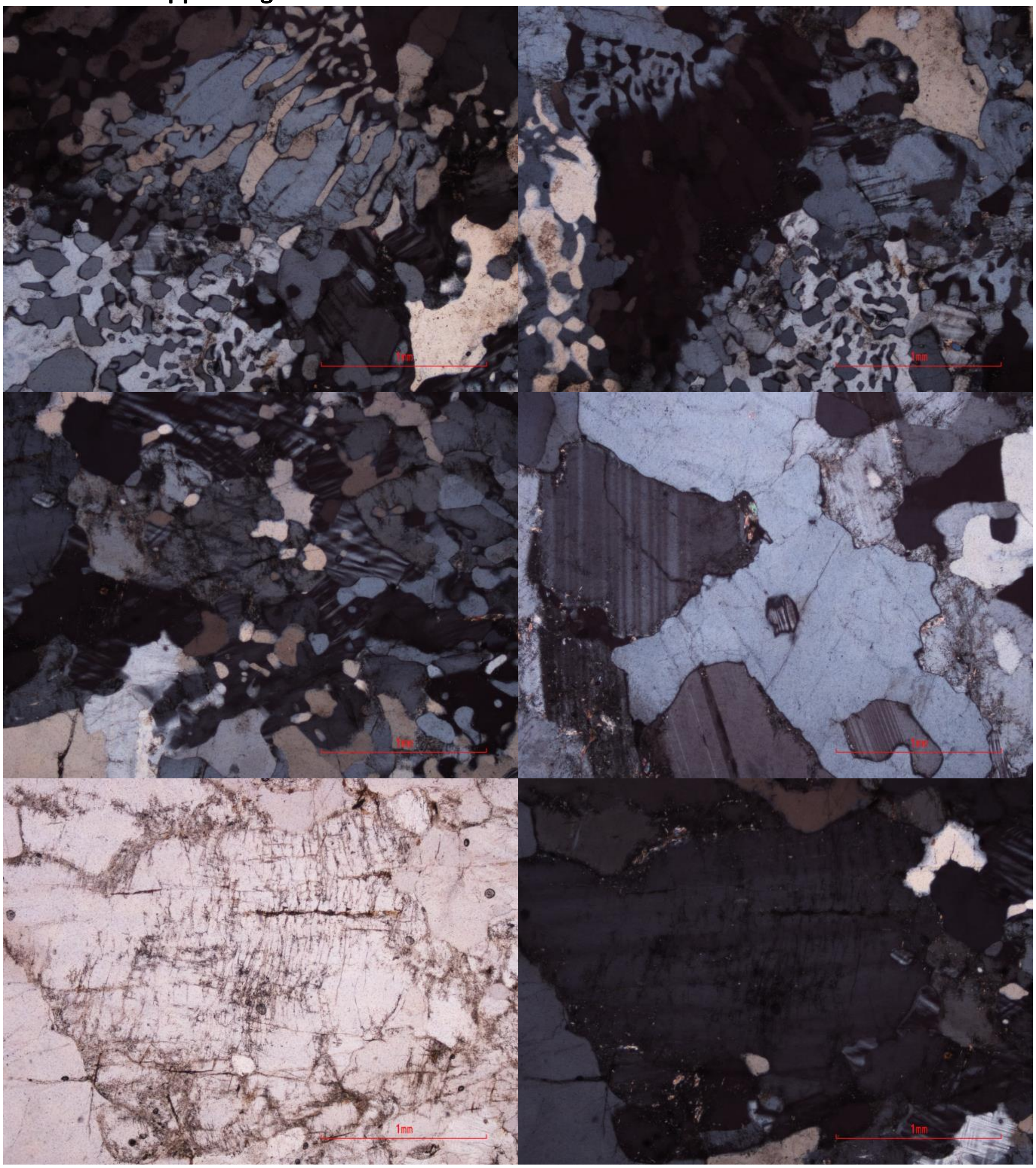

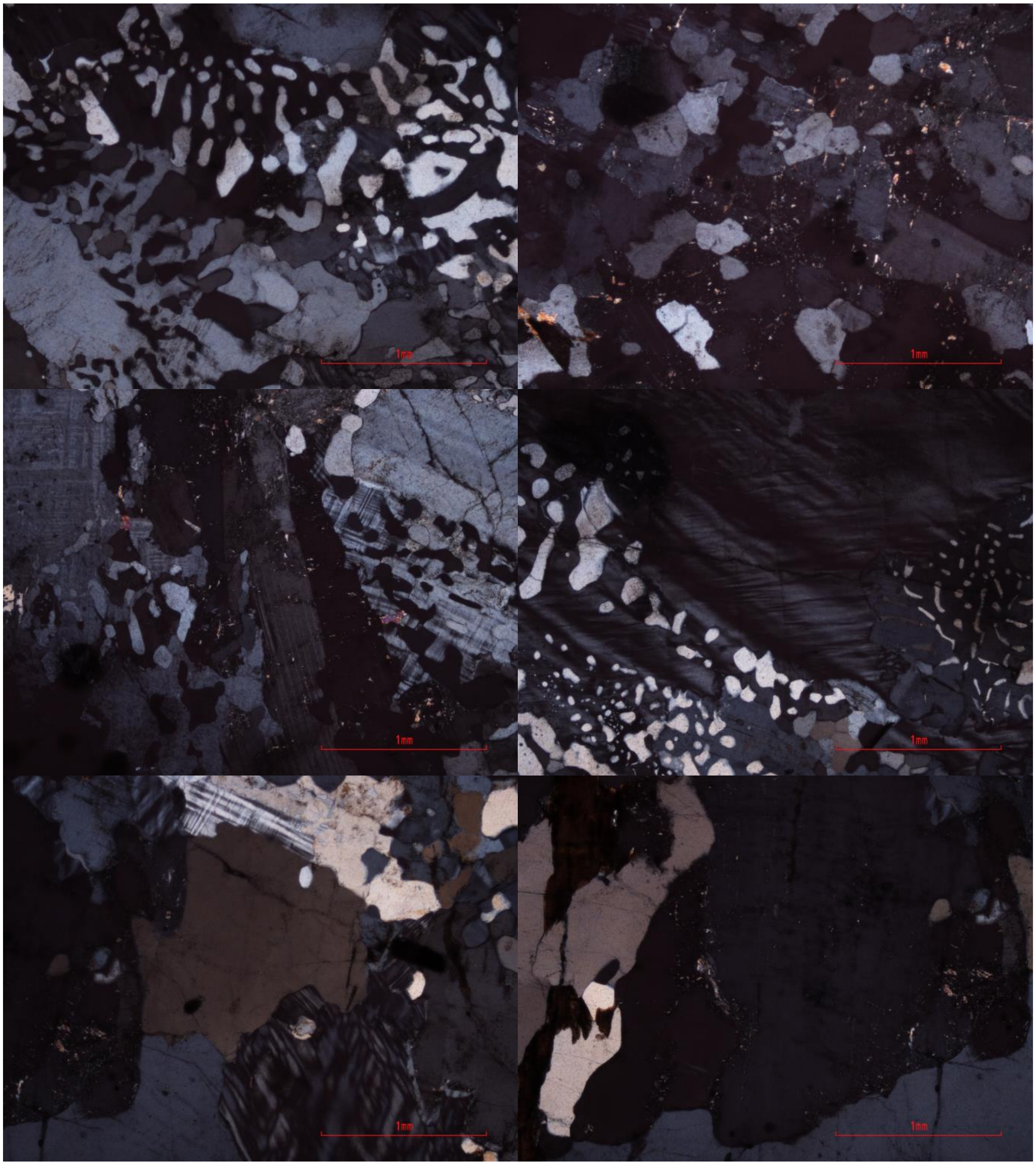
1mm
1mm
1mm
1mm
1mm
1mm

070aB - Dalmatian Granite

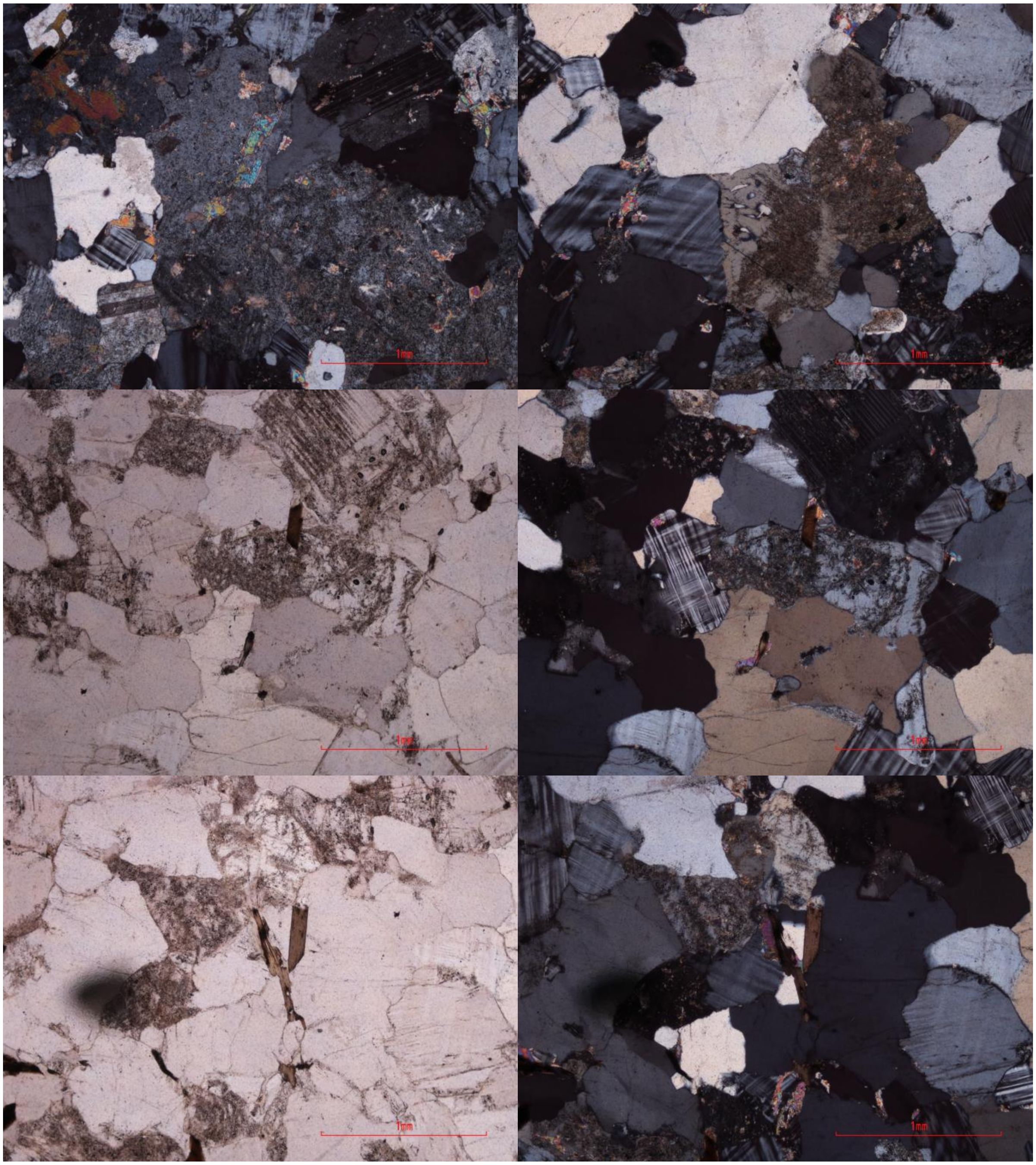

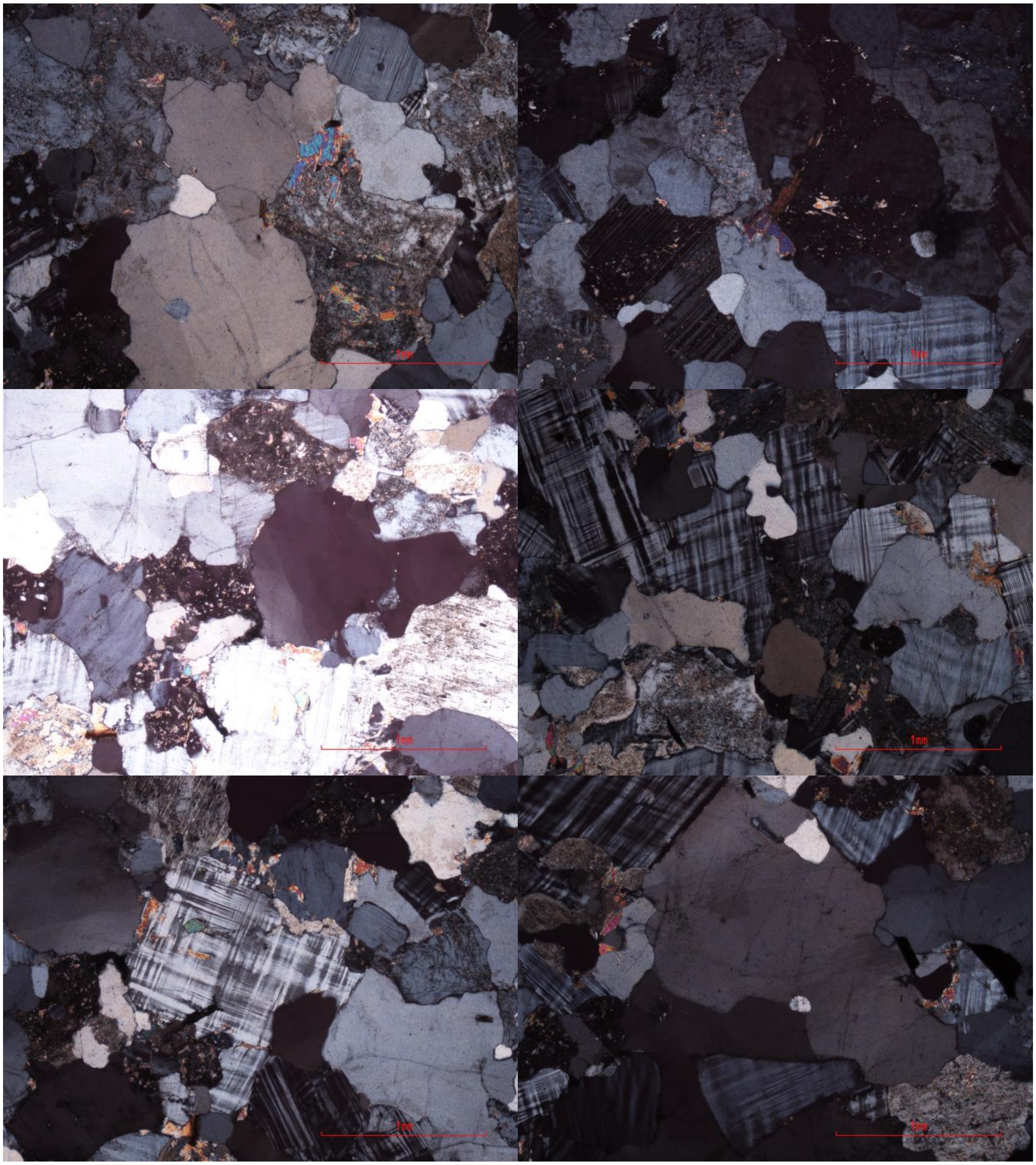

071aA - Salknappen Pegmatite

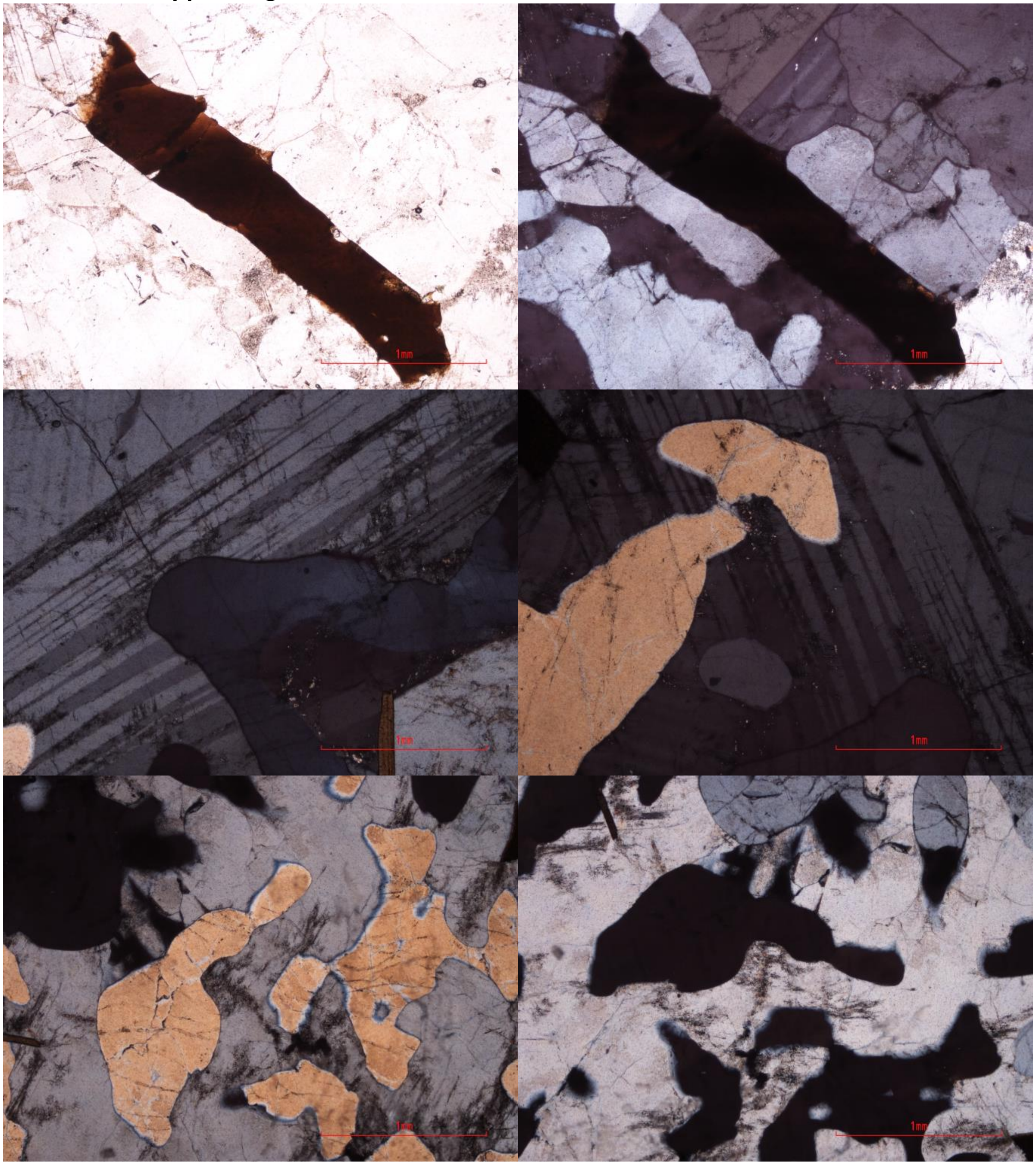

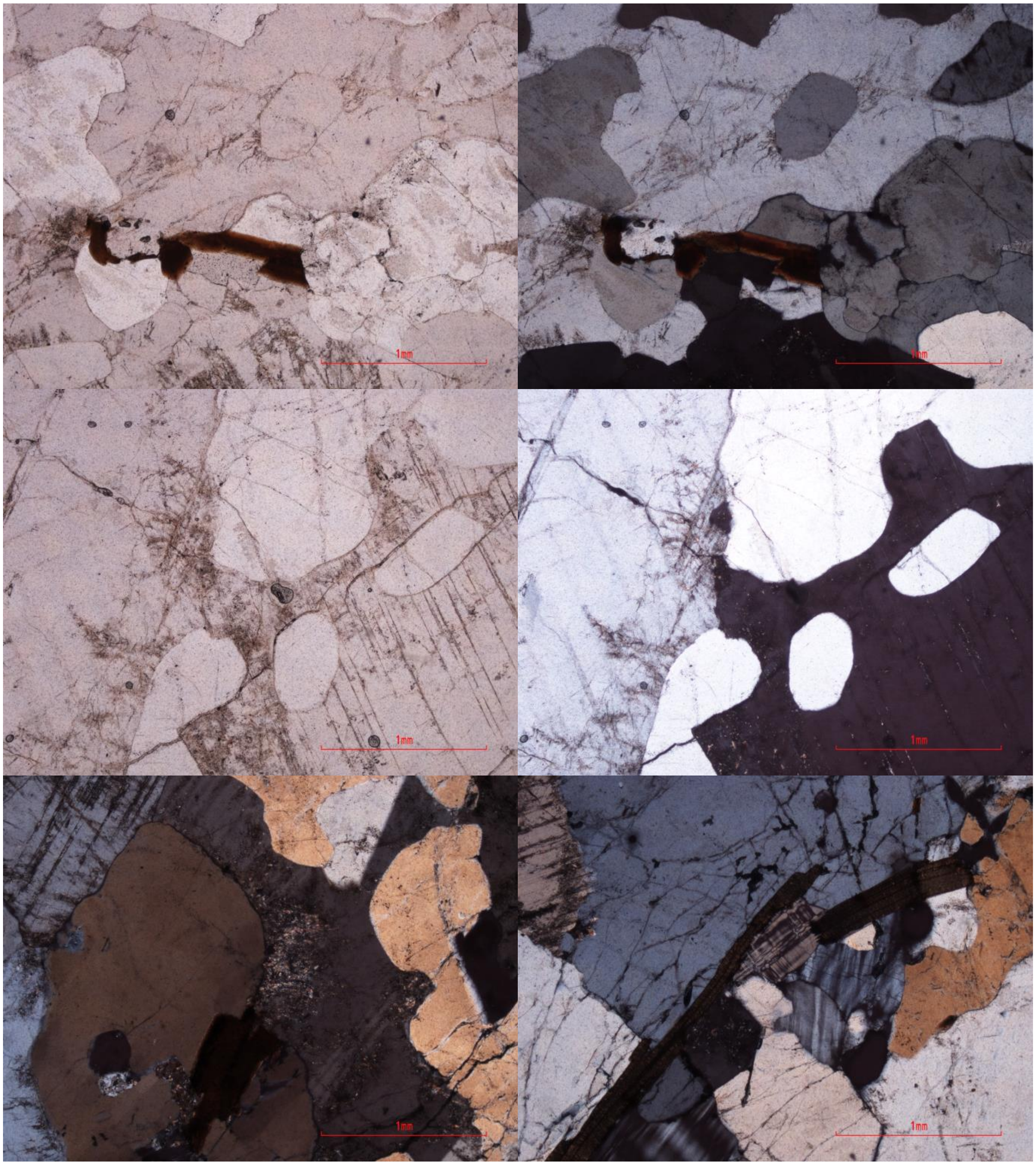
1mm
1mm
1mm
1mm
1mm
1mm

072aA - Salknappen Pegmatite

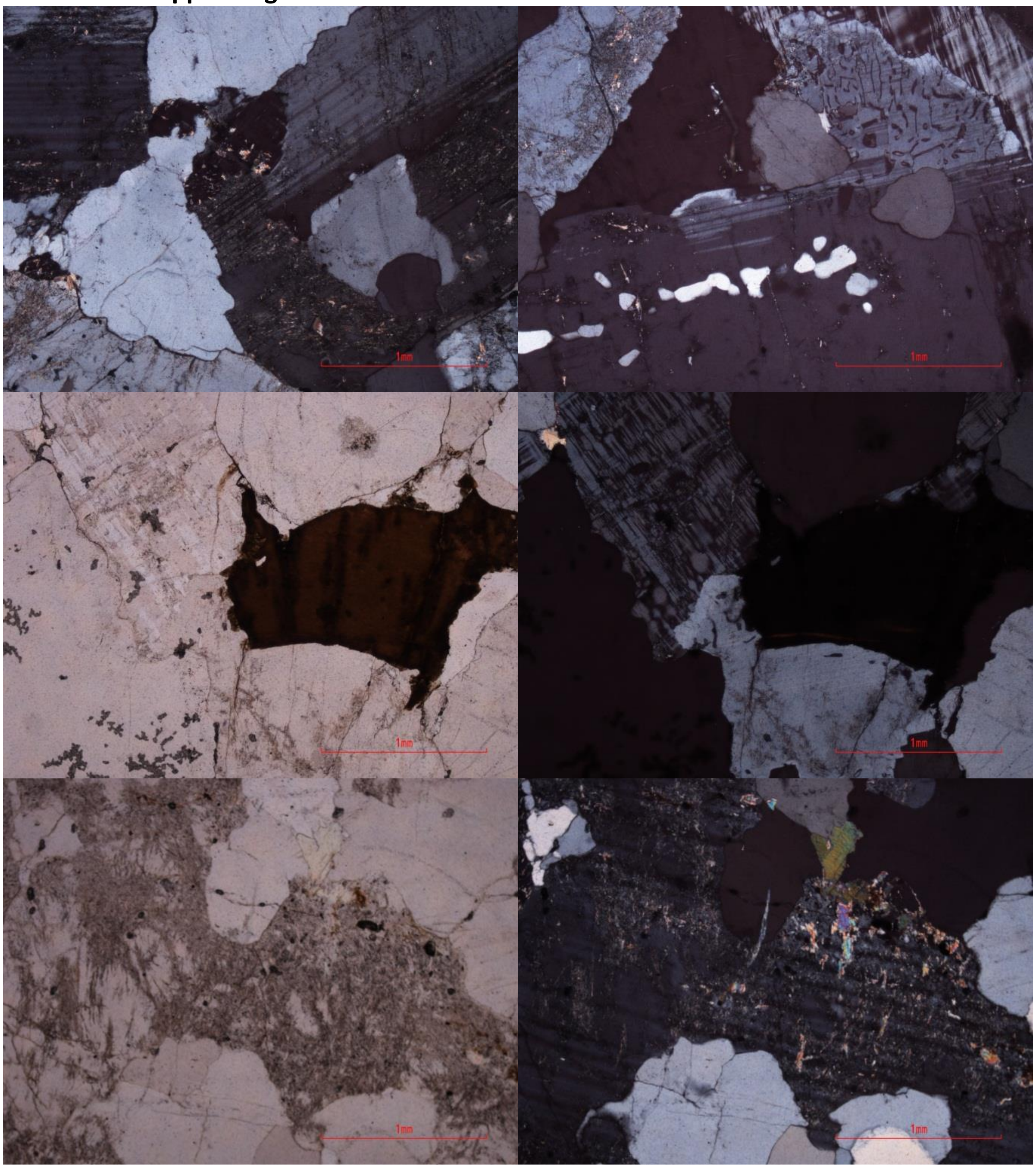

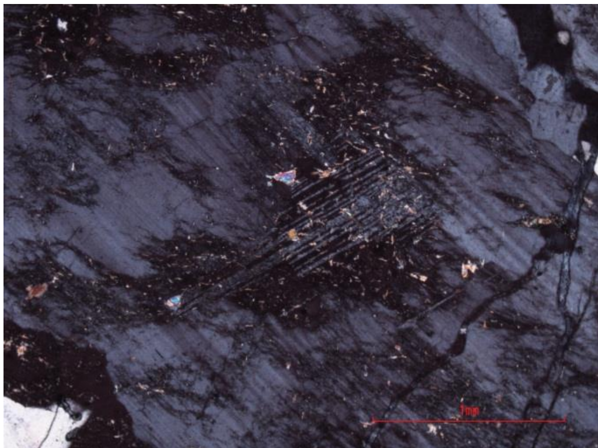
1mm
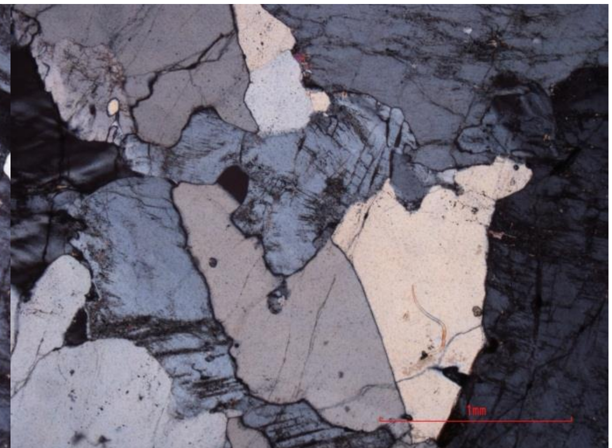
1mm
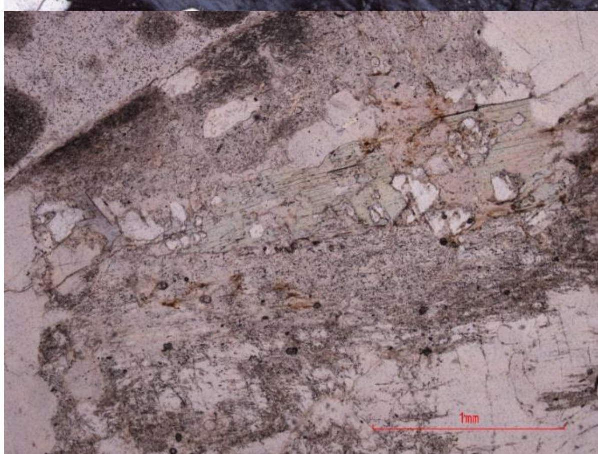
1mm
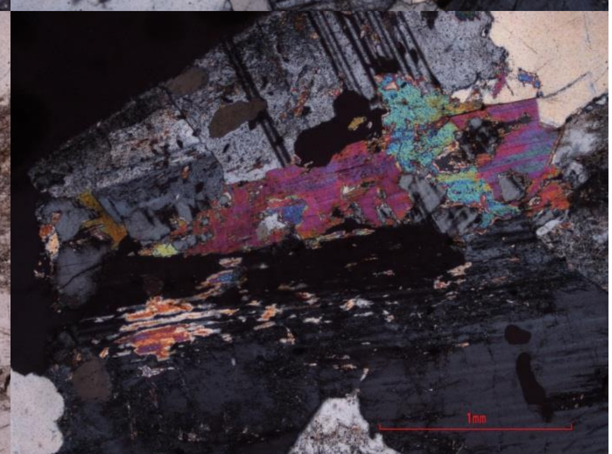
1mm
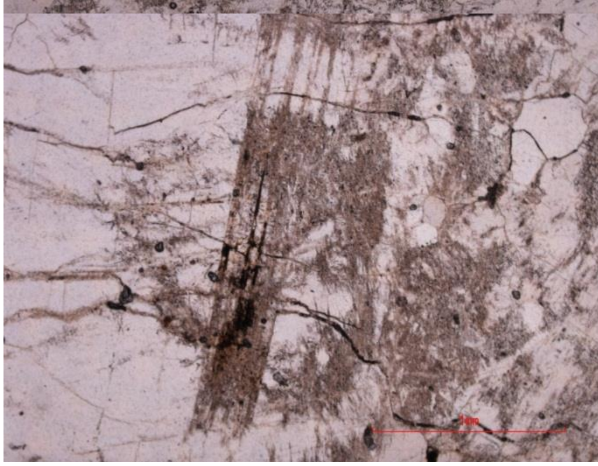
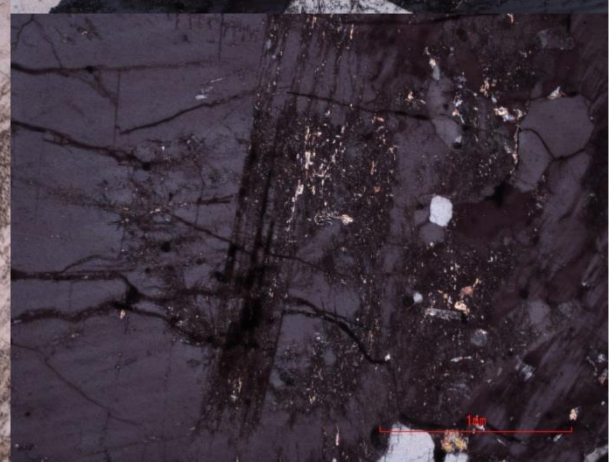

075aA - Salknappen Pegmatite

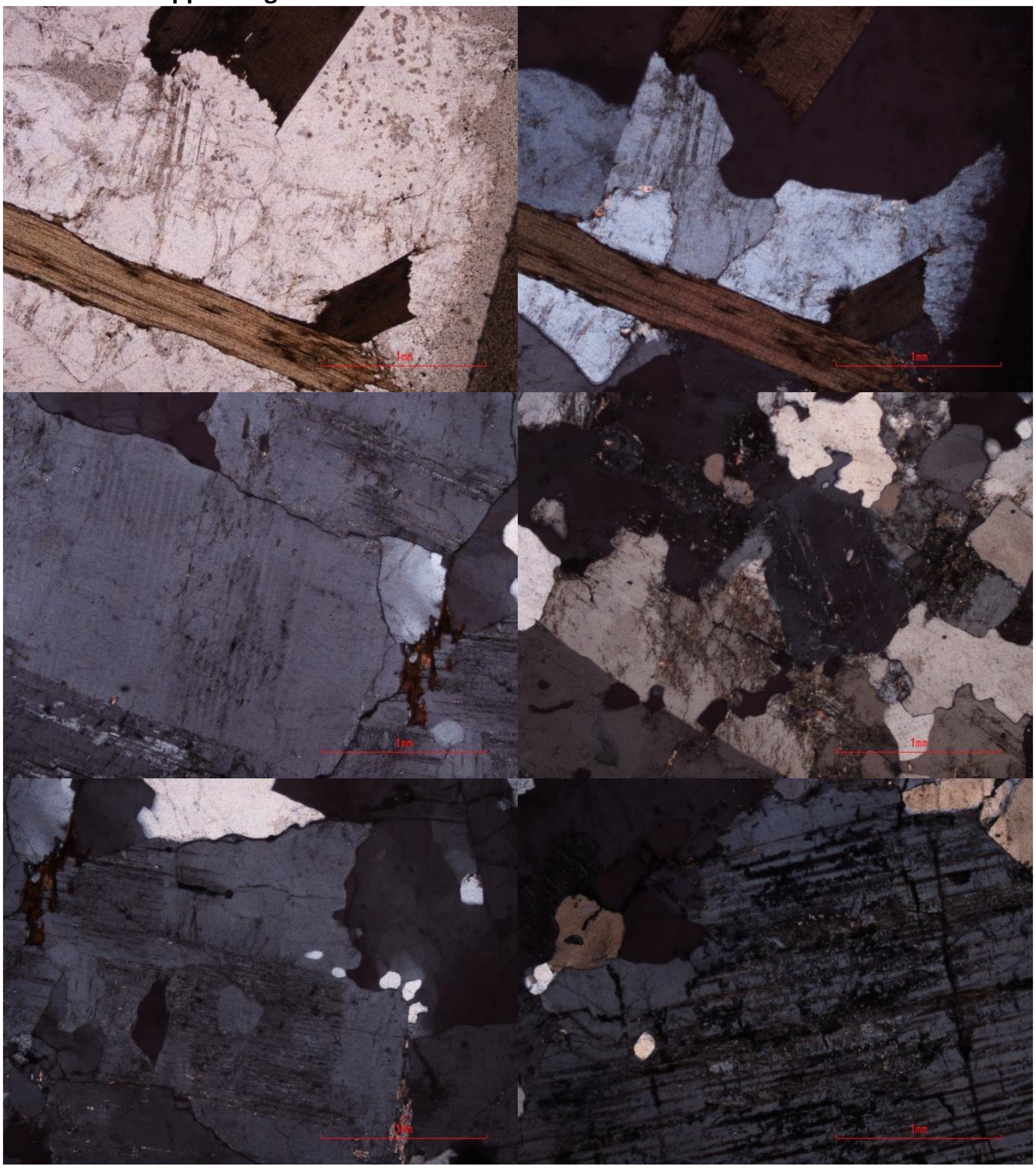

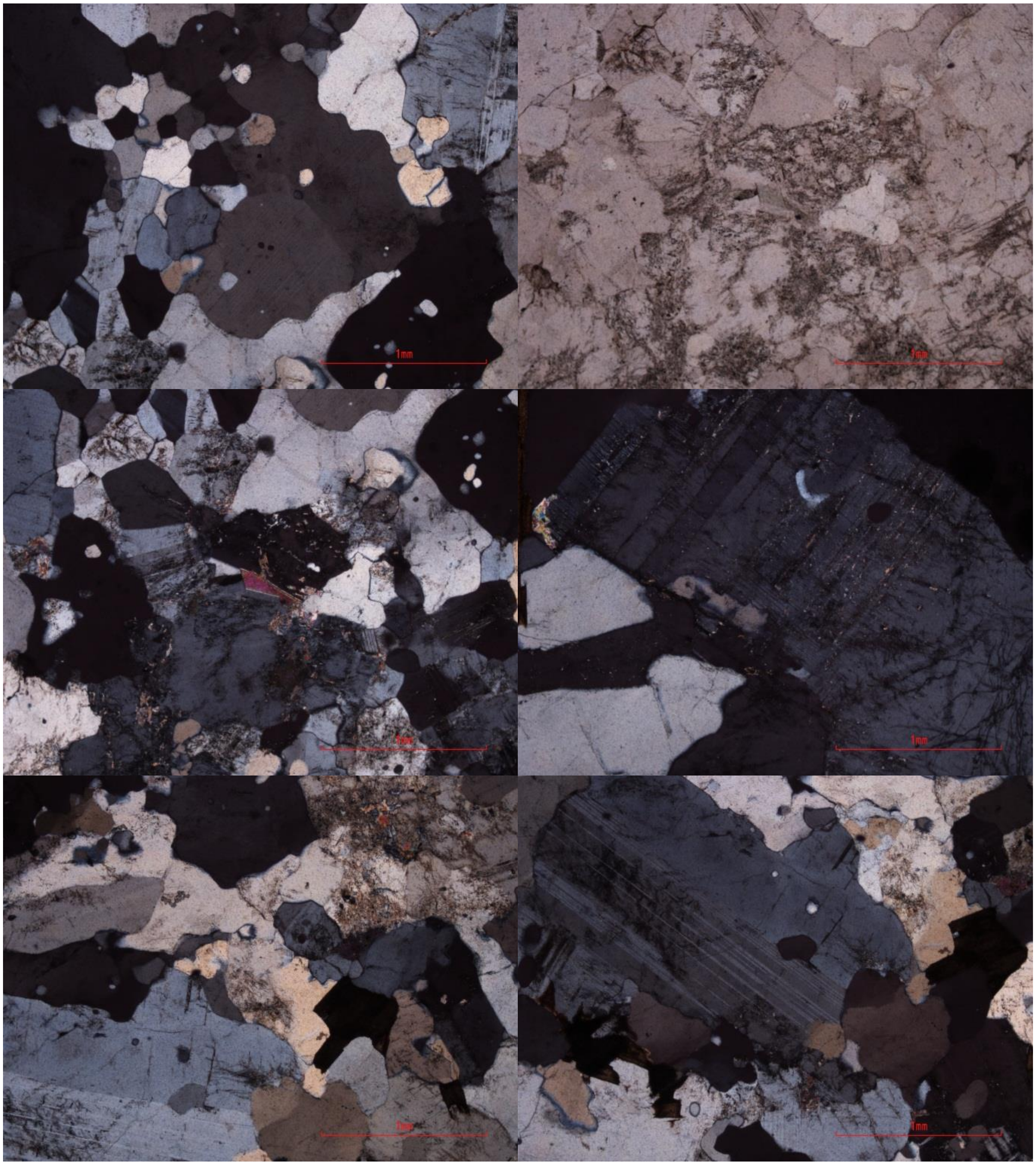
1mm
1mm
1mm

076aA - Salknappen Pegmatite

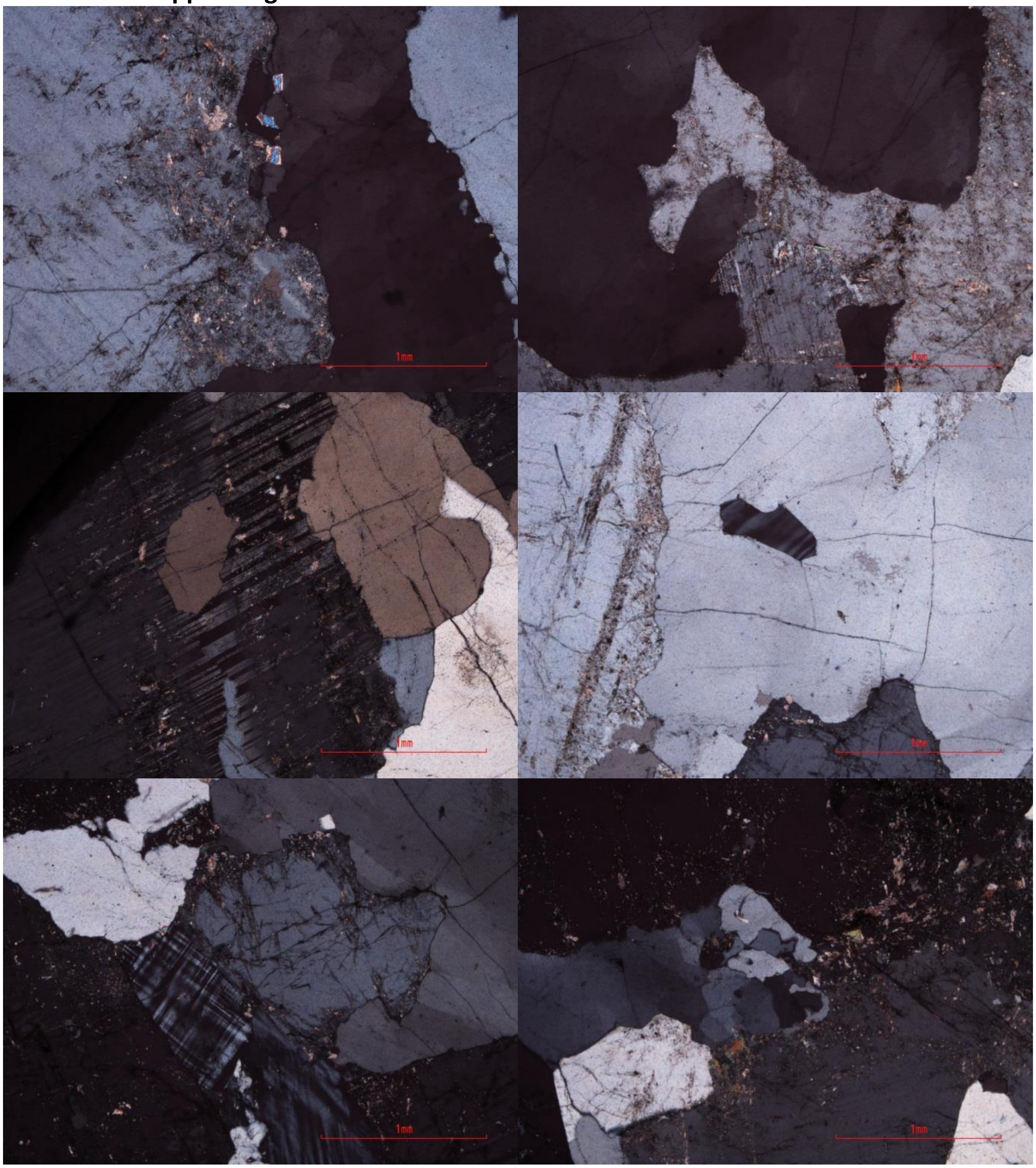

078aB - Salknappen Pegmatite

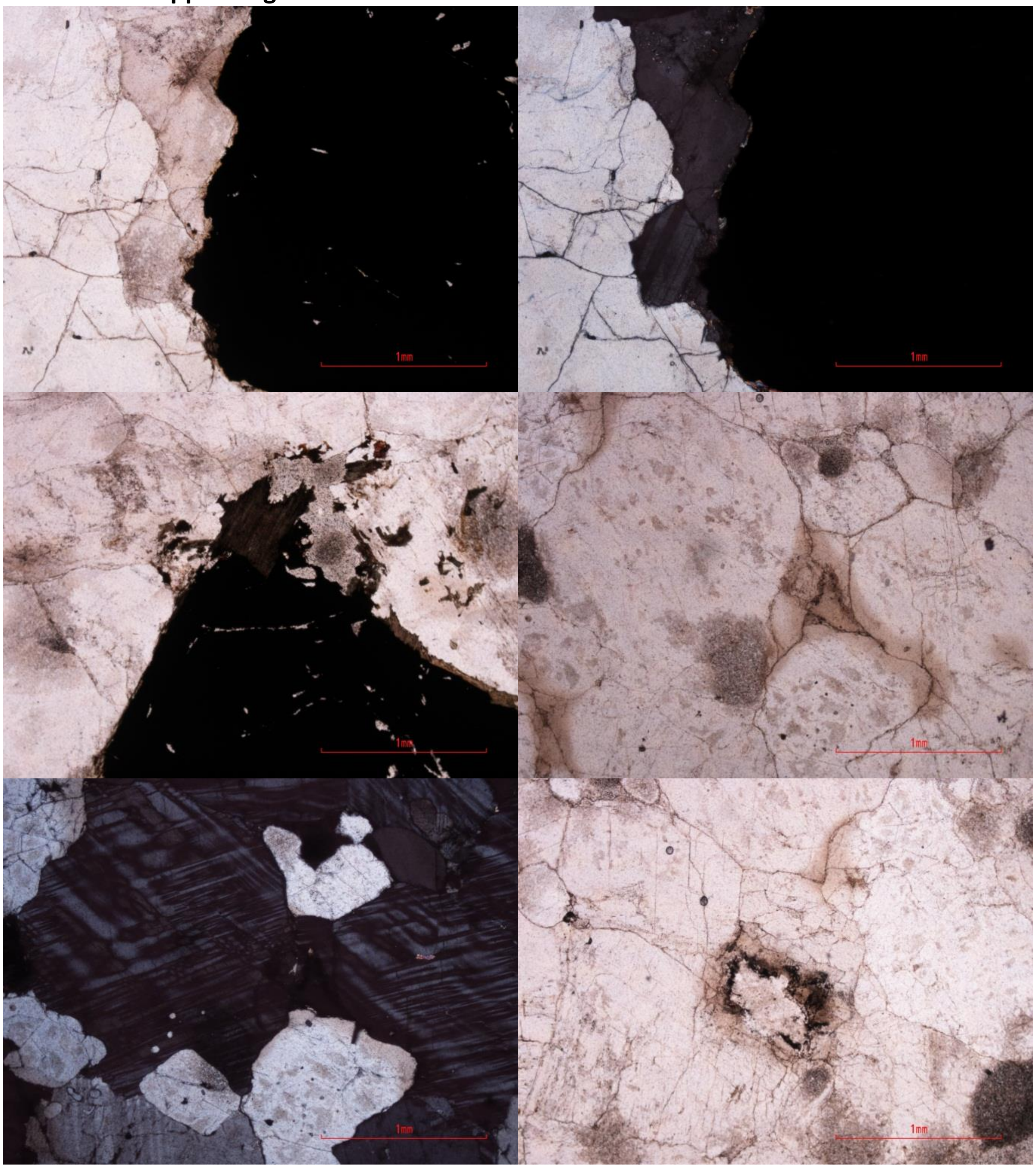

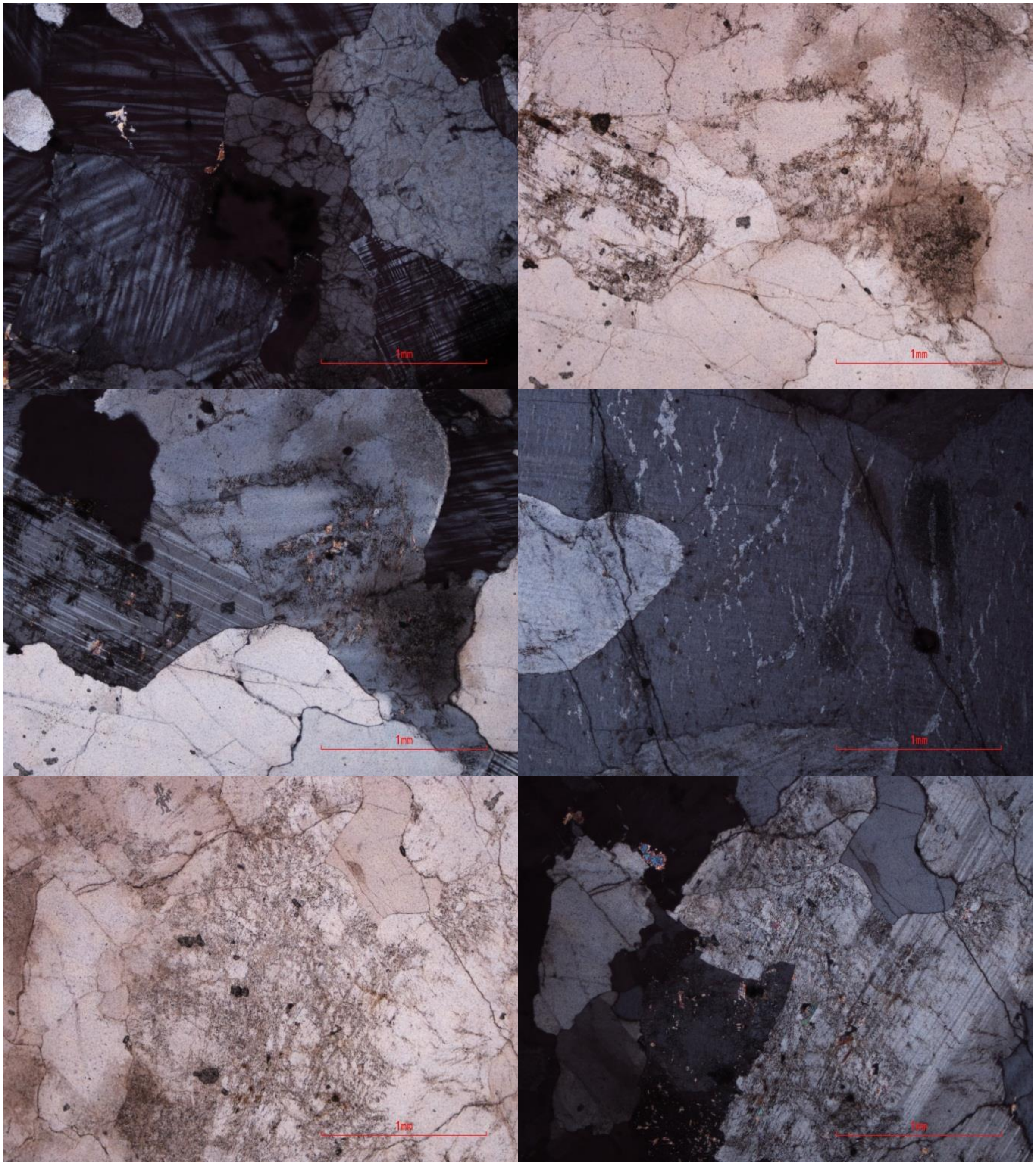

082aD - Salknappen Pegmatite

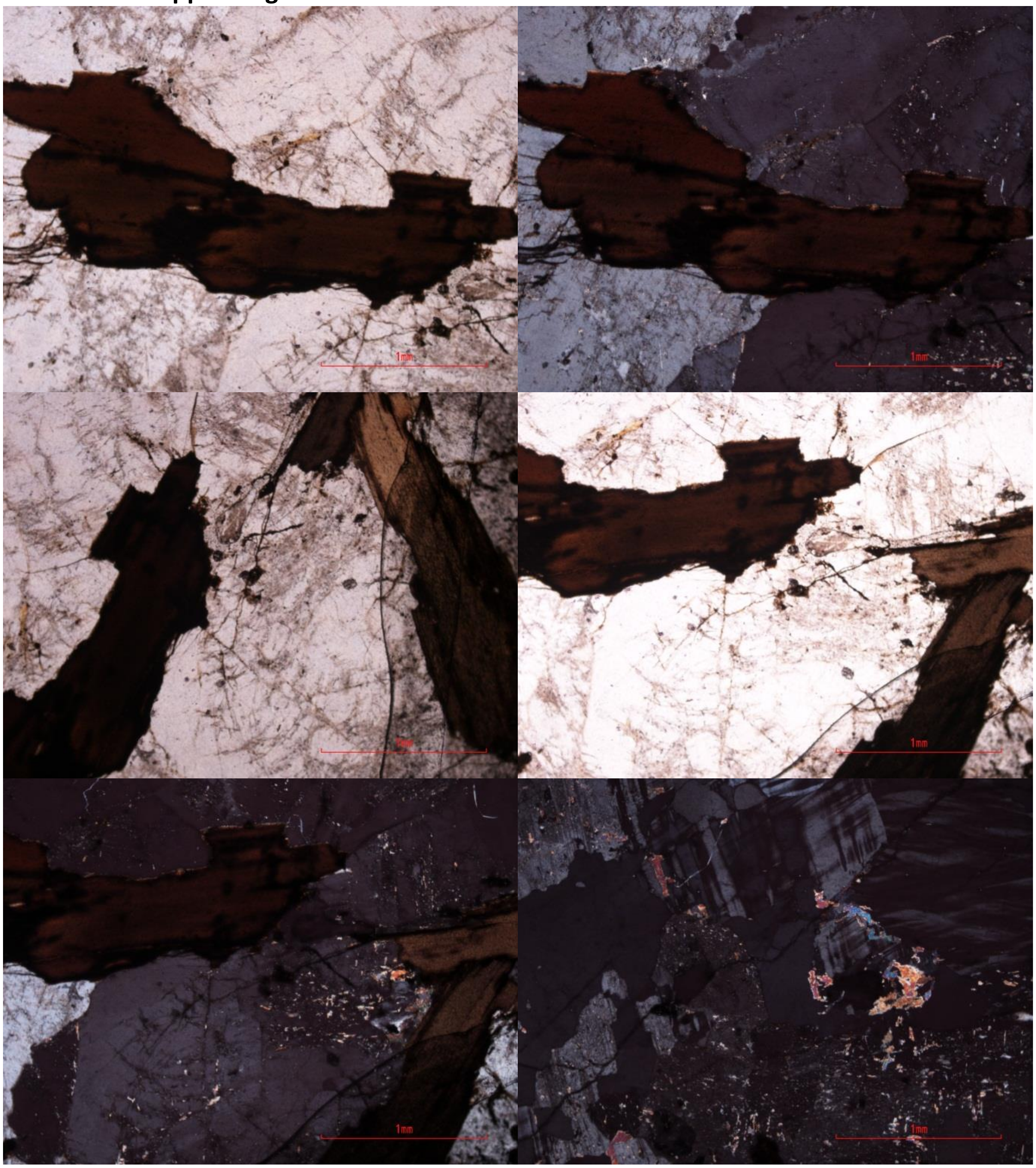

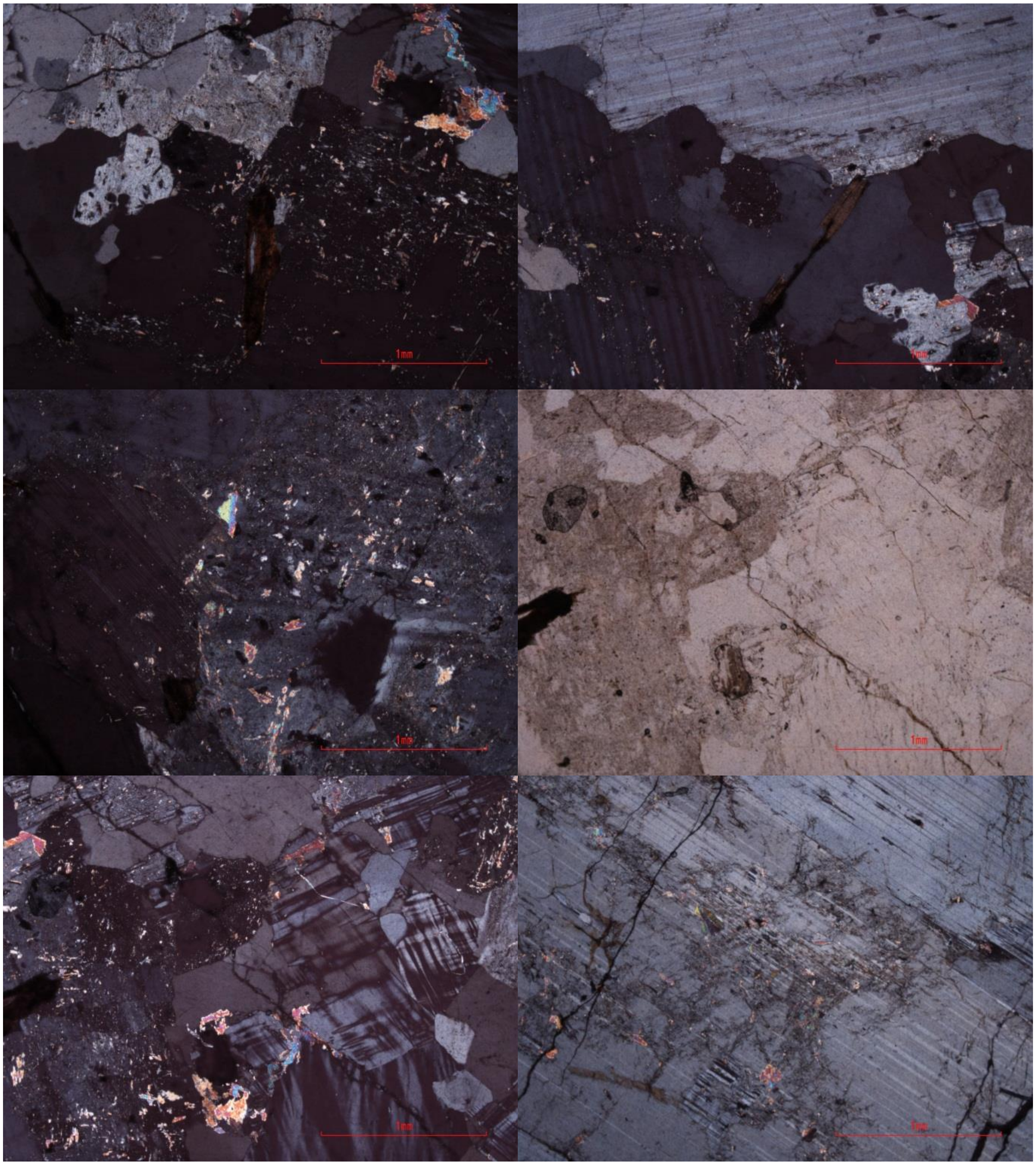
1mm
1mm
1mm
1mm

082bA - Salknappen Pegmatite

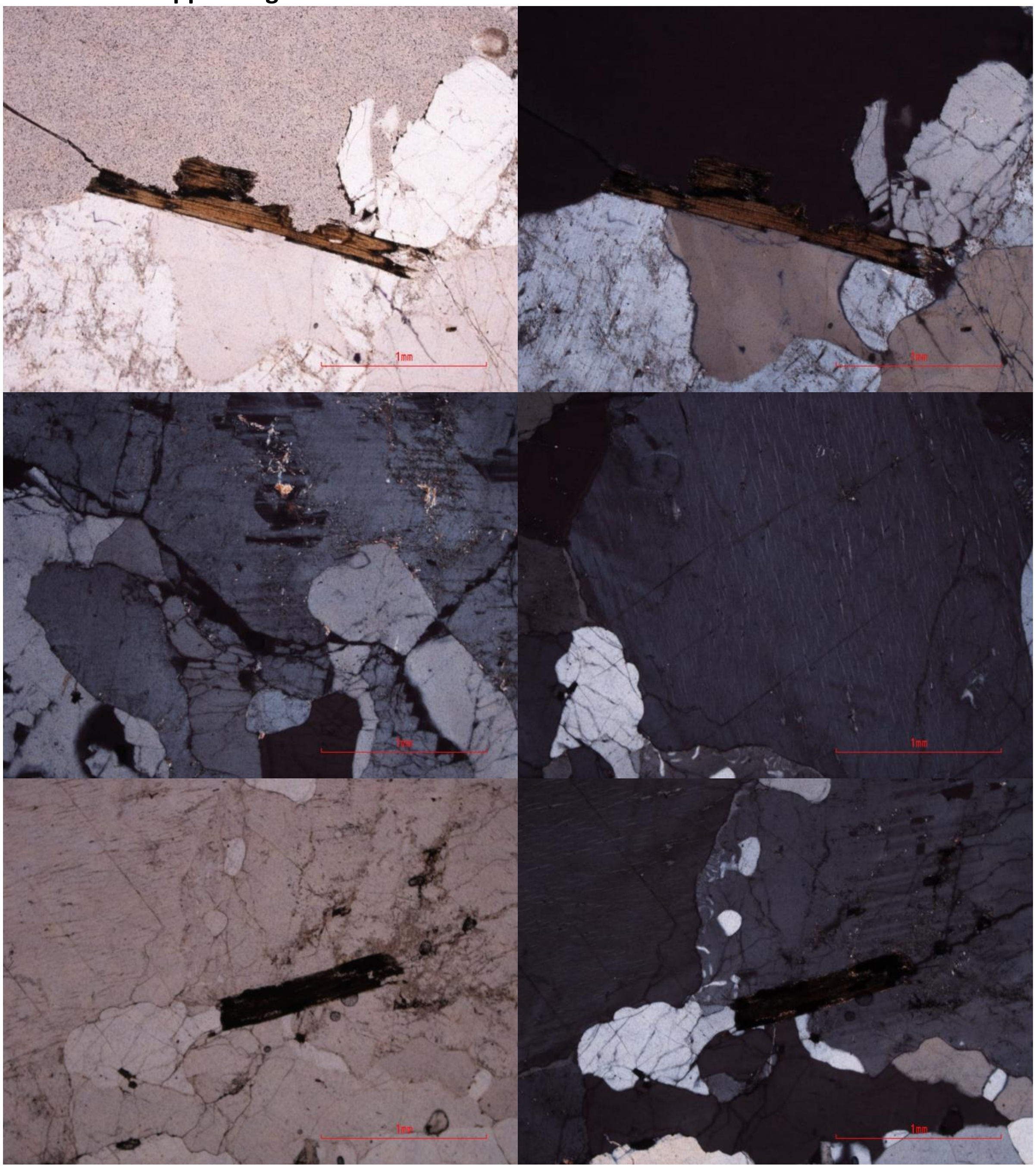

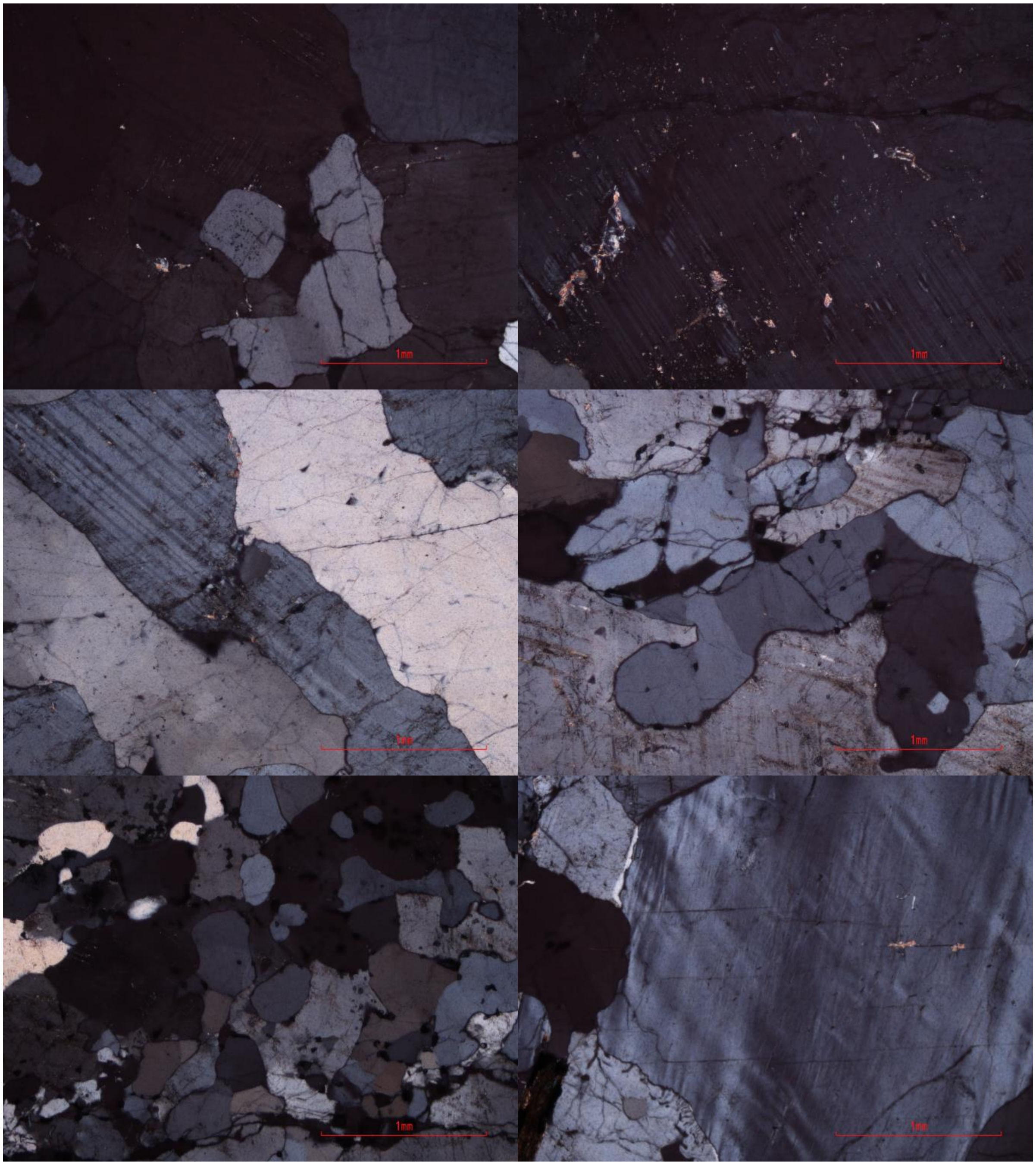
1mm
1mm
1mm
1mm
1mm
1mm

083aB - Dalmatian Granite

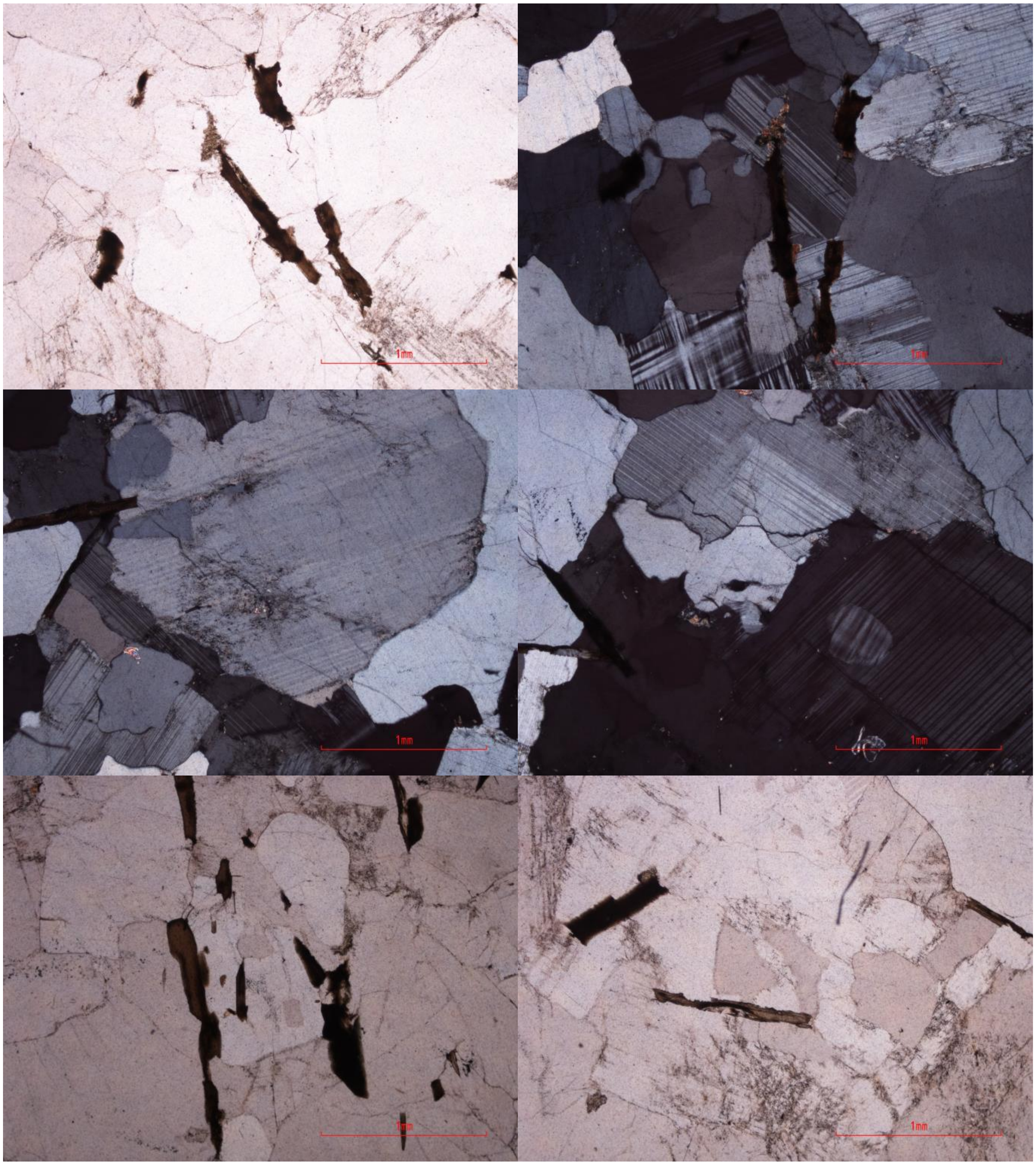

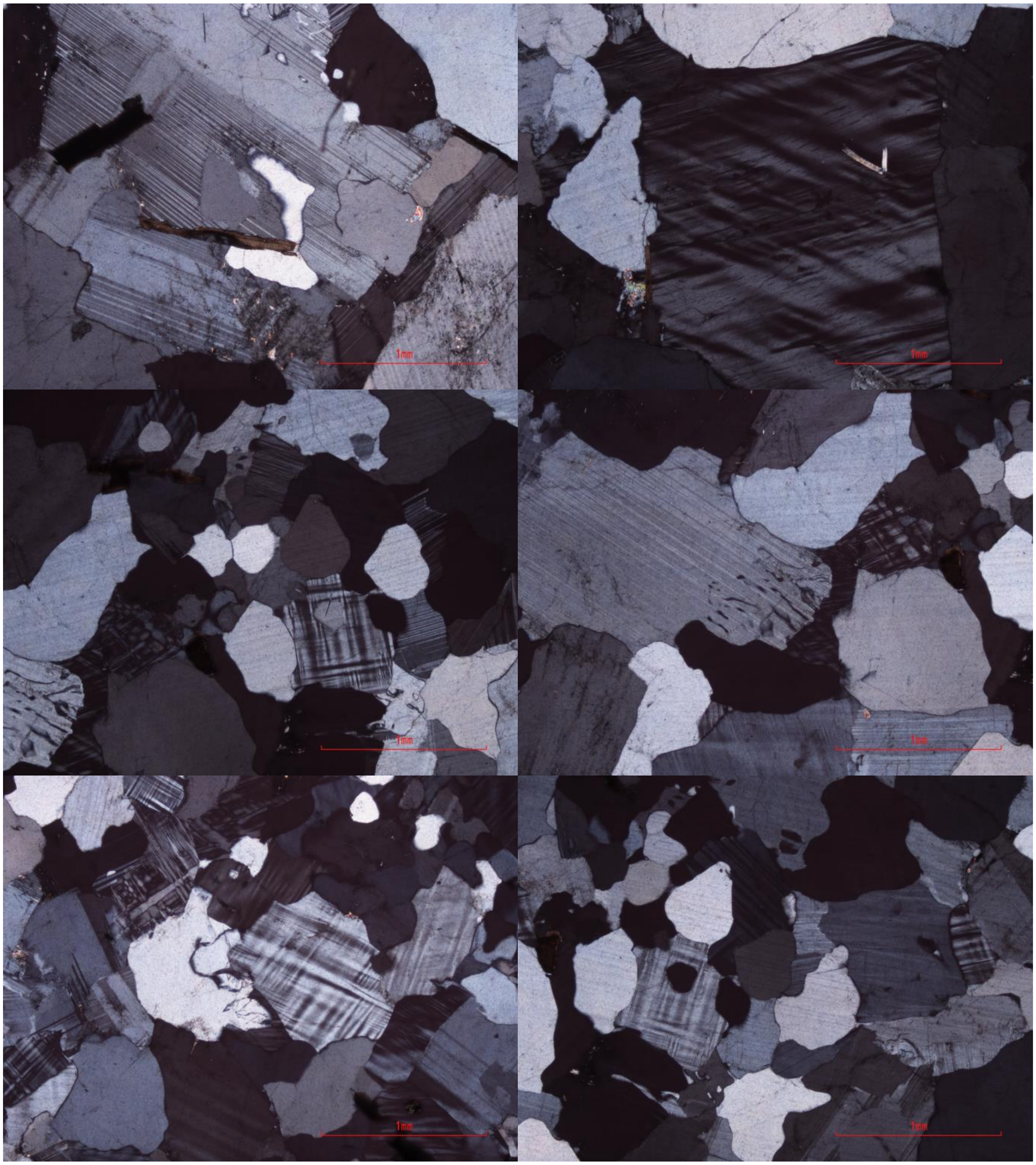
1mm
1mm
1mm
1mm
1mm
1mm

083bC - Salknappen Pegmatite

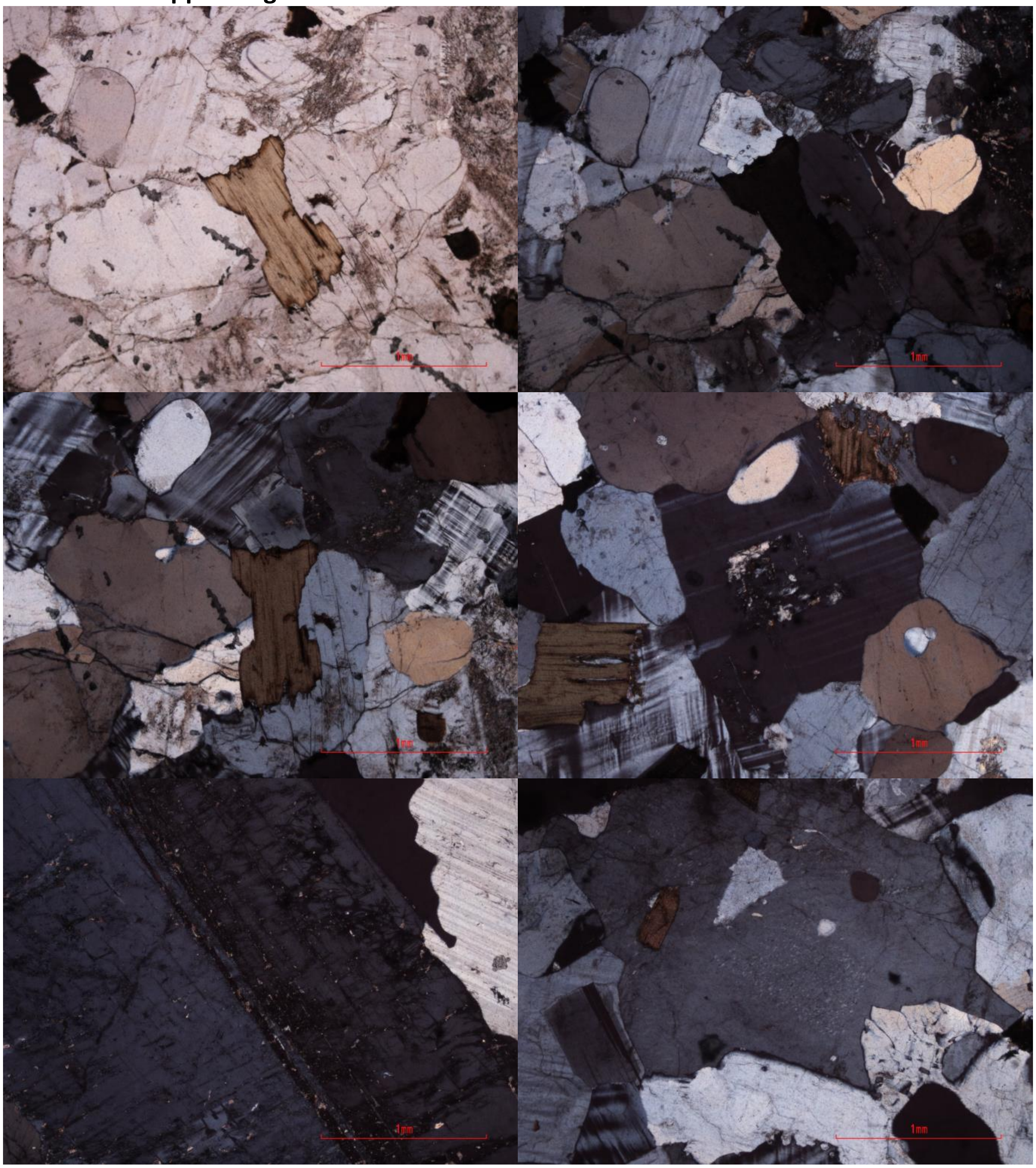

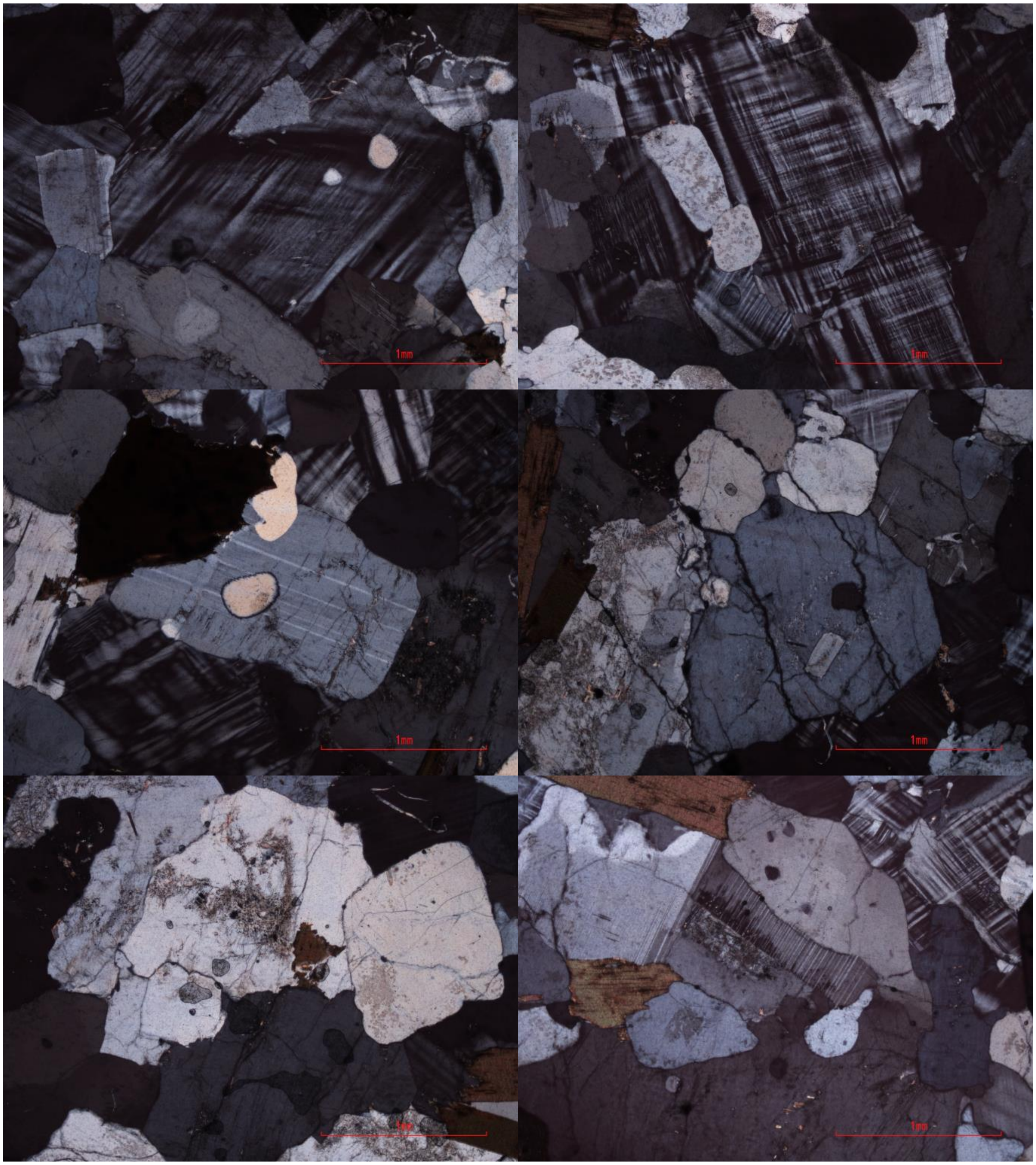
1mm
1mm
1mm
1mm
1mm
1mm

084aC - Salknappen Pegmatite

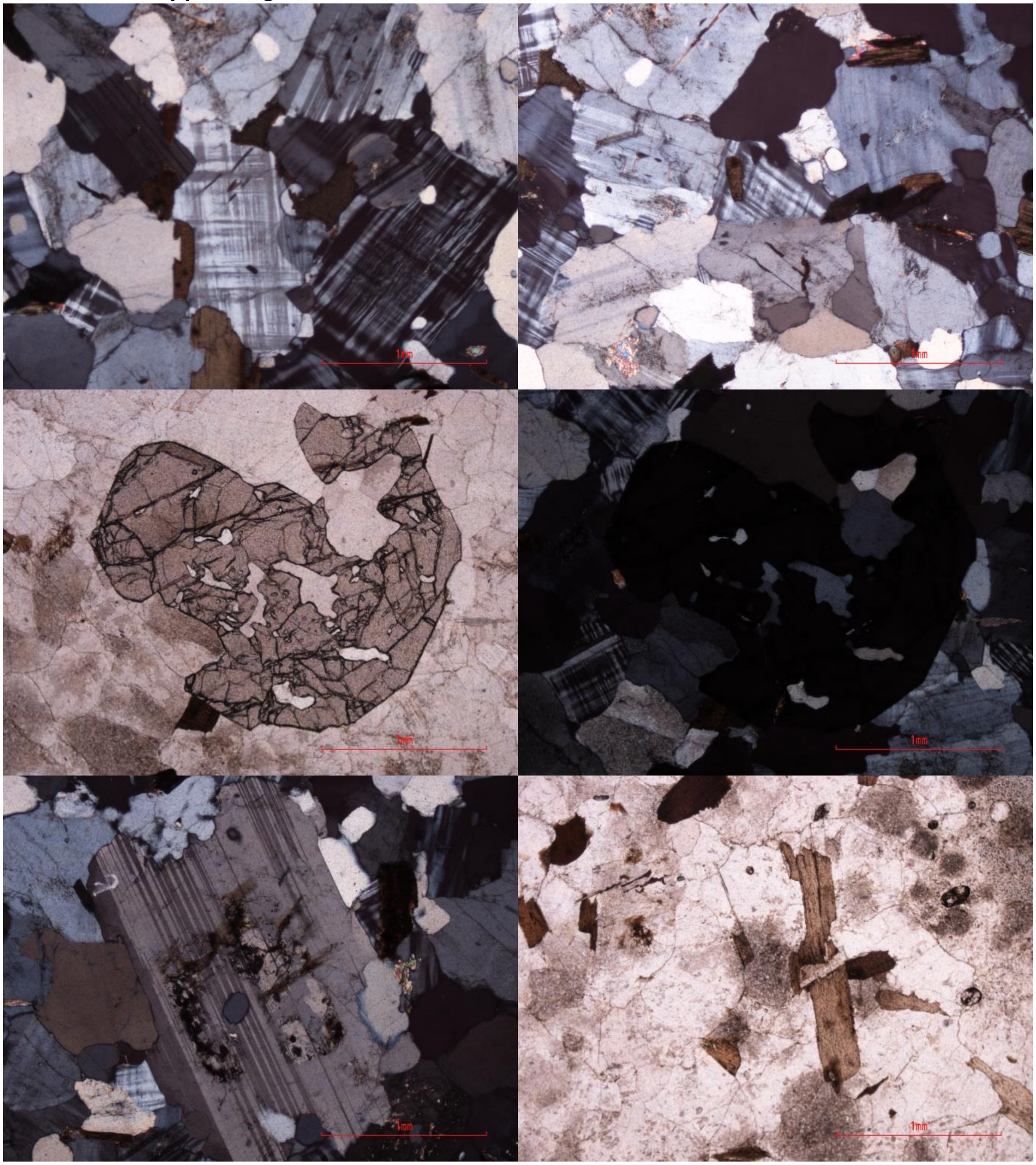

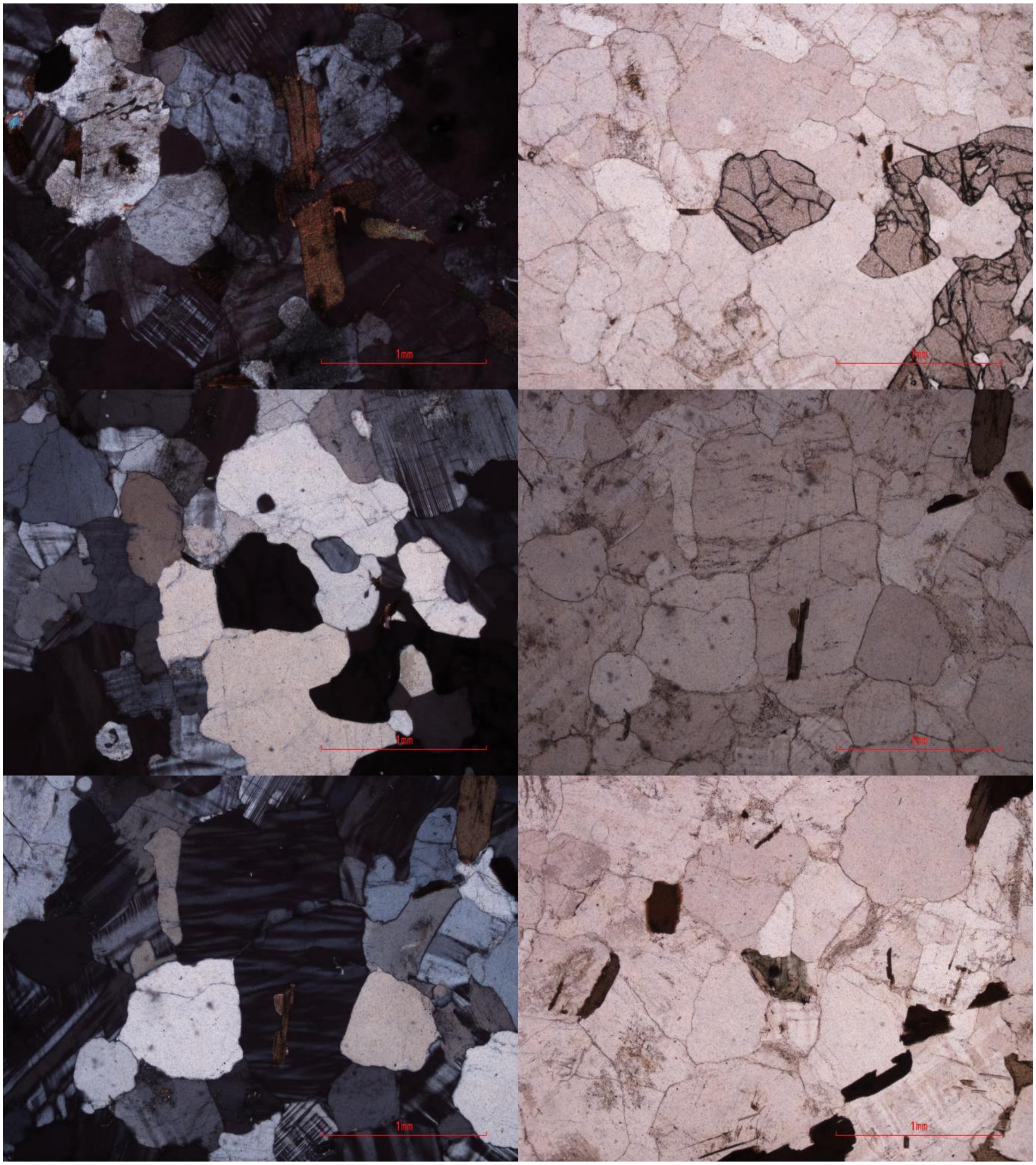
1mm
1mm
1mm
1mm
1mm
1mm

084bF - Dalmatian Granite

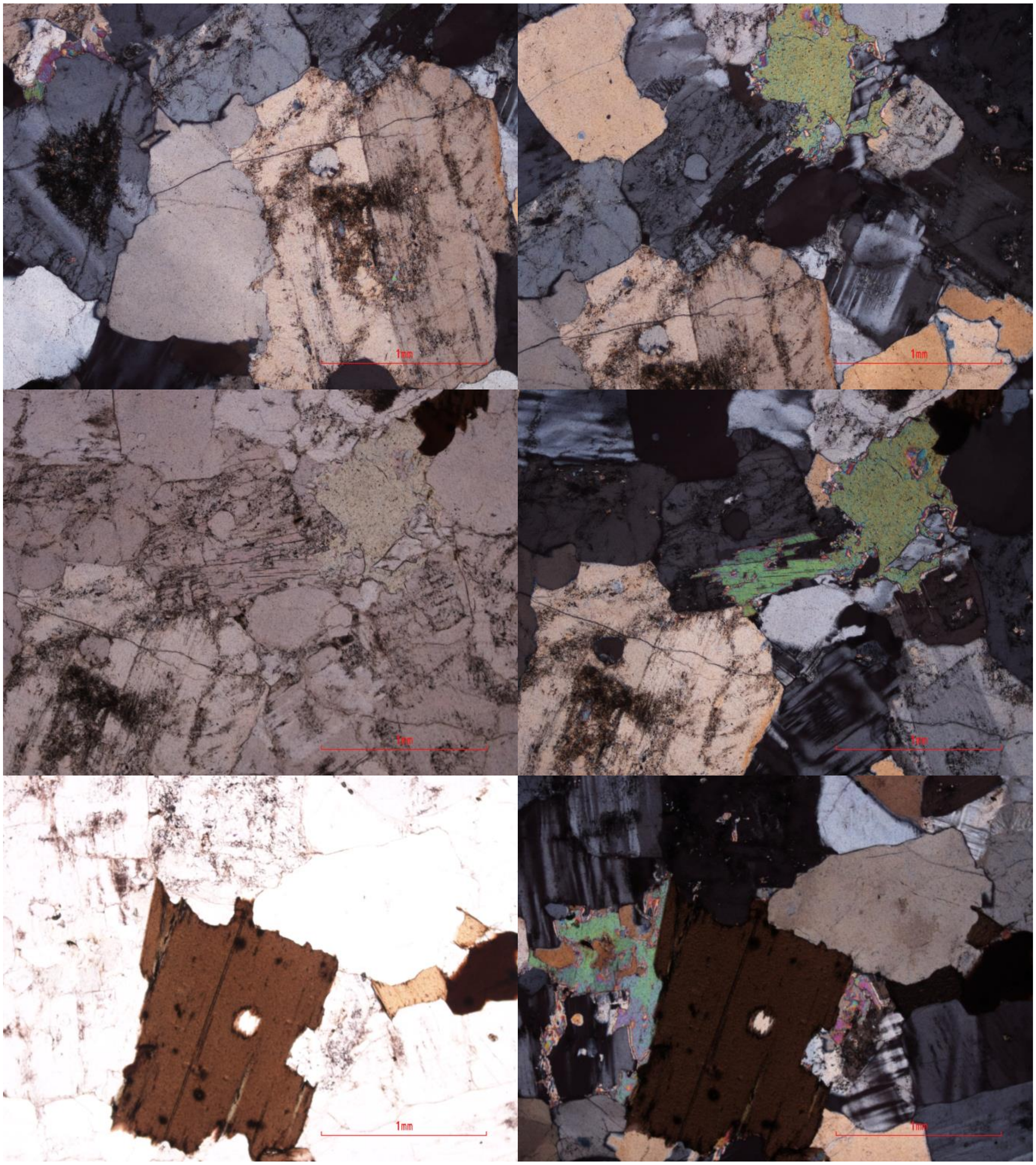


1mm
1mm
1mm